Environmental Chemistry for a Sustainable World 35

Mu. Naushad
Saravanan Rajendran
Eric Lichtfouse *Editors*

Green Methods for Wastewater Treatment

Springer

Environmental Chemistry for a Sustainable World

Volume 35

Other Publications by the Editors

Books
Environmental Chemistry
http://www.springer.com/978-3-540-22860-8

Organic Contaminants in Riverine and Groundwater Systems
http://www.springer.com/978-3-540-31169-0

Sustainable Agriculture
Volume 1: http://www.springer.com/978-90-481-2665-1
Volume 2: http://www.springer.com/978-94-007-0393-3

Book series
Environmental Chemistry for a Sustainable World
http://www.springer.com/series/11480

Sustainable Agriculture Reviews
http://www.springer.com/series/8380

Journals
Environmental Chemistry Letters
http://www.springer.com/10311

More information about this series at http://www.springer.com/series/11480

Mu. Naushad • Saravanan Rajendran
Eric Lichtfouse
Editors

Green Methods for Wastewater Treatment

Springer

Editors
Mu. Naushad
Department of Chemistry,
College of Science
King Saud University
Riyadh, Saudi Arabia

Saravanan Rajendran
Faculty of Engineering,
Department of Mechanical Engineering
University of Tarapacá
Arica, Chile

Eric Lichtfouse
Aix Marseille University
CNRS, IRD, INRA, Coll France,
CEREGE
Aix-en-Provence, France

ISSN 2213-7114 ISSN 2213-7122 (electronic)
Environmental Chemistry for a Sustainable World
ISBN 978-3-030-16426-3 ISBN 978-3-030-16427-0 (eBook)
https://doi.org/10.1007/978-3-030-16427-0

This Springer imprint is published by the registered company Springer Nature Switzerland AG.
The registered company address is: Gewerbestrasse 11, 6330 Cham, Switzerland

Preface

Water is the most precious gifts of the nature to mankind; it is difficult even to imagine a form of life that might exist without water. However, due to the rapid pace of industrialization and tremendous increase in the population, the contamination of water resources has occurred globally. Recently, several health organisation reports described various water-related diseases can easily kill more than millions of people every year including children.

In this scenario, this book is described in the detailed account of different green methods for wastewater treatment. The applications of various types of materials like mesoporous materials, TiO_2-based nanocomposites and magnetic nanoparticles for wastewater treatment are discussed in this book. The role of catalysts along with their chemical reactions, challenges, past developments and direction for further research of wastewater treatment methods has been also discussed in this book. Furthermore, various treatment methods like photo-Fenton, photocatalysis, electrochemical approach and adsorption were defined in more depth. Moreover, the bacterial infection and antibacterial solution have been also included in detail. I believe this book will be helpful for chemical engineers, environmental scientists, analytical chemist, materials scientists and all researchers who are working in the field of wastewater treatment.

Riyadh, Saudi Arabia — Mu. Naushad
Arica, Chile — Saravanan Rajendran
Aix-en-Provence, France — Eric Lichtfouse

Acknowledgements

First of all, we thank God for providing us good health and valuable opportunity to accomplish this book successfully.

In our journey towards this book, our heartfelt thanks to series editor and advisory board for accepting our book as a part of the series "Environmental Chemistry for a Sustainable World" and for their support and encouragement. We extend our sincere thanks to all authors and reviewers for providing hard work and genuine support to complete this book. We have great pleasure in acknowledging various publishers and authors for permitting us the copyright to use their figures and tables. We would still like to offer our deep apologies to any copyright holder if unknowingly their right is being infringed.

Dr. Mu. Naushad expresses his deep gratitude to the Chairman, Department of Chemistry, College of Science, King Saud University, Saudi Arabia, and extends his appreciation to the Deanship of Scientific Research at King Saud University for the support.

R. Saravanan would like to express his sincere thanks to Prof. Francisco Gracia (DIQBT, University of Chile), Prof. Lorena Cornejo Ponce (EUDIM, Universidad de Tarapacá) and Prof. Rodrigo Palma (Director, SERC) for their constant encouragement and valuable support that helped him to complete the task. He further extends his thanks to the Government of Chile (CONICYT-FONDECYT-Project No.: 11170414), SERC (CONICYT/FONDAP/15110019) and School of mechanical Engineering (EUDIM), Universidad de Tarapacá, Arica, Chile, for their financial support.

Mu. Naushad
Saravanan Rajendran
Eric Lichtfouse

Contents

About the Editors

Mu. Naushad is presently working as an Associate Professor in the Department of Chemistry, College of Science, King Saud University (KSU), Riyadh, Kingdom of Saudi Arabia. He obtained his M.Sc. and Ph.D. in Analytical Chemistry from Aligarh Muslim University, Aligarh, India, in 2002 and 2007, respectively. He has a vast research experience in the multidisciplinary fields of Analytical Chemistry, Materials Chemistry and Environmental Science. He holds several US patents, over 275 publications in the international journals of repute, 20 book chapters and several books published by renowned international publishers. He has >7200 citations with a Google Scholar h-index of >52. He has successfully run several research projects funded by the National Plan for Science, Technology and Innovation (NPST) and King Abdulaziz City for Science and Technology (KACST), Kingdom of Saudi Arabia. He is the Editor/Editorial Member of several reputed journals like *Scientific Reports* (Nature), *Process Safety and Environmental Protection* (Elsevier), *Journal of Water Process Engineering* (Elsevier) and *International Journal of Environmental Research and Public Health* (MDPI). He is also the Associate Editor for *Environmental Chemistry Letters* (Springer) and *Desalination and Water Treatment* (Taylor and Francis). He has been awarded the Scientist of the Year Award 2015 from the National Environmental Science Academy, New Delhi, India, Scientific Research Quality Award 2019, King Saud University and Almarai Award 2017, Saudi Arabia.

Saravanan Rajendran has received his Ph.D. in Physics-Material Science in 2013 from the Department of Nuclear Physics, University of Madras, Chennai, India. He was awarded the University Research Fellowship (URF) during the year 2009–2011 by the University of Madras. After working as an Assistant Professor in Dhanalakshmi College of Engineering, Chennai, India, during the year 2013–2014, he was awarded SERC and CONICYT-FONDECYT Postdoctoral Fellowship, University of Chile, Santiago, Chile, in the year 2014–2017. He has worked (2017–2018) in the research group of Professor John Irvine, School of Chemistry, University of St Andrews, UK, as a Postdoctoral Research Fellow within

the framework of an EPSRC-Global Challenges Research Fund for the removal of blue-green algae and their toxins. Currently, he is working as a Research Scientist in the School of Mechanical Engineering (EUDIM), University of Tarapacá, Arica, Chile, as well as a Research Associate in SERC, University of Chile, Santiago, Chile. He is Associate Editor for International Journal of Environmental Science and Technology (Springer). His research interests focuses in the area of nanostructured functional materials, photophysics, surface chemistry and nanocatalysts for renewable energy and waste water purification. He has published several international peer-reviewed journals, five book chapters and three books published by renowned international publishers.

Eric Lichtfouse (Ph.D.), born in 1960, is an Environmental Chemist working at the University of Aix-Marseille, France. He has invented carbon-13 dating, a method allowing to measure the relative age and turnover of molecular organic compounds occurring in different temporal pools of any complex media. He is teaching scientific writing and communication and has published the book *Scientific Writing for Impact Factor Journals*, which includes a new tool – the micro-article – to identify the novelty of research results. He is Founder and Chief Editor of scientific journals and series in environmental chemistry and agriculture. He got the Analytical Chemistry Prize by the French Chemical Society, the Grand Prize of the Universities of Nancy and Metz and a Journal Citation Award by the Essential Indicators.

About the Authors

Ali Akbari-Fakhrabadi Advanced Materials Laboratory, Department of Mechanical Engineering, University of Chile, Santiago, Chile

Muhamad I. Amal Research Center Metallurgy and Materials, Indonesian Institute of Sciences, Tangerang Selatan, Indonesia

Yaacov Ben-David Department of Biology and Chemistry, The Key Laboratory of Chemistry for Natural Products of Guizhou Province and Chinese Academy of Sciences, Guizhou, China

State Key Laboratory of Functions and Applications of Medicinal Plants, Guizhou Medical University, Guiyang, China

Madhumita Bhaumik Department of Applied Chemistry, University of Johannesburg, Johannesburg, South Africa

Arulvasu Chinnasamy Department of Zoology, University of Madras, Chennai, India

Raghunath Das Department of Applied Chemistry, University of Johannesburg, Johannesburg, South Africa

Lina J. Diguna Department of Renewable Energy Engineering, Prasetiya Mulya University, Tangerang, Indonesia

Babu Gajendran Department of Biology and Chemistry, The Key Laboratory of Chemistry for Natural Products of Guizhou Province and Chinese Academy of Sciences, Guizhou, China

State Key Laboratory of Functions and Applications of Medicinal Plants, Guizhou Medical University, Guiyang, China

Ealisha Jha Department of Physics and Physical Oceanography, Memorial University of Newfoundland, Newfoundland and Labrador, NL, Canada

R. Justin Joseyphus Magnetic Materials Laboratory, National Institute of Technology, Tiruchirappalli, Tamil Nadu, India

N. V. V. Jyothi Department of Chemistry, Sri Venkateswara University, Tirupati, Andhra Pradesh, India

Gurpreet Kaur Advanced Functional Materials Laboratory, Department of Nanotechnology, Sri Guru Granth Sahib World University, Fatehgarh Sahib, Punjab, India

Manjot Kaur Advanced Functional Materials Laboratory, Department of Nanotechnology, Sri Guru Granth Sahib World University, Fatehgarh Sahib, Punjab, India

S. Kaviya Department of Chemical Engineering, Indian Institute of Science (IISc), Bangalore, Karnataka, India

Akshay Kumar Advanced Functional Materials Laboratory, Department of Nanotechnology, Sri Guru Granth Sahib World University, Fatehgarh Sahib, Punjab, India

Yuly Kusumawati Chemistry Department, Sepuluh Nopember Institute of Technology, Surabaya, Indonesia

Wuling Liu Department of Biology and Chemistry, The Key Laboratory of Chemistry for Natural Products of Guizhou Province and Chinese Academy of Sciences, Guizhou, China

State Key Laboratory of Functions and Applications of Medicinal Plants, Guizhou Medical University, Guiyang, China

Yanmei Li Department of Biology and Chemistry, The Key Laboratory of Chemistry for Natural Products of Guizhou Province and Chinese Academy of Sciences, Guizhou, China

State Key Laboratory of Functions and Applications of Medicinal Plants, Guizhou Medical University, Guiyang, China

Arjun Maity Department of Applied Chemistry, University of Johannesburg, Johannesburg, South Africa

DST/CSIR National Centre for Nanostructured Materials, Council for Scientific and Industrial Research, Pretoria, South Africa

R. V. Mangalaraja Advanced Ceramics and Nanotechnology Laboratory, Department of Materials Engineering, Faculty of Engineering, University of Concepcion, Concepcion, Chile

Technological Development Unit (UDT), University of Concepcion, Coronel, Chile

Pritam Kumar Panda Division of Pediatric Hematology and Oncology, University Medical Center, University of Freiburg, Freiburg, Germany

Yashmin Pattnaik School of Biotechnology, KIIT Deemed to be University, Bhubaneswar, India

Prajita Paul School of Biotechnology, KIIT Deemed to be University, Bhubaneswar, India

Hugues Kamdem Paumo Department of Applied Chemistry, University of Johannesburg, Johannesburg, South Africa

Kriveshini Pillay Department of Applied Chemistry, University of Johannesburg, Johannesburg, South Africa

Eswaran Prabakaran Department of Applied Chemistry, University of Johannesburg, Johannesburg, South Africa

K. Prabakar Department of Electrical and Computer Engineering, Pusan National University, Busan, South Korea

Nurul Pratiwi Chemistry Department, Andalas University, Padang, Indonesia

Reza A. Putri Chemistry Department, Andalas University, Padang, Indonesia

Shepherd Sambaza Department of Applied Chemistry, University of Johannesburg, Johannesburg, South Africa

A. Dennyson Savariraj Advanced Ceramics and Nanotechnology Laboratory, Department of Materials Engineering, Faculty of Engineering, University of Concepcion, Concepcion, Chile

Mrutyunjay Suar School of Biotechnology, KIIT Deemed to be University, Bhubaneswar, India

Anup Thakur Department of Basic and Applied Sciences, Punjabi University, Patiala, Punjab, India

Arun Thirumurugan Advanced Materials Laboratory, Department of Mechanical Engineering, University of Chile, Santiago, Chile

Krishnapriya Madhu Varier Department of Medical Biochemistry, Dr. ALM PGIBMS, University of Madras, Chennai, India

Department of Zoology, University of Madras, Chennai, India

T. Vasantha Department of Chemistry, Sri Venkateswara University, Tirupati, Andhra Pradesh, India

Suresh K. Verma School of Biotechnology, KIIT Deemed to be University, Bhubaneswar, India

Institute of Environmental Medicine, Karolinska Institutet, Stockholm, Sweden

C. Viswanathan Department of Nanoscience and Technology, Bharathiar University, Coimbatore, India

Diana V. Wellia Chemistry Department, Andalas University, Padang, Indonesia

Chapter 1
Visible-Light-Responsive Nanostructured Materials for Photocatalytic Degradation of Persistent Organic Pollutants in Water

Hugues Kamdem Paumo, Raghunath Das, Madhumita Bhaumik, and Arjun Maity

Contents

Abstract Persistent organic pollutants (POPs) such as polychlorinated biphenyls and polycyclic aromatic hydrocarbons consist of a group of synthetic compounds that are characterized by their resistance to degradation, important long-range transportation, and harmful effects to the ecosystems and human well-being. Certainly, we cannot think about progress in human civilization without industrialization. However, the rapid evolution in chemical, agrochemical, and petrochemical industries and the population exponential growth in the last century have given rise to an important number of toxic, bioaccumulative, and persistent organic chemicals in the environment. Effective removal of persistent organic pollutants (POPs) from

H. K. Paumo · R. Das · M. Bhaumik
Department of Applied Chemistry, University of Johannesburg, Johannesburg, South Africa

A. Maity (✉)
Department of Applied Chemistry, University of Johannesburg, Johannesburg, South Africa

DST/CSIR National Centre for Nanostructured Materials, Council for Scientific and Industrial Research, Pretoria, South Africa
e-mail: amaity@csir.co.za

M. Naushad et al. (eds.), *Green Methods for Wastewater Treatment*, Environmental Chemistry for a Sustainable World 35, https://doi.org/10.1007/978-3-030-16427-0_1

wastewater represents one key approach that could limit their potential environmental impacts. Among a variety of techniques reported for the treatment of organic compound-contaminated wastewater, heterogeneous photocatalytic method using visible-light-responsive semiconductors has been articulated as an efficient technology that holds good potential for the removal of POPs. This chapter gives an overview of the latest development in the design and synthesis of unique semiconductors with visible-light-driven catalytic degradation of POPs. Contextual information on the basic principles of heterogeneous photocatalysis, paths of visible-light response, and photocatalytic performance of innovative semiconductor materials are presented.

Keywords Persistent organic pollutants · Heterogeneous photocatalysis · Visible-light response

Abbreviations

POPs	Persistent organic pollutants
BPA	Bisphenol A
DDT	Dichlorodiphenyl trichloroethane
PFOA	Perfluorooctanoic acid
HCB	Hexachlorobenzene
PFOS	Perfluorooctane sulfonate
PCBs	Polychlorinated biphenyls
TNF-α	Tumor necrosis factor α
PCDFs	Polychlorinated dibenzofurans
HepG2	Human hepatoblastoma cell line
PCDDs	Polychlorinated dibenzodioxins
AOPs	Advanced oxidation processes
PBBs	Polybrominated biphenyls
CB	Conduction band
PFOS	Perfluorooctane sulfonate
VB	Valence band
PFOSF	Perfluorooctane sulfonyl fluoride
TTIP	Titanium tetraisopropoxide
BDE209	Decabromodiphenyl ether
GO	Graphene oxide
PAHs	Polycyclic aromatic hydrocarbons
UV	Ultraviolet

1.1 Background

Water is worldwide regarded as the most vital of natural resources for the sustainability of life, yet freshwater systems are directly threatened by human activities. Rapid industrialization has led to the generation of a massive amount of synthetic chemicals, mostly of organic nature and beneficial in crop production and pest and disease control (Naushad 2014). However, the occurrence of some of these compounds into the natural environment has also been found to cause solemn damage to wildlife, aquatic life, and human well-being through food web or drinking water resources (Verhaert et al. 2017; Carlsson et al. 2016; Net et al. 2015). These organic compounds are fat-soluble and susceptible to bio-magnification and trans-boundary transportation. Recognized as persistent organic pollutants (POPs), their fate and activities have engrossed extensive scientific and political interest, principally when the local discharges have proceeded in dispersed contamination far away from the origin place of release (Nadal et al. 2015). The inappropriate treatment of effluent from industries manufacturing or making use of POPs and overflows from fields and atmospheric depositions are some of the main reasons of POPs ubiquitous nature (Fig. 1.1). For example, although no homegrown source for POPs contamination was identified around Bear Island (Bjørnøya), a medium-term air sampling survey of this Arctic island within the period 1999–2003 revealed a total of 50 toxic organic compounds (Kallenborn et al. 2007). These consisted of manmade chemicals used as pesticides and compounds employed in several industrial applications. The presence of these organic pollutants was utterly ascribed to atmospheric long-range transportation. Another example is the elaborated data on the bio-magnification of POPs in subtropical aquatic ecosystems. The Olifants River basin, a tributary of the Limpopo River in the northeast of South Africa, was recently identified as a life-threatening

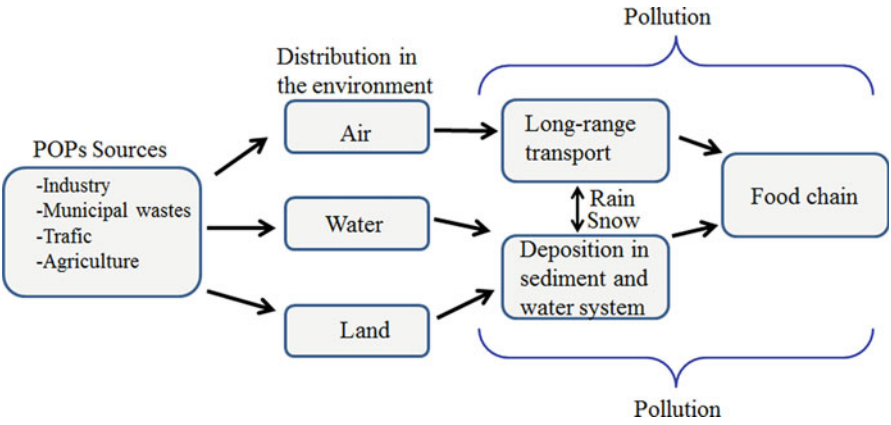

Fig. 1.1 Flow chart of POPs into the environment

river in the Southern African region, owing to the trophic magnification of the detected POPs (Verhaert et al. 2017). The Olifants River basin locality is South Africa's powerhouse with petrochemicals and mine companies. There is enough evidence suggesting that water quality in the Olifants River is impaired by the expansive coal mining in the area, agricultural return flows, and industrial wastewater releases downstream (Water Research Commission 2001). However, this catchment represents one of the main water resources for the residing populations of the Kruger National Park. It is also known for its substantial contribution to the national and regional economies.

1.2 Classifications of POPs

The worldwide concern about organic contaminant residues in the natural environment was initially addressed through a joined action of the global community under the Stockholm Convention in May 2001 (Haffner and Schecter 2014). The key provision, negotiated under the supports of the United Nations Environment Programme (UNEP) and ratified by 90 states and numerous regional economic integration organizations, was to decrease or even eliminate the production of a set of 12 POPs. These environmentally hazardous chemicals were grouped in three families according to their usage:

- Pesticides: dichloro-diphenyl-trichloroethane (DDT), hexachlorobenzene (HCB), aldrin, endrin, chlordane, toxaphene, dieldrin, heptachlor, and mirex
- Industrial substances: polychlorinated biphenyls (PCBs)

  PCBs were produced to serve as dielectric fluids for capacitors and transformers (Erickson and Kaley 2011). Owing to their propensity to enhance the stability and elasticity of polymers, PCBs were also employed as additives in products such as plastics, paints, and coatings.
- Industrial by-products: polychlorinated dibenzofurans and dibenzodioxins (PCDF/DDs)

Both PCDFs and PCDDs formation are associated to a range of incineration reactions in the presence of chlorine source and the production of a variety of chemical products (Altarawneh et al. 2009).

Since 2001, the number of these restricted organic chemicals has been increased considerably. At the fourth meeting of the POPs Review Committee in 2008 in Geneva, Switzerland, for example, amendment to the Stockholm Convention resulted in the addition of a new series of pesticides, including α-, β-, and ɣ-hexachlorocyclohexane, pentachlorobenzene, and chlordecone. Flame retardants such as polybrominated biphenyls (PBBs) and their ether derivatives as well as stain repelling surfactants perfluorooctane sulfonate (PFOS) and perfluorooctane sulfonyl fluoride (PFOSF) were equally listed by this subsidiary body (Wang et al. 2009). Later, the sixth meeting of the Review Committee, held in 2010, saw the inclusion of chemicals such as flame retardant hexabromocyclododecane and acaricide

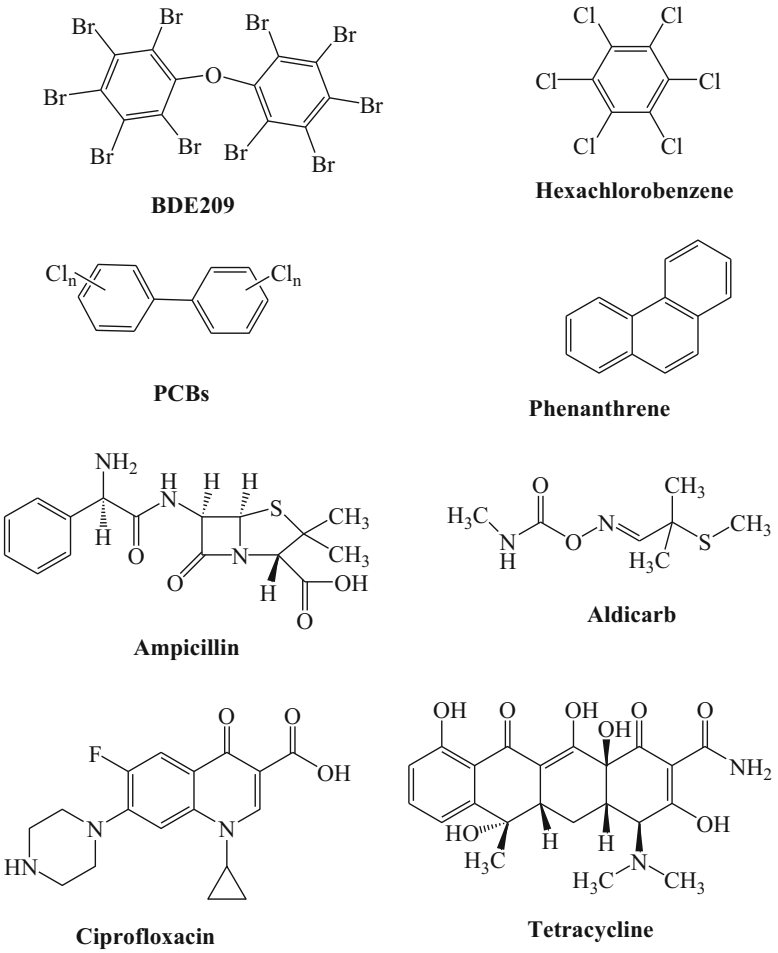

Fig. 1.2 Example of selected POPs

endosulfan. Recently in 2016, apprehension on the benign nature of decabromodiphenyl ether (BDE) was reviewed by the conference attendees during the twelveth meeting of the POPs Review Committee. This flame retardant was also itemized as POPs.

Polycyclic aromatic hydrocarbons (PAHs) are another important group of chemicals branded as POPs. These widespread environmental pollutants mainly occur from the incomplete combustion of vegetation and fossil fuels (Ruge et al. 2015). Accidental spillage during oil shipment has as well been viewed as significant anthropogenic source of PAHs into the environment (Fu et al. 2011). Generally, POPs structures are characterized by at least one aromatic or aliphatic ring, the presence of halogen substituents, and a lack of polar functionalities in some cases (Fig. 1.2).

Strangely, several reports on the evaluation of POPs chemical substitutes, based on internationally established scientific norms, have revealed that some of the proposed alternatives are equally very toxic and therefore not sustainable (Neumeister 2001).

Bisphenol A (BPA), on the other hand, an additive in various consumer and industrial products, although not yet listed by the POPs Review Committee, has frequently been labeled in several research articles as a persistent organic contaminant. In 2011, BPA was among the most produced chemicals in the world, with an estimation of over 5.5 million tons (Son et al. 2018). This synthetic organic compound is used as a monomer for the production of epoxy resins and polycarbonate plastics (Kahtani et al. 2019). The former are employed as tooth-filling materials and coatings for beverage cans, reusable bottles, and water pipes, while the latter are used in automotive components, digital optical discs, medical devices, and electronic equipment. BPA occurrence in the environment is attributed to leaching from the BPA-containing products (Klečka et al. 2009; Schecter et al. 2010; Gaw et al. 2014; Im and Löffler 2016).

The hefty production of antibiotics around the world, and subsequently their incidence in the freshwater systems, has raised concerns over the last decade (Liu et al. 2017a). Antibiotics are essentially employed in human medicine and animal husbandry. In China, for instance, more than 210 thousand tons of antibiotics are being manufactured every year (Luo et al. 2010). However, it has been reported that approximately 75% of the administered antibiotics are discharged in the environment as parent derivatives in urine, manure, and feces (Wang et al. 2014; Qiang et al. 2006).

1.3 Toxicity of POPs

The health effects of POPs are diverse. Exposure to residue of the insecticide DDT and its metabolites, for example, has been stated as hazardous to various mammals. Singh and co-workers reviewed the toxicological characteristics of organochlorinated compounds (Singh et al. 2016). Severe damage has been observed in the kidney, liver, and testicle of rats exposed to DDT. De Joode et al. (2001), on the other hand, reported a permanent deflation in the neurobehavioral operative and an upsurge of the psychiatric and neuropsychological symptoms in human exposed to DDT for more than 2 years. Similarly, a correlation has been established between long-term exposure to PCBs and the development of the type II diabetes by occupationally exposed employees (Silverstone et al. 2012). PCBs are also well-reported for their impact on human neurotransmitter (Gaum et al. 2014; Gaum et al. 2017), thyroid gland (Benson et al. 2018), and telomerase enzyme (Senthilkumar et al. 2012). On the other hand, the prenatal transfer of BDE has been found to cause a significant disruption of the thyroid endocrine system as well as the developmental abnormalities in zebrafish offspring (Han et al. 2017). So as to identify the mechanism of polybrominated diphenyl ethers (PBDEs) toxicity, Pereira and co-workers (2017) investigated their detrimental effects in human hepatoblastoma cell line (HepG2). The authors finding exposed an activation of the autophagic process.

Previously, Costa et al. (2015) also described caspase-dependent apoptosis in mouse cerebellar granule neurons, following PBDEs exposure. Perfluorooctanoic acid (PFOA) and perfluorooctane sulfonate (PFOS) have been found to inhibit the secretion of tumor necrosis factor α (TNF-α), following lipopolysaccharide stimulation, in cultured human leukocytes (Corsini et al. 2011). TNF-α is a cell signaling protein involved in systemic inflammation. Research findings also revealed that these perfluorinated compounds exhibit immunotoxic potential in vivo, as evidenced by the alteration of the hepatic immune system in mice exposed to PFOA-/PFOS-contaminated chow for 10 days (Qazi et al. 2010). PAHs, on the other hand, have been reported as substances with typical cancer-causing and DNA-damaging potential (Rengarajan et al. 2015; Singh and Agarwal 2018). For example, Ramesh's group (2010) reported an interaction between benzo[a]pyrene and the reproductive tissues of female Fischer 344 rats exposed to this environmental toxicant.

BPA is well-documented to act as an endocrine disruptor by mimicking naturally occurring hormones (Canle et al. 2017). The endocrine system is a key regulator of the body's metabolism, sexual development, and growth. Even at very low concentration, BPA has been found to competitively cohere to the estrogen receptor or membrane-bound estrogen receptor in cellular nucleus and promptly influence cellular function (Son et al. 2018). Environmental pollution triggered by the prevalence of antibiotics in the aquatic systems, on the other hand, has raised anxieties regarding their disposition to select for resistant bacteria and enable the establishment and intensification of pathogenic pools that could endanger public health (Luo et al. 2011; Pruden et al. 2006). To address the issues linked with all these anthropogenic organic pollutants, the development of effective technologies for the treatment of industrial and domestic wastewater containing POPs is of great interest within the industrial and scientific communities (Kumar et al. 2017).

1.4 Traditional Water Treatment Processes for the Removal of POPs

Several processes, including bioremediation, coagulation/flocculation, membrane filtration, activated carbon adsorption, ozonation, and advanced oxidation, have been reported for POPs removal from diverse contaminated milieu (Pi et al. 2018; Ji et al. 2014; Durán and Esposito 2000). However, some of these technologies have noteworthy limitations.

Bioremediation is often well-described as the most promising approach for POPs removal, owing to the metabolic potential of microorganisms and their aptitude to interact with organic contaminants even in extreme conditions (Gaur et al. 2018). Although highly valued for its cost-effectiveness, this process is also associated with disadvantages such as reduced bioavailability of pollutants on temporal and spatial scales and scarcity of bench-mark values for efficiency evaluation (Pariatamby and Kee 2016). Another effectve approach for the removal of organic pollutants is the coagulation-flocculation technique. This process involves the use of coagulants that

neutralize by mutual collision with counter ions and agglomerate the charged particles in colloidal suspension. However, this approach usually leads to the production of undesired high volume of sludge (Pariatamby and Kee 2016). Likewise, the use of membrane filtration and activated carbon adsorption also generate membrane retentate and spent activated carbon which must be disposed properly. Nevertheless, activated carbon adsorption and ozonation or UV-based oxidation procedures are the most frequently used methods in effluent treatment plants.

Ozonation makes use of unstable gas ozone (O_3) as a strong oxidant for organic pollutants degradation (Quero-Pastor et al. 2014). Ozone molecules are obtained via dissociation of oxygen molecules by powerful electric discharge, followed by binding collision of the obtained oxygen atoms with other available oxygen molecules. Subsequent to their formation, ozone molecules promptly undergo decomposition to generate highly reactive radicals such as hydroxyl (OH•), superoxide ($O_2^{\bullet -}$), and peroxyl (OOH•) in aqueous medium (Eqs. 1.1, 1.2, and 1.3) (Von Gunten 2003; Gardoni et al. 2012). Due to their strong oxidation potential, these species are able to instantaneously react with organic contaminants (Litter and Quici 2010).

$$O_3 + OH^- \rightarrow HO_2^- + O_2 \tag{1.1}$$

$$O_3 + HO_2^- \rightarrow OH \cdot + O_2 \cdot^- + O_2 \tag{1.2}$$

$$O_3 + OH \cdot \rightarrow OOH \cdot + O_2 \tag{1.3}$$

Ozone can also be combined with UV-light irradiation, hydrogen peroxide (H_2O_2), and catalysts, with the purpose of improving the interaction process with organic contaminants. This combination of oxidation procedures is known as advanced oxidation processes (AOPs). The method is capable of complete decomposition of organic contaminants into less toxic products or their mineralization into CO_2 and water. However the foremost drawback associated with AOPs has always been the relatively higher cost of reagents like ozone or UV light. Therefore, the use of visible-light irradiation as a source of energy is being considered as a model approach to reduce the costs (Dong et al. 2015; Cates 2017). Lately, the development of visible-light-sensitive catalysts for organic contaminants remediation in water has gained tremendous popularity.

Among AOPs, photocatalytic procedure appears as the most promising for the removal of POPs. This technology makes use of photons from a specific light source and a catalyst to generate reactive species. In water treatment, the catalyst can either be soluble (homogeneous photocatalysis) or in solid state (heterogeneous photocatalysis). However, in homogeneous catalysis and green chemical procedures, the catalyst removal or its retrieval from the reaction medium for the reusability purpose is a key concern (Feng et al. 2018; Qin et al. 2017; Gnanasekaran et al. 2016; Romero Sáez et al. 2017; Saravanan et al. 2011, 2018). For the fact that this shortcoming could be alleviate in heterogeneous photocatalysis, this approach can be applied for the sustainable treatment of effluent containing recalcitrant organic compounds like POPs, following the principles of green chemistry.

Heterogeneous photocatalysis takes place in five different stages, namely, (1) diffusion of the organic pollutant from the bulk of the aqueous solution to the surface of the catalyst (semiconductor), (2) adsorption on to the catalyst surface, (3) semiconductor catalyst surface irradiation-induced chemical reaction, (4) desorption of the product from the surface, and (5) removal from the boundary section to the bulk of the solution (Canle et al. 2017). The third stage entails the formation of reactive species, which may either react directly at the semiconductor surface with adsorbed molecules of the organic pollutants or lead to the generation of other reactive species such as oxygen radicals. Although it is always reported that there are numerous reactive species involved during the degradation of organic pollutants in photocatalytic systems, the most active species in most cases appears to be OH•. Hence this radical must be generated in situ unceasingly for the degradation procedure to accomplish the complete destruction of the pollutants. The fundamental attribute of semiconductors in photocatalysis is easily apprehended using the concept of energy band structure (Yan et al. 2013).

1.5 Fundamental of Heterogeneous Photocatalysis

Within a semiconductor, the electronic energy organization involves two distinct regimes, that is, the conduction band (CB) and the valence band (VB). The difference between these two bands is referred as the band gap of the semiconductor. Irradiation of a semiconductor surface with photons carrying sufficient energy to overcome its band gap (Eg) initiates the excitation of VB electrons (e^-) to the CB, leaving behind an equal number of positively charged holes (h^+), as illustrated in Fig. 1.3.

As a result of light irradiation, the photo-oxidizing ability of semiconductors is based upon the potential of photogenerated e^-/h^+ pairs to engender the activated radicals that are responsible for organic pollutants degradation. While the reaction of an adsorbed hydroxyl ion (OH^-) and/or a water molecule with h^+ generates a hydroxyl radical (Eqs. 1.5 and 1.6), adsorbed oxygen molecule (O_2) produces a superoxide radical by interacting with an excited-state electron (Eq. 1.7). In general, the sequence of chain oxidative/reductive reactions that arise at the photon-induced activated surface of a semiconductor photocatalyst has been proposed as follows (Dong et al. 2015):

$$\text{Semiconductor photocatalyst} \xrightarrow{h\nu \geq Eg} h^+ + e^- \tag{1.4}$$

$$h^+ + H_2O \rightarrow \ OH\cdot + H^+ \tag{1.5}$$

$$h^+ + OH^- \rightarrow OH\cdot \tag{1.6}$$

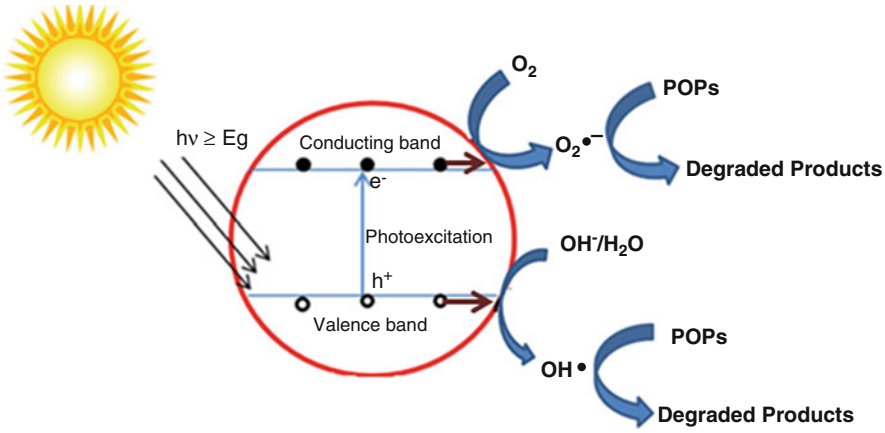

Fig. 1.3 Basic principle of heterogeneous photocatalysis

$$e^- + O_2 \rightarrow O_2 \cdot^- \tag{1.7}$$

$$O_2 \cdot^- + H^+ \rightarrow OOH \cdot \tag{1.8}$$

$$2OOH \cdot \rightarrow H_2O_2 + O_2 \tag{1.9}$$

$$H_2O_2 + O_2 \cdot^- \rightarrow OH^- + OH \cdot + O_2 \tag{1.10}$$

$$POP + (h^+, OH \cdot, O_2 \cdot^-, OOH \cdot \text{Or} H_2O_2) \rightarrow \text{Degraded Products} \tag{1.11}$$

Alongside the importance of energy band gap in photocatalytic process, the semiconductor morphology, crystallinity, and surface properties also play remarkable roles. For example, the morphology and surface properties can dictate the adsorption phase. Furthermore, the recombination ratio of photogenerated e^-/h^+ pairs can be subjected to the semiconductor photocatalyst crystallinity.

The key reaction parameters that are equally reported to influence the heterogeneous photocatalysis of POPs include the temperature, light intensity, semiconductor load, O_2 availability, organic pollutants concentration, and solution pH.

An increase in temperature significantly reduces the solubility of molecular oxygen in the bulk solution, thereby promoting the recombination of electron-hole and dropping the photocatalyst performance (Spasiano et al. 2015). The solution pH, on the other hand, directly impacts the surface charge of the photocatalyst and the position of CB and VB (Ahmad et al. 2016). A decrease in pH renders the CB positively charged holes more operative, owing to the lower amount of hydroxyl ions in the reaction milieu. Under basic or neutral conditions, an increased number of these hydroxyl ions are expected to generate more OH• radicals as foremost species for POPs degradation. Furthermore, the choice of an ideal light intensity is always required to accomplish a high performance in photocatalytic response (Tseng et al. 2010). Semiconductor implicates in photocatalysis do not absorb all the irradiated photons, as a result of light scattering and refraction phenomena. Hence, an upsurge

in light intensity usually increases the rate of reaction up until the mass transfer limitation is attained. Moreover, owing to the fact that heterogeneous photocatalysis is a surface interaction, an increase of the specific surface area of the semiconductor can serve as valuable tool that may lead to improved catalytic process.

With regard to the chemical kinetics that bring about the experimental estimation and analysis of the amount of residual contaminant as a function of time, it is always assumed that POPs adsorption proceeds at quasi-equilibrium, modeled by the Langmuir isotherm. Hence, the Langmuir–Hinshelwood model is usually exploited to describe the reaction progression. The photocatalytic rate of degradation "r" is expressed by the following equation (Spasiano et al. 2015):

$$r = K_r \times \theta_x = K_r \times \frac{K \times [\text{POPs}]}{1 + K \times [\text{POPs}]} \tag{1.12}$$

where K_r, [POPs], and K denote the reaction rate constant, the concentration of POPs, and the Langmuir adsorption constant, respectively. However, if the initial [POPs] is low, as it is in most degradation studies, the equation can be simplified to an apparent first-order as represented below (Spasiano et al. 2015):

$$r = K_{\text{app}} \times [\text{POPs}] = -\frac{d[\text{POPs}]}{dt} \tag{1.13}$$

By bringing together concentration terms, the following equation is obtained:

$$-\frac{d[\text{POPs}]}{[\text{POPs}]} = K_{\text{app}} dt \tag{1.14}$$

Integration of Eq. 1.11 results in:

$$\ln\left(\frac{[\text{POPs}]_o}{[\text{POPs}]_t}\right) = K_{\text{app}} t \tag{1.15}$$

The value of K_{app}, the apparent pseudo-first-order rate constant, can therefore be estimated from the slope of a plot of $\ln([\text{POPs}]_o/[\text{POPs}]_t$ against time t.

1.6 Overview of Visible-Light-Responsive Photocatalysts

In visible-light-responsive photocatalysis, the semiconductor should be able to absorb more profuse visible light (400 nm < λ < 800 nm), and its band gap should be sufficiently narrow (Eg < 3.0 eV) to allow excitation of electrons by the irradiated photons. Furthermore, the high crystallinity of the designed visible-light-driven photocatalyst can encourage mobility of the charge carriers to the surface and

suppress the recombination ratio for an improved activity (Joo et al. 2012). However, lower crystallinity in some cases has also been reported as a plausible motive for the enhanced photocatalytic, owing to the manifestation of surface defects that increases light absorption (Cen et al. 2014). The surface character of visible-light-responsive photocatalysts is known to significantly influence the oxidative/reductive reactions that are set to take place during the degradation process.

1.6.1 TiO_2-Based Photocatalysts for Visible-Light-Assisted Degradation of POPs

Among numerous oxides used for the photocatalytic degradation of POPs, titanium dioxide (TiO_2) is the most extensively investigated semiconductor, owing to its unique properties (Tian et al. 2014; Zheng et al. 2018). These include nontoxicity, strong oxidizing potency, and relatively high physicochemical stability. Moreover, defect chemistry of TiO_2 demonstrates its nonstoichiometric nature (Bak et al. 2006). The oxygen vacancies are the principal defects at near-atmospheric oxygen pressure, and their presence results in excess electrons as charge carriers and the description of an n-type semiconductor (Morgan and Watson 2010). Hitherto, the n-type TiO_2 direct application in photocatalytic degradation of organic contaminants has been consistently labeled as substandard for a number of reasons. TiO_2 with a wide band gap of 3.2 eV can only be activated under more expensive and hazardous UV-light irradiation which contributes very less (5%) to the natural solar spectrum (Zhang et al. 2015; Pelaez et al. 2012; Meng et al. 2012). Furthermore, fast recombination proportion of photoexcited e^- and h^+ has also been reported to significantly reduce its photocatalytic efficiency. To overcome these drawbacks, semiconductor TiO_2 coupling and/or doping have been proposed. Representative TiO_2-containing photocatalysts with distinguished activity toward POPs under visible-light irradiation are presented below.

Coupling

Performing suitable band engineering by coupling TiO_2 nanostructures with materials of good visible-light-harvesting potential are of great benefit for the development of visible-light-responsive photocatalysts. For example, Nguyen and Doong described the binary p-n semiconducting $ZnFe_2O_4/TiO_2$ nanocomposite ($ZnFe_2O_4$ weight ratio 1%), obtained by the solvothermal process, as excellent photocatalyst for BPA degradation in aqueous environment under visible-light illumination at 465 nm (Nguyen and Doong 2017). $ZnFe_2O_4$ is a p-type semiconductor with magnetic properties and a comparatively narrow band gap (1.9 eV). In p-type semiconductor, positively charged holes are mainstream charge carriers. The use of 1.0 g/L $ZnFe_2O_4/TiO_2$ heterojunction afforded complete destruction of toxic BPA

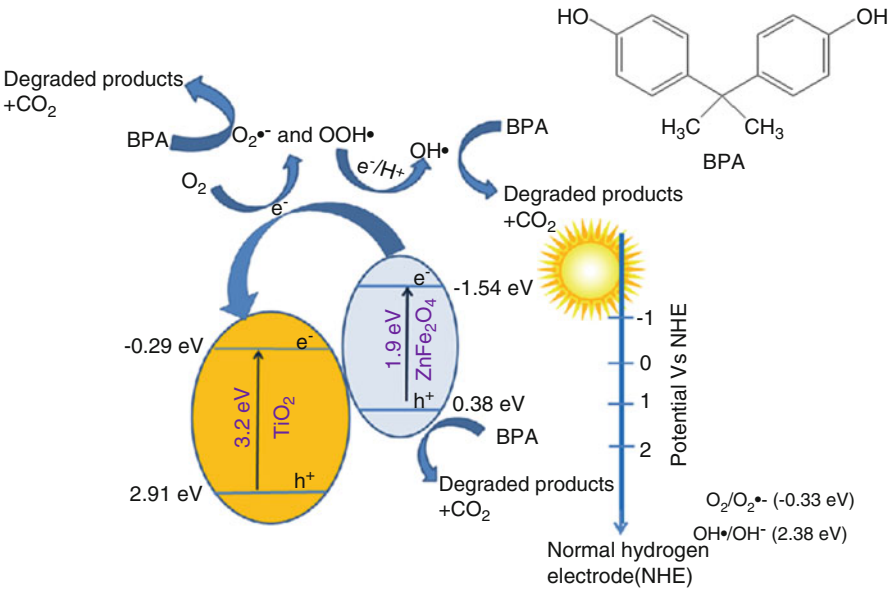

Fig. 1.4 Schematic diagram for the photodegradation of BPA using p-n heterojunction $ZnFe_2O_4$/TiO_2 under visible-light irradiation

(10 mg/L at pH 7) in 20 mL solution after 20 min. The radical trapping investigation revealed that photogenerated h^+ and both $OH•/O_2•^-$ radicals were the reactive species (Fig. 1.4). In addition, the reusability examination indicated that $ZnFe_2O_4$/TiO_2 material could be reapplied for not less than ten recurrent cycles of reaction.

Fabrication of p-n junction is well-reported as an efficient strategy to achieve improved photocatalytic activity, owing to an induced inner electric field which extends the e- and h^+ lifetime (Chen et al. 2011; Wei et al. 2011). The build-in electric field allows the movement of e- and h^+ in opposite directions in the space-charge region to accomplish their separation.

Shao et al. (2017) took advantage of the photosensitivity of silver halides and reported the synthesis of spherical-like AgI-deposited TiO_2 with visible-light ($\lambda > 420$ nm) photodegradation activity toward BDE209. The ideal TiO_2/AgI catalyst (AgI mass ratio 30%) exhibited a pseudo-first-order kinetic constant of about 0.29 h^{-1}. The debromination of BDE209 occurred as a result of the movement of photoexcited electrons from AgI to BDE209 via TiO_2 conduction band. Likewise, TiO_2/Ag_2O sheet loaded on natural polymer chitosan stabilized onto polypropylene matrix was described as photocatalytic film with impressive visible-light absorption at 545 nm and catalytic activity against antibiotics under irradiation with a 150 W tungsten/halogen lamp (Zhao et al. 2017). The complete decomposition of ampicillin (20 mg/L) in 40 mL solution took place within 180 min. The prepared multilayer photocatalyst with 2.4 eV energy band gap was found to owe its activity to the formation of p-n-type Ag_2O-TiO_2 heterojunctions and transfer of electrons from

TiO_2 to Ag_2O when their Fermi levels matches. The Fermi level represents the highest energy level occupied by valence band electrons.

Coupling TiO_2 with carbonaceous materials, exhibiting wide visible-light absorption, has also been reported as a tool for the improvement of quantum efficiency in TiO_2 photocatalytic systems (Liang et al. 2014; Li et al. 2015a). Graphene-containing semiconductors have been extensively investigated in the development of photocatalysts with visible-light response ability toward recalcitrant organic contaminants (Xie et al. 2015). When combine to semiconductor such as TiO_2, graphene can act as a sink that capture and shuttle electrons, thereby diminishing the charge recombination phenomenon (Sher Shah et al. 2012). Furthermore, grapheme has also been reported to decrease the energy band gap of grapheme-fused semiconductors through atomic d-π orbital hybridization and formation of additional band states (Zhang et al. 2008; Zhang et al. 2010; Li et al. 2013). For example, the solvothermal procedure involving the use of P123 nonionic surfactant, $TiCl_4$/titanium tetraisopropoxide (TTIP) solution, and graphene oxide (GO) yielded the nanocrystalline graphene/TiO_2 composite with high catalytic activity ($k = 0.25\ min^{-1}$) against aldicarb under visible-light irradiation ($\lambda > 400$ nm) (Li et al. 2013). *N*-methyl carbamate aldicarb is a chemical substitute to the restricted pesticides aldrin and heptachlor (Neumeister 2001). Fu et al. (2018) also described the graphite oxide-TiO_2-$Sr(OH)_2/SrCO_3$ nanocomposite as a novel catalyst with strong photodegradation activity toward PAH phenanthrene, under simulated sunlight irradiation (light intensity 100 mW/cm^2). The reported activity of this multicomponent material was attributed to a synergetic action of the three constituents within the composite during photocatalytic process. A redshift of the optical absorption as well as a divergent drive of the photogenerated e^- and h^+ was induced via hybridization of $Sr(OH)_2/SrCO_3$ and TiO_2. Graphite oxide repressed the charge recombination as outlined in the literature precedent (Li et al. 2013).

Tungsten trioxide (WO_3), unveiling a relatively smaller band gap of 2.8 eV, has also been coupled with TiO_2 for POPs photodegradation in water medium. For example, TiO_2/WO_3/GO nanoparticles, prepared via the hydrothermal procedure using Degussa P25, graphene oxide, and ammonium metatungstate, were reported as composited material with excellent BPA photodegradation in aqueous solution at pH 7 under visible-light illumination ($\lambda > 400$ nm) (Hao et al. 2017). As outlined by the authors, WO_3 effected an improved visible-light absorption, followed by the generation of $e-/h^+$. The GO surface acted as photogenerated electrons acceptor and restrained the pair charge carriers recombination.

Doping

Doping plays an essential role in amending the optical properties of semiconductor photocatalysts and allows for the use of sunlight energy. For example, cobalt-loaded titanate nanotubes, fabricated through the hydrothermal treatment of cobalt (II) chloride hexahydrate ($CoCl_2 \cdot 6H_2O$) and TiO_2 nanoparticles followed by calcination of the resultant precipitate, displayed ten times more catalytic activity than

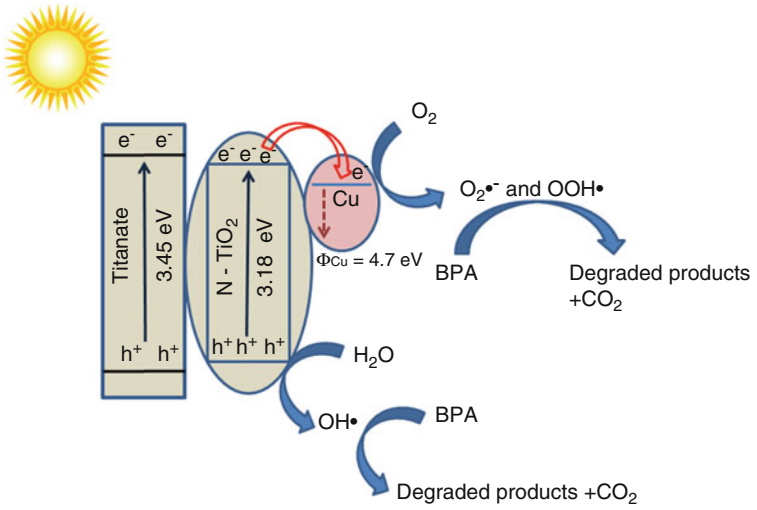

Fig. 1.5 Schematic diagram for the photodegradation of BPA using Cu-deposited N-TiO_2/titanate under visible-light irradiation

P25 TiO_2 for the degradation of phenanthrene in water under simulated sunlight irradiation (light intensity 85 ± 0.5 mW/cm^2) at 25 °C (Zhao et al. 2016). The percentage of phenanthrene (200 μg/L) removal by this Co-modified titanate nanomaterial (Co mass ratio 2.26%) was estimated around 98.6% after 12 h of contact time using 1 g/L dose. Interestingly, cobalt(II) oxide (CoO), generated as a result of the existence of cobalt(II) ions in titanate nanotubes during the calcination procedure, was proven to perform as photoexcited electrons transfer mediator, thereby hindering the $e-/h^+$ recombination.

Cu-N-codoped TiO_2/titanate nanotubes, fabricated via the microwave-assisted hydrothermal treatment of ST-01 TiO_2 nanoparticles and calcination in the presence of copper(II) ions under N_2/NH_3 atmosphere, were evaluated as photocatalyst for the removal of BPA in water medium (Doong and Liao 2017a). Relative to P25, nano-sized Cu-N-TiO_2/titanate exhibited remarkable activity under visible-light illumination ($\lambda = 420 \pm 20$ nm) with complete degradation of BPA after 120 min. The high efficiency of Cu^0-deposited, N-TiO_2/titanate nanotubes (Cu mass ratio 6%) was ascribed to their ability to extend the production of radical OH• for more than 5 min. As shown in Fig. 1.5, the deposited Cu^0 enhanced trapping of electrons that reacted with adsorbed oxygen to produce superoxide and subsequently peroxyl radicals. Metallic copper ability to remove high-energy electron from TiO_2 results from its higher work function value 4.7 eV (Doong and Liao 2017b). TiO_2 work function was estimated to be 4.2 eV. The nitrogen doping, on the other hand, resulted in reduced energy band gap of TiO_2 (3.18 eV).

It has been established that doping TiO_2 with nonmetallic elements, including N, C, and F, could serve as an efficient strategy to manipulate its band structure and enhance its photo-response ability into the visible region (Livraghi et al. 2006; Li

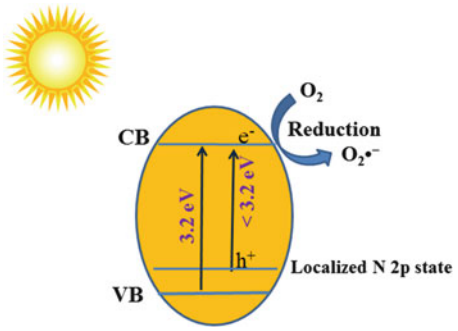

Fig. 1.6 Derivation of improved photocatalytic activity of N-doped TiO_2 in visible light

et al. 2005). With regard to nitrogen doping, for example, the electron paramagnetic resonance (EPR) spectra analysis and density functional theory (DFT) calculations of N-doped TiO_2 have established that the presence of localized N 2p states (neutral paramagnetic and charged diamagnetic) just above TiO_2 VB plays a critical role in the absorption of visible light, ease promotion of electrons to CB, and increased production of superoxide radicals (Fig. 1.6).

The visible-light photocatalytic evaluation of N,F-codoped TiO_2 nanoparticles toward BPA exposed a threefold more potential in contrast to pristine TiO_2 nanoparticles (He et al. 2016). These nonmetal-doped TiO_2 nanoparticles of 10.6 nm average size, 136 m^2/g estimated specific surface area, and 2.87 eV band gap were fabricated through the sol-gel procedure using EDTA and Zonyl® FS-300 fluorosurfactant as the nitrogen and fluorine sources, respectively. The pronounced activity of this engineered TiO_2 photocatalyst was ascribed to high specific surface area-to-volume ratio, enhanced visible-light absorption due to N-doping, and more surface acidity owing to F-doping. An increase in the photocatalyst surface acidity was found to increase BPA adsorption. Moreover, the displacement of oxygen atom of TiO_2 with fluorine bearing one extra electron could levitate the Fermi level, thus narrowing the band gap for a superior conversion of visible light (Wen et al. 2017; Fang et al. 2014).

Fe(III)-doped TiO_2 spheres at the polysulfone ultrafiltration membranes, obtained via the hydrothermal and phase inversion procedure, have also been reported to exhibit a relatively improved visible-light photocatalytic degradation of BPA, complemented with a self-cleaning capability (Wang et al. 2017). The use of 0.20 g of the optimized catalyst (Fe-TiO_2 mass ratio 20%) achieved 90.8% of BPA (10 mg/L in 250 mL) removal within 180 min under illumination with a 500 W xenon lamp. This effective BPA removal was ascribed to the electrostatic adsorption of the contaminant at the surface of the polymer support and its decomposition by Fe(III)-TiO_2 nanocatalyst. A recent study on the Fe(III)-doped TiO_2 visible-light response mechanism revealed that its activity relates with a narrow band gap (Jaihindh et al. 2018). This can be attributed to the d–d transition of Fe(III) due to 3*d*-orbital splitting and the charge transfer transitions between interacting Fe(III) ions to create Fe(II) and Fe(VI) electronic states across the band gap of TiO_2 (Khan and Swati 2016). During the photocatalytic process, these cations [Fe(III), Fe(II),

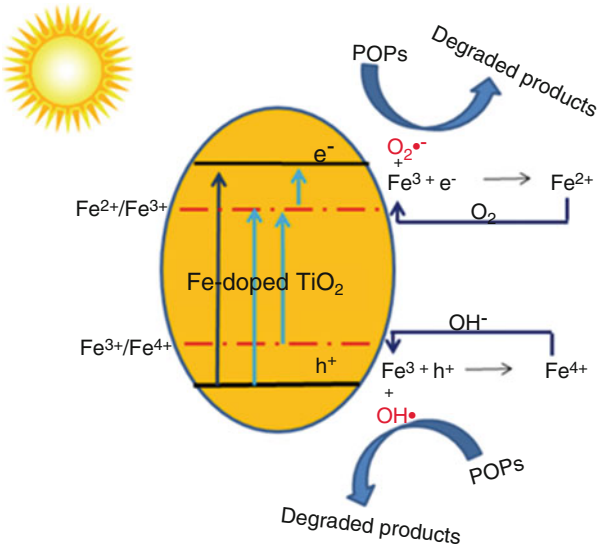

Fig. 1.7 Schematic diagram for the enhanced photocatalytic activity of Fe-doped TiO_2 under visible-light irradiation

and Fe(VI)] are anticipated to also act as the e^- and h^+ trapping sites and therefore facilitate the charge carriers separation. Figure 1.7 illustrates a proposed mechanism for the superior photocatalytic activity of Fe (III)-doped TiO_2 under visible-light illumination.

Ag-doped TiO_2 (25 mg), fabricated by Hlekelele et al. (2018) using a deposition-precipitation method, exhibited 91% photodegradation activity toward BPA (60 ppm) in 50 ml aqueous solution irradiated with visible light ($\lambda > 420$ nm). As compared to pristine TiO_2 and TiO_2/zeolite composite prepared during the same investigation, the Ag-TiO_2 increased photocatalytic behavior was attributed to the noble metal Ag nanoparticles ability to absorb visible light by means of surface plasmon resonance (SPR). SPR is known as the resonance coherent oscillations of electrons in the conduction band of a metal particle, stimulated by the electromagnetic field of an incident light as shown in Fig. 1.8 (Zhou et al. 2012). With regard to Ag and Au nanoparticles, this resonance falls within the visible region.

1.6.2 Alternative Photocatalysts for Visible-Light-Assisted Degradation of POPs

Multicomponent metal oxyhalides have also been found to demonstrate outstanding catalytic activity against organic pollutants in water medium under visible-light treatment (Zhu et al. 2017; Liu et al. 2017b; Yuan et al. 2016). For example, Yin

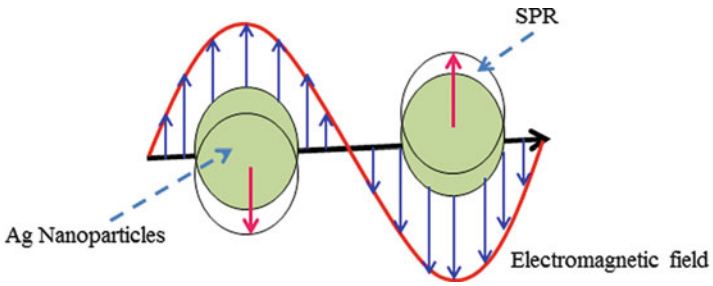

Fig. 1.8 Schematic representation of SPR in Ag nanoparticle interacting with the electromagnetic field of an incident light

and his group (2017) reported the synthesis and visible-light-driven catalytic activity of microsphere-like $PbBiO_2Cl$ with 49.56 m^2/g specific surface area and 2.18 eV band gap for the degradation of antibiotics. This perovskite-like multicomponent photocatalyst was obtained by the solvothermal process using ionic liquid 1-hexadecyl-3-methylimidazolium chlorine and a specific amount (0.15 g) of poly (N-vinyl-2-pyrrolidone) (PVP) complex system. As a photocatalyst, the $PbBiO_2Cl$ microspheres could achieve up to 89% decomposition of ciprofloxacin (10 mg/L) in aqueous solution, under visible-light illumination (300 W xenon lamp, $\lambda = 400$ nm). The apparent pseudo-first-order rate constant was evaluated to be 0.036 min^{-1}. Furthermore, the use of data obtained with the free radical scavengers (isopropanol for OH•, benzoquinone for $O_2^{\bullet -}$, and EDTA-2Na for h^+) revealed a high interaction of photoengendered h^+ and $O_2^{\bullet -}$ species with the representative persistent organic pollutant.

The p-type bismuth oxybromide (BiOBr) microspheres of diameters 1–3 μm, absorption discontinuity wavelength of 446 nm, and 2.64 eV estimated band gap were also synthesized using the solvothermal approach and assessed for their potential to act as photocatalyst for the removal of POPs in wastewater (Tian et al. 2012). 0.5 g/L of this ternary compound semiconductor, in 5 mL solution of BPA (20 mg/L) under virtual sunlight irradiation (800 W xenon lamp), achieved complete degradation of the contaminant after 90 min. Remarkably, only 50% degradation was accomplished with Degussa P25 under similar reaction conditions. The as-prepared BiOBr high activity was ascribed to the sandwich-like structure that facilitates the separation of charge carriers. On the other hand, aiming at improving BiOBr photocatalytic activity through the Fenton-like progression, Zhou et al. (2018) developed a series of pH-dependent $Co_xFe_yO_4$-BiOBr hybrid photocatalysts for the degradation of BPA under visible-light illumination. 50 mg of the optimized semiconductor, fabricated at pH 3, exhibited 78% degradation of BPA (10 mg/L) in 100 mL aqueous solution. According to the authors' findings, this hybrid material demonstrated a 3.4 times higher rate constant than pristine BiOBr prepared under the same reaction conditions. The catalytic activity was postulated to progress via in situ production of H_2O_2, induced by BiOBr, and then Fenton-like sequences to generate the hydroxyl and oxygen radicals (OH• and $O_2^{\bullet -}$) (Fig. 1.9).

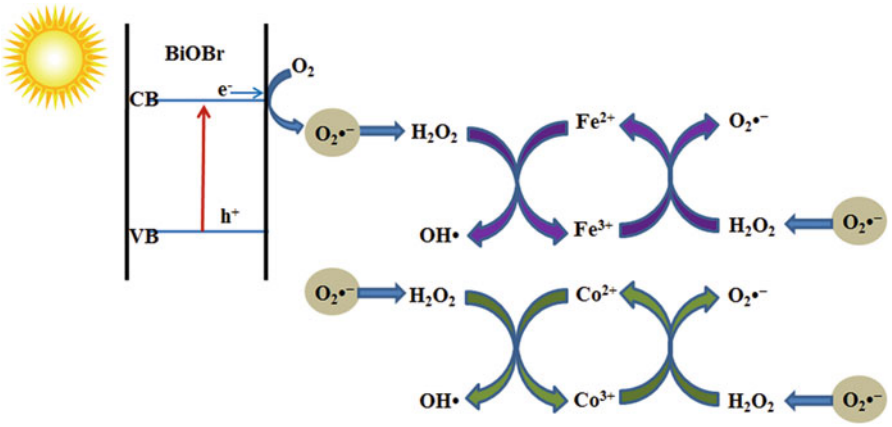

Fig. 1.9 Schematic diagram for the improved photoactivity of $Co_xFe_yO_4$-BiOBr through the formation of H_2O_2 and Fenton-like cycles

In a separate study, the grafting of Fe_3O_4 nanoparticles with 10 nm diameters onto mixed valent bismuth oxide Bi_2O_4 nanorods with average diameters of 120 nm, at the molar ratio 1:2.5 (Bi_2O_4:Fe_3O_4), afforded a nanocomposite with an impressive photocatalytic degradation toward anti-inflammatory medication ibuprofen in aqueous solution under 15 W fluorescent lamp illumination (light intensity: 326.0 μW. cm^{-2}) (Xia and Lo 2016). This nanocomposite was obtained by a two-step method involving the hydrothermal treatment of sodium bismuthate powder ($NaBiO_3$) to generate Bi_2O_4 and the in situ growth of superparamagnetic Fe_3O_4 particles using Fe^{2+}/Fe^{3+} salts mixtures. The incorporation of nano-sized Fe_3O_4 facilitates the isolation of the spent photocatalyst from the aqueous milieu by simple application of an external magnet. Additionally, during the ibuprofen degradation at the magnetic Bi_2O_4/Fe_3O_4 photocatalyst, the use of scavengers such as sodium oxalate (h^+), isopropanol (OH•), 4-hydroxy-2,2,6,6-tetramethylpiperidine-1-oxyl ($O_2•^-$), Fe(II)-EDTA (H_2O_2), and Cr(VI) (e-), to identify the important role of the reactive radicals, revealed that h^+, $O_2•^-$, and H_2O_2 were the most energetic species. A schematic representation for this process was proposed as shown in Fig. 1.10.

When coupled with other light-sensitive semiconductors, n-type bismuth tungstate has also been described as an attractive material with visible-light-driven properties for the photodegradation of refractory organic pollutants (Phuruangrat et al. 2018; Jonjana et al. 2018; Gao et al. 2018). For instance, Xia et al. (2014) reported the synthesis of the spherical-like Bi_2WO_6/BiOBr composite and its improved activity, relative to the bare constituents, in visible-light photocatalytic degradation of BPA. This heterojunction material was fabricated via the solvothermal method using sodium tungstate dihydrate ($Na_2WO_4.2H_2O$), bismuth nitrate pentahydrate ($Bi(NO_3)_3.5H_2O$), and ionic liquid 1-hexadecyl-3-methylimidazolium bromide ([C_{16}mim]Br) as solvent, reactant, and template. The photoluminescence spectra analysis indicated that as compared to BiOBr and Bi_2WO_6, a coupling of both materials eased the charge carrier separation, leading to increased catalytic activity.

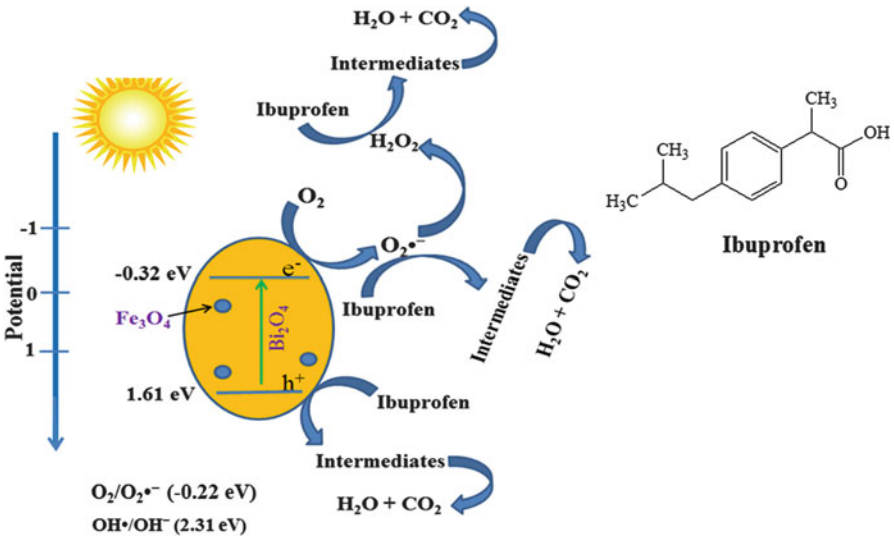

Fig. 1.10 Schematic diagram for the photodegradation of ibuprofen using Bi_2O_4/Fe_3O_4 under visible-light irradiations

Alongside the capability of graphitic carbon nitride (g-C_3N_4) to initiate water splitting for the hydrogen gas (H_2) production when composited with semiconductors such as TiO_2 (Liu and Lu 2018) and SnO_2 (Seza et al. 2018), this material has also been reported as support for the synthesis of hybrids with commendable photodegradation performance toward POPs. For example, Fe_3O_4-g-C_3N_4 (Fe_3O_4 mass ratio 4%), obtained by in situ growth of Fe_3O_4 nanoparticles at the surface of pre-synthesized C_3N_4 sheet, revealed a pseudo-first-order kinetic constant of 1.33 h^{-1} for BDE209 debromination under visible-light illumination ($\lambda > 420$ nm) (Shao et al. 2018). The dehalogenation process was proposed to evolve through the transfer of g-C_3N_4 photoexcited electrons to BDE209 via the conduction band of Fe_3O_4. In addition, the magnetization curve of Fe_3O_4-g-C_3N_4 hybrid exposed the distinctive superparamagnetic properties, and this photocatalyst could easily be isolated and reused four times without a significant loss of efficiency. To also achieve a material that could be easily removed from the reaction milieu after usage in photocatalytic system, Li et al. (2015b) reported the fabrication of hollow spherical Fe_2O_3/ZnO printed onto a filter paper. The bimetal oxide were obtained through the solvothermal method using the iron(III) chloride ($FeCl_3$) and zinc acetate ($Zn(Ac)_2$) precursors. Subsequently, their dispersion on a paper was effected with a household sprayer. The as-developed material was described as an outstanding photocatalyst for the removal of 2,4,6-trichlorophenol (rate constant of 0.014 min^{-1}) in aqueous solution in simulated sunlight irradiation (200 W xenon lamp) at 25 °C. In addition, the Fe_2O_3/ZnO-embedded filter paper was found to preserve its high efficiency after ten repeated photodegradation experiments.

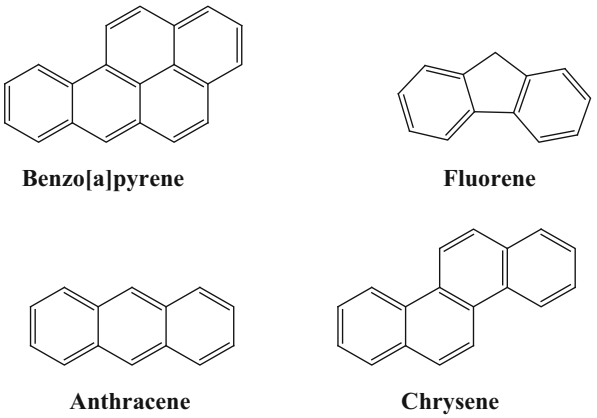

Fig. 1.11 Chemical structures of selected PAHs

Following previous reports on the ability of the metal hexacyanoferrate complexes to act as adsorbents and heterogeneous photocatalysts for the removal of organic pollutants (Shanker et al. 2016; Jassal et al. 2015), Shanker and co-workers (2017) described potassium zinc hexacyanoferrate nanocubes as efficient material for the removal of a variety of PAHs at neutral pH under natural sunlight irradiation (light intensity: 10.04 kW/m^2). This coordination complex was prepared following a green approach using zinc nitrate, potassium ferrocyanide $K_4[Fe(CN)_6]$, and an aqueous extract of plant *Sapindus mukorossi* as a bio-surfactant. The use of potassium zinc hexacyanoferrate nanocubes (25 mg) effected 70–93% degradation of phenanthrene, benzo[a]pyrene, fluorene, chrysene, and anthracene (50 mg/L) in aqueous media within 48 h (Fig. 1.11).

1.7 Conclusion

The fast growth in industries during the last century has resulted in the release of a huge number of POPs into the environment. Owing to their demonstrated potential for long-range transport, persistency, and bioaccumulation, POPs have proven to be highly toxic. There are enough data to conclude that adverse effects have occurred in wildlife and human well-being exposed to POPs. These potential human health effects and their consequences in developing and developed countries are of global concern. To remediate this situation, a comprehensive approach that takes into consideration the technical and economic point of view consists of treating the wastewaters before their discharge into the natural environment. At that point, relatively small volumes of POPs-contaminated water are to be attended, while the decontamination of polluted natural water streams would be very problematic or even unreasonable. For this purpose several technologies have been proposed. In this chapter, we have exposed that heterogeneous photocatalytic process represents a very proficient procedure for the nearly complete removal of refractory POPs in

aqueous medium. Moreover the development of visible-light-responsive heterogeneous photocatalysts is gaining momentum globally owing to the fact that these semiconductors are considered to be able to convert natural solar energy to chemical energy. Henceforth, visible-light-driven heterogeneous photocatalysis could be described as eco-friendly and relatively low-cost technique for efficient degradation of POPs in wastewater. However, to promote the practicability of this remarkable technology at industrial scale, the design of effective reactor for the full exploitation of natural solar radiation and optimization of the process have to be addressed. Furthermore, the design of an applicable photocatalyst immobilization technique to provide a productive solid-liquid separation still remains a challenge.

References

Ahmad R, Ahmad Z, Khan AU, Mastoi NR, Aslam M, Kim J (2016) Photocatalytic systems as an advanced environmental remediation: recent developments, limitations and new avenues for applications. J Environ Chem Eng 4(4):4143–4164. https://doi.org/10.1016/j.jece.2016.09.009

Al-Kahtani AA, Alshehri SM, Naushad M, Ruksana TA (2019) Fabrication of highly porous N/S doped carbon embedded with ZnS as highly efficient photocatalyst for degradation of bisphenol. Int J Biol Macromol 121:415–423. https://doi.org/10.1016/j.ijbiomac.2018.09.199

Altarawneh M, Dlugogorski BZ, Kennedy EM, Mackie JC (2009) Mechanisms for formation, chlorination, dechlorination and destruction of polychlorinated dibenzo-p-dioxins and dibenzofurans (PCDD/Fs). Prog Energy Combust Sci 35(3):245–274. https://doi.org/10.1016/j.pecs.2008.12.001

Bak T, Nowotny J, Nowotny MK (2006) Defect disorder of titanium dioxide. J Phys Chem B 110 (43):21560–21567. https://doi.org/10.1021/jp063700k

Benson K, Yang E, Dutton N, Sjodin A, Rosenbaum PF, Pavuk M (2018) Polychlorinated biphenyls, indicators of thyroid function and thyroid autoantibodies in the Anniston Community Health Survey I (ACHS-I). Chemosphere 195:156–165. https://doi.org/10.1016/j.chemosphere.2017.12.050

Canle M, Pérez MI, Santaballa JA (2017) Photocatalyzed degradation/abatement of endocrine disruptors. Curr Opin Green Sustain Chem 6:101–138. https://doi.org/10.1016/j.cogsc.2017.06.008

Carlsson P, Crosse JD, Halsall C, Evenset A, Heimstad ES, Harju M (2016) Perfluoroalkylated substances (PFASs) and legacy persistent organic pollutants (POPs) in halibut and shrimp from coastal areas in the far north of Norway: small survey of important dietary foodstuffs for coastal communities. Marine Poll Bull 105(1):81–87. https://doi.org/10.1016/j.marpolbul.2016.02.053

Cates EL (2017) Photocatalytic water treatment: so where are we going with this? Environ Sci Technol 51:757–758. https://doi.org/10.1021/acs.est.6b06035

Cen W, Xiong T, Tang C, Yuan S, Dong F (2014) Effects of morphology and crystallinity on the photocatalytic activity of $(BiO)_2CO_3$ nano/microstructures. Ind Eng Chem Res 53 (39):15002–15011. https://doi.org/10.1021/ie502670n

Chen CJ, Liao CH, Hsu KC, Wu YT, Wu JC (2011) P–N junction mechanism on improved NiO/TiO_2 photocatalyst. Catal Commun 12(14):1307–1310. https://doi.org/10.1016/j.catcom.2011.05.009

Corsini E, Avogadro A, Galbiati V, Dell'Agli M, Marinovich M, Galli CL, Germolec DR (2011) In vitro evaluation of the immunotoxic potential of perfluorinated compounds (PFCs). Toxicol Appl Pharmacol 250(2):108–116. https://doi.org/10.1016/j.taap.2010.11.004

Costa LG, Pellacani C, Dao K, Kavanagh TJ, Roque PJ (2015) The brominated flame retardant BDE-47 causes oxidative stress and apoptotic cell death in vitro and in vivo in mice. Neurotoxicology 48:68–76. https://doi.org/10.1016/j.neuro.2015.03.008

De Joode BV, Wesseling C, Kromhout H, Monge P, Garcia M, Mergler D (2001) Chronic nervous-system effects of long-term occupational exposure to DDT. Lancet 357(9261):1014–1016. https://doi.org/10.1016/S0140-6736(00)04249-5

Dong S, Feng J, Fan M, Pi Y, Hu L, Han X, Liu M, Sun J, Sun J (2015) Recent developments in heterogeneous photocatalytic water treatment using visible light-responsive photocatalysts: a review. RSC Adv 5(19):14610–14630. https://doi.org/10.1039/c4ra13734e

Doong RA, Liao CY (2017a) Enhanced visible-light-responsive photodegradation of bisphenol A by Cu, N-codoped titanate nanotubes prepared by microwave-assisted hydrothermal method. J Hazard Mater 322:254–262. https://doi.org/10.1016/j.jhazmat.2016.02.065

Doong RA, Liao CY (2017b) Enhanced photocatalytic activity of Cu-deposited N-TiO_2/titanate nanotubes under UV and visible light irradiations. Sep Purif Technol 179:403–411. https://doi.org/10.1016/j.seppur.2017.02.028

Durán N, Esposito E (2000) Potential applications of oxidative enzymes and phenoloxidase-like compounds in wastewater and soil treatment: a review. Appl Catal B 28(2):83–99. https://doi.org/10.1016/S0926-3373(00)00168-5

Erickson MD, Kaley RG (2011) Applications of polychlorinated biphenyls. Environ Sci Pollut Res 18(2):135–151. https://doi.org/10.1007/s11356-010-0392-1

Fang WQ, Wang XL, Zhang H, Jia Y, Huo Z, Li Z, Zhao H, Yang HG, Yao X (2014) Manipulating solar absorption and electron transport properties of rutile TiO_2 photocatalysts via highly n-type F-doping. J Mater Chem A 2(10):3513–3520. https://doi.org/10.1039/c3ta13917d

Feng W, Huang T, Gao L, Yang X, Deng W, Zhou R, Liu H (2018) Textile-supported silver nanoparticles as a highly efficient and recyclable heterogeneous catalyst for nitroaromatic reduction at room temperature. RSC Adv 8(12):6288–6292. https://doi.org/10.1039/c7ra13257c

Fu J, Sheng S, Wen T, Zhang ZM, Wang Q, Hu QX, Li QS, An SQ, Zhu HL (2011) Polycyclic aromatic hydrocarbons in surface sediments of the Jialu River. Ecotoxicology 20(5):940–950. https://doi.org/10.1007/s10646-011-0622-4

Fu J, Kyzas GZ, Cai Z, Deliyanni EA, Liu W, Zhao D (2018) Photocatalytic degradation of phenanthrene by graphite oxide-TiO_2-$Sr(OH)_2$/$SrCO_3$ nanocomposite under solar irradiation: effects of water quality parameters and predictive modeling. Chem Eng J 335:290–300. https://doi.org/10.1016/j.cej.2017.10.163

Gao X, Zhang R, Shang Y, Fei J, Fu F (2018) Synergism of 3D g-C_3N_4 decorated Bi_2WO_6 microspheres with efficient visible light catalytic activity. J Phys Chem Solids 119:19–28. https://doi.org/10.1016/j.jpcs.2018.03.032

Gardoni D, Vailati A, Canziani R (2012) Decay of ozone in water: a review. Ozone Sci Eng 34 (4):233–242. https://doi.org/10.1080/01919512.2012.686354

Gaum PM, Esser A, Schettgen T, Gube M, Kraus T, Lang J (2014) Prevalence and incidence rates of mental syndromes after occupational exposure to polychlorinated biphenyls. Int J Hyg Environ Health 217(7):765–774. https://doi.org/10.1016/j.ijheh.2014.04.001

Gaum PM, Gube M, Schettgen T, Putschögl FM, Kraus T, Fimm B, Lang J (2017) Polychlorinated biphenyls and depression: cross-sectional and longitudinal investigation of a dopamine-related Neurochemical path in the German HELPcB surveillance program. Environ Health 16(1):106. https://doi.org/10.1186/s12940-017-0316-3

Gaur N, Narasimhulu K, Pydisetty Y (2018) Recent advances in the bio-remediation of persistent organic pollutants and its effect on environment. J Clean Prod 198:1602–1631. https://doi.org/10.1016/j.jclepro.2018.07.076

Gaw S, Thomas KV, Hutchinson TH (2014) Sources, impacts and trends of pharmaceuticals in the marine and coastal environment. Philos Trans R Soc Lond Ser B Biol Sci 369(1656):20130572. https://doi.org/10.1098/rstb.2013.0572

Gnanasekaran L, Hemamalini R, Saravanan R, Ravichandran K, Gracia F, Gupta VK (2016) Intermediate state created by dopant ions (Mn, Co and Zr) into TiO_2 nanoparticles for

degradation of dyes under visible light. J Mol Liq 223:652–659. https://doi.org/10.1016/j.molliq.2016.08.105

Haffner D, Schecter A (2014) Persistent organic pollutants (POPs): a primer for practicing clinicians. Curr Environ Health Rep 1(2):123–131. https://doi.org/10.1007/s40572-014-0009-9

Han Z, Li Y, Zhang S, Song N, Xu H, Dang Y, Liu C, Giesy JP, Yu H (2017) Prenatal transfer of decabromodiphenyl ether (BDE-209) results in disruption of the thyroid system and developmental toxicity in zebrafish offspring. Aquat Toxicol 190:46–52. https://doi.org/10.1016/j.aquatox.2017.06.020

Hao X, Li M, Zhang L, Wang K, Liu C (2017) Photocatalyst TiO_2/WO_3/GO nano-composite with high efficient photocatalytic performance for BPA degradation under visible light and solar light illumination. J Ind Eng Chem 55:140–148. https://doi.org/10.1016/j.jiec.2017.06.038

He X, Aker WG, Pelaez M, Lin Y, Dionysiou DD, Hwang HM (2016) Assessment of nitrogen–fluorine-codoped TiO_2 under visible light for degradation of BPA: implication for field remediation. J Photochem Photobiol A 314:81–92. https://doi.org/10.1016/j.jphotochem.2015.08.014

Hlekelele L, Franklyn PJ, Dziike F, Durbach SH (2018) Novel synthesis of Ag decorated TiO_2 anchored on zeolites derived from coal fly ash for the photodegradation of bisphenol-A. New J Chem 42(3):1902–1912. https://doi.org/10.1039/c7nj02885g

Im J, Löffler FE (2016) Fate of bisphenol A in terrestrial and aquatic environments. Environ Sci Technol 50(16):8403–8416. https://doi.org/10.1021/acs.est.6b00877

Jaihindh DP, Chen CC, Fu YP (2018) Reduced graphene oxide-supported Ag-loaded Fe-doped TiO_2 for the degradation mechanism of methylene blue and its electrochemical properties. RSC Adv 8(12):6488–6501. https://doi.org/10.1039/c7ra13418e

Ji SS, Ren Y, Buekens A, Chen T, Lu SY, Cen KF, Li XD (2014) Treating PCDD/Fs by combined catalysis and activated carbon adsorption. Chemosphere 102:31–36. https://doi.org/10.1016/j.chemosphere.2013.12.008

Jonjana S, Phuruangrat A, Thongtem T, Kuntalue B, Thongtem S (2018) Decolorization of rhodamine B photocatalyzed by Ag_3PO_4/Bi_2WO_6 nanocomposites under visible radiation. Mater Lett 218:146–149. https://doi.org/10.1016/j.matlet.2018.01.176

Joo JB, Zhang Q, Dahl M, Lee I, Goebl J, Zaera F, Yin Y (2012) Control of the nanoscale crystallinity in mesoporous TiO_2 shells for enhanced photocatalytic activity. Energy Environ Sci 5(4):6321–6327. https://doi.org/10.1039/c1ee02533c

Kallenborn R, Christensen G, Evenset A, Schlabach M, Stohl A (2007) Atmospheric transport of persistent organic pollutants (POPs) to Bjørnøya (Bear island). J Environ Monit 9(10):1082–1091. https://doi.org/10.1039/b707757m

Khan H, Swati IK (2016) Fe^{3+-}doped anatase TiO_2 with d–d transition, oxygen vacancies and Ti^{3+} centers: synthesis, characterization, UV–vis photocatalytic and mechanistic studies. Ind Eng Chem Res 55(23):6619–6633. https://doi.org/10.1021/acs.iecr.6b01104

Klečka GM, Staples CA, Clark KE, van der Hoeven N, Thomas DE, Hentges SG (2009) Exposure analysis of bisphenol A in surface water systems in North America and Europe. Environ Sci Technol 43(16):6145–6150. https://doi.org/10.1021/es900598e

Kumar A, Naushad M, Rana A et al (2017) ZnSe-WO3 nano-hetero-assembly stacked on Gum ghatti for photo-degradative removal of Bisphenol A: Symbiose of adsorption and photocatalysis. Int J Biol Macromol 104:1172–1184. https://doi.org/10.1016/j.ijbiomac.2017.06.116

Li D, Haneda H, Labhsetwar NK, Hishita S, Ohashi N (2005) Visible-light-driven photocatalysis on fluorine-doped TiO_2 powders by the creation of surface oxygen vacancies. Chem Phys Lett 401(4–6):579–584. https://doi.org/10.1016/j.cplett.2004.11.126

Li K, Xiong J, Chen T, Yan L, Dai Y, Song D, Lv Y, Zeng Z (2013) Preparation of graphene/TiO_2 composites by nonionic surfactant strategy and their simulated sunlight and visible light photocatalytic activity towards representative aqueous POPs degradation. J Hazard Mater 250:19–28. https://doi.org/10.1016/j.jhazmat.2013.01.069

Li X, Lin H, Chen X, Niu H, Zhang T, Liu J, Qu F (2015a) Fabrication of TiO_2/porous carbon nanofibers with superior visible photocatalytic activity. New J Chem 39(10):7863–7872. https://doi.org/10.1039/c5nj01189b

Li Y, Wang K, Wu J, Gu L, Lu Z, Wang X, Cao X (2015b) Synthesis of highly permeable Fe_2O_3/ZnO hollow spheres for printable photocatalysis. RSC Adv 5(107):88277–88286. https://doi.org/10.1039/c5ra17765k

Liang D, Cui C, Hu H, Wang Y, Xu S, Ying B, Li P, Lu B, Shen H (2014) One-step hydrothermal synthesis of anatase TiO_2/reduced graphene oxide nanocomposites with enhanced photocatalytic activity. J Alloys Compd 582:236–240. https://doi.org/10.1016/j.jallcom.2013.08.062

Litter M, Quici N (2010) Photochemical advanced oxidation processes for water and wastewater treatment. Rec Patents Eng 4:217–241. https://doi.org/10.2174/187221210794578574

Liu Z, Lu X (2018) Multifarious function layers photoanode based on g-C_3N_4 for photoelectrochemical water splitting. Chin J Catal 39(9):1527–1533. https://doi.org/10.1016/S1872-2067(18)63079-7

Liu S, Zhao H, Lehmler HJ, Cai X, Chen J (2017a) Antibiotic pollution in marine food webs in Laizhou Bay, North China: trophodynamics and human exposure implication. Environ Sci Technol 51(4):2392–2400. https://doi.org/10.1021/acs.est.6b04556

Liu C, Dong X, Hao Y, Wang X, Ma H, Zhang X (2017b) Efficient photocatalytic dye degradation over Er-doped BiOBr hollow microspheres wrapped with graphene nanosheets: enhanced solar energy harvesting and charge separation. RSC Adv 7(36):22415–22423. https://doi.org/10.1039/c7ra02402a

Livraghi S, Paganini MC, Giamello E, Selloni A, Di Valentin C, Pacchioni G (2006) Origin of photoactivity of nitrogen-doped titanium dioxide under visible light. J Am Chem Soc 128(49):15666–15671. https://doi.org/10.1021/ja064164c

Luo Y, Mao D, Rysz M, Zhou Q, Zhang H, Xu L, JJ Alvarez P (2010) Trends in antibiotic resistance genes occurrence in the Haihe River, China. Environ Sci Technol 44(19):7220–7225. https://doi.org/10.1021/es100233w

Luo Y, Xu L, Rysz M, Wang Y, Zhang H, Alvarez PJ (2011) Occurrence and transport of tetracycline, sulfonamide, quinolone, and macrolide antibiotics in the Haihe River Basin, China. Environ Sci Technol 45(5):1827–1833. https://doi.org/10.1021/es104009s

Meng F, Hong Z, Arndt J, Li M, Zhi M, Yang F, Wu N (2012) Visible light photocatalytic activity of nitrogen-doped $La_2Ti_2O_7$ nanosheets originating from band gap narrowing. Nano Res 5(3):213–221. https://doi.org/10.1007/s12274-012-0201-x

Morgan BJ, Watson GW (2010) Intrinsic n-type defect formation in TiO_2: a comparison of rutile and anatase from GGA+U calculations. J Phys Chem C 114(5):2321–2328. https://doi.org/10.1021/jp9088047

Nadal M, Marquès M, Mari M, Domingo JL (2015) Climate change and environmental concentrations of POPs: a review. Environ Res 143:177–185. https://doi.org/10.1016/j.envres.2015.10.012

Naushad M (2014) Surfactant assisted nano-composite cation exchanger: development, characterization and applications for the removal of toxic Pb2+ from aqueous medium. Chem Eng J 235:100–108. https://doi.org/10.1016/j.cej.2013.09.013

Net S, El-Osmani R, Prygiel E, Rabodonirina S, Dumoulin D, Ouddane B (2015) Overview of persistent organic pollution (PAHs, Me-PAHs and PCBs) in freshwater sediments from Northern France. J Geochem Explor 148:181–188. https://doi.org/10.1016/j.gexplo.2014.09.008

Neumeister L (2001) Beyond POPs: evaluation of the UNEP chemical substitutes of the POPs pesticides regarding their human and environmental toxicity. Study on Behalf of the Environmental Agency, Hamburg

Nguyen TB, Doong RA (2017) Heterostructured $ZnFe_2O_4$/TiO_2 nanocomposites with a highly recyclable visible-light-response for bisphenol A degradation. RSC Adv 7(79):50006–50016. https://doi.org/10.1039/c7ra08271a

Pariatamby A, Kee YL (2016) Persistent organic pollutants management and remediation. Procedia Environ Sci 31:842–848. https://doi.org/10.1016/j.proenv.2016.02.093

Pelaez M, Nolan NT, Pillai SC, Seery MK, Falaras P, Kontos AG, Dunlop PS, Hamilton JW, Byrne JA, O'shea K, Entezari MH (2012) A review on the visible light active titanium dioxide photocatalysts for environmental applications. Appl Catal B 125:331–349. https://doi.org/10.1016/j.apcatb.2012.05.036

Pereira LC, Duarte FV, Varela AT, Rolo AP, Palmeira CM, Dorta DJ (2017) An autophagic process is activated in HepG2 cells to mediate BDE-100-induced toxicity. Toxicology 376:59–65. https://doi.org/10.1016/j.tox.2016.05.022

Phuruangrat A, Dumrongrojthanath P, Thongtem S, Thongtem T (2018) Hydrothermal synthesis of I-doped Bi_2WO_6 for using as a visible-light-driven photocatalyst. Mater Lett 224:67–70. https://doi.org/10.1016/j.matlet.2018.04.082

Pi Y, Li X, Xia Q, Wu J, Li Y, Xiao J, Li Z (2018) Adsorptive and photocatalytic removal of Persistent Organic Pollutants (POPs) in water by metal-organic frameworks (MOFs). Chem Eng J 337:351–371. https://doi.org/10.1016/j.cej.2017.12.092

Pruden A, Pei R, Storteboom H, Carlson KH (2006) Antibiotic resistance genes as emerging contaminants: studies in northern Colorado. Environ Sci Technol 40(23):7445–7450. https://doi.org/10.1021/es0604131

Qazi MR, Abedi MR, Nelson BD, DePierre JW, Abedi-Valugerdi M (2010) Dietary exposure to perfluorooctanoate or perfluorooctane sulfonate induces hypertrophy in centrilobular hepatocytes and alters the hepatic immune status in mice. Int Immunopharmacol 10(11):1420–1427. https://doi.org/10.1016/j.intimp.2010.08.009

Qiang Z, Macauley JJ, Mormile MR, Surampalli R, Adams CD (2006) Treatment of antibiotics and antibiotic resistant bacteria in swine wastewater with free chlorine. J Agric Food Chem 54 (21):8144–8154. https://doi.org/10.1021/jf060779h

Qin J, Yang C, Cao M, Zhang X, Saravanan R, Limpanart S, Mab M, Liu R (2017) Two-dimensional porous sheet-like carbon-doped ZnO/g-C_3N_4nanocomposite with high visible-light photocatalytic performance. Mater Lett 189:156–159. https://doi.org/10.1016/j.matlet.2016.12.007

Quero-Pastor MJ, Garrido-Perez MC, Acevedo A, Quiroga JM (2014) Ozonation of ibuprofen: a degradation and toxicity study. Sci Total Environ 466:957–964. https://doi.org/10.1016/j.scitotenv.2013.07.067

Ramesh A, Archibong AE, Niaz MS (2010) Ovarian susceptibility to benzo[a]pyrene: tissue burden of metabolites and DNA adducts in F-344 rats. J Toxicol Environ Health A 73(23):1611–1625. https://doi.org/10.1080/15287394.2010.514225

Rengarajan T, Rajendran P, Nandakumar N, Lokeshkumar B, Rajendran P, Nishigaki I (2015) Exposure to polycyclic aromatic hydrocarbons with special focus on cancer. Asian Pac J Trop Biomed 5(3):182–189. https://doi.org/10.1016/S2221-1691(15)30003-4

Romero-Sáez M, Jaramillo LY, LY RS, Benito N, Pabón E, Mosquera E, Gracia F (2017) Notable photocatalytic activity of TiO_2-polyethylene nanocomposites for visible light degradation of organic pollutants. Express Polym Lett 11(11):899–909. https://doi.org/10.3144/expresspolymlett.2017.86

Ruge Z, Muir D, Helm P, Lohmann R (2015) Concentrations, trends, and air–water exchange of PAHs and PBDEs derived from passive samplers in Lake Superior in 2011. Environ Sci Technol 49(23):13777–13786. https://doi.org/10.1021/acs.est.5b02611

Saravanan R, Shankar H, Prakash T, Narayanan V, Stephen A (2011) ZnO/CdO composite nanorods for photocatalytic degradation of methylene blue under visible light. Mater Chem Phys 125(1–2):277–280. https://doi.org/10.1016/j.matchemphys.2010.09.030

Saravanan R, Manoj D, Qin J, Naushad M, Gracia F, Lee AF, MansoobKhan MM, Gracia-Pinilla MA (2018) Mechanothermal synthesis of Ag/TiO_2 for photocatalytic methyl orange degradation and hydrogen production. Process Saf Environ Prot 120:339–347. https://doi.org/10.1016/j.psep.2018.09.015

Schecter A, Malik N, Haffner D, Smith S, Harris TR, Paepke O, Birnbaum L (2010) Bisphenol a (BPA) in US food. Environ Sci Technol 44(24):9425–9430. https://doi.org/10.1021/es102785d

Senthilkumar PK, Robertson LW, Ludewig G (2012) PCB153 reduces telomerase activity and telomere length in immortalized human skin keratinocytes (HaCaT) but not in human foreskin keratinocytes (NFK). Toxicol Appl Pharmacol 259(1):115–123. https://doi.org/10.1016/j.taap.2011.12.015

Seza A, Soleimani F, Naseri N, Soltaninejad M, Montazeri SM, Sadrnezhaad SK, Mohammadi MR, Moghadam HA, Forouzandeh M, Amin MH (2018) Novel microwave-assisted synthesis of porous g-C_3N_4/SnO_2 nanocomposite for solar water-splitting. Appl Surf Sci 440:153–161. https://doi.org/10.1016/j.apsusc.2018.01.133

Jassal V, Shanker U, Kaith BS, Shankar S (2015) Green synthesis of potassium zinc hexacyanoferrate nanocubes and their potential application in photocatalytic degradation of organic dyes. RSC Adv 5(33):26141–26149. https://doi.org/10.1039/c5ra03266k

Shanker U, Jassal V, Rani M (2016) Catalytic removal of organic colorants from water using some transition metal oxide nanoparticles synthesized under sunlight. RSC Adv 6(97):94989–94999. https://doi.org/10.1039/c6ra17555d

Shanker U, Jassal V, Rani M (2017) Degradation of toxic PAHs in water and soil using potassium zinc hexacyanoferrate nanocubes. J Environ Manag 204:337–348. https://doi.org/10.1016/j.jenvman.2017.09.015

Shao YY, Ye WD, Sun CY, Liu CL, Wang Q (2017) Visible-light-induced degradation of polybrominated diphenyl ethers with AgI–TiO_2. RSC Adv 7(62):39089–39095. https://doi.org/10.1039/c7ra07106j

Shao YY, Ye WD, Sun CY, Liu CL, Wang Q, Chen CC, Gu JY, Chen XQ (2018) Enhanced photoreduction degradation of polybromodiphenyl ethers with Fe_3O_4-gC_3N_4 under visible light irradiation. RSC Adv 8(20):10914–10921. https://doi.org/10.1039/c8ra01356j

Sher Shah MS, Park AR, Zhang K, Park JH, Yoo PJ (2012) Green synthesis of biphasic TiO_2–reduced graphene oxide nanocomposites with highly enhanced photocatalytic activity. ACS Appl Mater Interfaces 4(8):3893–3901. https://doi.org/10.1021/am301287m

Silverstone AE, Rosenbaum PF, Weinstock RS, Bartell SM, Foushee HR, Shelton C, Pavuk M, Anniston Environmental Health Research Consortium (2012) Polychlorinated biphenyl (PCB) exposure and diabetes: results from the Anniston Community Health Survey. Environ Health Perspect 120(5):727–732. https://doi.org/10.1289/ehp.1104247

Singh L, Agarwal T (2018) PAHs in Indian diet: assessing the cancer risk. Chemosphere 202:366–376. https://doi.org/10.1016/j.chemosphere.2018.03.100

Singh Z, Kaur J, Kaur R, Hundal SS (2016) Toxic effects of organochlorine pesticides: a review. Am J Biosci 4(3–1):11–18. https://doi.org/10.11648/j.ajbio.s.2016040301.13

Son S, Nam K, Kim H, Gye MC, Shin I (2018) Cytotoxicity measurement of Bisphenol A (BPA) and its substitutes using human keratinocytes. Environ Res 164:655–659. https://doi.org/10.1016/j.envres.2018.03.043

Spasiano D, Marotta R, Malato S, Fernandez-Ibanez P, Di Somma I (2015) Solar photocatalysis: materials, reactors, some commercial, and pre-industrialized applications. A comprehensive approach. Appl Catal B 170:90–123. https://doi.org/10.1016/j.apcatb.2014.12.050

Tian H, Li J, Ge M, Zhao Y, Liu L (2012) Removal of bisphenol A by mesoporous BiOBr under simulated solar light irradiation. Catal Sci Technol 2(11):2351–2355. https://doi.org/10.1039/c2cy20303k

Tian J, Zhao Z, Kumar A, Boughton RI, Liu H (2014) Recent progress in design, synthesis, and applications of one-dimensional TiO_2 nanostructured surface heterostructures: a review. Chem Soc Rev 43(20):6920–6937. https://doi.org/10.1039/c4cs00180j

Tseng TK, Lin YS, Chen YJ, Chu H (2010) A review of photocatalysts prepared by sol-gel method for VOCs removal. Int J Mol Sci 11(6):2336–2361. https://doi.org/10.3390/ijms11062336

Verhaert V, Newmark N, D'Hollander W, Covaci A, Vlok W, Wepener V, Addo-Bediako A, Jooste A, Teuchies J, Blust R, Bervoets L (2017) Persistent organic pollutants in the Olifants

River Basin, South Africa: bioaccumulation and trophic transfer through a subtropical aquatic food web. Sci Total Environ 586:792–806. https://doi.org/10.1016/j.scitotenv.2017.02.057

Von Gunten U (2003) Ozonation of drinking water: part I. Oxidation kinetics and product formation. Water Res 37(7):1443–1467. https://doi.org/10.1016/S0043-1354(02)00457-8

Wang T, Wang Y, Liao C, Cai Y, Jiang G (2009) Perspectives on the inclusion of perfluorooctane sulfonate into the Stockholm convention on persistent organic pollutants. Environ Sci Technol 43:5171–5175. https://doi.org/10.1021/es900464a

Wang N, Guo X, Xu J, Kong X, Gao S, Shan Z (2014) Pollution characteristics and environmental risk assessment of typical veterinary antibiotics in livestock farms in Southeastern China. J Environ Sci Health B 49(7):468–479. https://doi.org/10.1080/03601234.2014.896660

Wang Q, Yang C, Zhang G, Hu L, Wang P (2017) Photocatalytic Fe-doped TiO_2/PSF composite UF membranes: characterization and performance on BPA removal under visible-light irradiation. Chem Eng J 319:39–47. https://doi.org/10.1016/j.cej.2017.02.145

Water Research Commission (2001) State of the rivers report: Crocodile, Sabie-Sand and Olifants River systems. Report No. TT 147/01. Water Research Commission. Pretoria

Wei L, Shifu C, Huaye Z, Xiaoling Y (2011) Preparation, characterization of p–n heterojunction photocatalyst $CuBi_2O_4/Bi_2WO_6$ and its photocatalytic activities. J Exp Nanosci 6(2):102–120. https://doi.org/10.1080/17458081003770295

Wen L, Ding K, Huang S, Zhang Y, Li Y, Chen W (2017) Why does F-doping enhance the photocatalytic water-splitting performance of $mBiVO_4$? – a density functional theory study. New J Chem 41(3):1094–1102. https://doi.org/10.1039/c6nj02400a

Xia D, Lo IM (2016) Synthesis of magnetically separable Bi_2O_4/Fe_3O_4 hybrid nanocomposites with enhanced photocatalytic removal of ibuprofen under visible light irradiation. Water Res 100:393–404. https://doi.org/10.1016/j.watres.2016.05.026

Xia J, Di J, Yin S, Xu H, Zhang J, Xu Y, Xu L, Li H, Ji M (2014) Facile fabrication of the visible-light-driven Bi_2WO_6/BiOBr composite with enhanced photocatalytic activity. RSC Adv 4 (1):82–90. https://doi.org/10.1039/c3ra44191a

Xie X, Kretschmer K, Wang G (2015) Advances in graphene-based semiconductor photocatalysts for solar energy conversion: fundamentals and materials engineering. Nanoscale 7 (32):13278–13292. https://doi.org/10.1039/c5nr03338a

Yan H, Wang X, Yao M, Yao X (2013) Band structure design of semiconductors for enhanced photocatalytic activity: the case of TiO_2. Prog Nat Sci Mater Int 23(4):402–407. https://doi.org/10.1016/j.pnsc.2013.06.002

Yin S, Wu T, Li M, Di J, Ji M, Wang B, Chen Y, Xia J, Li H (2017) Controllable synthesis of perovskite-like $PbBiO_2Cl$ hollow microspheres with enhanced photocatalytic activity for antibiotic removal. Cryst Eng Comm 19(32):4777–4788. https://doi.org/10.1039/c7ce00993c

Yuan D, Huang L, Li Y, Xu Y, Xu H, Huang S, Yan J, He M, Li H (2016) Synthesis and photocatalytic activity of gC_3N_4/BiOI/BiOBr ternary composites. RSC Adv 6 (47):41204–41213. https://doi.org/10.1039/c6ra05565f

Zhang LW, Fu HB, Zhu YF (2008) Efficient TiO_2 photocatalysts from surface hybridization of TiO_2 particles with graphite-like carbon. Adv Funct Mater 18(15):2180–2189. https://doi.org/10.1002/adfm.200701478

Zhang H, Lv X, Li Y, Wang Y, Li J (2010) P25-graphene composite as a high performance photocatalyst. ACS Nano 4(1):380–386. https://doi.org/10.1021/nn901221k

Zhang W, Zou L, Dionysio D (2015) A parametric study of visible-light sensitive TiO_2 photocatalysts synthesis via a facile sol–gel N-doping method. J Exp Nanosci 10 (15):1153–1165. https://doi.org/10.1080/17458080.2014.985751

Zhao X, Cai Z, Wang T, O'Reilly SE, Liu W, Zhao D (2016) A new type of cobalt-deposited titanate nanotubes for enhanced photocatalytic degradation of phenanthrene. Appl Catal B 187:134–143. https://doi.org/10.1016/j.apcatb.2016.01.010

Zhao Y, Tao C, Xiao G, Su H (2017) Controlled synthesis and wastewater treatment of Ag_2O/TiO_2 modified chitosan-based photocatalytic film. RSC Adv 7(18):11211–11221. https://doi.org/10.1039/c6ra27295a

Zheng X, Xu S, Wang Y, Sun X, Gao Y, Gao B (2018) Enhanced degradation of ciprofloxacin by graphitized mesoporous carbon (GMC)-TiO_2 nanocomposite: strong synergy of adsorption-photocatalysis and antibiotics degradation mechanism. J Colloid Interface Sci 527:202–213. https://doi.org/10.1016/j.jcis.2018.05.054

Zhou X, Liu G, Yu J, Fan W (2012) Surface plasmon resonance-mediated photocatalysis by noble metal-based composites under visible light. J Mater Chem 22(40):21337–21354. https://doi.org/10.1039/c2jm31902k

Zhou T, Xu Y, Wang X, Huang S, Xie M, Xia J, Huang L, Xu H, Li H (2018) Construction of solid–liquid interfacial Fenton-like reaction under visible light irradiation over etched $Co_xFe_yO_4$–BiOBr photocatalysts. Cat Sci Technol 8(2):551–561. https://doi.org/10.1039/c7cy01915g

Zhu SR, Qi Q, Zhao WN, Wu MK, Fang Y, Tao K, Yi FY, Han L (2017) Hierarchical core–shell SiO_2@PDA@BiOBr microspheres with enhanced visible-light-driven photocatalytic performance. Dalton Trans 46(34):11451–11458. https://doi.org/10.1039/c7dt01581j

Chapter 2
Surface Modification of Highly Magnetic Nanoparticles for Water Treatment to Remove Radioactive Toxins

Arun Thirumurugan, Ali Akbari-Fakhrabadi, and R. Justin Joseyphus

Contents

Abstract Magnetic materials have received much attention due to their use in various applications such as biomedical, waste water treatment, photocatalytic, and electrocatalytic applications. Among the magnetic materials, Fe_3O_4 magnetic nanoparticles (MNPs) are the finest choice, due to their easy preparation process and flexible magnetic characteristics with adjustable morphology and size. Surface modifications of Fe_3O_4 MNPs with suitable surface modifier are necessary to utilize the hybrid materials for any specific required applications. The selection of surface modifier is important, as it is having a major role for the specific applications. The MNPs with higher saturation magnetization are essential for any magnetic field-assisted applications even with the surface modifier. In this chapter, the progresses on the surface modifications of Fe_3O_4 for the potential use in the heavy metal ion and

A. Thirumurugan (✉) · A. Akbari-Fakhrabadi
Advanced Materials Laboratory, Department of Mechanical Engineering, University of Chile, Santiago, Chile
e-mail: arunthiruvbm@gmail.com; aliakbarif@uchile.cl

R. J. Joseyphus
Magnetic Materials Laboratory, National Institute of Technology, Tiruchirappalli, Tamil Nadu, India
e-mail: rjustinj@nitt.edu

M. Naushad et al. (eds.), *Green Methods for Wastewater Treatment*, Environmental Chemistry for a Sustainable World 35, https://doi.org/10.1007/978-3-030-16427-0_2

radioactive toxin ion removal from water solutions are discussed. The possibility for the development of highly magnetic surface-modified MNPs of Fe–Fe_3O_4–Prussian blue system as a recoverable adsorbent is proposed.

Keywords Magnetic nanoparticles · Fe_3O_4 · Core–shell · Chemical synthesis · Surface modification · Adsorption · Detoxification · Saturation magnetization

2.1 Introduction

2.1.1 Magnetic Materials

Materials can exhibit ferromagnetic, diamagnetic, paramagnetic, ferrimagnetic, and antiferromagnetic behavior according to their magnetic nature. Soft and hard magnetic materials are the two types of classification based on the coercivity exhibited by them. To consider ferromagnetic materials for practical applications, coercivity is one of the most sensitive properties, which is extrinsic in nature. The materials with high magnetocrystalline anisotropy are hard magnetic materials which also have high coercivity, and the materials with low magnetocrystalline anisotropy are known as soft magnetic material. The coercivity is a function of particle size, which reaches a maximum value, when they are in the critical single domain (Ds) size. The coercivity reaches zero when the particle size reduces much below the single domain size due to superparamagnetism (Bean and Livingston 1959). Superparamagnetism is an outcome of the dominance of thermal energy over anisotropy energy. The anisotropy energy density is given as $E = KV\ sin2\theta$, where K is the anisotropy constant and V is the particle volume, for an assembly of uniaxial and single domain particles. The energy barrier required for the separation of two energy minima at $\theta = 0$ and $\theta = \pi$, which are corresponding to the parallel or antiparallel magnetization, respectively, to the easy axis, is $\Delta E\mathrm{B} = KV$. The particle freely fluctuates with the limit of $kBT >> KV$, where kB is Boltzmann's constant and T is temperature. This limit is called as isotropic superparamagnetic limit (Bean and Livingston 1959). The particle size will have a sizable influence on the magnetization dynamics with decreasing temperature. The energy limit reaches $kBT \approx KV$ and then finally to $kBT < KV$, and this state is called as blocked state.

In the blocked state, the direction of magnetization would swing among the two energy minima with a frequency, f, or a representative relaxation time, given by the Neel–Brown expression (Sorensen 2001), $\tau = \tau 0\ exp\ (KV/kBT)$, where $\tau 0 \sim 10^{-10}$ s is the relaxation time constant. From the above equation, it is obvious that the particle size plays an important role in determining the relaxation time. Figure 2.1 shows the relationship between coercivity (Hc) and particle size in a ferro-/ferrimagnetic material. The coercivity is lowest at the superparamagnetic (SPM) regime, reaches the highest at a critical size with a single domain, and decreases with

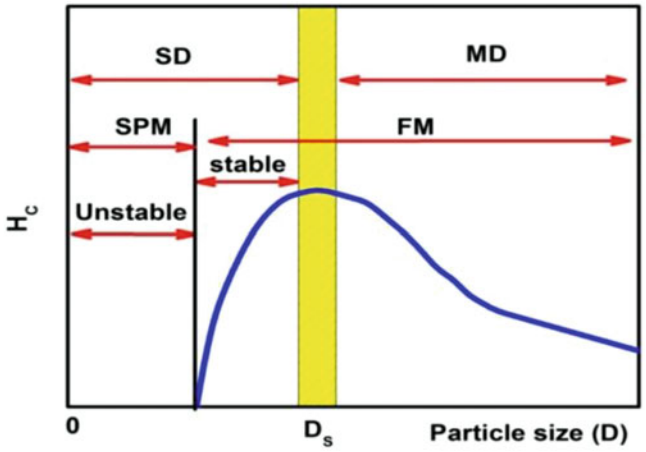

Fig. 2.1 Schematic diagram showing the relationship between coercivity (Hc) and particle size

the size of particle in the multidomain (MD) regime as shown in Fig. 2.1. From Fig. 2.1, it is also illustrated that the ferro-/ferrimagnetic (FM) particles become unstable when they become superparamagnetic particles. The unstable nature of superparamagnetic nanoparticles makes them unsuitable for recording application. Crossing the superparamagnetic limit by creating magnetic exchange coupling between ferromagnetic and antiferromagnetic surface (Skumryev et al. 2003) is one way of utilizing magnetic nanoparticles (MNPs) for high-density data storage. Developing synthetic routes for the synthesis of ferromagnetic nanoparticles with high anisotropy constants is another way to overcome the thermal fluctuations for the use in ultrahigh-density storage media (Weller and Moser 1999) and permanent magnets (Zeng et al. 2002). On the other hand, superparamagnetic nanoparticles with high saturation magnetization in low applied field and negligible remanent magnetization are used for biomedical applications (Pankhurst et al. 2003) such as targeted drug delivery (Lubbe et al. 1996; Gu et al. 2007; Mohapatra et al. 2014), localized heating of cancerous cells (hyperthermia) (Hergt et al. 2004), magnetic resonance imaging (MRI) contrast enhancement (Bjørnerud and Johansson, 2004), and medical diagnosis and therapy (Mornet et al. 2004).

The development of size-controlled and chemically stable MNPs has become one of the most essential and crucial factors for biomedical applications. Especially the MNPs with high saturation magnetization are important for applications such as targeted drug delivery and other magnetic field-assisted applications such as waste water purification including heavy metal ions and radioactive toxin removal or any other magnetic separation process which used magnetic nanoparticle and magnetic field.

2.1.2 Magnetite

Among the magnetic materials, Fe_3O_4 is found to be a common choice for surface modification due to easy process of size tuning and the attachment of surface modifier. Fe_3O_4 belongs to the class of ferrimagnetic materials with the spinel structure, and it is important because of the spontaneous magnetization like ferromagnetic materials. The spontaneous magnetization will be destroyed above the Curie temperature, which is 850 K for Fe_3O_4. The magnetic properties of the ferrites are dependent on the net magnetic moment of the ions present in the spinel structure. The maximum saturation magnetization of bulk Fe_3O_4 is 92 emu/g (Cullity 2009) and the saturation magnetization gets reduced with a reduction in particle size which is due to the surface spin effects even with a larger applied magnetic field. The surface spin effect on the particle is leading to spontaneously magnetized core and the misaligned surface spin forming the magnetic dead layer as shown in Fig. 2.2.

2.1.3 Surface Modification

Surface modification is important to improve the characteristics of nanoparticles such as dispersion of nanoparticles, improving the biocompatibility and obtaining other physicochemical properties. With the help of surface modification, we could be able to adjust the physical, chemical, and biological characteristics of the nanomaterials which can be used for industrial and biological applications. Although few properties could be improved with the surface modification, some of the core magnetic particle properties such as saturation magnetization might get suppressed due to surface modification with nonmagnetic surface modifier, and this is the major problem in the surface modification of MNPs. Preparing highly MNPs for the

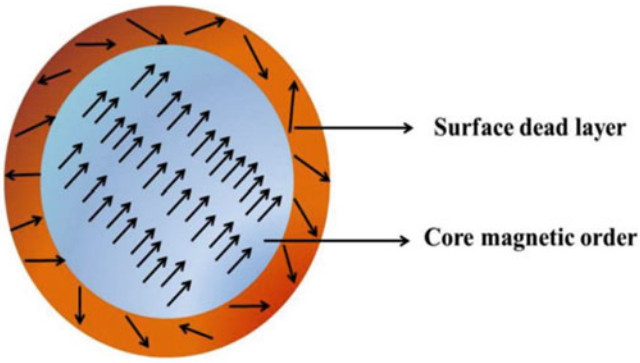

Fig. 2.2 Schematic diagram showing a particle exhibiting surface spin effects

surface modification would be the solution to have magnetic characteristics after the surface modification. Highly magnetic nanomaterials only could be able to response with surface modification even with lower applied magnetic field. The MNPs were surface modified with PVA, PEG, PVP, SiO_2, TiO_2, and various noble metals (Shan et al. 2003;Gupta and wells 2004; D'Souza et al. 2004; Ma et al. 2006; Chen and Chen 2005; Xuan et al. 2009; Mandal et al. 2005; Lu et al. 2007; Wu et al. 2008; Wilson et al. 2012; Laurent et al. 2008) for various applications including drug delivery, photocatalytic, and sensing. However, there are many potential uses of surface-modified MNPs in applications such as magnetic separation (reusable adsorbent in waste water purification or toxic ion removal) and magnetic field-assisted drug delivery which requires specific MNPs with higher saturation magnetization.

2.1.4 Water Purification

Water purification is one of the essential processes to avoid water scarcity for human use. The treatment processes for the purification of water are demonstrated by various stages of purification process, and the technologies are in the developing stage to meet the water standard proposed by the governing agencies (Alqadami et al. 2016a, b). New water treatment processes are being developed by various research groups throughout the world by introducing various nanomaterials into the water purification process (Naushad et al. 2016). Even though few water treatment methods are established, the efficiency of the nanomaterials in the water purification could be improved by developing novel filtration membrane, high surface area adsorbents, and other processes. Various processes were identified for the development of water purification technologies including several separation processes, coagulation, sedimentation, filtration, chemical purification, ion exchange, reverse osmosis, etc. (Daneshvar et al. 2017). The objective of all these processes is the removal of contaminants from water and to provide clean water. Numerous nanomaterials have been attempted to validate the removal efficiency and to reduce the cost of the overall process. Even though the commercially available nanomaterial has been utilized for water purification process, several research groups are in the process of synthesizing or developing various nanomaterial systems to improve the efficiency by obtaining various morphologies and different hybrid system. The use of magnetic nanomaterials is advantageous over other nanomaterials due to the easy way of collection and reuse of the nanomaterial. The water treatment by using nanomaterials as an adsorbent is shown schematically in Fig. 2.3. The adsorption process could happen through physical, chemical, or biological process. The adsorption capacity during the adsorption process may vary with different parameters such as pH, amount of adsorbent used, coexisting ions, temperature, and the interaction time of adsorbent with the polluted water.

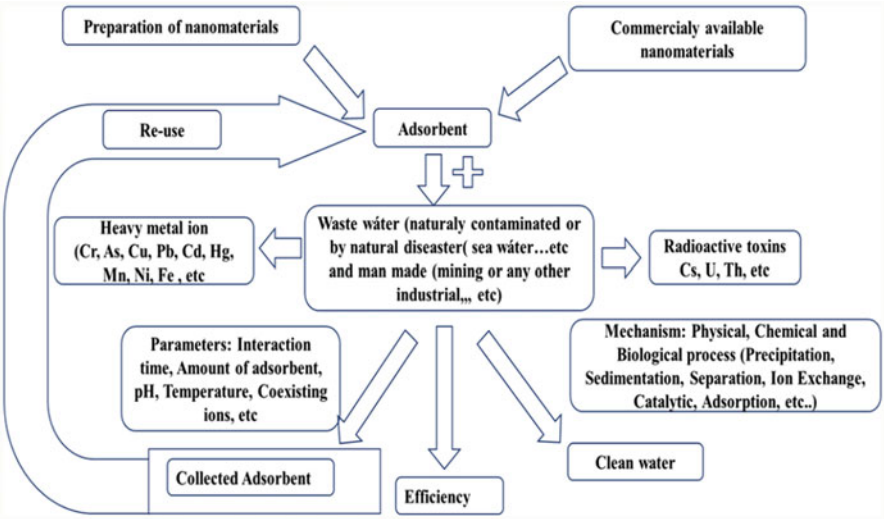

Fig. 2.3 Flow chart of nanoparticles for the toxic ion removal process

2.2 Fe_3O_4 for Heavy Metal Ion Removal

Fe_3O_4 was found as one of the best adsorbents for the removal of various heavy metals due to the easy preparation and tuning of the magnetic properties of the nanomaterials. For further improvement in the adsorption capacity, Fe_3O_4 MNPs were surface modified with several surface modifiers and found the significant improvement. Table 2.1 shows the use of Fe_3O_4 for the removal of heavy metal ions from waste water solutions. Fe_3O_4 MNPs were surface modified with various surface modifiers such as SiO_2, Al_2O_3, polypyrrole, humic acid, hematite, chitosan, EDTA, graphene, and graphene oxide, various functional materials, and their combinations. Even though bare Fe_3O_4 has the tendency to adsorb heavy metal ions, the adsorption capacity was observed as less for heavy metal ions. The surface-modified Fe_3O_4 MNPs showed good adsorption and removal efficiency toward the removal of copper, nickel, chromium, zinc, manganese, silver, cadmium, lead, arsenic, and mercury. From the available reports, it is understood that the adsorption capacity is increasing significantly due to the selection of suitable surface modifier for surface modifications.

2.3 Fe_3O_4 for Radioactive Toxic Ion Removal

As the Fe_3O_4 has the tendency to attract various heavy metal ions, it gave the opportunity to use it for the radioactive toxic ion removal. In the case of radioactive toxic metal ion removal, the utilization of bare Fe_3O_4 nanoparticle was very limited

Table 2.1 Bare and surface-modified Fe_3O_4 for removal of toxic ions

Magnetic material	Saturation magnetization (emu/g)	Type of metal removed	Efficiency or adsorption capacity	References
Fe_3O_4	40	As (V)	16.56 mg/g	Liyun Feng et al. (2012)
		As(III)	46.06 mg/g	
Fe_3O_4 nanoparticles	–	Ni(II)	95.6%	Y.F. Shena et al. (2009)
		Cu(II)	99.9%	
		Cd(II)	94.5%	
		Cr(VI)	97.3%	
Mesoporous Fe_3O_4 spheres	77.5	Cr(VI)	9 mg/g	Madhu Kumari et al. (2015)
		Pb(II)	19 mg/g	
Fe_3O_4 nanocrystals	–	As(III)	99.2%	Cafer T. Yavuz et al. (2006)
		As(V)	98.4	
Fe_3O_4@TAS	41.4	Cd(II), Cr (III), and Co(II)	286, 370, and 270	Alqadami et al. (2017a)
Fe_3O_4@TSC	55.4	Cr(III) and Co (II)	–	Alqadami et al. (2016a, b)
Fe_3O_4@silica	18.29	Hg(II)	0.588 mgL^{-1}	Haibo Hu et al. (2010)
Polypyrrole/Fe_3O_4	–	Cr(IV)	209.89 mg/g	Madhumita Bhaumik et al. (2013)
Humic acid (HA)-coated Fe_3O_4	68.1	Hg(II)	99.9%	Jing-Fu Liu et al. (2008)
		Pb(II)	99.5%	
Hematite–Fe_3O_4	27	Sb(III)	36.7 mg/g	Chao Shan et al. (2014)
Hematite-coated Fe_3O_4 particles	36	As(III), As(V)	1.0 ug/mg	K. Simeonidisa et al. (2011)
			2.1 ug/mg	
Chitosan–Fe_3O_4 nanoparticles	–	Cu(II)	21.5 mg/g	Yang-Chuang Chang and D.H. Chen (2005)
Fe_3O_4@EDTA	–	Ag(I), Hg (II)	112 mg/g for removal of all	Ensieh Ghasemi and A.H.M. Sillanpää (2017)
Fe_3O_4–RGO–MnO_2	48.57	As (III)	14.04 mg/g	Xubiao Luo et al. (2012)
		As (V)	12.22 mg/g	
Fe_3O_4–3-aminopropyl triethoxysilane (APTES)–glutaraldehyde (GA)	48.4	Cu (II)	61.07 mg/g	Mustafa Ozmen et al. (2010)
Fe_3O_4@SiO_2–NH_2	34	Cu(II)	0.69 mmol/g	Jiahong Wang et al. (2010)
		Pb(II)	0.54 mmol/g	
		Cd(II)	0.33 mmol/g	

(continued)

Table 2.1 (continued)

Magnetic material	Saturation magnetization (emu/g)	Type of metal removed	Efficiency or adsorption capacity	References
EDTA-functionalized Fe_3O_4	81.45	Cu(II)	46.27 mg/g	Yan Liu et al. (2013)
Fe_3O_4@$Al(OH)_3$	15.8	Fluoride	68 mg/g	Xiaoli Zhao et al. (2010)
Amine-functionalized mesoporous Fe_3O_4 nanoparticles	75	Cd(II)	446.4 mg/g	Xiaodong Xin et al. (2012)
		Pb(II)	369.0 mg/g	
Fe_3O_4–graphene	0.88	As (V)	240 mg/g	Liangqia Guo et al. (2015)
Fe_3O_4–graphene oxide	–	As (IV)	42.9 mg/g	Yeojoon Yoon et al. (2016)
		As(V)	18.8 mg/g	
Fe_3O_4-reduced graphene oxide			29.8 mg/g	
			8.42 mg/g	
Fe_3O_4–thiol-functionalized mesoporous silica material	38.8	Hg	260 metal/g	Guoliang Li et al. (2011)
		Pb	91.5 metal/g	
Fe_3O_4–3-aminopropyltriethoxysilane (APS) and copolymers of acrylic acid (AA) and crotonic acid (CA)	52	Cd^{2+}	29.6 mg/g	Fei Ge et al. (2012)
		Pb^{2+}	166.1 mg/g	
		Cu^{2+}	126.9 mg/g	
Poly(1-vinylimidazole)-grafted Fe_3O_4@SiO_2	44.7	Cd (II)	42.1 mg/g	Chao Shan et al. (2015a, b)
Fe_3O_4-reduced graphene oxides aerogels	39.771	As (III)	11.3 mg/g	Yong Li et al. (2016)
EDTA-modified chitosan/SiO_2/Fe_3O_4	18.2	Cu(II)	44.4 mg/g	Yong Ren et al. (2013)
		Pb(II)	63.3 mg/g	
		Cd(II)	123 mg/g	
Fe_3O_4@SiO_2–EDTA	34.49	Pb(II), Cd (II)	114.94 mg/g	Yu Liu et al. (2016)
			50.25 mg/g	
PANI/Fe_3O_4/PES (polyethersulfone)	–	Cu(II)	75%	Parisa Daraei et al. (2012)
Poly(1-vinylimidazole)-grafted Fe_3O_4@SiO_2	44.7	Hg(II)	346 mg/g	Chao Shan et al (2015a, b)
Fe_3O_4–chitosan–glycidyl methacrylate macromolecular hybrid material	19.1	Hg(II)	2.02 mmol/g	Khalid Z. Elwakeel and E. Guibal (2015)
Sulfate-doped Fe_3O_4/Al_2O_3	16	Fluoride	70.4 mg/g	Liyuan Chai et al. (2013)
Fe_3O_4@glycine–polypyrrole	2.2	Cr(VI)	238 mg/g	N. Ballav et al. (2014)
Thiol-modified Fe_3O_4@SiO_2	20.47	Hg	148.8 mg/g	Shengxiao Zhang et al. (2013)

due to the less adsorption capacity toward the radioactive toxic metal ion. But with the help of surface modification, radioactive toxic metal ion removal was succeeded using hybrid materials of Fe_3O_4 with various surface modifiers such as graphene, graphene oxide, TiO_2, WO_3, alginate, fungus, SiO_2, EDTA, Prussian blue, and other functional groups. These surface-modified Fe_3O_4 showed good adsorption capacity toward the removal of uranium, strontium, thorium, and cesium. Table 2.2 shows the efficiency of surface-modified Fe_3O_4 toward the radioactive toxic ion removal in the recent reports.

As we have seen from Tables 2.1 and 2.2, the saturation magnetization of Fe_3O_4 MNPs was varying with size, morphology, and surface modifier. Even though the adsorption capacity or efficiency of the surface-modified Fe_3O_4 is high, the saturation magnetizations of the final hybrid materials are less due to the nonmagnetic surface modifier. The saturation magnetization of any MNPs is important for the magnetic field-assisted application in a large scale. From the available literature, it is understood that achieving the saturation magnetization more than 82 emu/g for surface-modified Fe_3O_4 will be difficult. It is important to have a hybrid magnetic nanoparticle with higher saturation magnetization to show good response for the magnetic separation even after surface modification. To achieve this, there are two options: the first one is to have a highly magnetic core phase that can provide higher saturation magnetization after the surface modification with nonmagnetic surface modifier and the second option is to choose another magnetic material as a surface modifier to get a combined saturation magnetization from the core and shell or surface modifier. However, the choice of surface modifier also has important role for the water purification, and it should have a tendency to attract toxic ions from the water solutions. Further we will discuss about the possibility of utilizing Prussian blue as a surface modifier for the potential application in the cesium ion removal from the water solutions.

2.4 Prussian Blue and Its Use for Cs Ion Removal

Prussian blue is a blue pigment used as paint in drawings. Prussian blue was considered as the first synthetic coordination compound which was synthesized in Berlin around the year 1706. Prussian blue is an inorganic compound with the formula of $Fe_7(CN)_{18}$, which also contains variable quantity of water molecules within the crystal structure. With water molecule, the chemical stoichiometry of Prussian blue is written as $Fe_7(CN)_{18}(H_2O)x$, $(14 \leq x \leq 16)$. To determine the crystal structure of Prussian blue, various experiments were done, and the crystal structure of Prussian blue was demonstrated similar to coordination compounds such as $Mn_3[Co(CN)_6]_2$ and also $Co_3[Co(CN)_6]_2$. Prussian blue contains Fe(II)-CN-Fe(III) connections, with a distance of 1.92 Å for Fe(II)-C, 2.03 Å for Fe(III)-N, and 5.1 Å for Fe (II)-Fe (III). The crystal structure of Prussian blue having eight

Table 2.2 Surface-modified Fe_3O_4 for the removal of radioactive ions

Magnetic material	Saturation magnetization (emu/g)	Type of metal removed	Efficiency or adsorption capacity	References
Fe_3O_4/graphene	45.6	U(VI)	176.47	Donglin Zhao et al. (2018)
Fe_3O_4/graphene oxide	31.2	U(VI)	69.49 mg/g	Pengfei Zong et al. (2013)
Fe_3O_4–NH_2	–	Uranium (U)	268.49 mg/g	G. W. Peng et al. (2014)
Fe_3O_4@WO_3	–	Sr(II)	44.178 mg/g	Wanjun Mu et al. (2017)
		Cs(II)	53.175 mg/g	
Alginate/Fe_3O_4	8.6	Sr	12.5 mg/g	Hye-Jin Hong et al. (2016)
Fe_3O_4@AMCA–MIL53(Al)	49.7	U(VI), Th(IV)	227.3, 285.7	Alqadami et al. (2017b)
Fungus–Fe_3O_4	51.18	U(II)	171 mg/g	La Li et al. (2015)
Fe_3O_4–SiO_2	–	U(VI)	52 mg/g	Fang-Li Fan et al. (2012)
Polyacrylamide–Fe_3O_4	62.3	U(VI)	220.9 mg/g	Wencheng Song et al. (2014)
Prussian blue/Fe_3O_4	12.07	Cs	280.82 mg/g	Jiseon Jang and Dae Sung Lee (2016)
Fe_3O_4 particle-modified sawdust	–	Sr (II)	12.59 mg/g	Zihong Cheng et al. (2012)
Prussian blue-functionalized Fe_3O_4	27.5	^{137}Cs	99.76%	Hee-Man Yang et al. (2016)
Ammonium-pillared montmorillonite Fe_3O_4	36.295	Cs^+	26.79 mg/g	Xianming Zheng et al. (2017)
Coal fly ash–Fe_3O_4	–	U(VI)	1.38 mmol/g	Zhongshan Chen et al. (2017)

TiO_2/Fe_3O_4/graphene	–	U (VI)	14%	Zi-Jie Li et al. (2017)
PVA/Fe_3O_4/SiO_2/APTES	–	Th (IV)	62.5 mg/g	Gholam Hossein Mirzabe and Ali Reza Keshtkar (2015)
Covalent triazine polymer–Fe_3O_4	–	Sr(II)	128 mg/g	Arunkumar Rengaraj et al. (2017)
EDTA-functionalized Fe_3O_4/graphene oxide	39.47	U (VI)	277.43 mg/g	Donglin Zhao et al. (2017)
Amino-functionalized Fe_3O_4/graphene oxide	29.3	U(VI)	141.2 mg/	Lili Chen et al. (2016)
Diacrylamidoxime triaethylenetetralevopimaramide–Fe_3O_4	74	Th(IV)	666 mg/g	A.M. Atta and Z.F. Akl (2015)
Fe_3O_4/P(GMA–AA–MMA)–PO_4	7.3	U(VI)	274.7 mg/g	Dingzhong Yuan et al. (2016)
Amidoxime-functionalized Fe_3O_4@SiO_2	50.2	U(VI)	0.441 mmol/g	Yingguo Zhao et al. (2014)
Prussian blue/Fe_3O_4 cubes	80	Cs	22 mg/g	T. Arun and R.J. Joseyphus (2014)

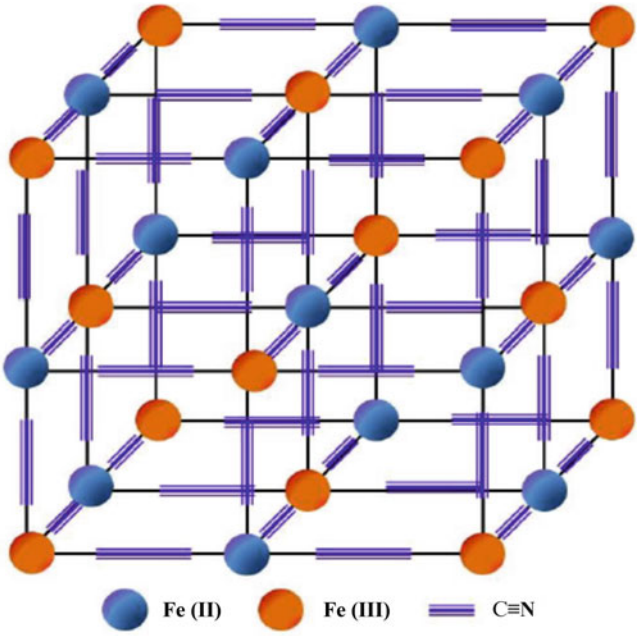

Fig. 2.4 Crystal structure of Prussian blue

channels is named as A site with a diameter of 0.32 nm. Figure 2.4 shows the crystal structure of Prussian blue. The composition may vary with the water molecules within the crystal structure.

The variation in the composition of Prussian blue is attributed to the low solubility of Prussian blue which leads to quick precipitation without attaining the equilibrium state between solid and liquid. Prussian blue is classified as soluble and insoluble, based on the colloidal forming tendency. The soluble Prussian blue has a chemical formula of $KFeFe(CN)_6$, and the insoluble Prussian blue has chemical formula of $Fe_4[Fe(CN)_6]_3$. Between these two forms, insoluble Prussian blue is in demand due to its unusual characteristics of charge transfer within, electro-chromic behavior, and the tendency of absorbing radioactive cesium ions. Even though the Prussian blue has the cyanide group within the crystal structure, the cyanide group is not easily breakable, which makes the Prussian blue nontoxic.

Radioactive cesium isotopes might be released from the nuclear reactor due to various reasons and can be easily enter to the food cycle via water source and plants. Among the cesium isotopes, ^{137}Cs and ^{134}Cs are having longer half-life period (Emery et al. 1972). The physical half-life period of ^{137}Cs is 30.2 years with 2 months of biological half-life. The ^{137}Cs used in radiation sources is regularly in the form of cesium chloride, and the cesium chloride is effortlessly dispersed in the environment. Cesium chloride and other cesium compounds are easily soluble in water or other solvents and immediately absorbed from the lungs and gastrointestinal tract and also through wounds. The high solubility and long half-life time make the ^{137}Cs to spread

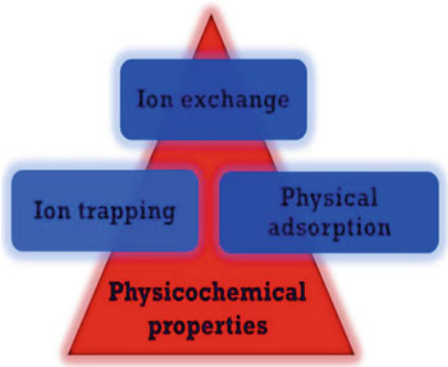

Fig. 2.5 Possible mechanisms for the attachment of Cs with Prussian blue

evenly throughout the biological body and cause health issues like cancer. It is proved that the Prussian blue is the effective drug for the ^{137}Cs poisoning of human beings by the US Food and Drug Administration (FDA). The effective dosage of Prussian blue is showed as 10 g/day for the radioactive ^{137}Cs absorption (Thompson and Church 2001; Lawrence and Kirk 2007; Hong et al. 2012). It is also noted that the Prussian blue is not much effective for the detoxification of any other radioactive metal ions.

As like other metal ion adsorbing mechanism, the adsorption of cesium ion with the Prussian blue also happens by combinations of various attachment mechanisms. Barton et al. demonstrated that the attachment of cesium ion with Prussian blue through physical adsorption of cesium ions into the crystal lattice due to the electrostatic interaction (Barton et al. 1958). Recently, the absorption of Cs ion with the Prussian blue is explained by the ion trapping by chemical adsorption through the hydrophilic lattice defect locations with proton elimination from the coordination water (Ishizaki et al. 2013). The open structure of Prussian blue results in high rate of adsorption capability. Hydrated ions easily move through the channels between the A sites. The basic principle for the ion exchange is that the ions in the solution are electronically charged and the charged ions could be attracted to the available locations on a solid material which is having an opposite charge. The solid material is named as sorbent, and the locations are named as binding sites. The physiochemical characteristics of Prussian blue would be the main reason for the adsorption of cesium ions which are ion exchange, ion trapping, and physical adsorption processes as illustrated in Fig. 2.5.

2.5 Fe_3O_4–Prussian Blue for Cesium Removal

The adsorption capacity of Cs by Prussian blue is found to be good and explained in detail by various mechanisms. But, the nonmagnetic nature of the material makes the Prussian blue unsuitable for magnetic field-assisted applications. Considering the absorption of Cs through the guts and their deposition in the lumens, it has to be

eliminated effectively in detoxification applications. One of the best options is to develop the Prussian blue-modified MNPs for detoxification of radioactive ion removal. Prussian blue–Fe_3O_4–PDDA composite was developed by Namiki et al. (Namiki et al. 2012) which was utilized for the removal of cesium ions and reached the maximum removal of 35%. Several reports are mainly focused on the attachment of Cs using Prussian blue (Prout et al. 1985; Lilga et al. 1997; Rassat et al. 1999; Lilga et al. 2001; Lin et al. 2001; Chen et al. 2007; Chang et al. 2008; Sangvanich et al. 2010; Parab and Sudersanan 2011; Arisaka and Nankawa 2012; Delchet et al. 2012; Namiki et al. 2012). The removal of cesium-attached adsorbent from the water solutions is still progressing. The removal of Prussian blue-attached Fe_3O_4 from waste water solutions are need to establish with different size and morphology as the size and morphology of the adsorbent also influence the adsorption efficiency and also the variation in the saturation magnetization. To establish the effect of MNP size on the adsorption capacity of cesium, we have developed Prussian blue-modified Fe_3O_4 with different sizes. Fe_3O_4 nanoparticles were prepared by using modified chemical oxidation method with optimized experimental conditions. Fe_3O_4 nanoparticle size was tuned between 10 and 100 nm by introducing the ferric ions, during the chemical reactions. The saturation magnetization of Fe_3O_4 was tuned from 62 to 90 emu/g by varying the particle size. The prepared Fe_3O_4 nanoparticles were used for the surface modification with Prussian blue, and the surface modification was achieved with optimized experimental conditions. The saturation magnetization of Fe_3O_4 with Prussian blue modification was 21–80 emu/g for various particle sizes. Figure 2.6 shows the MNP attraction toward a permanent magnet for (a) Fe_3O_4, (b) Prussian blue–Fe_3O_4 within few seconds, (c) Prussian blue–Fe_3O_4 after few seconds, and (d) Prussian blue.

We have used the Prussian blue-modified Fe_3O_4 nanoparticles for the cesium removal and found that the efficiency in terms of adsorption capacity is 22 mg/g. It is noted that the maximum value of adsorption capacity from the commercially available Prussian blue was observed as 29.3 mg/g (Torad et al. 2012). The adsorption capacity value of Prussian blue-modified Fe_3O_4 suggests that it could be used for the Cesium ion removal and also it can be used for magnetic field-assisted application as it has the Fe_3O_4 nanoparticles with higher saturation magnetization.

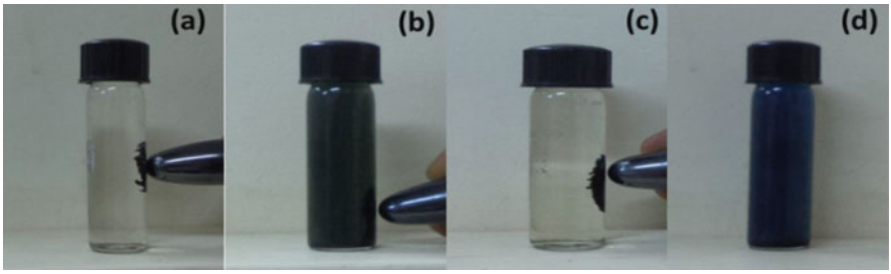

Fig. 2.6 MNP attraction toward a permanent magnet for (**a**) Fe_3O_4, (**b**) Prussian blue–Fe_3O_4 within few seconds, (**c**) Prussian blue–Fe_3O_4 after few seconds, and (**d**) Prussian blue

2.6 Fe–Fe_3O_4–Prussian Blue for Cesium Removal

Highly MNP systems are required for the water purification in a larger scale. Further our interest is to improve the magnetic characteristics of the nanoparticle within the hybrid system. Achieving higher saturation magnetization is possible by utilizing Fe MNPs in the hybrid systems. Synthesis of pure Fe magnetic nanoparticle is difficult as the pure Fe nanoparticles are easily get oxidized which will have the advantageous for the preparation of Fe–Fe_3O_4. Fe nanoparticles are not stable in many environments. Fe by itself reacts with air and water and forms various oxides such as Fe_3O_4, α- Fe_2O_3, γ-Fe_2O_3, and $Fe(OH)_2$. Fe nanoparticles exhibit interesting and useful magnetic properties, which is due to the high saturation magnetization of 218 emu/g. The crystal structure of Fe is body-centered cubic (bcc) below 1185 K, and above this temperature, it transforms to face-centered cubic (fcc) structure (Bramfitt and Benscoter 2002). The Curie temperature of Fe is 1044 K which is below the bcc–fcc phase transition temperature. The preparation of Fe nanoparticle with Fe_3O_4 shell would be the best possible way to achieve the highly magnetic nanoparticle with Fe_3O_4 surface characteristics. The surface-modified Fe nanoparticles with Prussian blue or any other surface modifier could give us a higher saturation magnetization, when compared to pure Fe_3O_4 with the same size. The occurrence of iron oxide layer on the surface of Fe is providing advantage for the surface modification and also for numerous applications. As the attachment of Prussian blue on the surface of Fe_3O_4 with suitable experimental procedure was successful, now we are able to use the highly magnetic Fe nanoparticles with a shell of Fe_3O_4 for the surface modification. To achieve this hybrid system, first we need to develop Fe–Fe_3O_4 system with high saturation magnetization and then surface modification with Prussian blue with optimized experimental conditions. Fe nanoparticles could be prepared by polyol process, and the oxide shell could be achieved by mild heating of Fe nanoparticles. Another way of getting iron oxide layer on the surface of Fe nanoparticles is to use higher amount of nucleating agent which will be used for the size reduction in lower concentration. Fe nanoparticles were prepared by using polyol process with $FeCl_2.4H_2O$ and NaOH at 170 °C. Platinum solutions were utilized as a nucleating agent to evaluate the size reduction. The lesser Pt concentration results in the size reduction of Fe nanoparticle, and higher concentration results in the reduction in particle size as well as the formation of oxide layer on the Fe nanoparticles. Figure 2.7 shows the TEM micrograph of Fe nanoparticles prepared by polyol process with and without Pt nucleating agent. With increasing Pt concentration, the size of Fe nanoparticle is reducing, and the oxide layer thickness on Fe nanoparticle is increasing. With this experimental procedure, we could be able to prepare various sizes of Fe nanoparticle with variable thickness of iron oxide shell.

Recently, the attachment of Prussian blue on the iron oxide surface was demonstrated based on the surface charge mechanism (Arun et al. 2013). The surface charge from the Fe_3O_4 could be due to the presence of ferrous and ferric ions on the surface of Fe_3O_4. It is also demonstrated that the Prussian blue easily gets

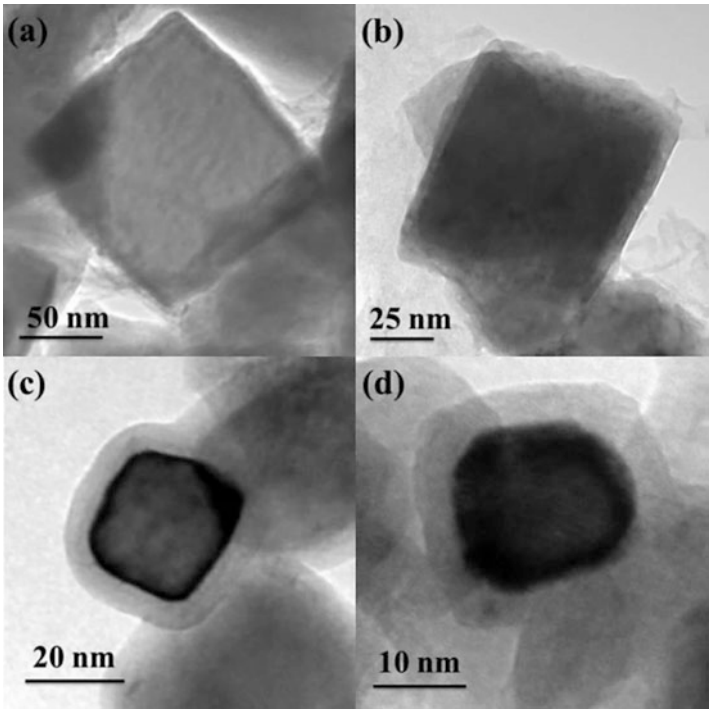

Fig. 2.7 Fe and Fe–Fe_3O_4 core–shell MNPs with different shell thickness

attached to the surface of Fe_3O_4 irrespective of surface charge on the Fe_3O_4, even in the hydrous or anhydrous environment. The possible way of Prussian blue attachment on Fe_3O_4 is shown in Fig. 2.8.

The attachment of Prussian blue can be easily adjusted by varying the HCl concentration. The saturation magnetization of smaller-sized Fe–Fe_3O_4 was observed as 168 emu/g. Fe–Fe_3O_4 nanoparticles were surface modified with Prussian blue, and the saturation magnetization was observed as 110 emu/g. The saturation magnetization of Fe–Fe_3O_4–Prussian blue was higher than that of bare Fe_3O_4. The Prussian blue fraction also could be adjusted by varying the HCl concentration. The advantageous over adjusting the fraction of Prussian blue and tuning of Fe_3O_4 shell thickness on the Fe nanoparticles providing opportunity to have a Fe- Fe_3O_4-Prussian blue system with adjustable saturation magnetization. Fe- Fe_3O_4-Prussian blue system with higher saturation magnetization could be the better candidate for any magnetic field assisted applications especially for the removal of cesium ions from water solutions. The development of Fe–Fe_3O_4–Prussian blue is shown in a schematic way as shown in Fig. 2.9. The system could be the suitable candidate for the water purification as it can be collected easily with the help of magnetic field and could be used again with a number of times.

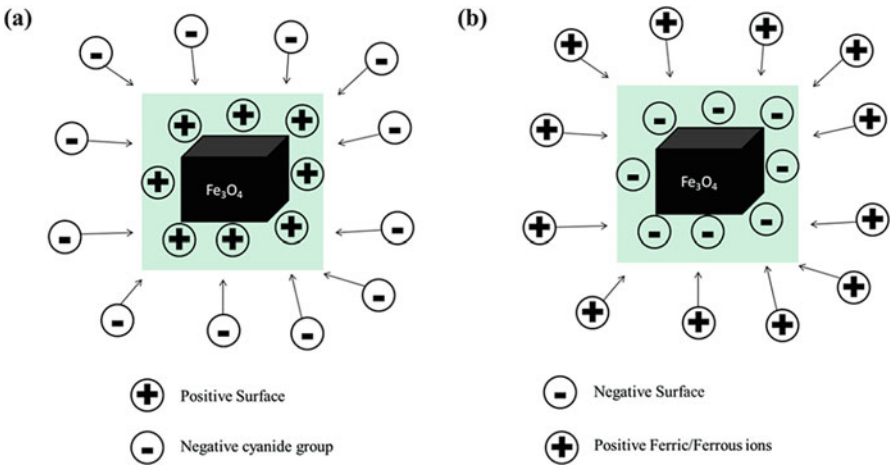

Fig. 2.8 Prussian blue attachment mechanism on Fe_3O_4 surface

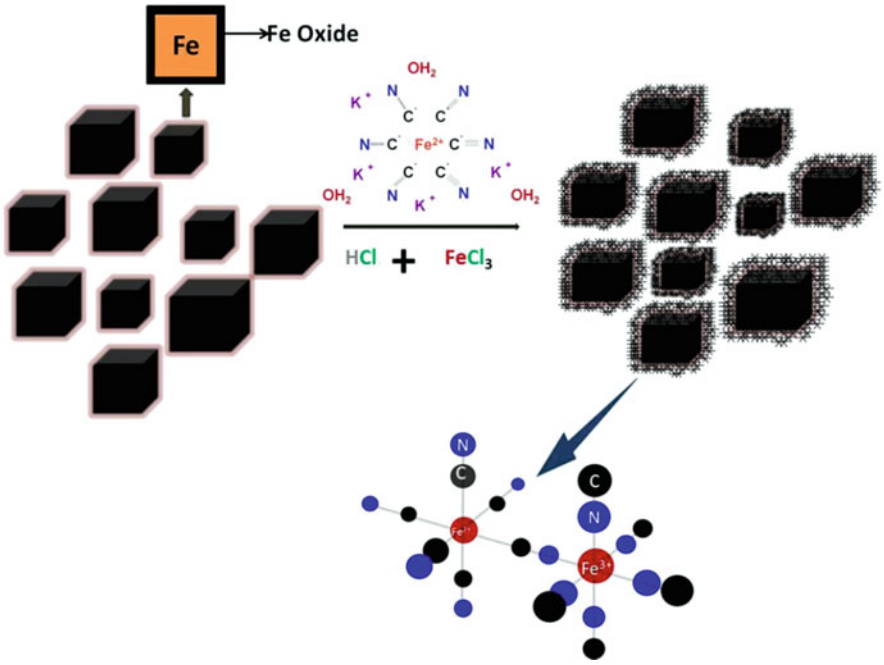

Fig. 2.9 Schematic diagram for the preparation of Fe–Fe_3O_4–Prussian blue

2.7 Summary

In this chapter, the progress on surface-modified Fe_3O_4 for the heavy metal ion and radio-toxic metal ion removal was discussed. The use of Prussian blue-modified Fe_3O_4 on the radio-toxic metal ion removal was shown by developing Fe_3O_4–Prussian blue nanoparticle hybrid system. The importance of Fe within Fe_3O_4 nanoparticles has been discussed in terms of saturation magnetization for the magnetic field-assisted applications. The new hybrid system of Fe–Fe_3O_4–Prussian blue is proposed for the better choice for cesium ion removal from waste water solutions and any magnetic field-assisted applications.

Acknowledgments The author T.A and A.A acknowledge FONDECYT Postdoctoral Research Project No. 3170696, Government of Chile, for the financial support.

References

Alqadami AA, Naushad M, Abdalla MA et al (2016a) Adsorptive removal of toxic dye using Fe3O4−TSC nanocomposite: equilibrium, kinetic, and thermodynamic studies. J Chem Eng Data 61(11):3806–3813. https://doi.org/10.1021/acs.jced.6b00446

Alqadami AA, Naushad M, Abdalla MA et al (2016b) Synthesis and characterization of Fe3O4 @TSC nanocomposite: highly efficient removal of toxic metal ions from aqueous medium. RSC Adv 6:22679–22689. https://doi.org/10.1039/C5RA27525C

Alqadami AA, Naushad M, Abdalla MA et al (2017a) Efficient removal of toxic metal ions from wastewater using a recyclable nanocomposite: a study of adsorption parameters and interaction mechanism. J Clean Prod 156:426–436. https://doi.org/10.1016/j.jclepro.2017.04.085

Alqadami AA, Naushad M, Alothman ZA, Ghfar AA (2017b) Novel metal-organic framework (MOF) based composite material for the sequestration of U(VI) and Th(IV) metal ions from aqueous environment. ACS Appl Mater Interfaces 9(41):36026–36037. https://doi.org/10.1021/acsami.7b10768

Arisaka M, Nankawa T (2012) Preparation of a film of copper hexacyanoferrate nanoparticles for electrochemical removal of cesium from radioactive wastewater. Electrochem Commun 25:23–25. https://doi.org/10.1016/j.elecom.2012.09.012

Arun T, Joseyphus RJ (2014) Prussian blue modified nanoparticles for Cs detoxification. J Mater Sci 49:7014–7022. https://doi.org/10.1007/s10853-014-8406-x

Arun T, Prakash K, Kuppusamy R, Joseyphus RJ (2013) Magnetic properties of Prussian blue modified Fe3O4 nanocubes. J Phys Chem Solids 74:1761–1768. https://doi.org/10.1016/j.jpcs.2013.07.005

Atta AM, Akl ZF (2015) Removal of thorium from water using modified magnetite nanoparticles capped with rosin amidoxime. Mater Chem Phys 163:253–261

Ballav N, Choi HJ, Mishra SB, Maity A (2014) Synthesis, characterization of Fe_3O_4@glycine doped polypyrrole magnetic nanocomposites and their potential performance to remove toxic Cr (VI). J Ind Eng Chem 20:4085–4093. https://doi.org/10.1016/j.jiec.2014.01.007

Barton GB, Hepworth JL, McClanahan ED, Moore RL, VanTuyl HH (1958) Chemical processing wastes, recovering fission products. J Ind Eng Chem 50:212–216. https://doi.org/10.1021/ie50578a039

Bean CP, Livingston JD (1959) Superparamagnetism. J Appl Phys 30:S120–S129. https://doi.org/10.1063/1.2185850

Bhaumik M, Setshedi K, Maity A, Onyango MS (2013) Chromium(VI) removal from water using fixedbed column ofpolypyrrole/Fe_3O_4 nanocomposite. Sep Purif Technol 110:11–19. https://doi.org/10.1016/j.seppur.2013.02.037

Bjørnerud A, Johansson L (2004) The utility of superparamagnetic contrast agents in MRI: theoretical consideration and applications in the cardiovascular system. NMR Biomed 17:465–477. https://doi.org/10.1002/nbm.904

Bramfitt BL, Benscoter AO (2002) Metallographer's guide: practice and procedures for iron and steels. ASM International, Materials Park

Chai L, Wang Y, Zhao N, Yang W (2013) Sulfate-doped Fe_3O_4/Al_2O_3 nanoparticles as a novel adsorbent for fluoride removal from drinking water. Water Res 47:4040–4049. https://doi.org/10.1016/j.watres.2013.02.057

Chang YC, Chen DH (2005) Preparation and adsorption properties of monodisperse chitosan-bound Fe_3O_4 magnetic nanoparticles for removal of Cu(II) ions. J Colloid Interface Sci 283:446–451. https://doi.org/10.1016/j.jcis.2004.09.010

Chang CY, Chau LK, Hu WP, Wang CY, Liao JH (2008) Nickel hexacyanoferrate Multilayer's on functionalized mesoporous silica supports for selective sorption and sensing of cesium. Microporous Mesoporous Mater 109:505–512. https://doi.org/10.1016/j.elecom.2012.09.012

Chen CT, Chen YC (2005) Fe_3O_4/TiO_2 core/shell nanoparticles as affinity probes for the analysis of phospho peptides using TiO2 surface-assisted laser desorption/ionization mass spectrometry. Anal Chem 77:5912–5919. https://doi.org/10.1021/ac050831t

Chen H, Kaminski MD, Liu X, Mertz CJ, Xie Y, Torno MD, Rosengart AJ (2007) A novel human detoxification system based on nanoscale bioengineering and magnetic separation techniques. Med Hypotheses 68:1071–1079. https://doi.org/10.1016/j.mehy.2005.04.047

Chen L, Zhao D, Chen S, Wang Z, Chen C (2016) One-step fabrication of amino functionalized magnetic graphene oxide composite for uranium(VI) removal. J Colloid Interface Sci 472:99–107. https://doi.org/10.1016/j.jcis.2016.03.044

Chen Z, Wang J, Pu Z, Zhao Y, Jia D, Chen H, Wen T, Hu B, Alsaedi A, Hayat T, Wang X (2017) Synthesis of magnetic Fe_3O_4 CFA composites for the efficient removal of U(VI) from wastewater. Chem Eng J 320:448–457. https://doi.org/10.1016/j.cej.2017.03.074

Cheng Z, Gao Z, Ma W, Sun Q, Wang B, Wang X (2012) Preparation of magnetic Fe_3O_4 particles modified sawdust as the adsorbent to remove strontium ions. Chem Eng J 209:451–457. https://doi.org/10.1016/j.cej.2012.07.078

Cullity BD (2009) Introduction to magnetic materials. Wiley, Hoboken

Daneshvar E, Vazirzadeh A, Niazi A et al (2017) Desorption of Methylene blue dye from brown macroalga: effects of operating parameters, isotherm study and kinetic modeling. J Clean Prod 152:443–453. https://doi.org/10.1016/j.jclepro.2017.03.119

Daraei P, Madaeni SS, Ghaemi N, Salehi E, Khadivi MA, Moradian R, Astinchap B (2012) Novel polyethersulfone nanocomposite membrane prepared by PANI/Fe_3O_4 Nanoparticles with enhanced performance for Cu(II) removal from water. J Membr Sci 415–416:250–259. https://doi.org/10.1016/j.memsci.2012.05.007

Delchet C, Tokarev A, Dumail X, Toquer G, Barre Y, Guari Y, Guerin C, Larionova J, Grandjean A (2012) Extraction of radioactive cesium using innovative functionalized porous materials. RSC Adv 2:5707–5716. https://doi.org/10.1039/C2RA00012A

D'Souza AJ, Schowen RL, Topp EM (2004) Polyvinylpyrrolidone-drug conjugate: synthesis and release mechanism. J Control Release 94:91–100. https://doi.org/10.1016/j.jconrel.2003.09.014

Elwakeel KZ, Guibal E (2015) Selective removal of Hg(II) from aqueous solution by functionalized magnetic-macromolecular hybrid material. Chem Eng J 281:345–359. https://doi.org/10.1016/j.cej.2015.05.110

Emery JF, Reynolds SA, Wyatt EI, Gleason GI (1972) Half-lives of radionuclides. IV. Nucl Sci Eng 48:319–323. https://doi.org/10.13182/NSE72-A22489

Fan FL, Qin Z, Bai J, Rong WD, Fan FU, Tian W, Wu XL, Wang Y, Zhao L (2012) Rapid removal of uranium from aqueous solutions using magnetic Fe_3O_4@SiO_2 composite particles. J Environ Radioact 106:40–46. https://doi.org/10.1016/j.jenvrad.2011.11.003

Feng L, Cao M, Ma X, Zhu Y, Hu C (2012) Superparamagnetic high-surface-area Fe_3O_4 nanoparticles as adsorbents for arsenic removal. J Hazard Mater 217–218:439–446. https://doi.org/10.1016/j.jhazmat.2012.03.073

Ge F, Li MM, Ye H, Zhao BX (2012) Effective removal of heavy metal ions Cd^{2+}, Zn^{2+}, Pb^{2+}, Cu^{2+} from aqueous solution by polymer-modified magnetic nanoparticles. J Hazard Mater 211–212:366–372. https://doi.org/10.1016/j.jhazmat.2011.12.013

Ghasemi E, Sillanpää AHM (2017) Superparamagnetic Fe_3O_4@EDTA nanoparticles as an efficient adsorbent for simultaneous removal of Ag(I), Hg(II), Mn(II), Zn(II), Pb(II) and Cd(II) from water and soil environmental samples. Microchem J 131:51–56. https://doi.org/10.1016/j.microc.2016.11.011

Gu FX, Karnik R, Wang AZ, Alexis F, Nissenbaum EL, Hong S, Langer RS, Farokhazad OC (2007) Targeted nanoparticles for cancer therapy. Nano Today 2:14–21. https://doi.org/10.1016/S1748-0132(07)70083-X

Guo L, Ye P, Wang J, Fu F, Wu Z (2015) Three-dimensional Fe_3O_4-graphene macroscopic composites for arsenic and arsenate removal. J Hazard Mater 298:28–35. https://doi.org/10.1016/j.jhazmat.2015.05.011

Gupta AK, Wells S (2004) Surface-modified superparamagnetic nanoparticles for drug delivery: preparation, characterization, and cytotoxicity studies. IEEE Trans NanoBiosci 3:66–73. https://doi.org/10.1109/TNB.2003.820277

Hergt R, Hiergeist R, Hilger I, Kaiser WA, Lapatnikov Y, Margel S, Richter U (2004) Maghemite nanoparticles with very high AC-losses for application in RF-magnetic hyperthermia. J Magn Magn Mater 270:345–357. https://doi.org/10.1016/j.jmmm.2003.09.001

Hong JY, Oh WK, Shin KY, Kwon OS, Son S, Jang J (2012) Spatially controlled carbon sponge for targeting internalized radioactive materials in human body. Biomaterials 33:5056–5066. https://doi.org/10.1016/j.biomaterials.2012.03.064

Hong HJ, Jeong HS, Kim BG, Hong J, Park IS, Ryu T, Chung KS, Kim H, Ryu J (2016) Highly stable and magnetically separable alginate/Fe_3O_4composite for the removal of strontium (Sr) from seawater. Chemosphere 165:231–238. https://doi.org/10.1016/j.chemosphere.2016.09.034

Hu H, Wang Z, Pan L (2010) Synthesis of monodisperse Fe_3O_4@silica core–shell microspheres and their application for removal of heavy metal ions from water. J Alloys Compd 492:656–661. https://doi.org/10.1016/j.jallcom.2009.11.204

Ishizaki M, Akiba S, Ohtani A, Hoshi Y, Ono K, Matsuba M, Togashi T, Kananizuka K, Sakamoto M, Kawamoto T, Tanaka H, Watanabe M, Arisaka M, Nankawa T, Kurihara M (2013) Proton-exchange mechanism of specific Cs+ adsorption via lattice defect sites of Prussian blue filled with coordination and crystallization water molecules. Dalton Trans 42:16049–16055. https://doi.org/10.1039/C3DT51637G

Jang J, Lee DS (2016) Magnetic Prussian blue nanocomposites for effective Cesium removal from aqueous solution. Ind Eng Chem Res 55:3852–3860. https://doi.org/10.1021/acs.iecr.6b00112

Laurent S, Forge D, Port M, Roch A, Robic C, Elst LV, Muller RN (2008) Magnetic iron oxide nanoparticles: synthesis, stabilization, vectorization, physicochemical characterizations, and biological applications. Chem Rev 108:2064–2110. https://doi.org/10.1021/cr068445e

Lawrence DT, Kirk MA (2007) Chemical terrorism attacks: update on antidotes. Emerg Med Clin North Am 25:567–595. https://doi.org/10.1016/j.emc.2007.02.002

Li G, Zhao Z, Liu J, Jiang G (2011) Effective heavy metal removal from aqueous systems by thiol functionalized magnetic mesoporous silica. J Hazard Mater 192:277–283. https://doi.org/10.1016/j.jhazmat.2011.05.015

Li L, Xu M, Chubik M, Chubik M, Gromov A, Wei G, Han W (2015) Entrapment of radioactive uranium from wastewater by using fungus- Fe_3O_4 bionanocomposites. RSC Adv 5:41611–41616. https://doi.org/10.1016/j.chemosphere.2016.09.034

Li Y, Zhang R, Tian X, Yang C, Zhou Z (2016) Facile synthesis of Fe_3O_4 nanoparticles decorated on 3D grapheneaerogels as broad-spectrum sorbents for water treatment. Appl Surf Sci 369:11–18. https://doi.org/10.1016/j.apsusc.2016.02.019

Li ZJ, Huang ZW, Guo WL, Wang L, Zheng LR, Chai ZF, Shi WQ (2017) Enhanced photocatalytic removal of uranium(VI) from aqueous solution by magnetic TiO_2/Fe_3O_4 and its Graphene composite. Environ Sci Technol 51:5666–5674. https://doi.org/10.1021/acs.est.6b05313

Lilga MA, Orth RJ, Sukamto JPH, Haight SM, Schwartz DT (1997) Metal ion separations using electrically switched ion exchange. Sep Purif Technol 11:147–158. https://doi.org/10.1016/S1383-5866(97)00017-8

Lilga MA, Orth RJ, Sukamto JPH, Rassat SD, Genders JD, Gopal R (2001) Cesium separation using electrically switched ion exchange. Sep Purif Technol 24:451–466. https://doi.org/10.1016/S1383-5866(01)00145-9

Lin Y, Fryxell GE, Wu H, Englhard M (2001) Selective sorption of cesium using self-assembled monolayers on mesoporous supports. Environ Sci Technol 35:3962–3966. https://doi.org/10.1021/es010710k

Liu JF, Shanzhao Z, Binjiang G (2008) Coating Fe_3O_4 magnetic nanoparticles with humic acid for high efficient removal of heavy metals in water. Environ Sci Technol 42:6949–6954. https://doi.org/10.1021/es800924c

Liu Y, Chen M, Hao Y (2013) Study on the adsorption of Cu(II) by EDTA functionalized Fe_3O_4 magnetic nano-particles, Yan Liu, Man Chen, Yongmei Hao. Chem Eng J 218:46–54. https://doi.org/10.1016/j.cej.2012.12.027

Liu Y, Fu R, Sun Y, Zhou X, Baig SA, Xi X (2016) Multifunctional nanocomposites Fe_3O_4@SiO_2-EDTA for Pb(II) andCu(II) removal from aqueous solutions. Appl Surf Sci 369:267–276. https://doi.org/10.1016/j.apsusc.2016.02.043

Lu AH, Salabas EL, Schth F (2007) Magnetic nanoparticles: synthesis, protection, functionalization, and application. Angew Chem Int Ed 46:1222–1244. https://doi.org/10.1002/anie.200602866

Lubbe AS, Bergemann C, Huhnt W, Fricke T, Riess H, Brock JW, Huhn D (1996) Preclinical experiences with magnetic drug targeting: tolerance and efficacy. Cancer Res 56:4694–4701

Luo X, Cheng C, Luo WS, Dong R, Tu X, Zeng G (2012) Adsorption of As (III) and As (V) from water using magnetite Fe_3O_4-reduced graphite oxide–MnO_2 nanocomposites. Chem Eng J 187:45–52. https://doi.org/10.1016/j.cej.2012.01.073

Ma D, Guan J, Normandin F, Denommee S, Enright G, Veres T, Simard B (2006) Multifunctional nano-architecture for biomedical applications. Chem Mater 18:1920–1927. https://doi.org/10.1021/cm052067x

Madhu Kumari, Pittman CU, Mohan D (2015) Heavy metals [chromium (VI) and lead (II)] removal from water using mesoporous magnetite (Fe_3O_4) nanospheres. J Colloid Interface Sci 442:120–132. https://doi.org/10.1016/j.jcis.2014.09.012

Mandal M, Kundu S, Ghosh SK, Panigrahi S, Sau TK, Yusuf SM, Pa T (2005) Magnetite nanoparticles with tunable gold or silver shell. J Colloid Interface Sci 286:187–194. https://doi.org/10.1016/j.jcis.2005.01.013

Mirzabe GH, Keshtkar AR (2015) Application of response surface methodology for thorium adsorption on PVA/Fe_3O_4/SiO_2/APTES nanohybrid adsorbent. J Ind Eng Chem 26:277–285. https://doi.org/10.1016/j.jiec.2014.11.040

Mohapatra A, McGraw G, Morshed B, Jennings J, Haggard W, Bumgardner J, Mishra S (2014) Electric stimulus response of chitosan microbeads embedded with magnetic nanoparticles for controlled drug delivery. In 36th IEEE EMBS Special Topic conference on Healthcare Innovation & Point-of-Care Technologies, Seattle, WA, USA

Mornet S, Vasseur S, Grasset F, Duguet E (2004) Magnetic nanoparticle design for medical diagnosis and therapy. J Mater Chem 14:2161–2175. https://doi.org/10.1039/B402025A

Mu W, Yu Q, Li X, Wei H, Jian Y (2017) Efficient removal of Cs^+ and Sr^{2+} from aqueous solution usinghierarchically structured hexagonal tungsten trioxide coated Fe_3O_4. Chem Eng J 319:170–178. https://doi.org/10.1016/j.cej.2017.02.153

Namiki Y, Namiki T, Ishii Y, Koido S, Nagase Y, Tsubota A, Tada N, Kitamoto Y (2012) Inorganic-organic magnetic nanocomposites for use in preventive medicine: a rapid and reliable elimination system for cesium. Pharm Res 29:1404–1418. https://doi.org/10.1007/s11095-011-0628-x

Naushad M, Ahamad T, Sharma G et al (2016) Synthesis and characterization of a new starch/SnO2 nanocomposite for efficient adsorption of toxic Hg2+ metal ion. Chem Eng J 300:306–316. https://doi.org/10.1016/j.cej.2016.04.084

Ozmen M, Can K, Arslan G, Tor A, Cengeloglu Y, Ersoz M (2010) Adsorption of Cu(II) from aqueous solution by using modified Fe_3O_4 magnetic nanoparticles. Desalination 254:162–169. https://doi.org/10.1016/j.desal.2009.11.043

Pankhurst QA, Connolly J, Jones SK, Dobson J (2003) Applications of magnetic nanoparticles in biomedicine. J Phys D Appl Phys 36:R167–R181. https://doi.org/10.1088/0022-3727/36/13/201

Parab H, Sudersanan M (2011) Engineering a lignocellulosic biosorbent – coir pith for removal of cesium from aqueous solutions: equilibrium and kinetic studies. Water Res 44:854–860. https://doi.org/10.1016/j.watres.2009.09.038

Peng GW, Ding DX, Xiao FZ, Wang XL, Hun N, Wang YD, Dai YM, Cao Z (2014) Adsorption of uranium ions from aqueous solution by amine group functionalized magnetic Fe_3O_4 nanoparticle. J Radioanal Nucl Chem 301:781–788. https://doi.org/10.1007/s10967-014-3278-8

Prout MS, Provan WM, Green T (1985) Species differences in response to trichloroethylene: I. Pharmacokinetics in rats and mice. Toxicol Appl Pharmacol 79:389–400. https://doi.org/10.1016/0041-008X(85)90137-1

Rassat SD, Sukamto JH, Orth RJ, Lilga MA, Hallen RT (1999) Development of an electrically switched ion exchange process for selective ion separations. Sep Purif Technol 15:207–222. https://doi.org/10.1016/S1383-5866(98)00102-6

Ren Y, Abbood HA, He F, Peng H, Huang K (2013) Magnetic EDTA-modified chitosan/SiO_2/Fe_3O_4 adsorbent: preparation, characterization, and application in heavy metal adsorption. Chem Eng J 226:300–311. https://doi.org/10.1016/j.cej.2013.04.059

Rengaraj A, Haldorai Y, Puthiaraj P, Hwang SK, Ryu T, Shin J, Han YK, Ahn WS, Huh YS (2017) Covalent Triazine polymer− Fe_3O_4 Nanocomposite for strontium ion removal from seawater. Ind Eng Chem Res 56:4984–4992. https://doi.org/10.1021/acs.iecr.7b00052

Sangvanich T, Sukwarotwat V, Wiacek RJ, Grudzien RM, Fryxell GE, Addleman RS, Timchalk C, Yantasee W (2010) Selective capture of cesium and thallium from natural waters and simulated wastes with copper ferrocyanide functionalized mesoporous silica. J Hazard Mater 182:225–231. https://doi.org/10.1016/j.jhazmat.2010.06.019

Shan GB, Xing JM, Luo MF, Liu HZ, Chen JY (2003) Immobilization of Pseudomonas delafieldii with magnetic polyvinyl alcohol beads and its application in biodesulfurization. Biotechnol Lett 25:1977–1981. https://doi.org/10.1023/B:BILE.0000004388.15751.8c

Shan C, Ma Z, Tong M (2014) Efficient removal of trace antimony(III) through adsorption by hematite modified magnetic nanoparticles. J Hazard Mater 268:229–236. https://doi.org/10.1016/j.jhazmat.2014.01.020

Shan C, Ma Z, Tong M (2015a) Efficient removal of free and nitrilotriacetic acid complexed Cd(II) from water by poly(1-vinylimidazole)-grafted Fe_3O_4@SiO_2magneticnanoparticles. J Hazard Mater 299:479–485. https://doi.org/10.1016/j.jhazmat.2015.07.024

Shan C, Ma Z, Tong M, Ni J (2015b) Removal of Hg(II) by poly(1-vinylimidazole)-grafted Fe_3O_4@SiO_2 magnetic nanoparticles. Water Res 69:252–260. https://doi.org/10.1016/j.watres.2014.11.030

Shena YF, Tanga J, Nie ZH, Wang YD, Renc Y, Zuo L (2009) Preparation and application of magnetic Fe_3O_4 nanoparticles for wastewater purification. Sep Purif Technol 68:312–319. https://doi.org/10.1016/j.seppur.2009.05.020

Simeonidisa K, Gkinis T, Tresintsi S, Martinez-Boubeta C, Vourlias G, Tsiaoussis I, Stavropoulos G, Mitrakas M, Angelakeris M (2011) Magnetic separation of hematite-coated Fe_3O_4 particles used as arsenic adsorbents. Chem Eng J 168:1008–1015. https://doi.org/10.1016/j.cej.2011.01.074

Skumryev V, Stoyanov S, Zhang Y, Hadjipanayis G, Givord D, Nogues J (2003) Beating the superparamagnetic limit with exchange bias. Nature 423:850–853. https://doi.org/10.1038/nature01687

Song W, Liu M, Hu R, Tan X, Li J (2014) Water-soluble polyacrylamide coated- Fe_3O_4 magnetic composites for high-efficient enrichment of U(VI) from radioactive wastewater. Chem Eng J 246:268–276. https://doi.org/10.1016/j.cej.2014.02.101

Sorensen CM (2001) In: Klabunde KJ (ed) Magnetism in nano scale materials in chemistry. Wiley-Interscience Publication, New York

Thompson DF, Church CO (2001) Prussian blue for treatment of radiocesium poisoning. Pharmacotherapy 21:1364–1367. https://doi.org/10.1592/phco.21.17.1364.34426

Torad NL, Hu M, Imura M, Naito M, Yamauchi Y (2012) Large Cs adsorption capability of nanostructured Prussian blue particles with high accessible surface areas. J Mater Chem 22:18261–18267. https://doi.org/10.1039/C2JM32805D

Wang J, Zheng S, Shao Y, Liu J, Xu Z, Zhu D (2010) Amino-functionalized Fe_3O_4@SiO_2 core–shell magnetic nanomaterial as a novel adsorbent for aqueous heavy metals removal. J Colloid Interface Sci 349:293–299. https://doi.org/10.1016/j.jcis.2010.05.010

Weller D, Moser A (1999) Thermal effect limits in ultrahigh-density magnetic recording. IEEE Trans Magn 35:4423–4439. https://doi.org/10.1109/20.809134

Wilson A, Mishra SR, Gupta R, Ghosh K (2012) Preparation and photocatalytic properties of hybride core-shell reusable CoFe2O4-ZnO nanospheres. J Magn Magn Mater 324:2597–2601. https://doi.org/10.1016/j.jmmm.2012.02.009

Wu W, He Q, Jiang C (2008) Magnetic iron oxide nanoparticles: synthesis and surface functionalization strategies. Nanoscale Res Lett 3:397–415. https://doi.org/10.1007/s11671-008-9174-9

Xiaodong Xin, Wei Q, Yang J, Yan L, Feng R, Chen G, Du B, Li H (2012) Highly efficient removal of heavy metal ions by amine-functionalized mesoporous Fe O nanoparticles. Chem. Eng. J. 184: 132–140 https://doi.org/10.1016/j.cej.2012.01.016

Xuan S, Jiang W, Gong X, Hu Y, Chen Z (2009) Magnetically separable Fe3O4/TiO2 hollow spheres: fabrication and photocatalytic activity. J Phys Chem C 113:553–558. https://doi.org/10.1021/jp8073859

Yang HM, Jang SC, Hong SM, Lee KW, Roh C, Huh YS, Seo BK (2016) Prussian blue-functionalized magnetic nanoclusters for the removal of radioactive cesium from water. J Alloys Compd 657:387–393. https://doi.org/10.1016/j.jallcom.2015.10.068

Yavuz CT, Mayo JT, Yu WW, Prakash A, Falkner JC, Yean S, Cong L, Shipley HJ, Kan A, Tomson M, Natelson D, Colvin VL (2006) Low-field magnetic separation of monodisperse Fe_3O_4 nanocrystals. Science 314:964–967. https://doi.org/10.1126/science.1131475

Yoon Y, Park WK, Hwang TM, Yoon DH, Yang WS, Kang JW (2016) Comparative evaluation of magnetite–graphene oxide and magnetite-reduced graphene oxide composite for As(III) and As (V) removal. J Hazard Mater 304:196–204. https://doi.org/10.1016/j.jhazmat.2015.10.053

Yuan D, Xiong X, Chen L, Lv Y, Wang Y, Yuan L, Liao S, Zhang Q (2016) Removal of uranium from aqueous solution by phosphate functionalized superparamagnetic polymer microspheres Fe_3O_4/P(GMA–AA–MMA). J Radioanal Nucl Chem 309:729–741. https://doi.org/10.1007/s10967-015-4682-4

Zeng H, Li J, Liu JP, Wang ZL, Sun S (2002) Exchange-coupled nanocomposite magnets by nanoparticle self-assembly. Nature 420:395–398. https://doi.org/10.1038/nature01208

Zhang S, Zhang Y, Liu J, Xu Q, Xiao H, Wang X, Xu H, Zhou J (2013) Thiol modified Fe_3O_4@SiO_2 as a robust, high effective, and recycling magnetic sorbent for mercury removal. Chem Eng J 226:30–38. https://doi.org/10.1016/j.cej.2013.04.060

Zhao X, Wang J, Wu F, Wang T, Cai Y, Shi Y, Jiang G (2010) Removal of fluoride from aqueous media by Fe_3O_4@$Al(OH)_3$ magnetic nanoparticles. J Hazard Mater 173:102–109. https://doi.org/10.1016/j.jhazmat.2009.08.054

Zhao Y, Li J, Zhao L, Zhang S, Huang Y, Wu X, Wang X (2014) Synthesis of amidoxime-functionalized Fe_3O_4@SiO_2 core–shell magnetic microspheres for highly efficient sorption of U (VI). Chem Eng J 235:275–283. https://doi.org/10.1016/j.cej.2013.09.034

Zhao D, Zhang Q, Xuan H, Chen Y, Zhang K, Feng S, Alsaedic A, Hayatcd T, Chen C (2017) EDTA functionalized Fe_3O_4 graphene oxide for efficient removal of U(VI)from aqueous solutions. J Colloid Interface Sci 506:300–307. https://doi.org/10.1016/j.jcis.2017.07.057

Zhao D, Zhu H, Wu C, Feng S, Alsaedi A, Hayat T, Chen C (2018) Facile synthesis of magnetic Fe_3O_4/graphene composites for enhanced U(VI) sorption. Appl Surf Sci 444(30):691–698. https://doi.org/10.1016/j.apsusc.2018.03.121

Zheng X, Dou J, Yuan J, Qin W, Hong X, Ding A (2017) Removal of Cs^+ from water and soil by ammonium-pillared montmorillonite Fe_3O_4 composite. J Environ Sci 56:12–24. https://doi.org/10.1016/j.jes.2016.08.019

Zong P, Wang S, Zhao Y, Wang H, Pana H, He C (2013) Synthesis and application of magnetic graphene/iron oxides composite for the removal of U(VI) from aqueous solutions. Chem Eng J 220:45–52. https://doi.org/10.1016/j.cej.2013.01.038

Chapter 3
FeS_2 Pyrite Nanostructures: An Efficient Performer in Photocatalysis

Gurpreet Kaur, Manjot Kaur, Anup Thakur, and Akshay Kumar

Contents

Abstract Water pollution is expanding at regular pace and the entire world is in grip of cancer-causing contaminants. Thus, there is urgent demand to develop an alternate technology for water treatment; herewith, photocatalysis has emerged as an efficient removal process. This chapter concentrates on the emerging area of utilization of pyrite nanostructures for photodegradation of wide variety of water pollutants and discusses the mechanism of photocatalysis process. This chapter can serve as a useful reference for those new to this field of research. The functionalization of FeS_2 material can be achieved with particular components such as catalytically active species, specific binding sites, or with supplementary functional groups. The insight of modification of pyrite to enhance the photocatalytic properties of pyrite is also elaborated in this chapter. Lastly, the chapter explains the photocatalytic activity in different reaction parameters and provides an overview of the environmental applications of pyrite nanostructures.

G. Kaur · M. Kaur · A. Kumar (✉)
Advanced Functional Materials Laboratory, Department of Nanotechnology, Sri Guru Granth Sahib World University, Fatehgarh Sahib, Punjab, India

A. Thakur
Department of Basic and Applied Sciences, Punjabi University, Patiala, Punjab, India

M. Naushad et al. (eds.), *Green Methods for Wastewater Treatment*, Environmental Chemistry for a Sustainable World 35, https://doi.org/10.1007/978-3-030-16427-0_3

Keywords Iron pyrite · FeS_2 · Nanostructures · Photocatalysis · Water treatment · Photocatalytic material

3.1 Background

Iron disulfide (FeS_2) has been developing as one of the most prospective semiconductors which has been used in various applications involving photocatalysis and photovoltaics (Talapin et al. 2010; Tian et al. 2015). Due to nontoxic nature, inexpensive FeS_2 has been progressively researched in the recent years. Metal sulfides (SnS_2, CdS, FeS_2) can absorb light in visible region which makes them a perfect candidate for visible light-driven photocatalysis. FeS_2 has been immensely studied among the transition metal sulfides due to its easy production and environment-friendly nature. FeS_2 exists in various polymorphs such as pyrite and marcasite. Pyrite (fool's gold) has cubic structure similar to sodium chloride structure with Fe^{2+} and S^{2-} ions in octahedral coordination. Pyrite FeS_2 is a semiconductor with direct bandgap of ~ 0.95 eV and high absorption coefficient of 6×10^{-5} cm^{-1} for energies greater than 1.1 eV which makes it mainly promising photocatalyst. The parameters needed to be addressed during synthesis are bandgap tuning, mobility of charge carriers, and band positions in order to improve photocatalytic activity.

FeS_2 nanostructures have been synthesized with number of different composition and phases. Most of the research has been focused onto the synthesis of these nanomaterials in the last decade. Several publications have described the efficient synthesis routes for controlling shape, size, morphology, as well as stability. Many prevalent methods including hydrothermal (Allen et al. 1912; Darr et al. 2017), hot injection (Guo et al. 2015), solvothermal (E'jazi and Aghaziarati 2012), and sulfidation (Shi et al. 2015) have been used for preparation of superior quality FeS_2 nanomaterial.

Organic contaminants, responsible for polluting aquatic environments, pose a serious threat to humanity and aquatic species (Gnanasekaran et al. 2018; Albadarin et al. 2017). Various removal techniques have been developed to manage the negative effects of these pollutants (Kumar et al. 2017). Pyrite has property of oxidizing easily and acidic conditions that are advantageous for removal of contaminants. The primary lacks in water treatment techniques are summed up as higher concentration of pollutants, lower degradation efficiency, and less recovery of photocatalyst from water that bring hurdles in progress of commercialization. Regardless of all the disadvantages, research and evolution are progressing rapidly. This chapter presents role of pyrite and its composites in the field of photocatalysis. The role of modification for enhancing the photocatalytic property is elucidated briefly in chapter.

3.2 Mechanism for Dye Degradation Followed by Pyrite

FeS_2 material can absorb visible light using mechanism described in Fig. 3.1. FeS_2 generate electron and hole pairs by absorbing visible light hν (Eq. 3.1). The production of $OH^{\cdot}$ radical was due to reaction of holes with the electron donor such as water (Eq. 3.2) (Khataee et al. 2016).

The thermodynamic stability of pyrite in aqueous environment was not good enough and leads to the oxidation of pyrite and generation of $OH^{\cdot}$ and H_2O_2 (Eqs. 3.3, 3.4, 3.5, 3.6, 3.7, 3.8, 3.9, 3.10, 3.11, 3.12, 3.13, 3.14, 3.15 and 3.16) (Choi et al. 2014a). Thus, the generated $OH^{\cdot}$ radicals result in the decomposition of organic pollutants and dyes. The $OH^{\cdot}$ radical acts as very powerful oxidizing agent and attacks the organic pollutants represented by the equations below.

$$FeS_2 + hv \rightarrow e^- + h^+ \tag{3.1}$$

$$h^+ + H_2O \rightarrow H^+ + OH^{\bullet} \tag{3.2}$$

$$O_2 + e^- \rightarrow O_2^{-\bullet} \tag{3.3}$$

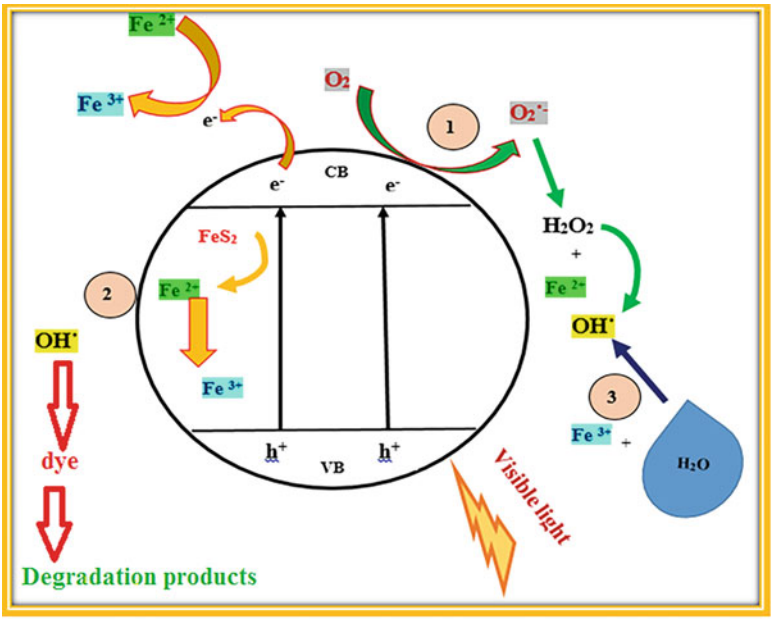

Fig. 3.1 Schematic representation of dye degradation mechanism of FeS_2 material. (Reprinted with permission from Ref. (Kaur et al. 2016). Copyright 2016 Royal Society of Chemistry)

$$2FeS_2 + 7O_2 + 2H_2O \rightarrow 2Fe^{2+} + 4SO_4^{2-} + 4H^+ \quad (3.4)$$

$$FeS_2 + 14Fe^{3+} + 8H_2O \rightarrow 15Fe^{2+} + SO_4^{2-} + 16H^+ \quad (3.5)$$

$$2Fe_{aq}^{2+} + \frac{1}{2}O_2 + 2H^+ \rightarrow 2Fe_{aq}^{3+} + 2SO_4^{2-} + H_2O \quad (3.6)$$

$$Fe^{3+} + e_{cb}^- \rightarrow Fe^{2+} \quad (3.7)$$

$$Fe_{aq}^{2+} + O_2 \rightarrow Fe_{aq}^{3+} + O_2^{-\bullet} \quad (3.8)$$

$$Fe_{aq}^{2+} + O_2 + 2H^+ \rightarrow Fe_{aq}^{3+} + H_2O_2 \quad (3.9)$$

$$Fe_{pyrite}^{2+} + H_2O_2 \rightarrow Fe_{pyrite}^{3+} + OH^- + OH^{\bullet} \quad (3.10)$$

$$Fe_{pyrite}^{2+} + O_2 \rightarrow Fe_{pyrite}^{3+} + O_2^{-\bullet} \quad (3.11)$$

$$Fe_{pyrite}^{2+} + O_2^{-\bullet} \rightarrow Fe_{pyrite}^{3+} + H_2O_2 \quad (3.12)$$

$$Fe_{pyrite}^{3+} + H_2O \rightarrow Fe_{pyrite}^{2+} + OH^{\bullet} + 2H^+ \quad (3.13)$$

$$2O_2^{-\bullet} + 2H^+ \rightarrow O_2 + H_2O_2 \quad (3.14)$$

$$H_2O_2 + e_{cb}^- \rightarrow OH^{\bullet +} + OH^- \quad (3.15)$$

$$H_2O_2 + h\nu \rightarrow 2OH^{\bullet} \quad (3.16)$$

The release of iron species such as Fe^{2+} and Fe^{3+} can be occurred due to readily oxidation of FeS_2 (pyrite) under ambient air conditions (Diao et al. 2015). Oxygen help in generation of reactive oxygen species such as superoxide radicals, hydrogen peroxide, and hydroxyl radicals via accepting an electron from ferrous ions (Zhang et al. 2015). The more reactive oxygen species can be produced by inducing the FeS_2 pyrite catalyst using the visible light irradiation. The hydroxyl radicals result from the transformation of products, i.e., hydrogen peroxide (H_2O_2) and superoxide radical. The reactive oxygen species $OH^{\cdot}$ induced the attack on dye molecule (Diao et al. 2013, 2015). Consequently, decomposition of dye molecules results in a series of intermediates with smaller molecular sizes. Lastly, the mineralization of these intermediates results in formation of carbon dioxide (CO_2) and water (H_2O). Thus, degradation of dye was achieved via Fenton-like process, and sequences of degradation procedure can be described in the above reactions (Eqs. 3.1, 3.2, 3.3, 3.4, 3.5, 3.6, 3.7, 3.8, 3.9, 3.10, 3.11, 3.12, 3.13, 3.14, 3.15 and 3.16).

Fe^{2+} ions were formed by inducing FeS_2 pyrite with help of water (H_2O) and H^+ (Tian et al. 2015). Further, Fe^{2+} species transformed into Fe^{3+} ions on the surface of pyrite. Concludingly, the as-formed Fe^{3+} species could react with water H_2O to form $OH^{\cdot}$ (Eq. 3.13). Thus, dye was degraded by forming $OH^{\cdot}$ radical (Eq. 3.17).

$$\text{Dye} + \text{OH}^{\bullet} \rightarrow \text{degradation} \tag{3.17}$$

Fenton process is an advanced oxidation process which utilizes ferrous ions and hydrogen peroxide to produce the second most powerful oxidant, i.e., hydroxyl radical ($OH^{\cdot}$) in aqueous solution (Balcioglu et al. 2001; Sharma et al. 2017).

3.3 Photodegradation of Contaminants

Water contamination is noteworthy issue in worldwide context. It has been recommended that it is the main reason for end of lives and diseases and that it represents the deaths of more than 14,000 persons every day. Contaminants may involve organic and inorganic wastes. Some of the hazardous water pollutants are herbicides or pesticides that involve various organohalide compounds, textile industry waste water, polyaromatic hydrocarbons, heavy metals, medical wastes, etc. (Fig. 3.2). These pollutants are noxious to aquatic life or environment by affecting the life span of environment-friendly microorganisms. In perspective of the previously mentioned issues, consideration has been focused around the improvement of more efficient, inexpensive, strong techniques for wastewater treatment.

3.3.1 Organohalide Compounds

Organohalide compounds, one of the most common pollutants, are used in industries as solvents and refrigerant precursors (Jiao et al. 2009), (Choi and Lee 2009). These contaminants polluted water streams, posing a serious danger to environment due to their carcinogenic and stable nature. Tetrachloroethylene, trichloroethylene, dichloroethane, and carbon tetrachloride are well-known pollutants of organochlorine

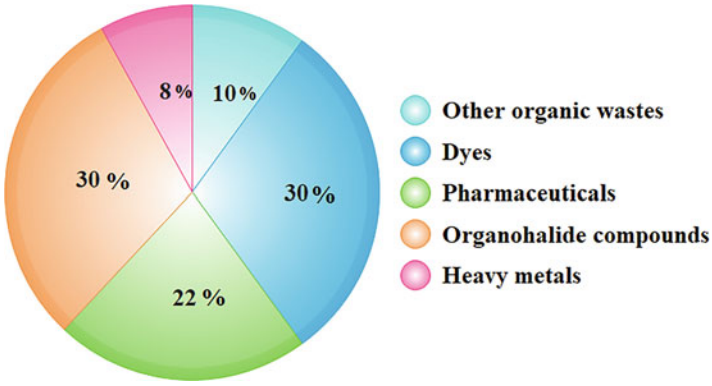

Fig. 3.2 Pie chart shows the release of various contaminants in water globally every year

solvents. The degradation of organochlorine compounds has been achieved using Fenton process as it involves the prevailing oxidizing ability and environment-friendly reagents (Duesterberg and Waite 2006; Li et al. 2005).

The premature end of degradation reaction, due to quick precipitation of iron hydroxide at neutral pH, is limitation of Fenton process (Pignatello et al. 2006). This limitation can be overcome by modifying the classical Fenton system with use of chelating ligands such as chitosan with glutaraldehyde and ethylenediaminetetraacetic acid to form stable complexes (Kang and Hua 2005), (Lipczynska-Kochany and Kochany 2008), (Furman et al. 2009). Che et al. (Che and Lee 2011) investigated that pyrite can particularly degrade organochlorine compounds through oxidative and reductive degradation mechanisms. With contrast to Fe (III), Fe (II) source played a significant role in removal of carbon tetrachloride. The high pH was proved to be more competent in reductive degradation, while acidic pH was required in case of oxidative degradation of organochlorine compounds. Alachlor (2-chloro-2′, 6′-diethyl-N-(methoxymethyl) acetanilide), generally used chloroacetanilide herbicide, was successfully degraded by pyrite/H_2O_2 system. The activation of molecular oxygen was brought by ferrous ions present on surface that enabled enhanced oxidation of alachlor. Therefore, the generation of superoxide radical was favored in order to quicken the Fe^{2+}/Fe^{3+} cycle on its surface for alachlor removal (Liu et al. 2015a).

3.3.2 Pharmaceuticals

Due to noteworthy upsurge in use of pharmaceuticals (ibuprofen, diclofenac, acetylsalicylic acid, and naproxen), traces are present in environment and waste water (Ternes 1998; Buser et al. 1999; Heberer 2002). Diclofenac (2-[2,6-dicholrophenyl) amino]phenylacetic acid) is one of the most common used pharmaceuticals (Buser et al. 1999). Only a very less amount of pharmaceutical are removed and hence polluted the groundwater through sewage treatment plants (Suarez et al. 2008). Bae and Kim (2013) demonstrated the complete removal of diclofenac with pyrite catalyzed Fenton reaction in just 120 s without further generation of toxic secondary products. The appropriate pH conditions as well as aqueous Fe (II) were responsible for 100% removal of diclofenac. The $HO^{\bullet}$ radical helps to degrade the aromatic intermediates such as 2-chloroaniline, 2-chlorophenol, and 2,6-dichlorophenol and finally mineralized to HCl and CO_2.

Ciprofloxacin (CIP), an antibiotic drug, was degraded up to 100% using 1.25 g/L FeS_2/SiO_2 catalyst loading in 60-min irradiation under UV light at 3-pH value and 0.10 mM ciprofloxacin concentration (Fig. 3.3). As the H_2O_2 concentration was increased from 3 mM to 60 mM, 100% of ciprofloxacin (0.15 mM) was removed in just 30 min with a less amount of catalyst loading (1.0 g/L). FeS_2/SiO_2 microspheres could facilitate the persistent release of ferrous ion, resulting in the reaction of ferrous ion and H_2O_2 (Diao et al. 2017).

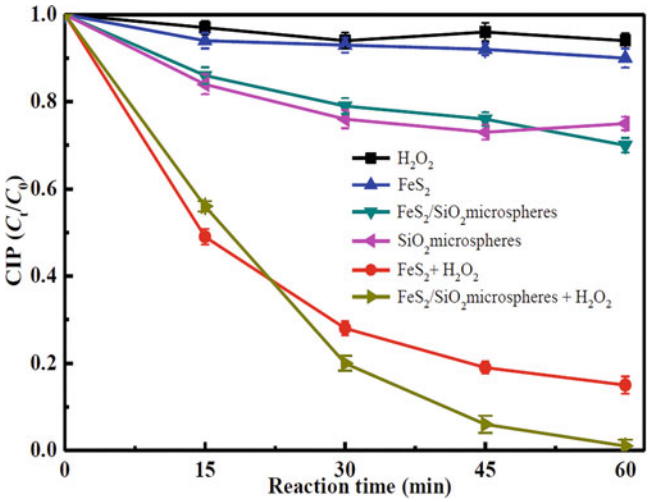

Fig. 3.3 Degradation of CIP by various systems. Reaction conditions: $[CIP]_0 = 0.10$ mM, $[H_2O_2]_0 = 3$ mM, $[catalyst]_0 = 1.25$ g/L, pH = 3.0. (Reprinted with permission from Ref.(Diao et al. 2017). Copyright 2017 Elsevier)

3.3.3 Dyes

Dyes are major pollutant from industries such as textile, leather, etc. AHPS (4-Amino-3-hydroxy-2-p-tolylazo-naphthalene-1-sulfonic acid; $C_{17}H_{15}O_4N_3S$) azo dye was removed up to 90% using electro-pyrite Fenton system. The rapid regeneration of ferrous ion facilitated the fast removal of AHPS synthetic dye (Labiadh et al. 2015). Anthraquinone dye reactive blue 69 (RB69) was degraded with heterogeneous sono-Fenton method using pyrite nanorods. The appropriate conditions for removal of RB69 were found to be ~ 5 pH, H_2O_2 concentration (1 mM), plasma-modified pyrite concentration (0.6 g/L), dye concentration (20 mg/L), and ultrasonic power (300 W) in 40 min (Khataee et al. 2016).

Liu et al. investigated photocatalytic activity of FeS_2 on some organic dyes such as methylene blue (MB), safranine T, methyl orange (MO), rhodamine B (Rh B), and pyronine B. The adsorption ability had resulted in provoking as well as hindering effects on photocatalytic degradation efficiency. The energy band of semiconductor and oxidation reduction potential of adsorbate also could affect the photocatalytic degradation rate of catalyst. This would be reason behind the lower degradation rates of different dyes (methyl orange, rhodamine B, and pyronine B), while their adsorption rates were better for photocatalysis. 1 g/L FeS_2 catalyst was dispersed in different dye solutions (each dye having same concentration of 1×10^{-5} mol/L) and irradiated under 40 W UV light for given time duration (Liu et al. 2013). A noticeable photocatalytic activity on decomposition of Rose Bengal dye under 100 W tungsten lamp was demonstrated for FeS_2 film. FeS_2 film deposited using single source precursor displayed high degradation rate (84%) in 300 min exposure

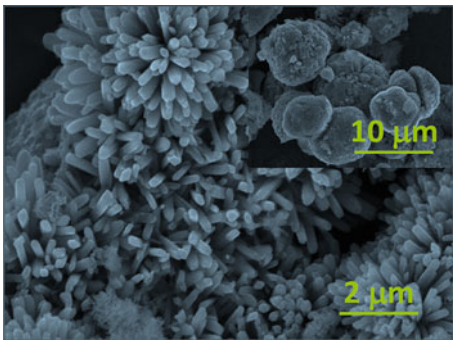

Fig. 3.4 SEM images of FeS_2 nanoparticles. (Reprinted with permission from Ref. (Morales-Gallardo et al. 2016). Copyright 2016 Elsevier)

of light (Bhar et al. 2013). Kirkeminde et al. prepared pyrite nanocrystals to control shape and morphology through thermodynamic parameters such as reaction temperature and chemical precursors. The metal-terminated facet (100) is less sensitive to photodegradation and photooxidation in water than (111) plane. As the pyrite plates did not show any oxidation process and their reactive nature which favored its use in photocatalytic cells while (111) nanospheres and even the (100) cubes proved to be beneficial for photovoltaics because of sulfur defects (Kirkeminde and Ren 2013).

Starch/AlOOH/FeS_2 mesoporous nanocomposite has been considered as prospective adsorbent for efficient removal of Congo red dye. The adsorption data was fitted well to pseudo first-order reaction. The solution pH, contact time, concentration, and temperature affected the adsorption process, i.e., spontaneous and endothermic in nature (Kumar et al. 2014). Cobalt-doped FeS_2 could degrade methylene blue as cobalt doping affected the lattice constants and might result in defects in FeS_2. The particle size decreased, and surface area increased when FeS_2 doped with cobalt, therefore leading to enhance the photocatalytic activity (Long et al. 2015).

The nanorod arrays (Fig. 3.4) showed enhanced photocatalytic activity, and almost 95% of methylene blue was degraded within 60-min illumination under UV light source 10 W LED lamp. The degradation reaction followed pseudo first-order kinetic with high correlation coefficient ($R^2 > 0.99$). The photogenerated electrons and holes contributed in oxidation–reduction reactions, which result in reactive hydroxyl radical ($OH^{\bullet}$), could efficiently decompose all organic dyes into simple products (Morales-Gallardo et al. 2016). Preferentially grown iron pyrite (111) with different catalyst dose showed high photocatalytic activity toward methylene blue and a textile dye Synazol yellow K-HL. The degradation mechanism was based on Fenton-like process to generate reactive oxygen species. FeS_2 catalyst ($1gL^{-1}$) degraded the methylene blue dye with efficacy of 95.90% (Fig. 3.5) and synazol yellow with efficacy of 99.29% in just 120 min under visible light irradiation (Kaur et al. 2016). FeS_2 is found to be preferential grown along (111) plane with least packing density and present more active sites in comparison to other planes. As the number of grains of preferred orientations in a specific plane is more as compared to other planes, it leads to high surface area of FeS_2 with large number of active sites, resulting in increased production of $OH^{\cdot}$ radicals and therefore increased

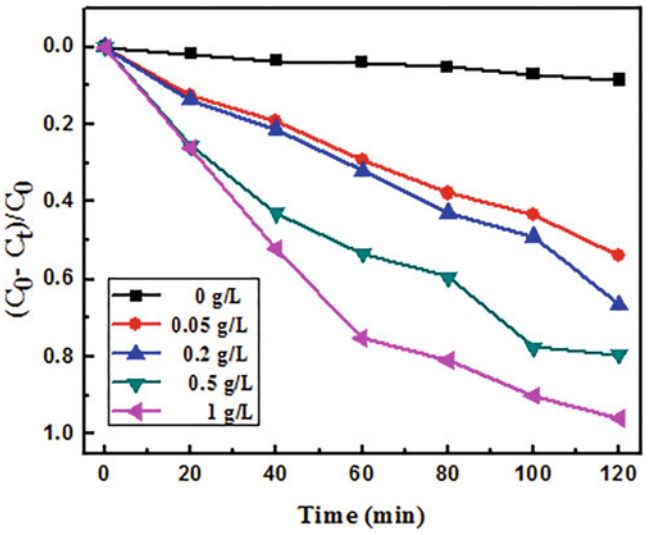

Fig. 3.5 Photocatalytic degradation efficiency of different concentrations of FeS_2 catalyst loading to methylene blue (1 mg/L) dye solution. (Reprinted with permission from Ref. (Kaur et al. 2016). Copyright 2016 Royal Society of Chemistry)

degradation of dyes during photo catalysis (Kaur et al. 2016). Thus, preferential growth plays a significant contribution toward the enhanced photocatalytic behavior.

Iron disulfide nanostructures successfully degraded methyl orange (93.09% in 120 min) as well as textile industry used dye Novacron yellow (98.15% in 80 min) in very less period of time (Kaur et al. 2017b). The degradation of very fast color textile NRH dye (1 mg/L) with Au@FeS_2 (1 g/L) loading catalyst was observed to be approximately 96.02% under visible light irradiation in just 60 min as compared to pure FeS_2 (95.63% in 120 min). Au@FeS_2 (1.00 g/L) was found to remove NRH dye (1 mg/L) in very less period of time as compared to FeS_2. The dye degradation process followed first-order kinetics. It was indicated from recyclability experiment Au@FeS_2 was found to be extremely active and suitable recyclable photocatalyst.

The functionalization of iron pyrite with gold showed excellent photocatalyst for degradation of a fast color textile dye Novacron red due to its synergistic effect. As due to large surface area and surface plasmon resonance, gold could act as receptor of electrons. The modification of FeS_2 with gold helps to create separation centers for electron/hole pairs as well as active sites (Fig. 3.6). The electrochemical performance also sustained the boosted photocatalytic activity (Fig. 3.7) (Kaur et al. 2017a). Au helps to trap electrons which leads to prevention of electrons and holes recombination. Along with Au, concentrated iron species scavenge the reactive oxygen species which lead to reduction in amount of hydroxyl radical and cause the degradation efficiency to decrease. It also suggests that Au can enhance the photocatalytic activity of FeS_2. Fusion of Au into a photocatalyst conveys extreme boost in photocatalytic activity due to its

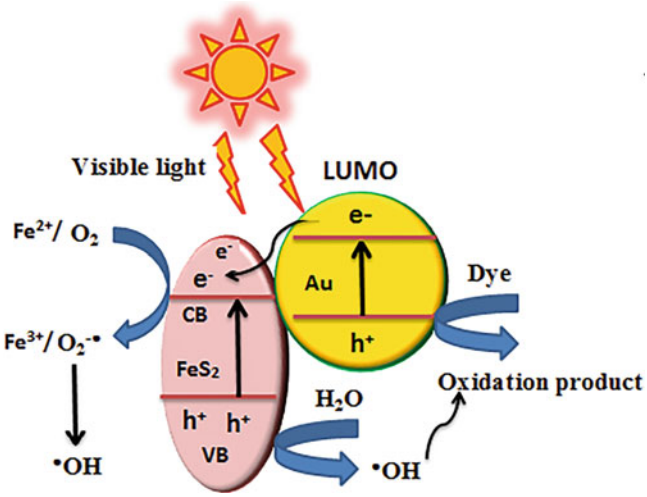

Fig. 3.6 Schematic representation of proposed mechanism of Au@FeS_2. (Reprinted with permission from Ref. (Kaur et al. 2017a). Copyright 2017 Royal Society of Chemistry)

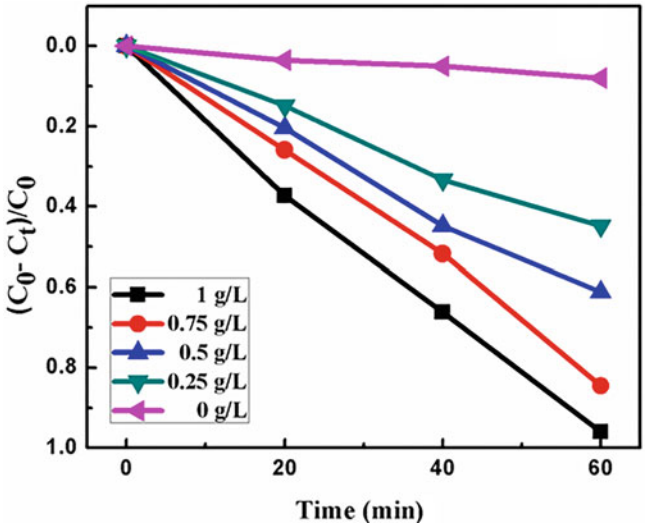

Fig. 3.7 Degradation efficiency comparison of different concentrations of Au@FeS_2 catalyst for Novacron red huntsman dye (1 mg/L). (Reprinted with permission from Ref. (Kaur et al. 2017a). Copyright 2017 Royal Society of Chemistry)

localized SPR effect, proficient photogenerated charge separation, and reduced electron–hole pair diffusion length (Kaur et al. 2017a).

Fan et al. (2017) degraded organic dyes MB, MO, and Rh B and factory waste water through direct electrolysis on anode using graphene supported $Fe_{1-x}Co_xS_2$

Table 3.1 FeS_2 nanostructures for removal of dye pollutants by photocatalysis method

Pollutant	Material used	Removal efficiency (%)	References
Rose Bengal dye	FeS_2 average pore diameter 40.33 Å and fairly high surface area of 49.53 m^2/g	80% degradation achieved in 300 min under 100 W clear glass tungsten lamp	Bhar et al. (2013)
Methyl orange dye	FeS_2 with (100) plane	50% in 80 min under Xenon light source	Kirkeminde and Ren (2013)
Methylene blue, safranine T, methyl orange, rhodamine B, and pyronine B	FeS_2	99.2% of MB degraded in 24 h irradiated under 40 W UV light	Liu et al. (2013)
Malachite green (MG), Cr(VI)	FeS_2	75% MG at low pH values (acidic conditions) in 120 min under UV light irradiation, 96.7% MG degraded in the presence of 10 mg/L of Cr(VI).	Sun and Cheng (2015)
Methylene blue	Cobalt-doped FeS_2 ($Co_{0.333}Fe_{0.666}S_2$)	48.9% in 210 min	Long et al. (2015)
Methylene blue, Synazol Yellow	FeS_2 of different catalyst dose	95.90%, 99.29%, respectively, in 120 min under visible light	Kaur et al. (2016)
Methylene blue	FeS_2 with nanorods morphology	95% in 60 min irradiation in 10 W LED lamp	Morales-Gallardo et al. (2016)
Methyl orange, Novacron yellow	FeS_2 of different catalyst dose	methyl orange (93.09% in 120 min), Novacron yellow (98.15% in 80 min) under visible light	Kaur et al. (2017b)
Novacron red	Au@FeS_2	96.02% in just 60 min under visible light	Kaur et al. (2017a)
Methylene blue	FeS_2/TiO_2	100% degradation in 150 min under sunlight	Rashid et al. (2018)
Methylene blue, methyl orange, and rhodamine B	Fe_2GeS_4	99.4% MB in 10 min (0.3 g/L Fe_2GeS_4, H_2O_2 of 50 mmol/L and pH of 7)	Shi et al. (2018)

system. The acidic ions could act as cathodic resource to produce H_2, while organic dyes act as anodic loss to balance the reaction that provide a dual benefit to energy and environment demand. The incorporation of reduced graphene oxide as the promoter of electron transfer was done in order to enhance the conductivity of cobalt-doped FeS_2. A number of reports about the use of iron disulfide pyrite in photocatalysis are summarized in Table 3.1. FeS_2/TiO_2 nanocomposite was proved as efficient photocatalyst, as it makes available effective separation of electron and holes to prevent recombination of charge carriers (Rashid et al. 2018). FeS_2 possessed the highest catalytic activity for indigo carmine dye degradation (88%)

among CuS and NiS_2 (Huerta-Flores et al. 2018). Ternary sulfur iron compound such as Fe_2GeS_4 nanoparticles could excellently degrade different organic dyes such as MB, MO, and Rh B on the basis of heterogeneous Fenton system (Shi et al. 2018).

These reported works undoubtedly reveal that pyrite has a potential application in remediation of environment polluted by organic and industrial dyes.

3.3.4 Heavy Metals

Heavy metals are well-known pollutants with high toxicity. Diao et al. (2013) demonstrated the simultaneous removal of malachite green (MG) dye as well as heavy metal Cr (VI) under UV light irradiation. While studying the role of dissolved oxygen supply in photocatalytic system, it was observed that presence of dissolved oxygen could increase the degradation ratio from 29.5% to 96.2%. The presence of oxygen proved as a favorable condition for generation of reactive species results in improved degradation rate. The photo Fenton-like process results in generation of reactive oxygen species, which helps in simultaneous degradation of MG and conversion of Cr (VI) to Cr (III). The reaction pathway followed by pyrite for degradation of heavy metal as well as dye is shown in Fig. 3.8.

The arsenic (arsenite As (III) and arsenate As (V)) from water was removed successfully using pyrite. The As (V) was more rapidly removed as compared to As (III) and explained on basis of Langmuir adsorption model. As pH increased in the range 7–10, arsenite removal process was found to be also increased. The effect of contact time and pH value on sorption and desorption of arsenic were studied in detailed manner in an anaerobic chamber ($95\%N_2/5\%H_2$) for removal of As (V) and

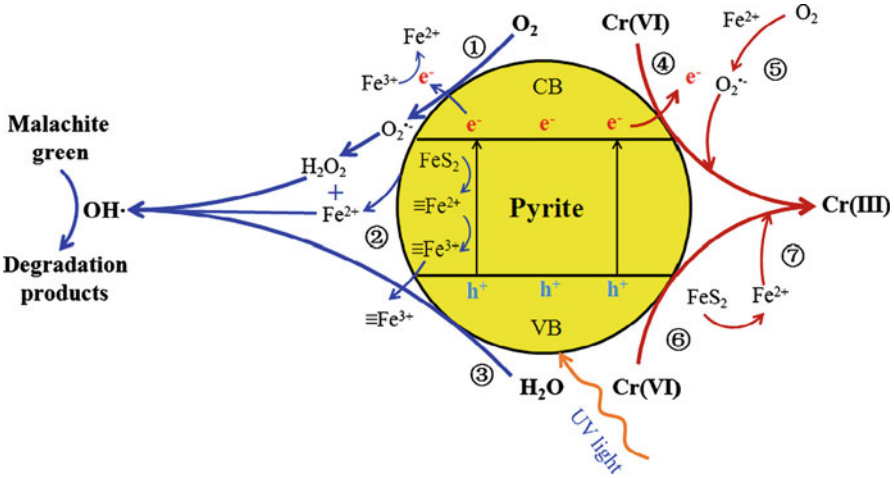

Fig. 3.8 Reaction pathway of MG degradation and Cr(VI) reduction in pyrite-based photocatalytic systems. (Reprinted with permission from Ref (Diao et al. 2015). Copyright 2015 Elsevier)

As (III) at specified time intervals. Sorption experiment for As (III) reveals that removal was increased with pH and exhibited moderate irreversibility as pH was titrated backward. For As (V) removal, removals increased as pH decreases, and moderate to high levels of irreversibility were found as pH elevated to its initial values. The arsenic could easily be removed from water with pyrite as arsenic was found to be strongly bonded with pyrite that led to formation of strong inner-sphere complexes (Dong Suk Han et al. 2013).

3.3.5 Other Organic Compounds

Phenolic compounds are major outcome of olive oil mills and consume dissolved oxygen level in aquatic bodies. Other organic compounds such as pectins, polyphenols, and polyalcohols also pollute the environment due to their organic nature as well as toxicity (Justino et al. 2012). Polycyclic aromatic hydrocarbons and aromatic contaminants are mutagenic and persistent nature. Pyrene and cetylpyridinium chloride (CPC) were removed effectively using pyrite Fenton system (Choi et al. 2014b). Pyrite could degrade 80% of nitrobenzene in 5 h on the basis of Fenton system. The continued formation of $^{\bullet}OH$ creates hindrance for quenching reaction in pyrite system. The acidic pH environment was a suitable condition for pyrite Fenton system (Zhang et al. 2014). Tyrosol (4-hydroxyphenylethanol) is one of these phenolic compounds released from olive oil mills waste water. Its toxic nature toward aquatic life poses a danger to the environment. Ammara et al. (2015) reported the effective degradation of tyrosol using pyrite Fenton catalyst due to self-management of iron concentration. There is no requirement of acidic conditions in this system relative to classic Fenton system and therefore proved to be a cleaner method. The effect of current on mineralization was also investigated as the upsurge in current led to rapid decline in mineralization current efficiency. Tyrosol of 0.30 mM was mineralized up to 76% in 6 h at 50 mA. The degradation kinetics for removal of tyrosol followed first-order reaction with rate constant value $3.57 \times 10^9\ M^{-1}\ s^{-1}$. The aromatic products as well as carboxylic acids (generated while oxidation of tyrosol) were removed completely. The photodegradation of terephthalic acid using electrochemically prepared FeS_2 films was accomplished up to 95% removal in 170 min (Jana et al. 2015). 4-chlorophenol was effectively degraded using FeS_2@GO. One hundred percent of 4-clorophenol was degraded in 60 min with 0.8 g/L FeS_2@GO in acidic to alkaline conditions (pH ~ 7.0) (Liu et al. 2015b). Bisphenol-A could be degraded efficiently using FeS_2@SiO_2 under UV radiation with persulfate system. $SO_4^{-\bullet}$, a predominant reactive oxygen species, played a significant role in degradation of bisphenol-A (Diao et al. 2018).

3.4 Conclusion and Outlook

Thorough and considerable studies on pyrite in photocatalysis in recent years have shown their significance to water treatment methods and their limitations. The literature survey shows that the higher recombination rate between photogenerated holes and electrons is the major limitation for photocatalytic efficiency. The enhancement in photocatalytic activity of FeS_2 is significant subject of interest in the field of photocatalysis. Modification with photocatalytic active material is driven its endeavor or effort to achieve the increase in photocatalytic efficiency due to its synergistic effect. Besides, pyrite displayed a high capacity of photocatalytic oxidation and reduction due to great synergistic impact of simultaneous degradation of organic contaminants. These findings revealed that pyrite has a potential application in environmental remediation which could lead to new way for developing an efficient photocatalytic material.

References

Albadarin AB, Charara M, Abu Tarboush BJ et al (2017) Mechanism analysis of tartrazine biosorption onto masau stones; a low cost by-product from semi-arid regions. J Mol Liq 242:478–483. https://doi.org/10.1016/j.molliq.2017.07.045

Allen ET, Crenshaw JL, Johnston J, Larsen ES (1912) The mineral sulphides of iron; with crystallographic study by E. S. Larsen. Am J Sci Ser 4 V:169–236. https://doi.org/10.2475/ajs.s4-33.195.169

Ammara S, Oturan A, Labiadhd ML et al (2015) Degradation of tyrosol by a novel electro-Fenton process using pyrite as heterogeneous source of iron catalyst. Water Res 74:77–87. https://doi.org/10.1016/j.watres.2015.02.006

Bae S, Kim D (2013) Degradation of diclofenac by pyrite catalyzed Fenton oxidation. Appl Catal B Environ 134–135:93–102. https://doi.org/10.1016/j.apcatb.2012.12.031

Balcioglu IA, Arslan I, Sacan MT (2001) Homogenous and heterogenous advanced oxidation of two commercial reactive dyes. Environ Technol 22:813–822. https://doi.org/10.1080/095933322086180323

Bhar SK, Jana S, Mondal A, Mukherjee N (2013) Photocatalytic degradation of organic dye on porous iron sulfide film surface. J Colloid Interface Sci 393:286–290. https://doi.org/10.1016/j.jcis.2012.10.049

Buser H-R, Poiger T, Müller MD (1999) Occurrence and environmental behavior of the chiral pharmaceutical drug ibuprofen in surface waters and in wastewater. Environ Sci Technol 33:2529–2535. https://doi.org/10.1021/es981014w

Che H, Lee W (2011) Selective redox degradation of chlorinated aliphatic compounds by Fenton reaction in pyrite suspension. Chemosphere 82:1103–1108. https://doi.org/10.1016/j.chemosphere.2010.12.002

Choi K, Lee W (2009) Reductive dechlorination of carbon tetrachloride in acidic soil manipulated with iron(II) and bisulfide ion. J Hazard Mater 172:623–630. https://doi.org/10.1016/j.jhazmat.2009.07.041

Choi K, Bae S, Lee W (2014a) Degradation of off-gas toluene in continuous pyrite Fenton system. J Hazard Mater 280:31–37. https://doi.org/10.1016/j.jhazmat.2014.07.054

Choi K, Bae S, Lee W (2014b) Degradation of pyrene in cetylpyridinium chloride-aided soil washing wastewater by pyrite Fenton reaction. Chem Eng J 249:34–41. https://doi.org/10.1016/j.cej.2014.03.090

Darr JA, Zhang J, Makwana NM, Weng X (2017) Continuous hydrothermal synthesis of inorganic nanoparticles: applications and future directions. Chem Rev 117:11125–11238. https://doi.org/10.1021/acs.chemrev.6b00417

Diao Z, Li M, Zeng F et al (2013) Degradation pathway of malachite green in a novel dual-tank photoelectrochemical catalytic reactor. J Hazard Mater 260:585–592. https://doi.org/10.1016/j.jhazmat.2013.05.037

Diao Z-H, Xu X-R, Liu F-M et al (2015) Photocatalytic degradation of malachite green by pyrite and its synergism with Cr(VI) reduction: performance and reaction mechanism. Sep Purif Technol 154:168–175. https://doi.org/10.1016/j.seppur.2015.09.027

Diao Z-H, Xu X-R, Jiang D et al (2017) Enhanced catalytic degradation of ciprofloxacin with FeS_2/SiO_2 microspheres as heterogeneous Fenton catalyst: kinetics, reaction pathways and mechanism. J Hazard Mater 327:108–115. https://doi.org/10.1016/j.jhazmat.2016.12.045

Diao Z-H, Wei-Qian Zeng-Hui D, Guo P-R et al (2018) Photo-assisted degradation of bisphenol A by a novel FeS_2@SiO_2 microspheres activated persulphate process: synergistic effect, pathway and mechanism. Chem Eng J 349:683–693. https://doi.org/10.1016/j.cej.2018.05.132

Duesterberg CK, Waite TD (2006) Process optimization of Fenton oxidation using kinetic modeling. Environ Sci Technol 40:4189–4195. https://doi.org/10.1021/es060311v

E'jazi N, Aghaziarati M (2012) Determination of optimum condition to produce nanocrystalline pyrite by solvothermal synthesis method. Adv Powder Technol 23:352–357. https://doi.org/10.1016/j.apt.2011.04.010

Fan Y, Wang D, Han D et al (2017) Integrated hydrogen evolution and water-cleaning via a robust graphene supported noble-metal-free $Fe_{1-x}Co_xS_2$ system. Nanoscale 9:5887–5895. https://doi.org/10.1039/C7NR00665A

Furman O, Laine DF, Blumenfeld A et al (2009) Enhanced reactivity of superoxide in water−solid matrices. Environ Sci Technol 43:1528–1533. https://doi.org/10.1021/es802505s

Gnanasekaran L, Hemamalini R, Naushad M (2018) Efficient photocatalytic degradation of toxic dyes using nanostructured TiO_2/polyaniline nanocomposite. Desalin Water Treat 108:322–328. https://doi.org/10.5004/dwt.2018.21967

Guo J, Liang S, Shi Y et al (2015) Electrocatalytic properties of iron chalcogenides as low-cost counter electrode materials for dye-sensitized solar cells. RSC Adv 5:72553–72561. https://doi.org/10.1039/C5RA13147B

Han DS, Song JK, Batchelor B, Abdel-Wahab A (2013) Removal of arsenite(As(III)) and arsenate (As(V)) by synthetic pyrite (FeS_2): Synthesis, effect of contact time, and sorption/desorption envelopes. J Colloid Interface Sci 392:311–318. https://doi.org/10.1016/j.jcis.2012.09.084

Heberer T (2002) Occurrence, fate, and removal of pharmaceutical residues in the aquatic environment: a review of recent research data. Toxicol Lett 131:5–17. https://doi.org/10.1016/S0378-4274(02)00041-3

Huerta-Flores AM, Torres-Martínez LM, Moctezuma E, Singh AP et al (2018) Green synthesis of earth-abundant metal sulfides (FeS_2, CuS, and NiS_2) and their use as visible-light active photocatalysts for H_2 generation and dye removal. J Mater Sci Mater Electron 29:11613–11626. https://doi.org/10.1007/s10854-018-9259-x

Jana S, Mondal P, Tripathi S et al (2015) Electrochemical synthesis of FeS_2 thin film: an effective material for peroxide sensing and terephthalic acid degradation. J Alloys Compd 646:893–899. https://doi.org/10.1016/j.jallcom.2015.06.168

Jiao Y, Qiu C, Huang L et al (2009) Reductive dechlorination of carbon tetrachloride by zero-valent iron and related iron corrosion. Appl Catal B Environ 91:434–440. https://doi.org/10.1016/j.apcatb.2009.06.012

Justino CIL, Freitas AC, Freitas AC et al (2012) Olive oil mill wastewaters before and after treatment: a critical review from the ecotoxicological point of view. Ecotoxicology 21:615–629. https://doi.org/10.1007/s10646-011-0806-y

Kang N, Hua I (2005) Enhanced chemical oxidation of aromatic hydrocarbons in soil systems. Chemosphere 61:909–922. https://doi.org/10.1016/j.chemosphere.2005.03.039

Kaur G, Singh B, Singh P et al (2016) Preferentially grown nanostructured iron disulfide (FeS_2) for removal of industrial pollutants. RSC Adv 6:99120–99128. https://doi.org/10.1039/C6RA18838A

Kaur G, Devi P, Kumar M et al (2017a) Electrochemical aspects of photocatalysis: Au@FeS_2 nanocomposite for removal of industrial pollutant. Phys Chem Chem Phys 19:32412–32420. https://doi.org/10.1039/C7CP06289C

Kaur G, Singh B, Singh P et al (2017b) Iron disulfide (FeS_2): a promising material for removal of industrial pollutants. Chem Sel 2:2166–2173. https://doi.org/10.1002/slct.201700087

Khataee A, Gholami P, Sheydaei M et al (2016) Preparation of nanostructured pyrite with N_2 glow discharge plasma and the study of its catalytic performance in the heterogeneous Fenton process. New J Chem 40:5221–5230. https://doi.org/10.1039/C5NJ03594E

Kirkeminde A, Ren S (2013) Thermodynamic control of iron pyrite nanocrystal synthesis with high photoactivity and stability. J Mater Chem A 1:49–54. https://doi.org/10.1039/C2TA00498D

Kumar R, Rashid J, Barakat MA (2014) Synthesis and characterization of a starch–AlOOH–FeS_2 nanocomposite for the adsorption of congo red dye from aqueous solution. RSC Adv 4:38334–38340. https://doi.org/10.1039/C4RA05183A

Kumar A, Kumar A, Sharma G et al (2017) Sustainable nano-hybrids of magnetic biochar supported g-C3N4/FeVO4for solar powered degradation of noxious pollutants- synergism of adsorption, photocatalysis & photo-ozonation. J Clean Prod 165:431–451. https://doi.org/10.1016/j.jclepro.2017.07.117

Labiadh L, Oturan MA, Panizza M et al (2015) Complete removal of AHPS synthetic dye from water using new electro-Fenton oxidation catalyzed by natural pyrite as heterogeneous catalyst. J Hazard Mater 297:34–41. https://doi.org/10.1016/j.jhazmat.2015.04.062

Li YC, Bachas LG, Bhattacharyya D (2005) Kinetics studies of trichlorophenol destruction by chelate-based Fenton reaction. Environ Eng Sci 22:756–771. https://doi.org/10.1089/ees.2005.22.756

Lipczynska-Kochany E, Kochany J (2008) Effect of humic substances on the Fenton treatment of wastewater at acidic and neutral pH. Chemosphere 73:745–750. https://doi.org/10.1016/j.chemosphere.2008.06.028

Liu S, Li M, Li S et al (2013) Synthesis and adsorption/photocatalysis performance of pyrite FeS_2. Appl Surf Sci 268:213–217. https://doi.org/10.1016/j.apsusc.2012.12.061

Liu W, Wang Y, Ai Z, Zhang L (2015a) Hydrothermal synthesis of FeS_2 as a high-efficiency Fenton reagent to degrade alachlor via superoxide-mediated Fe(II)/Fe(III) cycle. ACS Appl Mater Interfaces 7:28534–28544. https://doi.org/10.1021/acsami.5b09919

Liu W, Xu L, Li X et al (2015b) High-dispersive FeS_2 on graphene oxide for effective degradation of 4-chlorophenol. RSC Adv 5:2449–2456. https://doi.org/10.1039/C4RA11354C

Long F, He J, Zhang M et al (2015) Microwave-hydrothermal synthesis of Co-doped FeS_2 as a visible-light photocatalyst. J Mater Sci 50:1848–1854. https://doi.org/10.1007/s10853-014-8747-5

Morales-Gallardo MV, Ayala AM, Pal M et al (2016) Synthesis of pyrite FeS_2 nanorods by simple hydrothermal method and its photocatalytic activity. Chem Phys Lett 660:93–98. https://doi.org/10.1016/j.cplett.2016.07.046

Pignatello JJ, Oliveros E, MacKay A (2006) Advanced oxidation processes for organic contaminant destruction based on the Fenton reaction and related chemistry. Crit Rev Environ Sci Technol 36:1–84. https://doi.org/10.1080/10643380500326564

Rashid J, Saleem S, Awan SU, et al (2018) Stabilized fabrication of anatase-TiO_2/FeS_2 (pyrite) semiconductor composite nanocrystals for enhanced solar light-mediated photocatalytic degradation of methylene blue

Sharma G, Kumar A, Naushad M et al (2017) Photoremediation of toxic dye from aqueous environment using monometallic and bimetallic quantum dots based nanocomposites. J Clean Prod 172:2919–2930. https://doi.org/10.1016/j.jclepro.2017.11.122

Shi X, Tian A, Xue X et al (2015) Synthesis of FeS_2 (pyrite) nanotube through sulfuration of Fe_2O_3 nanotube. Mater Lett 141:104–106. https://doi.org/10.1016/j.matlet.2014.11.084

Shi X, Tian A, You J et al (2018) Degradation of organic dyes by a new heterogeneous Fenton reagent – Fe_2GeS_4 nanoparticle. J Hazard Mater 353:182–189. https://doi.org/10.1016/j.jhazmat.2018.04.018

Suarez S, Carballa M, Omil F, Lema JM (2008) How are pharmaceutical and personal care products (PPCPs) removed from urban wastewaters. Rev Environ Sci Bio/Technol 7:125–138. https://doi.org/10.1007/s11157-008-9130-2

Sun Y, Cheng H (2015) Photocatalytic degradation of malachite green by pyrite and its synergism with Cr (VI) reduction : performance and reaction mechanism. Sep Purif Technol 154:168–175. https://doi.org/10.1016/j.seppur.2015.09.027

Talapin DV, Lee J-S, Kovalenko MV, Shevchenko EV (2010) Prospects of colloidal nanocrystals for electronic and optoelectronic applications. Chem Rev 110:389–458. https://doi.org/10.1021/cr900137k

Ternes TA (1998) Occurrence of drugs in German sewage treatment plants and rivers1 Dedicated to Professor Dr. Klaus Haberer on the occasion of his 70th birthday.1. Water Res 32:3245–3260. https://doi.org/10.1016/S0043-1354(98)00099-2

Tian A, Xu Q, Shi X et al (2015) Pyrite nanotube array films as an efficient photocatalyst for degradation of methylene blue and phenol. RSC Adv 5:62724–62731. https://doi.org/10.1039/C5RA07434G

Zhang Y, Zhang K, Dai C et al (2014) An enhanced Fenton reaction catalyzed by natural heterogeneous pyrite for nitrobenzene degradation in an aqueous solution. Chem Eng J 244:438–445. https://doi.org/10.1016/j.cej.2014.01.088

Zhang Y, Tran HP, Hussain I et al (2015) Degradation of p-chloroaniline by pyrite in aqueous solutions. Chem Eng J 279:396–401. https://doi.org/10.1016/j.cej.2015.03.016

Chapter 4
Green Synthesized Metal Oxide Nanomaterials Photocatalysis in Combating Bacterial Infection

Prajita Paul, Yashmin Pattnaik, Pritam Kumar Panda, Ealisha Jha, Suresh K. Verma, and Mrutyunjay Suar

Contents

Abstract With the unprecedented progresses of nanotechnology, metallic nanoparticles (MNPs) synthesized by green approaches have received global attention due to their low toxicity for the mankind. The advent in nanomaterial studies and their applications provoked issue of their toxicity and biocompatibility with respect to ecosystem and human health. This chapter provides glimpse to green synthesis and functionalization of nanoparticles used for the environmental

P. Paul · Y. Pattnaik · M. Suar (✉)
School of Biotechnology, KIIT Deemed to be University, Bhubaneswar, India
e-mail: msuar@kiitbiotech.ac.in

P. K. Panda
Division of Pediatric Hematology and Oncology, University Medical Center, University of Freiburg, Freiburg, Germany

E. Jha
Department of Physics and Physical Oceanography, Memorial University of Newfoundland, Newfoundland and Labrador, NL, Canada

S. K. Verma (✉)
School of Biotechnology, KIIT Deemed to be University, Bhubaneswar, India

Institute of Environmental Medicine, Karolinska Institutet, Stockholm, Sweden

M. Naushad et al. (eds.), *Green Methods for Wastewater Treatment*, Environmental Chemistry for a Sustainable World 35, https://doi.org/10.1007/978-3-030-16427-0_4

remediation as well as highlights the "state of the art" in exploring various environment-friendly synthesis approaches. However, the field of nanoscience has blossomed over the last two decades to unfold to unleash its power on our day-to-day lives of various nanotechnological production processes. Also new strategies have been applied for synthesis and industrial preparation. In particular, this chapter discusses green nanotechnology-based production of biocompatible Ag and Au nanoparticles and their biomedical applications and also enlightens the platform for innovative antibacterial efficacy and its cytotoxicity.

Keywords Nanotechnology · Metallic nanoparticles · Green synthesis · Antibacterial · Biocompatible · Cytotoxicity

4.1 Introduction

The amalgamation of science, engineering, and technology at nanoscale level gave birth to the field of nanotechnology. The term nano is obtained from the Greek word "nanos" which implies small and refers to particles above subatomic measurements nearly 1 billionth of a meter. It's a science which involves the study of extremely small things and further engineering them to have potential utility in various other scientific fields (Mazhar et al. 2017). Nanotechnology has been a developing area since a decade or two and finding extensive applications due to its enhanced properties of being lightweight as well as showing a greater chemical reactivity than their larger-scale counterparts (Naushad et al. 2017). Chemical synthesis of nanoparticles makes them toxic and renders them unsuitable for applications in medical fields (Prabu 2015). When nanoparticles are manufactured by synthetic routes using organic solvents and in harsh chemical conditions, it leads to accumulation of toxic residues which subsequently pose a threat to the environment (Molnár et al. 2018). To resolve the issues associated with chemical synthesis routes, green methods of synthesis came into role. Green nanobiotechnology refers to an eco-friendly route of synthesis of nanomaterials utilizing plants, microorganisms, and even their by-products like lipids and proteins (Patra and Baek 2014). The diagram below lists out the different methods of nanoparticles synthesis Fig. 4.1.

At present, due to the nontoxic effects, nonexpensive, and eco-friendly nature, researchers are more interested in introducing new approaches in the field of biology.

4.2 Scopes for Green Synthesis of Metal Nanoparticles

Various routes of biosynthesized green nanoparticles include algae, microbes (diatoms), plants, some biocompatible agents, and heterotrophic human cell lines which are known as green nanofactories and especially exploited for the production of inorganic nanoparticles (Narayanan and Sakthivel 2011; Prabu 2015; Shirsat et al. 2016). Thus the approach for biosynthesized nanoparticles follows the principles of

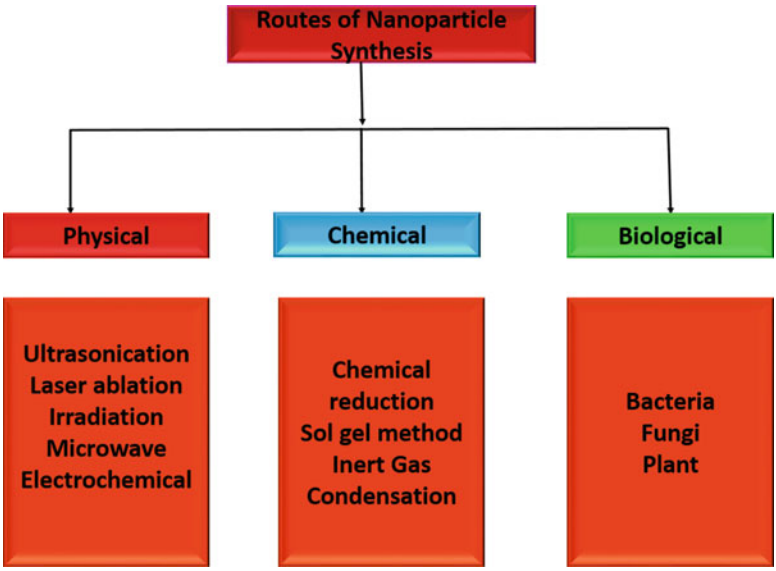

Fig. 4.1 Different routes for synthesis of nanoparticles

green chemistry. However, plants and plant resources are advantageous as sources of nanomaterials synthesis over prokaryotic microbes which further need downstream processing (Narayanan and Sakthivel 2011).

The principles of green chemistry have proved to be a promising alternate to produce biocompatible and steady nanoparticles having the added advantages of being nontoxic and environment-friendly (Parveen et al. 2016). With the advancement of green methods of nanoparticles synthesis, the scope of developments in other scientific fields like medicine has also increased multifold (Patra and Baek 2014). This chapter focusses on the strong cross-link between nanotechnology and its significant contribution to therapeutics especially in treating bacterial infections.

Recent years have shown immense increase in the production of gold nanoparticles, and their applications in biomedical spheres have also increased (Keighron and Keating 2010). Biogenic method of synthesis of silver and gold nanoparticles is seeking more attention owing to their intense antibacterial action as well as for their property of getting reduced to salts easily (Wang and Hu 2017). Biogenic Ag and Au nanoparticles act as good conduction centers and thereby facilitate transfer of electrons. The colloidal route of synthesis of silver and gold is predicted to create ion channels in between the prosthetic groups and to help the protein to acquire a favorable orientation.

The applications of nanoparticles in the area of medical science are known to be expanding due to their high stability both chemically and biologically and can be administered through almost all routes unlike other drugs which have certain limitations (Bao 2004). Introduction of nanoparticles into the cell generates a lot of structural modifications which often can lead to non-specific interactions between

the shell of the nanoparticles and proteins circulating in the bloodstream. Therefore an ideal nanoparticle used for therapeutics should be nontoxic, stable, non-immunogenic, biocompatible, noninflammatory, and biodegradable to ensure its potency and efficacy (Farkhani et al. 2014).

4.3 Biological Effect of Metal Nanoparticles

Following Table 4.1 listed below shows biosynthesis of nanoparticles from different bacteria. The extensive use of metallic oxide nanoparticles has shown remarkable applications in various areas such as antibacterial, antifungal, drug delivery, tissue engineering, wound healing, etc. (Martin-Ortigosa et al. 2014). In view of concern related to biocompatibility, green synthesized nanoparticles have been used (Vadlapudi et al. 2014). As far as beneficial effects are concerned, green synthesized metal nanoparticles have been studied for their antibacterial activities against pathogenic as well as nonpathogenic strains. The approach of green synthesis has been taken in prior to enhance the antibacterial activity of a metal nanoparticles like AgNPs, AuNPs, etc. However, their toxic effects can be ignored upon high usage and accumulation. Moreover, the toxic effect advances toward the environmental aspects and spread to other biotic factors of the ecosystem.

Table 4.1 Biosynthesis of nanoparticles from bacteria

Bacterial strains	Metal nanoparticles	Size	References
Pseudomonas stutzeri	AgNPs	100–200 nm	11
Lactobacillus sp.	AgNPs	15–30 nm	12
Morganella sp.	AgNPs	20–21 nm	13
Bacillus subtilis	AgNPs	5–50 nm	14
Bacillus indicus	AgNPs	2.5–13.3 nm	15
Pseudomonas antarctica	AgNPs	3–33 nm	15
Pseudomonas fluorescens	AgNPs	80–85 nm	16
Salmonella typhimurium	AgNPs	85–110 nm	17
Bacillus thuringiensis	AgNPs	20–30 nm	18
S. aureus	AgNPs	30–40 nm	18
S. typhimurium	AgNPs	40–50 nm	18
Bacillus subtilis	AuNPs	5–25 nm	19
Lactobacillus sp.	AuNPs	20–50 nm	20
Pseudomonas aeruginosa	AuNPs	15–30 nm	21
Escherichia coli	AuNPs	20–25 nm	22
Klebsiella pneumoniae	AuNPs	35–65 nm	23
Salmonella Typhimurium	AuNPs	20–40 nm	17

4.3.1 *Antibacterial Effects of Green Synthesized Metal Nanoparticles (AgNPs and AuNPs)*

Recently, successful biosynthesis of silver and gold nanoparticles was carried out by researchers via green route of methodology varying with morphology and desired size through natural reducing, capping, and stabilizing agents. These biosynthesized processes are widely favored due to their nontoxic, low-cost, naturally derived, eco-elegant features (Feng et al. 2000; Taylor et al. 2010) Fig. 4.2. The extracts such as amino acids, polysaccharides, enzymes/proteins, and vitamins from various organisms are found to be bioreduce with metallic ions in combinations with several biomolecules which are environmentally sustainable. However, several research groups reported green synthesis of Ag and Au metallic nanoparticles using bacteria, biological routes, and extraction of plant products. The biosynthesis of Au and Ag metallic nanoparticles is properly channelized through the organic compounds present in plant extracts for lower concentration of nanoparticles. The underlying molecular mechanism that permits inhibitory properties of biosynthesized Au and Ag nanoparticles cause reduction of ionic form of gold to its atomic state and ionic form of silver to its atomic state. This bioreduction occurs by absence of hydrogen due to OH groups present in the polyphenol molecules. The biosynthesis of such silver and gold nanoparticles can be achieved through different routes.

Successful synthesis of biogenic silver nanoparticles (AgNPs) was carried out by a group of researchers in an eco-friendly manner. For example, the root extract of plant named *Zingiber officinale* were used in presence of metallic ion. The change in change indicated the formation of biosynthesized silver nanoparticles (AgNPs)

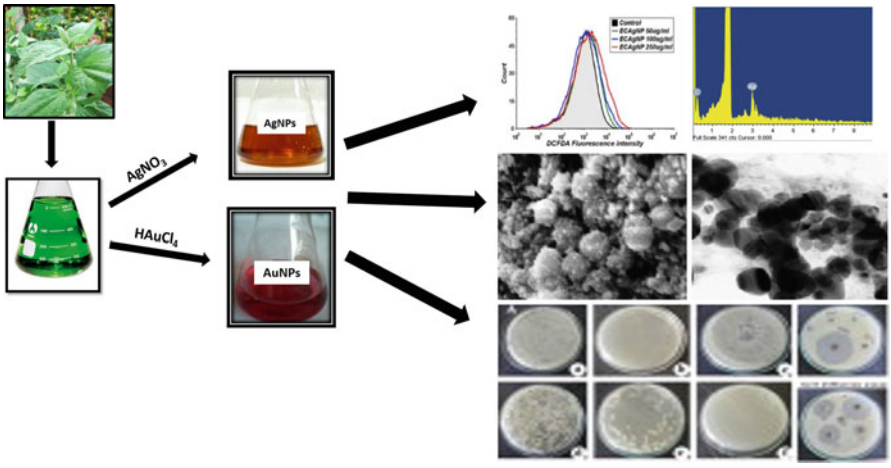

Fig. 4.2 Process outline for the synthesis of AgNPs and AuNPs along with its characterization techniques and antimicrobial activity

(Velmurugan et al. 2014). Another method of synthesis of AgNPs was done out by Ahmed group using plant extracts of *Azadirachta indica* (Ahmed et al. 2015). This plant extract functions as capping as well as reducing agent. For this method, leaves of plant extract were first cleaned by distilled water and air dried at room temperature. The leaves were boiled later in distilled water for 30 min, and the extract was stored in the refrigerator before use. This group also proposed a new, basic, one-step, easier, and quicker method for synthesizing of biogenic AgNPs by using plant extracts of *Crotalaria retusa* as well as *Terminalia arjuna* as reducing and stabilizing agents (Ahmed and Ikram 2015; Ahmed et al. 2016b). The biogenic silver nanoparticles (AgNPs) exhibited greater catalytic activity as well as excellent antibacterial premises against both Gram-negative and Gram-positive microorganisms.

Biosynthesis of gold nanoparticles (AuNPs) was also carried out by using environment-friendly material such as the plant extracts. For example, the plant extract of *Sphaeranthus indicus* was first washed, then transferred into conical of purified boiling water, and kept for 10 min. The plant extract was then filtered for further process. To it 1 mM of $HAuCl_4$ solution along with *S. indicus* plant extract was added and mixed well for 30 min; the change in color from light yellow to wine red indicated synthesis of Au NPs (pH 5.4) (Balalakshmi et al. 2017). Another set of synthesis of AuNPs were performed by different research group where they collected leaf, bark, stem, root, etc. These plant parts were properly cleaned with water, cut into small parts, and then allowed to boil in distilled water to obtain extract. Further, the purified extract is mixed with the metallic $HAuCl_4$ salt solution at room temperature to obtain Au NPs in a one-pot reaction (Ahmed et al. 2016a).

4.3.2 Cytotoxicity of Green Synthesized Metal Nanoparticles (AgNPs and AuNPs)

Cytotoxicity of a nanoparticle is defined as the alteration in cellular morphology leading to toxic effect of nanoparticle. Cytotoxicity has been considered as an important modality for proposing any nanomaterial for clinical applications. Nowadays both in vitro and in vivo biological models are being used to evaluate the cytotoxicity effect of engineered nanoparticles. In vitro evaluation has been described as the determination of cytotoxicity or in negative termed called as biocompatibility using mammalian cell lines as model, while in vivo evaluation describes the cytotoxicity determination in live models like mouse, rat, and zebrafish. Metallic nanoparticles such as silver and gold have been reported to exhibit cytotoxicity apart from their antibacterial efficacy. A number of studies have reported the cytotoxic effects of Ag NPs on neuronal cell, rat liver (Hussain 2005; Hussain et al. 2006), murine stem cells (Braydich-Stolle et al. 2005), and human lung epithelial cell (Lam et al. 2004; Asharani et al. 2009). The basic mechanism of AgNP toxicity has been understood since long time, yet detail

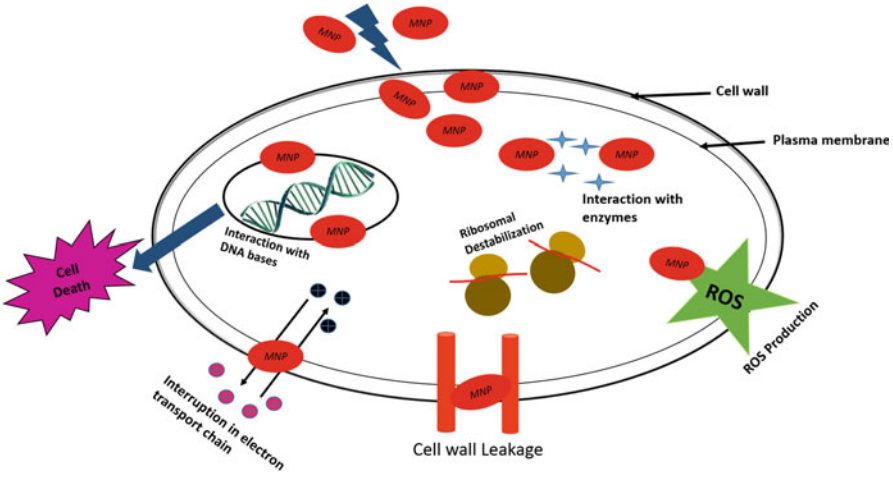

Fig. 4.3 Antibacterial mechanism of metal nanoparticles

explanation is still lacking. Ag NPs that get internalized inside cell through permeation of cell membrane create greater level of intracellular Ag+, leading toward genotoxic and cytotoxic effects carried out through the interruption of cell transport (Choi and Hu 2008). Smaller AgNP penetrates cell walls and membranes, while larger AgNP gets internalized through endosomal pathway (Xia et al. 2006). Through these basic mechanisms, the whole processes have been defined by many researchers. The mechanisms have been described in terms of three major cellular phenomena happening during their exposure: (1) generation of reactive oxygen species (ROS), (2) DNA damage, and (3) modulation of immunological factors like cytokine production. Uptake of AgNP can induce the generation of ROS at higher level which results toward oxidative stress and genotoxic effects. Induction of ROS proceeds toward disruption of flux of ions and electrons across the mitochondrial membrane leading to either apoptosis or necrosis (Asharani et al. 2009; Arora et al. 2008). The ROS induction, however, varies according to the physiochemical properties of the AgNPs Fig. 4.3.

As far as genotoxicity induced by AgNP is concerned, the toxic effects are induced by DNA damage as shown in case of human lung fibroblast, IMR90, and human glioblastoma cells, U251, by increasing ROS production or by diminishing energy production due to depleted ATP generation (Hsin et al. 2008). Apart from this, the mechanism of AgNP cytotoxicity has also been reported due to change in immunological responses. AgNP has been reported to elicit both stimulatory and suppressive effects on the production of cytokines associated with the inflammatory response and is found to be dependent on physiological parameters like size, dose, and cell types. Studies showed enhanced production of proinflammatory response mediators (TNF-α, MIP-2, and IL-1β) and an increase in IL-1β, IL-6, IL-8, and TNF-α in human epidermal cells (Carlson et al. 2008; Greulich et al. 2009).

Though the in vitro studies have provided detail information, in vivo studies have verified the toxicity of AgNP with regard to their exposure and organism basis. At gene level, the genes responsible for apoptosis and inflammation pathways have also been found to be in elicited regulation on AgNP exposure [24]. The toxicity of AgNP has also been reported in embryonic zebrafish model. Moreover, changes in morphology like abnormal organ formation, pericardial edema, and slow development have also been reported (Verma et al. 2017a, b). In brief, the mechanism of toxicity of AgNP has been defined with respect of both in vitro and in vivo model; however, the detailed understanding has come mostly from in vitro studies. In vivo studies have enlightened the detail but need to be excavated in more intensive and molecular way.

Similar to AgNP, the cytotoxic effects of AuNP have also been the matter of discussion with regard to their extensive studies. The toxicity of AuNPs has been discussed in frame of both in vitro and in vivo studies. Knowledge about toxicity in in vitro models have been done on a large scale on each and every types of cell lines. A group of researchers showed the in vitro biocompatibility of AuNPs obtained from tea flavonoids in PC-3 prostate cancer cells and MCF-7 breast cancer cells that marked up increase level of gold concentrations (Nune et al. 2009). Another group of researchers showed use of soybean phytochemical mediated AuNP biocompatibility toward fibroblast cell lines. For clinical purpose of AuNPs, it is necessary to unravel the mechanism of in vivo toxicity and biodistribution. Furthermore, this group also showed that mice injected with AuNPs synthesized from plant extract of *Lantana montevidensis* (LM) did not reveal in vivo toxicity as compared with untreated mice (Nune et al. 2009). Both serum histopathological evaluation and biochemical parameters were normal and without any symptoms of toxicity. All these in vivo results thus generated infer that AuNPs were nontoxic in animal models and can be recommended for biomedical applications. A group of researchers showed cinnamon phytochemical-derived AuNP biocompatibility toward animal models. They also demonstrated the in vivo biocompatibility of AuNPs after intraperitoneal injection (i.p.) in male Wistar rats (Ahmed et al. 2016a) where the major accumulation of these nanoparticles was observed in liver and spleen followed by kidneys and lungs. So far all the published articles gave evidence that AuNPs may serve as promising and secure to increase level of in vivo concentrations and potential in the field of pharmaceuticals and biomedical applications.

4.3.3 Biomedical Application of AgNP and AuNP

In the field of biology, metallic nanoparticles (MNPs) have drawn several promising applications owing to their catalytic properties, biocompatibility, optical nature, conductivity, surface volume, and density (Li and Li 2014; Boote et al. 2014). As compared to route of colloidal metallic nanoparticles (MNPs), biosynthesized NPs are superior to colloidal stability and their proficiency to conjugate with organic molecules. Metallic nanoparticles (MNPs) have been used in various applications

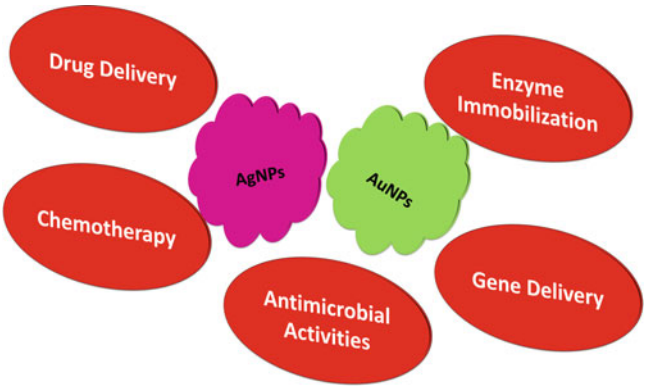

Fig. 4.4 Biomedical applications of AgNPs and AuNPs

such as drug delivery, enzyme immobilization, gene delivery, chemotherapy, and antimicrobial activity (Fig. 4.4).

Drug Delivery

This method includes targeted drug delivery and traditional mechanisms. Targeted drug delivery are preferred more than traditional drug delivery mechanisms since the drugs are chosen at a distinct affected area and doses are administrated locally without any undesirable effects. Several groups of work have been carried forward by scientists following these traditional drug delivery mechanisms (Li and Li 2014; Anandhakumar et al. 2012). The importance of metallic nanoparticles (MNPs) for efficient drug delivery mechanisms implies because of their distinct biophysical and biochemical properties with strong binding attraction for carboxylic acid aptamers, proteins, thiols, and disulfides. Therefore, they have been recommended for anticancer therapy. The toxicity of MNP depends on the surface coating, route of synthesis, size, shape, charge, and functionalized molecules, but its cytotoxicity relies at a minimal acceptable level of nanoparticles. The flexibility of MNPs involves their monolayers to provide an efficient system (Ajnai et al. 2014).

Enzyme Immobilization

The process of enzyme immobilization has been applied on solvent media for intensifying enzyme activity and stability (Iyer and Ananthanarayan 2008). In the field of biotechnology, the immobilization of enzyme seeks attention for their minimal expenses in industrial-based operational stability and ease of separation of products for long period (Mateo et al. 2007). Enormous scale of immobilization techniques can be used for covalent and adsorption on solid supports (Alonso et al. 2005). This method can be achieved by selecting matrix support and designing the

carrier. To be utilized as host matrices, MNPs such as gold and silver are used due to their surface stability and good electronic properties. Both these MNPs serve as good conduction centers to facilitate transfer of electrons (Chi et al. 2008). The enzyme immobilization of biogenic nanoparticle depends on solid supports either as isolated cells or whole cell enzymes, such as lysozyme (Vertegel et al. 2004), aminopeptidase, as well as alcohol dehydrogenase (Keighron and Keating 2010) and glucose oxidase (Li and Xu 2014).

Gene Delivery

The mechanism of gene delivery technique implies on gene of interest to specify its encoded protein into an appropriate host cell (Li and Xu 2014). Several types of gene delivery techniques are transfection, electroporation, and use of vectors such as retroviruses and adenoviruses (Farkhani et al. 2014). The gene delivery machinery in viral vectors occurs by introduction of nucleic acid sequences into the desired host genome of interest excluding any side effects. Therefore, these methods are secure in biomedical applications based on improvements in their efficiency (Martin-Ortigosa et al. 2014). In basic science, several nanoparticles have been applied, particularly to in vitro cells for stimulating the transfection efficiency. As a consequence, composite nanoparticles and nucleic acid are first supplied into in vitro cell medium and toward the surface of the cell followed by the magnetic force. Conditions due to the presence of higher toxicity of these nanoparticle biomedical applications are limited toward in vivo and in vitro conditions (Syu et al. 2014). Therefore, nanoparticles are encrusted with molecules, such as proteins and carbohydrates, synthetic organic polyethylene glycol, polyvinyl alcohol, poly-L-lactic acid, and silica to minimize toxic effect (Bao 2004). The process of developing new nonviral methods facilitates rate of transfection efficiency. At present, biosynthesized NPs hold an alternative approach for gene transfection (Seisenbaeva et al. 2017; Cai et al. 2008).

Chemotherapy

Chemotherapy is drug therapy for anticancer treatment of varied types. The main obstacles in cancer treatment are its toxic effect on healthy proliferating cells acquired by multidrug resistance (Gottesman et al. 2002). Therefore it is required for appropriate concentrations of anticancer drugs to be administered for reducing the toxic side effects (Maeda 2001). In these days, nanotechnology field has achieved the only alternative approach to overcome such problems by the application of nanotherapeutics, particularly for delivering drug to gene, siRNA, and antitumor therapy, biosensing, and bioimaging. Apart from MNPs, AuNPs also play an important role in drug delivery applications because of their size, shapes, surface-dependent properties, and minimal cytotoxic effects (Ghosh et al. 2008; Han et al. 2007). Therefore, nanoparticles can be recommended for efficient therapy toward drug delivery of targeted cancer cells.

Antimicrobial Activities

Due to the presence of high antimicrobial properties, metallic nanoparticles (MNPs) are used against various microorganisms. At present in the field of medical and pharmaceutical industries, inert nanomaterials serve as antimicrobial drugs. Compared to several metallic nanoparticles (MNPs), AgNPs showed effective bactericidal activity toward Gram-ve and Gram+ve bacteria including those antimicrobial-resistant strains (Li and Li 2014). AgNPs and its corresponding ions have drawn attention owing to their antibacterial nature either bacteriocidal or bacteriostatic and are also considered "oligo dynamic." Based on observation ionic form of Ag (silver) inactivates the interaction with thiol groups of essential proteins/enzymes. It is therefore known that ionic form of silver interaction with bacteria permits depolarization in the cell membrane, thereby inhibiting DNA replication machinery (Elechiguerra et al. 2005).

4.4 Conclusion and Future Outlook

This chapter primely focusses on eco-friendly biosynthesis of silver and gold nanoparticles as an alternative approach with relevant biomedical implications. These biogenic NPs have been used in the photocatalytic degradation of dyes. Therefore, metal/metal oxide hybrid nanocomposites might be use as a photocatalyst with enhanced antimicrobial activity. These nanoparticles have explored the therapy of nanomedicine which can be perceived from advancements of several AgNP- and AuNP-based nanomedicines. Green synthesized nanoparticles have been proved as beneficial in respect of high antibacterial efficacy with a biocompatibility at same platform. Furthermore, for the stability of in vitro and in vivo biodistribution, both AgNPs and AuNPs were used. This chapter highlights a novel opportunity with scope in advancement of designing convenient techniques to fabricate silver and gold nanoparticles with appropriate features to ensemble antibacterial activities, anticancer treatment, and therapeutic applications. Therefore, the potent role of these NPs should deliberate as cost worthy for therapeutic applications in the field of bioscience and biomedicine in the near future.

References

Ahmed S, Ikram S (2015) Silver nanoparticles: one pot green synthesis using terminalia arjuna extract for biological application. J Nanomed Nanotechnol 6:309. https://doi.org/10.4172/2157-7439.1000309

Ahmed S, Ullah S, Ahmad M, Swami BL (2015) Green synthesis of silver nanoparticles using *Azadirachta indica* aqueous leaf extract. J Radiat Res Appl Sci 9:1–7. https://doi.org/10.1016/j.jrras.2015.06.006

Ahmed S, Annu, Ikram S, Yudha S (2016a) Biosynthesis of gold nanoparticles: a green approach. J Photochem Photobiol B Biol 161:141–153. https://doi.org/10.1016/j.jphotobiol.2016.04.034

Ahmed S, Manzoor K, Ikram S (2016b) Synthesis of silver nanoparticles using leaf extract of Crotalaria retusa as antimicrobial green catalyst. J Bionanosci 10:282–287. https://doi.org/10.1166/jbns.2016.1376

Ajnai G, Chiu A, Kan T et al (2014) Trends of gold nanoparticle-based drug delivery system in cancer therapy. J Exp Clin Med 6:172–178. https://doi.org/10.1016/j.jecm.2014.10.015

Alonso N, Fernando L, Betancor L et al (2005) Immobilization and stabilization of glutaryl acylase on aminated sepabeads supports by the glutaraldehyde crosslinking method. J Mol Catal B Enzym 35:57–61. https://doi.org/10.1016/j.molcatb.2005.05.007

Anandhakumar S, Mahalakshmi V, Raichur AM (2012) Silver nanoparticles modified nanocapsules for ultrasonically activated drug delivery. Mater Sci Eng C 32:2349–2355. https://doi.org/10.1016/j.msec.2012.07.006

Arora S, Jain J, Rajwade JM, Paknikar KM (2008) Cellular responses induced by silver nanoparticles: in vitro studies. Toxicol Lett 179:93–100. https://doi.org/10.1016/j.toxlet.2008.04.009

Asharani PV, Low G, Mun K et al (2009) Cytotoxicity and genotoxicity of Silver. ACS Nano 3:279–290

Balalakshmi C, Gopinath K, Lokesh R et al (2017) Green synthesis of gold nanoparticles using a cheap Sphaeranthus indicus extract: impact on plant cells and the aquatic crustacean Artemia nauplii. J Photochem Photobiol B Biol 173:598–605. https://doi.org/10.1016/j.jphotobiol.2017.06.040

Bao G (2004) Functionalization and peptide-based delivery of magnetic nanoparticles as an intracellular MRI contrast agent. J Biol Inorg Chem 9:706–712. https://doi.org/10.1007/s00775-004-0560-1

Boote BW, Byun H, Kim J, Lib C (2014) Silver – gold bimetallic nanoparticles and their applications as optical materials. J Nanosci Nanotechnol 14:1563–1577. https://doi.org/10.1166/jnn.2014.9077

Braydich-Stolle L, Hussain S, Schlager JJ, Hofmann MC (2005) In vitro cytotoxicity of nanoparticles in mammalian germline stem cells. Toxicol Sci 88:412–419. https://doi.org/10.1093/toxsci/kfi256

Cai X, Conley S, Naash M (2008) Nanoparticle applications in ocular gene therapy. Vis Res 48:319–324. https://doi.org/10.1016/j.visres.2007.07.012

Carlson C, Hussain SM, Schrand AM et al (2008) Unique cellular interaction of silver nanoparticles: size-dependent generation of reactive oxygen species. J Phys Chem B 112:13608–13619

Chi M, Lyu R, Lin L, Huang H (2008) Characterization of Bacillus kaustophilus leucine aminopeptidase immobilized in Ca-alginate/k-carrageenan beads. Biochem Eng J 39:376–382. https://doi.org/10.1016/j.bej.2007.10.008

Choi O, Hu Z (2008) Size dependent and reactive oxygen species related nanosilver toxicity to nitrifying bacteria. Environ Sci Technol 42:4583–4588

Elechiguerra JL, Burt JL, Morones JR et al (2005) Interaction of silver nanoparticles with HIV-1. J Nanobiotechnol 10:1–10. https://doi.org/10.1186/1477-3155-3-6

Farkhani SM, Valizadeh A, Karami H et al (2014) Nanoparticles, nanocarriers, therapeutic and diagnostic molecules. Peptides 57:1–17. https://doi.org/10.1016/j.peptides.2014.04.015

Feng QL, Wu J, Chen GQ et al (2000) A mechanistic study of the antibacterial effect of silver ions on Escherichia coli and *Staphylococcus aureus*. J Biomed Mater Res 52(4):662–668

Ghosh P, Han G, De M et al (2008) Gold nanoparticles in delivery applications ☆. Adv Drug Deliv Rev 60:1307–1315. https://doi.org/10.1016/j.addr.2008.03.016

Gottesman MM, Fojo T, Bates SE (2002) Multidrug resistance in cancer: role of ATP-dependent transporters. Nat Rev Cancer 2:48–58. https://doi.org/10.1038/nrc706

Greulich C, Kittler S, Epple M et al (2009) Studies on the biocompatibility and the interaction of silver nanoparticles with human mesenchymal stem cells (hMSCs). Langenbeck's Arch Surg 394:495–502. https://doi.org/10.1007/s00423-009-0472-1

Han G, Ghosh P, Rotello VM (2007) Functionalized gold nanoparticles for drug delivery. Nanomedicine 2:113–123

Hsin Y, Chen C, Huang S et al (2008) The apoptotic effect of nanosilver is mediated by a ROS- and JNK-dependent mechanism involving the mitochondrial pathway in NIH3T3 cells. Toxicol Lett 179:130–139. https://doi.org/10.1016/j.toxlet.2008.04.015

Hussain SM (2005) In vitro toxicity of nanoparticles in BRL 3A rat liver cells. Toxicol In Vitro 19:975–983. https://doi.org/10.1016/j.tiv.2005.06.034

Hussain SM, Javorina AK, Schrand AM et al (2006) The interaction of manganese nanoparticles with PC-12 cells induces dopamine depletion. Toxicol Sci 92:456–463. https://doi.org/10.1093/toxsci/kfl020

Iyer PV, Ananthanarayan L (2008) Enzyme stability and stabilization — aqueous and non-aqueous environment. Process Biochem 43:1019–1032. https://doi.org/10.1016/j.procbio.2008.06.004

Keighron JD, Keating CD (2010) Enzyme: nanoparticle bioconjugates with two sequential enzymes: stoichiometry and activity of malate dehydrogenase and citrate synthase on Au nanoparticles. Langmuir 26:18992–19000. https://doi.org/10.1021/la1040882

Lam C, James JT, Mccluskey R, Hunter RL (2004) Pulmonary toxicity of single-wall carbon nanotubes in mice 7 and 90 days after intratracheal instillation. Toxicol Sci 134:126–134. https://doi.org/10.1093/toxsci/kfg243

Li Q, Li X (2014) Nanosilver particles in medical applications: synthesis, performance, and toxicity. Int J Nanomedicine 9:2399–2407

Li H, Xu D (2014) Trends in analytical chemistry silver nanoparticles as labels for applications in bioassays. Trends Anal Chem 61:67–73. https://doi.org/10.1016/j.trac.2014.05.003

Maeda H (2001) SMANCS and polymer-conjugated macromolecular drugs: advantages in cancer chemotherapy. Adv Drug Deliv Rev 46:169–185

Martin-Ortigosa S, Peterson DJ, Valenstein JS, Victor S, Lin Y, Brian G, Trewyn L, Lyznik A, Wang K (2014) Mesoporous silica nanopa intracellular Cre protein delivery for maize genome editing via loxP site excision. Plant Physiol. https://doi.org/10.1104/pp.113.233650

Mateo C, Palomo JM, Fernandez-lorente G et al (2007) Improvement of enzyme activity, stability and selectivity via immobilization techniques. Enzym Microb Technol 40:1451–1463. https://doi.org/10.1016/j.enzmictec.2007.01.018

Mazhar T, Shrivastava V, Tomar RS (2017) Green synthesis of bimetallic nanoparticles and its applications: a review. J Pharm Sci Res 9:102–110

Molnár Z, Bódai V, Szakacs G et al (2018) Green synthesis of gold nanoparticles by thermophilic filamentous fungi. Sci Rep 8:1–12. https://doi.org/10.1038/s41598-018-22112-3

Narayanan KB, Sakthivel N (2011) Green synthesis of biogenic metal nanoparticles by terrestrial and aquatic phototrophic and heterotrophic eukaryotes and biocompatible agents. Adv Colloid Interf Sci 169:59–79. https://doi.org/10.1016/j.cis.2011.08.004

Naushad M, Ahamad T, Al-Maswari BM et al (2017) Nickel ferrite bearing nitrogen-doped mesoporous carbon as efficient adsorbent for the removal of highly toxic metal ion from aqueous medium. Chem Eng J 330:1351–1360. https://doi.org/10.1016/j.cej.2017.08.079

Nune SK, Chanda N, Shukla R et al (2009) Green nanotechnology from tea: phytochemicals in tea as building blocks for production of biocompatible gold nanoparticles †. J Mater Chem 19:2912–2920. https://doi.org/10.1039/b822015h

Parveen K, Banse V, Ledwani L (2016) Green synthesis of nanoparticles: their advantages and disadvantages. AIP Conf Proc 1724:020048. https://doi.org/10.1063/1.4945168

Patra JK, Baek K (2014) Green nanobiotechnology: factors affecting synthesis and characterization techniques. J Nanomater 2014:417305

Prabu IJHJ (2015) Green synthesis and characterization of silver nanoparticles by leaf extracts of *Cycas circinalis*, Ficus amplissima, *Commelina benghalensis* and *Lippia nodiflora*. Int Nano Lett 5:43–51. https://doi.org/10.1007/s40089-014-0136-1

Seisenbaeva GA, Fromell K, Vinogradov VV et al (2017) Dispersion of TiO_2 nanoparticles improves burn wound healing and tissue regeneration through specific interaction with blood serum proteins. Sci Rep 7:1–11. https://doi.org/10.1038/s41598-017-15792-w

Shirsat S, Kadam A, Jadhav VV et al (2016) An eco-friendly physicocultural-based rapid synthesis of selenium nanoparticles. RSC Adv 6:48420–48426. https://doi.org/10.1039/C6RA08275K

Syu Y, Hung J, Chen J, Chuang H (2014) Plant physiology and biochemistry impacts of size and shape of silver nanoparticles on Arabidopsis plant growth and gene expression. Plant Physiol Biochem 83:57–64. https://doi.org/10.1016/j.plaphy.2014.07.010

Taylor P, Jha AK, Prasad K (2010) Green synthesis of silver nanoparticles using Cycas leaf. Int J Green Nanotechnol: Phys Chem 1:37–41. https://doi.org/10.1080/19430871003684572

Vadlapudi V, Behara M, Devamma MN (2014) Green synthesis and biocompatibility of nanoparticles. Rasayan J Chem 7:219–223

Velmurugan P, Anbalagan K, Manosathyadevan M (2014) Green synthesis of silver and gold nanoparticles using *Zingiber officinale* root extract and antibacterial activity of silver nanoparticles against food pathogens. Bioprocess Biosyst Eng 37:1935–1943. https://doi.org/10.1007/s00449-014-1169-6

Verma SK, Jha E, Sahoo B et al (2017a) RSC advances mechanistic insight into the rapid one-step facile biofabrication of antibacterial silver nanoparticles from bacterial release and their biogenicity and. RSC Adv 7:40034–40045. https://doi.org/10.1039/C7RA05943D

Verma SK, Panda PK, Jha E, Suar M (2017b) Altered physiochemical properties in industrially synthesized ZnO nanoparticles regulate oxidative stress; induce in vivo cytotoxicity in embryonic zebrafish by apoptosis. Sci Rep 7:1–16. https://doi.org/10.1038/s41598-017-14039-y

Vertegel AA, Siegel RW, Dordick JS (2004) Silica nanoparticle size influences the structure and enzymatic activity of adsorbed lysozyme. Langmuir 20(16):6800–6807

Wang L, Hu C (2017) The antimicrobial activity of nanoparticles: present situation and prospects for the future. Int J Nanomedicine 12:1227–1249

Xia T, Kovochich M, Brant J et al (2006) Comparison of the abilities of ambient and manufactured nanoparticles to induce cellular toxicity according to an oxidative stress paradigm. Nano Lett 6 (8):1794–1807

Chapter 5
Progression in Fenton Process for the Wastewater Treatment

S. Kaviya

Contents

Abstract The presence of industrial contaminants in water bodies leads unfit for domestic and irrigation process. The contaminated water treatment becomes even more problematical if the process encompasses high volumes of effluents. Advanced oxidation process (AOP) is a favorable technique for the wastewater treatment owing to its eco-friendly processing. This chapter gives a detailed discussion about the classical Fenton process; its progress/modifications such as photo-Fenton, microbially driven Fenton, electro-Fenton, and sono-Fenton and their combinations; and different nanocomposite materials used for this process.

Keywords Fenton process · Wastewater treatment · Advanced oxidation process · Classification of Fenton · Photo-Fenton · Electro-Fenton · Sono-Fenton · Microbially driven Fenton · Electro-photo-Fenton · Sono-electro-Fenton · Sono-photo-Fenton

S. Kaviya (✉)
Department of Chemical Engineering, Indian Institute of Science (IISc), Bangalore, Karnataka, India

M. Naushad et al. (eds.), *Green Methods for Wastewater Treatment*, Environmental Chemistry for a Sustainable World 35, https://doi.org/10.1007/978-3-030-16427-0_5

5.1 Introduction

Water management is a universal question nowadays with the growing demand of freshwater caused by increasing population, domestic usage, and emerging industrial needs (Awual et al. 2015). The discharged wastewater is the foremost environmental issue caused by the industry (Wang et al. 2018). Generally owing to the low elimination of contaminants by the conservative wastewater systems, the chemical contaminants end up in soil and water bodies (Matamoros et al. 2012; Veloutsou et al. 2014). The incomplete mineralization of the toxic chemicals may cause the generation of supplementary hazardous chemicals (Escher et al. 2006). Industrial wastewater requires posttreatment after biological digestion due to its high recalcitrant chemical oxygen demand (COD). Various physical-chemical-biological process have been used for the wastewater treatment such as absorption, ion exchange, membrane filtration, coagulation and flocculation, reverse osmosis, oxidation, electrochemical treatment, chemical precipitation, aerobic and anaerobic process, etc. (Naushad and Alothman 2015; Ghasemi et al. 2014a, b). Among them advanced oxidation process (AOP) is the most favorable alternate which overcomes the disadvantages of other methods. It is beneficial for cleaning lethal and nondegradable organic materials in contaminated water (Oppenlander 2003). Advanced oxidation process takes place with the in situ formation of hydroxyl ($OH^{\cdot}$) radicals which have a robust oxidation capability of 2.80 V versus standard hydrogen electrode (Oturan and Aaron 2014; Wang and Xu 2012). Under this process, the hydroxide radical oxidizes the organic contaminant either by small organic or complete mineralization into water (H_2O) and carbon dioxide (CO_2) (Kaviya and Prasad 2016).

AOP is a Fenton process which is commonly used due to non-toxic, great production, simple operation at room temperature and pressure. Moreover, it is used for the demolition of large quantities of toxic pollutants (Gogate and Pandit 2004). The Fenton process has effectively and efficiently removed the drugs to concentration below the detection limit (Velasquez et al. 2014; Mackulak et al. 2015). Besides, it has been used as a pre-management to increase the biodegradability of pollutants, specifically in the handling of concentrated wastewaters comprising recalcitrant compounds. Fenton reagent contains Fe^{2+} and H_2O_2 where Fe^{2+} is used as a catalyst and H_2O_2 used as an oxidant. The mechanism of the reaction (Eq. 5.1) is given below:

$$Fe^{2+} + H_2O_2 \rightarrow Fe^{3} + OH^{\cdot} + OH^{-} \tag{5.1}$$

Fenton reaction-produced $^{\cdot}OH$ radical have been utilized to treat an extensive range of harmful organic compounds, comprising landfill leachates (7), groundwater contaminated with chlorinated aliphatics and aromatics (8, 9), dry cleaning solvents (10, 11), PCB congeners (12), nitroaromatic compounds (13, 14), azo dyes (15), and PCP (16). The Fenton reaction is autocatalytic under acidic condition (Halliwell and Gutteridge 1986). In $^{\cdot}OH$ reaction working at pH > 5, the constant adding of Fe

(II) also consequences in the formation of huge amount of particulate Fe(III), which subsidizes to slurry discarding difficulties (Kim and Vogelpohl 1998).

5.2 Classification of Fenton Process

In order to increase the efficacy of classical Fenton, it is combined with other techniques such as electrochemical, photocatalytic, and ultrasonic waves. Figure 5.1 depicts the classification of Fenton process, and Table 5.1 gives an idea about various types of Fenton process for the degradation/removal of pollutant. The detailed discussion is discussed below.

5.2.1 Homogeneous Fenton Process

Tabai et al. (2017) studied the homogeneous Fenton reaction toward the deprivation of Acid Orange 7 (AO7) dye in aqueous solution using hydrogen peroxide by $HFe_{2.5}P_2W_{18}O_{62}$ $23.H_2O$ as a catalyst. They have examined the factors like pH, H_2O_2 concentration, the catalyst mass, and the concentration of the dye on the degradation. The operational pH range of the Fe(III)/H_2O_2 system was extended up to pH 8.5 using phosphotungstate $\left(PW_{12}O_{40}^{3-}\right)$ for the deprivation of organic compounds by homogeneous Fenton process (Lee and Sedlak 2009). It should be

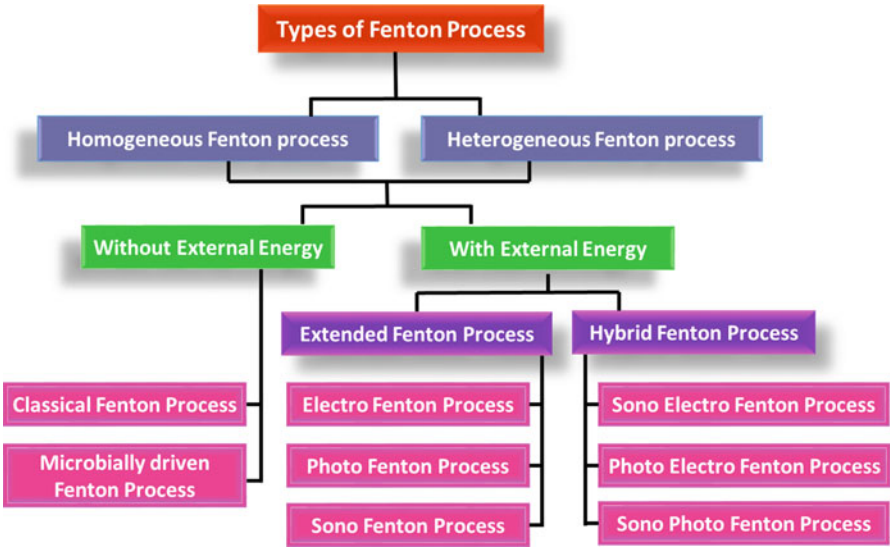

Fig. 5.1 Graphical illustration of classification of Fenton process

Table 5.1 Various types of Fenton process for the degradation/removal of pollutant

Pollutant	Category	Type of catalyst	Experimental condition	Source of energy	Remarks and findings	References
Acid Blue 113	Visible light photo-Fenton process	$MoS_2/MnFe_2O_4$	pH 6.3; 0.6 ml H_2O_2, 6.59 mg MoS_2/$MnFe_2O_4$; 25 mg L^{-1} dye	50 W white light-emitting diode (LED) lamp	99% of the dye was removed at 42 min	Samakchi et al. (2018)
α-Methylphenylglycine (α-MPG)	Solar photo-Fenton and solar photoelectro-Fenton	Fe(II)	500 mgL^{-1} α-MPG; pH 2.8–3; 25 °C; 36.3, 72.5 and 145.0 mM H_2O_2; 10 mg L^{-1} Fe^{2+}	Irradiance from 1000 W m^{-2} at noon to 400 W m^{-2} at 5 pm	70% and 90% of TOC by solar photoelectro-Fenton and solar photo-Fenton process, respectively	Serra et al. (2011)
Reactive Blue 19 (RB19)	Solar photo-Fenton process	La and Ce doped hydroxyl FeAl intercalated montmorillonite (FeAl-Mt)	RB19 of 0.12 mM, 14.7 mM H_2O_2, catalyst dosage 0.5 g L^{-1}, pH 3.0	Sunlight	Optimum amount of the doped Ce or La for the enhancement of the catalytic reactivity is 1.0%	Huang et al. (2014)
Methylene blue	Visible and solar photo-Fenton process	Fe–Ni/SiO_2	H_2O_2 3.0 mM L^{-1}; 0.85 g L^{-1} of Fe–Ni/SiO_2; pH 3; MB of 20 mg L^{-1}	Simulated solar light λ =300–800 nm; visible light intensity 115.5 mW cm^{-2}	Degradation and TOC efficiency are 99.80% and 86.19% under solar light; 99.01% and 75.71% under visible light	Ahmed et al. (2016)
Benzene, toluene, ethyl benzene and xylene, (BTEX) in waste gas	UV-Fenton process	Fe(II)	pH 3; H_2O_2 5.6 mmol L^{-1}; Fe^{2+}/H_2O_2 molar ratio 0.091; benzene, toluene, ethyl benzene, and o-xylene (C_{inlet} = 420, 683, 430, and 844 mg m^{-3}, respectively	UV lamp 40 W, λ at 254 nm	Removal efficiencies of benzene, toluene, ethyl benzene, and o-xylene were always maintained above 84%, 92%, 96%, and 97%, respectively, in 240 min	Wang et al. (2018)

Methylene blue	UV light photo-Fenton process	Graphite carbon coating hollow $CuFe_2O_4$ spheres	30 mg L^{-1} MB; 10 mg of catalyst; 0.2 mL H_2O_2	300 W UV-curing lamp ($\lambda > 400$ nm)	97% MB degradation	Guo et al. (2017)
Methylene blue and methyl orange (MO)	Solar photo-Fenton process	Fe/Al_2O_3–MCM-41	10^{-5} M of H_2O_2; pH 11; 100 mg L^{-1} MB; catalyst 1.0 g L^{-1}	Sunlight (light intensity 104,000 Lx)	Degradation and TOC for MB are 100% and 83%, and MO is 50% and 35%	Pradhan and Parida (2012)
Orange II	Sono-Fenton process	4A-zeolite supported α-Fe_2O_3 (Fe-4A)	Fe-4A 0.5 g/L; 10 mg/L of Orange II; no H_2O_2; ultrasound at a frequency of 40 kHz; 100 W	–	Fe-4A composite, with a practical α-Fe_2O_3 content of 24.9%, shows the maximum sono-Fenton reactivity to Orange II	Chen et al. (2010)
Industrial textile wastewater	Sono-Fenton process	Fe (II)	0.05 g L^{-1} of Fe (II); 1.65 g L^{-1} H_2O_2; pH 3; ultrasound at a frequency of 40 kHz	–	99% of decolorization at 60 min and 90 min for COD	Cetinkaya et al. (2018)
Reactive Orange 107 (RO107)	Sono-Fenton process	Fe_3O_4	0.8 g/L of Fe_3O_4; pH 5; 10 mM of H_2O_2; 300 W/L ultrasonic power; 100 mg/L of RO107	–	87% mineralization and COD is reduced from 2360 mg/L to 489.5 mg/L at 180 min	Jaafarzadeh et al. (2018)
Tri(2-chloroethyl)phosphate (TCEP)	Microwave-heterogeneous Fenton process	Iron oxide containing waste	100.0 mL TCEP; H_2O_2 and iron; MW frequency of 2450 MHz	–	TOC was 98.8% after 35 min reaction	Exposito et al. (2017)
Orange II	Heterogeneous Fenton process	Carbon-Fe	0.1 mM of Orange II; 30% of 6 mM H_2O_2; 30 °C; Catalyst 0.2 g/L;	–	Mineralization degrees as high as 90%	Ramirez et al. (2007)

(continued)

Table 5.1 (continued)

Pollutant	Category	Type of catalyst	Experimental condition	Source of energy	Remarks and findings	References
Phenol	Electro-Fenton process	Iron foam	working electrode PTFE-CC; counter electrode (Pt sheet 20 cm^2; Ag/AgCl reference electrode; scan rate of 10 mV s^{-1}; 50 mM TPP electrolyte; H_2O_2 (30%); Fe-F 0.5–4 g L^{-1}; phenol 1.4 mM; pH 6; airflow rate 0.50 L min^{-1}	–	56.25% degradation was achieved in 60 min	Deng et al. (2018)
Carbamazepine	Microbial electro-Fenton process	Fe-Mn catalyst	CBZ 5, 8, and 10 mg/L; acetate 300, 600, 800, and 1000 mg/L; voltage output of >20 mV; 30 °C; 5 g/L Na_2SO_4; resistance of 10 Ω	–	The CBZ removal rate in the MeFC was 10–100 times faster than that in other biological treatment processes	Wang et al. (2018)
Industrial electronics wastewater	Electro-Fenton process	Graphene-based gas diffusion cathode	29 mA cm^{-2}, 0.2 mM of Fe^{2+} and 0.2 L min^{-1} airflow; PTFE-CC-GDE cathode; platinum sheet anode; current density 14–-57 mA cm^{-2}; 50 mM K_2SO_4; pH 3	–	80% of mineralization of electronics wastewater in 180 min	Rodriguez et al. (2018)

Phenol	Electro-Fenton process	Iron electrodes and activated carbon	250 mg/L of phenol; electrical conductivity 125 μS/cm; stirring speed 100 rpm, current density 0.8 mA/cm^2 and inter-electrode gap 4 cm; pH 3; 2 mM Na_2SO_4	–	COD and TOC removals is 84% and 75%	Khatri et al. (2018)
Acetylsalicylic acid	Electro-Fenton process	Gas diffusion electrode with carbon nanotube	pH 3; 100 mA; 0.05 mM Na_2SO_4; catalyst layer was 0.15 g CNT and 93.75 mL PTFE; flow rate 0.25 L min^{-1}	–	Degradation 100% after 10 min and TOC 62% at 1 h	Yang et al. (2018)
Carbamazepine (CBZ)	Sono-photo-Fenton process	Ferrioxalate complex	H_2O_2 150 mg/L; Fe^{+2} 2.5 mg/L/ $[(COOH)_2 = 12.1$ mg/L; pH 5; 3. 15 mg/L of CBZ; ultrasound at a frequency of 20 kHz; 1000 W	Solar light	80% of TOC was removed	Exposito et al. (2018)
C.I. Acid Orange 7 (AO7)	Sono-photo-Fenton process	Fe_2O_3/SBA-15	pH 2; AO7 100 mg L^{-1}; 8 mmol L^{-1} H_2O_2 (30%); [Fe_2O_3/SBA-15] = 0.3 g L^{-1}; ultrasound at a frequency of 20 kHz,: 80 W	The UV light tube; 4 W; λ =254 nm	COD removal 32.6% and decolorization efficiency is 84.9%	Yan et al. (2016)
Phenol	Sono-photo-Fenton process	Crystalline hematite embedded on a mesostructured SiO2	$FeCl_3$.6H2O; silica; 22 °C; 35 mM H_2O_2; ultrasound at a	Mercury lamp; 150 W; λ =313 nm	90% TOC reduction are achieved	Segura et al. (2009)

(continued)

Table 5.1 (continued)

Pollutant	Category	Type of catalyst	Experimental condition	Source of energy	Remarks and findings	References
		support (Fe_2O_3/SBA-15)	frequency 20 KHz; power 0.13 W/mL			
Azure-B	Sono-photo-Fenton process	$FeCl_3$	pH 1.5–2.7; 1.33×10^{-4} M azure-B; 5×10^{-4} M $FeCl_3$; ultrasound at a frequency of 40 kHz; 0.5 mL H_2O_2	Tungsten lamp; light intensity 75.5 mW cm^{-2}; 200 W	The photochemical decomposition rate of azure-B is markedly increased in the presence of ultrasound	Vaishnave et al. (2014)
Bisphenol A (BPA)	Sono-photo-Fenton process	$FeSO_4.7H_2O$	100 ppm of BPA: H_2O_2 30%; $FeSO_4.7H_2O$; pH 2; 0.36 mM $Fe2^+$, 7.85 mM H_2O_2; amplitude of the ultrasound wave 1.9 bar	Mercury UV lamp; λ =365 nm	Strong convection generated by ultrasound and cavitation assists enhancement of interaction between BPA molecules and radicals generated through Fenton reactions. UV radiation can break the Fe(III)-hydroxy complexes to generate extra OH radicals	Chakma and Moholkar (2014)
Sodium alginate (NaAlg)	Sono-photo-Fenton process	TiO_2 NPs + Iron sulfate heptahydrate	pH 2.9; 25 °C; 0.35 g/L of H_2O_2 (30%); 0.05 mmol of iron sulfate heptahydrate; 0.05 to 0.5 gL^{-1} TiO_2; 10 gL^{-1}; ultrasound power 150 W	UV reactor;100 W; λ = 365 nm	Reaction order of NaAlg degradation (n) is 0.51	Zhou et al. (2017)

Municipal wastewater effluent containing antipyrine	Sono-photo-Fenton process	$FeSO_4.7H_2O$ (Panreac)	pH 2.7; 500 mg L^{-1} H_2O_2; 27 mg L^{-1} of Fe (II); ultrasound at a frequency 24 kHz, power 200 W	Heraeus UV Hg immersed lamp TNN 15/32; 15 W, λ =254 nm	TOC removal was 79% in 50 min	Exposito et al. (2017)
Di-n-butyl phthalate (DBP)	Sono-photo-Fenton process	$FeSO_4.7H_2O$	pH (2–9); Fe^{2+} (0–0.5 mM); 0.01 mM DBP; ultrasound at a frequency of 400 kHz; power 0.03 W mL^{-1}	Monochromatic UV light at 254 nm	The optimal dosage of Fe^{2+} is 0.1 mM at lower pH	Xu et al. (2014)
Bisphenol-A (BPA)	Sono-photo-Fenton process	$LaFeO_3$ perovskite	H_2O_2 of 2.38 mM; pH 6.7; ultrasound at a frequency of 20 kHz; 40 W; 15 ppm of BPA; 0.5 g/dm^3 $LaFeO_3$	Visible light lamp; 150 W	Degradation degree and a chemical oxygen demand (COD) reduction of 21.8% and 11.2%	Davididou et al. (2017)

noted that the homogeneous Fenton method has a substantial drawback: the reactions require up to 50–80 ppm of Fe ions in solution, which is higher the European Union instructions that permit only 2 ppm of Fe ions in processed water to be discarded into the surroundings (Sabhi and Kiwi 2001). The treatment has to be done at acidic pH conditions especially between 2.5 and 3.5. There is a possibility of unwanted side reaction and the disintegration of H_2O_2 to water and oxygen (Hartmann et al. 2010). The exclusion/management of the sludge-comprising Fe ions at the end of the contaminated water management is costly and necessities huge quantity of chemicals and manpower. Moreover, catalyst recycling is challenging.

5.2.2 Heterogeneous Fenton Process

To overcome the drawbacks of homogeneous Fenton reaction, the heterogeneous Fenton reaction has been developed. Different types of heterogeneous catalyst are used in Fenton reaction such as ferrihydrite, hematite, pyrite ash, goethite, electric arc furnace dust, magnetite, clay, pyrite, etc. Some attempts have been made by combining Fe ions or Fe oxides into inert support or the porous materials such as clay (Hassan and Hameed 2011), carbon material (Ramirez et al. 2007), mesoporous silica (Pham et al. 2009), alumina (Lim et al. 2006), zeolite (Arimi 2017), etc. so that the catalyst ions are slowly released from the support to the reaction sites. The heterogeneous catalysts are simply detached from the waste and slurry for recycle. The catalyst works over a wide range of pH. For example, carbon materials were utilized as a support for the deprivation of azo dye Orange II where activated carbon which is prepared from olive stone and carbon aerogel (Ramirez et al. 2007). The results revealed that carbon aerogel have shown good catalytic performance and mineralization effect than activated carbon. The technical complication and high budget production limits the large scale application of the catalyst. So as to increase the catalytic performance and economic value, Fe_3O_4 magnetic nanoparticles have been incorporated with activated carbon resulting from the recycled rice straw for the treatment of real coal gasification wastewater (Zhuang et al. 2016). The size and shape, crystallization, surface area, active site of the catalyst, reaction temperature, pH, and concentration of the contaminant are the main factors to determine the reaction rate (Kaviya and Prasad 2015; Arimi 2017; Hassani et al. 2018c). Heterogeneous Fenton catalyst was developed using pellets of natural zeolite which is modified by pre-treatment before inserting on them on Fe^{2+} ion (Arimi 2017). The catalyst is used for the exclusion of colored recalcitrant in molasses distillery wastewater (MDW). The effect of pH and temperature on the reaction also examined. The catalysts have shown 90% decolorization and 60% total organic carbon (TOC) elimination at 150 g/L catalyst dosage, 2 g/L H_2O_2 at 25 °C. Moreover, it is improved in the biodegradability of anaerobic effluent. Different shapes of the catalyst also used for the better performance. Ultra-small α-FeOOH nanorod have been utilized for the degradation of an azo dye, methyl orange and observed 98% of the degradation (Liu et al. 2018) which is relatively higher than the large sized

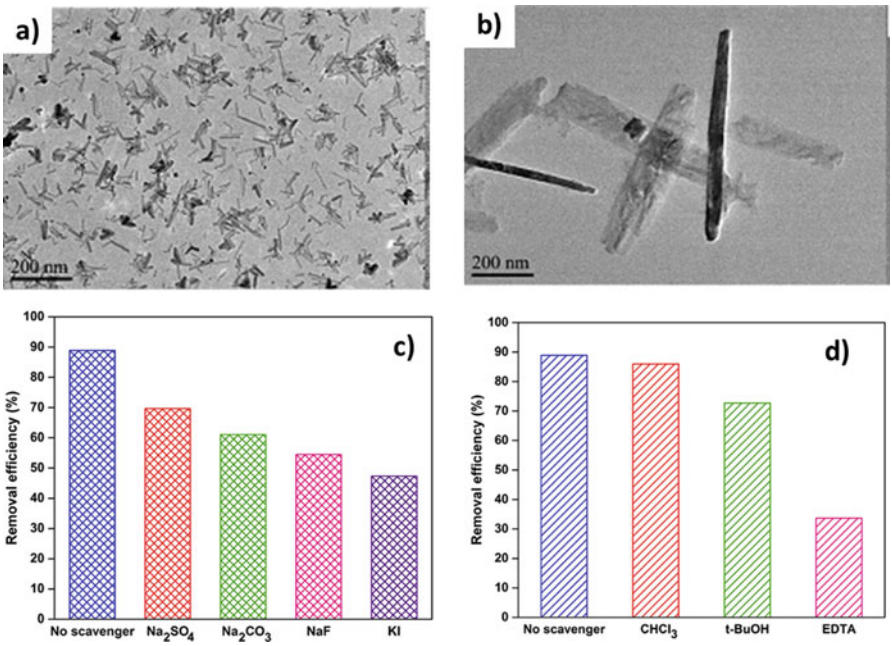

Fig. 5.2 Transmission electron microscopic image of (**a**) small α-FeOOH nanorod (**b**) large α-FeOOH nanorods, the effect of (**c**) inorganic and (**d**) organic scavengers on the removal of ciprofloxacin by heterogeneous Fenton process. (Liu et al. 2018; Hassani et al. 2018c)

α-FeOOH nanorods (Fig. 5.2a, b). The effect of ball milling time on the performance of magnetite (Fe_3O_4) nanoparticle toward the removal of ciprofloxacin (CIP) was studied by Hassani et al. (2018c). Furthermore, they have discovered that the incorporation of organic and inorganic scavengers significantly decreased the CIP removal efficacy (Fig. 5.2c, d).

The critical issue in the heterogeneous catalyst is leaching of ion from the support. Interestingly, the catalyst with higher catalytic performance, stability at a realistic cost. In order to enhance the pollutant degradation efficacy, exterior energy in the form of UV, sunlight, electricity and ultrasound are combined with the classical Fenton process.

5.2.3 Microbially Driven Fenton Reaction

Microbially focused Fenton reactions established on fabrication of H_2O_2 through microbial O_2 respiration and Fe(II) by microbial Fe(III) reduction which excludes the addition of H_2O_2 and UV radiation to recreate Fe(II) (Kim et al. 2006; Stefan and Bolton 1998). Figure 5.3 represents the overall strategy in the microbially focused Fenton Reaction. H_2O_2 basically generated by aerobically respiring bacteria through

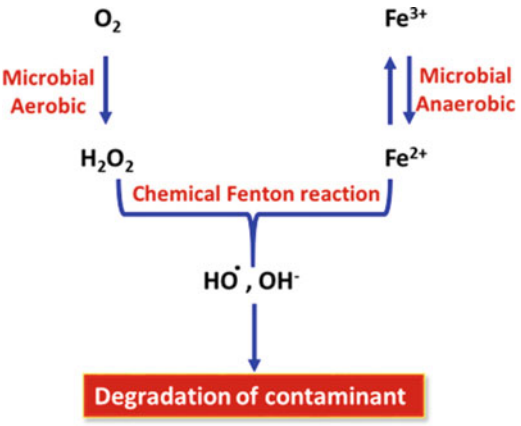

Fig. 5.3 Overall scheme for the microbially driven Fenton reaction

O_2 stimulation pathway (Eqs. 5.2 and 5.3) and also by Fe(II) autoxidation pathway under aerobic condition (Eqs. 5.4 and 5.5) (Stumm and Morgan 1996) which is given below. A. M. Mckinzi and T. J.

DiChristina examined the oxidative degradation of pentachlorophenol using *Shewanella putrefaciens* strain 200 under neutral pH condition. The microbe is acted as a catalyst for Fe(III) reduction and H_2O_2 fabrication by flashing amid anaerobic and aerobic situations in batch cultures accompanied with Fe(III). The scheme was established on a free radical-producing Fenton reaction among bacterially manufactured Fe(II) and H_2O_2 (Mckinzi and DiChristina 1999). In another work, Sekar and T. J. DiChristina scrutinized the generation of OH radical by *S. oneidensis* focussed Fenton reaction for the degradation of 1,4-dioxane. Here, Fe(II) formed through anaerobic phases interacts chemically by the Fenton reaction with H_2O_2 formed in aerobic phases to yield OH radicals that oxidatively degrade 1,4-dioxane (Sekar and DiChristina 2014). Gu and his research group studied the degradation of Tetrabromobisphenol using biogenic Fenton process by *Pseudomonas* sp. Fz through extracellular H_2O_2 and Fe(II) (Gu et al. 2016). Research have performed microbial degradation of organic contaminant in anaerobic circumstances, and the deprivation rates in nitrate-, iron-, and sulfate-reducing situations are remarkably slow (Steffan 2007). Moreover, studies revelled that the direct application of the reagent to microbes leads their cell death by the attack of radicals (Miller et al.1996).

$$O_2 + e^- \rightarrow O_2^{\cdot -} \tag{5.2}$$

$$O_2 + O_2^{\cdot -} \rightarrow H_2O_2 \tag{5.3}$$

$$Fe(II) + O_2 \rightarrow Fe(III) + O_2^{\cdot -} \tag{5.4}$$

$$Fe(II) + O_2^{\cdot -} + 2H^+ \rightarrow H_2O_2 + Fe(III) \tag{5.5}$$

5.2.4 *Photo-Fenton Process*

Heterogeneous Fenton process having the limitations such as decrease in the concentration of iron ion and the formation of hydroxide radical rely on Fe^{3+} and H_2O_2 reaction (Zhao et al. 2010).

The process of coupling light energy (UV or visible or sunlight) with classical Fenton process is called photo-Fenton process (Senn et al. 2014) (Fig. 5.4). It, overcoming the limitations from classical Fenton process by irradiation of light energy, increases the efficacy of Fenton reaction owing to renewal of the consumed Fe^{2+} ions and direct H_2O_2 photolysis (Ruppert et al. 1993). Figure 5.5 depicts the photochemical renewal of Fe^{2+} ions by photoreduction of Fe^{3+} ions under UV radiation (Faust and Hoigne 1990). In photo-Fenton process, Fe ions, Fe oxides, and Fe clusters may act as active sites, whereas in Fenton process, Fe ions are deliberated as principal active sites.

Iron and Iron oxide NPs have been utilized as a catalyst for heterogeneous photo-Fenton reaction for the degradation of various organic dyes (Zhao et al. 2013; Pradhan et al. 2013). The activity of the catalyst was enhanced by loading nanoparticles (Fe and Iron oxide) into mesoporous materials. Studies have been performed with Fe_3O_4@SiO_2 (Tan et al. 2015), Fe_3O_4@-rGO@TiO_2 (Yang et al. 2015), $FePO_4$ (Gao et al. 2015), α-Fe_2O_3-TiO_2 (Shao et al. 2015), Fe/MCM-41 (Lam and Hu 2007), Fe/Al_2O_3-MCM-41 (Pradhan and Parida 2012), etc. Fe-like metals such as mono- (Mn, Co, Fe) and bimetallic (Mn-Fe, Mn-Co, Co-Fe) nanoparticles are added into the mesoporous system for the degradation of dyes and mixture of dyes. Pradhan et al. examined the catalytic performance of Co-Fe/Al_2O_3-MCM-41 nanocomposite for the degradation of Methylene blue + Congo red at pH 10 under visible light irradiation. The catalyst has shown 100% of degradation efficacy in 60 min (Pradhan et al. 2016). Bimetallic iron-copper catalyst also attracted much attention. The mixture of iron with copper displays an enhanced catalytic activity synergic effects of two metal-redox pairs (Qin et al. 2018). In photo-Fenton process,

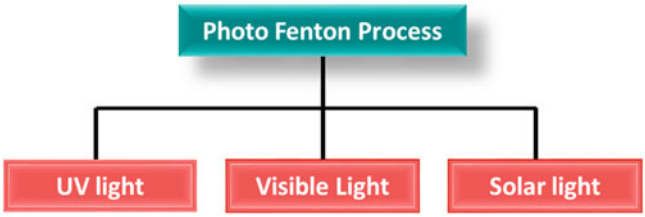

Fig. 5.4 Classification of photo-Fenton process

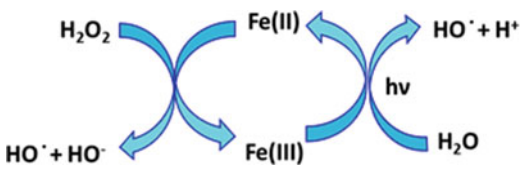

Fig. 5.5 Photo-Fenton reaction

the presence of suspended matter affects the penetration of light radiation and there by decrease the removal efficiency. The viability of photo-Fenton reaction depends on the intensity, wavelength of radiation, distribution of light inside the photoreactor, and catalyst.

UV Photo-Fenton Process

The recovery of Fe^{2+} via classical Fenton process is tremendously low (Minella et al. 2014). The regeneration of Fe^{2+} and more number of OH radical formation are possible only under UV light irradiation (Ramirez et al. 2010). UV radiation is commonly utilized in the water treatment and for the removal of contaminant from the wastewater. UV-Fenton and modified UV-Fenton process was examined in the real drilling wastewater at pH 3 and neutral pH, respectively, by Chen et al. (2016). In this study, they have utilized carboxymethyl β-cyclodextrin (CMCD) as a biodegradable complexing agent instead of commonly used ethylenediaminetetraacetic acid (EDTA) which could cause the secondary environmental risk. The results revealed that the UV-Fenton process with CMCD was measured more appropriate for biological oxidation process, owing to the lower intake of H_2O_2. UV radiation is categorized as vacuum UV (100–200 nm), UV-C (200–280 nm), UV-B (280–315 nm), and UV-A (315–400 nm). Light-emitting diode (LED)-based artificial illumination of UVA radiation was also used for the exclusion of micropollutant from wastewater which eliminates the influence of environmental conditions and annual solar light (Davididou et al. 2017). Obra et al. (2017) utilized UVA light from LED for the removal of micropollutant from urban contaminated water. They have studied with three different wavelengths (365, 385, and 400 nm), two different liquid depths (5 and 15 cm), and two iron concentrations (5 and 11 mg L^{-1}) for two different liquid depths (5 and 15 cm). Similarly, the effect of reaction circumstances like pH, H_2O_2 concentration, and $[H_2O_2]/[Fe^{2+}]$ ratio was examined for the degradation of dyes using UVC radiation (Manu and Mahamood 2011). The UV-based AOP reactions are based on the external chemicals which are considered as a limiting actor for their applications. Utilization of vacuum ultraviolet (VUV) radiation is a less chemical process, and radicals are formed from the photolysis of water (Eqs. 5.6 and 5.7) (Gonzalez and Braun 1995). Additionally, VUV light generates ozone by the photolysis of molecular oxygen which would enhance the removal of pollutant (Eqs. 5.8 and 5.9) (Moussavi et al. 2014).

$$H_2O \underset{h\nu=185\ nm}{\rightarrow} {}^{\cdot}OH + H^{\cdot} \tag{5.6}$$

$$H_2O \underset{h\nu=185\ nm}{\rightarrow} {}^{\cdot}OH + H^{+} + e^{-}_{eq} \tag{5.7}$$

$$O_2 \underset{h\nu=185\ nm}{\rightarrow} 2O^{\cdot} \tag{5.8}$$

$$O^{\cdot} + O_2 \rightarrow O_3 \tag{5.9}$$

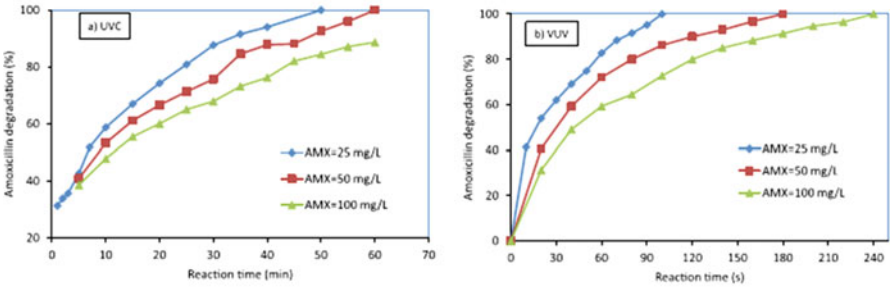

Fig. 5.6 Effect of amoxicillin initial concentration on its deprivation in (**a**) UVC and VUV (**b**) processes as a function of reaction time (pH7). (Pourakbar et al. 2016)

The performance of VUV-based photo-Fenton process was examined toward various natural and organic contaminants. Comparative study also performed to analyze the efficiency of VUV and UVC radiation toward the degradation and mineralization of amoxicillin (AMX) which is an antibiotic (Pourakbar et al. 2016) (Fig. 5.6). The results have shown that the deprivation of AMX has happened in 3 min or VUV process when compared to UVC. Moreover, the removal efficacy depends on the pH, and higher rate was accomplished at higher pH.

Visible Photo-Fenton Process

Unluckily, only 4–5% of sunlight contains UV light, and 45% is visible light energy (Hou et al. 2013). Adaptation of visible light is cheap when using light source to generate UV radiation. Hence, visible light energy-mediated photo-Fenton process is contemplated for the degradation of contaminant in the wastewater (Lv et al. 2010). Zinc ferrite ($ZnFe_2O_4$) is projected as a potential catalyst for the deprivation of contaminant because it is inexpensive and has a narrow band gap (1.9 eV) and peroxidase-resembling activity. Cai et al. investigated the heterogeneous photo-Fenton reaction using $ZnFe_2O_4$ catalyst for the deprivation of Orange II in water and visible light irradiation (Cai et al. 2016). Moreover, they have investigated the influence of pH, concentration of H_2O_2, dosage of the catalyst, and power of the light source on the deprivation of the dye. In order to enhance the performance of the catalyst under visible light, plasmonic material was incorporated with the photo-Fenton catalyst due to its surface plasmon resonance (Kaviya and Prasad 2015a, b). Liu and his research group investigated the performance of Ag/AgCl-Fe-sepiolite for the degradation of bisphenol A using visible light radiation (Liu et al. 2017). Ag/AgX nanomaterials lead the loss of photocatalytic efficiency owing to the charge recombination (Xu et al. 2016). Here, Ag/AgCl stimulate the charge transfer between Fe(III)/Fe(II) by encouraging photogenerated electrons and promoting the catalytic performance under visible irradiation. The catalyst has shown better catalytic activity than Ag/AgCl and Fe-sepiolite due to the synergistic effect and also the formation of active species such as $^{\cdot}OH$ radical and holes.

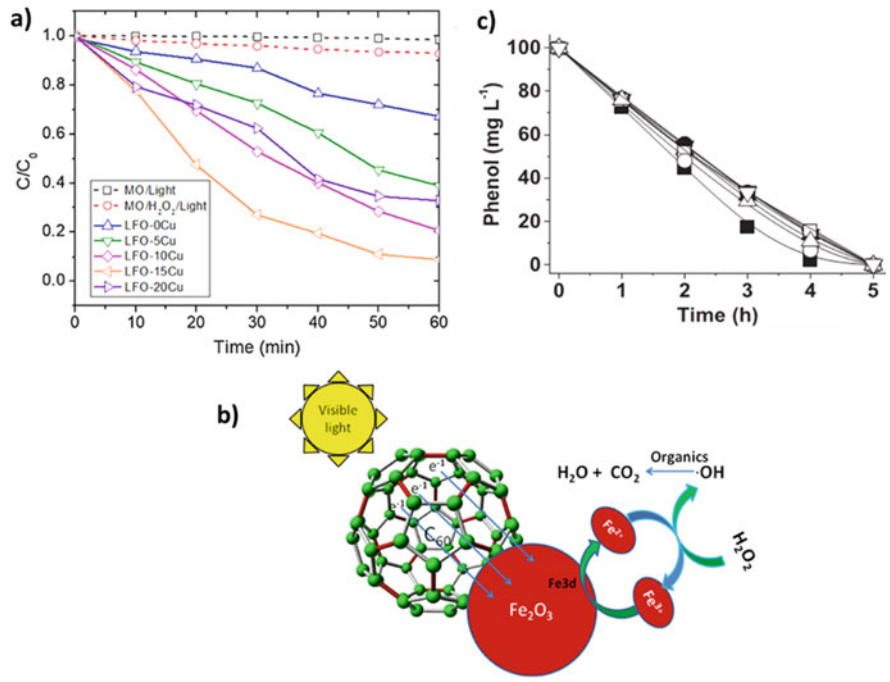

Fig. 5.7 (**a**) Photocatalytic degradation of methyl orange as a function of illumination time by using $LaFeO_3$ and Cu doped $LaFeO_3$; (**b**) schematic visible light-mediated photo-Fenton reaction mechanism of C_{60}-Fe_2O_3 catalyst; (**c**) Fe_{ox}/D3 catalyst reusability for phenol disappearance at pH 4 (recycled it for eight times). (Phan et al. 2018; Zou et al. 2018; Espinosa et al. 2018)

Cu doped $LaFeO_3$ was used for the complete decolorization of methyl orange, methylene blue, and rhodamine B solutions in visible light (Phan et al. 2018) (Fig. 5.7a). The perovskite oxide $LaFeO_3$ (XYO_3 structure) is extensively studied because of its nontoxicity, firmness, and small band gap energy. In order to improve the catalytic activity, replacing the element X and Y in the XYO_3 structure. Doping of metal into the perovskite oxide is not only reducing the band gap but also leads oxygen vacancy which prevent the recombination of charge carriers (Kaviya and Prasad 2015a). Fe_2O_3 is an n-type semiconductor with the band gap of 2.2 eV (Barroso et al. 2011). Fullerene [60] (C60) is a three-dimensional structure with delocalized electrons which allows a high electron mobility and absorbs weekly in the visible region. Moreover, it induces the charge separation and slows down the charge recombination (Li et al. 2013). The composite of C_{60}-Fe_2O_3 was used for the deprivation of methylene blue (MB), rhodamine B (RhB), methyl orange (MO), and phenol in the existence of H_2O_2 under visible light radiation over a wide range of pH (Zou et al. 2018). Furthermore, they have done the mineralization, leaching, and recycling experiments and achieved excellent catalytic performance due to the formation of ˙OH radical in the whole process (Fig. 5.7b). The main problem associated with the metal doping on the support are leaching of metal from the

support, poor stability under strong oxidation conditions and using of carbon materials as a support leads lower efficiency (Dhakshinamoorthy et al. 2012). Hence, developing a stable support which anchor and immobilize the dopant without decreasing the performance is a deal. Research have been performed by doping of Cu NP on diamond (D3) support as a heterogeneous photo-Fenton catalyst in visible irradiation (Espinosa et al. 2016). Though, the catalyst is deactivated upon recycle owing to the oxidation of the active reduced copper species to inactive Cu(II). Espinosa and co-worker have studied the immobilization of iron oxide NPs on the hydroxylated exterior of improved diamond nanoparticles (Espinosa et al. 2018). The catalyst has shown superior activity than iron oxide/TiO_2 and carbon materials such as activated carbon and graphite. Moreover, it exhibits comparable performance to Ag/D3 and higher stability and reusability than Cu/D3 (Fig. 5.7c).

Solar Photo-Fenton Process

Solar disinfection method is one of the processes in water treatment (Giannakis et al. 2016). Solar photo-Fenton process has been used for the removal of bacteria and micropollutants in contaminated water (Lonfat et al. 2016; Lasso et al. 2012). This technique is performed at neutral pH because acidic pH is toxic to the environs and the microorganism. Guzman et al. examined the removal of *Escherichia coli* and other micropollutants from municipal wastewater (Guzman et al. 2017). For this purpose, they have used mineral ions in place of iron salt and with natural organic acids such as citric, tartaric, ascorbic, and caffeic. Lime and orange juice are used as additives. Lime-based additives have produced photoactive compounds with more activity and led to the inactivation of bacteria after 48 h (Fig. 5.8a). The effect of solution pH and the catalyst, for example, Fe-citrate, was studied toward the inactivation of *Escherichia coli* (Lonfat et al. 2016). The bacterial inactivation rate i.e., the formation of OH radical is higher in the case of homogeneous photo-Fenton reaction when compared to heterogeneous photo-Fenton reaction using Fe-citrate complex at near neutral pH condition. Studies were investigated with stimulated solar light rather than natural sunlight where TiO_2 have used as a photocatalyst and resorcinol, hydroquinone were used as a natural organic matter for the degradation (Lasso et al. 2012). The reaction was carried out in the presence and absence of bacteria such as *Escherichia coli*, *Shigella sonnei*, *and Salmonella typhimurium*. The results revealed that the bacterial inactivation is less effected when organic maters are present in the medium. The parameters such as temperature, dosage of the reagent (iron, H_2O_2), pH, light irradiation, types of microorganism, and organic and inorganic materials present in the water determine the photocatalytic activity and inactivation of microorganism by the reaction. Experiment was performed to discover the effect of the above factors such as pH, concentration of the reagent, mechanical stress, and types of irradiation like UVA light in addition to the combined effects of UVA-Fe, solar-UVA, and UVA-H_2O_2 for the treatment of wastewater containing *Escherichia coli* and total coliforms (Gomez et al. 2014) (Fig. 5.8b). The complete disinfection was achieved by solar-UVA with H_2O_2.

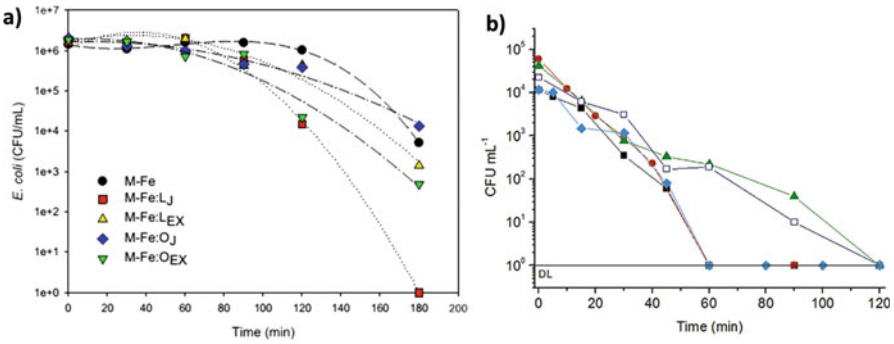

Fig. 5.8 (**a**) *E. coli* inactivation using solar photo-Fenton by a natural material of iron (M-Fe) and natural products (lime juice (LJ) and aqueous extraction (LEX); orange juice (OJ) and aqueous extraction (OEX)); (**b**) total coliforms inactivation by photo-Fenton replicas with secondary effluents of a municipal wastewater treatment plant attained on five different days over 1 year. (Guzman et al. 2017; Gomez et al. 2014)

Similarly, gram-positive bacteria, viruses, spores, protozoa, and fungi are incapacitated by photo-Fenton reaction (Ibanez et al. 2003; Lasso et al. 2008; Byrne et al. 2011). Moreover, this technique has been used for the degradation of dyes. For example, the deprivation of methylene blue was explored under visible and solar photo-Fenton process using Fe-Ni/SiO_2 catalyst (Ahmed et al. 2016). The results have shown that the degradation and total organic carbon (TOC) removal efficiency were greater in the case of sunlight irradiation compared to visible light.

5.2.5 *Electro-Fenton Process*

Electrooxidation/electrochemical oxidation is a favorable method for wastewater treatment owing to the simple operation, adaptability, and biocompatibility (Goyes et al. 2015). When compared to the classical Fenton process, it has the advantage of in-site incessant electrogeneration of H_2O_2, short reaction time, rapid degradation rate, and continuous Fe^{2+} renewal over cathodic reduction. In this method, organic molecules are oxidized by either direct oxidation, i.e., anodic oxidation on anodic surface, or indirect oxidation, i.e., electro-Fenton (EF). In direct oxidation method, $^{\cdot}OH$ radicals are produced via water oxidation on a high O_2 over voltage anode (Eq. 5.10). In the case of electro-Fenton process, $^{\cdot}OH$ radicals are produced by Fenton reagent.

$$H_2O \rightarrow {}^{\cdot}OH + H^+ + e^- \tag{5.10}$$

The electro-Fenton process comprises the addition of Fenton reagent to electrooxidation reaction (Altin 2008). Hence, the electrogenerated hydrogen

peroxide reacts with Fe^{2+} and leads the generation of $^{\cdot}OH$ radices. Electro-Fenton process is utilized for the removal of Acid Red 18 azo dye which is examined by Malakootian and Moridi (2017). They have examined the effects of various factors on the dye removal efficacy and achieved 99% and 90% removal efficacy for the synthetic and real sample, respectively (contaminated water from the Asia wool knitting factory). The comparative studies of Fenton process and electro-Fenton reaction were analyzed toward the phenol degradation (Gumus and Akbal 2016). They observed that the degradation and mineralization proficiency improved with an intensification in H_2O_2 concentration and current density and declined with an upturn in initial phenol concentration and pH. The outcomes directed that the classical Fenton process produces 59% mineralization, whereas electro-Fenton yields 93%. Additionally, the study showed that electro-Fenton reaction is additional reasonable for the treatment of phenol in contaminated water. EF process also utilized for the treatment of insecticide in water. For example, magnetic chitosan bead was used for the elimination of chlordimeform insecticide (Rezgui et al. 2018).

The effect of air pressure on the EF process was estimated by two organic substances such as malic acid and Acid Orange 7 (Perez et al. 2018). One set of the experiment was conducted by a conventional carbon felt as a cathode (Fig. 5.9a). They have observed a slow removal of malic acid along with the formation of formic acid. On the other hand, the exclusion of maleic acid was intensely accelerated, and the formation of formic acid was not sensed under pressurized air. They have achieved a rapid and almost greater than 95% elimination of TOC using the deposition of carbon black + polytetrafluoroethylene mixture and in the presence of pressurized air. In another work, graphene@graphite-based gas diffusion electrode (G-GDE) with good conductivity and an excellent electrocatalytic activity was made for the degradation of rhodamine B by EF process (Zhang et al. 2018). Further, they have compared the activity with graphite-based gas diffusion cathode (GDE) and graphite sheet cathode (GE) (Fig. 5.9b). The result demonstrated that, G-GDE electrode have shown excellent removal of the dye and low energy consumption due

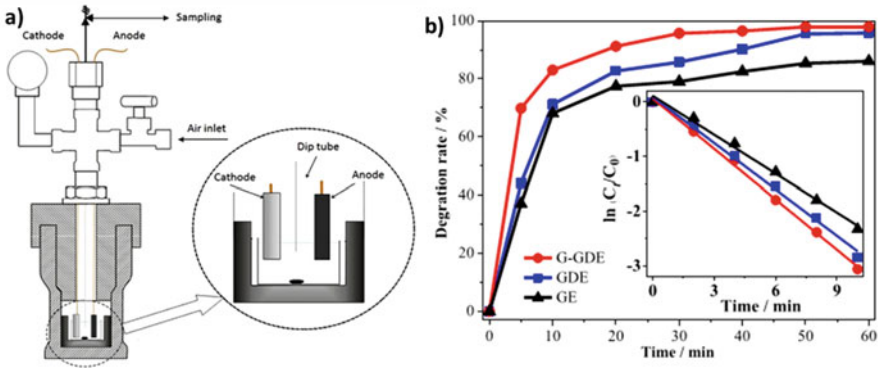

Fig. 5.9 (**a**) Graphical depiction of the pressurized reactor; (**b**) rhodamine B removal by G-GDE, GDE, and GE. (Perez et al. 2018; Zhang et al. 2018)

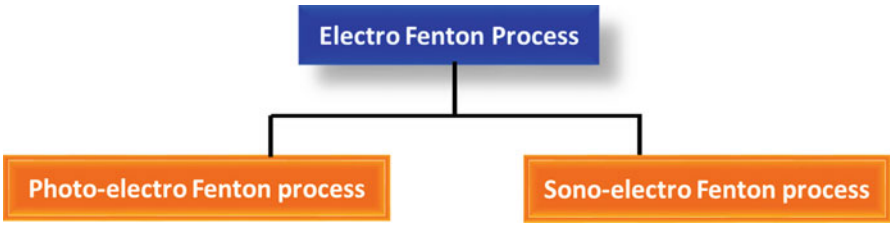

Fig. 5.10 Classification of electro-Fenton process

to its higher conductivity, porous nature and corrosion resistance when compared to other electrodes.

The efficacy of electro-Fenton process is increased by coupling with ultrasound and light energy. (Fig. 5.10).

Photoelectro-Fenton Process

The drawback of electro-Fenton process is the generation of Fe(III)-carboxylate complex which is difficult to rescind by $^{\cdot}OH$ radicals. It can be solved by irradiating the solution. This process is called as photoelectro-Fenton process. It leads to the enrichment of Fe^{2+} renewal and OH radicals generation via photoreduction of Fe $(OH)^{2+}$ and the photodecarboxylation of Fe(III)-carboxylate (Eqs. 5.11 and 5.12) (Huitle and Brillas 2015; Khataee et al. 2013).

$$Fe(OH)^{2+} + h\nu \rightarrow Fe^{2+} + {}^{\cdot}OH \tag{5.11}$$

$$Fe(OOCR)^{2+} + h\nu \rightarrow Fe^{2+}CO_2 + R^{\cdot} \tag{5.12}$$

Metal-organic frameworks (MOF) and modified MOF have been used for the effluent purification (Hasan and Jhung 2015) and electrocatalytic studies, for example, oxygen evolution reaction (OER) and oxygen reduction reaction (ORR) (Wang et al. 2014). In order to advance the ORR activity, numerous carbon materials such as activated carbon, graphite, carbon sponge, carbon aerogel, and gas diffusion electrodes are incorporated with MOF. Among them, carbon aerogel is a unique porous electrode which contains a three-dimensional network, high-surface area, and excellent electrical conductivity. Moreover, the addition of metal and organic linkers to MOF increases the absorption of solar light and enhances the photocatalytic performance (Zhang et al. 2015). By considering the above facts, Zhao and his research group (2017) worked on the photoelectro-catalytic performance of bifunctional MOF(2Fe/Co)/carbon aerogel as a cathode in acidic condition toward the degradation of rhodamine B and dimethyl phthalate (Fig. 5.11a). They observed that the addition of MOF increases the formation of H_2O_2, and the catalyst is independent of pH with excellent catalytic performance. Boron-doped diamond is used as an anode for the solar light-driven photo-Fenton (SPEF) reaction which is performed in

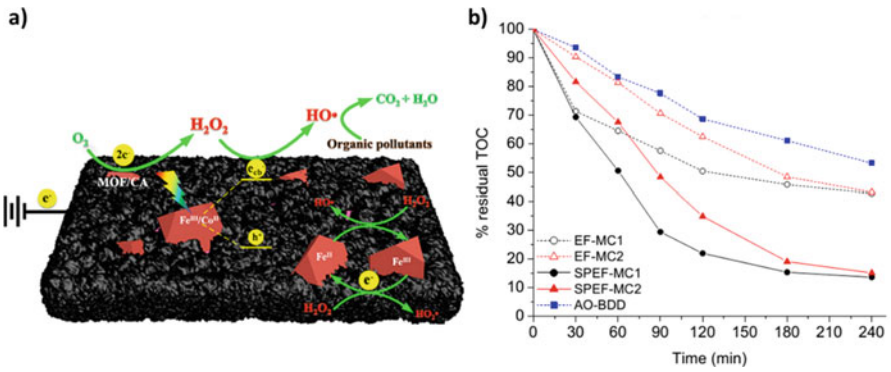

Fig. 5.11 (**a**) Graphical representation of solar-photoelectro-Fenton mechanism with MOF (2Fe/Co)/carbon aerogel cathode; (**b**) percentage of residual TOC by AO-BDD, EF, and SPEF toward the degradation of amoxicillin. (Zhao et al. 2017; Campos et al. 2018)

a batch cell rector (GilPavas et al. 2018) where titanium electrode is a cathode in nonpolar configuration (Fig. 5.11b). The utilization of boron-doped diamond as an anode having the features such as corrosion resistance, thermal stability, inert surface, hardness, low adsorption, electrical conductivity, and wide potential in aqueous and nonaqueous electrolytes (Montilla et al. 2002). The process yielded total decolorization, 83% of chemical oxygen demand (COD) reduction, 70% of total organic carbon (TOC) mineralization (in 15 min), and an extremely oxidized and biocompatible effluent. The operational cost is 1.56 USD/m^3 which is a cost-effective and proficient alternative for processing of industrial wastewater.

Campos et al. (2018) studied the performance of air diffusion mesoporous carbon electrode (ADE-MC) as cathode in electro-Fenton and photoelectro-Fenton process toward the deprivation of amoxicillin. The outcomes showed that the catalyst is good for *in-situ* electrogeneration of hydrogen peroxide. It gives the whole deprivation and mineralization percentages of 55% and 85% with electro-Fenton and solar electro photo-Fenton processes, respectively.

5.2.6 Sono-Fenton Process

Water molecules are produced ˙OH radical through cavitation phenomenon during sonication (Eq. 5.13) (Yang 2015). When we transmit the ultrasonic (US) waves into the solution, it produces microbubbles with high localized temperature and pressure (hot spot approach) (Weng et al. 2013). The volatile organic molecules are deprived by pyrolysis where the interior of the cavitation bubble is deprived at high temperature and the bubble liquid boundary by oxidation with ˙OH radicals. However, non-volatile compounds are ruined by oxidation with ˙OH radicals at the bulk liquid (Dukkanci 2018). Moreover, the catalyst surface is cleaned because of sonication. The sonication process has been used for the treatment of dyes and drugs (Kruger

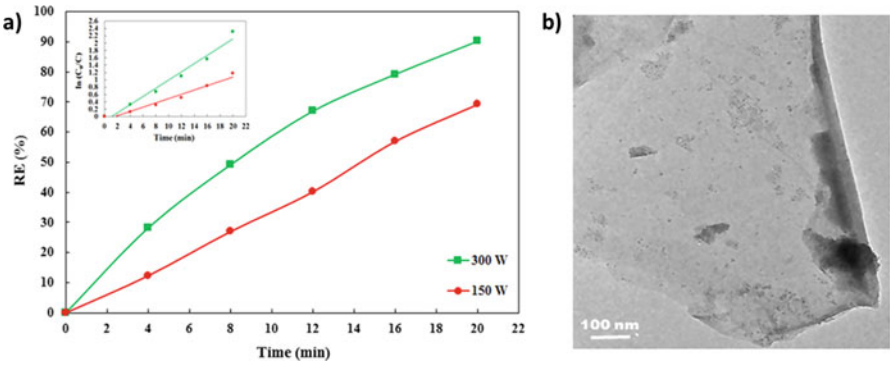

Fig. 5.12 (**a**) Impact of ultrasonic power on the removal efficiency of phenazopyridine; (**b**) TEM images of $CoFe_2O_4$-rGO nanocomposite. (Khataee et al. 2016; Hassani et al. 2018b)

et al. 1999). Conversely, it requires high energy due to its low deprivation rate and mineralization. Hence, it should be combined with Fenton process for the better performance (Zhang et al. 2009).

$$H_2O \overset{)))}{\rightarrow} {}^{\cdot}OH + H^{\cdot} \tag{5.13}$$

The plasma-modified clinoptilolite (PMC) nanorods were used for the treatment of phenazopyridine (PhP) (Khataee et al. 2016) by sono-Fenton method (Fig. 5.12a). Clinoptilolite is a zeolite which is extensively used in the AOP process due to cheap, nontoxic nature and low surface area which disturbs the mass transfer during the process (Chauhan et al. 2012). Moreover, they have examine the catalytic performance of PMC with natural clinoptilolite and found the greater activity with PMC. Magnetic nanoparticles were used for the treatment of contaminant by sono-Fenton process owing to the ease in the separation of catalyst from the system (Wang et al. 2015). The treatment of basic violet 10 (BV10) was employing by nano-sized magnetite (Fe_3O_4) using sono-Fenton process (Hassani et al. 2018a). The nano-sized magnetite (Fe_3O_4) particle was synthesized by milling of magnetite mineral by a high-energy planetary ball milling procedure. The results revealed that the catalyst has shown an excellent removal of BV10 due to ${}^{\cdot}OH$ radicals which are the main oxidative species and also with the presence of $O_2^{\cdot-}/HO_2^{\cdot}$ radicals. In another work, monodispersed magnetic cobalt ferrite ($CoFe_2O_4$) nanoparticle-reduced graphene oxide composite (Fig. 5.12b) was used for the elimination of organic dyes such as AO7, AR17, BR46, and BY28 from an aqueous solution by ultrasonic radiation (Hassani et al. 2018b). They have studied the effect of parameters, for example, pH, catalyst dosage, H_2O_2 concentration, concentration of the dye, ultrasonic power, and reaction time on the exclusion of dyes. The trapping experiments exhibited that $O_2^{\cdot-}$ radical is the main reactive oxygen species in the exclusion of dyes. Li et al. (2018) investigated the decolorization of rhodamine B ultrasound with Fenton process.

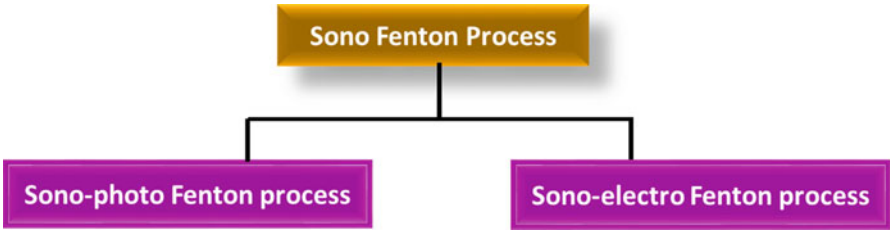

Fig. 5.13 Classification of sono-Fenton process

Here, they have used iron forms which having a porous structure. Conversely, the thermodynamic instability of iron in the company of H_2O and/or O_2 causes the oxidation and precipitation of iron on the surface (Kanel et al. 2006). Several reports suggest that the formation of passive layer is retarded in the presence of organic acids (Riverohuguet and Marshall 2009). Hence, they have executed a reaction with oxalic acid and iron foam which is anticipated to dissolve the oxides on the Fe^0 exterior and, subsequently, progresses its performance. The results show that $O_2^{\cdot}$ and H_2O_2 served a major role in the removal of rhodamine B. In order to develop the performance, sono-Fenton is further classified into sono-photo-Fenton process and sono-electro-Fenton process (Fig. 5.13).

Sono-electro-Fenton Process

The coupling among ultrasonic waves and in situ electro formation of Fenton reagent is called sono-electro-Fenton process. Enhancement in the sono-electro Fenton (SEF) method is owing to (i) enhanced mass transmission rate of both reactants (Fe^{3+} and O_2) at the cathode for the electrochemical formation of Fenton's reagent (Fe^{2+} + H_2O_2) and its transmission into the solution which further improve the reaction kinetics by growing the OH fabrication rate and speed up the demolition method, (ii) the extra formation of OH by sonolysis, (iii) pyrolysis of organics because of the cavitation produced by ultrasound waves (Oturan et al. 2008). Studied the sono-electrochemical supported Fenton reaction for the treatment of organic compounds such as herbicides 2,4-dichlorophenoxyacetic acid (2,4-D), 4,6-dinitro-o-cresol (DNOC), and azobenzene (AB). They have used an electrolytic cell with a Pt anode and a 3D carbon-felt cathode for an electro-Fenton (EF) process at constant current, which leads to the formation of excessive amounts of $^{\cdot}$OH radicals. Low- and high-frequency ultrasound waves were used for the process. The results demonstrated that the herbicides 4,6-dinitro-o-cresol (DNOC) and 2,4-dichlorophenoxyacetic acid (2,4-D) are considerably accelerated, whereas no enhancement is detected for the deprivation of the dye azobenzene (AB). The decomposition of reactive black (RB 5), removal of chemical oxygen demand (COD) (Sahinkaya 2013) and cationic red X-GRL (Li et al. 2010) from synthetic textile was conducted under various functioning settings by SEF process.

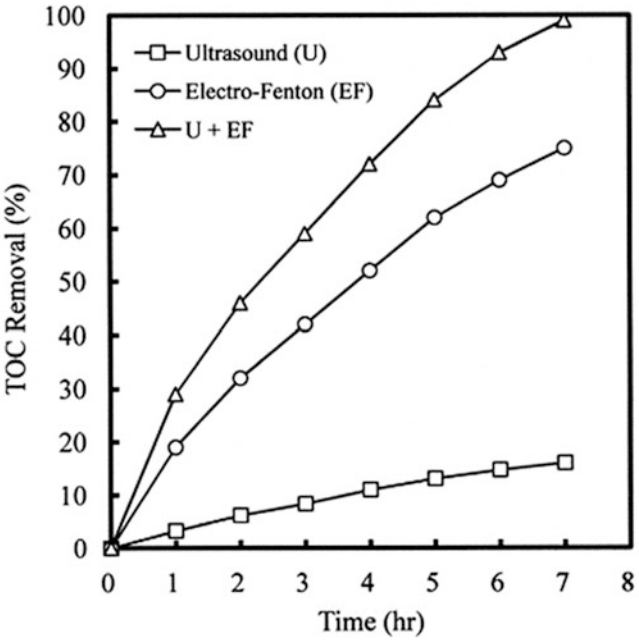

Fig. 5.14 Removal efficacy of total organic carbon by means of sonolysis, electro-Fenton, and sono-electro-Fenton processes. (Chen and Huang 2014)

Decomposition of dinitrotoluene (DNT) and 2,4,6-trinitrotoluene (TNT) in contaminated water is conducted by Chen and Huang (2014). Further, they have compared the performance by sono-electrochemical and sono-electro-Fenton reaction (Fig. 5.14). Also, examined was the impact of various parameters on the sono-electrolytic activity, such as electrode potential, Fe^{2+} dosage, sono-electrolytic temperature, acidity of wastewater, and O_2 dosage. They have observed the considerable improved mass transfer rate of oxygen to the cathode by ultrasonic waves which resulted in the excellent yield of H_2O_2. Hence, the sono-electro-Fenton reaction has shown better activity than the sono-electrochemical process.

Sono-photo-Fenton Process

The synergetic effect of sono-photocatalysis (US/UV) and sono-Fenton reaction (US/Fe^{2+}) has been effectively improved the degradation process by Fenton, photocatalyst and ultrasound by producing ore $^{\cdot}OH$ radical (Torres et al. 2007). Iron-loaded mesoporous silica (Fe_2O_3/SBA-15) was used as a heterogeneous catalyst for the decolorization of C.I Acid Orange 7 (AO7) by sono-photo-Fenton process (Zhong et al. 2011). They have investigated the effect of pH, US power,

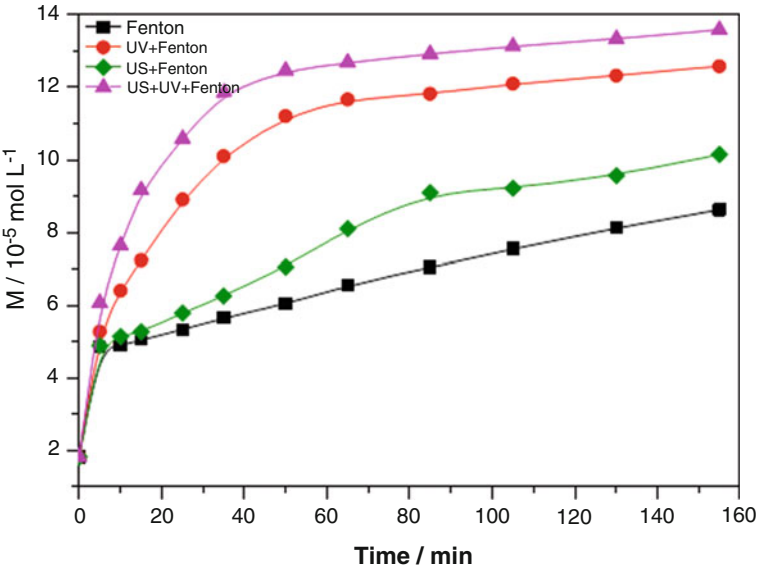

Fig. 5.15 Effect of different assist systems on sodium alginate deprivation during Fenton process. (Zhou et al. 2017)

Fe_2O_3/SBA-15 loading, and H_2O_2 concentration on the decolorization of the dye molecule. The results revealed that the efficacy of decolorization is amplified with the intensification of H_2O_2 concentration, US power, and the catalyst loading. In contrary, it reduced with rise of pH and the dye concentration. The performance of sono-photo-Fenton reaction was investigated toward the degradation of di-n-butyl phthalate (Xu et al. 2014). The study was performed with ultrasound at 400 kHz, UV radiation at 254 nm, and without using the external hydrogen peroxide.

They have found that US/Fe^{2+} process is improved the degradation of di-n-butyl phthalate and more proficient in utilizing Fe^{2+} related to the classical Fenton reaction. The degradation of high molecular weight sodium alginate was done by Zhou and his co-workers (2017) using TiO_2 nanoparticles (Fig. 5.15). Furthermore, they have compared the performance of the catalyst through sono-Fenton, sono-photo-Fenton, and photo-Fenton process. The results conclude that sono-photo-Fenton reaction provides an effective way for the degradation of sodium alginate into low molecular weight. Dukkanci (2018) has studied the sono-photo-Fenton reaction under visible light irradiation using $LaFeO_3$ as a catalyst for the oxidation of bisphenol A. The perovskite catalyst is with lower band gap than semiconductor photocatalyst. Hence, it could absorb the radiation in the visible region. The energy analysis shows that the energy consumption is high in this proses related to sono-Fenton and photo-Fenton reaction.

5.3 Conclusion

The performance of classical-Fenton and various hybrid Fenton processes on the degradation of contaminant in the wastewater was discussed, and their performance was compared. Compared to classical-Fenton process, hybrid methods have shown an excellent removal efficacy toward the contaminants. The experimental parameters such as initial pH, concentration of the dye, catalyst dosage, ultrasonic power, scavengers, H_2O_2 concentration, anode, cathode, and nature of light irradiation have shown an impact on the progress of the reaction. Conversely, a wide range of assessment is required because it can afford powerful economic and environmental assistance for the improvement of pilot-/industrial-scale Fenton processes.

Acknowledgments S.K. thanks SERB, Govt. of India, for SERB-National postdoctoral fellowship and Dr. S. Venugopal, Assistant professor, Department of Chemical Engineering, Indian Institute of Science (IISc), for his constant support.

References

Ahmed Y, Yaakob Z, Akhtar P (2016) Degradation and mineralization of methylene blue using a heterogeneous photo-Fenton catalyst under visible and solar light irradiation. Cat Sci Technol 6 (4):1222–1232. https://doi.org/10.1039/C5CY01494H

Altin A (2008) An alternative type of photoelectro-Fenton process for the treatment of landfill leachate. Sep Purif Technol 61(3):391–397. https://doi.org/10.1016/j.seppur.2007.12.004

Arimi MM (2017) Modified natural zeolite as heterogeneous Fenton catalyst in treatment of recalcitrants in industrial effluent. Prog Nat Sci Mater Int 27(2):275–282. https://doi.org/10.1016/j.pnsc.2017.02.001

Awual MR, Hasan MM, Naushad M et al (2015) Preparation of new class composite adsorbent for enhanced palladium(II) detection and recovery. Sensors Actuators B Chem 209:790–797. https://doi.org/10.1016/j.snb.2014.12.053

Barroso M, Cowan AJ, Pendlebury SR, Gratzel M, Klug DR, Durrant JR (2011) The role of cobalt phosphate in enhancing the photocatalytic activity of α-Fe_2O_3 toward water oxidation. J Am Chem Soc 133(38):14868–14871. https://doi.org/10.1021/ja205325v

Byrne JA, Ibanez PAF, Dunlop PSM, Alrousan DMA, Hamilton JWJ (2011) Photocatalytic enhancement for solar disinfection of water: a review. Int J Photoenergy 2011:798051–798063. https://doi.org/10.1155/2011/798051

Cai C, Zhang Z, Liu J, Shan N, Zhang H, Dionysiou DD (2016) Visible light-assisted heterogeneous Fenton with $ZnFe_2O_4$ for the degradation of Orange II in water. Appl Catal B Environ 182:456–468. https://doi.org/10.1016/j.apcatb.2015.09.056

Campos BG, Acosta DM, Ramirez AH, Mar JLG, Reyes LH, Manriquez J, Ruiz EJR (2018) Air diffusion electrodes based on synthetized mesoporous carbon for application in amoxicillin degradation by electro-Fenton and solar photo electro-Fenton. Electrochim Acta 269:232–240. https://doi.org/10.1016/j.electacta.2018.02.139

Cetinkaya SG, Morcali MH, Akarsu S, Ziba CA, Dolaz M (2018) Comparison of classic Fenton with ultrasound Fenton processes on industrial textile wastewater. Sustain Environ Res 28 (4):165–170. https://doi.org/10.1016/j.serj.2018.02.001

Chakma S, Moholkar VS (2014) Investigations in synergism of hybrid advanced oxidation processes with combinations of sonolysis + Fenton Process + UV for degradation of bisphenol A. Ind Eng Chem Res 53(16):6855–6865. https://doi.org/10.1021/ie500474f

Chauhan NL, Das J, Jasra RV, Parikh PA, Murthy ZVP (2012) Synthesis of small-sized ZSM-5 zeolites employing mixed structure directing agents. Mater Lett 74:115–117. https://doi.org/10.1016/j.matlet.2012.01.094

Chen WS, Huang CP (2014) Decomposition of nitrotoluenes in wastewater by sonoelectrochemical and sonoelectro-Fenton oxidation. Ultrason Sonochem 21(2):840–845. https://doi.org/10.1016/j.ultsonch.2013.10.026

Chen F, Li Y, Cai W, Zhang J (2010) Preparation and sono-Fenton performance of 4A-zeolite supported α-Fe_2O_3. J Hazard Mater 177(1–3):743–749. https://doi.org/10.1016/j.jhazmat.2009.12.094

Chen W, Zou C, Li X, Li L (2016) The treatment of phenolic contaminants from shale gas drilling wastewater: a comparison with UV-Fenton and modified UV-Fenton processes at neutral pH. RSC Adv 6(93):90682–90689. https://doi.org/10.1039/c6ra18662a

Davididou K, Monteagudo JM, Chatzisymeon E, Duran A, Exposito AJ (2017) Degradation and mineralization of antipyrine by UV-A LED photo-Fenton reaction intensified by ferrioxalate with addition of persulfate. Sep Purif Technol 172:227–235. https://doi.org/10.1016/j.seppur.2016.08.021

Deng F, Rodriguez OG, Vargas HO, Qiu S, Lefebvre O, Yang J (2018) Iron-foam as a heterogeneous catalyst in the presence of tripolyphosphate electrolyte for improving electro-Fenton oxidation capability. Electrochim Acta 272:176–183. https://doi.org/10.1016/j.electacta.2018.03.160

Dhakshinamoorthy A, Navalon S, Alvaro M, Garcia H (2012) Metal nanoparticles as heterogeneous Fenton catalyst. ChemSusChem 5(1):46–64. https://doi.org/10.1002/cssc.201100517

Dukkanci M (2018) Sono-photo-Fenton oxidation of bisphenol-A over a $LaFeO_3$ perovskite catalyst. Ultrason Sonochem 40:110–116. https://doi.org/10.1016/j.ultsonch.2017.04.040

Escher BI, Bramaz N, Richter M, Lienert J (2006) Comparative ecotoxicological hazard assessment of beta-blockers and their human metabolites using a mode-of-action-based test battery and a QSAR approach. Environ Sci Technol 40(23):7402–7408. https://doi.org/10.1021/es052572v

Espinosa JC, Navalon S, Alvaro M, Garcia H (2016) Copper nanoparticles supported on diamond nanoparticles as a cost-effective and efficient catalyst for natural sunlight assisted Fenton reaction. Cat Sci Technol 6(19):7077–7085. https://doi.org/10.1039/C6CY00572A

Espinosa JC, Catalaa C, Navalona S, Ferrera B, Alvaroa M, Garcia H (2018) Iron oxide nanoparticles supported on diamond nanoparticles as efficient and stable catalyst for the visible light assisted Fenton reaction. Appl Catal B Environ 226:242–251. https://doi.org/10.1016/j.apcatb.2017.12.060

Exposito AJ, Monteagudo JM, Duran A, Fernandez A (2017) Dynamic behavior of hydroxyl radical in sono-photo-Fenton mineralization of synthetic municipal wastewater effluent containing antipyrine. Ultrason Sonochem 35:185–195. https://doi.org/10.1016/j.ultsonch.2016.09.017

Exposito AJ, Monteagudo JM, Duran A, Martin IS, Gonzalez L (2018) Study of the intensification of solar photo-Fenton degradation of carbamazepine with ferrioxalate complexes and ultrasound. J Hazard Mater 342:597–605. https://doi.org/10.1016/j.jhazmat.2017.08.069

Faust B, Hoigne J (1990) Photolysis of Fe (III)-hydroxy complexes as sources of OH radicals in clouds, fog and rain. Atmos Environ A 24(1):79–89. https://doi.org/10.1016/0960-1686(90)90443-Q

Gao Y, Wang Y, Zhang H (2015) Removal of Rhodamine B with Fe-supported bentonite as heterogeneous photo-Fenton catalyst under visible irradiation. Appl Catal B 178:29–36. https://doi.org/10.1016/j.apcatb.2014.11.005

Ghasemi M, Naushad M, Ghasemi N, Khosravi-fard Y (2014a) A novel agricultural waste based adsorbent for the removal of Pb(II) from aqueous solution: kinetics, equilibrium and thermodynamic studies. J Ind Eng Chem 20:454–461. https://doi.org/10.1016/j.jiec.2013.05.002

Ghasemi M, Naushad M, Ghasemi N, Khosravi-fard Y (2014b) Adsorption of Pb(II) from aqueous solution using new adsorbents prepared from agricultural waste: adsorption isotherm and kinetic studies. J Ind Eng Chem 20:2193–2199. https://doi.org/10.1016/j.jiec.2013.09.050

Giannakis S, Lopez MIP, Spuhler D, Perez JAS, Ibanez PF, Pulgarin C (2016) Solar disinfection is an augmentable, in situ-generated photo-Fenton reaction – Part 1: A review of bacterial inactivation by hν/H_2O_2/Fe, at near-neutral pH. Appl Catal B 199:431–446. https://doi.org/10.1016/j.apcatb.2016.06.009

GilPavas E, Gomez ID, Garcia MAG (2018) Optimization of solar-driven photo-electro-Fenton process for the treatment of textile industrial wastewater. J Water Process Eng 24:49–55. https://doi.org/10.1016/j.jwpe.2018.05.007

Gogate PR, Pandit AB (2004) A review of imperative technologies for wastewater treatment I: oxidation technologies at ambient conditions. Adv Environ Res 8(3–4):501–551. https://doi.org/10.1016/S1093-0191(03)00032-7

Gomez EO, Garcia BE, Martin MMB, Ibanez PF, Perez JAS (2014) Inactivation of natural enteric bacteria in real municipal wastewater by solar photo-Fenton at neutral pH. Water Res 63:316–324. https://doi.org/10.1016/j.watres.2014.05.034

Gonzalez MC, Braun AM (1995) VUV photolysis of aqueous solutions of nitrate and nitrite. Res Chem Intermed 21(8–9):837–859. https://doi.org/10.1163/156856795X00512

Goyes REP, Arenas JV, Palma ART, Ostos C, Ferraro F, Gonzalez I (2015) The abatement of indigo carmine using active chlorine electrogenerated on ternary Sb_2O_5-doped Ti/RuO_2-ZrO_2 anodes in a filter-press FM01-LC reactor. Electrochim Acta 174:735–744. https://doi.org/10.1016/j.electacta.2015.06.037

Gu C, Wang J, Liu S, Liu G, Lu H, Jin R (2016) Biogenic Fenton-like reaction involvement in cometabolic degradation of tetrabromobisphenol A by *Pseudomonas* sp. fz. Environ Sci Technol 50(18):9981–9989. https://doi.org/10.1021/acs.est.6b02116

Gumus D, Akbal F (2016) Comparison of Fenton and electro-Fenton processes for oxidation of phenol. Process Saf Environ Prot 103:252–258. https://doi.org/10.1016/j.psep.2016.07.008

Guo X, Wang K, Li D, Qin J (2017) Heterogeneous photo-Fenton processes using graphite carbon coating hollow $CuFe_2O_4$ spheres for the degradation of methylene blue. Appl Surf Sci 420:792–801. https://doi.org/10.1016/j.apsusc.2017.05.178

Guzman PV, Giannakis S, Rtimi S, Grandjean D, Bensimon M, Alencastro LF, Palma RT, Pulgarin C (2017) A green solar photo-Fenton process for the elimination of bacteria and micropollutants in municipal wastewater treatment using mineral iron and natural organic acids. Appl Catal B Environ 219:538–549. https://doi.org/10.1016/j.apcatb.2017.07.066

Halliwell B, Gutteridge JMC (1986) Oxygen free radicals and iron in relation to biology and medicine: some problems and concepts. Arch Biochem Biophys 246(2):501–524. https://doi.org/10.1016/0003-9861(86)90305-X

Hartmann M, Kullmanna S, Keller H (2010) Wastewater treatment with heterogeneous Fenton-type catalysts based on porous materials. J Mater Chem 20(41):9002–9017. https://doi.org/10.1039/C0JM00577K

Hasan Z, Jhung SH (2015) Removal of hazardous organics from water using metal-organic frameworks (MOFs): plausible mechanisms for selective adsorptions. J Hazard Mater 283:329–339. https://doi.org/10.1016/j.jhazmat.2014.09.046

Hassan H, Hameed BH (2011) Fe-clay as effective heterogeneous Fenton catalyst for the decolorization of Reactive Blue 4. Chem Eng J 171(3):912–918. https://doi.org/10.1016/j.cej.2011.04.040

Hassani A, Karaca C, Karaca SS, Khataee A, Acisli O, Yılmaz B (2018a) Enhanced removal of basic violet 10 by heterogeneous sono-Fenton process sing magnetite nanoparticles. Ultrason Sonochem 42:390–402. https://doi.org/10.1016/j.ultsonch.2017.11.036

Hassani A, Çelikdag G, Eghbali P, Sevim M, Karaca S, Metin O (2018b) Heterogeneous sono-Fenton-like process using magnetic cobalt ferrite reduced graphene oxide (CoFe2O4-rGO) nanocomposite for the removal of organic dyes from aqueous solution. Ultrason Sonochem 40:841–852. https://doi.org/10.1016/j.ultsonch.2017.08.026

Hassani A, Karaca M, Karaca S, Khataee A, Acisli O, Yılmaz B (2018c) Preparation of magnetite nanoparticles by high-energy planetary ball mill and its application for ciprofloxacin degradation through heterogeneous Fenton process. J Environ Manag 211:53–62. https://doi.org/10.1016/j.jenvman.2018.01.014

Hou Y, Li XY, Zhao QD, Chen GH (2013) $ZnFe_2O_4$ multi-porous microbricks/graphene hybrid photocatalyst: facile synthesis, improved activity and photocatalytic mechanism. Appl Catal B Environ 142–143:80–88. https://doi.org/10.1016/j.apcatb.2013.04.062

Huang Z, Wu P, Li H, Li W, Zhua Y, Zhu N (2014) Synthesis and catalytic properties of La or Ce doped hydroxy-FeAl intercalated montmorillonite used as heterogeneous photo Fenton catalysts under sunlight irradiation. RSC Adv 4(13):6500–6507. https://doi.org/10.1039/c3ra46729e

Huitle CAM, Brillas E (2015) Decontamination of wastewaters containing synthetic organic dyes by electrochemical methods. An updated review. Appl Catal B Environ 166–167:603–643. https://doi.org/10.1016/j.apcatb.2014.11.016

Ibanez JA, Litter MI, Pizarro RA (2003) Photocatalytic bactericidal effect of TiO_2 on *Enterobacter cloacae* comparative study with other Gram (−) bacteria. J Photochem Photobiol A 157 (1):81–85. https://doi.org/10.1016/S1010-6030(03)00074-1

Jaafarzadeh N, Takdastan A, Jorfi S, Ghanbari F, Ahmadi M, Barzegar G (2018) The performance study on ultrasonic/Fe_3O_4/H_2O_2 for degradation of azo dye and real textile wastewater treatment. J Mol Liq 256:62–470. https://doi.org/10.1016/j.molliq.2018.02.047

Kanel SR, Greneche JM, Choi H (2006) Arsenic(V) removal from groundwater using nano scale zero-valent iron as a colloidal reactive barrier material. Environ Sci Technol 40(6):2045–2050. https://doi.org/10.1021/es0520924

Kaviya S, Prasad E (2015a) Biogenic synthesis of ZnO-Ag nano custard apple for efficient photocatalytic degradation of methylene blue by sunlight irradiation. RSC Adv 5 (22):17179–17185. https://doi.org/10.1039/C4RA15293J

Kaviya S, Prasad E (2015b) Sequential detection of Fe^{3+} and As^{3+} ions by biosynthesized AuNPs: a study of aggregation and disaggregation process. Anal Methods 7(1):168–174. https://doi.org/10.1039/C4AY02342K

Kaviya S, Prasad E (2016) Eco-friendly synthesis of ZnO Nano pencils in aqueous medium: a study of photocatalytic degradation of methylene blue under direct sunlight. RSC Adv 6 (40):33821–33827. https://doi.org/10.1039/C6RA04306B

Khataee A, Khataee A, Fathinia M, Vahid B, Joo SW (2013) Kinetic modeling of photoassisted-electrochemical process for degradation of an azo dye using boron-doped diamond anode and cathode with carbon nanotubes. J Ind Eng Chem 19(6):1890–1894. https://doi.org/10.1016/j.jiec.2013.02.037

Khataee A, Rad TS, Vahid B, Khorram S (2016) Preparation of zeolite nanorods by corona discharge plasma for degradation of phenazopyridine by heterogeneous sono-Fenton-like process. Ultrason Sonochem 33:37–46. https://doi.org/10.1016/j.ultsonch.2016.04.015

Khatri I, Singh S, Garg A (2018) Performance of electro-Fenton process for phenol removal using Iron electrodes and activated carbon. J Environ Chem Eng 6:7368. https://doi.org/10.1016/j.jece.2018.08.022

Kim SM, Vogelpohl A (1998) Degradation of organic pollutants by the photo-Fenton-process. Chem Eng Technol 21:187–191. https://doi.org/10.1002/(SICI)1521-4125(199802)21:2<187::AID-CEAT187>3.0.CO;2-H

Kim CG, Seo HJ, Lee BR (2006) Decomposition of 1,4-dioxane by advanced oxidation and biochemical process. J Environ Sci Health A Tox Hazard Subst Environ Eng 41(4):599–611. https://doi.org/10.1080/10934520600574807

Kruger O, Schulze TL, Peters D (1999) Sonochemical treatment of natural ground water at different high frequencies: preliminary results. Ultrason Sonochem 6(1–2):123–128. https://doi.org/10.1016/S1350-4177(98)00031-5

Lam FLY, Hu X (2007) A high performance bimetallic catalyst for photo-Fenton oxidation of Orange II over a wide pH range. Catal Commun 8(12):2125–2129. https://doi.org/10.1016/j.catcom.2007.04.025

Lasso AM, Pulgarin C, Benitez N (2008) Degradation of DBPs' precursors in river water before and after slow sand filtration by photo-Fenton process at pH 5 in a solar CPC reactor. Water Res 42 (15):4125–4132. https://doi.org/10.1016/j.watres.2008.07.014

Lasso AM, Arismendi LEM, Herrera JAR, Sanabria J, Benitez N, Pulgarin C (2012) The detrimental influence of bacteria (*E. coli, Shigella and Salmonella*) on the degradation of organic compounds (and *vice versa*) in TiO_2 photocatalysis and near-neutral photo-Fenton processes under simulated solar light. Photochem Photobiol Sci 11(5):821–827. https://doi.org/10.1039/c2pp05290c

Lee C, Sedlak DL (2009) A novel homogeneous Fenton-like system with Fe(III)-phosphotungstate for oxidation of organic compounds at neutral pH values. J Mol Catal A Chem 311(1–2):1–6. https://doi.org/10.1016/j.molcata.2009.07.001

Li H, Lei H, Yu Q, Li Z, Feng X, Yang B (2010) Effect of low frequency ultrasonic irradiation on the sonoelectro-Fenton degradation of cationic red X-GRL. Chem Eng J 160(2):417–422. https://doi.org/10.1016/j.cej.2010.03.027

Li G, Jiang B, Li X, Lian ZC, Xiao SN, Zhu J, Zhang DQ, Li HX (2013) $C_{60}/Bi_2TiO_4F_2$ heterojunction photocatalysts with enhanced visible-light activity for environmental remediation. ACS App Mater Interfaces 5(15):7190–7197. https://doi.org/10.1021/am401525m

Li G, Qiu S, Ma F, Jia Y, Jiang X (2018) Degradation of RhB by a sono-Fenton-like process with an iron-foam in the presence of oxalic acid. Anal Methods 10(32):3976–3983. https://doi.org/10.1039/c8ay00839f

Lim H, Lee J, Jin S, Kim J, Yoon J, Hyeon T (2006) Highly active heterogeneous Fenton catalyst using iron oxide nanoparticles immobilized in alumina coated mesoporous silica. Chem Commun 28(4):463–465. https://doi.org/10.1039/B513517F

Liu Y, Mao Y, Tang X, Xu Y, Li C, Li F (2017) Synthesis of Ag/AgCl/Fe-S plasmonic catalyst for bisphenol A degradation in heterogeneous photo-Fenton system under visible light irradiation. Chin J Catal 38(10):1726–1735. https://doi.org/10.1016/S1872-2067(17)62902-4

Liu Z, Zhang L, Dong F, Dang J, Wang K, Wu D, Zhang J, Fang J (2018) Preparation of ultra-small goethite nanorods and their application as heterogeneous Fenton reaction catalysts in the degradation of azo dyes. ACS Appl Nano Mater 1(8):4170–4178. https://doi.org/10.1021/acsanm.8b00930

Lonfat CR, Barona JF, Sienkiewicz A, Velez J, Benitez LN, Pulgarin C (2016) Bacterial inactivation with iron citrate complex: a new source of dissolved iron in solar photo-Fenton process at near-neutral and alkaline pH. Appl Catal B Environ 180:379–390. https://doi.org/10.1016/j.apcatb.2015.06.030

Lv H, Ma L, Zeng P, Ke D, Peng T (2010) Synthesis of floriated $ZnFe_2O_4$ with porous nanorod structures and its photocatalytic hydrogen production under visible light. J Mater Chem 20 (18):3665–3672. https://doi.org/10.1039/B919897K

Mackulak T, Mosny M, Grabic R, Golovko O, Koba O, Birosova L (2015) Fenton- like reaction: a possible way to efficiently remove illicit drugs and pharmaceuticals from wastewater. Environ Toxicol Pharmacol 39(2):483–488. https://doi.org/10.1016/j.etap.2014.12.016

Malakootian M, Moridi A (2017) Efficiency of electro-Fenton process in removing Acid Red 18 dye from aqueous solutions. Process Saf Environ Prot 111:138–147. https://doi.org/10.1016/j.psep.2017.06.008

Manu B, Mahamood S (2011) Enhanced degradation of paracetamol by UV-C supported photo-Fenton process over Fenton oxidation. Water Sci Technol 64(12):2433–2438. https://doi.org/10.2166/wst.2011.804

Matamoros V, Arias CA, Nguyen LX, Salvado V, Brix H (2012) Occurrence and behavior of emerging contaminants in surface water and a restored wetland. Chemosphere 88 (9):1083–1089. https://doi.org/10.1016/j.chemosphere.2012.04.048

Mckinzi AM, DiChristina TJ (1999) Microbially driven Fenton reaction for transformation of pentachlorophenol. Environ Sci Technol 33(11):1886–1891. https://doi.org/10.1021/es980810z

Miller CM, Valentine RL, Roehl MC, Alvarez PJJ (1996) Chemical and microbiological assessment of pendimethalin-contaminated soil after treatment with Fenton's reagent. Water Res 30 (11):2579–2586. https://doi.org/10.1016/S0043-1354(96)00151-0

Minella M, Marchetti G, Laurentiis ED, Malandrino M, Maurino V, Minero C, Vione D, Hanna K (2014) Photo-Fenton oxidation of phenol with magnetite as iron source. Appl Catal B Environ 154–155:102–109. https://doi.org/10.1016/j.apcatb.2014.02.006

Montilla F, Michaud PA, Morallon E, Vazquez JL, Comninellis C (2002) Electrochemical oxidation of benzoic acid at boron-doped diamond electrodes. Electrochim Acta 47(21):3509–3513. https://doi.org/10.1016/S0013-4686(02)00318-3

Moussavi G, Hossaini H, Jafari SJ, Farokhi M (2014) Comparing the efficacy of UVC, UVC/ZnO and VUV processes for oxidation of organophosphate pesticides in water. J Photochem Photobiol A 290:86–93. https://doi.org/10.1016/j.jphotochem.2014.06.010

Naushad M, Alothman ZA (2015) Separation of toxic Pb^{2+} metal from aqueous solution using strongly acidic cation-exchange resin: analytical applications for the removal of metal ions from pharmaceutical formulation. Desalin Water Treat 53:2158–2166. https://doi.org/10.1080/19443994.2013.862744

Obra IDL, Garcia BE, Sanchez JLG, Lopez JLC, Perez JAS (2017) Low cost UVA-LED as a radiation source for the photo-Fenton process: a new approach for micropollutant removal from urban wastewater. Photochem Photobiol Sci 16(1):72–78. https://doi.org/10.1039/c6pp00245e

Oppenlander T (2003) Photochemical purification of water and air. Wiley VCH, Weinheim

Oturan MA, Aaron JJ (2014) Advanced oxidation processes in water/wastewater treatment: principles and applications – a review. Crit Rev Environ Sci Technol 44(23):2577–2641. https://doi.org/10.1080/10643389.2013.829765

Oturan MA, Sires I, Oturan N, Perocheau S, Laborde JL, Trevin S (2008) Sonoelectro-Fenton process: a novel hybrid technique for the destruction of organic pollutants in water. J Electroanal Chem 624(1–2):329–332. https://doi.org/10.1016/j.jelechem.2008.08.005

Perez JF, Sabatino S, Galia A, Rodrigo MA, Llanos J, Saez C, Scialdone O (2018) Effect of air pressure on the electro-Fenton process at carbon felt electrodes. Electrochim Acta 273:447–453. https://doi.org/10.1016/j.electacta.2018.04.031

Pham ALT, Lee C, Doyle FM, Sedlak DL (2009) A silica-supported iron oxide catalyst capable of activating hydrogen peroxide at neutral pH values. Environ Sci Technol 43(23):8930–8935. https://doi.org/10.1021/es902296k

Phan TTN, Nikoloski AN, Bahri PA, Li D (2018) Heterogeneous photo-Fenton degradation of organics using highly efficient Cu-doped $LaFeO_3$ under visible light. J Ind Eng Chem 61:53–64. https://doi.org/10.1016/j.jiec.2017.11.046

Pourakbar M, Moussavi G, Shekoohiyan S (2016) Homogenous VUV advanced oxidation process for enhanced degradation and mineralization of antibiotics in contaminated water. Ecotoxicol Environ Saf 125:72–77. https://doi.org/10.1016/j.ecoenv.2015.11.040

Pradhan AC, Parida KM (2012) Facile synthesis of mesoporous composite Fe/Al_2O_3-MCM-41: an efficient adsorbent/catalyst for swift removal of methylene blue and mixed dyes. J Mater Chem 22(15):7567–7579. https://doi.org/10.1039/C2JM30451A

Pradhan GK, Sahu N, Parida KM (2013) Fabrication of S, N co-doped α-Fe_2O_3 nanostructures: effect of doping, OH radical formation, surface area, [110] plane and particle size on the photocatalytic activity. RSC Adv 3(21):7912–7920. https://doi.org/10.1039/C3RA23088K

Pradhan AC, Sahoo MK, Bellamkonda S, Parida KM, Rao GR (2016) Enhanced photodegradation of dyes and mixed dyes by heterogeneous mesoporous $Co–Fe/Al_2O_3$-MCM-41 nanocomposites: nanoparticles formation, semiconductor behavior and mesoporosity. RSC Adv 6(96):94263–94277. https://doi.org/10.1039/C6RA19923B

Qin Q, Liu Y, Li X, Suna T, Xu Y (2018) Enhanced heterogeneous Fenton-like degradation of methylene blue by reduced $CuFe_2O$. RSC Adv 8(2):1071–1077. https://doi.org/10.1039/C7RA12488K

Ramirez JH, Hodar FJM, Cadenas AFP, Castilla CM, Costa CA, Madeira LM (2007) Azo-dye Orange II degradation by heterogeneous Fenton-like reaction using carbon-Fe catalysts. Appl Catal B Environ 75(3–4):312–323. https://doi.org/10.1016/j.apcatb.2007.05.003

Ramirez JH, Vicente MA, Madeira LM (2010) Heterogeneous photo-Fenton oxidation with pillared clay-based catalysts for wastewater treatment: a review. Appl Catal B Environ 98(1–2):10–26. https://doi.org/10.1016/j.apcatb.2010.05.004

Rezgui S, Amranea A, Fourcadea F, Assadia A, Monserb L, Adhoum N (2018) Electro-Fenton catalyzed with magnetic chitosan beads for the removal of chlordimeform insecticide. Appl Catal B Environ 226:346–359. https://doi.org/10.1016/j.apcatb.2017.12.061

Riverohuguet M, Marshall WD (2009) Influence of various organic molecules on the reduction of hexavalent chromium mediated by zero-valent iron. Chemosphere 76(9):1240–1248. https://doi.org/10.1016/j.chemosphere.2009.05.040

Rodriguez OG, Lee YY, Vargas HO, Deng F, Wang Z, Lefebvre O (2018) Mineralization of electronic wastewater by electro-Fenton with an enhanced graphene-based gas diffusion cathode. Electrochim Acta 276:12–20. https://doi.org/10.1016/j.electacta.2018.04.076

Ruppert G, Bauer R, Heisler G (1993) The photo-Fenton reaction – an effective photochemical wastewater treatment process. J Photochem Photobiol A73(1):75–78. https://doi.org/10.1016/1010-6030(93)80035-8

Sabhi S, Kiwi J (2001) Degradation of 2,4-dichlorophenol by immobilized iron catalysts. Water Res 35(8):1994–2002. https://doi.org/10.1016/S0043-1354(00)00460-7

Sahinkaya S (2013) COD and color removal from synthetic textile wastewater by ultrasound assisted electro-Fenton oxidation process. J Ind Eng Chem 19(2):601–605. https://doi.org/10.1016/j.jiec.2012.09.023

Samakchi S, Chaibakhsh N, Shoeili ZM (2018) Synthesis of $MoS_2/MnFe_2O_4$ nanocomposite with highly efficient catalytic performance in visible light photo-Fenton-like process. J Photochem Photobiol A Chem 367:420–428. https://doi.org/10.1016/j.jphotochem.2018.09.003

Segura Y, Molina R, Martínez F, Melero JA (2009) Integrated heterogeneous sono-photo Fenton processes for the degradation of phenolic aqueous solutions. Ultrason Sonochem 16(3):417–424. https://doi.org/10.1016/j.ultsonch.2008.10.004

Sekar R, DiChristina TJ (2014) Microbially driven Fenton reaction for degradation of the widespread environmental contaminant 1,4-dioxane. Environ Sci Technol 48(21):12858–12867. https://doi.org/10.1021/es503454a

Senn AM, Russo YM, Litter MI (2014) Treatment of wastewater from an alkaline cleaning solution by combined coagulation and photo-Fenton processes. Sep Purif Technol 132(6):552–560. https://doi.org/10.1016/j.seppur.2014.06.006

Serra A, Domenech X, Brillas E, Peral J (2011) Life cycle assessment of solar photo-Fenton and solar photoelectro-Fenton processes used for the degradation of aqueous α-methylphenylglycine. J Environ Monit 13(1):167–174. https://doi.org/10.1039/c0em00552e

Shao P, Tian J, Liu B, Shi W, Gao S, Song Y, Ling M, Cui F (2015) Morphology-tunable ultrafine metal oxide nanostructures uniformly grown on graphene and their applications in the photo-Fenton system. Nanoscale 7(34):14254–14263. https://doi.org/10.1039/C5NR03042K

Stefan MI, Bolton JR (1998) Mechanism of the degradation of 1,4-dioxane in dilute aqueous solution using the UV hydrogen peroxide process. Environ Sci Technol 32(11):1588–1595. https://doi.org/10.1021/es970633m

Steffan R (2007) Biodegradation of 1,4-dioxane. SERDP, August

Stumm W, Morgan JJ (1996) Aquatic chemistry. Wiley, New York

Tabai A, Bechiri Q, Abbessi M (2017) Degradation of organic dye using a new homogeneous Fenton-like system based on hydrogen peroxide and a recyclable Dawson-type heteropolyanion. Int J Ind Chem 8(1):83–89. https://doi.org/10.1007/s40090-016-0104-x

Tan X, Lu L, Wang L, Zhang J (2015) Facile synthesis of bimodal mesoporous $Fe_3O_4@SiO_2$ composite for efficient removal of methylene blue. Eur J Inorg Chem 2015(18):2928–2933. https://doi.org/10.1002/ejic.201500267

Torres RA, Petrier C, Combet E, Moulet F, Pulgarin C (2007) Bisphenol A mineralization by integrated ultrasound-UV-iron (II) treatment. Environ Sci Technol 41(1):297–302. https://doi.org/10.1021/es061440e

Vaishnave P, Kumar A, Ameta R, Punjabi PB, Ameta SC (2014) Photo oxidative degradation of azure-B by sono-photo-Fenton and photo-Fenton reagents. Arab J Chem 7(6):981–985. https://doi.org/10.1016/j.arabjc.2010.12.019

Velasquez M, Santander IP, Contreras DR, Yanez J, Zaror C, Salazar RA, Moya MP, Mansilla HD (2014) Oxidative degradation of sulfathiazole by Fenton and photo-Fenton reactions. J Environ Sci Health A 49(6):661–670. https://doi.org/10.1080/10934529.2014.865447

Veloutsou S, Bizani E, Fytianos K (2014) Photo-Fenton decomposition of β-blockers atenolol and metoprolol; study and optimization of system parameters and identification of intermediates. Chemosphere 107:180–186. https://doi.org/10.1016/j.chemosphere.2013.12.031

Wang JL, Xu LJ (2012) Advanced oxidation processes for wastewater treatment: formation of hydroxyl radical and application. Crit Rev Environ Sci Technol 42(3):251–325. https://doi.org/10.1080/10643389.2010.507698

Wang H, Yin F, Li G, Chen B, Wang Z (2014) Preparation, characterization and bifunctional catalytic properties of MOF(Fe/Co) catalyst for oxygen reduction/evolution reactions in alkaline electrolyte. Int J Hydrog Energy 39(28):16179–16186. https://doi.org/10.1016/j.ijhydene.2013.12.120

Wang W, Jiao T, Zhang Q, Luo X, Hu J, Chen Y, Peng Q, Yan X, Li B (2015) Hydrothermal synthesis of hierarchical core-shell manganese oxide nanocomposites as efficient dye adsorbents for wastewater treatment. RSC Adv 5(69):56279–56285. https://doi.org/10.1039/C5RA08678G

Wang W, Lu Y, Luo H, Liu G, Zhang R, Jin S (2018) A microbial electro-Fenton cell for removing carbamazepine in wastewater with electricity output. Water Res 139:58–65. https://doi.org/10.1016/j.watres.2018.03.066

Weng CH, Lin YT, Chang CK, Liu N (2013) Decolourization of direct blue 15 by Fenton/ultrasonic process using a zero-valent iron aggregate catalyst. Ultrason Sonochem 20(3):970–977. https://doi.org/10.1016/j.ultsonch.2012.09.014

Xu LJ, Chu W, Graham N (2014) Degradation of di-n-butyl phthalate by a homogeneous sono-photo-Fenton process with in situ generated hydrogen peroxide. Chem Eng J 240:541–547. https://doi.org/10.1016/j.cej.2013.10.087

Xu YQ, Huang SQ, Xie M, Li YP, Jing LQ, Xu H, Zhang Q, Li HM (2016) Core–shell magnetic Ag/AgCl@Fe_2O_3 photocatalysts with enhanced photoactivity for eliminating bisphenol A and microbial contamination. New J Chem 40(4):3413–3422. https://doi.org/10.1039/C5NJ02898A

Yan L, Liu J, Feng Z, Zhao P (2016) Continuous degradation of BTEX in landfill gas by the UV-Fenton reaction. RSC Adv 6(2):1452–1459. https://doi.org/10.1039/c5ra22585j

Yang CW (2015) Degradation of bisphenol A using electrochemical assistant Fe (II) activated peroxydisulfate process. Water Sci Technol 8(2):139–144. https://doi.org/10.1016/j.wse.2015.04.002

Yang X, Chen W, Huang J, Zhou Y, Zhu Y, Li C (2015) Rapid degradation of methylene blue in a novel heterogeneous Fe_3O_4 @rGO@TiO_2-catalyzed photo-Fenton system. Sci Rep 5:10632–10642. Article number: 10632

Yang H, Zhou M, Yang W, Ren G, Ma L (2018) Rolling-made gas diffusion electrode with carbon nanotube for electro-Fenton degradation of acetylsalicylic acid. Chemosphere 206:439–446. https://doi.org/10.1016/j.chemosphere.2018.05.027

Zhang H, Fu H, Zhang D (2009) Degradation of CI Acid Orange 7 by ultrasound enhanced heterogeneous Fenton-like process. J Hazard Mater 172(2–3):654–660. https://doi.org/10.1016/j.jhazmat.2009.07.047

Zhang CH, Ai LH, Jiang J (2015) Solvothermal synthesis of MIL–53(Fe) hybrid magnetic composites for photoelectrochemical water oxidation and organic pollutant photodegradation under visible light. J Mater Chem A 3(6):3074–3081. https://doi.org/10.1039/C4TA04622F

Zhang Z, Meng H, Wang Y, Shi L, Wang X, Chai S (2018) Fabrication of graphene@graphite-based gas diffusion electrode for improving H_2O_2 generation in Electro-Fenton process. Electrochim Acta 260:112–120. https://doi.org/10.1016/j.electacta.2017.11.048

Zhao Y, Jiangyong H, Chen H (2010) Elimination of estrogen and its estrogenicity by heterogeneous photo-Fenton catalyst β-FeOOH/resin. J Photochem Photobiol A 212(2–3):94–100. https://doi.org/10.1016/j.jphotochem.2010.04.001

Zhao Y, Pan F, Li H, Niu T, Xu G, Chen W (2013) Facile synthesis of uniform α-Fe_2O_3 crystals and their facet-dependent catalytic performance in the photo-Fenton reaction. J Mater Chem A 1 (24):7242–7246. https://doi.org/10.1039/C3TA10966F

Zhao H, Chen Y, Peng Q, Wang Q, Zhao G (2017) Catalytic activity of MOF(2Fe/Co)/carbon aerogel for improving H_2O_2 and •OH generation in solar photo–electro–Fenton process. Appl Catal B Environ 203:127–137. https://doi.org/10.1016/j.apcatb.2016.09.074

Zhong X, Royer S, Zhang H, Huang Q, Xiang L, Valange S, Barrault J (2011) Mesoporous silica iron-doped as stable and efficient heterogeneous catalyst for the degradation of C.I. Acid Orange 7 using sono–photo-Fenton process. Sep Purif Technol 80(1):163–171. https://doi.org/10.1016/j.seppur.2011.04.024

Zhou Q, Liu Y, Yu G, He F, Chen K, Xiao D, Zhao X, Feng Y, Li J (2017) Degradation kinetics of sodium alginate via sono-Fenton, photo-Fenton and sono-photo-Fenton methods in the presence of TiO_2 nanoparticles. Polym Degrad Stab 135:111–120. https://doi.org/10.1016/j.polymdegradstab.2016.11.012

Zhuang H, Hong X, Shan S, Yuan X (2016) Recycling rice straw derived, activated carbon supported, nanoscaled Fe3O4 as a highly efficient catalyst for Fenton oxidation of real coal gasification wastewater. RSC Adv 6(97):95129–95136. https://doi.org/10.1039/C6RA20952A

Zou C, Meng Z, Ji W, Liu S, Shen Z, Zhang Y, Jiang N (2018) Preparation of a fullerene[60]-iron oxide complex for the photo-Fenton degradation of organic contaminants under visible-light irradiation. Chin J Catal 39(6):1051–1059. https://doi.org/10.1016/S1872-2067(18)63067-0

Chapter 6
Electrochemical Aspects for Wastewater Treatment

A. Dennyson Savariraj, R. V. Mangalaraja, K. Prabakar, and C. Viswanathan

Contents

A. D. Savariraj (✉)
Advanced Ceramics and Nanotechnology Laboratory, Department of Materials Engineering, Faculty of Engineering, University of Concepcion, Concepcion, Chile

R. V. Mangalaraja
Advanced Ceramics and Nanotechnology Laboratory, Department of Materials Engineering, Faculty of Engineering, University of Concepcion, Concepcion, Chile

Technological Development Unit (UDT), University of Concepcion, Coronel, Chile

K. Prabakar
Department of Electrical and Computer Engineering, Pusan National University, Busan, South Korea

C. Viswanathan
Department of Nanoscience and Technology, Bharathiar University, Coimbatore, India

M. Naushad et al. (eds.), *Green Methods for Wastewater Treatment*, Environmental Chemistry for a Sustainable World 35, https://doi.org/10.1007/978-3-030-16427-0_6

Abstract Water has been an inevitable part of human life and its civilization, and water contamination is caused by pollution from industrial wastes such as effluents, dyes, and heavy metals and sewage water due to human activities. Therefore, cost-effective treatment of wastewater has to be carried out without giving any by-products. This chapter is aimed at explaining the different ways of electrochemically treating the wastewater and degrading the contaminants. Electrochemical treatment is advantageous over other methods as it is inexpensive and is a green technique. The mechanism of degradation through anodic oxidation has been explained in details. The incorporation of microorganisms toward water treatment and using them for different kinds of sensors to detect the contaminants opens a new window to address this issue. Along with microorganisms, nanomaterials and ionic liquids are also used in sensing the pollutants and in removing and converting them into energy as well.

Keywords Water contamination · Pollution · Industrial waste · Dyes · Heavy metals · Electrochemical

6.1 Introduction

Water has been the backbone of human civilization, and it is part and parcel of our day today life. With increasing global population, better living standard and scarcity of water sources make water a rare commodity. In addition to the above, the vast industrial establishments and the pollution caused eventually draw the attention of researchers around the world as the availability of freshwater and access to portable water are becoming a serious issue of the present day (Alothman et al. 2012). Inorganic chemicals and microorganisms are the crucial parameters to monitor the quality of water as they do influence on plants/organisms present in the aqua system and human body (Mao et al. 2015). The industrial effluents and sewage from townships and human activities give out heavy metals, pesticides, detergents, and dyes which all contaminate the water reservoirs like lakes, river, canal, and groundwater (Tiwari 2016; Kaur et al. 2017; Naushad et al. 2015). The wastage often leave harmful carcinogenic dyes particularly azo dyes in aquatic ecosystems and cause different kinds of health hazards, as dyes make the water anoxic for aquatic inhabitants by bringing down the dissolved oxygen concentration (Habibi et al. 2005; Dakiky and Nemcova 2000). There are different types of methods such as physical and chemical separation and biological methods which incorporate several techniques like adsorption, oxidation, filtration, coagulation, and flocculation by which the water contaminants can be addressed (Shahat et al. 2015). The essential prerequisite for an effective treatment is that it should be environmentally friendly and cost-effective and should not yield any harmful by-products. The main advantage of electrochemical photocatalysis in detoxifying the pollutants, over the above-stated methods, is that it leads to complete mineralization and degradation of the effluents (Kaur et al. 2017).

Azo dyes are a multifaceted group of colored organic compounds, employed extensively for industrial applications like gasoline, paper, leathers, cosmetics, additives, and foodstuffs and in analytical chemistry. In addition, phenolic compounds from oil refinery, drug manufacturing industries, and phenol-formaldehyde resin are often biologically nondegradable which should undergo prior treatment before discharging into the environment. The chemical pollutants from the industrial wastewater comprise of phenol and phenolic compounds, which come from the effluents of oil refineries, polymeric resins, pharmaceuticals, coal conversion plants, coal tar distillation, petrochemicals, etc. (Rajkumar and Palanivelu 2004). Phenolic compounds not only curtail the microbial activities but also negatively influence biological treatment process. Besides being highly toxic, they also cause sweating and cyanosis and finally result in death due to respiratory problem (Woodworth et al. 1998). Phenolic wastes are treated using physical, chemical, biological, and electrochemical processes; however, biological processes are ineffective for higher concentrations of phenols in the wastewater (Suidan et al. 1983; Fedorak and Hrudey 1986; Blum et al. 1986). Pollutants like bacteria, anions, and heavy metals are to be rapidly detected as it is important in maintaining the quality and control that necessitate an outstanding detection of contaminant in water as the present technologies suffer from certain limitations (Mao et al. 2015). Table 6.1 gives an account of different types of nanomaterials used in sensing water pollutants.

6.2 Advantages of Electrochemical Methods

In addressing environmental issues, electrochemical methods stand superior over other methods in recycling harmful chemicals. These methods are widely employed for sterilization, disinfection, deodorization, and microbiological application of similar type. Since electron is the reagent without additional reagents used in the electrochemical methods, it stands out to be a clean and green method (Rajeshwar and Ibanez 1997). Besides that, electrochemical methods are operated at temperature lower than other non-electrochemical methods and without forming harmful by-products. The water pollutants are treated by electrochemical method via oxidation process which is subdivided into two ways: (1) direct oxidation and (2) indirect oxidation. In the direct oxidation process, the treatment of pollutants occurs on the anode via oxidation as initially the pollutants are adsorbed on the electrode's surface (anode) whereby the pollutants are neutralized via anodic electron transfer. On the other hand in the indirect oxidation method, the pollutants are treated via oxidation in the bulk solution by the oxidants generated using strong accidents like hydrogen peroxide, ozone, and hypochlorite/chlorine which are generated electrochemically (Rajeshwar et al. 1994). The present water quality monitoring mostly takes place either at the point of water supply or in water treatment plant which is more essential and relevant rather than along the distribution line of water and at the usage point is very much essential. Therefore, continuous monitoring with accurate and accessible

Table 6.1 An account of optical and electronic sensors based on nanomaterial toward quick water contaminant detection

Sensor type	Sensing material	Contaminant (water sample unless stated otherwise)	LOD	Working range	Detection time	References
Optical sensors	Au NP	Pb^{2+}	3 nM	3 nM to 1 μM	6 min	Wang et al. (2008)
	Au NP	Pb^{2+}	100 nM	0.1–50 μM	25 min	Chai et al. (2010)
	GO QD	Pb^{2+}	0.09 nM	0.1–1000 nM	20 min	Li et al. (2013)
	Au NP	Hg^{2+}	1 nM	1 nM to1 mM	15 min	Darbha et al. (2008)
	Au NP	Hg^{2+}	9.9 nM	9.9–600 nM	10 min	Darbha et al. (2007), Huang et al. (2007)
	Au NP	Hg^{2+}	5 nM	50 nM to 10 μM	10 min	Huang et al. (2007)
	Au NP	As^{2+}	0.13 nM	0.13 nM to 0.65 μM	10 min	Kalluri et al. (2009)
Electronic sensors	Au NP/graphene	Pb^{2+} (1 M HEPES buffer)	20 pM	20 pM to 100 nM	Tens of seconds	Wen et al. (2013)
	Au NP/RGO	Pb^{2+}	10 nM	10 nM to 10 μM	Few seconds	Zhou et al. (2014)
	Au NP/RGO	Hg^{2+}	25 nM	25 nM to 14.2 μM	seconds	Chen et al. (2012)
	Graphene	Hg^{2+}	50 nM		20 min	Zhang et al. (2010)
	RGO	Hg^{2+}	0.1 nM	0.1–30 nM	Several min	Yu et al. (2013)
	RGO	Hg^{2+}	1 nM	1–28 nM	Tens of seconds	Sudibya et al. (2011)
	SWCNT (no probe)	Hg^{2+}	10 nM	10 nM to 1 mM	Few seconds	Kim et al. (2009)
	CNT	Cd^{2+}	88 nM	88 nM to 8.8 μM	30 min	Chouteau et al. (2004)

	SiNW	Pb^{2+}	1 nM	1–10^4 nM	Few seconds	Bi et al. (2009)
	SiNW	Hg^{2+}	10^{-7} M	10^{-7} to 10^{-3} M	Several min	Luo et al. (2009)
		Cd^{2+}	10^{-4} M	10^{-4} to 10^{-2} M	Several min	
	SWCNT	*E. coli* DH5a	3×10^3 CFU mL^{-1}	3×10^3–1×10^6 CFU mL^{-1}	20 min	So et al. (2008)
	Graphene	*E. coli* K12	10 CFU mL^{-1}	10–10^5 CFU mL^{-1}	30 min	Huang et al. (2011)
	RGO	*E. coli* O157:H7	803 CFU mL^{-1}	803–10^7 CFU mL^{-1}	25 min	Chen et al. (2014)
	RGO	*E. coli* O157:H7	10 CFU mL^{-1}	10–10^4 CFU mL^{-1}	2 s	Chang et al. (2013)
Electrochemical sensors	Au	As^{3+} (1 M HCl)	0.26 nM	0.26–195 nM	100 s	Kumar Jena and Retna Raj (2008)
		Hg^{2+} (1 M HCl)	0.1 nM	0.1–75 nM		
	Au–Pt NP	Hg^{2+} (1 M HCl)	0.04 nM	0.04–10 nM	100 s	Gong et al. (2010b)
	Au NP/CNT	Hg^{2+} (0.1 M $HClO_4$)	0.3 nM	0.5 nM to 1.25 μM	2 min	Xu et al. (2008)
	Au NP/graphene	Hg^{2+} (1 M HCl)	0.03 nM	0.04–300 nM	110 s	Gong et al. (2010a)
	Carbon NP	Hg^{2+} (1 M HCl)	4.95 nM	4.95–49.5 nM	2 min	Aragay et al. (2011)
	CNT	Pb^{2+} (1 M HCl)	0.96 nM	9.6–480 nM	180 s	Injang et al. (2010)
		Cd^{2+} (1 M HCl)	7.04 nM	17.6–880 nM		
	Bi–CNT	Pb^{2+} (0.1 M acetate buffer)	6.24 nM	9.6–480 nM	300 s	Hwang et al. (2008)
		Cd^{2+} (0.1 M acetate buffer)	6.16 nM	17.6–880 nM		
	$MgSiO_3$	Pb^{2+} (0.1 M NaAc–HAc)	0.247 nM	0.1–1.0 μM	Tens of seconds	Xu et al. (2013)
		Cd^{2+} (0.1 M NaAc–HAc)	0.186 nM	0.2 nM to 1.0 μM	Several min	
		Hg^{2+} (0.1 M NaAc–HAc)	0.375 nM	0.4 nM to 2.0 μM		

(continued)

Table 6.1 (continued)

Sensor type	Sensing material	Contaminant (water sample unless stated otherwise)	LOD	Working range	Detection time	References
	Graphene nanodots	Cu^{2+} (ammonium acetate solution)	9 nM	9 nM to 4 μM	15 min	Zhu et al. (2015)
		Pb^{2+} (ammonium acetate solution)	6 nM	6 nM to 2.5 μM		
	MWCNT/GO	Pb^{2+} (0.1 M NaAc–HAc)	0.96 nM	0.96–144 nM	3 min	Huang et al. (2014)
		Cd^{2+} (0.1 M NaAc–HAc)	0.88 nM	0.88–264 nM		
	Titanate nanosheet	Hg^{2+} (0.1 M HCl)	0.025 nM	0.2–200 nM	80 s	Yuan et al. (2013)
	Graphene/ Nafion	Pb^{2+} (0.1 M acetate buffer)	0.096 nM	2.4–240 nM	300 s	Li et al. (2009)
		Cd^{2+} (0.1 M acetate buffer)	0.176 nM	1.32–264 nM		
	Fe_3O_4 /RTIL	As^{3+} (acetate buffer)	0.01 nM	13.3–133 nM	Few min	Gao et al. (2013)
	Nanosized hydroxyapatite	Pb^{2+} (0.2 M HAc-NaAc)	1 nM	5.0 nM to 0.8 μM	10 min	Pan et al. (2009)
	Nanosized Co	$H_2PO_4 -$ (KH_2PO_4 solution)		10–5 to 10–2 M	1 min or less	Zou et al. (2007)

Adopted from Mao et al. (2015)

detection technologies is required. This necessitates the implementation of sensors that monitor water rapidly and continuously sense contaminants to give warning in advance (Mao et al. 2015).

The electrochemical treatment of wastewater involves both recycling/decomposing and sensing aspects, and it is a custom-made method where cells and electrodes are designed to minimize the loss in power because of poor current distribution with controlled potential avoiding side reaction (Rajeshwar et al. 1994). The basic criteria for electrochemical methods are sensitivity and selectivity which can avoid production of unwanted side-products. Production of high concentration of electroactive species is necessary for zero-effluent technology that hinges on the electrolytic cell's design.

Several advantages of nanomaterials as electrode materials have been attested for the analysis of diversified chemicals of cancer investigation, food quality, clinical, pharmaceutical, clinical and environmental interest. Nanomaterials possess many advantages that make them suitable for the analysis of various chemicals of food quality, clinical and pharmaceutical applications, cancer investigation, and environmental importance (Gupta et al. 2013). The elimination of most environmental pollutants is carried out by converting them into nontoxic materials by different processes. The successful elimination and immediate conversion of several environmental pollutants can be achieved by one or more processes including electrochemical oxidation and reduction, advanced electrochemical process, electrocoagulation/flotation, and electrodialysis (Feng et al. 2016).

6.3 Electrochemical Oxidation

Electrochemical oxidation is an efficient method to break up highly resistant organic compounds into small nontoxic fragments and anodic oxidation and is one of the oxidation methods for treating organic compounds by direct and indirect oxidation. Based on the nature of the pollutants, the treatment is executed using primary, secondary, and tertiary methods. The possibility of electrochemical treatment of organic substrates in wastewater and several studies are made by Dabrowski in the 1970s; Kirk, Stucki, Kotz, Chettiar, and Watkinson in the 1980s; and Comninellis in the early 1990s till this date (Martinez-Huitle and Ferro 2006).

Though electrochemical oxidation is carried out similar to chemical method using strong oxidants, the in situ electrogeneration occurring in electrochemical oxidation makes it advantageous over the chemical method yielding better results in the absence of organic substrates. To elaborate further, it is the nature of the electrode material used in the electrochemical oxidation that determines the efficiency, and Comninellis brought out a mechanism in this regard, taking into account different stabilizations applied by the electrode material over the electrosorbed hydroxyl radical which justifies the results obtained (Martinez-Huitle et al. 2004). Depending on the electrode properties, the electrodes have been divided into active and non-active electrodes the oxidation process as direct oxidation and indirect

oxidation, and nevertheless based on the strong activity of strong oxidizing species like $Cl^{\cdot}$, $S_2O_8^{\cdot}$, and $Ce^{IV\cdot}$, they are also addressed as mediated electrochemical oxidation (Juttner et al. 2000; Marselli et al. 2003; Galla et al. 2000). Both direct and indirect anodic oxidation have been applied to treat organic contaminants.

6.4 Mechanism of Degradation

Comninellis proposed a suitable mechanism for the degradation of organic compound on metal oxide anode (Comninellis 1994). This process takes place in two steps. In the first step, H_2O is discharged at the surface of the anode yielding adsorbed hydroxyl radicals followed by a metal oxide layer as explained by Eqs. (6.1) and (6.2). The formation of passivation layer is inhibited by the oxide layer on the electrode (Gattrell and Kirk 1993).

$$MO_x + H_2O \rightarrow MO_x(OH^{\cdot}) + H^+ + e^- \tag{6.1}$$

$$MO_x(OH^{\cdot}) \rightarrow MO_{x+1} + H^+ + e^- \tag{6.2}$$

Oxygen is produced when any oxidizable organics are absent as presented in the Eqs. (6.3) and (6.4):

$$MO_x\ (OH^{\cdot}) \rightarrow MO_x + \tfrac{1}{2}\, O_2 + H^+ + e^- \tag{6.3}$$

$$MO_{x+1} \rightarrow MO_x + \tfrac{1}{2}\, O_2 \tag{6.4}$$

Combine reactions (6.1), (6.2), (6.3), and (6.4) to get the overall Eq. (6.5):

$$2H_2O \rightarrow 4H^+ + O_2 + 4e^- \tag{6.5}$$

When the oxidizable organic compound R is present, the reaction occurring will be as follows:

$$R + MO_x\ (OH^{\cdot})_n \rightarrow CO_2 + nH^+ + ne^- + MO_x \tag{6.6}$$

$$R + MO_{x+1} \rightarrow MO_x + RO \tag{6.7}$$

And a detailed schematic representation of the electrochemical degradation pathways of organic compounds on Pt electrodes is presented in Fig. 6.1.

The degradation route for organic compounds depends on the anode materials and specific interaction of the anode material with the compounds in solution (Torres et al. 2003).

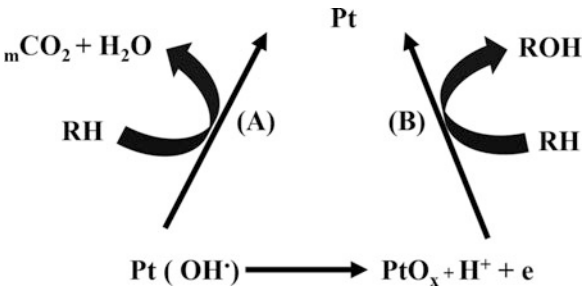

Fig. 6.1 Electrochemical degradation pathways of phenols, RH, by Pt electrodes. (Reproduced from (Torres et al. 2003) with permission from Elsevier.)

6.4.1 Direct Anodic Oxidation

In this method, the treatment and destruction of pollutants are carried out solely using electrons whereby the pollutants are adsorbed on the anode's surface without incorporating any other elements. Theoretically speaking, the negative potential required for this process is much more than that required for water spitting and oxygen evolution. The requirement for more negative potential results in catalytic poisoning of the electrode as a layer of polymer covers its surface, which eventually brings down the overall performance of treating the pollutants (Rodrigo et al. 2001; Chatzisymeon et al. 2009). This catalytic poisoning is very much evident when platinum electrode has been used to treat phenol, where phenol gets adsorbed on to the surface of the platinum electrode in voltammetry and chronoamperometry and subsequently arresting the catalytic activity as the adsorption of phenol is irreversible (Feng et al. 2016; Gattrell and Kirk 1993). James D. et al. investigated the mechanism of anode poisoning by chlorinated phenols, compared the structure vs reactivity for phenols varying in the degree of chlorination, and studied its influence to regulate oxidation to oxidation mechanism made with different electrodes (Rodgers et al. 1999).

6.4.2 Indirect Anodic Oxidation

This method proceeds via oxygen evolution as intermediate which is advantageous over the direct method, avoiding the need for an oxidizing agent, without any by-products. In this technique, both physically adsorbed "active oxygen" (adsorbed hydroxyl radicals ·OH) and chemisorbed "active oxygen" (oxygen in the lattice of a metal oxide (MO) anode) play very vital role to electrochemically destruct the species at the anode either partically or completely. The hydroxyl radical OH stands next to fluorine in terms of its ability to oxidize, possessing a very high potential of $E_0 = 2.80$ V vs SHE. Therefore when the complete destruction of organic compounds occurs the chemisorbed "active oxygen" involves the formation of certain oxidation products (Johnson et al. 1999; Chang and Johnson 1990). The efficiency of the process and the selectivity of the electrode depends solely on the nature of the

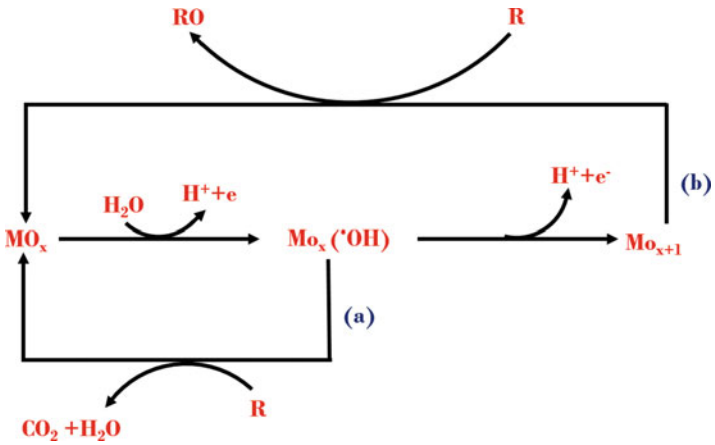

Fig. 6.2 Schematic illustration of the electrochemical oxidation of organic compounds on (**a**) "active" and (**b**) "non-active" anodes. (Reproduced from (Feng et al. 2016) with permission from The Royal Society of Chemistry)

anode material. The active anode materials such as RuO_2, IrO_2, and Pt make selective and partial oxidation feasible with low oxygen evolution over potential. On the other hand, non-active anode materials like SnO_2, PbO_2, and boron-doped diamond (BDD) make complete combustion possible with very high oxygen evolution over potential as shown in Fig. 6.2 (Feng and Li 2003; Comninellis 1994).

6.5 Platinum (Pt) Electrodes

Platinum is a well-known metal known for its electrocatalytic properties because of appreciable conductivity and chemical stability. Therefore it is used for several applications, including as counter electrode for solar cells and oxidation of organic compounds (pollutants) on the platinum anodes. Platinum has been used for treatment of water pollutant and presented in several reports. CH. Comninellis et al. have used Pt electrodes at constant pH of 12 or 2.5, for the oxidation of phenol which is an effluent from refineries, coke plants, plastic, and chemical plants. The reaction proceeds via two parallel pathways: electrogenerated hydroxyl radical-assisted chemical oxidation and direct combustion of adsorbed phenol and/or conversion of its aromatic intermediates to CO_2 (Comninellis and Pulgarin 1991). 1-Aminonaphthalene-3,6-disulphonic acid is produced while synthesizing H-acid is used for the synthesis of different dyes. A. Socha et al. used Pt electrode to treat 1-aminonaphthalene-3,6-disulphonic acid varying temperature and pH (Socha et al. 2005). A modification of Pt electrode was carried out by making Pt support on titanium electrodes of Pt/Ti composition and used for the degradation of Novacron Yellow C-RG by both direct and indirect oxidation. The electrochemical degradation

of the above compound by Pt/Ti electrode was compared with that of boron-doped diamond (BDD), and it was found that BDD performs better than Pt/Ti; however the latter does the color removal better than the former by fragmenting the azo dyes (Rocha et al. 2014).

6.6 Microbial Electrochemistry for Water Treatment

Microbial electrochemistry is a branch of electrochemistry that incorporates microorganisms into electrochemical reactions. Microbial electrochemical technology (MET) is an environmentally friendly process which can contribute potentially. The microbial fuel cell (MFC) is one of the best examples for resource recovery from water. The organic compounds are oxidized by microorganisms to generate electrical current at the anode, while oxygen is reduced at the cathode giving rise to flow of electricity (Logan et al. 2006). Microbial electrochemical technologies (MET) make use of electroactive bacteria in the solid-state electrodes for the metabolic activity to oxidize different types of compounds leading to the synthesis of chemicals, bioremediation of polluted matrices, degradation of contaminants, and conversion to different types of energy forms to make it more productive (Ramirez-Vargas et al. 2018). Bioelectrochemical system (BES) is used for the generation of electricity, synthesis of other by-products, and environmental services including soil bioremediation, desalination, and treatment of wastewater (Arends and Verstraete 2012; Sharma et al. 2014). The microbial electrochemistry is based on the interaction of bacteria with the insoluble electron donors or acceptors which rely on the exchange of metabolic electrons either removed from an electron donor or donated to an electron acceptor via an electroconductive material (Rabaey et al. 2007; Rosenbaum and Franks 2014). Either through capacitive interaction or Faraday interactions, the living microbial cells interact with electrodes, whereby the lipid layer of a microorganism enters in contact and replaces the ions and water molecules, because of the change in the double-layer capacity of electrodes. Figure 6.3 presents a schematic illustration of different branches of the biochemistry field and the interrelations with bioelectrochemical systems and their applications as microbial electrochemical technologies.

6.7 The Challenges Faced by Microbial Electrochemical Technologies (MET)

1. METs demand heavy investments over conventional reactors for water treatment due to the requirement of electrodes, current collectors, and wiring and membranes. When an MET is to substitute an activated sludge system either partially or completely, the value resulting from the product and the savings from reduced

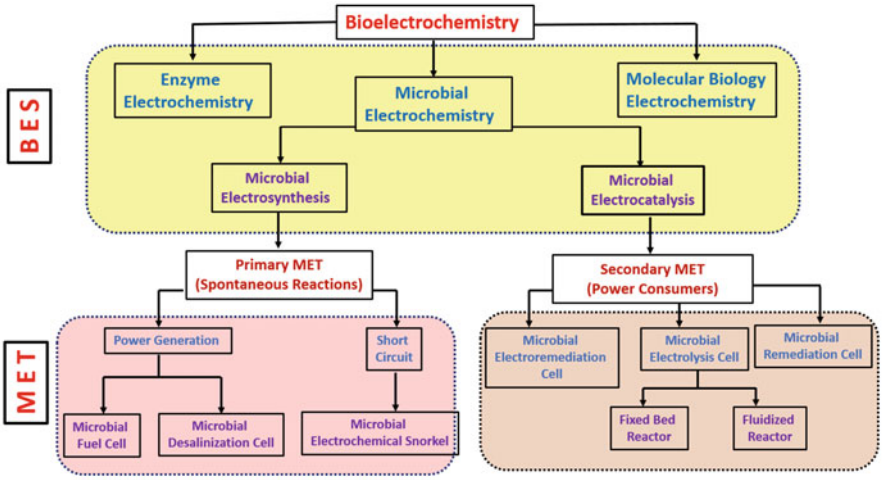

Fig. 6.3 Diagram illustrating the disciplines of the biochemistry field, the interrelations with bioelectrochemical systems, and their applications as microbial electrochemical technologies. (Adopted from Ramirez-Vargas et al. 2018)

aeration requirements should be sufficient to permit a reasonable payback time of the initial investment in the system (Escapa et al. 2012; Modin and Gustavsson 2014).

2. The real wastewater treatment bears low performance, and, on the other hand, when the reactors are operated with synthetic nutrient media containing acetate, the current density is high, yielding better energy efficiencies (Fan et al. 2012). In the domestic water, the conductivity is usually low resulting in large potential losses and eventually lower performance. In addition to the above, the microbial activity can be restricted with a decline in pH due to low alkalinity. The issue of clogging pipes and poisoning of separators is caused by the excess microbial growth and particles (Liu and Cheng 2014). The additional factors that decide the current generation are that of the competitive interaction between microorganisms. When glucose is used in MFC, the conversion of glucose to acetate takes place in the first step by fermentation that serves as substrates for electroactive bacteria-assisted current generation, and similar process takes place when ethanol is fed. A negative consequence in current generation occurs due to the competition between electroactive bacteria and methanogens. Hydrogen-utilizing methanogens stand out to be a strong competitor to electroactive bacteria, and their activities can bring down the coulombic efficiencies of biological anodes. Methanogens make use of hydrogen and acetate as substrates (Freguia et al. 2008; Parameswaran et al. 2009).
3. Inadequate effluent quality. The wastewater treatment is aimed at meeting certain effluent limits, which is more preferred than energy efficiency when considering the treatment plant operation. The effluent coming out from MET has to be

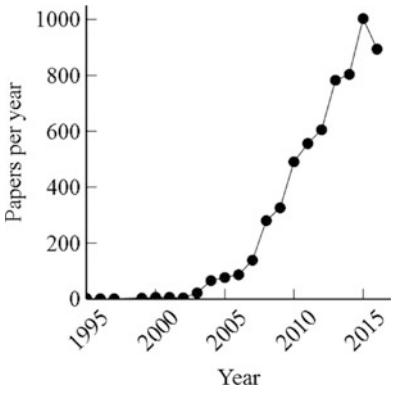

Fig. 6.4 The graph drawn between year and the numbers of papers published. (Reproduced from (Modin and Aulenta 2017) with permission from The Royal Society of Chemistry)

subjected to post-treatment to meet the limits for biochemical oxygen demand (BOD), nitrogen, and phosphorous (He et al. 2016).

4. Competition from existing processes. The sole purpose of MET is to increase the energy recovery from wastewater which is carried out by a mature process called anaerobic digestion, operating at higher COD removal rates. Moreover, production of renewable energy in large scale is achieved by different types of technologies like wind turbines, photovoltaics, and water and wave power.
   The large-scale energy conversion from wastewater using microbial electrochemistry has several other potential applications such as nutrient removal, desalination, chemical production, and degradation of recalcitrant pollutants. Figure 6.4 gives the account of the number of papers published on biosystem-based wastewater treatment coupled with energy harvesting.

6.8 Microbiology-Based Electrochemical Sensors

MET has been considered as a suitable sensor because it is easy to record the electrical current and potential over a range of parameters. It has been researched as sensor for BOD, volatile fatty acids (VFA), microbial cell numbers, corrosion, toxicity extraterrestrial life, activity, and individual chemical compounds and for detection of electronegative microorganisms. The most relevant parameters in water sectors are BOD and VFA (Abrevaya et al. 2015; Yang et al. 2015: Modin and Aulenta 2017).

6.8.1 BOD Sensors

BOD sensors based on MFC were developed as early as in the 1970s and MFC-based sensors with biological anodes exhibited long-term stability beyond

5 years (Kim et al. 2003). The measure of the concentration of biodegradable organic compound water is called BOD. Online sensors with high reliability are more preferred and it is easy to use. Although these sensors have several advantages, they do have certain drawbacks. The sensors based on immobilized cells on oxygen suffer from operational instability that makes it handicapped of longtime operation due to the growth in the immobilized layer (Jouanneau et al. 2014; Liu and Mattiasson 2002). Those employed based on pH shifts and luminescence have the limitation to be used in real wastewater with complex composition or organic compounds (Murakami et al. 1998; Sakaguchi et al. 2003). Although bioreactor-type sensors seem to be most powerful and commercially available, however their large size and several components make them less preferred (Jouanneau et al. 2014).

The BOD sensors developed in the initial days had a very low response time although they had better stability, and this forced the researchers to make efforts to improve the sensors with fast response time and simple design. In order to achieve the above said goals, continuous feeding up was done in MFC where the measure of the current corresponding to BOD concentration was developed instead of feeding in batches followed by measuring the electric charge (Chang et al. 2004). MET-based BOD sensors do have some drawbacks: They are (i) BODs cannot replace conventional BODs but they can be used to infer some data from the wastewater plant that limits its usages; (ii) the incomplete conversion of organic compounds from wastewater into electricity because there is a competition between methanogens and electroactive microorganisms for substrate (Ahn and Logan 2010; Kaur et al. 2014); and (iii) in MFCs, the aerobic oxidation of the substrate arising from the oxygen, passing from cathode to anode and the non-electroactive electrodes' consumption of organic compounds which all will reflect in reduced output (Modin and Aulenta 2017).

When designing sensors, the following aspects have to be kept in mind:

(i) They should be operated in such a way that the activities of electroactive microorganisms are to be promoted over other functional groups.
(ii) Using anodes with high surface area to volume ratio.
(iii) Anode potential-controlled operation.
(iv) Using a gel matrix where electroactive microorganisms are embedded that might also improve the storage of bioelectrodes (Arends 2017).

6.8.2 VFA Sensors

In anaerobic digesters, accumulation of VFAs will result in reaction failure because of a drop in pH, and therefore VFAs are to be monitored. Both offline techniques like high-pressure liquid chromatography and gas chromatography and online techniques like pH titration are used to the total measure of VFAs and get its total concentration, respectively (Feitkenhauer et al. 2002), and the individual VFAs can be detected using headspace chromatography (Boe et al. 2006). Acetate has been widely used as the substrate in most sensors using microbial electrochemical systems (Freguia et al.

2010; Liu et al. 2005a). The ratio between acetate and propionate concentration is the key factor, sensors can also be designed to make them specific to acetate or propionate, altering this ratio would affect anaerobic digester, and maintaining electroactive microbial communities that are specifically active toward acetate or propionate is not so easy (Modin and Aulenta 2017).

6.8.3 Toxic Sensors

Detection and biological treatment of toxic substances found in wastewater are a must as they can be a serious threat to aquatic system which affects people and animals that depend on it. Mostly MFC-based sensors have been employed for the detection of the toxicity in natural and synthetic water (Kim et al. 2007). The interaction of organophosphate insecticide, polychlorinated biphenyl, and heavy metals such as Pb and Hg with MFC brings a drop in the current generation (Stein et al. 2012) that itself is an indication of toxicity apart from polarization curves fitted to kinetic curve; however electroactive biofilms do not respond at concentrations equal or higher than the typical levels in wastewater (Patil et al. 2010).

6.9 Electronic Sensors Based on Nanomaterials

Electronic sensors are made by incorporating nanomaterials such as MoS_2, carbon nanotubes (CNT), and layered materials like graphene and $MoSe_2$ in their single-layer form after exfoliation into single layer. Nanomaterial-based electronic FET sensors show very high sensitivity and quick response towards water pollutants owing to their high carrier mobility and high sensitivity to electronic perturbations, outdoing the present technologies. When the contaminant comes in contact with the semiconducting materials in the channel of the transistors, the contaminants are detected based on the change in the semiconducting material's conductivity. The concentration of the contaminants corresponds to the extent of the amplitude of conductivity (Mao et al. 2015). These FET sensors made up of nanomaterials have three terminals, namely, source terminal, the drain terminal, and the gate terminal, and the semiconducting nanomaterial forms the sensing channel that connects the source and drain terminals. The position of the gates can be made either on top or back position depending on the composition of the sensors. The sensitivity of the 1D and 2D semiconducting nanomaterials to the chemical contaminants makes them to be incorporated in chemical and biosensors. When water contaminants such as heavy metals and bacteria come into contact with FET-based sensors, it stimulates a change in the electrical characteristics, and the difference in the electrical behavior is used to detect both the presence and the extent of contamination. The age-old techniques to detect heavy metal ions such as Hg^{2+} and Cd^{2+} found from food industries to environmental science are spectroscopy and fluorescence which are not only

expensive but also hardly portable. Therefore, the alternative device that can detect Hg^{2+} and Cd^{2+} reliably and rapidly is using a FET device where 1D SiNW is synthesized using bottom-up approach employed as channel (Cui et al. 2001; Luo et al. 2009).

6.10 Bioelectrochemical Systems (BESs)

Bioelectrochemical systems (BESs) are based on the interaction of bacteria with electrodes making use of electrons that are either supplied or removed through an external electrical circuit. Microbial fuel cells (MFC) are a very productive form of generating power from electron donors present in the water as contaminants through extracellular electron transfer by bacteria, with respect to metals like iron and manganese. The role of bacteria and its interaction with electron and its due mechanisms are explored to understand the process of energy conversion process and building a green environment although several aspects are yet to be discovered.

The interaction of bacteria with insoluble terminal electron and acceptor donors is very similar to chemical system. In MFC bacteria oxidize the electron donors where anodic electrode is an electron acceptor with the electron flow takes place from the anode through the external circuit. The electron flow is directed toward a high-redox electron acceptor such as oxygen at the electrode, and the cations equate the charge balance by diffusing from anode to cathode via a charge-selective separator (Rabaey and Verstraete 2005). At the surface of the electrode, bacteria consume electrons accompanied with the electrochemical reduction of electron acceptor like nitrate, perchlorate, or metals (Gregory et al. 2004; Gregory and Lovley 2005; Clauwaert et al. 2007).

In every anodic and cathodic case, the utmost driving force is extracellular electron transfer that is required as and when the entry of an electron acceptor or donor into the cell is restricted and its extracellular electrons are transferred to insoluble Fe (III) or Mn(IV) oxides or to humic substances which are too large to enter into the cells (Lovley et al. 1987; Myers and Nealson 1988).

The bacterial cell yield is determined by the energy accessible to bacteria which corresponds to the potential difference between the electron donor and acceptor (Heijnen et al. 1999). The Nernst equation is used to determine the difference in potential between donor and acceptor which is related to the extent of the availability of oxidized and reduced compound (Rabaey and Verstraete 2005).

In BES anodes, the anodic potential defines the potential of the electron acceptor and in the cathode the cathodic potential is defined by electron donor potential. The yield by the bacteria is determined by many factors including the resistance of the electrolyte. Here a closer interaction between bacteria and the electrode is inevitable to minimise the activation losses that lead to imperfect oxidation and reduction. Butler–Volmer equation describes the activation loss at the electrode, either toward or away from an insoluble acceptor or donor, and the parameters of the equation can

be determined via linearization, followed by calculating the gain for bacteria depending on an electron flux.

6.11 Zinc-Based Electrochemical Sensors

Zinc oxide of different morphologies is employed in electrochemical sensors especially in the detection of p-nitroaniline (pNA), that is, the derivate of aniline used in dye, polymer, rubber, painting, gasoline, and pharmaceutical industries (Ahmad et al. 2017). When the pNA discharge is excess in the environment, it leads to the catastrophic effect to both human being and environment. ZnO nano rod assembly grown on FTO (electrode) with seed layer assisted has been used both with and without binder by Rafiq Ahmad et.al was used for the detection of pNA). They reported that the nanorods grown directly on the electrode without binder seem to bear better surface with enhanced electrocatalytic activity. In phosphate buffer saline solution (PBS), the dissolved oxygen gets adsorbed onto the surface of ZnO nanorod, ionic species (O_2^-, OH^-, etc.) are generated on the surface, and the ionic species generated absorb electrons from the conduction band and migrate to the surface of the ZnO NR. The chemisorbed ionic species (OH^-) combine with pNA and yield CO_2 and H_2O by oxidation while forming several intermediate reactions (Ahmad et al. 2016, 2017; Sun et al. 2007). Gupta et al. synthesized ZnO nanoparticles and used modified electrode of the following composition: ZnO/NP sonic liquid–carbon paste electrode (ZnO/NPs/IL/CPE) toward the detection of droxidopa in pharmaceutical and urine samples (Gupta et al. 2013).

6.12 Ionic Liquids in Electrochemical Sensing

Ionic liquids have been employed in electrochemical sensing because of their unusual physicochemical properties such as low volatility, high intrinsic conductivity, high thermal stability, wide electrochemical windows, and appreciable solvability. The kinds of sensing ionic liquids that have been used include the sensing of biomolecules, such as nucleic acids, enzymes and proteins, sensing gas, and various important ions, among other chemo-sensing platforms, and they are most widely used for electrochemical sensing of CO_2 which has become an inevitable part of human life (Behera et al. 2015). Ionic liquids are, in liquid state, comprised of salts of their weekly coordinated ions at temperatures below 100C. They mostly consist of a bulky organic cation (e.g., alkyl-substituted ammonium, imidazolium, pyrrolidinium, etc.) paired with an inorganic or organic anion (e.g., acetate, hexafluorophosphate, halide ions, tetrafluoroborate, etc.). They possess two asymmetrical ions with opposite charges which are loosely fit together (Wei and Ivaska 2008). They possess many archetypal properties, like low volatility, high chemical

and thermal stability, wide electrochemical window, wide liquid range, good electrical conductivity, high polarity, and appreciable ability to dissolve in several compounds, and therefore they remain stable when used under conditions, while the organic solvents fail. They work well on wide electrochemical windows as 4.5 V compared with 1.2 V in most aqueous electrolytes can be used for several compounds which would otherwise be inaccessible (Fuller et al. 1997; Hapiot and Lagrost 2008; Quinn et al. 2002; Wei and Ivaska 2008). The physical and chemical properties of the ionic liquids can be tuned by tuning the structure of the cation and/or anion and selecting appropriate cation or anion to suit a specific requirement (Behera et al. 2015; Greaves and Drummond 2008; Kyo et al. 2005; Plechkova and Seddon 2008; Seddon 2003; Wasserscheid 2006; Welton 1999). These ionic liquids are environmentally friendly and play a dual role of acting as solvent and electrolyte as well and in addition they are used as alternative electrolyte material for several electrochemical devices like solar cells; fuel cells; batteries; supercapacitors; sensing biomolecules like proteins, enzymes, and nucleic acids; and several gases including O_2, CO, CO_2, SO_2, NO_2, H_2S, and Cl_2 (Behera et al. 2015). Ionic liquids can be divided into two groups based on their solubility in water, namely, hydrophilic and hydrophobic. The immiscible hydrophobic ionic liquids have been coated on glassy carbon electrode which in turn can be used for electrochemical sensing. The hydrophobic ionic liquids make nonpolarizable interfaces when in contact with water which has the advantage of being easily prepared in aqueous solution. In some cases, dry ionic liquids have been used without moisture, depending on the requirement, and hydrophilic (water-miscible) ionic liquids had been sidelined for a long time, owing to its stability issue in aqueous solution. In the recent days, hydrophilic ionic liquids are also made as film on glassy carbon electrodes to be used in aqueous media for electrochemical sensing (Yu et al. 2005). The anions present on the ILs determine the miscibility of ILs (Seddon et al. 2000; Anthony et al. 2001). The anions that make the ILs miscible in water are Cl^-, Br^-, I^-, NO_3^-, $CH3COO^-$, and CF_3COO^-, and those ILs having Tf_2^- and PF_6 groups on the contrary make them immiscible, while the ILs with BF_4^- and CF_3SO_3 depend on the structure of the cations though they have miscibility in water to some extent. The miscibility of ILs in water is indirectly proportional to length of the cation chain. The shorter the chain length, the greater is the miscibility, and the longer the chain length, lesser the miscibility as the length of the cation chain corresponds to the surface tension (Fitchett et al. 2005). IL-based electrochemical analysis is applied for two types of sensors as far as water treatment is concerned:

(a) Ion-selective or potentiometric sensors: Potentiometric or ion-selective sensors make use of solid-state planar reference electrodes based on ILs and Ag/AgCl planar microelectrodes embedded with PVC membranes. This method is fast, accurate, and cost-effective. IL-based sensors, with PEDOT-based electrode, exhibit linear anionic potentiometric response in KCL solution, and such electrodes show high selectivity to anions such as sulfate (Wei and Ivaska 2008).
(b) Voltammetric sensors are a complementary class of sensors to potentiometric sensors which use ILS to detect ions voltammetrically. Techniques such as linear

sweep, square wave, and cathodic stripping voltammetry are used to determine trace amount of chloride (Wei and Ivaska 2008; Villagran et al. 2004). In voltammetric sensors IL-type carbon paste electrode (Liu et al. 2005b) and imidazolium salt-functionalized polyelectrolyte were utilized (Shen et al. 2007). The configuration is set up with working electrode, reference electrode, and counter electrode which were all kept in close proximity to one another and covered with a thin film of IL insoluble in water. From the carrier stream, the electroactive components to be detected and determined need to diffuse into the ionic liquid first and then into the surface of the working electrode (Yu et al. 2005).

6.13 Metal Removal

From the wastewater, the metal contaminants contaminate drinking water, and therefore there is a need to prevent contamination and recover valuable metals from it. The different metal contaminants such as cadmium, mercury, lead, copper, lithium, indium, cobalt, platinum- group metals, aluminum, and steel were sent out from different kinds of industries manufacturing various articles (Modin and Aulenta 2017; Nabi et al. 2009). The different sources releasing metal-containing wastewater are petroleum refining; photographic operations which releases several metals, inorganic pigment, and dye manufacturing; wood processing; treatment process; and printed circuit board manufacturing (Barakat 2011). In addition to the above listed processes, metal wastes from mining industries and metal-containing leachates also give out wastewater containing metal contaminants (Akcil and Koldas 2006; Van der Bruggen et al. 1998). The different techniques used for the removal of metals from wastewater are, ion exchange, membrane separation, electrodialysis, chemical precipitation, photocatalysis, and adsorption. In order to recover metals from highly concentrated wastewater sources, electrochemical processes are employed, and to recover specific metals in their elemental form, electrochemical recovery by reduction of metal ions on cathode is adopted and used. For these processes to be efficient and economical, the metal concentration has to be very high (Modin and Aulenta 2017).

6.14 Microbial Electro Chemical Metal Recovery

For the recovery of metal particles, different kinds of microbial electrochemical reactors are being used, and the organic compounds/sulfides are oxidized on the microbial anode, the reduction of the metal ions takes place at the abiotic cathode, and they are reduced as solid metal. The schematic representation is given in Fig. 6.5.

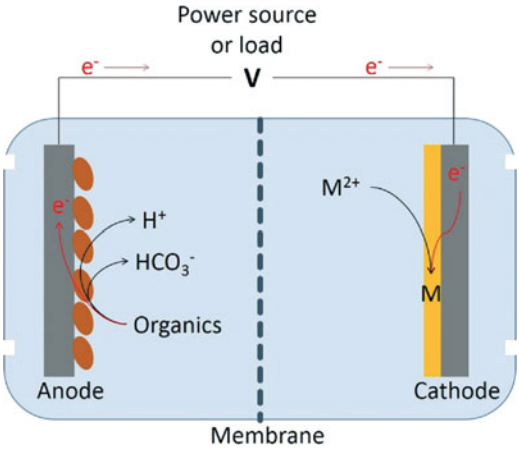

Fig. 6.5 Schematic diagram illustrating of a microbial electrochemical reactor with a microbial anode oxidizing organics and an abiotic cathode reducing metal ions. (Reproduced from (Modin and Aulenta 2017) with permission from The Royal Society of Chemistry)

This type of system has dual advantage of combining the treatment of organic wastewater at the anode and the recovery of metal at the cathode. The operating potential of the anodes is usually from -0.2 to 0 V whereas the reduction potential of Cu^{2+}/Cu is 0.34 V vs. the standard hydrogen electrode SHE, which is higher than the former and therefore the system could be used with MFC to recover Cu along with the generation of electricity. The recovery of Cu by the above system has a highest efficiency of >99.88%, and such removal techniques are used to recover Au, Ag, Ni, Pb, Cd, and Zn using biological anodes and abiotic cathodes (Heijne et al. 2010; Tao et al. 2011; An et al. 2014; Cheng et al. 2013; Wu et al. 2016; Choi and Hu 2013; Choi and Cui 2012; Qin et al. 2012). In order to recover the metals with low reduction potentials such as Ni, Pb, Cd, and Zn, MFCs use the electrical energy as the input. In a mixed solution containing metals like Cu, Pb, Cd, and Zn, the metals are extracted using applied potentials ranging between 0 V and 1.7 V (Modin and Aulenta 2017). The metals are obtained whether as soluble ions or as precipices by reduction reaction occurring at the cathode, and in the case of lithium batteries the Co^{2+} ions from lithium cobalt oxides from the used lithium batteries are discharged using MFC (Huang et al. 2013), which was also used to convert VO_2^+ to VO^{2+} of reduced toxicity by precipitation (Zhang et al. 2009). In exceptional cases intermediates are generated at the cathode which interact with metals and in the case of reduction of Cr(IV) to Cr(III) by the intermediate H_2O_2 formed by the reduction of O_2 on a cathode in MFC (Liu et al. 2011). For the precipitation of $Co(OH)_2$, it was also carried out by hydroxide ion generated by the reduction of O_2 in a MFC (Huang et al. 2015). For the reduction of metals, microorganisms can also be employed as catalysts in few cases, and the microorganisms influence the thermodynamics of the reaction (Modin and Aulenta 2017; Varia et al. 2014).

6.15 Conclusion

Over the past several decades, researchers have discovered and developed a number of technologies, to investigate sense and detect and treat the pollutants. These conventional detection techniques lack rapid and in situ sensing, and these were made possible by using nanomaterials in sensors which offer several advantages like very high sensitivity, quick response, easy detection, small size, and cost-effectiveness. Adopting electrochemistry for the treatment of wastewater is an environmentally friendly method and cost-effective. It is most effective because of adopting different strategies of oxidation and technologies to mineralize the non-biodegradable organic matter. In anodic oxidation, indirect oxidation is more beneficial than direct oxidation since indirect oxidation proceeding via intermediates of oxygen production will not be subjected to catalytic poisoning or corrosion, subsequently influencing the selectivity and efficiency positively which depend on the nature of the electrode. The extracellular electron transfer by microorganism can be understood through BES, and it can open new ways for biogeochemical cycles to facilitate clean and green environment. BES can be an efficient tool for the removal of nitrate, perchlorate, sulfur, and other compounds. The removal of organic compounds and pollutants from water effluents can be innovatively treated using microbial electrochemical technologies which generate power besides degrading the pollutants. Electrochemical treatment of wastewater that offers a better platform to build a clean environment can be improved by restructuring the technique to treat a large quantity of wastewater for the cost-effective and productive degradation of the contaminants.

Acknowledgment The authors A. Dennyson Savariraj and R.V. Mangalaraja gratefully acknowledge FONDECYT Post-doctoral Project No. 3170640, Government of Chile, Santiago, for the financial assistance.

References

Abrevaya XC, Sacco NJ, Bonetto MC, Hilding-Ohlsson A, Corton E (2015) Analytical applications of microbial fuel cells. Part II: toxicity, microbial activity and quantification, single analyte detection and other uses. Biosens Bioelectron 63:591–601. https://doi.org/10.1016/j.bios.2014.04.053

Ahmad R, Tripathy N, Khan MY, Bhat KS, Ahn M, Hahn Y (2016) Ammonium ion detection in solution using vertically grown ZnO nanorod based field-effect transistor. RSC Adv 6 (60):54836–54840. https://doi.org/10.1039/C6RA09731F

Ahmad R, Tripathy N, Ahn M, Hahn Y (2017) Development of highly-stable binder-free chemical sensor electrodes for p-nitroaniline detection. J Colloid Interface Sci 494:300–306. https://doi.org/10.1016/j.jcis.2017.01.099

Ahn Y, Logan BE (2010) Effectiveness of domestic wastewater treatment using microbial fuel cells at ambient and mesophilic temperatures. Bioresour Technol 101(2):469–475. https://doi.org/10.1016/j.biortech.2009.07.039

Akcil A, Koldas S (2006) Acid mine drainage (AMD): causes, treatment and case studies. J Clean Prod 14(12):1139–1145. https://doi.org/10.1016/j.jclepro.2004.09.006

Alothman ZA, Ali R, Naushad M (2012) Hexavalent chromium removal from aqueous medium by activated carbon prepared from peanut shell: adsorption kinetics, equilibrium and thermodynamic studies. Chem Eng J 184:238–247. https://doi.org/10.1016/j.cej.2012.01.048

An Z, Zhang H, Wen Q, Chen Z, Du M (2014) Desalination combined with copper(II) removal in a novel microbial desalination cell. Desalination 346:115–121. https://doi.org/10.1016/j.desal.2014.05.012

Anthony JL, Maginn EJ, Brennecke JF (2001) Solution thermodynamics of imidazolium-based ionic liquids and water. J Phys Chem B 105(44):10942–10949. https://doi.org/10.1021/jp0112368

Aragay G, Pons J, Merkoci A (2011) Enhanced electrochemical detection of heavy metals at heated graphite nanoparticle-based screen-printed electrodes. J Mater Chem 21(12):4326–4331. https://doi.org/10.1039/C0JM03751F

Arends JBA (2017) The next step towards usable microbial bioelectrochemical sensors? Microb Biotechnol 11(1):20–21. https://doi.org/10.1111/1751-7915.12590

Arends JBA, Verstraete W (2012) 100 years of microbial electricity production: three concepts for the future. Microb Biotechno 5(3):333–346. https://doi.org/10.1111/j.1751-7915.2011.00302.x

Barakat MA (2011) New trends in removing heavy metals from industrial wastewater. Arab J Chem 4(4):361–377. https://doi.org/10.1016/j.arabjc.2010.07.019

Behera K, Pandey S, Kadyan A, Pandey S (2015) Ionic liquid-based optical and electrochemical carbon dioxide sensors. Sensors (Basel) 15(12). https://doi.org/10.3390/s151229813

Bi X, Agarwal A, Yang K (2009) Oligopeptide-modified silicon nanowire arrays as multichannel metal ion sensors. Biosens Bioelectron 24(11):3248–3251. https://doi.org/10.1016/j.bios.2009.04.007

Blum DJW, Hergenroeder R, Parkin GF, Speece RE (1986) Anaerobic treatment of coal conversion wastewater constituents: biodegradability and toxicity. J Water Pollut Control Fed 58 (2):122–131. https://doi.org/10.2307/25042863

Boe K, Batstone DJ, Angelidaki I (2006) An innovative online VFA monitoring system for the anerobic process, based on headspace gas chromatography. Biotechnol Bioeng 96(4):712–721. https://doi.org/10.1002/bit.21131

Chai F, Wang C, Wang T, Li L, Su Z (2010) Colorimetric detection of Pb^{2+} using glutathione functionalized gold nanoparticles. ACS Appl Mater Interfaces 2(5):1466–1470. https://doi.org/10.1021/am100107k

Chang H, Johnson DC (1990) Electrocatalysis of anodic oxygen-transfer reactions: activation of electrodes in by addition of bismuth(III) and arsenic(III,V). J Electrochem Soc 137 (8):2452–2457. https://doi.org/10.1149/1.2086959

Chang IS, Jang JK, Gil GC, Kim M, Kim HJ, Cho BW, Kim BH (2004) Continuous determination of biochemical oxygen demand using microbial fuel cell type biosensor. Biosens Bioelectron 19 (6):607–613. https://doi.org/10.1016/S0956-5663(03)00272-0

Chang J, Mao S, Zhang Y, Cui S, Zhou G, Wu X, Yang C, Chen J (2013) Ultrasonic-assisted self-assembly of monolayer graphene oxide for rapid detection of bacteria. Nanoscale 5 (9):3620–3626. https://doi.org/10.1039/C3NR00141E

Chatzisymeon E, Dimou A, Mantzavinos D, Katsaounis A (2009) Electrochemical oxidation of model compounds and olive mill wastewater over DSA electrodes: 1. The case of Ti/IrO2 anode. J Hazard Mater 167(1):268–274. https://doi.org/10.1016/j.jhazmat.2008.12.117

Chen K, Lu G, Chang J, Mao S, Yu K, Cui S, Chen J (2012) Hg(II) ion detection using thermally reduced graphene oxide decorated with functionalized gold nanoparticles. Anal Chem 84 (9):4057–4062. https://doi.org/10.1021/ac3000336

Chen Y, Michael ZP, Kotchey GP, Zhao Y, Star A (2014) Electronic detection of bacteria using holey reduced graphene oxide. ACS Appl Mater Interfaces 6(6):3805–3810. https://doi.org/10.1021/am500364f

Cheng S, Wang B, Wang Y (2013) Increasing efficiencies of microbial fuel cells for collaborative treatment of copper and organic wastewater by designing reactor and selecting operating parameters. Bioresour Technol 147:332–337. https://doi.org/10.1016/j.biortech.2013.08.040

Choi C, Cui Y (2012) Recovery of silver from wastewater coupled with power generation using a microbial fuel cell. Bioresour Technol 107:522–525. https://doi.org/10.1016/j.biortech.2011.12.058

Choi C, Hu N (2013) The modeling of gold recovery from tetrachloroaurate wastewater using a microbial fuel cell. Bioresour Technol 133:589–598. https://doi.org/10.1016/j.biortech.2013.01.143

Chouteau C, Dzyadevych S, Chovelon J, Durrieu C (2004) Development of novel conductometric biosensors based on immobilised whole cell microalgae. Biosens Bioelectron 19(9):1089–1096. https://doi.org/10.1016/j.bios.2003.10.012

Clauwaert P, Rabaey K, Aelterman P, De Schamphelaire L, Pham TH, Boeckx P, Boon N, Verstraete W (2007) Biological denitrification in microbial fuel cells. Environ Sci Technol 41 (9):3354–3360. https://doi.org/10.1021/es062580r

Comninellis C (1994) Electrocatalysis in the electrochemical conversion/combustion of organic pollutants for waste water treatment. Electrochim Acta 39(11):1857–1862. https://doi.org/10.1016/0013-4686(94)85175-1

Comninellis C, Pulgarin C (1991) Anodic oxidation of phenol for waste water treatment. J Appl Electrochem 21(8):703–708. https://doi.org/10.1021/es062580r

Cui Y, Wei Q, Park H, Lieber CM (2001) Nanowire nanosensors for highly sensitive and selective detection of biological and chemical species. Science 293(5533):1289. https://doi.org/10.1126/science.1062711

Dakiky M, Nemcova I (2000) Aggregation of o,o′- Dihydroxy azo Dyes III. Effect of Cationic, Anionic and Non-Ionic Surfactants on the Electronic Spectra of 2-Hydroxy-5-Nitrophenylazo-4-[3-Methyl-1-(4ϩ-sulfophenyl)-5-pyrazolone]. Dyes Pigments 44(3):181–193. https://doi.org/10.1016/S0143-7208(99)00086-8

Darbha GK, Ray A, Ray PC (2007) Gold nanoparticle-based miniaturized nanomaterial surface energy transfer probe for rapid and ultrasensitive detection of mercury in soil, water, and fish. ACS Nano 1(3):208–214. https://doi.org/10.1021/nn7001954

Darbha GK, Singh AK, Rai US, Yu E, Yu H, Chandra Ray P (2008) Selective detection of mercury (II) ion using nonlinear optical properties of gold nanoparticles. J Am Chem Soc 130 (25):8038–8043. https://doi.org/10.1021/ja801412b

Escapa A, Gomez X, Tartakovsky B, Moran A (2012) Estimating microbial electrolysis cell (MEC) investment costs in wastewater treatment plants: case study. Int J Hydrog Energy 37 (24):18641–18653. https://doi.org/10.1016/j.ijhydene.2012.09.157

Fan Y, Han S, Liu H (2012) Improved performance of CEA microbial fuel cells with increased reactor size. Energy Environ Sci 5(8):8273–8280. https://doi.org/10.1039/C2EE21964F

Fedorak PM, Hrudey SE (1986) Anaerobic treatment of phenolic coal conversion wastewater in semicontinuous cultures. Water Res 20(1):113–122. https://doi.org/10.1016/0043-1354(86)90222-8

Feitkenhauer H, von Sachs J, Meyer U (2002) On-line titration of volatile fatty acids for the process control of anaerobic digestion plants. Water Res 36(1):212–218. https://doi.org/10.1016/S0043-1354(01)00189-0

Feng YJ, Li XY (2003) Electro-catalytic oxidation of phenol on several metal-oxide electrodes in aqueous solution. Water Res 37(10):2399–2407. https://doi.org/10.1016/s0043-1354(03)00026-5

Feng Y, Yang L, Liu J, Logan BE (2016) Electrochemical technologies for wastewater treatment and resource reclamation. Environ Sci Water Res Technol 2(5):800–831. https://doi.org/10.1039/C5EW00289C

Fitchett BD, Rollins JB, Conboy JC (2005) Interfacial tension and electrocapillary measurements of the room temperature ionic liquid/aqueous interface. Langmuir 21(26):12179–12186. https://doi.org/10.1021/la051997s

Freguia S, Rabaey K, Yuan Z, Keller J (2008) Syntrophic processes drive the conversion of glucose in microbial fuel cell anodes. Environ Sci Technol 42(21):7937–7943. https://doi.org/10.1021/es800482e

Freguia S, Teh EH, Boon N, Leung KM, Keller J, Rabaey K (2010) Microbial fuel cells operating on mixed fatty acids. Bioresour Technol 101(4):1233–1238. https://doi.org/10.1016/j.biortech.2009.09.054

Fuller J, Carlin RT, Osteryoung RA (1997) The room temperature ionic liquid 1-ethyl-3-methylimidazolium tetrafluoroborate: electrochemical couples and physical properties. J Electrochem Soc 144(11):3881–3886. https://doi.org/10.1149/1.1838106

Galla U, Kritzer P, Bringmann J, Schmieder H (2000) Process for total degradation of organic wastes by mediated electrooxidation. Chem Eng Technol 23(3):230–233. https://doi.org/10.1002/(SICI)1521-4125(200003)23:3<230::AID-CEAT230>3.0.CO;2-3

Gao C, Yu X, Xiong S, Liu J, Huang X (2013) Electrochemical detection of arsenic(III) completely free from noble metal: Fe_3O_4 microspheres-room temperature ionic liquid composite showing better performance than gold. Anal Chem 85(5):2673–2680. https://doi.org/10.1021/ac303143x

Gattrell M, Kirk DW (1993) A study of the oxidation of phenol at platinum and preoxidized platinum surfaces. J Electrochem Soc 140(6):1534–1540. https://doi.org/10.1149/1.2221598

Gong J, Zhou T, Song D, Zhang L (2010a) Monodispersed Au nanoparticles decorated graphene as an enhanced sensing platform for ultrasensitive stripping voltammetric detection of mercury(II). Sens Actuators B Chem 150(2):491–497. https://doi.org/10.1016/j.snb.2010.09.014

Gong J, Zhou T, Song D, Zhang L, Hu X (2010b) Stripping voltammetric detection of mercury (II) based on a bimetallic Au-Pt inorganic-organic hybrid nanocomposite modified glassy carbon electrode. Anal Chem 82(2):567–573. https://doi.org/10.1021/ac901846a

Greaves TL, Drummond CJ (2008) Protic ionic liquids: properties and applications. Chem Rev 108(1):206–237. https://doi.org/10.1021/cr068040u

Gregory KB, Lovley DR (2005) Remediation and recovery of uranium from contaminated subsurface environments with electrodes. Environ Sci Technol 39(22):8943–8947. https://doi.org/10.1021/es050457e

Gregory JM, Ingram WJ, Palmer MA, Jones GS, Stott PA, Thorpe RB, Lowe JA, Johns TC, Williams KD (2004) A new method for diagnosing radiative forcing and climate sensitivity. Geophys Res Lett 31(3). https://doi.org/10.1029/2003GL018747

Gupta VK, Sadeghi R, Karimi F (2013) A novel electrochemical sensor based on ZnO nanoparticle and ionic liquid binder for square wave voltammetric determination of droxidopa in pharmaceutical and urine samples. Sensors Actuators B Chem 186:603–609. https://doi.org/10.1016/j.snb.2013.06.048

Habibi MH, Hassanzadeh A, Mahdavi S (2005) The effect of operational parameters on the photocatalytic degradation of three textile azo dyes in aqueous TiO2 suspensions. J Photochem Photobiol A 172(1):89–96. https://doi.org/10.1016/j.jphotochem.2004.11.009

Hapiot P, Lagrost C (2008) Electrochemical reactivity in room-temperature ionic liquids. Chem Rev 108(7):2238–2264. https://doi.org/10.1021/cr0680686

He W, Wallack MJ, Kim K, Zhang X, Yang W, Zhu X, Feng Y, Logan BE (2016) The effect of flow modes and electrode combinations on the performance of a multiple module microbial fuel cell installed at wastewater treatment plant. Water Res 105:351–360. https://doi.org/10.1016/j.watres.2016.09.008

Heijne AT, Liu F, Rvd W, Weijma J, Buisman CJN, Hamelers HVM (2010) Copper recovery combined with electricity production in a microbial fuel cell. Environ Sci Technol 44(11):4376–4381. https://doi.org/10.1021/es100526g

Heijnen HFG, Schiel AE, Fijnheer R, Geuze HJ, Sixma JJ (1999) Activated platelets release two types of membrane vesicles: microvesicles by surface shedding and exosomes derived from exocytosis of multivesicular bodies and alpha-granules. Blood 94(11):3791. http://www.bloodjournal.org/content/94/11/3791.abstract

Huang C, Yang Z, Lee K, Chang H (2007) Synthesis of highly fluorescent gold nanoparticles for sensing mercury(II). Angew Chem 119(36):6948–6952. https://doi.org/10.1002/ange.200700803

Huang Y, Dong X, Liu Y, Li L, Chen P (2011) Graphene-based biosensors for detection of bacteria and their metabolic activities. J Mater Chem 21(33):12358–12362. https://doi.org/10.1039/C1JM11436K

Huang L, Li T, Liu C, Quan X, Chen L, Wang A, Chen G (2013) Synergetic interactions improve cobalt leaching from lithium cobalt oxide in microbial fuel cells. Bioresour Technol 128:539–546. https://doi.org/10.1016/j.biortech.2012.11.011

Huang H, Chen T, Liu X, Ma H (2014) Ultrasensitive and simultaneous detection of heavy metal ions based on three-dimensional graphene-carbon nanotubes hybrid electrode materials. Anal Chim Acta 852:45–54. https://doi.org/10.1016/j.aca.2014.09.010

Huang L, Liu Y, Yu L, Quan X, Chen G (2015) A new clean approach for production of cobalt dihydroxide from aqueous co(II) using oxygen-reducing biocathode microbial fuel cells. J Clean Prod 86:441–446. https://doi.org/10.1016/j.jclepro.2014.08.018

Hwang GH, Han WK, Park JS, Kang SG (2008) Determination of trace metals by anodic stripping voltammetry using a bismuth-modified carbon nanotube electrode. Talanta 76(2):301–308. https://doi.org/10.1016/j.talanta.2008.02.039

Injang U, Noyrod P, Siangproh W, Dungchai W, Motomizu S, Chailapakul O (2010) Determination of trace heavy metals in herbs by sequential injection analysis-anodic stripping voltammetry using screen-printed carbon nanotubes electrodes. Anal Chim Acta 668(1):54–60. https://doi.org/10.1016/j.aca.2010.01.018

Johnson SK, Houk LL, Feng J, Houk RS, Johnson DC (1999) Electrochemical incineration of 4-chlorophenol and the identification of products and intermediates by mass spectrometry. Environ Sci Technol 33(15):2638–2644. https://doi.org/10.1021/es981045r

Jouanneau S, Recoules L, Durand MJ, Boukabache A, Picot V, Primault Y, Lakel A, Sengelin M, Barillon B, Thouand G (2014) Methods for assessing biochemical oxygen demand (BOD): a review. Water Res 49:62–82. https://doi.org/10.1016/j.watres.2013.10.066

Juttner K, Galla U, Schmieder H (2000) Electrochemical approaches to environmental problems in the process industry. Electrochim Acta 45(15):2575–2594. https://doi.org/10.1016/S0013-4686(00)00339-X

Kalluri J, Arbneshi T, Afrin Khan S, Neely A, Candice P, Varisli B, Washington M, McAfee S, Robinson B, Banerjee S, Singh A, Senapati D, Ray P (2009) Use of gold nanoparticles in a simple colorimetric and ultrasensitive dynamic light scattering assay: selective detection of arsenic in groundwater. Angew Chem 121(51):9848–9851. https://doi.org/10.1002/anie.200903958

Kaur A, Boghani HC, Michie I, Dinsdale RM, Guwy AJ, Premier GC (2014) Inhibition of methane production in microbial fuel cells: operating strategies which select electrogens over methanogens. Bioresour Technol 173:75–81. https://doi.org/10.1016/j.biortech.2014.09.091

Kaur G, Devi P, Kumar M, Thakur A, Bala R, Kumar A (2017) Electrochemical aspects of photocatalysis: Au@FeS2 nanocomposite for removal of industrial pollutant. Phys Chem Chem Phys 19(48):32412–32420. https://doi.org/10.1039/C7CP06289C

Kim BH, Chang IS, Cheol Gil G, Park HS, Kim HJ (2003) Novel BOD (biological oxygen demand) sensor using mediator-less microbial fuel cell. Biotechnol Lett 25(7):541–545. https://doi.org/10.1023/A:1022891231369

Kim M, Sik Hyun M, Gadd GM, Joo Kim H (2007) A novel biomonitoring system using microbial fuel cells. J Environ Monit 9(12):1323–1328. https://doi.org/10.1039/b713114c

Kim TH, Lee J, Hong S (2009) Highly selective environmental nanosensors based on anomalous response of carbon nanotube conductance to mercury ions. J Phys Chem C 113(45):19393–19396. https://doi.org/10.1021/jp908902k

Kumar Jena B, Retna Raj C (2008) Gold nanoelectrode ensembles for the simultaneous electrochemical detection of ultratrace arsenic, mercury, and copper. Anal Chem 80(13):4836–4844. https://doi.org/10.1021/ac071064w

Kyo M, Usui-Aoki K, Koga H (2005) Label-free detection of proteins in crude cell lysate with antibody arrays by a surface Plasmon resonance imaging technique. Anal Chem 77 (22):7115–7121. https://doi.org/10.1021/ac050884a

Li J, Guo S, Zhai Y, Wang E (2009) High-sensitivity determination of lead and cadmium based on the Nafion-graphene composite film. Anal Chim Acta 649(2):196–201. https://doi.org/10.1016/j.aca.2009.07.030

Li M, Zhou X, Guo S, Wu N (2013) Detection of lead (II) with a "turn-on" fluorescent biosensor based on energy transfer from CdSe/ZnS quantum dots to graphene oxide. Biosens Bioelectron 43:69–74. https://doi.org/10.1016/j.bios.2012.11.039

Liu W, Cheng S (2014) Microbial fuel cells for energy production from wastewaters: the way toward practical application. J Zhejiang Univ Sci A 15(11):841–861. https://doi.org/10.1631/jzus.A1400277

Liu J, Mattiasson B (2002) Microbial BOD sensors for wastewater analysis. Water Res 36 (15):3786–3802. https://doi.org/10.1016/S0043-1354(02)00101-X

Liu H, Cheng S, Logan BE (2005a) Production of electricity from acetate or butyrate using a single-chamber microbial fuel cell. Environ Sci Technol 39(2):658–662. https://doi.org/10.1021/es048927c

Liu H, He P, Li Z, Sun C, Shi L, Liu Y, Zhu G, Li J (2005b) An ionic liquid-type carbon paste electrode and its polyoxometalate-modified properties. Electrochem Commun 7 (12):1357–1363. https://doi.org/10.1016/j.elecom.2005.09.018

Liu L, Yuan Y, Li F, Feng C (2011) In-situ Cr(VI) reduction with electrogenerated hydrogen peroxide driven by iron-reducing bacteria. Bioresour Technol 102(3):2468–2473. https://doi.org/10.1016/j.biortech.2010.11.013

Logan BE, Hamelers B, Rozendal R, Schroder U, Keller J, Freguia S, Aelterman P, Verstraete W, Rabaey K (2006) Microbial fuel cells: methodology and technology. Environ Sci Technol 40 (17):5181–5192. https://doi.org/10.1021/es0605016

Lovley DR, Stolz JF, Nord GL Jr, Phillips EJP (1987) Anaerobic production of magnetite by a dissimilatory Iron-reducing microorganism. Nature 330:252. https://doi.org/10.1038/330252a0

Luo L, Jie J, Zhang W, He Z, Wang J, Yuan G, Zhang W, Wu L, Man C, Lee S (2009) Silicon nanowire sensors for Hg^{2+} and Cd^{2+} ions. Appl Phys Lett 94(19):193101. https://doi.org/10.1063/1.3120281

Mao S, Chang J, Zhou G, Chen J (2015) Nanomaterial-enabled rapid detection of water contaminants. Small 11(40):5336–5359. https://doi.org/10.1002/smll.201500831

Marselli B, Garcia-Gomez J, Michaud P-A, Rodrigo MA, Comninellis C (2003) Electrogeneration of hydroxyl radicals on boron-doped diamond electrodes. J Electrochem Soc 150(3):D79–D83. https://doi.org/10.1149/1.1553790

Martinez-Huitle CA, Ferro S (2006) Electrochemical oxidation of organic pollutants for the wastewater treatment: direct and indirect processes. Chem Soc Rev 35(12):1324–1340. https://doi.org/10.1039/B517632H

Martinez-Huitle CA, Ferro S, De Battisti A (2004) Electrochemical incineration of oxalic acid: role of electrode material. Electrochim Acta 49(22):4027–4034. https://doi.org/10.1016/j.electacta.2004.01.083

Modin O, Aulenta F (2017) Three promising applications of microbial electrochemistry for the water sector. Environ Sci Water Res Technol 3(3):391–402. https://doi.org/10.1039/C6EW00325G

Modin O, Gustavsson DJI (2014) Opportunities for microbial electrochemistry in municipal wastewater treatment – an overview. Water Sci Technol 69:1359–1372. https://doi.org/10.2166/wst.2014.052

Murakami Y, Kikuchi T, Yamamura A, Sakaguchi T, Yokoyama K, Ito Y, Takiue M, Uchida H, Katsube T, Tamiya E (1998) An organic pollution sensor based on surface photovoltage. Sensors Actuators B Chem 53(3):163–172. https://doi.org/10.1016/S0925-4005(99)00010-6

Myers CR, Nealson KH (1988) Bacterial manganese reduction and growth with manganese oxide as the sole electron acceptor. Science 240(4857):1319. https://doi.org/10.1126/science.240.4857.1319

Nabi SA, Naushad M, Bushra R (2009) Synthesis and characterization of a new organic-inorganic Pb2+ selective composite cation exchanger acrylonitrile stannic(IV) tungstate and its analytical applications. Chem Eng J 152:80–87. https://doi.org/10.1016/j.cej.2009.03.033

Naushad M, Alothman ZA, Inamuddin, Javadian H (2015) Removal of Pb(II) from aqueous solution using ethylene diamine tetra acetic acid-Zr(IV) iodate composite cation exchanger: kinetics, isotherms and thermodynamic studies. J Ind Eng Chem 25:35–41. https://doi.org/10.1016/j.jiec.2014.10.010

Pan D, Wang Y, Chen Z, Lou T, Qin W (2009) Nanomaterial/ionophore-based electrode for anodic stripping voltammetric determination of lead: an electrochemical sensing platform toward heavy metals. Anal Chem 81(12):5088–5094. https://doi.org/10.1021/ac900417e

Parameswaran P, Torres C, Lee H, Krajmalnik-Brown R, Rittmann BE (2009) Syntrophic interactions among anode respiring bacteria (ARB) and non-ARB in a biofilm anode: electron balances. Biotechnol Bioeng 103(3):513–523. https://doi.org/10.1002/bit.22267

Patil S, Harnisch F, Schroder U (2010) Toxicity response of electroactive microbial biofilm – a decisive feature for potential biosensor and power source applications. ChemPhysChem 11 (13):2834–2837. https://doi.org/10.1002/cphc.201000218

Plechkova NV, Seddon KR (2008) Applications of ionic liquids in the chemical industry. Chem Soc Rev 37(1):123–150. https://doi.org/10.1039/B006677J

Qin B, Luo H, Liu G, Zhang R, Chen S, Hou Y, Luo Y (2012) Nickel ion removal from wastewater using the microbial electrolysis cell. Bioresour Technol 121:458–461. https://doi.org/10.1016/j.biortech.2012.06.068

Quinn BM, Ding Z, Moulton R, Bard AJ (2002) Novel electrochemical studies of ionic liquids. Langmuir 18(5):1734–1742. https://doi.org/10.1021/la011458x

Rabaey K, Verstraete W (2005) Microbial fuel cells: novel biotechnology for energy generation. Trends Biotechnol 23(6):291–298. https://doi.org/10.1016/j.tibtech.2005.04.008

Rabaey K, Rodriguez J, Blackall LL, Keller J, Gross P, Batstone D, Verstraete W, Nealson KH (2007) Microbial ecology meets electrochemistry: electricity-driven and driving communities. ISME J 1:9–18. https://doi.org/10.1038/ismej.2007.4

Rajeshwar K, Ibanez JG (1997) Environmental electrochemistry: fundamentals and applications in pollution abatement. Academic, San Diego. http://lib.ugent.be/catalog/rug01:000540457

Rajeshwar K, Ibanez JG, Swain GM (1994) Electrochemistry and the environment. J Appl Electrochem 24(11):1077–1091. https://doi.org/10.1007/BF00241305

Rajkumar D, Palanivelu K (2004) Electrochemical treatment of industrial wastewater. J Hazard Mater 113(1):123–129. https://doi.org/10.1016/j.jhazmat.2004.05.039

Ramirez-Vargas C, Prado A, Arias C, Carvalho P, Esteve-Nunez A, Brix H (2018) Microbial electrochemical technologies for wastewater treatment: principles and evolution from microbial fuel cells to bioelectrochemical-based constructed wetlands. Water 10(9). https://doi.org/10.20944/preprints201807.0369.v1

Rocha JHB, Gomes MMS, Santos EV, Moura ECM, Silva DR, Quiroz MA, Martinez-Huitle CA (2014) Electrochemical degradation of Novacron Yellow C-RG using boron-doped diamond and platinum anodes: direct and indirect oxidation. Electrochim Acta 140:419–426. https://doi.org/10.1016/j.electacta.2014.06.030

Rodgers JD, Jedral W, Bunce NJ (1999) Electrochemical oxidation of chlorinated phenols. Environ Sci Technol 33(9):1453–1457. https://doi.org/10.1021/es9808189

Rodrigo MA, Michaud PA, Duo I, Panizza M, Cerisola G, Comninellis C (2001) Oxidation of 4-chlorophenol at boron-doped diamond electrode for wastewater treatment. J Electrochem Soc 148(5):D60–D64. https://doi.org/10.1149/1.1362545

Rosenbaum MA, Franks AE (2014) Microbial catalysis in bioelectrochemical technologies: status quo, challenges and perspectives. Appl Microbiol Biotechnol 98(2):509–518. https://doi.org/10.1007/s00253-013-5396-6

Sakaguchi T, Kitagawa K, Ando T, Murakami Y, Morita Y, Yamamura A, Yokoyama K, Tamiya E (2003) A rapid BOD sensing system using luminescent recombinants of *Escherichia Coli*. Biosens Bioelectron 19(2):115–121. https://doi.org/10.1016/S0956-5663(03)00170-2

Seddon KR (2003) A taste of the future. Nature 2:363. https://doi.org/10.1038/nmat907

Seddon KR, Annegret S, Maria-Jose T (2000) Influence of chloride, water, and organic solvents on the physical properties of ionic liquids. Pure Appl Chem 72:2275. https://doi.org/10.1351/pac200072122275

Shahat A, Awual MR, Naushad M (2015) Functional ligand anchored nanomaterial based facial adsorbent for cobalt(II) detection and removal from water samples. Chem Eng J 271:155–163. https://doi.org/10.1016/j.cej.2015.02.097

Sharma M, Bajracharya S, Gildemyn S, Patil SA, Alvarez-Gallego Y, Pant D, Rabaey K, Dominguez-Benetton X (2014) A critical revisit of the key parameters used to describe microbial electrochemical systems. Electrochim Acta 140:191–208. https://doi.org/10.1016/j.electacta.2014.02.111

Shen Y, Zhang Y, Qiu X, Guo H, Niu L, Ivaska A (2007) Polyelectrolyte-functionalized ionic liquid for electrochemistry in supporting electrolyte-free aqueous solutions and application in amperometric flow injection analysis. Green Chem 9(7):746–753. https://doi.org/10.1039/B616452H

So H, Park D, Jeon E, Kim Y, Kim BS, Lee C, Choi SY, Kim SC, Chang H, Lee J (2008) Detection and titer estimation of *Escherichia coli* using aptamer-functionalized single-walled carbon-nanotube field-effect transistors. Small 4(2):197–201. https://doi.org/10.1002/smll.200700664

Socha A, Chrzescijanska E, Kusmierek E (2005) Electrochemical and photoelectrochemical treatment of 1-aminonaphthalene-3,6-disulphonic acid. Dyes Pigments 67(1):71–75. https://doi.org/10.1016/j.dyepig.2004.10.012

Stein NE, Hamelers HVM, van Straten G, Keesman KJ (2012) Effect of toxic components on microbial fuel cell-polarization curves and estimation of the type of toxic inhibition. Biosensors 2(3):255. https://doi.org/10.3390/bios2030255

Sudibya HG, He Q, Zhang H, Chen P (2011) Electrical detection of metal ions using field-effect transistors based on micropatterned reduced graphene oxide films. ACS Nano 5(3):1990–1994. https://doi.org/10.1021/nn103043v

Suidan MT, Strubler CE, Kao S, Pfeffer JT (1983) Treatment of coal gasification wastewater with anaerobic filter technology. Biotechnol Bioeng 55(10):1263–1270. https://doi.org/10.1002/bit.260250612

Sun J, Sun S, Fan M, Guo H, Qiao L, Sun R (2007) A kinetic study on the degradation of p-nitroaniline by Fenton oxidation process. J Hazard Mater 148(1):172–177. https://doi.org/10.1016/j.jhazmat.2007.02.022

Tao H, Liang M, Li W, Zhang L, Ni J, Wu W (2011) Removal of copper from aqueous solution by electrodeposition in cathode chamber of microbial fuel cell. J Hazard Mater 189(1):186–192. https://doi.org/10.1016/j.jhazmat.2011.02.018

Tiwari D (2016) Ferrate(VI) a greener solution: synthesis, characterization, and multifunctional use in treating metal-complexed species in aqueous solution. In: Anonymous, Ferrites and ferrates: chemistry and applications in sustainable energy and environmental remediation, American Chemical Society 1238(7):161–220. https://doi.org/10.1021/bk-2016-1238.ch007

Torres RA, Torres W, Peringer P, Pulgarin C (2003) Electrochemical degradation of p-substituted phenols of industrial interest on Pt electrodes.: attempt of a structure-reactivity relationship assessment. Chemosphere 50(1):97–104. https://doi.org/10.1016/S0045-6535(02)00487-3

Van der Bruggen B, Vogels G, Van Herck P, Vandecasteele C (1998) Simulation of acid washing of municipal solid waste incineration Fly ashes in order to remove heavy metals. J Hazard Mater 57(1):127–144. https://doi.org/10.1016/S0304-3894(97)00078-2

Varia J, Zegeye A, Roy S, Yahaya S, Bull S (2014) Shewanella Putrefaciens for the remediation of Au^{3+}, Co^{2+} and Fe^{3+} metal ions from aqueous systems. Biochem Eng J 85:101–109. https://doi.org/10.1016/j.bej.2014.02.002

Villagran C, Banks CE, Hardacre C, Compton RG (2004) Electroanalytical determination of trace chloride in room-temperature ionic liquids. Anal Chem 76(7):1998–2003. https://doi.org/10.1021/ac030375d

Wang Z, Lee JH, Lu Y (2008) Label-free colorimetric detection of Lead ions with a nanomolar detection limit and tunable dynamic range by using gold nanoparticles and DNAzyme. Adv Mater 20(17):3263–3267. https://doi.org/10.1002/adma.200703181

Wasserscheid P (2006) Volatile times for ionic liquids. Nature 439:797. https://doi.org/10.1038/439797a

Wei D, Ivaska A (2008) Applications of ionic liquids in electrochemical sensors. Anal Chim Acta 607(2):126–135. https://doi.org/10.1016/j.aca.2007.12.011

Welton T (1999) Room-temperature ionic liquids. Solvents for synthesis and catalysis. Chem Rev 99(8):2071–2084. https://doi.org/10.1021/cr980032t

Wen Y, Li FY, Dong X, Zhang J, Xiong Q, Chen P (2013) The electrical detection of Lead ions using gold-nanoparticle- and DNAzyme-functionalized graphene device. Adv Healthc Mater 2 (2):271–274. https://doi.org/10.1002/adhm.201200220

Woodworth JG, Munday BL, Campin D (1998) Evaluation of biomarkers for exposure of fish to eucalypt-based pulp mill effluent and for determination of routes of exposure. Environ Toxicol Water Qual 13(4):285–296. https://doi.org/10.1002/(SICI)1098-2256(1998)13:4<285::AID-TOX2>3.0.CO;2-3

Wu D, Huang L, Quan X, Li Puma G (2016) Electricity generation and bivalent copper reduction as a function of operation time and cathode electrode material in microbial fuel cells. J Power Sources 307:705–714. https://doi.org/10.1016/j.jpowsour.2016.01.022

Xu H, Zeng L, Xing S, Shi G, Xian Y, Jin L (2008) Microwave-radiated synthesis of gold nanoparticles/carbon nanotubes composites and its application to voltammetric detection of trace mercury(II). Electrochem Commun 10(12):1839–1843. https://doi.org/10.1016/j.elecom.2008.09.030

Xu R, Yu X, Gao C, Jiang Y, Han D, Liu J, Huang X (2013) Non-conductive nanomaterial enhanced electrochemical response in stripping voltammetry: the use of nanostructured magnesium silicate hollow spheres for heavy metal ions detection. Anal Chim Acta 790:31–38. https://doi.org/10.1016/j.aca.2013.06.040

Yang H, Zhou M, Liu M, Yang W, Gu T (2015) Microbial fuel cells for biosensor applications. Biotechnol Lett 37(12):2357–2364. https://doi.org/10.1007/s10529-015-1929-7

Yu P, Lin Y, Xiang L, Su L, Zhang J, Mao L (2005) Molecular films of water-miscible ionic liquids formed on glassy carbon electrodes: characterization and electrochemical applications. Langmuir 21(20):9000–9006. https://doi.org/10.1021/la051089v

Yu C, Guo Y, Liu H, Yan N, Xu Z, Yu G, Fang Y, Liu Y (2013) Ultrasensitive and selective sensing of heavy metal ions with modified graphene. Chem Commun 49(58):6492–6494. https://doi.org/10.1039/C3CC42377H

Yuan S, Peng D, Song D, Gong J (2013) Layered titanate nanosheets as an enhanced sensing platform for ultrasensitive stripping voltammetric detection of mercury(II). Sensors Actuators B Chem 181:432–438. https://doi.org/10.1016/j.snb.2013.01.092

Zhang B, Zhao H, Shi C, Zhou S, Ni J (2009) Simultaneous removal of sulfide and organics with vanadium(V) reduction in microbial fuel cells. J Chem Technol Biotechnol 84(12):1780–1786. https://doi.org/10.1002/jctb.2244

Zhang T, Cheng Z, Wang Y, Li Z, Wang C, Li Y, Fang Y (2010) Self-assembled 1-octadecanethiol monolayers on graphene for mercury detection. Nano Lett 10(11):4738–4741. https://doi.org/10.1021/nl1032556

Zhou G, Chang J, Cui S, Pu H, Wen Z, Chen J (2014) Real-time, selective detection of Pb^{2+} in water using a reduced graphene oxide/gold nanoparticle field-effect transistor device. ACS Appl Mater Interfaces 6(21):19235–19241. https://doi.org/10.1021/am505275a

Zhu H, Xu Y, Liu A, Kong N, Shan F, Yang W, Barrow CJ, Liu J (2015) Graphene nanodots-encaged porous gold electrode fabricated via ion beam sputtering deposition for electrochemical analysis of heavy metal ions. Sensors Actuators B Chem 206:592–600. https://doi.org/10.1016/j.snb.2014.10.009

Zou Z, Han J, Jang A, Bishop PL, Ahn CH (2007) A disposable on-chip phosphate sensor with planar cobalt microelectrodes on polymer substrate. Biosens Bioelectron 22(9):1902–1907. https://doi.org/10.1016/j.bios.2006.08.004

Chapter 7
TiO_2-Based Nanocomposites for Photodegradation of Organic Dyes

Eswaran Prabakaran, Shepherd Sambaza, and Kriveshini Pillay

Contents

Abstract The semiconductor metal oxide consisting of TiO_2 nanoparticles has been applied for the environmental remediation of toxic substances from environmental samples. TiO_2 nanoparticles have been used as a photocatalyst for the degradation of organic pollutants in wastewater samples and have demonstrated potential as an effective photocatalyst. This includes applications for the decontamination of compounds from contaminated samples under both UV and visible light irradiation. Although these nanoparticles have been easily utilized for this application, the electron–hole recombination rate and bandgap energy level could be very high. There are therefore numerous reports on TiO_2 nanoparticles coated onto biopolymers of chitosan, alginate, and carboxymethyl cellulose and conducting polymers of polypyrrole, polythiophene, and polyaniline to give polymer TiO_2 nanocomposites as the photocatalyst. Such studies have been implemented for the photocatalytic

E. Prabakaran · S. Sambaza · K. Pillay (✉)
Department of Applied Chemistry, University of Johannesburg, Johannesburg, South Africa
e-mail: kriveshinip@uj.ac.za

M. Naushad et al. (eds.), *Green Methods for Wastewater Treatment*, Environmental Chemistry for a Sustainable World 35, https://doi.org/10.1007/978-3-030-16427-0_7

degradation of organic dyes under UV and visible light irradiation in an attempt to improve the photocatalytic activity by lowering the electron–hole recombination rate and the bandgap energy. Moreover adsorptive photocatalytic degradation is favored since this provides a surface onto which the pollutants are adsorbed first and thereafter undergo photocatalytic degradation. This chapter therefore provides an overview of TiO_2 as a photocatalyst with respect to its advantages and disadvantages. In a critical review in the recent trends on supporting TiO_2, other support materials are discussed, and future research perspectives are also critically evaluated.

Keywords Biopolymers · Conduction polymers · TiO_2 nanocomposite · Photocatalyst · Organic dyes

7.1 Introduction

Environmental pollution has been identified as a global hazard because of growing industries and increases in population (Peirce et al. 1998; Sharma et al. 2017). Large amounts of organic pollutants like dyes are discharged into the surroundings via fabric and effluent industries. The organic dyes which are discharged from industrial effluent are classified as cationic, anionic, or neutral (Ming-Twang et al. 2017). The huge quantity of dyes which enter the environment from industrial wastewater per year enters surface waters, thereby leading to contaminated groundwater (Chaukura et al. 2017; Sharma et al. 2018). The degraded quality of groundwater has an effect on humans, animals, and environmental systems (Zhang et al. 2014). Due to this fact, environmental protection has become of prime importance to ensure the safety and security of all living organisms. Researchers are therefore placing an emphasis on environmental safety and remediation from poisonous pollution (Andreozzi et al. 1999; Pathania et al. 2016).

Many methods of environmental remediation with respect to the removal of pollutants from contaminated water have thus been developed by researchers (Pathania et al. 2015). The primary focus is on converting hazardous wastewater into safe potable drinking water. Among the various methods developed, the advanced oxidation method (AOM) is the most suitable for wastewater treatment. AOM is carried out for wastewater remediation in numerous industries by using chemical treatment processes. It has been used in the degradation of organic pollutants from the environmental wastewater samples because it produces efficient reactive and active oxidants from the ozone, photocatalyst, and H_2O_2 under UV light irradiation. The generation of more radicals results in the conversion of toxic organic matter to nontoxic matter (Yao 2013). AOM is an eco-friendly chemical process for the removal of wastewater treatment. It also has some advantages including fast degradation reaction rates and nonselective oxidation of organic pollutants and degrades the multiple toxic pollutants simultaneously in wastewater treatment. This method is primarily based on the Fenton reaction, ultrasound reaction, ozonation, and photocatalysts (Bremner et al. 2009). This advanced oxidation

process produces oxidizing agents which include hydroxyl radicals ($HO^{\cdot}$), superoxide radical (O_2^{-}), and hydrogen peroxide (H_2O_2), and these degrade the natural pollutants by oxidizing them (Chong et al. 2010).

In order to enhance the rate of the oxidation process, several photocatalysts have been employed. Among them, heterogeneous photocatalysts are a green technique for the photocatalytic degradation of poisonous pollutants (Khan et al. 2013). Nowadays, semiconductor substances have been used as photocatalysts for the wastewater remediation because of their low cost, fast degradation of organic pollutants, and eco-friendly nature (Cho et al. 2015; Ibhadon and Fitzpatrick 2013). Titanium dioxide in particular has demonstrated superior photocatalytic activity for the degradation of the poisonous organic pollutants and wastewater treatment because of its low cost, long-term stability, optical properties, biocompatibility, electricity storage potential, and nontoxicity (Khan et al. 2014a, b, c, d; Kalathil et al. 2013; Tatsuma et al. 2001; Sajan et al. 2016; Tong et al. 2012; Anpo and Tackeuchi 2003; Al-harbi et al. 2011). However, the TiO_2 nanocatalyst does not absorb light energy well in the UV and visible regions due to massive bandgap energy (3.2 eV) which has resulted in poor photocatalytic activity (Malato et al. 2009).

Nowadays, different approaches aimed at improving the photocatalytic behavior of TiO_2 nanoparticles have been adopted. These include surface change, doping, coupling, and creation of oxygen emptiness (Gua et al. 2014; Venieri et al. 2015; Wang et al. 2012; Gnanasekaran et al. 2016; Li et al. 2016; Saravanan et al. 2018a, b). The surface change on TiO_2 nanoparticles is vital for photocatalytic utility, wherein polymers blended into a TiO_2 nanocomposite have exhibited remarkable and unique activities as both sensors and photocatalysts (Camara et al. 2014; Li et al. 2012; Romero-Sáez et al. 2017; Shankar et al. 2011a, b).

In this book chapter, an emphasis is placed on biopolymers (chitosan, carboxymethyl cellulose, and sodium alginate) and conducting polymers (polyaniline, polythiophene, polypyrrole) coated on TiO_2 nanocomposites for the photocatalytic degradation of dyes. These polymers are coordinated with TiO_2 to present polymer TiO_2 nanocomposites. Polymer TiO_2 nanocomposites have the distinct advantages of ease of separation, decreased electron–hole recombination rate, and decreased bandgap energy leading to accelerated photocatalytic activity underneath both UV and visible light irradiation.

7.1.1 General View of Photocatalyst

The photocatalyst is defined as a catalyst which increases the rate of the chemical reaction under the light energy absorption without undergoing any structural changes (Serpone and Pelizzetti 1989; Khan et al. 2015). Titanium dioxides (TiO_2) are n-type semiconductor materials which have been extensively used as photocatalysts. These popular photocatalysts have demonstrated different properties along with different structures, low cost, less harm to the environment, easy material

preparation at room temperature, photostability, and narrow bandgap energy of 3.2 eV (Yu et al. 2005). Commonly, the development of TiO_2 photocatalysts involves the photocatalytic degradation response of environmental pollutants under UV light and visible light irradiation.

The mechanism of the photocatalytic reactions is dependent upon the excited state of the catalyst and ground state of the substrate (Ohama and Van Gemert 2011). Photocatalysts of the photochemical reaction include both homogenous and heterogeneous catalysts. However, the heterogeneous photocatalyst which is used as a solid state along with different phases of reactants is more commonly used and includes the TiO_2 semiconductor catalyst (Nursam et al. 2015). In this case the heterogeneous photocatalyst is used as a stable state along with distinct phases of reactants and TiO_2 semiconductor catalysts (Nursam et al. 2015). TiO_2 semiconductor material contains a valence band and a conduction band corresponding to holes and electrons occupied on it, respectively (Sahoo et al. 2015). The bandgap energy is calculated as the difference in energy barrier between the valence band (VB) and the conduction band (CB). This bandgap energy may be important for photocatalytic reactions under both UV and visible light irradiation and also provides an indicator of the quality of photocatalytic activity. TiO_2 nanoparticles are produced in the electron donor region of the conductance band and electron acceptor region of the valence band while absorbing light energy. Both bands of TiO_2 nanoparticles are involved in the redox reaction which degrades organic pollutants in the environment (Kharisov et al. 2016). The bandgap energy is either higher or lower than the original bandgap energy, while light energy is absorbed on TiO_2 semiconductor materials. A positive charge is formed at VB, and a negative charge of electrons is created at CB, when the electron moves from the VB to CB after energy absorbing (Evans et al. 2013). This kind of TiO_2 semiconductor catalyst is involved in the redox reaction with environmental pollutants (Qamar et al. 2015). This oxidation and reduction reaction for the degradation of pollutants results in a creation of positive charges (holes) on VB and negative charges (electrons) on CB (Sakar et al. 2016).

The oxidation reaction is driven by hydroxyl radicals ($^{\bullet}OH$) from water, and the reduction reaction proceeds via superoxide radicals ($O_2^{\bullet-}$) from oxygen molecules by using the TiO_2 catalyst. Both radicals enhance the oxidation power for the photocatalytic degradation of organic pollutants (Djokic et al. 2012). The recombination of electrons–holes occurs between VB and CB due to the production of heat energy and the loss of electron and holes. Sometimes, electron and holes result in opposite reactions which are carried out on the TiO_2 semiconductor material (Panda 2009). The recombination of electrons–holes involves two processes within the photochemical reaction such as non-radiative recombination and radiative recombination processes which are obeyed through the photochemical application. Light energy is produced by the radiative recombination method, and heat energy is generated by non-radiation recombination processes (Fulay 2016). The semiconductor of TiO_2 nanoparticles has been employed as a photocatalyst for the photochemical degradation of organic pollutants. However, it has attracted less interest due to a high electron–hole recombination charge (Ibhadon and Fitzpatrick 2013).

Fluorescence spectroscopy is an instrumental technique which is used for the determination of electron–hole recombination rate, electron–hole transfer, and trapping and migration of the TiO_2 photocatalyst. Pure TiO_2 nanoparticles have exhibited good photocatalytic abilities for the degradation of organic pollutants due to reduced luminescence and low electron–hole recombination charge rate (Ohtani 2013; Ma et al. 2011). The electron–hole recombination rate is based totally on the synthesis of the TiO_2 nanoparticle catalyst and different types of photodegradation of organic pollutants (Zhang and Yates 2012). The excitation of electrons which move from VB to CB and the holes created at VB depends on the extent of absorption of light energy by the TiO_2 nanoparticles and also results in either an equal or higher energy than the original bandgap energy. The electron–hole recombination rate is dependent on the extraordinary trapping states of the TiO_2 nanoparticles because of the excitation of electrons–holes.

The TiO_2 semiconductor catalyst exists in two types of trapping states which include the shallow and deep states, and these states are generated from defects and impurities. These types of states of TiO_2 nanoparticles have demonstrated good photocatalytic activity because of electron–hole charge carriers on the catalyst (Hall 1952; Shockley and Read 1952). The non-radiative recombination rate produces heat energy from light energy, and this is shown by time-resolved photoacoustic spectroscopy (TRPAS) (Schneider et al. 2014). The heat energy is formed within the agglomerated TiO_2 semiconductor nanoparticles. However these nanoparticles still display superior properties which include large surface area, better adsorption properties, and increased photocatalytic degradation rate of organic pollutants (Mendive et al. (2011).

The electron–hole recombination rate is determined by time-resolved absorption spectroscopy (TAS). The improvement of photocatalytic activity depends on the electron–hole recombination rate that is combined with a different property such as electron–hole trapping, interfacial charge transfer, and temperature (Skinner et al. 1995; Colombo and Bowman 1996; Katoh and Furube 2011). The detailed mechanism of photocatalytic degradation reaction is shown in Fig. 7.1.

7.1.2 Bandgap Energy Levels with Metal Oxide Semiconductors

Nowadays, the photocatalytic degradation of organic pollutants is accomplished with metal oxide semiconductor nanoparticles, which have a low bandgap energy (Mamba and Mishra 2016). Different metal oxides possess different bandgap energies, where TiO_2 has been extensively used as a photocatalyst for the degradation of environmental pollutants because of photostability, nontoxicity, low cost, eco-friendly nature, and thermal stability (Khan et al. 2014a, b, c, d; Sellappan 2013). Although TiO_2 nanoparticles have some inherent disadvantages such as fast electron–hole recombination rate and less quantum efficiency, these metal oxide

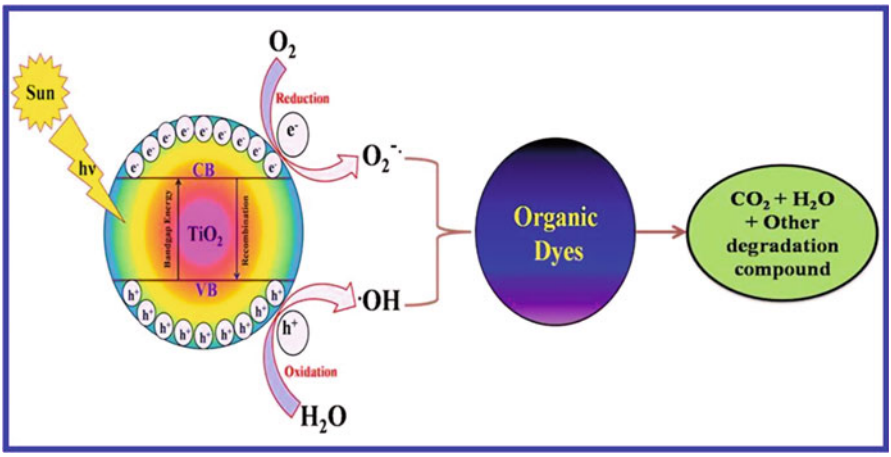

Fig. 7.1 Mechanism of photocatalytic degradation of organic dyes

nanoparticles are used under different types of light irradiation such as UV light, visible light, and infrared light irradiation (Chen et al. 2016a, b). It has been mostly used in the photocatalytic degradation of organic dyes under UV light irradiation because of its large bandgap energy (3.2 eV) (Daghrir et al. 2013). Researchers have developed modified TiO_2 nanoparticles with reducing the bandgap energy and electron–hole recombination rate for efficient catalytic degradation of organic dyes under UV and visible light irradiation (Wang et al. 2015). Thus different modified materials have been used for improving the photocatalytic activity of TiO_2 nanoparticles, and these include modifications with metals, nonmetals, noble metals, various semiconductors, and polymers. The different bandgap energies of various semiconductors are shown in Fig. 7.2.

7.1.3 Advantages of TiO_2 Photocatalyst Semiconductor

The semiconductor substances of TiO_2 nanoparticles have been used in adsorption, reverse osmosis, ion exchange, renewable power applications, and wastewater treatment (Nakata and Fujishima 2012; Konstantinou and Albanis 2004; Fujishima et al. 2000; Rajeshwar et al. 2008; Rehman et al. 2009). It is also used in hydrogen generation from environmental samples. The various applications are shown in Fig. 7.3. So, the applications of TiO_2 nanoparticles are by no means limited to photocatalytic applications.

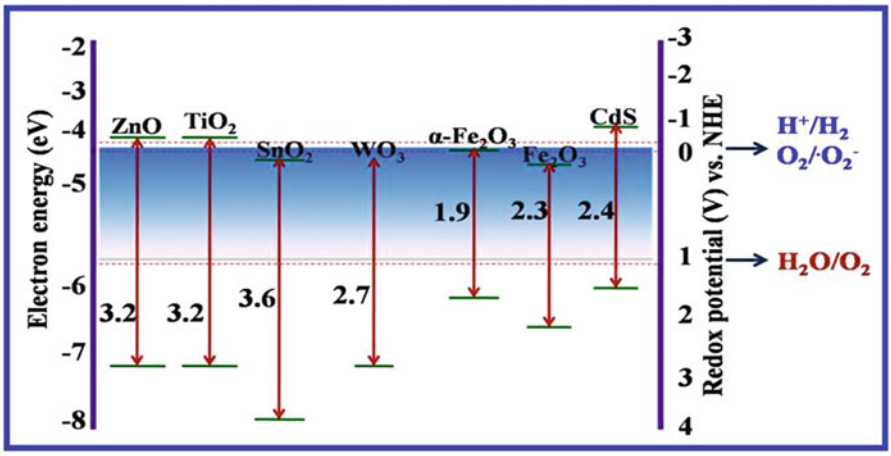

Fig. 7.2 Bandgap energy levels of different metal oxide nanoparticles

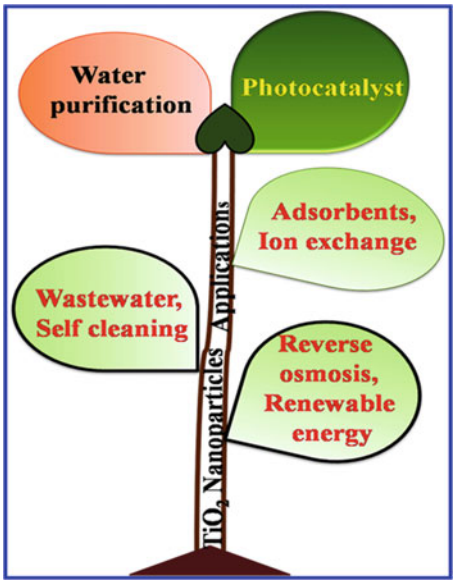

Fig. 7.3 Schematic diagram of TiO_2 photocatalyst applications

7.1.4 Doping of Photocatalyst

The distinctive metal oxide nanoparticles which have been used as photocatalysts for environmental water remediation are ZnO, SnO_2, CeO_2, ZrO_2, TiO_2, and CuO. Among them, TiO_2 nanoparticles have shown superior abilities as photocatalysts, with respect to good photostability and higher bandgap energy. Although it has a few drawbacks like higher electron–hole recombination rate (Rothenberger et al. 1985),

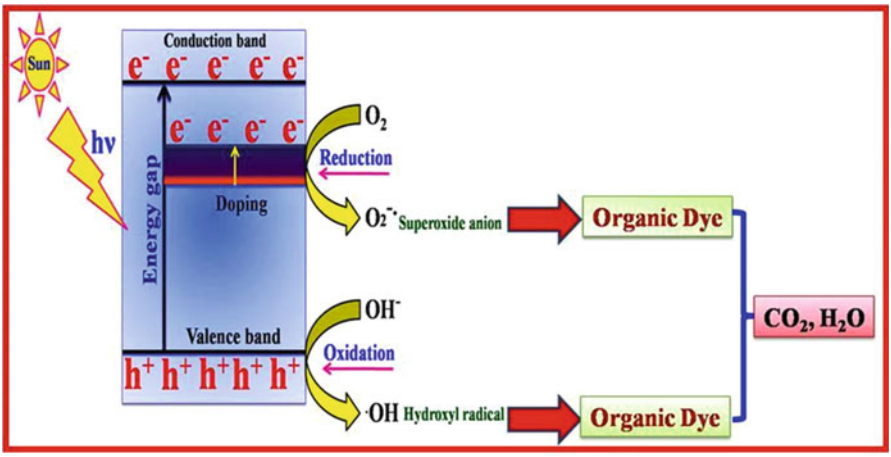

Fig. 7.4 Mechanism of doped photocatalyst for the degradation of organic dyes

UV light energy absorption, and less photocatalytic activity (Serpone et al. 1994), these problems have been overcome by a few surface amendments that are needed for the TiO_2 nanoparticles. The surface modifications include modifications with metals, metal oxides, nitrogen (N), sulfur (S), carbon (C), fluorine, and polymers which increase the photocatalytic activity under the visible light irradiation, reduce the bandgap energy, and minimize electron–hole recombination rate. The metal oxide doping on TiO_2 nanoparticles reduced the bandgap energy and enhanced the photocatalytic activity in the visible region (Saravanan et al. 2011). The combined structures of Au/TiO_2, ZnO/SnO_2, and CeO_2/Au had been shown the splendid photocatalytic activity (Khan et al. 2014a, b, c, d; Cun et al. 2002; Khan et al. 2014a, b, c, d). The polymer-based TiO_2 nanocomposites are PANI/TiO_2, PPy/TIO_2, and PT/TiO_2 (Salem et al. 2009; Zhang et al. 2014). These types of nanocomposite have decreased the drawbacks of pure metal oxide TiO_2 nanocomposite and resulted in high photostability, high visible light energy absorption, and high electron–hole transfer and reduced the electron–hole recombination rate. The schematic diagram of doping photocatalyst mechanism is shown in Fig. 7.4.

7.2 Polymer Nanocomposites for Photocatalytic Applications

The semiconductor TiO_2 nanoparticles have been used for the photocatalytic degradation of toxic pollutants in the solid phase, and these have shown less photocatalytic activity with low surface area (Vaez et al. 2012). Modified TiO_2 nanoparticles in the form of nanocomposite materials with carbon materials, silica particles, cellulose materials, and polymers have therefore been prepared and used in

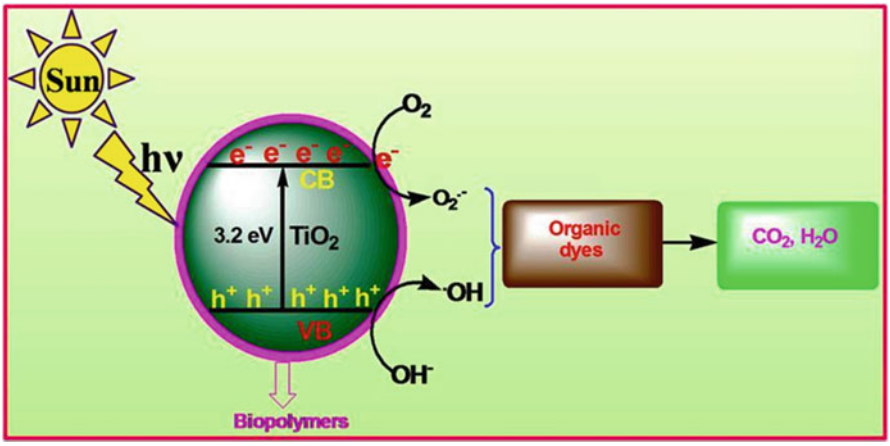

Fig. 7.5 Mechanism of photocatalytic degradation of organic dyes with biopolymer-capped TiO_2 nanocomposites as photocatalyst

photocatalytic applications. These polymer nanocomposites have performed better at the photocatalytic degradation of organic pollutants (Matos et al. 2007; Mansilla et al. 2006; Shironita et al. 2008; Jin et al. 2007, Sriwong et al. 2008). TiO_2 nanocomposites have improved surface areas, high degradation rate constants, and excesses of hydroxides radicals and thus have resulted in an increase in percentage of degradation efficiency (Shan et al. 2010). Among them, polymer-capped TiO_2 nanocomposites have demonstrated excellent photocatalytic degradation of organic dyes because of increased photocatalytic activity, low-cost materials, high abundance, photostability, inert materials, and good oxidation capability (Han and Bai 2009; Magalhães et al. 2011).

Biopolymer-capped TiO_2 nanocomposites have displayed great photocatalytic activities because of lower bandgap energy. These produce positive charge holes (h^+) within VB and the negative charge of the electron (e^-) in the CB when light energy is absorbed. Since biopolymers are used to reduce the bandgap energy and electron–hole recombination rate of TiO_2 nanoparticles, electrons are reacted with O_2 to form $O_2^{-\cdot}$radicals in the CB band, whereas VB produce the more positive charge of holes, and it is producing the excellent oxidation of H_2O to $^{\cdot}OH$ radicals. Both radicals of O_2^- and $^{\cdot}OH$ are excellent oxidizing agents for the degradation of organic dyes under sunlight irradiation and also result in complete mineralization into carbon dioxide and water (Afzal et al. 2016). Therefore, biopolymer-capped TiO_2 nanocomposites have shown excellent photocatalytic degradation of organic dyes under visible light irradiation as shown in Fig. 7.5.

The conducting polymer TiO_2 nanocomposites have been used as photocatalysts for the degradation of organic dyes under visible light irradiation. The conducting polymers are p-type semiconductors, and TiO_2 is an n-type semiconductor. P-type semiconductor polymers are absorbed under light energy and have created the hole in highest occupied molecular orbital (HOMO), and the electron in the lowest

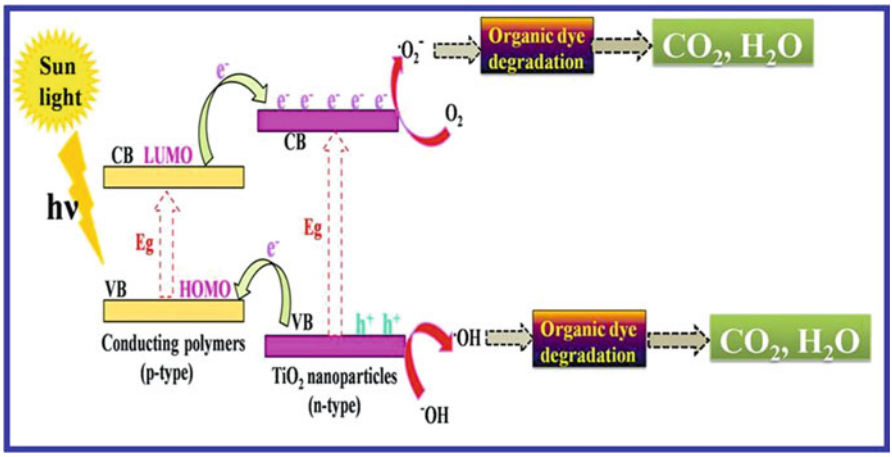

Fig. 7.6 Mechanism of photocatalytic degradation of organic dyes with conducting polymer-capped TiO_2 nanocomposites as photocatalyst

unoccupied molecular orbital (LUMO) has very energetic electrons, and it effortlessly transferred into the conduction band (CB) of n-type TiO_2 semiconductor nanoparticles. This results in the photoreduction of oxygen to superoxide anion. Whereas HOMO of hole collected electrons from the valence band (VB) of TiO_2 to create the recombination processes. As a result of a hole is produced in the VB of TiO_2 drives the photooxidation process (Liu et al. 2015). The number of electrons is added into the CB of TiO_2 nanoparticles, and more holes are created at the VB of TiO_2 nanoparticles. It becomes more oxidizing radicals on TiO_2 nanoparticles to increase the degradation of organic dyes under the visible light irradiation (Rasoulifard et al. 2017). The conducting polymer-capped TiO_2 nanocomposites exhibited the good photocatalyst under sunlight irradiation. Hence, these nanocomposites increased the photocatalytic activity under the sunlight irradiation because of conducting polymers, and biopolymers decreased the electron–hole recombination in the TiO_2 nanoparticles to enhance degradation of organic dyes (Lee et al. 2012; Abdelwahab and Helaly 2017). The schematic diagram of the photocatalytic mechanism of conducting polymer TiO_2 nanocomposites is shown in Fig. 7.6.

7.3 Biopolymers Based on TiO_2 Nanocomposites as Photocatalyst

Biopolymers are capping agents for TiO_2 nanoparticles, and these have been produced for reducing toxic organic dye concentrations from environmental samples. The TiO_2 nanoparticles have been capped with chitosan, carboxymethyl cellulose acetate, and sodium alginate, and these nanocomposites have shown superior photocatalytic activity when compared with pure TiO_2 semiconductor nanoparticles. Such biopolymers are also easily available; contain various functional groups of OH, NH_2, and COOH; are biocompatible and nontoxic; and have good coordination with TiO_2 nanoparticles. These nanocomposites have thus demonstrated the excellent photocatalytic activity for the degradation of dyes (Guibal 2005).

7.3.1 Chitosan Coated on TiO_2 Nanocomposite as Photocatalyst

These nanocomposites of TiO_2 nanoparticles have been utilized for the degradation of organic dyes and have also demonstrated superior characteristics such as lower energy of absorption, good resistance, and good photocatalytic activity and are prepared at room temperature (Ohtani et al. 1997). Although this has the important drawback of TiO_2 nanoparticles being not easily recovered and recycled after applied photocatalytic degradation of organic dyes, chitosan-capped TiO_2 nanocomposites easily solved the abovementioned problem due to easy recovery and reusability and also rendered a more efficient photocatalytic degradation of organic dyes. Such a material also demonstrated easily controlled size and improved the surface area and good adsorption capacities (Wan Ngah et al. 2011; Xiang et al. 2015). TiO_2 nanoparticles can exist in both rutile and anatase forms, and of these two forms, anatase exhibited the better photocatalytic activity under visible light irradiation when compared to the rutile structure. These anatase TiO_2 nanoparticles can without difficulty be modified to enhance photocatalytic efficiency and increase surface area and are easily size controlled (Bickley et al. 1991). Chitosan/TiO_2 nanocomposites confirmed that better adsorption and good photocatalytic degradation of organic dyes of methylene blue and benzopurpurin can be achieved due to the basic nature of the dyes that is bound and cationic nature of chitosan in the TiO_2 nanocomposite under UV light irradiation. This nanocomposite has delivered the excellent degradation of the basic organic dyes due to the reduced size of TiO_2 nanoparticles with acetate groups of chitosan easily coordinating with the TiO_2 nanoparticles (Haldorai and Shim 2014).

Chitosan/TiO_2 nanocomposite is mostly prepared by the chemical precipitation method, which has shown longer thermal stability and good crystalline nature. It has shown fast degradation of methylene blue under UV light irradiation within 3 h, and it showed a high percentage of degradation efficiency of about 90%, reusability, and

photostability, and it is easily recoverable (Zubieta et al. 2007). The photocatalytic studies of the degradation of methyl orange with chitosan/TiO_2 nanocomposites and TiO_2 nanoparticles under UV light irradiation were compared. Here it is noted that the chitosan/TiO_2 nanocomposite performed better at the photocatalytic degradation of methyl orange under UV light irradiation than pure TiO_2 nanoparticles because of the controlled size of the TiO_2 nanoparticles, the large surface area of TiO_2 nanoparticles, and the higher energy of absorption by using chitosan polymer as the surface. The above properties are also used to increase the photocatalytic degradation of methyl orange dyes under UV and visible light irradiation (Saravanan et al. 2018a, b). This nanocomposite had increased the surface area and feasible photocatalytic activity due to chitosan biopolymer as a surface support for TiO_2 nanoparticles. Chitosan/TiO_2 nanocomposite showed a decrease in photocatalytic activity with corresponding increase in the negative charge of methyl orange dye because of the negatively charged surface of chitosan/TiO_2 nanocomposite which increased the electrostatic repulsion between them (Fajriati et al. 2014). Chitosan/TiO_2 nanocomposite is also prepared as the multilayered coating on glass slides. The multilayered coating of the nanocomposite preparation processes is made with glass slides coated onto chitosan/TiO_2 solution. The multilayered coating of chitosan/TiO_2 nanocomposite on glass slides exhibited spherical shapes and a well-defined crystalline nature of metal oxide which was confirmed by X-ray diffraction. This material also exhibited improved photocatalytic activities for the degradation of methyl orange dye. This catalytic efficiency of methyl orange dye is dependent upon the thickness of chitosan/TiO_2 nanocomposite coated on the glass slides. The photocatalytic degradation rate decreased with increased coating layer thickness. It was also noted that the adsorption of properties of methyl orange increased and the photocatalytic activity reduced under UV light irradiation. Methyl orange is readily degraded by chitosan/TiO_2 nanocomposite under UV light irradiation due to its cationic nature and the negative charge of the chitosan/TiO_2 nanocomposite which promotes electrostatic interactions (Xiao et al. 2015).

Chitosan-supported TiO_2 nanocomposite is prepared by immobilization processes, wherein chitosan is an immobilization agent for the formation of the chitosan/TiO_2 nanocomposite. This nanocomposite acts as the photocatalyst for degradation of organic dyes and the effect of parameters such as the dosage of catalyst, and the pH of the solution of the dye have been investigated. This nanocomposite can be recovered and reused after photodegradation of dyes solution to a greater extent than pristine TiO_2 nanoparticles (Dhanya and Aparna 2016). This photocatalyst is therefore an effective tool for clean environments and purification of water. Toxic dyes of reactive red, methylene blue, and rhodamine B were converted from harmful to harmless forms by using the chitosan/TiO_2 nanocomposite catalyst under UV light irradiation (Essawy et al. 2017). Chitosan/TiO_2 nanocomposite has shown great photocatalytic activity with organic dyes under UV light irradiation due to the synergetic interaction between the biopolymer of chitosan and metal oxide of TiO_2 nanoparticles (Škoric et al. 2016). The photocatalytic activity of chitosan-capped TiO_2 nanocomposite has also been investigated with the different parameters such as catalyst dosage, pH variation, and initial concentration of dye. This

nanocomposite exhibited excellent percentage of degradation of dyes in the presence of H_2O_2, where H_2O_2 produces a lot of hydroxide radicals, and it also increases the photocatalytic activity. Additionally, chitosan/TiO_2 nanocomposite also shows good adsorption properties (Hasmath Farzan and Sankaran Meenakshi 2014).

Chitosan/TiO_2 nanocomposites with three-dimensional macroporous structures are prepared by using the template method. The three-dimensional macroporous structure is obtained with varying concentrations of the solutes chitosan and TiO_2 and varying freezing rate of chitosan/TiO_2 nanocomposite. Another scaffold macroporous morphology of chitosan/TiO_2 nanocomposite is prepared by the monolith method with a sol solution of anatase of TiO_2 nanoparticles and glycidoxypropyltrimethoxysilane (GPTMS) cross-linked. Potassium-titanate (K-TiO_2) and degussa P25 titanium dioxide (P25 TiO_2) are immobilized on the chitosan scaffold structure of polymer. These nanoparticles are incorporated onto the channel walls of the chitosan scaffold compound as a result of increases in the mechanical properties and increased photocatalytic activity. The chitosan/TiO_2 microstructure is prepared by monolith processes and increases the mechanical stability in chitosan/TiO_2 nanocomposite when compared to both potassium-titanate (K-TiO_2) and degussa P25 titanium dioxide (P25 TiO_2). This scaffold morphology of the chitosan/TiO_2 nanocomposite resulted in excellent photocatalytic activity for the degradation of methylene blue when compared to pure anatase TiO_2 nanoparticles (Suwanchawalit et al. 2009; Zhao et al. 2017).

7.3.2 *Alginate Coated on TiO_2 Nanocomposite as Photocatalyst*

TiO_2 nanoparticles were embedded onto the polyacrylamide/calcium alginate (PAM/CA) to give PAM/CA/TiO_2 nanocomposite for the degradation of the organic dye of methyl orange under visible light. This nanocomposite has special properties such as easy recovery from the degraded dye solution and increase in percentage of degradation efficiency (80.8%) in presence of sodium chloride concentration (Wei et al. 2016). TiO_2/calcium alginate (T/CA) nanocomposite is synthesized by using a cross-linker agent in aqueous solution. T/CA nanocomposite has good thermal stability and biocompatibility due to calcium alginate capped on TiO_2 nanoparticles and also proved to be an excellent photocatalyst for the degradation of the organic dye of methyl orange under UV light irradiation. For the photodegradation study, low catalyst dosage was needed for the degradation of the organic dye methyl orange dye. This nanocomposite was effortlessly recovered from the dyes after photocatalytic treatment and was also applied in wastewater treatment because of its low cost and very easy preparation method (Zhao et al. 2014). Alginate-supported TiO_2 nanocomposite (Alg/TiO_2) beads are characterized by their physicochemical stability when compared to pure alginate (Alg) under UV light irradiation in the aqueous medium. The diameter and mass of both beads of pure alginate and alginate/

TiO_2 nanocomposite are evaluated under UV light irradiation. The beads created the cavity for exposure to UV light irradiation. From the analysis pure alginate is easily broken from the glycosidic bond in biopolymer chain, but alginate/TiO_2 nanocomposite is not broken because of alginate's strong bond with TiO_2 metal oxide nanoparticles under UV light irradiation. Although TiO_2 nanoparticles can be easily separated from the beads by using an external environmental, it has shown excellent photocatalytic activity when compared to pure alginate. It is also used for the degradation of organic dyes from environmental samples. TiO_2 nanoparticles are incorporated with alginate beads, and it is applied in photocatalytic applications of the dye. Alg/TiO_2 nanocomposite has demonstrated good physicochemical stability and better photocatalytic degradation of the cationic dye solution under UV light irradiation. This nanocomposite has shown better photocatalytic under UV light irradiation when compared to TiO_2 nanoparticles (Lam et al. 2017).

Barium ion immobilization on the alginate/carboxymethyl cellulose (CMC) polymer composite is encapsulated on TiO_2 nanoparticles to give a (Ba/Alg/CMC/TiO_2) nanocomposite by using the dissipative convective method followed by the freeze-drying procedure. Ba/Alg/CMC/TiO_2 hydrogel nanocomposite has shown better photocatalytic activity for the degradation Congo red dye under sunlight irradiation (Thomas et al. 2017). This photocatalyst hydrogel nanocomposite is easily reused and recovered from the photocatalytic degradation of Congo red dye solution due to TiO_2 immobilization on barium/alginate/carboxymethylcellulose gels to perfect the crystalline material. Ba/Alg/CMC/TiO_2 nanocomposite hydrogel was used to degrade Congo red to harmless products, and it is also a low-cost material and eco-friendly material (Thomas et al. 2016). The photocatalyst paper sheet is prepared by using various ratios of TiO_2/sodium in the alginate nanocomposite. The modified photocatalyst paper with TiO_2/sodium alginate nanocomposite was tested for the chemical oxygen demand of wastewater treatment. It is also proved to be an efficient photocatalyst for the removal of chemical oxygen demand in wastewater treatment. The use of sodium alginate as a biopolymer increased the adhesion of nanoparticles to paper fibers and reduced the harmful effect of the photocatalyst on them. The obtained results confirmed the possible utilization of the modified paper in both hygienic and food packaging applications (Abdel Rehim et al. 2016).

7.3.3 Carboxymethyl Cellulose Based on TiO_2 Nanocomposite as Photocatalyst

TiO_2/carbon/cellulose fiber is prepared by the papermaking method. TiO_2 nanoparticles are coated on carbon fibers of cellulose fibers as raw materials, and also Na_2SiO_3 and $Al_2(SO_4)_3$ are used as adhesives to distribute the small carbon fiber. The TiO_2/carbon fiber paper catalyst enhanced the photocatalytic degradation of methyl orange in presence of adhesive sodium silicates than aluminum sulfate as adhesive. The TiO_2/carbon fiber nanocomposite paper catalyst demonstrated

excellent photocatalytic activity for the degradation of methyl orange dye when compared to poly(amidoamine-epichlorohydrin) (PAE) paper catalyst. TiO_2/carbon/cellulose fiber catalyst has exhibited good photocatalytic activity under UV light irradiation and can be used repeatedly. This simple procedure is promising for the manufacture of paper with high photocatalytic activity (Zhang et al. 2013). The photocatalytic activity of TiO_2 nanoparticles is exploited for the production of self-cleaning textiles. Cotton-based fabrics are functionalized with TiO_2 nanoparticle sols with differing surface properties, and their photocatalytic efficiency was tested in various experimental setups. The different types of TiO_2 nanoparticles surface were used for the photocatalytic degradation of dye and textile dyes under UV light irradiation. TiO_2 coated on a cellulose-based catalyst was more efficient for the photodegradation of both rhodamine B and textile dyes when compared to pure TiO_2 nanoparticles. The TiO_2-coated cellulose material has exhibited better reaction and good adsorption of the •OH for enhancement of the catalytic reduction of RhB (Ortelli et al. 2014).

7.4 Conducting Polymers Based on TiO_2 Nanocomposites as Photocatalysts

The conducting polymers have demonstrated different properties which include flexibility, electrical, optical properties, corrosion resistance, morphology, and tunable conductivity over their existing inorganic counterparts (Huang et al. 1986; McCullough et al. 1993). The conducting polymers are incorporated onto TiO_2 nanoparticles to give a nanocomposite which has the properties of electrical conductivity, optical and mechanical (Shirakawa 2001). The conducting polymers are joined with the inorganic substance of TiO_2 nanoparticles to offer nanocomposites, and these result in a large surface area of TiO_2 nanoparticles and good dispersion and increased the better performance for the photocatalytic degradation organic dyes under the UV and visible light irradiation. Here, the conducting polymers of polypyrrole, polythiophene, and polyaniline are combined with TiO_2 nanocomposites for photocatalytic degradation of organic dyes under UV light and visible light irradiation.

7.4.1 Polypyrrole Coated on TiO_2 Nanocomposite as Photocatalyst

Polypyrrole capped TiO_2 nanocomposite is prepared with the resource of an in situ polymerization technique with various ratios of PPy:TiO_2. It has been used as a photocatalyst for the photodegradation of the organic dye of methyl orange under visible light irradiation. This nanocomposite exhibited fabulous photodegradation of

methyl orange because of the synergetic impact of the polymer of PPy and TiO_2 nanoparticles (Wang et al. 2008). Polypyrrole–TiO_2 (PPy–TiO_2) nanocomposite is synthesized by oxidation polymerization method. Polypyrrole–TiO_2 nanocomposite has also been used for the photocatalytic degradation of methylene blue and methyl orange dyes under UV light irradiation. This nanocomposite is likewise evaluated with different catalyst dosage, the different initial concentrations of dye solution and pH of dye solution. The PPy–TiO_2 nanocomposite has shown efficient degradation of methylene blue and acid oranges dyes (Sangareswari and Meenakshi Sundaram 2015). PPy–TiO_2 nanocomposite was also used for the degradation of methylene blue under solar light irradiation. Enhanced photocatalytic degradation of methylene blue was observed under sunlight irradiation, and the PPy–TiO_2 nanocomposite was prepared through the chemical oxidation approach. This nanocomposite showed better photocatalytic activity of methylene blue under sunlight irradiation when compared to the other pure TiO_2 nanocomposite. The repeatability of photocatalytic activity was also examined. A possible mechanism was proposed and mentioned in the principle of experimental outcomes. The methylene blue dye therefore becomes successfully degraded by PPy–TiO_2 nanocomposite under the sunlight irradiation. The percentage of dye degradation was reported as 93% for PPy–TiO_2 nanocomposite (Sangareswari and Meenakshi Sundaram 2017).

PPy/TiO_2 nanocomposites are successfully prepared through the surface molecular imprinting method. The MIP/PPy/TiO_2 nanocomposites have shown better adsorption potential and selectivity that PPy/TiO_2 nanocomposites and the photocatalytic activity of MIP/PPy/TiO_2 are higher than that of PPy/TiO_2 due to the advent of the imprinted cavities at the surface of MIP/PPy/TiO_2 nanocomposites. The size and shape of MIP/PPY/TiO_2 nanocomposites and PPy/TiO_2 nanocomposites were confirmed with the aid of SEM and XRD, and also MIP/PPy/TiO_2 nanocomposite is in the anatase crystalline shape. UV–Vis diffuse reflectance spectra showed that the MIP/PPy/TiO_2 photocatalyst absorbed extra photons under visible light irradiation (Deng et al. 2012). TiO_2 nanoparticles included thin films of polypyrrole (ppy) on the air–water interface. Aqueous TiO_2 nanoparticles while treated with H_2O_2 and left in a chamber of pyrrole vapor resulted in the formation of a film at the interface and further to the bulk precipitate. The TiO_2 containing PPy composite while transferred onto glass substrates had already completed the photocatalyzed decomposition of aqueous organic dyes like methyl orange and methylene blue. The PPy–TiO_2 nanocomposite films catalyzed the reactions more efficiently than a suspension of TiO_2 nanoparticles (Chowdhury et al. 2005; He et al. 2014).

The solid nature of TiO_2/polypyrrole nanocomposites is synthesized through a simple one-step hydrothermal method. The nanocomposites are able to perform efficiently under visible light. The photocatalysis is driven via their morphology that makes use of an excessive amount of 4.5 nm TiO_2 nanoparticles electronically coupled to 200–300 nm polypyrrole granules. Polypyrrole acts because of the visible light photosensitizer, and the photoactivity of the nanocomposite arises from the electron transfer from the excited polypyrrole to TiO_2 nanoparticles and further through all the nanocomposite interfaces. The visible light photocatalysis was

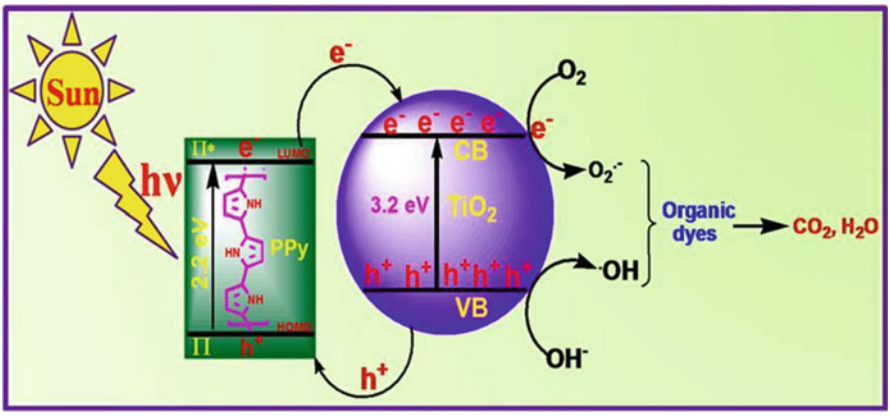

Fig. 7.7 Mechanism of photocatalytic degradation of organic dyes with PPy/TiO_2 nanocomposite as photocatalyst

verified by means of methylene blue degradation (Dimitrijevic et al. 2013). One pot synthesis of the polymer of polypyrrole and inorganic materials of TiO_2 nanoparticles are combined together to give PPy–TiO_2 nanocomposite with the chemical oxidation method. PPy–TiO_2 nanocomposite has displayed excellent photocatalytic activity for the degradation of methyl orange under visible light irradiation and additionally delivers a 100% degradation of methyl orange within 60 min which was higher than that of the pure TiO_2 nanoparticles (55%). This nanocomposite has also brought better photovoltaic performance than the pure TiO_2 nanoparticles. By comparing the physical mixture of the PPy–TiO_2 nanocomposite and TiO_2 nanoparticles, the improved activity of the PPy–TiO_2 nanocomposite may be attributed to the decreased charge transfer resistance, great electric conductance of the PPy, and nano-sized structure of TiO_2 and their synergetic impact (Baig et al. 2017). Titanium dioxide (TiO_2) was modified by a silane coupling agent to improve the dispersity before the polymerization. UV–visible analysis shows that the PPy/TiO_2 nanocomposites have a higher photocatalytic activity under natural light than virgin TiO_2 (Sun et al. 2013; Gao et al. 2016). The schematic diagram of the photocatalytic mechanism of PPy/TiO_2 nanocomposite is shown in Fig. 7.7.

7.4.2 Polythiophene Coated on TiO_2 Nanocomposite as Photocatalyst

The electron–hole recombination rate may be very high for pure TiO_2 nanoparticles and, additionally, less photocatalytic efficiency for the degraded organic dyes under UV light irradiation (Wu et al. 1998; Zhang et al. 2008). It has some disadvantages such as less adsorption of dyes, less binding with dyes, and poor stability (Wang et al. 2003). Polythiophene conducting polymer is easily bound with the metal oxide

of TiO_2 nanoparticles to give polythiophene/TiO_2 nanocomposite as a photocatalyst for degradation of organic dyes under the UV and visible light irradiation (Zhu and Dan 2010). The polymerization of thiophene is conducted by using in situ polymerization processes with TiO_2 nanoparticles to form a polythiophene/TiO_2 nanocomposite. This nanocomposite shows remarkable electron transfer at the same time as the absorption light energy and better photocatalysts for the degradation of the organic pollutants of methyl orange dye under UV light irradiation (Zhu et al. 2008). It has additionally brought the absorption peak at 400 nm, as a result of good photocatalytic degradation of methyl orange dye under solar light irradiation. Further, polythiophene/TiO_2 nanocomposite easily adsorbs the dye molecules because of the large surface area of TiO_2 nanoparticles, which is dependent on the conducting polymer of polythiophene activity. The concentration of polythiophene/TiO_2 nanocomposite increases with increasing photocatalytic efficiency and adsorption activity, and these types of activities are determined by the surface morphology of the polythiophene/TiO_2 nanocomposite. The photocatalytic efficiency study was investigated with the pure conducting polymer of polythiophene, pure TiO_2 nanoparticles, and polythiophene/TiO_2 nanocomposite, wherein polythiophene/TiO_2 nanocomposite gave the highest photocatalytic efficiency (56.6%) when compared to both pure polythiophene and pure TiO_2 nanoparticles. The photodegradation ability is due to the active site of TiO_2 nanoparticles, not polythiophene polymer. A large amount of polythiophene polymer on TiO_2 nanoparticles has reduced the photodegradation of the organic dye of methyl orange due to the fact active site TiO_2 nanoparticles blocking. Based on this observation, the large active sites are available in TiO_2 nanoparticles, and also photocatalytic degradation rate of methyl orange dye increased. Polythiophene/TiO_2 nanocomposite is mainly concentrated onto the surface property, which is associated with the amount of polythiophene and TiO_2 nanoparticles. The photocatalytic degradation observed is primarily based on the quantity of polythiophene polymer and accelerates the photocatalytic degradation of methyl orange dye (Li et al. 2008). The charge of polythiophene/TiO_2 nanocomposite and pure TiO_2 was determined by zeta potential measurements. The TiO_2 nanoparticles become positively charged after modification. These characterization methods are used to determine the ability of photocatalytic degradation of methyl orange dye, the adsorption properties, and low electron–hole recombination rate (Xu et al. 2010). Hence polythiophene/TiO_2 nanocomposite has exhibited the better adsorption activity and also good photocatalytic performance of methyl orange (Zhu et al. 2010). Polythiophene/TiO_2 nanocomposite was also tested for the photocatalytic degradation of methyl orange dye under visible light irradiation. Here, TiO_2 nanoparticles are mostly used in the photocatalytic application under UV light irradiation. However, polythiophene/TiO_2 nanocomposite was used for the photocatalytic degradation of methyl orange under visible light because of polythiophene acting as sensitizer and fast electron transfer to the CB band of TiO_2 nanoparticles. The CB band electron interacts with O_2 adsorbed on the TiO_2 nanoparticles to give a superoxide radical, which acts as a highly oxidizing agent to degrade the organic dye of methyl orange dye. The polymerization of polythiophene has been conducted using different

methods such as microemulsion and photoinduced polymerization of polythiophene, and those methods have resulted in extraordinary morphology (Wang and Zhang 2013).

Polythiophene–TiO_2 nanocomposite was prepared by the microemulsion method, wherein TiO_2 nanoparticles were used as coalescence. Polythiophene–TiO_2 nanocomposite was applied to the photocatalytic degradation of textile dyes of orange II and methyl orange under UV light irradiation. It showed better photocatalytic degradation of textile dyes of orange II and methyl orange due to low bandgap energy levels. The comparison of the photocatalytic ability was determined with polythiophene–TiO_2 nanocomposite and pure polythiophene polymer alone. Polythiophene–TiO_2 nanocomposite exhibited the highest photodegradation of efficiency of textile dyes of orange II and methyl orange because of the large surface area of the polythiophene–TiO_2 nanocomposite. The degradation rate of the polythiophene–TiO_2 nanocomposite was higher than the pure TiO_2 nanoparticles because of bandgap energy level 2.0 eV for polythiophene–TiO_2 nanocomposite and 3.2 eV for TiO_2 nanoparticles (Cheng et al. 2012). Polythiophene was coated on TiO_2 nanoparticles to give polythiophene–TiO_2 nanocomposite by the photoinduced polymerization method. But, the normal interface method of the polythiophene–TiO_2 nanocomposite is not stable for photocatalytic applications, so it depends on light energy to create charge separation. The photoinduced method has produced the polymer of polythiophene by using free radical polymerization and also preparation of the polymer–TiO_2 nanocomposite. This method is suitable for the preparation of polythiophene–TiO_2 nanocomposite because of the charge carrier between the TiO_2 and thiophene of monomer interface (Strandwitz et al. 2010; Weng and Ni 2008). The sulfur contents of thiophene monomer are the backbone for the synthesis of the polymer of polythiophene, and the TiO_2 nanoparticle is also used to prepare polythiophene–TiO_2 nanocomposite with the photoinduced polymerization method. The polythiophene–TiO_2 nanocomposite has exhibited the excellent photocatalytic activity of RhB under the UV and visible light irradiation (Xu et al. 2011).

Poly(3,4-propylenedioxy-2,2′:5′,2″-terthiophene)/TiO_2 nanocomposite and poly (3,4-(2,2-dimethylenepropylenedioxy)-2,2′:5′,2″-terthiophene)/TiO_2 nanocomposite have been synthesized by using the solid-state method. Moreover, the poly(3, 4-propylenedioxy thiophene)/TiO_2 and poly(3,4-2,2-dimethylenepropylenedioxythiophene)/TiO_2 nanocomposites have been synthesized under the abovesaid condition. The photocatalytic activities of the nanocomposites were tested for the degradation methylene blue under the UV and visible irradiation. FT-IR and UV-visible spectra confirmed that the composites showed the stable country approach. The poly(3,4-propylenedioxy-2,2′:5′,2″-terthiophene)/TiO_2 nanocomposite and poly(3,4-(2,2-dimethylenepropylenedioxy)-2,2′:5′,2-″-terthiophene)/TiO_2 nanocomposite had a better oxidation degree and conjugation length than others. This additionally indicated that the TiO_2 nanoparticles had no impact on the crystallinity of the composites. However these were properly embedded inside the polymer matrix. Moreover, the very best degradation efficiency of 90.5% occurred in the case of the poly(3,4-propylenedioxy-2,2′,5′,2″-terthiophene)/

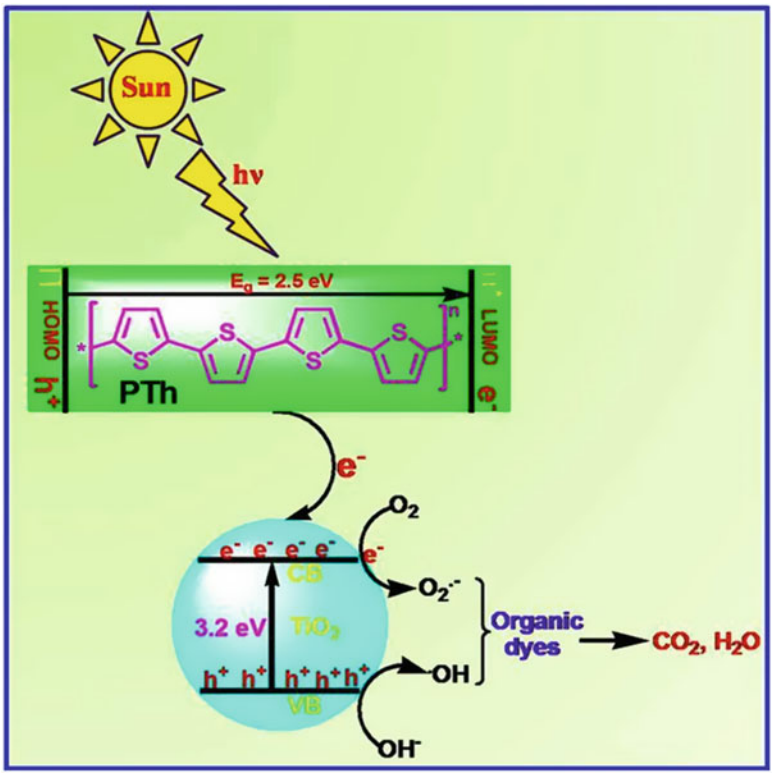

Fig. 7.8 Mechanism of photocatalytic degradation of organic dyes with PTh/TiO_2 nanocomposite as photocatalyst

TiO_2 nanocomposite (Jamal et al. 2014). The schematic diagram of the photocatalytic mechanism of PTh/TiO_2 nanocomposite is shown in Fig. 7.8.

7.4.3 Polyaniline Coated on TiO_2 Nanocomposite as Photocatalyst

PANI–TiO_2 nanocomposites have been organized by the template-free method with different contents of TiO_2 nanoparticles. This nanocomposite showed outstanding photocatalytic degradation of rhodamine B under visible light irradiation. Here 10% of TiO_2 coated on PANI nanocomposite exhibited higher photocatalytic degradation than pure TiO_2 nanoparticles and also lowered the recombination rate for electron–hole separation. Additionally, nanorods and nanotubes of TiO_2 coated on PANI nanocomposite increased the photocatalytic activity and adsorption activity due to

extending the surface of TiO_2. The photocatalyst of PANI–TiO_2 nanocomposite was prepared by a sol–gel method at room temperature because of the controlled size of TiO_2 nanoparticles (Olad et al. 2012; Jumat et al. 2017). PANI–TiO_2 polymer nanocomposite showed good photocatalytic degradation of methylene blue under UV light irradiation within 60 min and also excellent optimum degradation (87%) at pH 3. This PANI–TIO_2 nanocomposite was also used for the photodegradation of methylene blue with the different dosage, different concentrations of methylene blue, and various pH. Adsorption characteristics on the PANIi-TiO_2 surface and the aqueous solubility of the dyes also play an important role in the photodegradation of dye. The catalyst is involved in photocatalyst processes with two types of reactions for degrading the organic pollutants first for adsorption of dyes on the outer layer of catalyst, and the observed photodegradation of methylene blue was 21.5% with a ratio of PANI:TiO_2 of 65.5%. Hydroxyl groups are important for the photodegradation of methylene blue, in which they act as an oxidizing agent and behave as reaction intermediates. PANI–TiO_2 nanocomposite has demonstrated fast photocatalytic degradation of methylene blue and high percentage degradation efficiency. Photoreactivity of PANI–TiO_2 nanocomposite was studied as a function of pH of solution methylene blue solution, the dosage of catalyst, and concentration of dye. The reaction rate constant (r) and equilibrium binding constant (K) values are incredibly significant when compared to another catalyst (Ahmad and Mondal 2012).

The synthesis of PANI@TiO_2 nanocomposite powder is synthesized by in situ polymerization methods in which ammonium persulfate (APS) acts as an oxidizing agent and TiO_2 anatase powder as a precursor for nanoparticles under ice bath conditions. The stable-state photocatalytic degradation of PANI@TiO_2 nanocomposites was investigated under the ambient air for the development of a photodegradable polymer. The PANI@TiO_2 nanocomposite powders confirmed particularly superior photodegradation and also decreased the ratio PANI:TiO_2 nanocomposite. The ratio of PANI@TiO_2 (1:3) led to a weight loss of 6.8% under ambient conditions, but 0.3% weight loss after irradiation for 60 min was observed under ambient conditions (Zhang et al. 2016). The PANI@TiO_2 nanocomposites are the combination of various ratios of inorganic/organic compounds with the in situ polymerization method, and it was also applied for photocatalytic degradation under UV light irradiation. The present observation shows that the photocatalytic method can be effective for stable-segment PANI degradation and the PANI@TiO_2 nanocomposite has the capability for use as a photodegradable product. Photocatalytic degradation in the strong polymer matrix proceeded much quicker than the direct photolytic degradation under air. The photocatalytic experiment indicates that PANI@TiO_2 nanocomposite resulted in an enhanced absorption and photocatalytic performance compared with pure TiO_2 or PANI, due to the decreased recombination of the electron–hole pairs, efficient charge transport, and enhanced charge separation efficiency. It was suggested that the PANI@TiO_2 nanocomposites are able to act as good photocatalysts in environmental purification (Chen et al. 2016a, b; Gilja et al. 2017).

PANI/TiO_2 nanocomposite was also used for the photocatalytic degradation of rhodamine B, in which PANI/TiO_2–50 nanocomposites demonstrated that the excellent catalytic activity was achieved for the degradation of rhodamine B (RB) with a degradation efficiency of (92%). This nanocomposite was used for the photocatalytic degradation of organic pollutants like methylene blue. PANI is an important part of the nanocomposite which involves the synthesis of different structures of TiO_2 nanoparticles with carbonization processes. Pure TiO_2 has a rutile structure with 99% during the carbonization reaction. In the case, PANI/TiO_2 nanocomposite also adopts the rutile structure during the carbonization method. This finding suggests that the carbonization process leads to a PANI layer on the surface of the TiO_2 nanoparticles which have a good impact on their crystalline structure. The initial [TiO_2]/[PANI] mole ratio has a significant effect on the anatase to rutile crystalline ratio in carbonized PANI/TiO_2 nanocomposites. The carbonized PANI layer is observed on the surface of TiO_2 nanocrystals. The carbonization process induced a significant increase in the photocatalytic efficiencies of the nanocomposites. The 50:50 initial concentrations of the PANI/TiO_2 nanocomposite exhibited notable photocatalytic activity under UV light irradiation at 60 min, and it resulted in 99% degradation efficiency of methylene blue when compared to the non-carbonization of PANI/TiO_2 nanocomposite under 6 h degradation of dye of the methylene blue (57%) and pure TiO_2 nanoparticles. PANI/TiO_2 nanocomposite was also used for the photocatalytic degradation of rhodamine B, in which PANI/TiO_2–50 nanocomposites demonstrated that the excellent catalytic activity for the degradation of rhodamine B (RB) with a degradation efficiency of (92%) when compared to the non-carbonization with took 6 h for degradation irradiation time with 50% degradation. It has been shown that an increase of the preliminary [TiO_2]/[PANI] molar ratio (sample TPC-80) induced a maximum efficiency in the degradation process of methylene blue within 1 h. The obtained results revealed that the carbonized PANI/TiO_2 nanocomposites have a great potential for application in photocatalytic degradation of organic pollutants. Also, there is large space for enhancement of their photocatalytic activity through modifications in synthetic conditions (pH, acid dopant, etc.) of non-carbonized precursors and optimization of the carbonization process that would lead to a better dispersion of nanocomposites. These nanocomposites were used for the degradation processes of other types of synthetic dyes (acid, direct, and reactive) taking into account the enormous problem of nondegraded textile dyes in effluents and consequently in water resources (Kalikeri et al. 2018; Sarmah and Kumar 2011).

PANI/TiO_2 nanocomposite is prepared with in situ oxidation polymerization methods, and it has emerged in the degradation of methylene blue for photocatalytic activity based on a prepared pattern. PANI/TiO_2 nanocomposite is likewise more desirable in the photocatalytic activity with exceptional pH variant, dosage variation, and different initial dyes. PANI/TiO_2 nanocomposite has attracted two kinds of interests consisting of photosensitization and synergetic effects among TiO_2 and

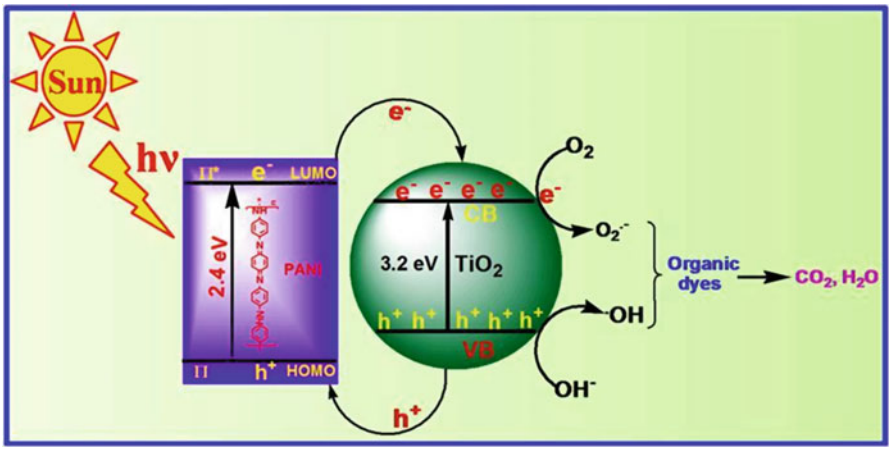

Fig. 7.9 Mechanism of photocatalytic degradation of organic dyes with PANI/TiO_2 nanocomposite as photocatalyst

PANI. This nanocomposite has the great photocatalytic activity and additionally implemented the industrial waste water treatment (Yang et al. 2017). The black anatase shape of TiO_2 nanoparticles is prepared by using hydrothermal techniques, and it has shown higher light absorption capacity and anticorrosivity activity toward light irradiation. The black anatase of TiO_2 nanoparticles integrated into polyaniline to give PANI/TiO_2 nanocomposite, and it confirmed the good photocatalytic degradation of methyl orange under visible light irradiation. It also established the enhancement of the electron switch compared to pure TiO_2 nanoparticles. The electron–hole recombination rate is reduced and additionally improved the photocatalytic activity and showed the efficient dye sensitizer solar cells (Kavil et al. 2017). The azo dye degradation was completed by nanofibers substances of PANI/TIO_2/PANI nanocomposite under visible light irradiation. These nanofibers are synthesized by the electrospinning technique and additionally exhibited the extremely good photodegradation efficiency (87%) after ten instances reused. PANI/TiO_2/PANI nanofibers showed higher degradation ability than the TiO_2/PANI nanofibers. These nanofibers also showed greater photocatalytic degradation of organic pollutants under visible light irradiation without lack of activity (Sedghi et al. 2017; Kumar et al. 2016; Lin et al. 2012). The schematic diagram of the photocatalytic mechanism of PTh/TiO_2 nanocomposite is shown in Fig. 7.9. The brief detail of different biopolymers and conducting polymer-based TiO_2 nanocomposites has been suggested for the photocatalytic degradation of organic dyes as shown in Table 7.1.

Table 7.1 Different biopolymers and conducting polymer-based TiO_2 nanocomposite as photocatalytic degradation of organic dyes

S. no.	TiO_2-based nanocomposites	Dyes	Light sources	Degradation (t)	(%) Degradation	References
1	TiO_2/CS nanocomposite	MB[a], MO[b]	Visible	120 min	63.58%	Saravanan et al. (2018a, b)
2	CS–TiO_2 scaffolds	MB Orange II	UV	20 h	–	Suwanchawalit et al. (2009)
3	Ag_2O/TiO_2/chitosan	Methyl orange	Visible	15 min	96%	Zhao et al. (2017)
4	[j]Ch/PMA/TiO_2 microparticles	Acid orange 7	UV	8 h	100%	Škoric et al. (2016)
5	CS/PVA/TiO_2 nanocomposite	Acid red 14	Visible	80 min	–	Rasoulifard et al. (2017)
6	Chitosan/TiO_2 composite	MO	UV	480 min	60%	Xiao et al. (2015)
7	Fe_3O_4/chitosan/TiO_2	MB	Visible	–	93%	Xiang et al. (2015)
8	Chitosan/TiO_2 nanohybrid	MB	UV	3 h	90%	
9	[k]Ch-g-PNMANI/TiO_2 nanocomposite	RR[c], RB-133[d]	Sun	120 min	93.56%	Essawy et al. (2017)
10	Ba/Alg/CMC/TiO_2 nanocomposite	Congo red	Solar	–	–	Thomas et al. (2016)
11	Sr/Alg/CMC/GO/TiO_2 nanocomposites	Congo red	Sun	240 min	98%	Thomas et al. (2017)
12	TiO_2/calcium alginate nanocomposite	MO	UV	120 min	82.25%	Zhao et al. (2014)
13	Nano-TiO_2/cellulose substrate	RhB[e]	UV	120 min	–	Ortelli et al. (2014)
14	TiO_2/CF/cellulose fiber	MO	UV	7 h	80%	Zhang et al. (2014)
15	PPy/TiO_2 nanocomposite	MO	Visible	160 min	–	Wang et al. (2008)
16	PPy/TiO_2 nanocomposites	RhB	Visible	8 h	97%	Gao et al. (2016)
17	PPy/TiO_2 nanocomposite	MB	Sun	90 min	93%	
18	PPy/TiO_2 nanocomposite	MO	Visible	60 min	100%	Baig et al. (2017)
19	[l]MIP–PPy/TiO_2 nanocomposite	RhB, Rh6G[f], MB	Visible	120 min	85 5%,	He et al. (2014)
					63%, 59%	
20	PTh derivatives/TiO_2 nanocomposites	MB	UV	7 h	51.5%	Jamal et al. (2014)
			Sun		90.5%	
21	PTh/TiO_2 composite particles	MO	Visible	10 h	95.1%	Xu et al. (2010)

22	Poly(3-hexylthiophene)/TiO_2 nanocomposite	MO	UV	150 min	92.7%	Zhu et al. (2010)
23	TiO_2/PANI nanocomposite	MO	Visible UV	120 min	49.9%	Olad et al. (2012)
				120 min	92.9%	
24	PANI/TiO_2 nanocomposites	RB5[g]	Visible	300 min	96%	Jumat et al. (2017)
25	PANI/TiO_2 nanocomposite	R45[h]	UV	60 min	98%	Gilja et al. (2017)
26	PANI/TiO_2 nanocomposites	MG	UV	360 min	99.4%	Sarmah and Kumar (2011)
27	PANI@TiO_2/GN nanocomposite	MB	Visible	175 min	91.6%	Kumar et al. (2016)
28	PANI-modifiedTiO_2 composite	MO	UV, visible	125 min	81.3%,	Lin et al. (2012)
				6 h	21.5%	
29	PANI/TiO_2 nanocomposite	RB-19[i]	UV, visible, solar	120 min	98.4%,	Kalikeri et al. (2018)
					86%	
30	PANI-black anatase	MO	Visible	40 min	–	Kavil et al. (2017)
31	PANI/TiO_2/polyacrylonitrile nanocomposite	MO	Visible	60 min	90%	Sedghi et al. (2017)

Note
[a]Methylene blue (MB)
[b]Methyl orange (MO)
[c]Red RR reactive dye (RR)
[d]Remazol red (RB-133)
[e]Rhodamine B (RhB)
[f]Rhodamine 6G (Rh6G)
[g]Reactive Black 5 Dye (RB5)
[h]Red 45 (R45)
[i]Reactive blue 19 (RB-19)
[j]Chitosan-based microparticles for immobilization of TiO_2 nanoparticles (Ch/PMA/TiO_2)
[k]Chitosan-grafted-polyN-methylaniline imprinted TiO_2 nanocomposites (Ch-g-PNMANI/TiO_2)
[l]Molecularly imprinted polypyrrole/titanium dioxide nanocomposites (MIP-PPy/TiO_2)

7.5 Conclusions

This chapter has reviewed the photocatalytic activity of composites of biopolymers and conducting polymers with semiconductor TiO_2 nanoparticles to polymer TiO_2 nanocomposites. Polymer TiO_2 nanocomposites are important photocatalysts for the effective elimination of toxic organic dyes from environmental samples. The developments of the photocatalytic activity of polymer TiO_2 nanocomposites have led to enhanced photocatalytic degradation of organic dyes under the UV and visible light irradiation. These polymer TiO_2 nanocomposites are recollected and reused after photocatalytic degradation approaches. These nanocomposites have been noted for photocatalytic performance, reusability, and photostability. Those polymer nanocomposites must now be applied for real industrial applications which warrant the need for further studies on a scale-up applications.

References

Abdel Rehim MH, El-Samahy MA, Badawy AA, Mohram ME (2016) Photocatalytic activity and antimicrobial properties of paper sheets modified with TiO_2/Sodium alginate nanocomposites. Carbohydr Polym 148:194–199. https://doi.org/10.1016/j.carbpol.2016.04.061

Abdelwahab NA, Helaly FM (2017) Simulated visible light photocatalytic degradation of Congo red by TiO_2 coated magnetic polyacrylamide grafted carboxymethylated chitosan. J Ind Eng Chem 50:162–171. https://doi.org/10.1016/j.jiec.2017.02.010

Afzal S, Samsudin EM, Julkapli NM, Hamid SBA (2016) Controlled acid catalyzed sol gel for the synthesis of highly active TiO_2-chitosan nanocomposite and its corresponding photocatalytic activity. Environ Sci Pollut Res 23:23158–23168. https://doi.org/10.1007/s11356-016-7507-2

Ahmad R, Mondal PK (2012) Adsorption and photodegradation of methylene blue by using PAni/TiO_2 nanocomposite. J Dispers Sci Technol 33(3):380–386. https://doi.org/10.1080/01932691.2011.567172

Al-Harbi LM, El-Mossalamy EH, Arafa HM, Al-Owais A, Shah MA (2011) TiO_2 nanoparticles with tetra-pad shape prepared by an economical and safe route at very low temperature. Mod Appl Sci 5(3):130–135. https://doi.org/10.5539/mas.v5n3p130

Andreozzi R, Caprio V, Insola A, Marotta R (1999) Advanced oxidation processes (AOP) for water purification and recovery. Catal Today 53(1):51–59. https://doi.org/10.1016/S0920-5861(99)00102-9

Anpo M, Tackeuchi M (2003) The design and development of highly reactive titanium oxide photocatalysts operating under visible light irradiation. J Catal 216(1–2):505–516. https://doi.org/10.1016/S0021-9517(02)00104-5

Baig U, Gondal MA, Ilyas AM, Sanagi MM (2017) Band gap engineered polymeric-inorganic nanocomposite catalysts: synthesis, isothermal stability, photo catalytic activity and photovoltaic performance. J Mater Sci Technol 33(6):547–557. https://doi.org/10.1016/j.jmst.2016.11.031

Bickley RI, Gonzalez-Carreno T, Lees JS, Palmisano RL, Tilley JD (1991) A structural investigation of titaniumdioxide photocatalysts. J Solid State Chem 92(1):178–190. https://doi.org/10.1016/0022-4596(91)90255-G

Bremner DH, Molina R, Martinez F, Melero J, Segura Y (2009) Degradation of phenolic aqueous solutions by high frequency sono-Fenton systems (Fe_2O_3/SBA-15-H_2O_2). Appl Catal B Environ 90(3–4):380–388. https://doi.org/10.1016/j.apcatb.2009.03.028

Camara RM, Crespo E, Portela R, Suarez S, Bautista L, Gutierrez-Martin F, Sanchez B (2014) Enhanced photocatalytic activity of TiO_2 thin films on plasma pretreated organic polymers. Catal Today 230:145–151. https://doi.org/10.1016/j.cattod.2013.10.049

Chaukura N, Edna C, Murimba EC, Gwenzi W (2017) Sorptive removal of methylene blue from simulated wastewater using biochars derived from pulp and paper sludge. Environ Technol Innov 8:132–140. https://doi.org/10.1016/j.eti.2017.06.004

Chen J, Cen J, Xu X, Li X (2016a) The application of heterogeneous visible light photocatalysts in organic synthesis. Cat Sci Technol 6:349–362. https://doi.org/10.1039/C5CY01289A

Chen X, Li H, Wu H, Wu Y, Shang Y, Pan J, Xiong X (2016b) Fabrication of TiO_2@PANI nanobelts with the enhanced absorption and photocatalytic performance under visible light. Mater Lett 172:52–55. https://doi.org/10.1016/j.matlet.2016.02.134

Cheng Y, Wang J, Bao YC, Ma YL, Wang GH (2012) Synthesis of polythiophene nanoparticles by microemulsion polymerization for photocatalysis. Adv Mater Res 399–401:1312–1319. https://doi.org/10.4028/www.scientific.net/AMR.399-401.1312

Cho KM, Kim KH, Choi HO, Jung HT (2015) A highly photoactive, visible-light-driven graphene/2D mesoporous TiO_2 photocatalyst. Green Chem 17(7):3972–3978. https://doi.org/10.1039/C5GC00641D

Chong MN, Jin B, Chow CW, Saint C (2010) Recent developments in photocatalytic water treatment technology: a review. Water Res 44(10):2997–3027. https://doi.org/10.1016/j.watres.2010.02.039

Chowdhury D, Paul A, Chattopadhyay A (2005) Photocatalytic Polypyrrole−TiO_2−nanoparticles composite thin film generated at the air−water Interface. Langmuir 21(9):4123–4128. https://doi.org/10.1021/la0475425

Colombo DP, Bowman RM (1996) Does interfacial charge transfer competes with charge carrier recombination? A femtosecond diffuses reflectance investigation of TiO_2 nanoparticles. J Phys Chem 100(47):18445–18449. https://doi.org/10.1021/jp9610628

Cun W, Jincai Z, Xinming W, Bixian M, Guoying S, Ping'an P, Jiamo F (2002) Preparation, characterization and photocatalytic activity of nano-sized ZnO/SnO_2 coupled photocatalysts. Appl Catal B 39(3):269–279. https://doi.org/10.1016/S0926-3373(02)00115-7

Daghrir R, Drogui P, Robert D (2013) Modified TiO_2 for environmental photocatalytic applications: a review. Ind Eng Chem Res 52(10):3581–3599. https://doi.org/10.1021/ie303468t

Deng F, Li Y, Luo X, Yang L, Tu X (2012) Preparation of conductive polypyrrole/TiO_2 nanocomposite via surface molecular imprinting technique and its photocatalytic activity under simulated solar light irradiation. Colloids Surf A Physicochem Eng Asp 395:183–189. https://doi.org/10.1016/j.colsurfa.2011.12.029

Dhanya A, Aparna K (2016) Synthesis and evaluation of TiO_2/chitosan based hydrogel for the adsorptional photocatalytic degradation of azo and anthraquinone dye under UV light irradiation. Proc Technol 24:611–618. https://doi.org/10.1016/j.protcy.2016.05.141

Dimitrijevic NM, Tepavcevic S, Liu Y, Rajh T, Silver SC (2013) Nanostructured TiO_2/polypyrrole for visible light photocatalysis. J Phys Chem C 117(30):15540–15544. https://doi.org/10.1021/jp405562b

Djokic V, Vujovic J, Marinkovic A, Petrovic R, Janackovic D, Onjia A, Mijin D (2012) A study of the photocatalytic degradation of the textile dye CI basic yellow 28 in water using a P160 TiO_2-based catalyst. J Serb Chem Soc 77(12):1747–1757. https://doi.org/10.2298/JSC121015130D

Essawy AA, Sayyah SM, El-Nggar AM (2017) Wastewater remediation by TiO_2-impregnated chitosan nano-grafts exhibited dual functionality: high adsorptivity and solar-assisted self-cleaning. J Photochem Photobiol B Biol 173:170–180. https://doi.org/10.1016/j.jphotobiol.2017.05.044

Evans RC, Douglas P, Burrow HD (2013) Applied photochemistry. Springer, Dordrecht

Fajriati I, Mudasir M, Wahyuni ET (2014) Photo-catalytic de-colorization study of methyl orange by TiO_2-chitosan nanocomposites. Indo J Chem 14(3):209–218. https://doi.org/10.22146/ijc.21230

Fujishima A, Rao TN, Tryk DA (2000) Titanium dioxide photocatalysis. J Photochem Photobiol C Photochem Rev 1(1):1–21. https://doi.org/10.1016/S1389-5567(00)00002-2

Fulay P (2016) Electronic, magnetic, and optical materials. CRC Press, Bosa Roca

Gao F, Hou X, Wang A, Chu G, Wu W, Chen J, Zou H (2016) Preparation of polypyrrole/TiO_2 nanocomposites with enhanced photocatalytic performance. Particuology 26:73–78. https://doi.org/10.1016/j.partic.2015.07.003

Gilja V, Novaković K, Travas-Sejdic J, Hrnjak-Murgić Z, Kraljić M, Roković K, Žic M (2017) Stability and synergistic effect of polyaniline/TiO_2 photocatalysts in degradation of azo dye in wastewater. Nano 7(12):412. https://doi.org/10.3390/nano7120412

Gnanasekaran L, Hemamalini R, Saravanan R, Ravichandran K, Gracia F, Gupta VK (2016) Intermediate state created by dopant ions (Mn, Co and Zr) into TiO_2 nanoparticles for degradation of dyes under visible light. J Mol Liq 223:652–659. https://doi.org/10.1016/j.molliq.2016.08.105

Gua Y, Xinga M, Zhang J (2014) Synthesis and photocatalytic activity of graphene based doped TiO_2 nanocomposites. Appl Surf Sci 319(1):8–15. https://doi.org/10.1016/j.apsusc.2014.04.182

Guibal E (2005) Heterogeneous catalysis on chitosan-based materials: a review. Prog Polym Sci 30 (1):71–109. https://doi.org/10.1016/j.progpolymsci.2004.12.001

Haldorai Y, Shim JJ (2014) Novel chitosan-TiO_2 nanohybrid: preparation, characterization, antibacterial, and photocatalytic properties. Polym Compos 35(2):327–333. https://doi.org/10.1002/pc.22665

Hall RN (1952) Electron-hole recombination in germanium. Phys Rev 87(2):387. https://doi.org/10.1103/PhysRev.87.387

Han H, Bai R (2009) Buoyant photocatalyst with greatly enhanced visible-light activity prepared through a low temperature hydrothermal method. Ind Eng Chem Res 48(6):2891–2898. https://doi.org/10.1021/ie801362a

Hasmath Farzan M, Meenakshi S (2014) Synergistic effect of chitosan and titanium dioxide on the removal of toxic dyes by the photodegradation technique. Ind Eng Chem Res 53(1):55–63. https://doi.org/10.1021/ie402347g

He MQ, Bao LL, Sun KY, Zhao DX, Li WB, Xia JX, Li HM (2014) Synthesis of molecularly imprinted polypyrrole/titanium dioxide nanocomposites and its selective photocatalytic degradation of rhodamine B under visible light irradiation. Express Polym Lett 8:850–861. https://doi.org/10.3144/expresspolymlett.2014.86

Huang WS, Humphrey BD, MacDiarmid AG (1986) Polyaniline, a novel conducting polymer. Morphology and chemistry of its oxidation and reduction in aqueous electrolytes. J Chem Soc Faraday Trans 1 82(8):2385–2400. https://doi.org/10.1039/F19868202385

Ibhadon AO, Fitzpatrick P (2013) Heterogeneous photocatalysis: recent advances and applications. Catalysts 3(1):189–218. https://doi.org/10.3390/catal3010189

Jamal R, Osman Y, Rahman A, Zhang AAY, Tursun A (2014) Solid-state synthesis and photocatalytic activity of Polyterthiophene derivatives/TiO_2 nanocomposites. Materials 7 (5):3786–3801. https://doi.org/10.3390/ma7053786

Jin F, Cao J, Kishida H, Moriya T, Enomoto H (2007) Impact of phenolic compounds on hydrothermal oxidation of cellulose. Carbohydr Res 342(8):1129–1132. https://doi.org/10.1016/j.carres.2007.02.013

Jumat NA, Wai PS, Joon Ching J, Basirun WJ (2017) Synthesis of polyaniline-TiO_2 nanocomposites and their application in photocatalytic degradation. Polym Polym Compos 25 (7):507–514. https://doi.org/10.1177/096739111702500701

Kalathil S, Khan MM, Ansari SA, Lee J, Cho MH (2013) Band gap narrowing of titanium dioxide (TiO_2) nano-crystals by electrochemically active biofilms and their visible light activity. Nanoscale 5(14):6323–6326. https://doi.org/10.1039/C3NR01280H

Kalikeri H, Kamath N, Gadgil DJ, Kodialbail VS (2018) Visible light-induced photocatalytic degradation of Reactive Blue-19 over highly efficient polyaniline-TiO_2nanocomposite: a comparative study with solar and UV photocatalysis. Environ Sci Pollut Res 25(4):3731–3744. https://doi.org/10.1007/s11356-017-0663-1

Katoh R, Furube A (2011) Tunneling-type charge recombination in nanocrystalline TiO_2 films at low temperature. J Phys Chem Lett 2(15):1888–1891. https://doi.org/10.1021/jz2008424

Kavil J, Ullattil SG, Alshahrie A, Periyata P (2017) Polyaniline as photocatalytic promoter in black anatase TiO_2. Sol Energy 158:792–796. https://doi.org/10.1016/j.solener.2017.10.049

Khan MM, Ansari SA, Amal MI, Lee J, Cho MH (2013) Highly visible light active Ag@TiO_2 nanocomposites synthesized using an electrochemically active biofilm: a novel biogenic approach. Nanoscale 5(10):4427–4435. https://doi.org/10.1039/C3NR00613A

Khan MM, Ansari SA, Pradhan D, Ansari MO, Han DH, Lee J, Cho MH (2014a) Band gap engineered TiO_2 nanoparticles for visible light induced photoelectrochemical and photocatalytic studies. J Mater Chem A 2(3):637–644. https://doi.org/10.1039/C3TA14052K

Khan MM, Ansari SA, Pradhan D, Ansari MO, Lee J, Cho MH (2014b) Band gap engineered TiO_2 nanoparticles for visible light induced photoelectrochemical and photocatalytic studies. J Mater Chem A 2(3):637–644. https://doi.org/10.1039/C3TA14052K

Khan MM, Lee J, Cho MH (2014c) Au@TiO_2 nanocomposites for the catalytic degradation of methyl orange and methylene blue: an electron relay effect. J Ind Eng Chem 20(4):1584–1590. https://doi.org/10.1016/j.jiec.2013.08.002

Khan MM, Ansari SA, Ansari MO, Min BK, Lee J, Cho MH (2014d) Biogenic fabrication of Au@CeO_2 nanocomposite with enhanced visible light activity. J Phys Chem C 118 (18):9477–9484. https://doi.org/10.1021/jp500933t

Khan MM, Adil SF, Al-Mayouf A (2015) Metal oxides as photocatalysts. J Saudi Chem Soc 19 (5):462–464. https://doi.org/10.1016/j.jscs.2015.04.003

Kharisov BI, Kharissova OV, Ortiz-Mendez U (2016) CRC concise encyclopedia of nanotechnology. CRC Press, Bosa Roca

Konstantinou IK, Albanis TA (2004) TiO_2-assisted photocatalytic degradation of azo dyes in aqueous solution: kinetic and mechanistic investigations. Appl Catal B 49(1):1–14. https://doi.org/10.1016/j.apcatb.2003.11.010

Kumar R, Ansari MO, Parveen N, Oves M, Barakat MA, Alshahri A, Khan MY, Cho MH (2016) Facile route to a conducting ternary polyaniline@TiO_2/GN nanocomposite for environmentally benign applications: photocatalytic degradation of pollutants and biological activity. RSC Adv 6 (112):111308–111317. https://doi.org/10.1039/C6RA24079H

Lam WH, Chong MN, Horri BA, Tey BT, Chan ES (2017) Physicochemical stability of calcium alginate beads immobilizing TiO_2 nanoparticles for removal of cationic dye under UV irradiation. J Appl Polym Sci 134(26):45002. https://doi.org/10.1002/app.45002

Lee JU, Jung JW, Jo JW, Jo WH (2012) Degradation and stability of polymer-based solar cells. J Mater Chem 22(46):24265–24283. https://doi.org/10.1039/C2JM33645F

Li Y, Lu A, Wang C, Wu X (2008) Characterization of natural sphalerite as a novel visible light-driven photocatalyst. Sol Energy Mater Sol Cells 92(8):953–959. https://doi.org/10.1016/j.solmat.2008.02.023

Li X, He G, Han Y, Xue Q, Wu X, Yang S (2012) Magnetic titania-silica composite-polypyrrole core-shell spheres and their high sensitivity toward hydrogen peroxide as electrochemical sensor. J Colloid Interface Sci 387(1):39–46. https://doi.org/10.1016/j.jcis.2012.07.071

Li J, Xu X, Liu X, Yu C, Yan D, Sun Z, Pan L (2016) Sn doped TiO_2 nanotube with oxygen vacancy for highly efficient visible light photocatalysis. J Alloys Compd 679:454–462. https://doi.org/10.1016/j.jallcom.2016.04.080

Lin Y, Li D, Hu J, Xiao G, Wang J, Li W, Fu X (2012) Highly efficient photocatalytic degradation of organic pollutants by PANI modified TiO_2 composite. J Phys Chem C 116(9):5764–5772. https://doi.org/10.1021/jp211222w

Liu X, Chen Q, Lv L, Feng X, Meng X (2015) Preparation of transparent PVA/TiO_2 nanocomposite films with enhanced visible-light photocatalytic activity. Catal Commun 58:30–33. https://doi.org/10.1016/j.catcom.2014.08.032

Ma CM, Lee YW, Hong GB, Shie JL, Chang CT (2011) Effect of platinum on the photocatalytic degradation of chlorinated organic compound. J Environ Sci 23(4):687–692. https://doi.org/10.1016/S1001-0742(10)60480-9

Magalhães F, Moura FCC, Lago RM (2011) TiO_2/LDPE composites: a new floating photocatalyst for solar degradation of organic contaminants. Desalination 276(1–3):266–271. https://doi.org/10.1016/j.desal.2011.03.061

Malato S, Fernández-Ibáñez P, Maldonado MI, Blanco J, Gernjak W (2009) Decontamination and disinfection of water by solar photocatalysis: recent overview and trends. Catal Today 147 (1):1–59. https://doi.org/10.1016/j.cattod.2009.06.018

Mamba G, Mishra A (2016) Graphitic carbon nitride ($g\text{-}C_3N_4$) nanocomposites: a new and exciting generation of visible light driven photocatalysts for environmental pollution remediation. Appl Catal B Environ 198:347–377. https://doi.org/10.1016/j.apcatb.2016.05.052

Mansilla HD, Bravo C, Ferreyra R, Litter MI, Jardim WF, Lizama C, Freer J, Fernandez J (2006) Photocatalytic EDTA degradation on suspended and immobilized TiO_2. J Photochem Photobiol A 181(2–3):188–194. https://doi.org/10.1016/j.jphotochem.2005.11.023

Matos J, Laine J, Herrmann J-M, Uzcategui D, Brito JL (2007) Influence of activated carbon upon titania on aqueous photocatalytic consecutive runs of phenol photodegradation. Appl Catal B Environ 70(1–4):461–469. https://doi.org/10.1016/j.apcatb.2005.10.040

McCullough RD, Lowe RD, Jayaraman M, Anderson DL (1993) Design, synthesis, and control of conducting polymer architectures: structurally homogeneous poly(3-alkylthiophenes). J Org Chem 58(4):904–912. https://doi.org/10.1021/jo00056a024

Mendive CB, Hansmann D, Bredow T, Bahnemann D (2011) New insights into the mechanism of TiO_2 photocatalysis: thermal processes beyond the electron-hole creation. J Phys Chem C 115 (40):19676–19685. https://doi.org/10.1021/jp112243q

Ming-Twang S, Zaini MAA, Salleh LM et al (2017) Potassium hydroxide-treated palm kernel shell sorbents for the efficient removal of methyl violet dye. Desalin Water Treat 84:262–270. https://doi.org/10.5004/dwt.2017.21206

Nakata K, Fujishima A (2012) TiO_2 photocatalysis: design and applications. J Photochem Photobiol C 13(3):169–189. https://doi.org/10.1016/j.jphotochemrev.2012.06.001

Nursam NM, Wang X, Caruso RA (2015) High-throughput synthesis and screening of titania-based photocatalysts. ACS Comb Sci 17(10):548–569. https://doi.org/10.1021/acscombsci.5b00049

Ohama Y, Van Gemert D (2011) Application of titanium dioxide photocatalysis to construction materials: state-of-the-art report of the RILEM Technical Committee 194-TDP, vol 5. Springer, Dordrecht

Ohtani B (2013) Titania photocatalysis beyond recombination: a critical review. Catalysts 3 (4):942–953. https://doi.org/10.3390/catal3040942

Ohtani B, Ogawa Y, Nishimoto S (1997) Photocatalytic activity of amorphous-anatase mixture of titanium (IV) oxide particles suspended in aqueous solutions. J Phys Chem B 101 (19):3746–3752. https://doi.org/10.1021/jp962702+

Olad A, Behboudi S, Entezami AA (2012) Preparation, characterization and photocatalytic activity of TiO_2/polyaniline core-shell nanocomposite. Bull Mater Sci 35(5):801–809. https://doi.org/10.1007/s12034-012-0358-7

Ortelli S, Blosi M, Albonetti S, Vaccari A, Dondi M, Costa AL (2014) TiO_2 based nano-photocatalysis immobilized on cellulose substrates. J Photochem Photobiol A Chem 276:58–64. https://doi.org/10.1016/j.jphotochem.2013.11.013

Panda S (2009) Microelectronics and optoelectronics technology. Laxmi Publications, New Delhi

Pathania D, Sharma G, Kumar A et al (2015) Combined sorptional–photocatalytic remediation of dyes by polyaniline Zr(IV) selenotungstophosphate nanocomposite. Toxicol Environ Chem 97:526–537. https://doi.org/10.1080/02772248.2015.1050024

Pathania D, Katwal R, Sharma G et al (2016) Novel guar gum/Al2O3 nanocomposite as an effective photocatalyst for the degradation of malachite green dye. Int J Biol Macromol 87:366–374. https://doi.org/10.1016/j.ijbiomac.2016.02.073

Peirce JJ, Weiner R, Vesilind PA (1998) Environmental pollution and control, 4th edn. Elsevier, Oxford. ISBN 978-0-7506-9899-3

Qamar M, Drmosh Q, Ahmed MI, Qamaruddin M, Yamani ZH (2015) Enhanced photoelectrochemical and photocatalytic activity of WO_3-surface modified TiO_2 thin film. Nanoscale Res Lett 10(54):1–6. https://doi.org/10.1186/s11671-015-0745-2

Rajeshwar K, Osugi ME, Chanmanee W, Chenthamarakshan CR, Zanoni M, Kajitvichyanukul P, Krishnan-Ayer R (2008) Heterogeneous photocatalytic treatment of organic dyes in air and aqueous media. J Photochem Photobiol C 9(4):171–192. https://doi.org/10.1016/j.jphotochemrev.2008.09.001

Rasoulifard MH, Dorraji MSS, Mozafari V (2017) Visible light photocatalytic activity of chitosan/poly(vinyl alcohol)/TiO2 nanocomposite for dye removal: taguchi-based optimization. Environ Prog Sustain Energy 36(1):66–72. https://doi.org/10.1002/ep.12438

Rehman S, Ullah R, Butt AM, Gohar ND (2009) Strategies of making TiO_2 and ZnO visible light active. J Hazard Mater 170(2–3):560–569. https://doi.org/10.1016/j.jhazmat.2009.05.064

Romero-Sáez M, Jaramillo LY, Saravanan R, Benito N, Pabón E, Mosquera E, Gracia F (2017) Notable photocatalytic activity of TiO_2-polyethylene nanocomposites for visible light degradation of organic pollutants. Express Polym Lett 11(11):899–909. https://doi.org/10.3144/expresspolymlett.2017.86

Rothenberger G, Moser J, Gratzel M, Serpone N, Sharma DK (1985) Charge carrier trapping and recombination dynamics in small semiconductor particles. J Am Chem Soc 107(26):8054–8059. https://doi.org/10.1021/ja00312a043

Sahoo DP, Rath D, Nanda B, Parida K (2015) Transition metal/metal oxide modified MCM-41 for pollutant degradation and hydrogen energy production: a review. RSC Adv 5(102):83707–83724. https://doi.org/10.1039/C5RA14555D

Sajan CP, Wageh S, Al-Ghamdi AA, Yu JG, Cao SW (2016) TiO_2 nanosheets with exposed {001} facets for photocatalytic applications. Nano Res 9(1):3–27. https://doi.org/10.1007/s12274-015-0919-3

Sakar M, Balakumar S, Saravanan P, Bharathkumar S (2016) Particulates vs. fibers: dimension featured magnetic and visible light driven photocatalytic properties of Sc modified multiferroic bismuth ferrite nanostructures. Nanoscale 8(2):1147–1160. https://doi.org/10.1039/C5NR06655G

Salem MA, Al-Ghonemiy AF, Zaki AB (2009) Photocatalytic degradation of allura red and quinoline yellow with polyaniline/TiO_2 nanocomposite. Appl Catal B Environ 91(1–2):59–66. https://doi.org/10.1016/j.apcatb.2009.05.027

Sangareswari M, Meenakshi Sundaram M (2015) Enhanced photocatalytic activity of conducting Polypyrrole-TiO_2 nanocomposite for degradation of organic dyes under UV light irradiation. J Nanosci Technol 1(1):9–12. https://doi.org/10.30799/jnst

Sangareswari M, Meenakshi Sundaram M (2017) Development of efficiency improved polymer-modified TiO_2 for the photocatalytic degradation of an organic dye from wastewater environment. Appl Water Sci 7(4):1781–1790. https://doi.org/10.1007/s13201-015-0351-6

Saravanan R, Shankar H, Prakash T, Narayanan V, Stephen A (2011) ZnO/CdO composite nanorods for photocatalytic degradation of methylene blue under visible light. Mater Chem Phys 125(1–2):277–280. https://doi.org/10.1016/j.matchemphys.2010.09.030

Saravanan R, Aviles J, Gracia F, Mosquera E, Gupta VK (2018a) Crystallinity and lowering band gap induced visible light photocatalytic activity of TiO_2/CS (Chitosan) nanocomposites. Int J Biol Macromol 109:1239–1245. https://doi.org/10.1016/j.ijbiomac.2017.11.125

Saravanan R, Manoj D, Qin J, Naushad M, Gracia F, Lee AF, Khan MM, Gracia-Pinilla MA (2018b) Mechanothermal synthesis of Ag/TiO_2 for photocatalytic methyl orange degradation and hydrogen production. Process Saf Environ Prot 120:339–347. https://doi.org/10.1016/j.psep.2018.09.015

Sarmah S, Kumar A (2011) Photocatalytic activity of polyaniline-TiO_2 nanocomposites. Indian J Phys 85(5):713–726. https://doi.org/10.1007/s12648-011-0071-1

Schneider J, Matsuoka M, Takeuchi M, Zhang J, Horiuchi Y, Anpo M, Bahnemann DW (2014) Understanding TiO_2 photocatalysis: mechanisms and materials. Chem Rev 114(19):9919–9986. https://doi.org/10.1021/cr5001892

Sedghi R, Moazzami HR, Davarani SSH, Nabid MR, Keshtkar AR (2017) A one step electrospinning process for the preparation of polyaniline modified TiO_2/polyacrylonitrile nanocomposite with enhanced photocatalytic activity. J Alloys Compd 695:1073–1079. https://doi.org/10.1016/j.jallcom.2016.10.232

Sellappan R (2013) Mechanisms of enhanced activity of model TiO_2/carbon and TiO_2/metal nanocomposite photocatalysts. Chalmers University of Technology, Göteborg

Serpone N, Pelizzetti E (1989) Photocatalysis: fundamentals and applications. Wiley, New York

Serpone N, Lawless D, Disdier J, Herrmann JM, Serpone N, Lawless D (1994) Spectroscopic, photoconductivity, and photocatalytic studies of TiO_2 colloids: naked and with the lattice doped with $Cr^{3+,}$ Fe^{3+}, and V^{5+} cations. Langmuir 10(3):643–652. https://doi.org/10.1021/la00015a010

Shan AY, Ghazi TIM, Rashid SA (2010) Immobilisation of titanium dioxide onto supporting materials in heterogeneous photocatalysis: a review. Appl Catal A Gen 389(1–2):1–8. https://doi.org/10.1016/j.apcata.2010.08.053

Shankar H, Saravanan R, Suresh V, Narayanan V, Rossi F, Stephen A (2011a) Investigation on the photocatalytic degradation of aqueous methyl orange using nano-titania loaded Mo-MCM-41 H. Int J Nanosci 10:1131–1135. https://doi.org/10.1142/S0219581X11009581

Shankar H, Saravanan R, Suresh V, Narayanan V, Rossi F, Stephen A (2011b) Synthesis and characterization of nano-titania photocatalyst loaded on Mo-MCM-41 support. Adv Sci Lett 4:89–95. https://doi.org/10.1166/asl.2011.1197

Sharma G, Naushad M, Kumar A et al (2017) Efficient removal of coomassie brilliant blue R-250 dye using starch/poly(alginic acid-cl-acrylamide) nanohydrogel. Process Saf Environ Prot 109:301–310. https://doi.org/10.1016/j.psep.2017.04.011

Sharma A, Sharma G, Naushad M et al (2018) Remediation of anionic dye from aqueous system using bio-adsorbent prepared by microwave activation. Environ Technol (UK) 39(7):917–930. https://doi.org/10.1080/09593330.2017.1317293

Shirakawa H (2001) The discovery of polyacetylene film: the dawning of an era of conducting polymers (Nobel Lecture). Angew Chem Int Ed Engl 40(14):2574–2580. https://doi.org/10.1002/1521-3773(20010716)40:14<2574::AID-ANIE2574>3.0.CO;2-N

Shironita S, Mori K, Shimizu T, Ohmichi T, Mimura N, Yamashita H (2008) Preparation of nano-sized platinum metal catalyst using photo-assisted deposition method on mesoporous silica including single-site photocatalyst. Appl Surf Sci 254(23):7604–7607. https://doi.org/10.1016/j.apsusc.2008.01.120

Shockley W, Read W Jr (1952) Statistics of the recombinations of holes and electrons. Phys Rev 87 (5):835. https://doi.org/10.1103/PhysRev.87.835

Skinner DE, Colombo DP Jr, Cavaleri JJ, Bowman RM (1995) Femtosecond investigation of electron trapping in semiconductor nanoclusters. J Phys Chem 99(20):7853–7856. https://doi.org/10.1021/j100020a003

Škoric ML, Terzić I, Milosavljevic N, Radetic M, Šaponjic Z, Radoičić M, Krušic MK (2016) Chitosan-based microparticles for immobilization of TiO_2 nanoparticles and their application for photodegradation of textile dyes. Eur Polym J 82:57–70. https://doi.org/10.1016/j.eurpolymj.2016.06.026

Sriwong C, Wongnawa S, Patarapaiboolchai O (2008) Photocatalytic activity of rubber sheet impregnated with TiO_2 particles and its recyclability. Catal Commun 9(2):213–218. https://doi.org/10.1016/j.catcom.2007.05.037

Strandwitz NC, Nonoguchi Y, Boettcher SW, Stucky GD (2010) In situ photopolymerization of pyrrole in mesoporous TiO_2. Langmuir 26(8):5319–5322. https://doi.org/10.1021/la100913e

Sun L, Shi YC, Li B, Li X, Wang Y (2013) Preparation and characterization of polypyrrole/TiO2nanocomposites by reverse microemulsion polymerization and its photocatalytic activity for the degradation of methyl orange under natural light. Polym Compos 34(7):1076–1080. https://doi.org/10.1002/pc.22515

Suwanchawalit C, Patil AJ, Krishna Kumar R, Wongnawa S, Mann S (2009) Fabrication of ice-templated macroporous TiO_2–chitosan scaffolds for photocatalytic applications. J Mater Chem 19(44):8478–8483. https://doi.org/10.1039/B912698H

Tatsuma T, Saitoh S, Ohko Y, Fujishima A (2001) TiO_2-WO_3 photoelectrochemical anticorrosion system with an energy storage ability. Chem Mater 13(9):2838–2842. https://doi.org/10.1021/cm010024k

Thomas M, Naikoo GA, Sheikh MUD, Bano M, Khan F (2016) Effective photocatalytic degradation of Congo red dye using alginate/carboxymethyl cellulose/TiO_2 nanocomposite hydrogel under direct sunlight irradiation. J Photochem Photobiol A Chem 327:33–43. https://doi.org/10.1016/j.jphotochem.2016.05.005

Thomas M, Natarajan TS, Sheikha MUD, Bano M, Khan F (2017) Self-organized graphene oxide and TiO_2 nanoparticles incorporated alginate/carboxymethyl cellulose nanocomposites with efficient photocatalytic activity under direct sunlight. J Photochem Photobiol A Chem 346:113–125. https://doi.org/10.1016/j.jphotochem.2017.05.037

Tong H, Ouyang SX, Bi YP, Umezawa N, Oshikiri M, Ye JH (2012) Nano-photocatalytic materials: possibilities and challenges. Adv Mater 24(2):229–251. https://doi.org/10.1002/adma.201102752

Vaez M, Moghaddam AZ, Mahmoodi NM, Alijani S (2012) Decolorization and degradation of acid dye with immobilized titania nanoparticles. Process Saf Environ Prot 90(1):56–64. https://doi.org/10.1016/j.psep.2011.07.005

Venieri D, Gounaki I, Binas V, Zachopoulos A, Kiriakidis G, Mantzavinos D (2015) Inactivation of MS_2 coliphage in sewage by solar photocatalysis using metal doped TiO_2. Appl Catal B Environ 178:54–64. https://doi.org/10.1016/j.apcatb.2014.10.052

Wan Ngah WS, Teong LC, MAKM H (2011) Adsorption of dyes and heavy metal ions by chitosan composites: a review. Carbohydr Polym 83(4):1446–1456. https://doi.org/10.1016/j.carbpol.2010.11.004

Wang J, Zhang D (2013) One-dimensional nanostructured polyaniline: syntheses, morphology controlling, formation mechanisms, new features, and applications. Adv Polym Technol 32 (S1):E323–E368. https://doi.org/10.1002/adv.21283

Wang P, Zakeeruddin SM, Moser JE, Nazeeruddin MK, Sekiguchi T, Grätzel M (2003) A stable quasi-solid-state dye-sensitized solar cell with an amphiphilic ruthenium sensitizer and polymergel electrolyte. Nat Mater 2(6):402–407. https://doi.org/10.1038/nmat925

Wang D, Wang Y, Li X, Luo Q, An J, Yue J (2008) Sunlight photocatalytic activity of polypyrrole–TiO_2 nanocomposites prepared by 'in situ' method. Catal Commun 9(6):1162–1166. https://doi.org/10.1016/j.catcom.2007.10.027

Wang Y, Zhang J, Liu L, Zhu C, Liu X, Su Q (2012) Visible light photocatalysis of V_2O_5/TiO_2 nanoheterostructures prepared via electrospinning. Mater Lett 75(1–2):95–98. https://doi.org/10.1016/j.apcatb.2007.04.001

Wang W, Huang G, Jimmy CY, Wong PK (2015) Advances in photocatalytic disinfection of bacteria: development of photocatalysts and mechanisms. J Environ Sci 34:232–247. https://doi.org/10.1016/j.jes.2015.05.003

Wei S, Zhang X, Zhao K, Fu Y, Li Z, Lin B, Wei J (2016) Preparation, characterization, and photocatalytic degradation properties of polyacrylamide/calcium alginate/TiO_2 composite film. Polym Compos 37(4):1292–1301. https://doi.org/10.1002/pc.23295

Weng Z, Ni X (2008) Oxidative polymerization of pyrrole photocatalyzed by TiO_2 nanoparticles and interactions in the composites. J Appl Polym Sci 110(1):109–116. https://doi.org/10.1002/app.28636

Wu T, Liu G, Zhao J, Hidaka H, Serpone N (1998) Photoassisted degradation of dye pollutants. V. self-photosensitized oxidative transformation of Rhodamine B under visible light irradiation in aqueous TiO_2 dispersions. J Phys Chem B 102(30):5845–5851. https://doi.org/10.1021/jp980922c

Xiang Y, Wang H, He Y, Song G (2015) Efficient degradation of methylene blue by magnetically separable Fe_3O_4/chitosan/TiO_2 nanocomposites. Desalin Water Treat 55(4):1018–1025. https://doi.org/10.1080/19443994.2014.922441

Xiao G, Su H, Tan T (2015) Synthesis of core–shell bioaffinity chitosan–TiO_2 composite and its environmental applications. J Hazard Mater 283:888–896. https://doi.org/10.1016/j.jhazmat.2014.10.047

Xu S, Zhu Y, Jiang L, Dan Y (2010) Visible light induced photocatalytic degradation of methyl orange by polythiophene/TiO_2 composite particles. Water Air Soil Pollut 213(1–4):151–159. https://doi.org/10.1007/s11270-010-0374-4

Xu S, Jiang L, Yang H, Song Y, Dan Y (2011) Structure and photocatalytic activity of polythiophene/TiO_2 composite particles prepared by photoinduced polymerization. Chin J Catal 32(3–4):536–545. https://doi.org/10.1016/S1872-2067(10)60207-0

Yang C, Dong W, Cui G, Zhao Y, Shi X, Xia X, Tang B, Wang W (2017) Enhanced photocatalytic activity of PANI/TiO_2 due to their photosensitization-synergetic effect. Electrochim Acta 247:486–495. https://doi.org/10.1016/j.electacta.2017.07.037

Yao H (2013) Application of advanced oxidation processes for treatment of air from livestock buildings and industrial facilities. Department of Engineering, Aarhus University, Denmark, Technical report BCE -TR-8, 36 pp

Yu JC, Ho WK, Yu JG, Yip H, Wong P, Zhao JC (2005) Efficient visible-light-induced photocatalytic disinfection on sulfur-doped nanocrystalline titania. Environ Sci Technol 39 (4):175–1179. https://doi.org/10.1021/es035374h

Zhang Z, Yates JT Jr (2012) Band bending in semiconductors: chemical and physical consequences at surfaces and interfaces. Chem Rev 112(10):5520–5551. https://doi.org/10.1021/cr3000626

Zhang X, Sun DD, Li G, Wanga Y (2008) Investigation of the roles of active oxygen species in photodegradation of azo dye AO7 in TiO_2 photocatalysis illuminated by microwave electrodeless lamp. J Photochem Photobiol A 199(2–3):311–315. https://doi.org/10.1016/j.jphotochem.2008.06.009

Zhang J, Liu W, Wang P, Qian K (2013) Photocatalytic behavior of cellulose-based paper with TiO_2 loaded on carbon fibers author links open overlay panel. J Environ Chem Eng 1 (3):175–182. https://doi.org/10.1016/j.jece.2013.04.022

Zhang Z, Yang RY, Gao YS, Zhao YF, Wang JY, Huang L, Guo J, Zhou TT, Lu P, Guo ZH, Wang Q (2014) Novel $Na_2Mo_4O_{13}$/MoO_3 hybrid material as highly efficient CWAO catalyst for dye degradation at ambient conditions. Sci Rep 4:6797–6809. https://doi.org/10.1038/srep06797

Zhang L, Liu P, Su Z (2016) Preparation of PANI/TiO_2 nanocomposites and their solid-phase photocatalytic degradation. Polym Degrad Stab 91(9):2213–2219. https://doi.org/10.1016/j.polymdegradstab.2006.01.002

Zhao K, Feng L, Li Z, Fu Y, Zhang X, Wei J, Wei S (2014) Preparation, characterization and photocatalytic degradation properties of a TiO_2/calcium alginate composite film and the recovery of TiO_2 nanoparticles. RSC Adv 4(93):51321–51329. https://doi.org/10.1039/C4RA08102A

Zhao Y, Tao C, Xiao G, Su H (2017) Controlled synthesis and wastewater treatment of Ag_2O/TiO_2 modified chitosan-based photocatalytic film. RSC Adv 7(18):11211–11221. https://doi.org/10.1039/C6RA27295A

Zhu Y, Dan Y (2010) Photocatalytic activity of poly(3-hexylthiophene)/titanium dioxide composites for degrading methyl orange. Sol Energy Mater Sol Cells 94:1658–1664. https://doi.org/10.1016/j.solmat.2010.05.025

Zhu Y, Xu S, Jiang L, Pan K, Dan Y (2008) Synthesis and characterization of polythiophene/titanium dioxide composites. React Funct Polym 68(10):1492–1498. https://doi.org/10.1016/j.reactfunctpolym.2008.07.008

Zhu Y, Xu S, Yi D (2010) Photocatalytic degradation of methyl orange using polythiophene/titanium dioxide. React Funct Polym 70(5):282–287. https://doi.org/10.1016/j.reactfunctpolym.2010.01.007

Zubieta CE, Messina PV, Luengo C, Dennehy M, Pieroni O, Schulz PC (2007) Reactive dyes emotion by porous TiO_2-chitosan materials. J Hazard Mater 152(2):765–777. https://doi.org/10.1016/j.jhazmat.2007.07.043

Chapter 8
Light-Activated Nanoparticles for Antibacterial Studies

Krishnapriya Madhu Varier, Wuling Liu, Yaacov Ben-David, Yanmei Li, Arulvasu Chinnasamy, and Babu Gajendran

Contents

K. M. Varier
Department of Medical Biochemistry, Dr. ALM PGIBMS, University of Madras, Chennai, India

Department of Zoology, University of Madras, Chennai, India

W. Liu · Y. Ben-David · Y. Li · B. Gajendran (✉)
Department of Biology and Chemistry, The Key Laboratory of Chemistry for Natural Products of Guizhou Province and Chinese Academy of Sciences, Guizhou, China

State Key Laboratory of Functions and Applications of Medicinal Plants, Guizhou Medical University, Guiyang, China

A. Chinnasamy
Department of Zoology, University of Madras, Chennai, India

M. Naushad et al. (eds.), *Green Methods for Wastewater Treatment*, Environmental Chemistry for a Sustainable World 35, https://doi.org/10.1007/978-3-030-16427-0_8

Abstract Photolysis or light activation of electrons to an energy excited state to aid a release of energy could be utilized in many applications like industries and semiconductors as well as for antimicrobial action. This electron transfer mechanism is widely being incorporated to metals and metal oxides or sometimes with nanoparticles (NPs) to increase its reactivity. However, three forms of NP formulations are used for antibacterial action like nanocomposites, doped NPs, and metal oxide NPs. The preparation, synthesis, and antimicrobial application of the metal oxide NPs are explained coherently in this chapter. Moreover, the future prospects of these NP-assisted light-activated antimicrobial actions are also dealt in detail.

Keywords Photolysis · Nanocomposites · Doped nanoparticles · Metal oxides · Metal oxides NP synthesis · Antimicrobial action

8.1 Introduction

The photocatalysis process gained attention in the scientific world, since Fujishima and Honda (1972) initially stated the use of TiO_2 as a catalyst for water splitting through solar energy conversion. Ever since, these suspended semiconductors have been used widely as an agent of pollutant degradation, water purification, indoor self-cleaning surfaces, as well antimicrobials (Kumar et al. 2018). In a natural purification system, photocatalysis is initiated by sunlight (the ultraviolet [UV] rays) by the breakdown of organic molecules. However, the antimicrobial effect of this system is restricted. Thus, to promote specific redox reactions on semiconductor surfaces through the employment of semiconductors and the incorporation of catalysts was introduced (Miller 1971). Since then, an enhancement in the purification process and antibacterial action could be achieved to the expected levels.

The photocatalytic reaction proceeds over a semiconductor powder through several steps (Fig. 8.1) in accordance with band theory (electron transfer theory) escorted by the interaction of photo-generated electrons and holes with the reactants which potentially occurs at low temperatures. The bandwidth of the reaction categorizes the desirable light energy, reducing ability and oxidizability of the products.

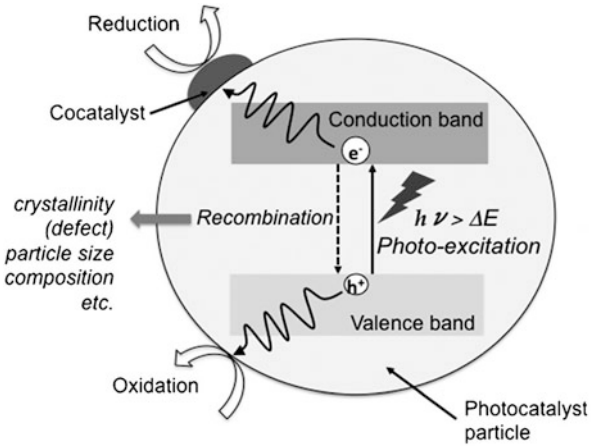

Fig. 8.1 Model of reaction, charge separation, and recombination over photocatalyst. (Tetsuya et al. 2011; open access)

This even contributes to the lifetime of the generated catalyst (Tetsuya et al. 2011; Saravanan et al. 2018a). Thus the activated electrons are highly reactive and could produce reactive oxygen species, causing oxidative stress to the cell membranes and thus the killing of bacteria. This may even happen through the interaction of such electrons to the functional enzymes or proteins of the bacterial cells and hence pose a threat to the progression of the microbes in their habitat (Tetsuya et al. 2011; Thakur et al. 2017). This can even be achieved by altering the hydrogen adsorption properties of metals. A recent study has demonstrated that silver (Ag)-decorated TiO_2 nanomaterials altered the hydrogen absorption and thereby the photocatalytic ability (Saravanan et al. 2018b). Moreover, the metal nanoparticle (NP)-assisted photocatalysts can be found in various industrial, medical, personal, and military applications (Jiang et al. 2009). However, this chapter deals with the antimicrobial action of the light-activated metal particles.

8.2 Nanoformulations for Antibacterial Action

It should be noted at this juncture that the properties of the NPs like composition, size, properties, and doping effect add on to the applications of the NP-assisted photocatalysis and its related antibacterial effect. The major three forms of NPs used for antibacterial action are nanocomposites, doped NPs, and metal oxides. The publications for various nanoformulation over past five yearrs are depicted in Fig. 8.2.

8.2.1 Nanocomposites

Nanocomposites are amalgams possessing dimensions in the nanometer range (1 nm = 10–9 m) and have emerged as suitable alternatives to incredulous

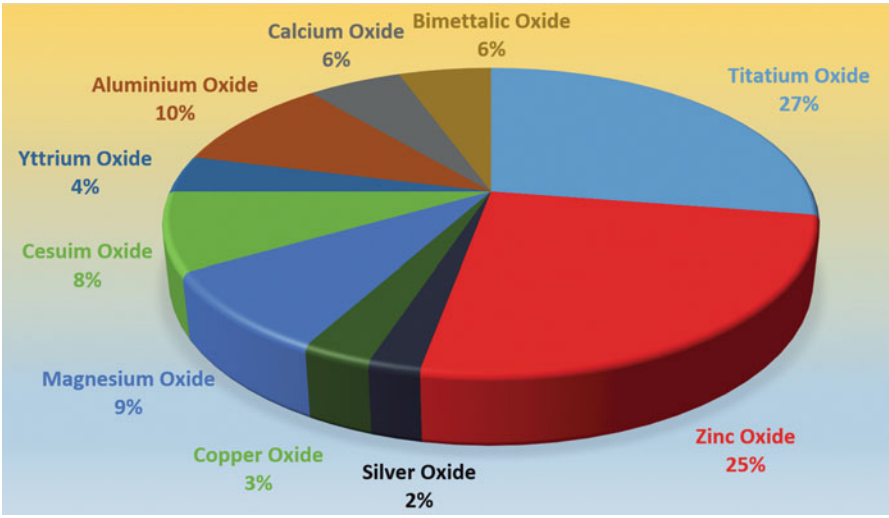

Fig. 8.2 Number of publications on Google Scholar on light-activated nanoparticles for antibacterial studies over the period 2013–2018 recovered from sources as a part of literature survey

Table 8.1 Different types of nanocomposites (Pedro et al. 2009; open access)

Class	Examples
Ceramic	Al_2O_3/SiO_2, SiO_2/Ni, Al_2O_3/TiO_2, Al_2O_3/SiC, Al_2O_3/CNT
Metal	Fe-Cr/Al_2O_3, Ni/Al_2O_3, Co/Cr, Fe/MgO, Al/CNT, Mg/CNT
Polymer	Thermoplastic/thermoset polymer/layered silicates, polyester/TiO_2, polymer/CNT, polymer/layered double hydroxides

restrictions of microcomposites and monolithic, due to their fundamental stoichiometry composition at microphase (Roy et al. 2010; Rajendran et al. 2018), looking to enter to the cell membranes of microorganisms and causing the desired effect. Since the twenty-first century, researchers have reported that design distinctiveness and proper combinations than conventional composites offer better applications in industrial and health-care clinics (Schmidt et al. 2002). Even though the first extrapolation of them was testified as early as 1992 (Gleiter), nowadays, nanocomposites deal innovative technology (Choa et al. 2003). As in the case of microcomposites, according to their matrix materials, nanocomposite materials can be categorized in three dissimilar classes as shown in Table 8.1, namely, ceramic matrix nanocomposites (CMNC), metal matrix nanocomposites (MMNC), and polymer matrix nanocomposites (PMNC) with examples. The report of Saravanan et al. (2016) has emphasized that an enhanced photocatalytic degradation and electrochemical detection competence were observed in a ZnO/CeO_2 (90:10) nanoformulation.

8.2.2 Doped Metal Oxide NPs

Various attempts were done to shift metal oxide NP absorption into a visible light region, which chiefly focus on the doping with transition metal ions (Choi et al. 1994; Nalage et al. 2015). Nonetheless, the limitations of doped metal oxide NPs, such as the inclination to form charged carrier recombination centers, thermal instability (Choi et al. 1994), and the exclusive accommodations for ion implantation, make metal-doped metal oxides unrealistic for its applications (Wang et al. 1999). During the last decade, anion doping of metal oxides was positively achieved using anions of nitrogen (Asahi et al. 2001), carbon (Sakthivel and Kisch 2003), sulfur (Umebayashi et al. 2002), phosphorus (Lin et al. 2005), and fluoride (Ho et al. 2006). Among these anion dopants, nitrogen appears to be the most operational because of its metastable AX center formation, similarity in size to oxygen, and lesser ionization energy (Park et al. 2002). The major long wavelength region (>700 nm) in N-doped TiO_2 and ZrO_2 of absorption spectra is the significantly improved absorption at which it offers better photocatalytic light activities at visible range (Qiu et al. 2007). The active, visible wavelength of TiO_{2-} and ZrO_2-doped complexes promises a varied array of antibacterial applications under visible lightening (Asahi et al. 2001).

8.2.3 Metal Oxide NPs

Due to the amplified reactivity and comfort of handling into useful electrode formats, NP metal oxide photocatalysts are striking. However, their preparation is quite tedious. The prompt bulk synthesis of photocatalytic NPs with consistent shape and size via the cathodic corrosion method is used for the nifty research through several composite metal oxides (Matthew et al. 2017).

Synthesis of Metal Oxide NPs

The method by which the metal oxide particles were synthesized is précised in Fig. 8.3. For the synthesis of H2WO4 particles, a tungsten wire is flooded with a KHSO4 solution (1 M). A voltage of 0 V to −10 V in the range square wave was applied between a W wire (working electrode) and a tall surface area Pt foil (counter electrode) occasioning in the instant materialization of the NPs. While submerged in a 10 M NaOH solution, TiO_2 nanowires were arranged with a titanium wire that was exposed to an AC square wave in the range of 0 V to −10 V with a frequency of 100 Hz. Similarly, the BiVO4 NPs were produced by means of a vanadium wire occupied in 10 mL of a mixture (1:1 by volume) of the saturated CaCl2 solution and MilliQ water, to which saturated Bi2O3 solution was supplemented successively, by

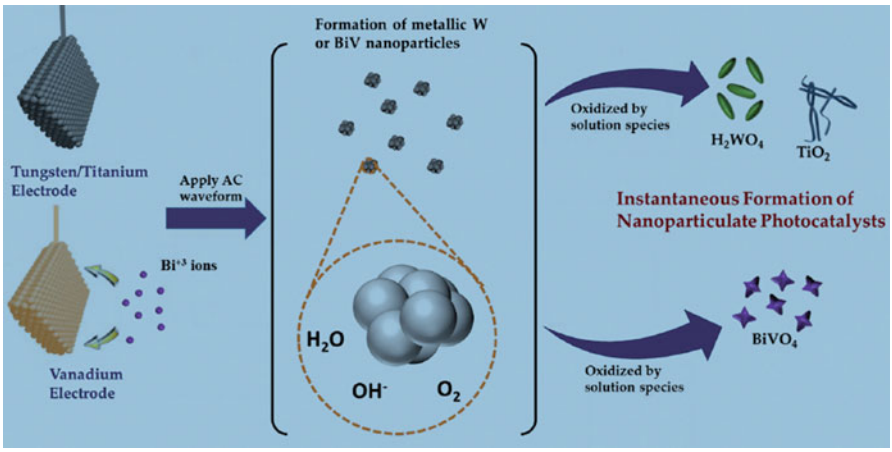

Fig. 8.3 Schematic depicting how cathodic corrosion was used to prepare H2WO4, TiO_2, and BiVO4 photocatalysts. (Matthew et al. 2017; copyright received)

applying a −8 V to 2 V. Once synthesized, the resulting suspensions of NPs were centrifuged at and elucidated in a UV-Vis spectrophotometer (Matthew et al. 2017).

8.3 Factors Affecting the Antimicrobial Action of NP Metal Oxides

Many factors affect the antimicrobial action of the synthesized metal oxide NPs which are light activated. The photocatalytic efficiency also varies according to the temperatures used for synthesis of nanocomposites, the nature of the doping materials, as well as methods used for synthesis of nanocomposites (Saravanan et al. 2013a, b, c). Some of the aspects are listed below.

8.3.1 Size

The smaller size of NPs synthesized in a photocatalytic manner encountered antimicrobial operations through fighting intracellular bacteria (Ranghar 2012). The drugs of ordinary size pose limited impact on intracellular microbes (Andrade et al. 2013). Because of antibiotics' condensed membrane transport, an improved treatment method using metal oxide NPs is developed to combat microorganisms, which could excite its electrons upon photoactivation posing an ROS threat to the microbes (Qi et al. 2013).

8.3.2 Protection

NP carriers like metal oxides (ZnO, CuO, etc.) could prevent the drug being resistant to targeted bacteria. The presence of metal oxides very often shelters the NPs from serious chemical reactions which are harmful for the potency of the assisted NPs for its action against microbial population. Moreover, healthier efflux and condensed endorsement of antibiotics in the bacterial cells (such as in *E. coli*, *P. aeruginosa*, etc.) are the normal and significant explanations for bacterial resistance than traditional antibiotics. Nevertheless, investigators have demonstrated that abundant NPs can incredulous this type of mechanisms (Muhling et al. 2009), preventing drug resistance. For example, Roy et al. (2010) estimated the influence of TiO_2 nanoparticles with different antibiotics against methicillin-resistant *Staphylococcus aureus* (MRSA). However, TiO_2 nanoparticles enhanced the antimicrobial effect of cephalosporins, beta-lactams, glycopeptides, aminoglycosides, macrolides, tetracycline, and lincosamides against MRSA.

8.3.3 Precision and Security

NP metal oxides can curtail side effects and precede antibiotics to the infection site. When we use a beneficial carrier, we can moderate the side effects (including drug toxicity) and can boost absorption at an anticipated site. The focused NP-based drug delivery demands either active targeting or passive targeting (Xiong et al. 2012).

8.3.4 Controllability

Well-regulated constant discharge of drugs can be achieved passively. With the appropriate NP drug release method, like metal oxide photocatalysts (Liu et al. 2016), they are operative even by dissimilar kinds of stimulatory factors (such as a light, heat, and pH) (Lim et al. 2018).

8.3.5 Shape

The shape of NPs accounts for antimicrobial activity by interacting with periplasmic enzymes causing gradations of bacterial cell damage, according to the shape of NPs (Cha et al. 2015). A comparison of pyramid-, plate-, and sphere-shaped ZnO NPs which exposed the β-galactosidase (GAL) rearrangement produced differential photocatalytic activity (Prasannakumar et al. 2015). *Pseudomonas desmolyticum* and *Staphylococcus aureus* were greatly affected with Y2O3 NP prismatic-shaped

owing to the straight interaction among the NPs and the bacterial cell membrane surface (Hong et al. 2016). Moreover, cube-shaped Ag NPs display tougher antibacterial activity than the sphere-shaped and wire-shaped Ag NPs with similar diameters, due to the specific facet reactivity and surface area (Actis et al. 2015) consuming a smaller effect on microbiota susceptibility (Talebian et al. 2014). In several studies, experimenters concluded that the nanostructures and its morphological variations primarily account for its photocatalytic properties (Thangaraj et al. 2017; Qin et al. 2017).

8.3.6 Roughness

Roughness is another key factor acting in NP-assisted antibacterial action. As the roughness of NPs rises, the size and the surface area-to-mass ratio upholding the adsorption of bacterial proteins, followed by a reduction in bacterial adhesion, occur (Sukhorukova et al. 2015).

8.3.7 Zeta Potential

Several researchers have authenticated the zeta potential of NPs has long-term influence on bacterial adhesion. For example, the electrostatic magnetism between the negatively charged cell membrane of bacteria and positively charged NPs has a positive charge on its surface which are disposed to get adsorbed to microbial surface (Pan et al. 2013) and enhances vascular permeability (Maeda 2010), through ion exchange by limiting attachment of the bacteria (Fang et al. 2015). When the negatively charged and neutral NPs are compared to its positively charged equivalents, it is proved that the positively charged metal oxide NPs enhance the ROS production, which primes to influential relations among the metal oxide NPs and the bacterial surfaces (Arakha et al. 2015)

8.3.8 Doping Modification

Doping modification is another effective strategy to regularize the interaction of bacteria with the desired type of NPs. The NPs used in clinics are now altered to disperse in hydrophilic or aqueous environment aggregations using doping modification techniques. For instance, the ZnO NPs doped with Au (Gold) to form ZnO/Au co-doped nanocomposites were directed to progress photocatalytic activity by

increasing ROS production. These effects are due to an altered metal oxide bandwidth, improved light absorption for gold's surface plasmon resonance wavelength, and photoinduced charge carrier reactivity causing amplified electron-carrying efficiency and its charge separation (He et al. 2014). The ZnO NPs have "O" content at the surface that regulates antimicrobial activity against both Gram-positive and Gram-negative bacteria (Mehmood et al. 2015).

8.3.9 Environmental Conditions

The environmental conditions in which the NPs should exhibit its action also affect its antimicrobial function. One such condition is the temperature, which could potentially alter the activity with respect to its effect on potential ROS production. When ZnO NPs are stimulated by temperature variations, electrons are captivated at its active site, which interact with oxygen molecules (O2), thereby advancing the antimicrobial efficacy of the metal oxide NPs. Another factor is the decrease in the pH, which potentates the rate of dissolute ZnO NPs production by elevating the antimicrobial properties (Saliani et al. 2015). Certain results projected the protonation of the imidazole molecules under acidic conditions which at times leads to surface charge switching. At lower pH, the surfaces of the NPs were positively charged being beneficial to the contact with the bacterial cell barrier stimulating strong electrostatic multivalent regulation. Moreover, Li and his coworkers (2012) proved that antibacterial tests in five types of media due to free Zn ions and zinc complexes are mainly through ZnO NPs (Khan et al. 2016).

8.4 Mechanisms Through Which Metal NP Oxides Express Antimicrobial Action

NPs attain its contact with the bacterial cells, the foremost step to achieve antibacterial action through van der Waals forces (Armentano et al. 2014), electrostatic attractions, 86 and receptor-ligand hydrogen bond formations (Gao et al. 2014), and hydrophobic interactions (Luan et al. 2016), ensuring its entry to the metabolic pathway and impelling the function and shape of its cell membranes. In tail with it, NPs communicate with the bacterial cell's basic components, such as enzymes, lysosomal organelles, as well as DNA, causing oxidative insults, cell membrane permeability alternations, heterogeneous changes, electrolyte balance loss, protein deactivation, enzyme inhibition, and even alterations in gene expression (Xu et al. 2016). However, the most frequently proposed mechanisms in the current NP research focus on oxidative stress (Gurunathan et al. 2012), metal ion release

(Zakharova et al. 2015), and non-oxidative mechanisms (Leung et al. 2014) about which is explained in detail in the following sections.

8.4.1 Oxidative Stress and ROS Generation

Oxidative stress, generated by ROS (reactive oxygen species), is an efficient reason for the antiseptic action of the synthesized metal oxide NPs. There are mainly four types of ROS produced like the superoxide radical (O_2^-), hydrogen peroxide (H_2O_2), the hydroxyl radical (·OH), and singlet oxygen (O_2) which reveal different levels of activity and crescendos. For example, CaO and MgO NPs can generate O_2^-, whereas ZnO NPs can generate H_2O_2 and OH but not O_2^-. In the meantime, CuO NPs can yield the four mentioned types of reactive oxygen species. Studies have indicated that O_2^- and H_2O_2 reason minute stress reactions which are acute and could be counteracted by the endogenous antioxidants, like superoxide and catalase enzymes, although ROS could aggravate the microbial death. The principal cause of ROS attacks is restructuring of cell membranes, defective sites, and oxygen vacancies in their crystal forms, owing to sites of electron replacements (Malka et al. 2013). In a normal cell, the assembly and disassembly of ROS are poised. In dissimilarity, with excessive ROS assembly, the situation gets unbalanced and cell ultimately favors oxidation, which damages the organelles of microbes (Li et al. 2012; Peng et al. 2013).

8.4.2 Dissolved Metal Ions

Metal ions of the metal oxide NPs were gradually loosened over time after adhering to the cell wall, monitored by uninterrupted interface with the functional groups of biomolecules, such as amino (–NH), mercapto (–SH), and carboxyl (–COOH) groups, enzyme inactivation, cell structure demolishment, and altering normal physiological processes, eventually constraining the microbial progression. However, the influence of metal ions on the pH of lipid vesicles is insignificant as far as the antibacterial course of metal oxide suspension is concerned. Thus, dissolved metal ions are not the foremost reason for the antimicrobial machinery of metal oxide NPs (Yu et al. 2014). By the same token, a study revealed that superparamagnetic iron oxide counteracts with microbial cells by unswervingly penetrating the membrane of the cell by interfering with the transmembrane electron transfer. Furthermore, heavy metal ions could incidentally perform as transporters of many antimicrobial substances (Hussein et al. 2014).

8.4.3 Non-oxidative Mechanisms

The pioneer study of Leung et al. (2014) revealed that antibacterial machineries of NPs are unconnected to the membrane lipid peroxidation followed by oxidative stress, based on the many observations, chiefly:

1. In the absence of intact cell membrane of microbes and surface pores are distinctly visible, metal oxide (MgO) NPs that are not detected in the cell. Moreover, the lack of presence of unwarranted Mg ions was invisible in energy-dependent X-ray spectroscopy studies, thus proving the inhibitory effect of metal oxides to disrupt the cell membrane.
2. The phosphatidylethanolamine (PE) and lipopolysaccharide (LPS) of the cell wall were unchanged due to MgO NP treatment, indicating that MgO failed to stimulate lipid peroxidation. Furthermore, the quantity of ROS-aggravated proteins in the cell remained constant.

However, many perilous cellular metabolic developments related to proteins, including amino acid metabolism, energy metabolism, carbohydrate metabolism, as well as nucleotide metabolism, are significantly abridged (Leung et al. 2014). This paved a way for biologists to think about alternative non-oxidative mechanisms causing microbial cell death by the NPs treatment. Some of such proposed mechanisms are described below.

The Interaction of the Cell Barriers

Cell walls and membranes are the physical and biological barriers to self-defense from the external environment, particularly providing a natural shape to organisms. The components of the cell membrane (for Gram-positive and Gram-negative bacteria are different) result in dissimilar adsorption pathways for NPs (Lesniak et al. 2013). LPS categorizes the structural uniqueness of the cell walls of Gram-negative bacteria which have a negatively charged constituency that appeals to NPs. In disparity, expression of teichoic acid in the Gram-positive bacteria's cell wall assists the NPs distribution beside the molecular phosphate chain opposing its aggregation (Sarwar et al. 2015). In one study, a nanocomposite of hydroxyapatite whisker and nano-zinc oxide (HAPw/n-ZnO) exhibited a durable antimicrobial effect on *Staphylococcus mutans*, *S. aureus*, and *Candida albicans* than to that on *E. coli* which is causing bacterial death as a dependent factor of components and structure, cell membrane, and NP interaction. Moreover, some elements specific to Gram-negative species, like LPS, can inhibit the linkage of ZnO NPs to the cell and may even normalize the stream of ions in and out of the membrane. However, the depth of the microbial cell wall in Gram-negative bacteria often hinders the antibacterial function of NPs (Yu et al. 2014). In another study, Wehling et al. (2014) considered the antibacterial activity of nano-diamonds in countless bacterial

surface structures with varied reactive groups by establishing covalent bonds with adjacent proteins and molecules on cell walls.

Inhibition of Bacterial Proteins as well as DNA Synthesis

The intervention of NPs with bacterial protein synthesis machinery progressively fascinated the microbiologists in the near future. The effect of CuO NPs on denitrification of bacterial enzymes was analyzed by Su et al. (2015) which could modify the manifestation of key proteins. When these NPs enter the cell, it resulted in the regulation of proteins tangled in electron transfer, nitrogen metabolism, or substance transport. Similarly, TiO_2 NPs enhance bacterial DNA degeneration, compression, and fragmentation resulting in the reduced physiological activities of the microbial genes (Zhukova 2015). Moreover the molecular docking studies betweenTiO_2 NPs have predicted the potential NPs to inhibit GC-rich regions of bacterial DNA (Iram et al. 2015). In addition, it may even lead to bacterial cell apoptosis, which is proved in *E. coli* model (Su et al. 2015). The study even revealed that around ten mutant genes are responsible for the gene expression and the molecular structure and functions, leading to ribosomal composition and RNA modification and protein expression. Furthermore, the gold-superparamagnetic iron oxide NPs inhibit some proteins in bacteria over a solid affinity formed by disulfide bonds affecting the metabolism and redox systems of the cells (Niemirowicz et al. 2014).

NPs Regulate the Expression of Metabolic Genes

Bacterial metabolic pathways are not secluded but reasonably are joined with the complex activity of living cells. For illustration, the metabolism of glucose in *S. mutans* is a significant mechanism that bases, various metabolic genes. Moreover, *Fusobacterium nucleatum* could use the amino acid metabolites, like butyric acid, which could enhance the advancement of periodontal disease. Thus, decisive variations in the metabolic rate of bacteria are used to control bacterial cell pathology by diverse mechanisms (Padmavathy and Vijayaraghavan 2011; Yu et al. 2014). Liquid hue spectrum of magnesium oxide nanoparticles (MgO NPs) altered the metabolic protein expressions, by upregulating action of weak thiamine ester-binding proteins as well as riboflavin metabolic protein. The downregulation of the protein charted to a critical signaling of cell metabolism also added its mechanism resulting in a decrease in metabolic cellular activity, suggesting NP's regulation in the processes of bacteria on target proteins (Leung et al. 2014). However, copper oxide NPs (CuO NPs) downregulated the protein expression of nitrate and nitrite reductases causing bacterial death (Su et al. 2015). Moreover, considerable evidences are there which proves the adhesive efficiency of titanium dioxide to the bacterial biofilms (Rogusha 2015) and disrupt its metabolite levels (Pan et al. 2015). For instance, d-alanine metabolism is indispensable for the formation and growth of *S. mutans* biofilm.

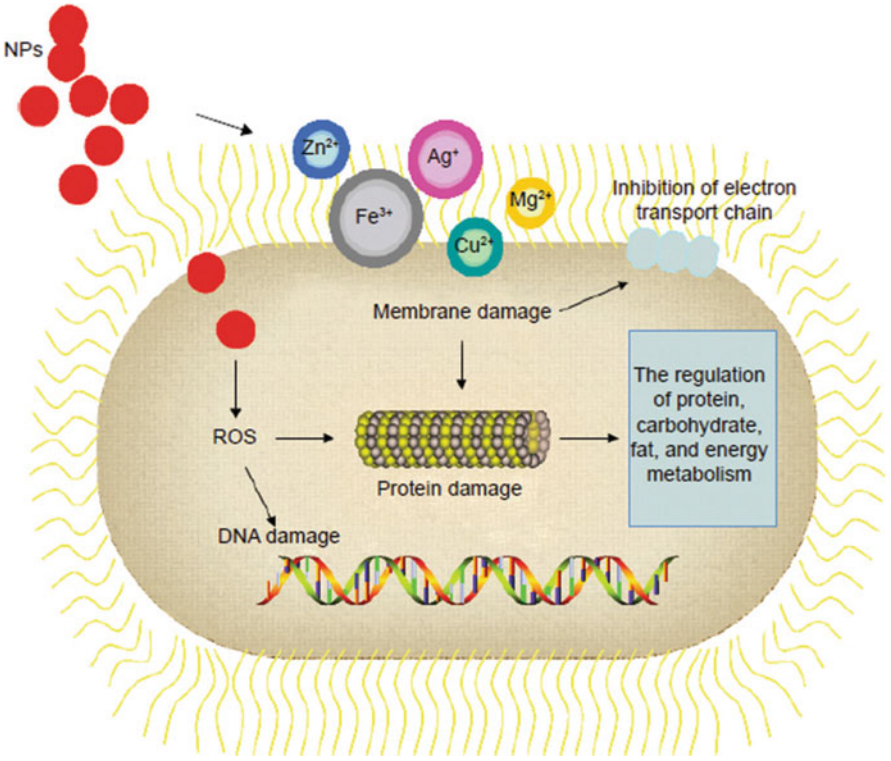

Fig. 8.4 Mechanisms of NP action in bacteria cells. **Notes:** NPs can attack bacteria cell through multiple mechanisms: the formation of ROS leading to membrane, protein, and DNA damage; direct interaction occurs with cell membrane because some metal-based NPs can generate metal ion via dissolving, for example, inhibition of electron transport chain; and the regulation of bacterial metabolic processes. **Abbreviations:** NPs, nanoparticles; ROS, reactive oxygen species. (Wang et al. 2017; open access)

Thus, NPs can attack through multiple mechanisms on bacteria cells, a diagrammatic representation of which is provided in Fig. 8.4.

8.5 Different Metal Oxides Exhibiting Antimicrobial Action

8.5.1 TiO_2 Metal Oxides

The photocatalytic disinfection has gained great research attraction in the last century. It was first reported with the NPs of TiO_2 by UV procedure which successfully inactivated many microorganisms, like bacteria and fungi such as *Micrococcus luteus*, *Escherichia coli*, *Bacillus subtilis (cells and spores)*,

Streptococcus faecalis (Melian et al. 2000), *Staphylococcus aureus* (Kuhn et al. 2003), *Candida albicans* (Kuhn et al. 2003), *Lactobacillus acidophilus* (Saito et al. 1992), and others. Moreover, the activation of TiO_2 with UV was found to be effective against parasites such as *Giardia intestinalis and Acanthamoeba castellanii* cysts (Sokemen et al. 2008).

The crystal structure, shape, and size of TiO_2 are connected with the antimicrobial activity (Haghighi et al. 2013). Sometimes, this may be due to the oxidative stress exerted by TiO_2 nanoparticles (anatase forms), causing specific DNA damage (Cioffi and Rai 2012; Roy et al. (2010) with dissimilar antibiotics assessed the antimicrobial effect of TiO_2 nanoparticles against methicillin-resistant *Staphylococcus aureus* (MRSA). They reported that TiO_2 NPs improved the antimicrobial effect of aminoglycosides, beta-lactams, glycopeptides, cephalosporins, lincosamides, macrolides, and tetracycline against MRSA.

TiO_2 nanoparticles possess photocatalytic properties which enhance the efficiency of them to eradicate the bacteria. Carré et al. (2014) measured the photocatalytic antibacterial activity that was accompanied by lipid peroxidation that grounds for membrane fluidity and cell integrity (Carre et al. 2014). However, doping them with metal oxide ions improves the antibacterial and photocatalytic properties of TiO_2 nanoparticles (Allahverdiyev et al. 2011; Zaleska 2008) by shifting TiO_2 NPs' light absorption to visible range so that UV light irradiation can be avoided. Conjugation of nontoxic polymers with TiO_2 nanoparticles is an alternative method to tackle toxicity issues. For instance, *Aeromonas hydrophila*-mediated TiO_2 were synthesized by Jayaseelan et al. (2013) which showed better zone of inhibition when compared to that of tetracycline treatment (Fig. 8.5 and Table 8.2).

8.5.2 ZnO Metal Oxides

ZnO nanoparticles projected many bactericidal effects on Gram-positive and Gram-negative bacterial strains which are at times even resistant to high temperature and pressure (Azam et al. 2012). The improved antibacterial activity of ZnO nanoparticles was attained due to the improved surface area (Xie et al. 2011), varying particle sizes (Padmavathy and Vijayaraghavan 2011), as well as interruption of transmembrane electron transportation. Moreover, studies have suggested that the antibacterial mechanism of ZnO nanoparticles in *C. jejuni* might be a result of the cell membrane disruption and ROS stress (Xie et al. 2011). The outcomes indicated that ZnO nanoparticles triggered considerable membrane leakage, morphological alterations, and upregulation (up to 52-fold) in oxidative stress-related gene expression in *C. jejuni.* In addition, the antimicrobial activity of the ZnO nanoglobules prepared using 0.05 M TWEEN80 was demonstrated by Rajendar et al. in 2017 (Fig. 8.6) which showed considerable antibacterial effects on four major microorganisms.

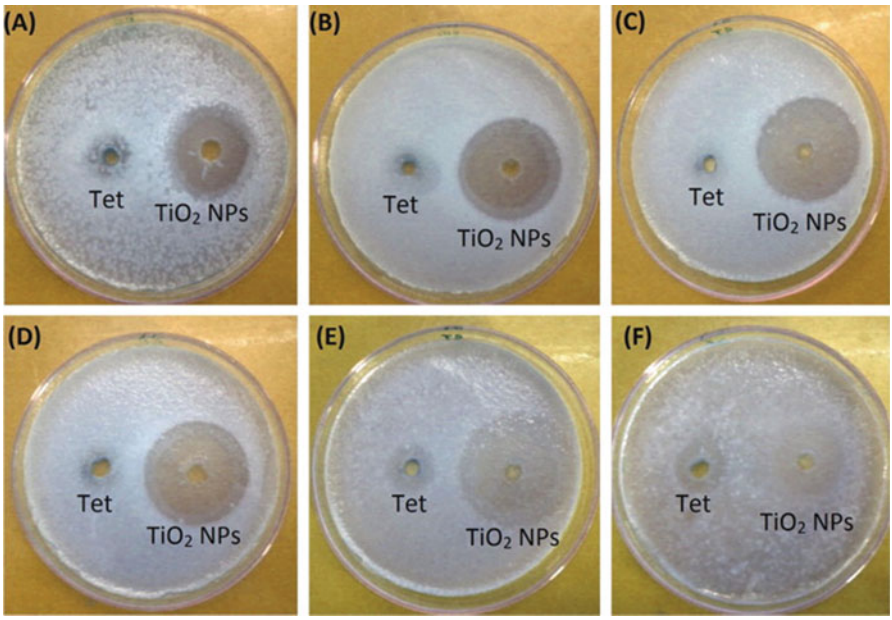

Fig. 8.5 Well diffusion assay for TiO_2 nanoparticles against *A. hydrophila* (**a**), *E. coli* (**b**), *P. aeruginosa* (**c**), *S. aureus* (**d**), *S. pyogenes* (**e**), and *E. faecalis* (**f**). (Jayaseelan et al. 2013; copyright received)

Table 8.2 Zone of inhibition (mm) and MIC (lg ml^1) of *A. hydrophila*-synthesized TiO_2 nanoparticles against various microorganisms (Jayaseelan et al. 2013; copyright received)

	A. hydrophila-synthesized TiO_2 nanoparticles		Tetracycline	
Microorganisms	Zone of inhibition (mm)	MIC (lg ml^1)	Zone of inhibition (mm)	MIC (lg ml^1)
A. hydrophila	23	25	14	20
E. coli	26	20	14	20
P. aeruginosa	25	30	12	25
S. pyogenes	31	10	15	15
S. aureus	33	10	15	10
E. faecalis	29	15	16	15

Even though ZnO moderates the viability of many human pathogenic bacteria, the precise machinery is not established till date. One such possibility was the cohort of hydrogen peroxide which act for ROS insult and thus antibacterial activity. The electrostatic force attraction between the metal oxides and the cell membrane could also be a reason (Zhang et al. 2008). Besides these two, other factors like membrane dysfunction due to nanoparticles internalization through zinc ion release also add to

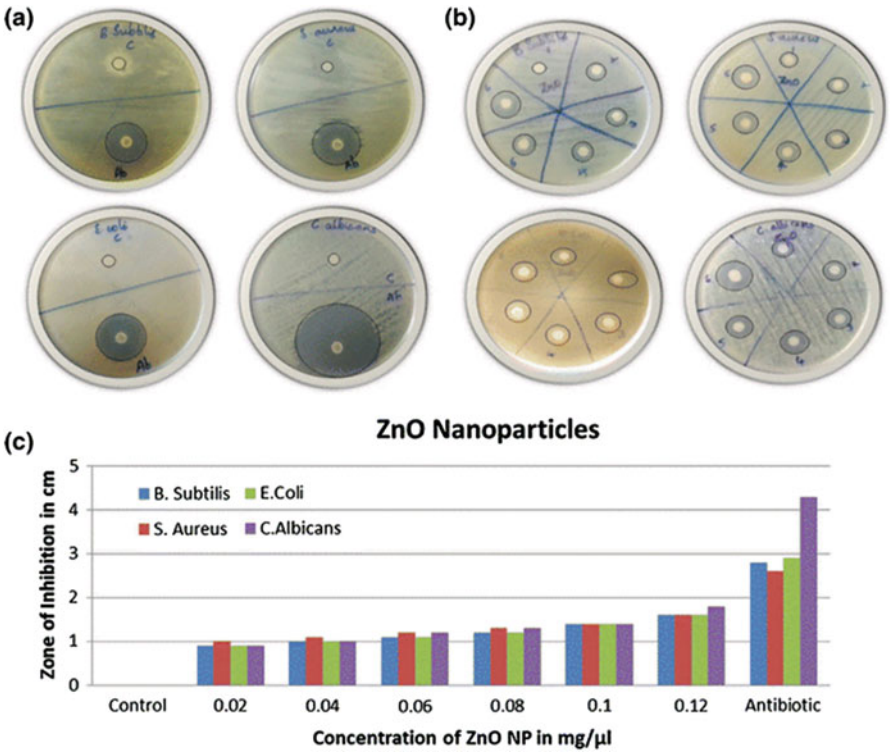

Fig. 8.6 Antimicrobial activity of the ZnO nanoglobules prepared using 0.05 M TWEEN80. (**a**) Positive and negative control for measuring the zone of inhibition, (**b**) antimicrobial activity of ZnO nanoglobules at various concentrations, (**c**) diameter of the zone of inhibition for different concentrations of ZnO nanoglobules. (Rajendar et al. 2017; copyright received)

a probable explanation of the cell damage (Rao et al. 2013). Moreover, the antibacterial activity of ZnO nanoparticles is contingent on the concentration and surface area. The metal oxide NPs in its higher concentrations and larger surface area demonstrated superior antibacterial action (Buzea et al. 2007). According to Hosseinkhani et al., as a result of particle size reduction, a considerable decrease in the bacteria number was observed against *Shigella dysenteriae* (Hosseinkhani et al. 2011). Emami-Karvani and Chehrazi (2011) evaluated that higher concentration and lesser particle size enhanced the antibacterial activity of ZnO nanoparticles.

8.5.3 Ag_2O Metal Oxides

Nowadays, Ag2O nanoparticles have been considered as an innovative substitute to the marketed antibiotics (Sathyanarayanan et al. 2013). Sondi and Salopek-Sondi

(2004) demonstrated that when *E. coli* was exposed to Ag2O NPs, genetic replication ability was lost and the cell cycle stopped at the G2/M phase. Further ROS insult occurred, followed by apoptosis. Furthermore, Ag had reported to be less toxic than many other disinfectants. In 2016, Qin et al. proved that the photocatalytic activity and stability gets enhanced when the rich Ag++ ion of Ag_3PO_4 formulates the surface plasmon resonance (SPR) of Ag NPs. Marambio-Jones and Hoek (2010) had reviewed the antibacterial machineries of the Ag NPs and its potential insinuations for the environment. Similarly, the antimicrobial activity of Ag NPs synthesized from *Linum usitatissimum L.* whole plant extract (WPE) and thidiazuron-induced callus extract (CE) is tested against many pathogenic microorganisms, which is depicted in Fig. 8.7 (Anjum and Abbasi 2016). Moreover, the supplementary investigation could be achieved to develop Ag-related compounds, composites, and metal co-dopants with maximum antimicrobial effect and minimum toxicity.

8.5.4 CuO Metal Oxides

The CuO nanoparticles were tested against various microbes like *Klebsiella pneumoniae*, *Salmonella paratyphi*, *P. aeruginosa*, and *Shigella* strains for its antibacterial activity (Mahapatra et al. 2008). As per their investigations, these nanoparticles specified appropriate antibacterial activity against all the selected microbes which were achieved through the microbial cell membrane passage by decomposing the vital bacterial enzymes which were crucial for triggering cell death. Moreover, a recent study by Pulicherla et al. (2017) reported that the bioinspired green synthesis of CuO NPs from the stem bark extract of *S. alternifolium* has potent antimicrobial effects (Figs. 8.8 and 8.9).

The size-dependent antibacterial activity of CuO nanoparticles was done by Azam et al. (2012). Their study with *S. aureus* and *B. subtilis*, *Pseudomonas aeruginosa*, and *E. coli* projected the bactericidal activity of CuO NPs influenced by their stability, size, as well as the concentration of the metal nanoparticles, which restricted the growth via transistors over nanometric pores on the bacterial cellular membranes. However, Ahamed et al.'s (2014) studies revealed that CuO nanoparticles (23 nm) had substantial antimicrobial activity in bacterial strains like *E. coli*, *K. pneumoniae*, *P. aeruginosa*, *Shigella flexneri*, *Enterococcus faecalis*, *S. typhimurium*, *S. aureus*, and *Proteus vulgaris*. But the nanoformulations were much more resistant to *K. pneumoniae*, while *E. coli* and *E. faecalis* disclosed the maximum sensitivity (Ahamed et al. 2014).

8.5.5 MgO Metal Oxides

Several scientists have proved the strong antimicrobial action of MgO nanoparticles through either cell membrane damage or oxidative stress (Jin and He 2011). Hewitt

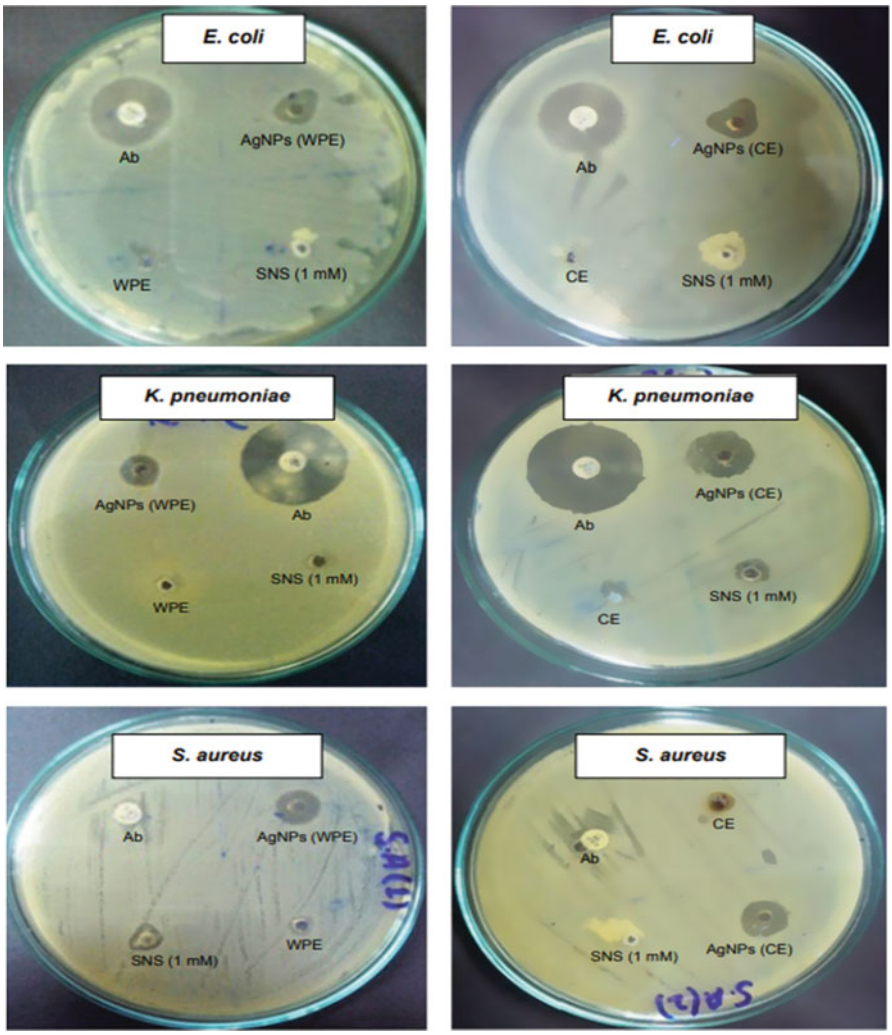

Fig. 8.7 Antibacterial assay of Ag NPs. Notes: zone of inhibition of WPE (10 mg mL-1), CE (10 mg mL-1), Ab (10 mg disk-1), WPE-mediated Ag NPs (10 mg mL-1), and CE-mediated Ag NPs (10 mg mL-1) against multiple drug-resistant bacterial strains was measured in mm. Abbreviations: Ag NPs, silver nanoparticles; WPE, whole plant extract; CE, callus extract; Ab, antibiotic; *E. coli*, *Escherichia coli*; *K. pneumoniae*, *Klebsiella pneumoniae*; *S. aureus*, *Staphylococcus aureus*; SNS, silver nitrate solution. (Anjum and Abbasi 2016; open access)

et al. (2001) stated that MgO introduced the changes in sensitivity against *E. coli* encouraged by active oxygen. However, Leung et al. declared the mechanism of MgO antimicrobial activity due to the damage of cell membranes (Leung et al. 2014). In recent studies, the MgO nanoparticles presented the bactericidal activity in contradicting both Gram-positive and Gram-negative bacteria (Vidic et al. 2013).

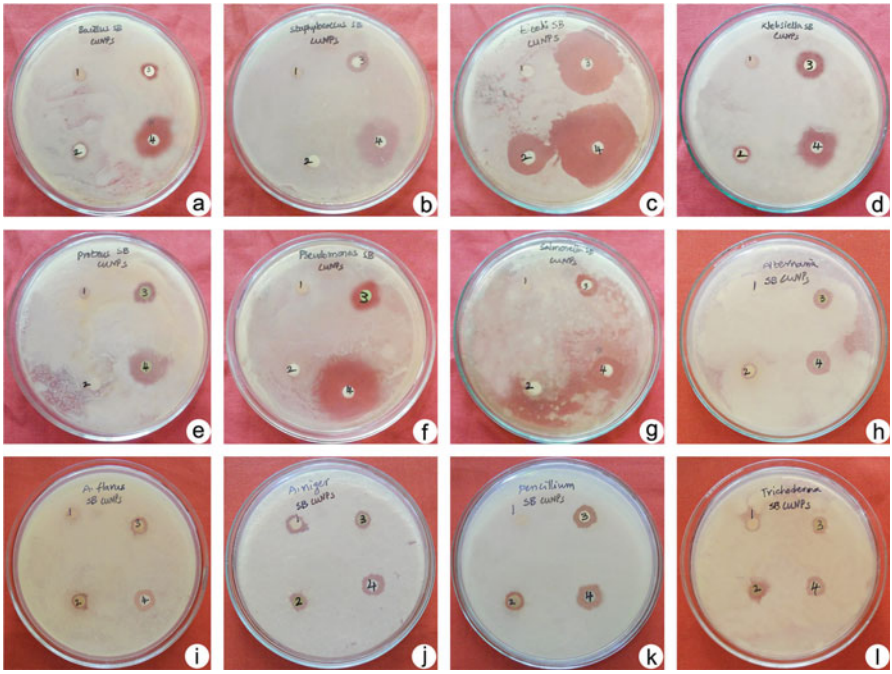

Fig. 8.8 Antimicrobial activity of synthesized CuO NPs. (**a**) *B. subtilis*, (**b**) *S. aureus*, (**c**) *E. coli*, (**d**) *K. pneumoniae*, (**e**) *P. vulgaris*, (**f**) *P. aeruginosa*, (**g**) *S. typhimurium*, (**h**) *A. solani*, (**i**) *A. flavus*, (**j**) *A. niger*, (**k**) *P. chrysogenum*, (**l**) *T. harzianum*; (1) plant extract, (2) CuSO4_5H2O, (3) CuO NPs, (4) streptomycin/fluconazole. (Pulicherla et al. 2017; Open access)

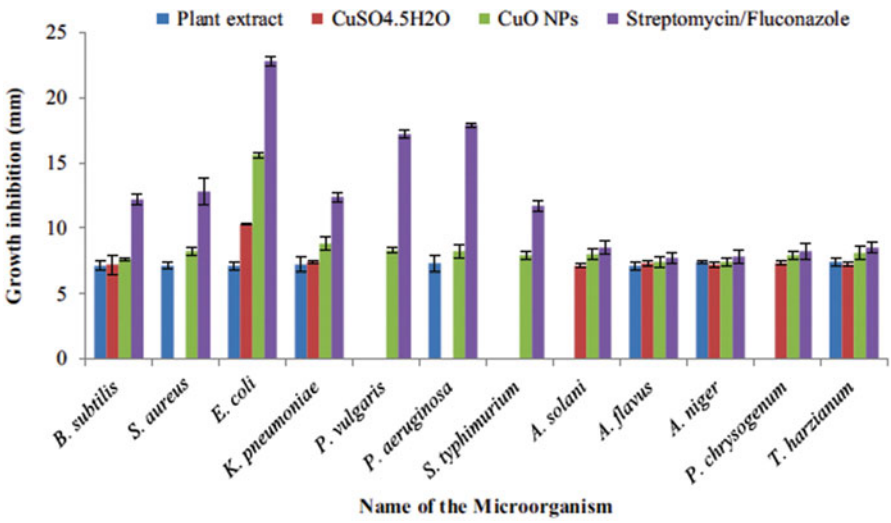

Fig. 8.9 Antimicrobial activity of bioinspired green synthesis of CuO NPs from stem bark extract of *Syzygium alternifolium (Wt.)* against various pathogens. (Pulicherla et al. 2017; Open access)

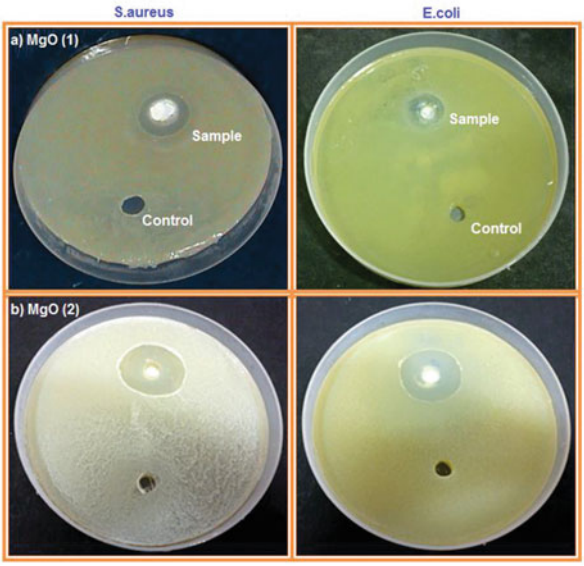

Fig. 8.10 Antibacterial studies of MgO (1) and MgO (2) nanoparticles. (From http://shodhganga.inflibnet.ac.in/bitstream/10603/56541/15/15_chapter%209.pdf; open access)

Sawai et al. (2000) examined the antibacterial activity of MgO against *E. coli or S. aureus.* They recommended that the manifestation of active oxygen, like superoxides, on the MgO NPs' surface as the primary aspect that marks the antibacterial activity (Fig. 8.10).

8.5.6 Cerium Oxide Nanoparticles (CeO_2 NPs)

The cerium oxide (CeO_2) is a nonstoichiometric compound having three and four oxidation states (Ce4+, Ce3+). Many reports in the literature state that the concentration of Ce3+ proliferations is more as compared to Ce4+ as the size of the particles decreases, the bioactivity also increases up to 6 nm of zone of inhibition. The oxidation states of these two CeO_2 NPs develop many oxygen vacancies which accompanies the Ce4+ form to Ce3+ reduction resulting in the oxygen molecule loss. These CeO_2 nanoparticles have a moral antimicrobial activity, as they can act as scavenger radicals and ROS production to eliminate bacteria (Dos Santos et al. 2014).

8.5.7 Yttrium Oxide Nanoparticles (Y_2O_3 NPs)

Yttrium oxide (Y2O3) has a cubic structural composition having the highest free energy value which is unconstrained from the oxide form, from the elemental form

(Kosfstad 1972) due to excessive oxidative stress (Atou et al. 1990) and its structure, size variations are able to cause death induced by stress in a way that seems to be dependent. The antibacterial behavior of synthesized Y2O3 NPs using *Acalypha indica* leaves extract was also demonstrated (Becker et al. 2002).

8.5.8 *Aluminum Oxide (Al_2O_3)*

Alumina forms temperature-resistant, stable NPs, having a hexagonal structure, containing oxygen and Al3+ ions filling around 60% of total octahedral sites of the structural network (Ganguly and Poole 2003). Alumina NPs possess an antioxidant activity and wedge the release of ROS, ramblingly by stalling apoptosis, before finalizing cellular death (Sadiq et al. 2009). The antibacterial activities of Al_2O_3 NPs against *E. coli*, *Proteus vulgaris*, *Staphylococcus aureus*, and *Streptococcus mutans* are demonstrated in Fig. 8.11 and Table 8.3.

Moreover, in a report of 2009, the authors stated that the pathogen inhibition of *E. coli* by alumina NPs in 10–1000 g/ml range acts as antimicrobials by paying the ROS generation, by disrupting bacterial cell wall. Moreover, Al2O3 NPs' radical scavenging possessions block ROS generation leding to bacterial death (Sadiq et al. 2009).

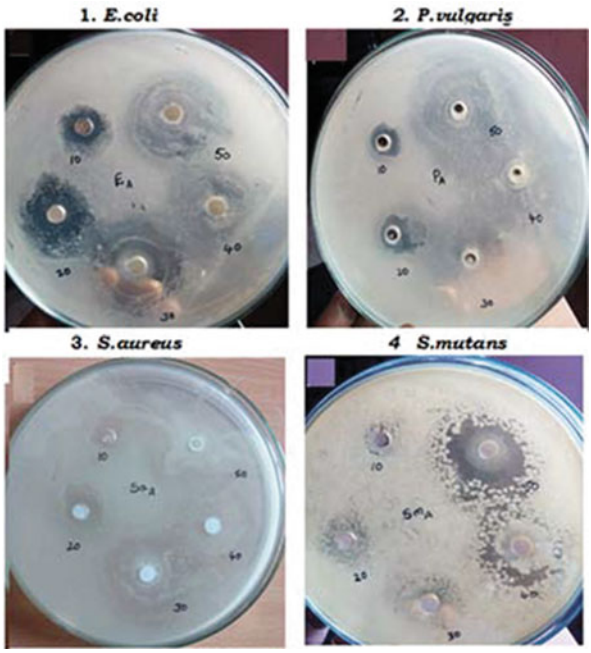

Fig. 8.11 Antibacterial activities of aluminum oxide nanoparticles against bacteria using the agar well diffusion method; the fig. showed (**1**) *E. coli*, (**2**) *Proteus vulgaris*, (**3**) *Staphylococcus aureus*, (**4**) *Streptococcus mutans.* (Manyasree et al. 2018; open access)

Table 8.3 Inhibition zones at different concentrations against two Gram-positive and two Gram-negative organisms (Manyasree et al. 2018; open access)

	Mean zones of inhibition [mm] ± SD [$n = 2$]				
Name of the organism	10 mg/ml	20 mg/ml	30 mg/ml	40 mg/ml	50 mg/ml
Escherichia coli	9 ± 0.20	18 ± 0.25	27 ± 0.25	31 ± 0.10	39 ± 0.35
Proteus vulgaris	5 ± 0.30	10 ± 0.40	15 ± 0.45	20 ± 0.20	26 ± 0.45
Staphylococcus aureus	6 ± 0.15	12 ± 0.10	18 ± 0.35	23 ± 0.25	29 ± 0.40
Streptococcus mutans	8 ± 0.35	14 ± 0.35	19 ± 0.30	25 ± 0.10	30 ± 0.30

8.5.9 CaO and CacO3 Nanoparticles

Under alkaline conditions, the CaO NPs confirmed a sturdy antimicrobial activity due to ROS by the NPs' hydration with water. The CaO NPs presented antimicrobial activity against both Gram-negative and Gram-positive bacteria like *E. coli* and *S. aureus* causing damage to cell membrane and leading to intracellular content leakage and cell death (Sawai 2003). Moreover, Jeong et al. (2007) inspected the antimicrobial efficacy of CaCO3 NPs. As per their results, CaCO3 often gets converted to CaO owing to temperature rise. The produced CaO nanoparticles designated a durable bactericidal activity against *E. coli*, *S. aureus*, *S. typhimurium*, and *B. subtilis* (Zhou et al. 2015).

8.5.10 Bimetallic Oxide Nanoparticles

Bimetallic oxides containing twofold active metal oxide NPs (Fe, Mg, Ni, Ag and Zn) have gathered special attention in the modern era owing to its extraordinary activity against Gram-negative and Gram-positive bacteria. For instance, Zn-MgO NPs are a unique bimetallic oxide NPs that displayed antimicrobial activity in *E. coli* and *B. subtilis* microbes. Moreover, Fe-Ag NPs had high antimicrobial activity against *E. coli*. The mechanics behind for both were explained as the ROS insult and cell wall damage. Thus, the combination therapy has enhanced the antimicrobial activity (Niemirowicz et al. 2014).

The formulation of metal ion-doped NPs could improve antimicrobial properties of metal NPs synthesized by the Ti-doped ZnO powders which resulted in an enhanced antibacterial accomplishment against *S. aureus* as well as *E. coli*. related to the particle size decrease and crystallinity. The antibacterial activity of CaCO3/MgO nanocomposites allowed superior antibacterial action against *S. aureus* than *E. coli* (Yamamoto et al. 2010). In addition, V_2O_5 when coupled with ZnO, these nanocomposites enhanced its photocatalytic activity (Saravanan et al. 2014). Moreover, Vidic et al. (2013) reported antimicrobial activity of co-doped nanostructure of ZnO-MgO against the same microbes suggesting a safe novel therapeutics for bacterial infections. Many results designated that MgO and CaO NPs blended with

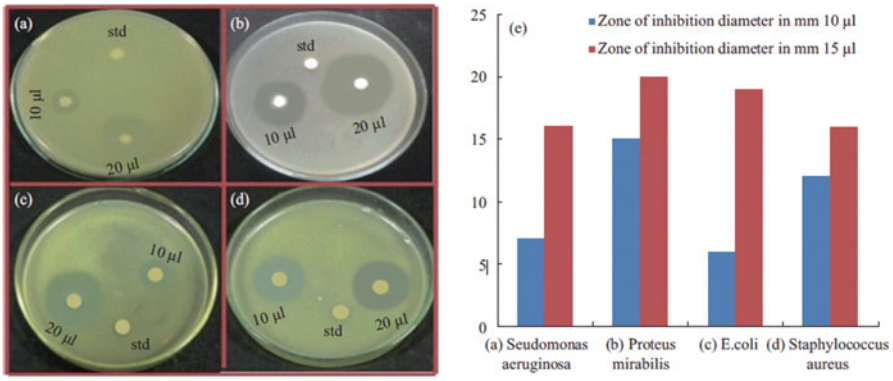

Fig. 8.12 (Color online) The photographic image of an inhibition zone produced by ZnO-CuO nanocomposite (3: 1 M) for (**a**) *Pseudomonas aeruginosa*, (**b**) *Proteus mirabilis*, (**c**) *E.coli*, and (**d**) *Staphylococcus aureus*. (**e**) Bar graph representing the size of the zone of inhibition formed around each disc, loaded with test samples, indicating the antibacterial activity toward the same for ZnO-CuO nanocomposite 3:1 M. (Saravanakkumar et al. 2018; open access)

supplementary disinfectants illustrated exceptional antibacterial effect (Leung et al. 2014). In addition, the ZnO-CuO nanocomposite (3: 1 M) formed zone of inhibition around each disc with loads test samples (Fig. 8.12). However, the presence of a third metal in bimetallic nanocomposite can also enhance the catalytic action. For instance, Mn^{2+} ion was able to increase photocatalysis of Mn-ZnS composite (Joicy et al. 2014).

8.6 Limitations and Future Prospects

The recombination between photo-generated electrons and holes in a photocatalyst is crucial for a successful reaction, as the lifetime of the charge separation decides the photocatalytic action. Consequently, a huge quantity of revisions is linked to the regulation of band structure and the charge separation. On the other hand, diminutive evidence regarding the adsorbed species and the intermediates in photocatalytic reactions is obtainable. Photocatalytic reactions may occur on the photocatalyst's surface or in the ordinary catalysts. The difference between the both is the driving force to stimulate the adsorbed reactants being photo-energy and thermal energy, respectively. Therefore, the kinetic clarification of surface structure, surface species, and surface property during the photoreaction is obligatory to comprehend the photocatalysis. Commonly a catalytic reaction contains many elementary steps like absorption of light in a photocatalytic reaction. Hence, there is identification of thermodynamic constraint in the photocatalysis than with the ordinary process. However, further clarification of the reaction mechanism is needed to get beneficial information on the additional development of the photocatalysis and novel insight on photocatalytic chemistry.

Many of the factors add to the future prospects of the photocatalysts. Countless NPs stabilize at least any one of the common resistance mechanisms. These possessions are due to specific physicochemical properties and bactericidal means of NPs (Chen et al. 2014). The uniquely small size helps NPs to interact with cells due to a larger surface area-to-mass ratio with the handy and manageable application, in disparity to traditional antibiotics. Besides the interruption of bacterial membranes, difficulty of biofilm formation is another significant mechanism, as they portray a major measure in the progress of bacterial resistance (Peulen and Wilkinson 2011). The distinctive structure and arrangement of bacterial biofilms deliver protection to the implanted microorganisms, assisting them to escape from most antibiotics. Moreover, bacterial biofilms act for regular resistance mutations and the interchange or variation of mutations among diverse bacterial cells (Khameneh et al. 2016). Studies have discovered that countless NPs can overcome biofilm formation, comprising Au-based NPs (Yu et al. 2016), NPs, CuO NPs (Miao et al. 2016), Ag-based NPs (Markowska et al. 2013), Mg-based NPs (Lellouche et al. 2012), NO NPs (Hetrick et al. 2009; Slomberg et al. 2013), and YF NPs (Lellouche et al. 2012). The best prevention of biofilms is attained by a lesser size and larger surface area-to-mass ratio, as well as the shape of NPs with an extraordinary outcome on biofilm obliteration (e.g., NPs with rodlike shape are more operative than NPs with spherical shape).

8.7 Conclusion

The usage of metal oxide NPs pooled with visible light irradiation unlocks innovative opportunities for surface decontamination. As described, it is promising to encompass the absorption constituency of the NPs to the red/NIR by doping with the transition metal ions or organic molecules. In cases where NPs might be toxic, it is promising to coat them with a massive selection of surfaces. This property is thus exploited as a solicitation by encountering many pathogenic microbes.

References

Actis L, Srinivasan A, Lopez-Ribot JL, Ramasubramanian AK, Ong JL (2015) Effect of silver nanoparticle geometry on methicillin susceptible and resistant Staphylococcus aureus, and osteoblast viability. J Mater Sci 26(7):210–215. https://doi.org/10.1007/s10856-015-5538-8

Ahamed M, Alhadlaq HA, Khan M, Karuppiah P, Aldhabi NA (2014) Synthesis, characterization and antimicrobial activity of copper oxide nanoparticles. J Nanomater 2014:1–4. https://doi.org/10.1155/2014/637858

Allahverdiyev AM, Abamor ES, Bagirova M, Ra-failovich M (2011) Antimicrobial effects of $TiO_{(2)}$ and $Ag_{(2)}O$ nanoparticles against drug-resistant bacteria and leishmania parasites. Future Microbiol 6:933–940. https://doi.org/10.2217/fmb.11.78

Andrade F, Rafael D, Videira M, Ferreira D, Sosnik A, Sarmento B (2013) Nanotechnology and pulmonary delivery to overcome resistance in infectious diseases. Adv Drug Deliv Rev 65(13–14):1816–1827. https://doi.org/10.1016/j.addr.2013.07.020

Anjum S, Abbasi BHD (2016) Thidiazuron-enhanced biosynthesis and antimicrobial efficacy of silver nanoparticles via improving phytochemical reducing potential in callus culture of *Linum usitatissimum* L. Int J Nanomed 11:715–728. https://doi.org/10.2147/IJN.S102359

Arakha M, Sweta P, Devyani S, Tapan KP, Bairagi CM, Krishna P, Bibekanand M, Suman J (2015) Antimicrobial activity of iron oxide nanoparticle upon modulation of nanoparticle-bacteria interface. Sci Rep 5:14813. https://doi.org/10.1038/srep14813

Armentano I, Arciola CR, Fortunati E, Davide F, Samantha M, Concetta FA, Jessica R, Jose MK, Marcello I, Livia V (2014) The interaction of bacteria with engineered nanostructured polymeric materials: a review. Sci World J 2014:410423. https://doi.org/10.1155/2014/410423

Asahi R, Morikawa T, Ohwaki T, Aoki K, Taga Y (2001) Visible-light photocatalysis in nitrogen-doped titanium oxides. Science 293:269–271. https://doi.org/10.1126/science.1061051

Atou T, Kusaba K, Fukuoka K, Kikuchi M, Syon YJ (1990) Shock-induced phase transition of M_2O_3 (M = Sc, Y, Sm, Gd, and In)-type compounds. Sol State Chem 89:378–384. https://doi.org/10.1016/0022-4596(90)90280-B

Azam A, Ahmed AS, Oves M, Khan M, Memic A (2012) Size-dependent antimicrobial properties of CuO nanoparticles against gram-positive and-negative bacterial strains. Int J Nanomed 7:3527. https://doi.org/10.2147/IJN.S29020

Becker S, Soukup J, Gallagher J (2002) Differential particulate air pollution induced oxidant stress in human granulocytes, monocytes and alveolar macrophages. Toxicol in Vitro 16:209–218. https://doi.org/10.1016/S0887-2333(02)00015-2

Buzea II, Pacheco K, Robbie K (2007) Nanomaterials and nanoparticles: sources and toxicity. Biointerphases 2:MR17–MR71. https://doi.org/10.1116/1.2815690

Carré G, Hamon E, Ennahar S, Estner M, Lett MC, Horvatovich P, Gies JP, Keller V, Keller N, Andre P (2014) TiO_2 photocatalysis damages lipids and proteins in Escherichia coli. Appl Environ Microbiol 80:2573–2581. https://doi.org/10.1128/AEM.03995-13

Cha SH, Hong J, McGuffie M, Yeom B, VanEpps JS, Kotov NA (2015) Shape-dependent biomimetic inhibition of enzyme by nanoparticles and their antibacterial activity. ACS Nano 9(9):9097–9105. https://doi.org/10.1021/acsnano.5b03247

Chen CW, Hsu CY, Lai SM, Syu WJ, Wang TY, Lai PS (2014) Metal nano bullets for multidrug resistant bacteria and biofilms. Adv Drug Deliv Rev 78:88–104. https://doi.org/10.1016/j.addr.2014.08.004

Choa YH, Yang JK, Kim BH, Jeong YK, Lee JS, Nakayama T, Sekino T, Niihara K (2003) Preparation and characterization of metal: ceramic nanoporous nanocomposite powders. J Magn Magn Mater 266(1–2):12–19. https://doi.org/10.1016/S0304-8853(03)00450-5

Choi WY, Termin A, Hoffmann MR (1994) The role of metal-ion dopants in quantum-sized Tio_2—correlation between photoreactivity and charge-carrier recombination dynamics. J Phys Chem 98(13):669–679. https://doi.org/10.1021/j100102a038

Cioffi N, Rai M (2012) Nano-antimicrobials. In: Cioffi N, Rai M (eds) Synthesis and characterization of novel nano antimicrobials. Springer, Berlin/Heidelberg. https://link.springer.com/content/pdf/bfm%3A978-3-642-24428-5%2F1%2F1.pdf

Dos Santos CC, Farias IAP, Albuquerque AJR, Silva PM, One GMC, Sampaio FC (2014) Antimicrobial activity of Nano cerium oxide (IV) (CeO_2) against Streptococcus Mutans. BMC Proc 8(Suppl 4):48. https://doi.org/10.1186/1753-6561-8-S4-P48

Emami-Karvani ZP, Chehrazi P (2011) Antibacterial activity of ZnO nanoparticle on gram positive and gram-negative bacteria. Afr J Microbiol Res 5:1368–1373. https://doi.org/10.5897/AJMR10.159

Fang B, Jiang Y, Nusslein K, Rotello VM, Santore MM (2015) Antimicrobial surfaces containing cationic nanoparticles: how immobilized, clustered, and protruding cationic charge presentation affects killing activity and kinetics. Coll Surf B 125:255–263. https://doi.org/10.1016/j.colsurfb.2014.10.043

Fujishima A, Honda K (1972) Electrochemical photolysis of water at a semiconductor electrode. Nature 238:37–38. https://doi.org/10.1038/238037a0

Ganguly P, Poole WJA (2003) In situ measurement of reinforcement stress in an aluminum-alumina metal matrix composite under compressive loading. Mater Sci Eng 352:46–54. https://doi.org/10.1016/S0921-5093(02)00450-1

Gao W, Thamphiwatana S, Angsantikul P, Zhang L (2014) Nanoparticle approaches against bacterial infections. Wires Nanomed Nanobi 6(6):532–547. https://doi.org/10.1002/wnan.1282. Epub 2014 Jul 15

Gleiter H (1992) Materials with ultrafine microstructures: retrospectives and perspectives. Nanostr Mat 1(1):1–19. https://doi.org/10.1016/0965-9773(92)90045-Y

Gurunathan S, Han JW, Dayem AA, Eppakayala V, Kim JH (2012) Oxidative stress-mediated antibacterial activity of graphene oxide and reduced graphene oxide in *Pseudomonas aeruginosa*. Int J Nanomedicine 7:5901–5914. https://doi.org/10.2147/IJN.S37397. Epub 2012 Nov 30

Haghighi F, Roudbar MS, Mohammadi P, Hosseinkhani S, Shipour R (2013) Antifungal activity of TiO_2 nanoparticles and EDTA on *Candida albicans* biofilms. Infect Epidemiol Med 1:33–38. https://pdfs.semanticscholar.org/d816/127a0b7d75797b3497f3009f690985932dbc.pdf

He W, Kim HK, Wamer WG, Melka D, Callahan JH, Yin JJ (2014) Photogenerated charge carriers and reactive oxygen species in ZnO/Au hybrid nanostructures with enhanced photocatalytic and antibacterial activity. J Am Chem Soc 36(2):750–757. https://doi.org/10.1021/ja410800y

Hetrick EM, Shin JH, Paul HS, Schoenfisch MH (2009) Anti-biofilm efficacy of nitric oxide-releasing silica nanoparticles. Biomaterials 30(14):2782–2789. https://doi.org/10.1016/j.biomaterials.2009.01.052

Hewitt CJ, Bellara SR, Andreani A, Nebe-von-Caron G, McFarlane CM (2001) An evaluation of the anti-bacterial action of ceramic powder slurries using multiparameter flow cytometry. Biotechnol Lett 23:667–675. https://doi.org/10.1023/A:1010379714673

Ho W, Yu JC, Lee S (2006) Synthesis of hierarchical nanoporous F-doped TiO_2 spheres with visible light photo-catalytic activity. Chem Commun 10:1115–1117. https://doi.org/10.1039/b515513d

Hong X, Wen J, Xiong X, Hu Y (2016) Shape effect on the antibacterial activity of silver nanoparticles synthesized via a microwave-assisted method. Environ Sci Pollut Res Int 23(5):4489–4497. https://doi.org/10.1007/s11356-015-5668

Hosseinkhani P, Zand A, Imani S, Rezayi M, Rezaei Zarchi S (2011) Determining the antibacterial effect of ZnO nanoparticle against the pathogenic bacterium, Shigella dysenteriae (type 1). Int J Nano Dimens 1:279–285. https://doi.org/10.7508/IJND.2010.04.006

Hussein Al Ali SH, Zowalaty EL, Hussein ME, Geilich BM, Webster TJ (2014) Synthesis, characterization, and antimicrobial activity of an ampicillin-conjugated magnetic nanoantibiotic for medical applications. Int J Nanomedicine 9:3801–3814. https://doi.org/10.2147/IJN.S61143

Iram NE, Khan MS, Jolly R, Mohammad A, Mahboob A, ParvezA RHK, Farha F (2015) Interaction mode of polycarbazole-titanium dioxide nanocomposite with DNA: molecular docking simulation and in-vitro antimicrobial study. J Photochem Photobiol 153:20–32. https://doi.org/10.1016/j.jphotobiol.2015.09.001

Jayaseelan C, Abdul AR, Selvaraj MR, Arivarasan VK, Jayachandran V, Se-Kwon K, Moorthy ICS (2013) A Biological approach to synthesize TiO_2 nanoparticles using *Aeromonas hydrophila* and its antibacterial activity. Spectrochimica Acta A Mole Biomol Spectrosc 107:82–89. https://doi.org/10.1016/j.saa.2012.12.083

Jeong S, Park JS, Song SH, Jang SB (2007) Characterization of antibacterial nanoparticles from the scallop, Ptinopecten yessoensis. Biosci Biotechnol Biochem 71:2242–2247. https://doi.org/10.1271/bbb.70228

Jiang W, Mashayekhi H, Xing B (2009) Bacterial toxicity comparison between nano- and microscaled oxide particles. Environ Pollut 157:1619–1625. https://doi.org/10.1021/cr00033a004

Jin T, He Y (2011) Antibacterial activities of magnesium oxide (MgO) nanoparticles against foodborne pathogens. J Nanopart Res 13:6877–6885. https://doi.org/10.1007/s11051-011-0595-5

Joicy S, Saravanan R, Prabhu D, Ponpandian N, Thangadurai P (2014) Mn^{2+} ion influenced optical and photocatalytic behaviour of Mn–ZnS quantum dots prepared by a microwave assisted technique. RSC Adv 4:44592–44599. http://pubs.rsc.org/en/Content/ArticleLanding/2014/RA/c4ra08757g#!divAbstract

Khameneh B, Diab R, Ghazvini K, Fazly Bazzaz BS (2016) Breakthroughs in bacterial resistance mechanisms and the potential ways to combat them. Microb Pathog 95:32–42. https://doi.org/10.1016/j.micpath.2016.02.009

Khan MF, Ansari AH, Hameedullah M, Ahmad E, Husain FM, Zia Q, Baig U, Zaheer MR, Alam MM, Khan AM, AlOthman ZA, Ahmad I, Ashraf GM, Aliev G (2016) Sol-gel synthesis of thorn-like ZnO nanoparticles endorsing mechanical stirring effect and their antimicrobial activities: potential role as nano-antibiotics. Sci Rep 6:27689. https://doi.org/10.1038/srep27689

Kofstad P (1972) Nonstoichiometry, diffusion, and electrical conductivity in binary metal oxides. Wiley-Interscience, New York. https://doi.org/10.1002/maco.19740251027

Kuhn KP, Chaberny IF, Massholder K, Manfred S, Volker WB, Hans-Gunther S, Lothar E (2003) Disinfection of surfaces by photocatalytic oxidation with titanium dioxide and UV-A light. Chemosphere 53:71–77. https://doi.org/10.1016/S0045-6535(03)00362-X

Kumar A, Kumar A, Sharma G et al (2018) Biochar-templated g-C_3N_4/Bi2O2CO3/CoFe2O4 nano-assembly for visible and solar assisted photo-degradation of paraquat, nitrophenol reduction and CO2 conversion. Chem Eng J 339:393–410. https://doi.org/10.1016/j.cej.2018.01.105

Lellouche J, Friedman A, Gedanken A, Banin E (2012) Antibacterial and antibiofilm properties of yttrium fluoride nanoparticles. Int J Nanomedicine 7:5611–5624. https://doi.org/10.2147/IJN.S37075

Lesniak A, Salvati A, Santos-Martinez MJ, Radomski MW, Dawson KA, Åberg C (2013) Nanoparticle adhesion to the cell membrane and its effect on nano-particle uptake efficiency. J Am Chem Soc 135(4):1438–1444. https://doi.org/10.1021/ja309812z

Leung YH, Ng A, Xu X, Shen Z, Gethings LA, Wong MT, Chan C, Guo MY, Ng YH, Djurišić YB (2014) Mechanisms of antibacterial activity of MgO: non-ROS mediated toxicity of MgO nanoparticles towards Escherichia coli. Small 10:1171–1183. https://doi.org/10.1002/smll.201302434

Li Y, Zhang W, Niu J, Chen Y (2012) Mechanism of photogenerated reactive oxygen species and correlation with the antibacterial properties of engineered metal-oxide nanoparticles. ACS Nano 6(6):5164–5173. https://doi.org/10.1021/nn300934k

Lim EK, Chung BH, Chung SJ (2018) Recent advances in pH-sensitive polymeric nanoparticles for smart drug delivery in cancer therapy. Curr Drug Targets 19(4):300–317. https://doi.org/10.2174/1389450117666160602202339

Lin L, Lin W, Zhu YX, Zhao BY, Xie YC (2005) Phosphor-doped titania- a novel photocatalyst active in visible light. Chem Lett 34:284–285. https://doi.org/10.1246/cl.2005.284

Liu J-L, Zhang W-J, Li X-D, Yang N, Pan W-S, Kong J, Zhang J-S (2016) Sustained-release Genistein from nanostructured lipid carrier suppresses human lens epithelial cell growth. Int J Opthalmol 9(5):643–649. https://doi.org/10.18240/ijo.2016.05.01

Luan B, Huynh T, Zhou R (2016) Complete wetting of graphene by biological lipids. Nanoscale 8(10):5750–5754. https://doi.org/10.1039/C6NR00202A

Maeda H (2010) Tumor-selective delivery of macromolecular drugs via the EPR effect: background and future prospects. Bioconjug Chem 21(5):797–802. https://doi.org/10.1021/bc100070g

Mahapatra OM, Bhagat C, Gopalakrishnan KD, Arunachalam (2008) Ultrafine dispersed CuO nanoparticles and their antibacterial activity. J Exp Nanosci 3:185–193. https://doi.org/10.1080/17458080802395460

Malka E, Perelshtein I, Lipovsky A, Shalom Y, Naparstek L, Perkas N, Patick T, Lubart R, Nitzan Y, Banin E, Gedanken A (2013) Eradication of multi-drug resistant bacteria by a novel Zn-doped CuO nanocomposite. Small 9(23):4069–4076. https://doi.org/10.1002/smll.201301081

Manyasree D, Kiranmayi P, Kumar R (2018) Synthesis, characterization and antibacterial activity of aluminium oxide nanoparticles. Int J Pharm Pharm Sci 10(1):32–35. https://doi.org/10.22159/ijpps.2018v10i1.20636

Marambio-Jones C, Hoek EMV (2010) A review of the antibacterial effects of silver nanomaterials and potential implications for human health and the environment. J Nanopart Res 12:1531–1551. https://doi.org/10.1007/s11051-010-9900-y

Markowska K, Grudniak AM, Wolska KI (2013) Silver nanoparticles as an alternative strategy against bacterial biofilms. Acta Biochim Pol 60(4):523–530. http://www.actabp.pl/pdf/4_2013/523.pdf

Matthew L, Kromer JM, Matthew L, Adam K, Zachary TG, Burton HS, Sara M, Alex Y, Joaquin RL, Paramaconi R (2017) High throughput preparation of metal oxide nanocrystals by cathodic corrosion and their use as active photocatalysts. Langmuir 33(46):13295–13302. https://doi.org/10.1021/acs.langmuir.7b0246531Oct2017

Mehmood S, Rehman MA, Ismail H, Mirza B, Bhatti AS (2015) Significance of post growth processing of ZnO nanostructures on antibacterial activity against gram-positive and gram-negative bacteria. Int J Nanomed 10:4521–4533. https://doi.org/10.2147/IJN.S83356

Melian JAH, Rodriguez JMD, Suarez AV, Rendon ET, Valdes C, Arana J, Perez P (2000) The photocatalytic disinfection of urban waste waters. Chemosphere 41:323–327. https://doi.org/10.1016/S0045-6535(99)00502-0

Miao L, Wang C, Hou J, Wang P, Ao Y, Li Y, Geng N, Yao Y, Luv B, Yang Y, You G, Xu Y (2016) Aggregation and removal of copper oxide (CuO) nanoparticles in wastewater environment and their effects on the microbial activities of wastewater biofilms. Bioresour Technol 216:537–544. https://doi.org/10.1016/j.biortech.2016.05.082

Miller KJ (1971) An introduction to semiconductor surfaces as catalysts. J Chem Educ 48:582–586. https://doi.org/10.1021/ed048p582

Muhling M, Bradford A, Readman JW, Somerfield PJ, Handy RD (2009) An investigation into the effects of silver nanoparticles on antibiotic resistance of naturally occurring bacteria in an estuarine sediment. Mar Environ Res 68(5):278–283. https://doi.org/10.1016/j.marenvres.2009.07.001

Nalage SR, Navale ST, Mane RS et al (2015) Preparation of camphor-sulfonic acid doped PPy-NiO hybrid nanocomposite for detection of toxic nitrogen dioxide. Synth Met 209:426–433. https://doi.org/10.1016/j.synthmet.2015.08.018

Niemirowicz K, Swiecicka I, Wilczewska AZ, Misztalewska I, Kalska-Szostko B, Bienias K, Bucki R, Car H (2014) Gold-functionalized magnetic nanoparticles restrict growth of *Pseudomonas aeruginosa*. Int J Nanomedicine 9:2217–2224. https://doi.org/10.2147/IJN.S56588. eCollection 2014

Padmavathy N, Vijayaraghavan R (2011) Interaction of ZnO nanopar-ticles with microbes – a physio and biochemical assay. J Biomed Nanotechnol 7(6):813–822. https://doi.org/10.1166/jbn.2011.1343

Pan X, Wang Y, Chen Z, Pan D, Cheng Y, Liu Z, Lin Z, Guan X (2013) Investigation of antibacterial activity and related mechanism of a series of nano-Mg(OH)2. ACS Appl Mater Interfaces 5(3):1137–1142. https://doi.org/10.1021/am302910q

Pan F, Xu A, Xia D, Yu Y, Chen G, Meyer M, Zhao D, Huang CH, Wu Q, Fu J (2015) Effects of octahedral molecular sieve on treatment performance, microbial metabolism, and microbial community in expanded granular sludge bed reactor. Water Res 87:127–136. https://doi.org/10.1016/j.watres.2015.09.022

Park CH, Zhang SB, Wei SH (2002) Origin of p-type doping difficulty in ZnO: the impurity perspective. Phys Rev B 66:073202–073207. https://doi.org/10.1103/PhysRevB.66.073202

Pedro HCC, Kestur GS, Fernando W (2009) Nanocomposites: synthesis, structure, properties and new application opportunities. Mater Res 12(1):1–39. https://doi.org/10.1590/S1516-14392009000100002

Peng Z, Ni J, Zheng K, Shen Y, Wang X, He G, Jin S, Tang T (2013) Dual effects and mechanism of TiO_2 nanotube arrays in reducing bacterial colonization and enhancing $C_3H_{10}T_{1/2}$ cell adhesion. Int J Nanomedicine 8:3093–3105. https://doi.org/10.2147/IJN.S48084. Epub 2013 Aug 14

Peulen TO, Wilkinson KJ (2011) Diffusion of nanoparticles in a biofilm. Environ Sci Technol 45 (8):3367–3373. https://doi.org/10.1021/es103450g

Prasannakumar JB, Vidya KS, Anantharaju G, Ramgopal H, Nagabhushana SC, Sharma B, Daruka Prasad SC, Prashantha RB, Basavaraj H, Rajanaik KL (2015) Bio-mediated route for the synthesis of shape tunable Y2O3:Tb3+ nanoparticles: photoluminescence and antibacterial properties. Spectrochim Acta A Mol Biomol Spectrosc 151:131–140. https://doi.org/10.1016/j.saa.2015.06.081

Pulicherla Y, Thirumalanadhuni V, Palempalli UMD, Nataru S (2017) Bioinspired green synthesis of copper oxide nanoparticles from Syzygium alternifolium (Wt.) Walp: characterization and evaluation of its synergistic antimicrobial and anticancer activity. Appl Nanosci 7:417–427. https://doi.org/10.1007/s13204-017-0584-9

Qi G, Li L, Yu F, Wang H (2013) Vancomycin-modified mesoporous silica nanoparticles for selective recognition and killing of pathogenic gram-positive bacteria over macrophage-like cells. ACS Appl Mater Interfaces 5(21):10874–10881. https://doi.org/10.1021/am403940d

Qin J, Zhang X, Yang C, Song A, Zhang B, Saravanan R, Ma M, Liu R (2016) Effect of Ag^+ and PO_4^{3-} ratios on the microstructure and photocatalytic activity of Ag_3PO_4. Funct Mater Lett 9 (5):1650063. http://www.worldscientific.com/doi/abs/10.1142/S1793604716500636

Qin J, Yang C, Cao M, Zhang X, Saravanan R, Limpanart S, Mab M, Liu R (2017) Two-dimensional porous sheet-like carbon-doped ZnO/g-C_3N_4nanocomposite with high visible-light photocatalytic performance. Mater Lett 189:156–159. http://www.sciencedirect.com/science/article/pii/S0167577X16318912

Qiu XF, Zhao YX, Burda C (2007) Synthesis and characterization of nitrogen-doped group IVB visible-light-photoactive metal oxide nanoparticles. Adv Mater 19:3995–3999. https://doi.org/10.1002/adma.200700511

Rajendar V, Shilpa CCH, Rajitha B, Venkateswara RK, Chandra Sekhar M, Purusottam RB, Si-Hyun P (2017) Effect of TWEEN 80 on the morphology and antibacterial properties of ZnO nanoparticles. J Mater Sci Mater Electron 28:3272–3277. https://doi.org/10.1007/s10854-016-5919-x

Rajendran S, Manoj D, Raju K et al (2018) Influence of mesoporous defect induced mixed-valent NiO ($Ni^{2+/}Ni^{3+}$)-TiO_2 nanocomposite for non-enzymatic glucose biosensors. Sens Actuators B Chem 264:27–37. https://doi.org/10.1016/j.snb.2018.02.165

Ranghar S (2012) Nanoparticle-based drug delivery systems: promising approaches against infections. Braz Arch Biol Technol 57:209–222. https://doi.org/10.1590/S1516-89132013005000011

Rao MC, Ravindranadha K, Rose Mary T (2013) Development of ZnO nanoparticles for clinical applications. J Chem Biol Phys Sci 4:469–473. www.jcbsc.org/admin/get_filephy.php?id=154

Roguska A, Belcarz A, Pisarek M, Ginalska G, Lewandowska M (2015) TiO_2 nanotube composite layers as delivery system for ZnO and Ag -nanoparticles – an unexpected overdose effect decreasing their antibacterial efficacy. Mater Sci Eng C Mater Biol Appl 51:158–166. https://doi.org/10.1016/j.msec.2015.02.046

Roy AS, Parveen A, Koppalkar AR, Prasad M (2010) Effect of nano-titanium dioxide with different antibiotics against methicillin-resistant Staphylococcus aureus. J Biomater Nanobiotechnol 1:37–41. https://doi.org/10.4236/jbnb.2010.11005

Sadiq IM, Chowdhury B, Chandrasekaran N, Mukherjee A (2009) Antimicrobial sensitivity of Escherichia coli to alumina nanoparticles. Biol Med 5:282–286. https://doi.org/10.1016/j.nano.2009.01.002

Saito T, Iwase T, Horie J, Morioka T (1992) Mode of photocatalytic bactericidal action of powdered semicon-ductor TiO_2 on Mutans streptococci. J Photochem Photobiol B 14:369–379. https://doi.org/10.1016/1011-1344(92)85115-B

Sakthivel S, Kisch H (2003) Daylight photocatalysis by carbon-modified titanium dioxide. Angew Chem Int Ed Eng 42:4908–4911. https://doi.org/10.1002/anie.200351577

Saliani M, Jalal R, Kafshdare Goharshadi E (2015) Effects of pH and temperature on antibacterial activity of zinc oxide nanofluid against Escherichia coli O157:H7 and Staphylococcus aureus. Jundish J Microbio 8(2):e17115. https://doi.org/10.5812/jjm.17115

Saravanakkumar D, Sivaranjani S, Kaviyarasu K, Ayeshamariam A, Ravikumar B, Pandiarajan S, Veeralakshmi C, Jayachandran M, Maaza M (2018) Synthesis and characterization of ZnO–CuO nanocomposites powder by modified perfume spray pyrolysis method and its antimicrobial investigation. J Semicond 39(3):1–7. https://doi.org/10.1088/1674-4926/39/3/032001

Saravanan R, Gupta VK, Narayanan V, Stephen A (2013a) Comparatives studies on photocatalytic activity of ZnO prepared by different methods. J Mol Liq 181:133–141. http://www.sciencedirect.com/science/article/pii/S0167732213000810

Saravanan R, Thirumal E, Gupta VK, Narayanan V, Stephen A (2013b) The photocatalytic activity of ZnO prepared by simple thermal decomposition method at various temperatures. J Mol Liq 177:394–401. http://www.sciencedirect.com/science/article/pii/S0167732212003662

Saravanan R, Prakash T, Gupta VK, Narayanan V, Stephen A (2013c) Synthesis, characterization and photocatalytic activity of novel Hg doped ZnO nanorods prepared by thermal decomposition method. J Mol Liq 178:88–93. http://www.sciencedirect.com/science/article/pii/S0167732212004114

Saravanan R, Gupta VK, Edgar M, Gracia F (2014) Preparation and characterization of V_2O_5/ZnO nanocomposite system for photocatalytic application. J Mol Liq 198:409–412. http://www.sciencedirect.com/science/article/pii/S0167732214003432

Saravanan R, Khan MM, Gracia F, Qin J, Gupta VK, Stephen A (2016) Ce^{3+}-ion-induced visible-light photocatalytic degradation and electrochemical activity of ZnO/CeO_2 nanocomposite. Nature-Sci Rep 6:31641. http://www.nature.com/articles/srep31641

Saravanan R, Aviles J, Gracia F, Mosquera E, Vinod KG (2018a) Crystallinity and lowering band gap induced visible light photocatalytic activity of TiO_2/CS (Chitosan) nanocomposites. Int J Biol Macromole 109:1239–1245. https://www.sciencedirect.com/science/article/pii/S0141813017323450

Saravanan R, Tuan KA, Hoang RB, Diaz-Droguett DE, Gracia F, Gracia-Pinilla MA, Akbari-Fakhrabadi A, Vinod KG (2018b) Hydrogen adsorption properties of Ag decorated TiO_2 nanomaterials. Int J Hydro Ener 43(5):2861–2868. https://www.sciencedirect.com/science/article/pii/S0360319917347195

Sarwar A, Katas H, Samsudin SN, Zin NM (2015) Regioselective sequential modification of chitosan via azide-alkyne click reaction: synthesis, characterization, and antimicrobial activity of ahitosan derivatives and nanoparticles. PLoS One 10(4):e0123084. https://doi.org/10.1371/journal.pone.0123084

Sathyanarayanan MB, Balachandranath R, Genji SY, Kannaiyan SK, Subbiahdoss G (2013) The effect of gold and iron-oxide nanoparticles on biofilm-forming pathogens. ISRN Microbiol 2013:1–5. https://doi.org/10.1155/2013/272086

Sawai J (2003) Quantitative evaluation of antibacterial activities of metallic oxide powders (ZnO, MgO and CaO) by conductimetric assay. J Microbiol Methods 54:177–182. https://doi.org/10.1016/S0167-7012(03)00037-X

Sawai J, Kojima H, Igarashi H, Hashimoto A, Shoji S, Sawaki T, Hakoda A, Kawada E, Kokugan T, Shimizu M (2000) Antibacterial characteristics of magnesium oxide powder. World J Microbiol Biotechnol 16:187–194. https://doi.org/10.1023/A:1008916209784

Schmidt D, Shah D, Giannelis EP (2002) New advances in polymer/layered silicate nanocomposites. Curr Opin Solid State Mater Sci 6(3):205–212. https://doi.org/10.1016/S1359-0286(02)00049-9

Slomberg DL, Lu Y, Broadnax AD, Hunter RA, Carpenter AW, Schoenfisch MH (2013) Role of size and shape on biofilm eradication for nitric oxide-releasing silica nanoparticles. ACS Appl Mater Interfaces 5(19):9322–9329. https://doi.org/10.1021/am402618w

Sokemen M, Degerli S, Aslan A (2008) Photocatalytic disinfection of Giardia intestinalis and Acanthamoeba castellani cysts in water. Exp Parasitol 119:44–48. https://doi.org/10.1016/j.exppara.2007.12.014

Sondi B, Salopek-Sondi (2004) Silver nanoparticles as antimicrobial agent: a case study on E. coli as a model for Gram-negative bacteria. J Colloid Interface Sci 275:177–182. https://doi.org/10.1016/j.jcis.2004.02.012

Su Y, Zheng X, Chen Y, Li M, Liu K (2015) Alteration of intracellular protein expressions as a key mechanism of the deterioration of bacterial denitrification caused by copper oxide nanoparticles. Sci Rep 5:15824. https://doi.org/10.1038/srep15824

Sukhorukova IV, Sheveyko AN, Kiryukhantsev-Korneev PV, Zhitnyak IY, Gloushankova NA, Denisenko EA, Filippovich SY, Ignatov SG, Shtansky DV (2015) Toward bioactive yet antibacterial surfaces. Coll Surf B 135:158–165. https://doi.org/10.1016/j.colsurfb.2015.06.059

Talebian N, Haddad S, Zavvare H (2014) Enhanced bactericidal action of SnO_2 nanostructures having different morphologies under visible light: influence of surfactant. J Photochem Photobio B Biol 130:132–139. https://doi.org/10.1016/j.jphotobiol.2013.10.018

Tetsuya S, Kentaro T, Tsunehiro T (2011) A unique photo-activation mechanism by "in situ doping" for photo-assisted selective NO reduction with ammonia over TiO_2 and photooxidation of alcohols over Nb2O5. Catal Sci Technol 1:541–551. https://doi.org/10.1039/c1cy00104c

Thakur M, Sharma G, Ahamad T et al (2017) Efficient photocatalytic degradation of toxic dyes from aqueous environment using gelatin-Zr(IV) phosphate nanocomposite and its antimicrobial activity. Colloids Surf B Biointerfaces 157:456–463. https://doi.org/10.1016/j.colsurfb.2017.06.018

Thangaraj P, Saravanan R, Balasubramanian K, Gracia F, Mansilla HD, Gracia-Pinilla MA, Viswanathan MR (2017) Sonochemical synthesis of CuO nanostructures and their morphology dependent optical and visible light driven photocatalytic properties. J Mater Sci Mater Electron 28:2448–2457. https://www.springerprofessional.de/sonochemical-synthesis-of-cuo-nanostructures-and-their-morpholog/10871786

Umebayashi T, Yamaki T, Itoh H, Asai K (2002) Band gap narrowing of titanium dioxide by sulfur doping. Appl Phys Lett 81:454–456. https://doi.org/10.1063/1.1493647

Vidic J, Stankic S, Haque F, Ciric D, Le Goffic R, Vidy A, Jupille J, Delmas B (2013) Selective antibacterial effects of mixed ZnMgO nanoparticles. J Nanopart Res 15:1–10. https://doi.org/10.1007/s11051-013-1595-4

Wang YQ, Cheng HM, Hao YZ, Ma JM, Li WH, Cai SM (1999) Photoelectrochemical properties of metal-ion-doped TiO_2 nanocrystalline electrodes. Thin Solid Films 349:120–125. https://doi.org/10.1016/S0040-6090(99)00239-4

Wang L, Hu C, Shao L (2017) The antimicrobial activity of nanoparticles: present situation and prospects for the future. Int J Nanomed 12:1227–1249. https://doi.org/10.2147/IJN.S121956

Wehling J, Dringen R, Zare R, Mass M, Rezwan K (2014) Bactericidal activity of partially oxidized nanodiamonds. ACS Nano 8(6):6475–6483. https://doi.org/10.1021/nn502230m

Xie Y, He Y, Irwin PL, Jin SL (2011) Antibacterial activity and mechanism of action of zinc oxide nanoparticles against campylobacter jejuni. Appl Environ Microbiol 77:2325–2331. https://doi.org/10.1128/AEM.02149-10

Xiong MH, Li YJ, Bao Y, Yang XZ, Hu B, Wang J (2012) Bacteria-responsive multifunctional nanogel for targeted antibiotic delivery. Adv Mater 24(46):6175–6180. https://doi.org/10.1002/adma.201202847

Xu Y, Wei MT, Ou-Yang HD, Walker SG, Wang HZ, Gordon CR, Guterman S, Zawacki E, Applebaum E, Brink PR, Rafailovich M, Mironava T (2016) Exposure to TiO_2 nanoparticles increases Staphylococcus aureus infection of HeLa cells. J Nanobio-Technol 14:34. https://doi.org/10.1186/s12951-016-0184-y

Yamamoto O, Ohira T, Alvarez K, Fukuda M (2010) Antibacterial characteristics of $CaCO_3$–MgO composites. Mater Sci Eng B 173:208–212. https://doi.org/10.1016/j.mseb.2009.12.007

Yu J, Zhang W, Li Y (2014) Synthesis, characterization, antimicrobial activity and mechanism of a novel hydroxyapatite whisker/nano zinc oxide biomaterial. Biomed Mater 10(1):015001. https://doi.org/10.1088/1748-6041/10/1/015001

Yu Q, Li J, Zhang Y, Wang Y, Liu L, Li M (2016) Inhibition of gold nanoparticles (AuNPs) on pathogenic biofilm formation and invasion to host cells. Sci Rep 6:26667. https://doi.org/10.1038/srep26667

Zakharova OV, Godymchuk AY, Gusev AA, Gulchenko SI, Vasyukova IA, Kuznetsov DV (2015) Considerable variation of antibacterial activity of Cu nanoparticles suspensions depending on the storage time, dispersive medium, and particle sizes. Biomed Res Int 2015:412–530. https://doi.org/10.1155/2015/412530

Zaleska A (2008) Doped-TiO_2: a review. Recent Pat Eng 2:157–164. https://doi.org/10.2174/187221208786306289

Zhang L, Ding Y, Povey M, York D (2008) ZnO nanofluids—A potential antibacterial agent. Prog Nat Sci 18:939–944. https://doi.org/10.1016/j.pnsc.2008.01.026

Zhou Y, Li L, Zhou Q, Yuan S, Wu Y, Zhao H, Wu H (2015) Lack of efficacy of prophylactic application of antibiotic-loaded bone cement for prevention of infection in primary total knee arthroplasty: results of a meta-analysis. Surg Infect 16(2):183–187. https://doi.org/10.1089/sur.2014.044

Zhukova LV (2015) Evidence for compression of Escherichia coli K12 cells under the effect of TiO_2 nanoparticles. ACS Appl Mater Interfaces 7(49):27197–27205. https://doi.org/10.1021/acsami.5b08042

Chapter 9
Green Technologies for Wastewater Treatment

T. Vasantha and N. V. V. Jyothi

Contents

T. Vasantha (✉) · N. V. V. Jyothi
Department of Chemistry, Sri Venkateswara University, Tirupati, Andhra Pradesh, India

M. Naushad et al. (eds.), *Green Methods for Wastewater Treatment*, Environmental Chemistry for a Sustainable World 35, https://doi.org/10.1007/978-3-030-16427-0_9

Abstract A metals accretion of solids, liquids, and gaseous toxic waste has upshot from a lack of improvement in toxic waste management. This has necessitated the design of an assortment of novel research works in water and wastewater treatment, industrialized dissipate management, ground water, and soil pollution subsistence. Simultaneously, increasing concerns about water sources are becoming a considerable matter, as a paucity of water has been seen all over the earth. A number of expanding technologies have the know-how to modernize our world of commercialization. Advanced Treatment Techniques for Industrial Wastewater is an innovative collection of research that covers the different aspects of environmental engineering in running water and wastewater treatment processes with the different techniques and systems for pollution management. A number of them are presently within the scope of improvement but there is lingering frustration to firmly implement them in civilization, and all are propitious solutions to some very authentic challenges facing the planet. The term "Green Technology" is relatively new and has been slowly adopted over the most recent decades; emerald is the present day system for a healthy life. This chapter illustrates different green technology challenges and their chance to enhance wastewater treatment technologies and trends toward progress.

Keywords Jade (Green) chemistry · Green technology · Wastewater treatment · Advantages and disadvantages of green technologies

9.1 Introduction

Water is one of the most precious resources on earth. All living organisms require water for survival. Without the presence of water, life would not exist on the globe. Water covers nearly 71% of the Earth's surface, but only 2.5% of it exists as freshwater. A huge volume of wastewater is released from the areas of urbanization and industrialization, and it was utilized more by irrigation resources in semi-urban and urban agriculture areas (Shahat et al. 2015). Economic activities drive countless lives, including for poor farmers, and this has dramatically changed the quality of water bodies (Marshall et al. 2007). Current awareness on the contaminant risk posed to natural water bodies has to expand so that efficient studies toward improved industrial development can be assessed. Because of increased industrial wastewater, the massive features of contaminants in organic and inorganic complex mixtures have increased, so there is a need to treat the concentration of pollutants in the wastewater and the environment by using a treatment process (Woisetschlager et al. 2013; Sires et al. 2014). It has become a crucial necessity for today's atmosphere to stop water from becoming polluted or expand the cost effectual curative scheme used for its defense (Awual et al. 2015). Owing to the hasty growth of the inhabitants in emerging countries, the offered predictable treatment for wastewater plants are being overloaded, and there will be no space obtainable for growth of the existing treatment plants. Reprocessing and reuse of air, water soil pollutants, and waste have been emerging topics throughout the 2010s, to shield innate resources and the atmosphere (Corder et al. 2015; Colling et al. 2016).

One of the foremost sources of wastewater is farming effluent that contains pollutants and contaminants, including chemicals, microorganisms, nutrients and other toxin, municipal runoff, and squall water. Sewage as wastewater includes water from cleaners, bathing, laundry, toilets, bathroom fittings, and sinks. Influent is the wastewater that flows into a treatment plant, reservoir, or basin. As this wastewater is inappropriately released into the river bodies, these pollutants can cause an ecological issue leading to health tribulations in humans and animals (Wongburi and Park 2018; Jhansi and Mishra 2013). Yet, wastewater also contains reusable wherewithal, such as carbon, nutrients, and water, that could be recovered or reused. For that reason, wastewater ought to be fittingly treated for elimination of pollutants to meet the effluent regulatory values. Moreover, the process should focus on resource recovery to lessen the carbon footprint and to be self-sustainable (Metcalf and Eddy 1991).

Some form of wastewater treatment has been used since antiquity; however, a variety of conventional methods used to treat the water have not been economical (Pawar Avinash Shivajirao 2012). Therefore, innovative green technology methods are being introduced to defeat the predictable methods of wastewater treatment (Zhou and Smith 2002; Turovskiy 2014).

Currently, the management of waste and superiority of water are significant concerns for human life. The accretion of technology in urbanization and

industrialization explains the increase in the percentage accumulation of waste all around the world and the discharge of heavy metals in water streams. The release of inadequately treated industrial waste containing heavy metals affects waterways and turns into a stern ecological problem in need of solution development (New Technologies in Wastewater Treatment 2014). The use of heavy metal polluted wastewater to irrigate poses a risk to civic health (Siddique et al. 2014). These destructive metals are produced from a variety of activities, such as waste disposal, industrial, agricultural, and others. Increasing the heavy metals content in wastewater streams has negative effects on human bodies, including death. Technology used in the handling of wastewater includes chemical precipitation, absorption, ion-exchange, coagulation flocculation, and membrane filtration; flotation and electrochemical and the added advanced oxidation process involve enormous outfitting and regulation overheads (Nabi et al. 2011; Gutha et al. 2015; Cheng et al. 2012; Javadian et al. 2014). Consequently, an outlay of effectual green skill toward the removal of these heavy metals as well as progress in the effluent standards is desired.

Energetic industrialization has resulted in a huge extent of wastewater from industrial zones, for instance paper, crop fruit, sugar, pulp, distilleries, cuisine processing, slaughterhouses, sago/starch, poultry farms, tanneries, dairies, etc. Regardless of the requirements for toxic waste manage events, this wastewater is usually dumped on territory or used to irrigate, devoid of enough treatment, and it consequently becomes a gigantic resource of ecological toxic waste and physical condition hazards. The wastewater organization in India has grown to be an extremely necessary regional hub owing to escalating health concerns and inhabitant's pressure. In spite of the wastewater sector witnessing major augmentation in the past decade due to escalating government support and private involvement, the scale of the problem remains vast. It is estimated that less than 20% of domestic and 60% of industrial wastewater is treated. Metros and big cities (more than 100,000 inhabitants) treat merely about 29.2% of their wastewater, whereas smaller cities treat only 3.7% of their wastewater. Manufacturing wastewater includes industrial effluents (with or without pre-treatment) and sometimes also cooling water from energy construction and mining water. The trivial enrichment in wastewater quantity is chiefly based on reduction in the production process and sometimes because of upgrading or edifice of effective treatment conveniences (Martin-Lara et al. 2014).

Within the present developing world, the term green technology has played a considerable function during the course of a nation's fiscal growth toward sustainability and provided an alternative socioeconomic model that will enable the current and upcoming generations to live in a hygienic as well as hale and hearty atmosphere, in accord with nature. Clean technology, furthermore identified as green technology, refers to the development and extension of the processes, practices, and applications to improve or replace the existing technology and facilitate society to meet their own requirements and at the same time substantially decrease the impact of humans on the globe amid ecological risks and environmental scarcity. The theory of green technology, if allowed to pervade the lives of all societies, will ease the aim

of the millennium improvement goals of keeping the environment intact and developing it for the long-term survival of civilization. Green Technologies and Environmental Sustainability are focused toward the goals of green technologies, which progressively give more importance to ensuring sustainability. This chapter shows altered perspectives of green technology in different zones, including energy, agriculture, waste management, and economics and contains current advancements ready for sustainable increases in the field of bio energy, green chemistry, nanotechnology, degraded land reclamation, and bioremediation.

Additionally, advanced manufacturing industries along with the emergent are allied by the superior treatment process, resulting in considerable development toward the versatility and the outlay of this process at the industrialized scale. By means of lifecycle investigation, for instance, (Wiesner et al. 1994) concluded that the outlay of new pressure-driven membrane filtration plants are predicted to be analogous with or smooth less than that of folks by means of a predictable treatment process with a capacity of 20,000 m^3/day.

To resolve the innovative challenge as well as enhance inexpensive wherewithal, a variety of advanced treatment technologies can be wished-for, tested, and applied to gather both modern and expected treatment needs. Amid them, membrane filtration, UV radiation, and advanced oxidation processes have been traditional for victorious deletion of an extensive range of taxing contaminants in irrigation and treatment of wastewater. This chapter focuses on the superior treatment of green technologies with an emphasis on their main applications, fundamentals, advantages, and disadvantages. The recent boundaries and future research desires related to this technology are discussed in this chapter (Fig. 9.1).

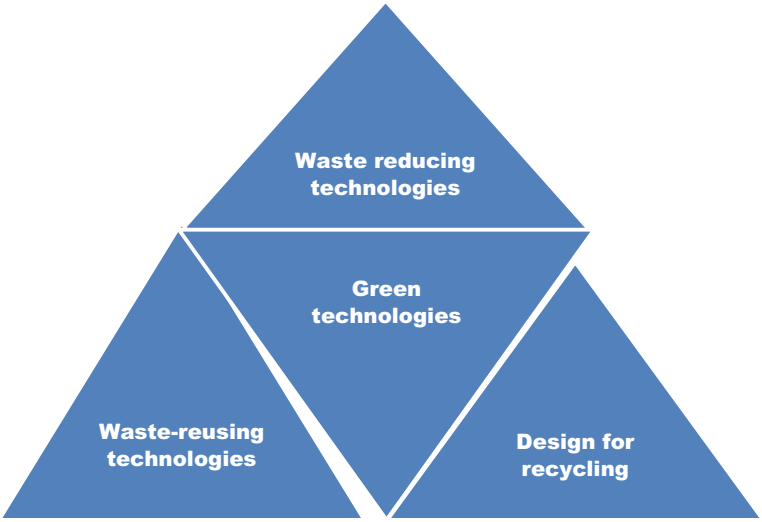

Fig. 9.1 Designing of green technologies

9.1.1 Characteristics and Treatment Technology of Wastewater

The features of wastewater containing heavy metals, such as the treatment level and pollution loading rate, are report to be intimately allied to industrialized characteristics. The industrial characteristics include geographical location, (Yu et al. 2003a, b, c; Yu et al. 2003a, b, c) departments in government, industrial sectors, grade of registration, and endeavor extent (large, medium, and small). The feature of water and extent of heavy metal content in wastewater is assorted to a great extent among different industrial sectors. For the most considerable large-scale and national-owned mineral endeavor, the irrigation utilization coefficients are usually elevated, whereas for the diminutive scale, rural community ownership, municipality, private and communal enterprise, the levels of treatment are very low (Yu et al. 2003a, b, c). The treatment level appears to be inferior and have a dwindling endeavor of extent with the geographical transition from east to west (Yu et al. 2003a, b, c). The pollutant concentrations are middling from the nonferrous industry and assorted greatly. The wastewater discharged from village and small town enterprises contains high concentrations of heavy metals; as a result they could not regularly congregate the expulsion (Sharma et al. 2015). Even though the summary metal emission quantity was low, wastewater without treatment from some diminutive civic and village enterprises resulted in astonishing metal toxic waste in a confined area, which ought to be proscribed.

9.1.2 Waste Management

The term ‘solid waste’ habitually relates to materials fashioned by human activity, and action is commonly undertaken to minimize theireffect on health, the atmosphere or aesthetics. Waste management is the utilization, purification, recycling, discarding, and treatment of solid waste that is looked after by the government or the verdict body of a city/town. There are diverse methods and fields of proficiency for each waste management involving solid, liquid, gaseous or radioactive substances. In some instances, green waste management is also carried out to recuperate assets.

Green waste management practices diverge for emergent nations, residential, and industrial producers, and they are also designed for urban and rural areas. The management for nonhazardous residential and institutional waste in metropolitan areas is habitually the liability of local government powers that be, while management for nonhazardous commercial and industrial waste is habitually the responsibility of the generator.

The waste management industry has been taking a leisurely pace toward new technology, such as radio frequency identification (RFID) tags, integrated software packages, and GPS, which enable a superior eminence data to be composed without

the use of assessment or manual data entry. Technology like RFID tags are currently being used to accumulate data on presentation rates for curb-side pick-ups, which is constructive when exploring the usage of recycle bins or similar. Benefits of GPS tracking is particularly apparent in view of the efficiency of ad hoc pick-ups where the anthology is finished on a customer request basis. Integrated software packages are constructive in aggregate with this data for use in optimization of waste collection operations.

Integrated waste administration with a life cycle study attempts to propose the best option for green waste management. The quantity of broad studies signify source severance, waste administration, and collection followed by reuse and recycling of the nonorganic portion, energy, and compost/fertilizer production of the organic waste partition via anaerobic digestion to be the chosen waste management decisions. Nonmetallic waste properties are not damaged by means of burning and are able to be reprocessed/recycled in a future source exhausted culture.

9.2 Green Chemistry

The term 'Green Chemistry' was coined by Anastas (Anastas and Kirchhoff 2002) from the US Environmental Protection Agency (EPA). It is the "design of chemical products and processes to reduce or eliminate the use and production of harmful substances" (Anastas and Warner 1998; Anastas 2007; Anastas and Williamson 1996). In 1993 the name 'US Green Chemistry Program' was formally adopted, which has served as a crucial point on behalf of performance around the United States, for instance, the Green Chemistry Challenge. This does not signify that research on green chemistry did not subsist earlier than the 1990s; simply that it did not have the forename. During the 1990s, both Italy and the United Kingdom launched a major initiative in green chemistry, and, more recently, Japan initiated the Green and Sustainable Chemistry Network. The initial version of the academic journal *Green Chemistry* was guaranteed by the Royal Society of Chemistry, which appeared in 1999. The essential feature of the term is the supposition of design. It includes systematic conception, planning, and novelty.

9.2.1 Need of Wastewater Treatment

As India hurtles in the direction of a new urbanized economy, a worsening status of our atmosphere has been observed. Unfortunately, swift industrialization has increased the amount of toxins in our surroundings. Administration of waste at wastewater treatment plants in India has become crucial for our cities today.

9.2.2 Benefits

Beneficial water treatment methods do not merely manufacture hygienic reusable irrigation water but also have the possibility to bring into being assorted further benefits. They have the possibility to condense a country's waste production, to harvest methane, and to fabricate natural manure, and for the waste collected through the method, the benefits are waste reduction, fertilizer production, and energy production.

9.2.3 Information About Waste Management

The technique of wastewater management was initially developed in reaction to the adverse conditions sourced by the liberation of wastewater into the surroundings and the distress caused to civic wellbeing. In addition, as cities became larger, restricted land exists for wastewater treatment as well as discarding, predominantly by irrigation and sporadic filtration. Besides, when a population grows, the scope of wastewater spawn rises rapidly, and the deteriorating quality of this gigantic quantity of wastewater surpasses the self purification capacity of the stream and waterway bodies. Consequently, additional methods of treatment are developed to step up the forces of the natural world beyond conditions in treatment amenities of relatively smaller size. Even though clear out is obligatory to avert further expulsion of contaminated wastes into the atmosphere, development of an outlay effect technology is desired for diligent use. Conventionally, the method employed for wastewater remediation consists of the abolition of metals by flocculation, ion exchange resins, filtration, and activated charcoal (Karthikeyan et al. 2005; Vijayaraghavan et al. 2007; Wang and Chen 2009).

Generally, since 1900 to untimely the 1970s, treatment objectives included: (i) the deletion of hovering and floatable matter from wastewater, (ii) elimination of disease-causing pathogenic micro-organisms, and (iii) the treatment of biodegradable organics (BOD). The deletion treatments focused on aesthetic and ecological disquiet. The former errands of diminution and deletion of BOD, hovering solids, and pathogenic microorganism have continued, but at larger levels. The deletion of nutrients, such as nitrogen and phosphorus, has also begun to be addressed, particularly in some of the streams and lakes. Major initiatives have been undertaken around the globe to accomplish more effectual and prevalent treatment of wastewater to maintain the excellence of the surface waters. The endeavor is owing to (i) a comprehension of the adverse long-term effects caused via the discharge of some of the specific constituents established in wastewater and (ii) an increase in the understanding of the environmental effects caused by the wastewater discharges. Since the 1990s, as a time of enlarged scientific awareness and an extended information base,

wastewater treatments have begun to focus on the health concerns associated with tainted and potentially noxious chemicals that are unconfined into the milieu. The waterway feature improved the objectives of the 1970s and has continued, but the emphasis has shifted to the definition as well as deletion of noxious and trace compounds that could feasibly be the origin of long-term health effects and adverse ecological impacts. As a result, though the past treatment objectives remain valid today, the imperative grade of treatment has increased drastically, with the addition of supplementary treatment objectives and goals.

The characteristics of Dewat's system consists of primary, secondary treatments and discarding (or utilization) of solids and treated water. The primary treatment might be as trouble-free as a septic tank, to eliminate settleable solids, and endow among restricted anaerobic treatment which canister should be used in the vicinity of poor soil and high groundwater. Modification of the over system enables aerobic treatment of the effluent and thwarts perched solids from inflowing to the secondary treatment. Because they are economical, and as a result have little continuance, they are prone to failure and even when in effective service may tranquilly secrete a pathogen rich waste stream. Secondary treatment options, based on sand filters, provide effectual deletion of pathogens in areas with deep permeable soils, but are ineffective in other locales with highly porous soil types. A noteworthy quantity of attention has been given to the use of organic systems meant for deletion of radio nuclides and heavy metals from solutions, and (Massoud et al. 2009; Parkinson and Tayler 2003) made a wide-ranging chapter on the existing treatment methods. A variety of predictable methods for wastewater treatment exist from primeval times, (Narmadha and Selvam Kavitha 2012; Pawar Avinash Shivajirao 2012; Turovskiy 2000); however, they are extremely pricey and thus not economical. The exceedingly developed newfangled green technology methods are being introduced to prevail over the conformist methods of wastewater treatment (Dangelico and Pujari 2010). The study chapter is allied to new green technological methods, which prove to be more advanced than the predictable methods.

9.2.4 Wastewater and the Necessity for Wastewater Management

Contaminated water is released from various industries. The sources of irrigation pollution are from sewage and industrialized waste. By means of these sources from the inhabitants of India, and the phenomenal swiftness of the escalation of its industrialized landscape, the volume of wastewater is also rising at an alarming rate. Adding to this the attenuation of freshwater sources, for instance, river, groundwater, and well water, so as to have an alarming circumstance. Very soon irrigation water may become a premium commodity.

The growing levels of wastewater have become of great consequence. Not only is it unfit for utilization but it also can mix with other sources and pollute them as well (Albadarin et al. 2017). For instance, the tainted water pollutes the river, and when this watercourse run downstream and it joins other water sources, such as other rivers, the contamination further spreads. Wastes also seep into the earth and contaminate the underground water source. Thus, now-a-days almost each source of water is heavily tainted, from the rivers to the coastal areas.

Water is essential and intended for all; therefore, the treatment of water is of the uttermost seriousness. Consumption of irrigation water is meant for all creatures. Irrigation water is essential to farming, the food industry, and livestock. To a minute degree, nature can react with reasonably fashioned noxious waste akin to human being and mammal waste. On the other hand, the enormous quantity of wastewater today cannot be managed by nature alone.

Several effects of rising levels of wastewater are summarized:

- Lack of drinking water
- Adverse effect on groundwater
- Harmful effect on river and marine life
- Soil pollution
- Superfluity of hazardous chemicals, some of which are unremitting
- Rise of pollution in coastal areas
- Increase in unremitting health circumstances associated with lethal chemicals, such as mercury and lead, in all creatures.

The investigative upshoot in the field of health related to water safeguards and a change in civilization environmental consciousness (type of weather and assets defense) obliged a new perspective concerning wastewater treatment. The plant designed for treating wastewater will become the source overhaul provider for human beings and water bodies (Millennium Ecosystem Assessment [MEA], 2005), vigor overhaul provider, and manufacturer of stipulated tilting products, including water fertilizers. Sustainable wastewater treatment consists of the subsequent safeguards (Schaum 2016; Schaum and Cornel 2016).

Health safeguard: Defense of sanitized necessities, including antibiotic resistant microorganisms acquiescence with features standards for daily handling in water bodies contributing hygienically harmless water for water reprocessing.

Water safeguard: The diminution of eutrophication via nutrient abolition (phosphorus and nitrogen) to the utmost feasible scope, abolition of nanoparticles, microplastics, and micropollutant for the safeguard of marine fauna and from the viewpoint of precautionary health care.

Resource safeguard: The diminution of source utilization for wastewater treatment, for instance, in service materials and vigor, reduction of ecological impact; source resurgence by consuming resources contained in wastewater, predominantly energy, nutrients, and water. To make all of this doable, it is crucial to coalesce skill and operation optimization; therefore, identifying synergy needs to be exploited.

9.2.5 The Physico-Chemical Treatment

Noxious wastes are habitually classified according to diverse techniques and size, where bigger particles are estranged during filtration, floatation, and gravity and smaller particles are much more complicated to detach. That is why this treatment is predominantly useful.

Chemicals known as coagulants and flocculants are used to detach them. This is a frequently used technique to treat industrialized waste. It is ideal for the deletion of hovering matter, such as grease, oil, metals, and liquefied material as well as non-living material.

9.2.6 Natal Treatment

In this method, a membrane based system is used for recycling the wastewater. A membrane bioreactor combines the use of the unproblematic science of ultra filtration with a bioreactor to treat wastewater. In short, the method coalesces the corporeal process with the natal method. This is a frequently used method in industrial and metropolitan wastewater management. Treated water is recycled for assorted intentions, such as irrigation.

9.2.7 Zilch Fluid Liberation Scheme

Several inhabitants analyze this as a periphery skill in wastewater management. It confiscates all liquefied solids from the wastewater, leaving purified water. A technique like RO is used to decontaminate the water. There is a large area where the necessity for wastewater management is great. Some of the areas of operation for wastewater treatment plants in India are:

- Metropolitan water management for urban and municipality
- Large building societies or colonies
- Desalination
- Designed for use in rural regions, such as irrigation
- Industrialized segment

Some of the challenges still faced in India are:

- Apathy by some governments
- Lack of civic confidential partnership on wastewater management
- Lack of awareness
- Disproportion in the quantity of wastewater and handling plants
- Lack of a cohesive nationwide campaign

In India, the treatment plants have become an imperative component of the countryside crucial for sustaining the health of our public and the earth. Green technology has brought new technology to the treatment of wastewater.

9.3 Green Technology (GT)

GT is an ecological curative technology that diminishes the ecological damage resulting from the products and technology for citizen's conveniences. Currently, advancement in corporations have lead to further thought toward GT, helping to enhance green capabilities (Hekkert and Negro 2009; Pujari 2009; Berrone et al. 2013). Green technology can improve material along with waste consumption, energy efficiency, and recycling.

In support of these benefits, GT not only enhances ecological features but also encourages the potency of a nation's financial system (Shrivastava 1995; Aithal 2015a, b, c). It is supposed that GT promises to develop farm effectiveness while simultaneously minimizing ecological degradation and conserving innate assets. GT is a sustainable technology that will not generate a footprint, and it is used for an assortment of processes. GT maintains the use of innate macrobiotic resources and stays away from the manufacture of emerald gas. GT also uses fewer sources and does not support enlarging the entropy of the earth. GT supports the mechanization of each process and hence avoids human interference.

The foremost technologies used in present day, including space technology, internet technology, atomic, nuclear technology, automobile technology, computer technology, aircraft technology, renewable energy technology, biotechnology, nanotechnology, telecommunication technology, etc., can be made green using the principles of green technology (Sridhar Acharya and Aithal 2015; Han and Liu 2009; Guoliang 2011; Aithal and Aithal 2015a, b). Such GT might enable solving both basic and superior problems. At the moment, industrial and technological progress in emergent countries is budding swiftly, and ecological problems as well as others must be considered. As a result, novel green technology research promotes ecological and monetary development (Hasper 2009). Inside this section, our aim is to present effectual green technology for treatment of waste.

9.3.1 Class of Green Technology

Jade technologies cover an extensive province of fabrication and utilization technologies. The espousal and use of green technologies entails making use of ecological technologies to observe and assess toxic waste deterrence, manage, remediation, and renovation. Thus, the monitoring and appraisal technologies are used to resolve and follow the circumstances of the environs, over and above, the expulsion of innate or anthropogenic supplies of a detrimental nature. Avoidance technology

evades the manufacture of environmentally perilous materials or alters traditions so as to lessen harm to the milieu; it encompasses product swap or the redesign of an intact creation development sooner than by means of the original portion. Risk management technology deals with things that are undisruptive earlier and then penetrate the surroundings. Remediation and reinstatement technologies exemplify the method proposed to advance the stipulation of ecosystems besmirched by unsurprisingly induced or anthropogenic things (2003 United Nations environment programme environmentally sound technologies for sustainable).

9.3.2 Sectors of Green Technology

1. Water and waste management: Solid waste management, Sewage treatment, Recycling technology, and Water purification.
2. Agriculture: Organic agriculture.
3. Building: Building performance technology and Sustainable building material.
4. Transportation: Electric vehicle and Rail transport.
5. Energy: Efficiency technology and Renewable energy technology.

9.3.3 Advantages of Green Technologies (AGTs) Toward Wastewater Management

This refers to the process of removing the contaminants and undesirable components in domestic, industrial, and polluted waters to safely return it to the environment for drinking, irrigation, industrial, and other uses. Today, the increase in ecological awareness and enhanced government regulation has made some conventional wastewater treatment systems questionable. To fill the gap left by less than adequate conventional technologies, AGTs are tested, vetted, and implemented as clean alternatives for wastewater treatment purposes.

Several steps are basically employed during any wastewater treatment process. The first consists of separating the solids from the liquid water. This is achieved through gravity as solids are heavier than the liquid water. Other solid components, such as oils and woods, which are less dense than liquid water, could be removed from the water surface through separation. Afterward, the liquid wastewater is subjected to filtration processes to dispose of any colloidal suspensions of fine solids, chemicals particulates, and impurities. The resulting filtered water is finally exposed to oxidation on the way to trim down or eradicate the toxicity of any remaining noxious waste and disinfect the wastewater before releasing it to the environment. Currently, a number of AGTs methods are tested and used for wastewater treatment either alone or in combination with other conventional methods.

9.3.4 Objectives of Advanced Green Technologies (OAGTs)

Advanced green technologies (AGTs) refer to a group of practical methodologies and materials based, among others, on nontoxic chemical processes, clean energies, and environmental monitoring to slow down or correct the negative impact induced by human activities. Advanced green technologies are aimed to provide better sustainability through securing our societal needs without further damaging or depleting the remaining natural resources. This could be achieved through:

- Setting up economical models to implement and commercialize related innovations by encouraging the creation of jobs and novel careers in the field.
- The recycling of manufactured goods and products.
- Development of clean alternative technologies and energies to replace those proven to negatively impact health and pollute the environment.
- Decreasing the pollution caused by the waste release as well as contamination through improving the behavior of human manufacturing and expenditures.

9.3.5 Green Technology Four Pillars Policy

Social: Get better quality of life for all (Luken and Van Rompaey 2008) through the use of technology.
Milieu: Marmalade and lessen the impact on the atmosphere.
Financial system: Augment the nationalized fiscal enhancement.
Vigor: Inquire about the route for arriving at vigor independently and encourage efficient exploitation.

9.3.6 Benefits of Green Technology

1. Does not produce hazardous wastes into the atmosphere.
2. Renewable; will never expire.
3. Be able to fetch monetary benefits to assured area.
4. Requires less upholding, so you do not need scores of capital to operate it.
5. Slow global warming by plummeting CO_2 emission.

9.3.7 Drawbacks of Adopting Green Technology

1. Lack of human resources and skills.
2. No known alternative process technology.
3. Lack of information.

4. High implementation costs.
5. Uncertainty about performance impacts.
6. No renowned unconventional chemical or unrefined fabric inputs.

9.4 Jade Industry Initiative

An association through the 'jade economy' and sustainable advancement concept, akin to the 'jade economy' and 'jade industry', is seen as a main and realistic alleyway toward accomplishing sustainable improvement. The influence of the 'jade economy' is to achieve enhanced human being welfare as well as public fairness, while simultaneously diminishing ecological jeopardy and protecting environmental scarcity. The 'jade industry' transforms a developed and associated diligence sector via introducing further efficient, source prolific, and dependable utilization of untreated resources. Consequently, they furnish extra efficiency toward sustainable industrialized enhancement.

The jade industry is the zone strategy intended to recognize the jade economy as well as jade augmentation, and eventually, toward a sustainable progress improvement opportunity. Presently, there are numerous benefits for pursuing a jade industry approach. The jade industry offers a sensible alleyway in the direction of long-term fiscal improvement and sustainable improvement, thereby unbolting enterprise progress to their source production as well as ecological presentation and ascertaining a pioneering operation so as to deliver ecological cargo and armed forces (create green industry). This is indispensable from social, monetary, and ecological perspectives, particularly as Green diligence ropes:

9.4.1 Revenue and Employment Formation

Superior dissipate executives, projects, renewable liveliness, resurgence services, stipulation of other ecological possessions, and services create jobs and provide a resource of revenue, including for underprivileged communities with inferior formal proficiency levels.

9.4.2 Gung Ho and Sustainable Trade

Condensed outfitted outlay owing to the abridged consumption of supplies, vigor, and stream, as well as of minimization of dissipate and secretion generation, while assuring a link of trade in illumination of tapering consumer necessities meant for ecological and social revelation and recital.

9.4.3 Innate Resource Precautions

Condensed exploitation of irrigation, supplies and stimulates alleviation of the stress lying on the now scant resources, which are all anticipated to become scarcer in days to come if current inhabitant, urbanization, and improvement tendencies persist in the future.

9.4.4 Ecological Executive

Condensed generation of dissipates and emissions lessen the contamination encumberment on the innate ambiance and biodiversity.

9.4.5 Industrial and Chemical Protection

Enhance operation, sustain, and deal with flora that make use of chemicals maturely to pose less jeopardy to recruits and community.

9.4.6 Visual Aid the Lane

Jade industry canister is achieved by a quantity of concerted proceedings:

9.5 A. Greening of Diligence

Allows and props up the entire diligence despite their region, magnitude or location, to jade their operations, methods, and products to:

9.5.1 Exploit Resources Powerfully

Elevate the productive utilization of resources, water, and vigor in industrialized invention, by such approaches as: dematerialization of products with worthy manacles; utilization of resources by means of longer overhaul of natural life; surrogate of virgin resources with cast-off supplies; recycling, reclaiming, and revitalization of materials; use of supplies, water and vigor as sustainably administered and/or low impact sources.

9.5.2 Lessen the Generation of Waste and Emission

Lessen and wherever possible eradicate the formation of waste and emissions inside factory, by such approaches as: enhancement in the method of maintenance, monitoring, and operation; dissipate minimization; application of superior process technology with superior effectiveness as well as specificity; recycling, recuperation, and reclaiming of process rivulet.

9.5.3 Lessen Peril Allied with Chemical and (Perilous) Waste

Lessen peril allied with fabrication, make use of and dispose of chemicals, by such approaches as: sound executive of chemical; phasing out of venomous and other environmentally detrimental substances; relevance of the most excellent ecological practice and most excellent accessible modus operandi to prevent unintended formation and emissions of pop and further perilous poisons; proxy of chemical processes by non-chemical processes (biological, physical, etc); and substitution with safer, extra specific, and/or more effectual unconventional chemicals.

9.6 B. Construction of Jade Industries Ascertains and Enlarges (Innovative) Jade Industries That Furnish Ecological Freight and Services To

9.6.1 Diminish, Recycle, and Reprocess Waste Materials

Shore up industry to develop and deliver superior incorporated waste executives, reprocess and resource revival technology, services and systems, for saleable, civic, edifice, demolition, industrialized and other definite waste streams, and generate trustworthy materials of recycled supplies and products.

9.6.2 Improve Industrial Vigor Efficiency and Create Use of Renewable Vigor

Shore up industries to management systems, products, equipment, deliver technology, recognize services that augment industrialized vigor efficiency and the use of renewable vigor (bio and solar, etc.) or extra low carbon vigor sources (in fastidious waste warmth).

9.6.3 Accumulate, Cope, and Arrange (Perilous) Waste and/or Emissions Within Environmentally Compatible Traditions

Prop up industry on the way to develop and deliver technology, equipment, executive systems, products, be acquainted with how services accumulate, cope and arrange, devoid of threats to the atmosphere, (perilous) waste and/or emissions, counting for exemplar chemical electronic waste, curative waste, etc.

9.7 New Technologies

9.7.1 Why We Need Advanced Treatment

The utilization of conservative irrigation water and wastewater treatment processes has become even more challenging through recognition of increasing noxious waste, fast augmentation of inhabitants, and industrialized tricks along with declining ease of use of the stream resources because the waste matter of unusual secondary treatment shows tranquil restraint of 20–40 mg/L BOD, which might be abhorrent to several streams. Hovering solids, which accumulate and contribute to biochemical oxygen demand (BOD), might perchance reconcile on the torrent bed and inhibit the aquatic existence. The BOD of discharge in a tributary by a low stream is able to cause harm to aquatic existence by tumbling the dissolved oxygen content. In addition, the secondary effluent contains a considerable amount of dissolved solids and plant nutrients. If the dissipate water is of industrialized derivation, it might also retain traces of unrefined chemicals, heavy metals, and additional contaminants. Diverse methods are used within advanced dissipate treatments to gratify any of the numerous specific goals, which comprise the erasure of (1) venomous substances, (2) BOD, (3) hovering solids, (4) dissolve solids, and (5) plant nutrients. These technologies make the option available for better civic health and the milieu. The emphasis is positioned on their basic ideology, focal relevance, and narrative improvement. Advantages and drawbacks of this technology are compared to emphasize their modern confines and future research requests. It can be considered that, along with the emergent familiarity and the advances in industrialized diligence, the relevance of these technologies will be increased at an unprecedented scale. These treatment technologies may be introduced at any juncture of the treatment process, such as in the casing of industrialized watercourse or might be used for the entire deletion of contaminants subsequent to secondary treatment.

9.7.2 Automated Chemostat Treatment (ACT)

Automated Chemostat treatment is a description scheme in the handling of slush. This skill is flexible and simple to integrate; it is totally computerized, controllable,

and significantly more efficient than the existing practice. The systematic concept of automated chemostat treatment is the use of a suitable bacterial cocktail in support of a known category of tainted irrigation water to get a novel chemostat. The process is maintained within an affirmed balance of bacterial escalation and natural composite degradation. Because of the low concentration of bacterial cells, no aggregate is fashioned and each bacterium acts when a single cell boosts the surface vacant for the method and enables the biodegradation at a much superior effectiveness. The domino effect is an almost slush gratis output of water that can be returned straight to the milieu or advanced to the next process. Automated chemostat reduces COD, hydrocarbons, suspended solids, and TOC from oily waters and slippery, parting fine effluents below industry regulation levels. On the basis of a water sample from the refinery, ACT determines the most efficient solution to treat the specific refinery issue. The hydraulic age and the bacterial age become equal, requiring a lower density of single cell bacteria. This ACT operates as an unremitting flow reactor devoid of activated sludge. The bioreactor can thus be relevant on site, where using accessible infrastructure with high suppleness for intonation for the method saves considerably in effectual and continuation outlay.

Advantages

The advantages of this simplify the scheme by plummeting chemical treatment and bio sludge as well as reducing black sludge formation. Its litheness and modularity permit it to embrace low and high capacity contamination, be used for fresh and salt water, be simply modified, and have augment capability. Production is nearly sludge free, gathering the strictest disposal values. This trailblazing "green" process is effortless to change and can be used in diverse sites, including oil refineries, oil storage farms, contaminated reservoirs, drilling sites, marine ports, and storage tanks.

Full Control from Any Point for Every Point

The completely automated system comprises an assortment of online sensors that feed the management unit information on different parameters for instance: dissolved oxygen, TOC, nitrogen, TPH, and temperature. The regulators ensure the finest process balance is upheld among the additives, organic compounds, degradation flow rate, and bacterial growth.

Application

1. These technologies directly address the three focal disadvantages of predictable water treatments in refineries: initially, there is no necessity to reactivate bio slush.

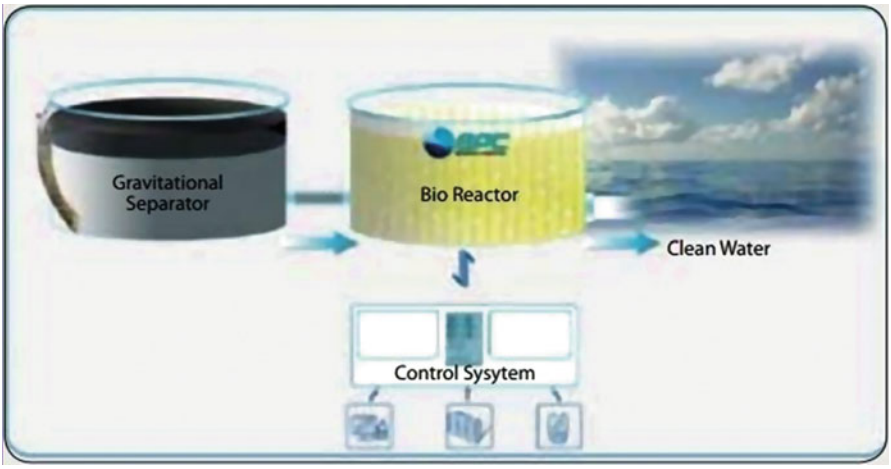

Fig. 9.2 Diagram for automated continuous flow system

2. ACT eliminates the requirement of the DAF process and saves time.
3. Productivity, which is practically sludge free, can be dumped directly in nature by tumbling bio slush sources and the creation of black slush, as well as adequately eradicating nitrogen. Its output meets the strictest discarding values, necessitating no further handling.
4. ACT offers a vastly effectual treatment of side torrent, which is regularly the origin of tragedy in conservative treatment processes. Side torrents impact the most, originate traffic jams, and further stern procedures.
5. It can be executed devoid of an inclusive extra treatment scheme.
6. Permits severance of heavily polluted rivulet and amplifies overall output.
7. Provides an efficient manner to rupture loss and PAH, eliminates oil, other organics, and phenols.
8. The patented process exploits inimitable bioremediation technology to trim down COD, hydrocarbons, TOC, and suspended solids from oily waters and slippery departure effluent of high quality reunion stringent industry values.
9. The bioreactor can be functional on-site (using the available infrastructure) owing to its elevated litheness in process intonation. This spectacularly lessens the equipment and maintenance outlay (Fig. 9.2).

9.7.3 Membrane Bio Reactor (MBR)

Membrane Bio Reactor (MBR) technology is based on the array of predictable activated mire handling together with a course of action filtration by a membrane with a pore volume between 10 nm and 0.4 microns (micro/ultra filtration), which

allows mire division. The membrane is a hurdle that retains all particles, colloids, bacteria, and viruses of treated irrigation water. Also, it can operate at upper concentrations of mire (up to 12 g/l as an alternative of the standard 4 g/l in predictable systems), which significantly reduces the volume of the reactors and mire formation. Although there are currently two leading procedure configurations of biomass rebuff MBRs, side stream (SMBR) and underwater or engrossed (IMBR), the engrossed configuration is the most extensively used in community wastewater solutions owing to the inferior related outlay of operation. Here, the component is located directly in the process reservoir and is therefore less energy intensive, while as an end result, it is only compulsory to generate a trivial vacuum within the membrane component, considered as trans membrane pressure (TMP) for filtration.

In support of the absorbed configuration, mostly two types of profitable membrane modules are obtainable: flat sheets (FS) and hollow fibers (HF). Hollow fibers permit a higher packing density due to thinner spaces among membranes compared to flat sheets. Nonetheless, these make it further vulnerable to membrane congestion and/or sludging, and it can also make crackdown extra tricky. The membrane materials used for an IMBR are fluorinated and sulfonated polymers (polyethersulfone, polyvinylidene, difluoride in fastidious), which dominate in saleable membrane MBR products. It is indispensable to cram the mechanism and factors that contribute to membrane fouling in MBR. Normally, these factors have been classified in four discrete groups: nature of the sludge, operating parameters, membrane/module characteristics, and feed wastewater.

9.7.4 Membrane Filtration

It involves the running of water containing impurities across a membrane. Running water pervades all the way through the membrane into a divided conduit for improvement. Because of the cross-flow collection of water and the overwhelming ingredients, resources at the back do not move up to the membrane surface but are passed out of the system for adjusted recovery or elimination. The watercourse transitory in the membrane is called pervade, although the water with more concentrated materials is called the concentrate or retentate (Fig. 9.3).

Membranes are constructed of roughage or other polymer matter, by means of a highest pore size put down during the industrialized process. It is necessary that the membranes elude passage of particles the size of microorganisms, or about 1 micron (0.001 millimeters), and therefore that they remain in the process. This means that the MBR system is fine for eradication of solid materials, but the deduction of a liquefied wastewater apparatus must done and facilitated by means of the accompanying management steps.

Membranes can be configured in a number of ways. For membrane application, two configurations are primarily frequently used for hollow fiber groups in bundles, as revealed in Fig. 9.4. The hollow fiber bundles are connected by manifolds in the unit so as to be calculated for easy alteration and service. This type of membrane

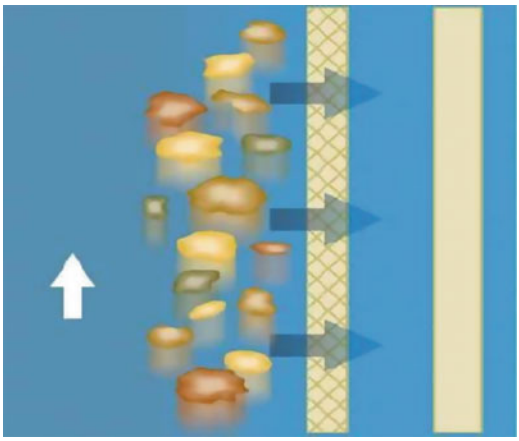

Fig. 9.3 Diagram for membrane filtration process

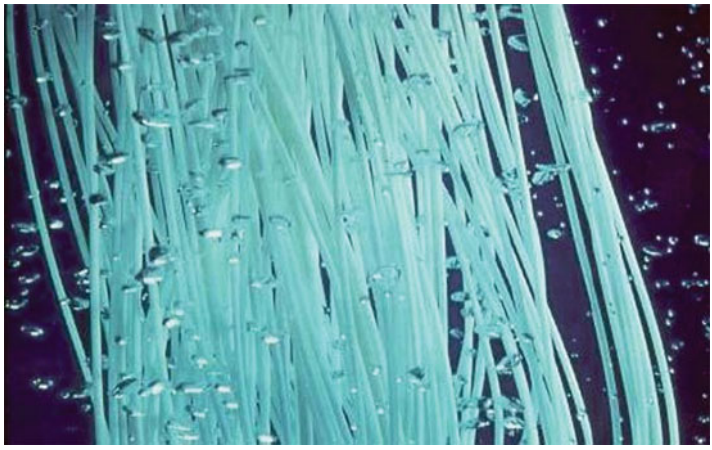

Fig. 9.4 Diagram for hollow-fiber membrane system

existence can be achieved, or even improved on, for 10 years. On the subject of permeability, a correlation of permeability loss and operation time was established from research, demonstrating that the membrane permeability reaches a nonoperative value after 7 years of operation (Sebastian et al. 2011).

9.7.5 Wet Air Oxidation (WAO)

In the aqueous industrial treatment, the misuse of effluents is a considerable and necessary procedure, with several techniques employed. WAO is one of the

available technologies for the management of aqueous wastewaters. In wet air oxidation, aqueous waste is oxidized in the liquid phase at high temperatures (400–573 K) and pressures (0.5–20 MPa) in the presence of an oxygen containing gas (usually air). This technology consists of techniques to heat transfer and the use of both homogeneous and heterogeneous catalysts to enhance reaction rate. WAO is a hydrothermal process suitable for the oxidation of organic and inorganic components or pollutants in aqueous misuse streams. High hotness and eminent pressure are requisite, commonly operated inside the superheated water range (<300 °C, <20 MPa). Usually, the higher the hotness, the higher the level of oxidation achieved, and the connected requirement of pressure is essential to maintain the fluid state. Oxygen limited pressure and residence time is also crucial to the degree of oxidation. Residence times can variety from seconds to hours depending upon the nature of the material to be oxidized, and obviously limited to the most difficult components to corrode when bearing in mind complex mixtures, such as industrial and municipal misuse streams.

Wet Air Oxidation of Wastewater Slush

In misuse water treatment, the primary use of alum (or alternatively ferric salts) is as a coagulant or as a phosphate precipitant, via formation of insoluble aluminum phosphate. Alum and phosphates may therefore be alienated from the fluid aqueous watercourse by WAO as a considerable economic benefit to this procedure. The organic module of the mire is significant in terms of proportion and overall quantity, and amongst other criteria it is essential to be detached from the aqueous watercourse. The analysis of COD provides a suitable measure of the organic matter. A primary benefit of this method is a considerable reduction in COD of the fluid output (Paul et al. 2012).

WAO Process

We recognize that wet air oxidation is the oxidation of soluble or perched gears in water using oxygen as the oxidizing agent (Fig. 9.5).

Features & Benefits

1. Pretreatment of high force wastewater to create eco-friendly residual organics.
2. Low operating costs and minimal air toxic waste discharges.
3. Destruction of specific compounds.
4. Removal of toxicity or reactivity.
5. Procedure fluid treatment for recycling/recovery.
6. Gross reduction of chemical oxygen demand (COD).

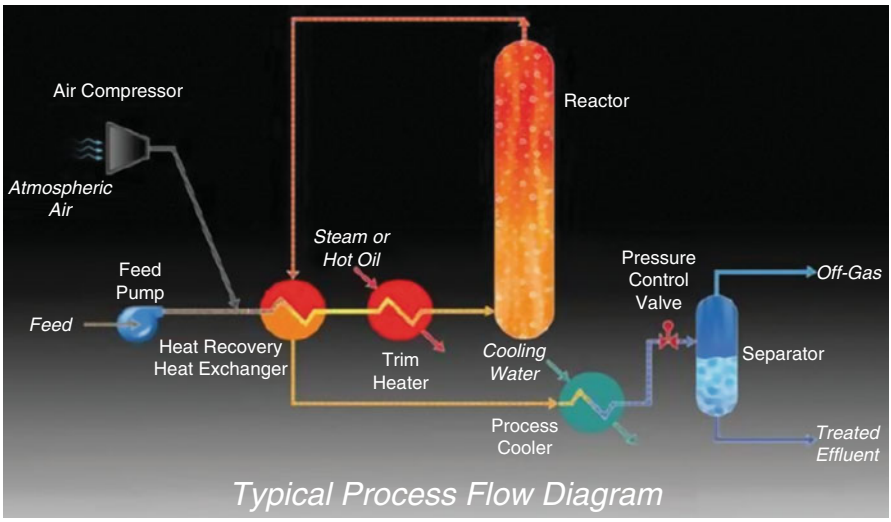

Fig. 9.5 A typical flow diagram of wet air oxidation process

Disadvantages

1. Elevated capital costs.
2. Safety implication connected with a scheme in action by such rigorous in service circumstances.
3. In the design of the procedure, equilibrium has to be reached connecting the improvement of the reaction rates with hotness and pressure adjacent to their consequences on capital cost and operational difficulties, such as deterioration and scaling of apparatus.

Application

1. Treatment of towering strength wastewater, comprises tired caustic streams create by ethylene off rockers and refineries.
2. In method, for treatment and recycling/recovery of procedure fluid streams.
3. Biological mire conditioning and demolition.

9.8 Technology Classification

Membrane separation is currently exploited as a support or surrogate planned for habitual watercourse and wastewater treatment technology, such as biological filtration or corporeal and chemical solutions. They are rapidly gaining acceptance all over the planet, and for the most part the victorious and reasonably priced water

Table 9.1 Taxonomy of membrane-based water filtration

	Membrane type	Configuration	Material
Membrane	Microfiltration (MF)	Pipe-shaped membranes: capillary, hollow fiber or tubular plate-shaped membranes: flat plate or spiral	Organic (Polymeric)
	Ultrafiltration (UF)	Plate-and-frame, spiral-wound, and tubular	Inorganic (Mineral)
Applications	Water Treatment (incl. Desalination) and Wastewater Treatment		
End users	Industries, Municipalities and communal applications, Desalination plants		

treatment schemes are easy to get to (Pall Corporation 2015). At first membrane separation was used for grounding of procedure water, though its services have expanded owing to its merit within wastewater solutions and intake water decontamination practices by means of the plan to retain microorganisms in desalination and irrigation water softening. Membrane separation is based on discerning filtration by pores of different sizes and consists of four leading membrane types: reverse osmosis, ultrafiltration, nanofiltration, and microfiltration. Every part of these types are disparate particles from the nourished watercourse. Ultra- and microfiltration is deployed generally for particle removal, while reverse osmosis along with nanofiltration is used for desalination and softening. Membranes for water filtration differ within stipulations of aperture size. The smaller the aperture, the greater the applied pressure disparity must be to squash the water course through the membrane. Relatively bulky particles can be alienated through ultra- and microfiltration. However, particularly in the cases of desalination andsoftening, there are minor particles which require exclusion. During such situations, the most appropriate solution is to deploy reverse osmosis or nanofiltration. These membranes are not permeable resources with defined pore size; however, the homogeneous polymer layer retains assured substances owing to their particular formation. The technology taxonomy of membrane-based water filtration is summarized in Table 9.1

9.8.1 Membrane-Based Technology

9.8.2 Membrane Filtration Systems

Membrane systems are crucial to the enlargement of superior water retrieval systems, and the progress of innovative and enhanced systems is predicted to continue. Engrossed micro- and ultrafiltration membranes afford an admirable pretreatment for RO, which can eliminate an extensive array of liquefied ingredients. Besides, the growth of membrane filtration systems have lead to the

improvement of both highly developed water treatment technologies and MBRs, which are swiftly attracting the diligent workhorse of water repossession.

Among MBRs, residence times of natal solids are augmented, making probable extra biological treatment and the upholding of pathogens; treatment by means of MBR produces an extremely elucidated effluent that can be merely sterile. Consequently, treatment with MBR is ideal for turning out non drinkable water. In favor of the retrieval of filtered water, MBR has to be followed by UV and RO treatments (Tao et al. 2005, 2006).

9.8.3 Ultra Filtration

Ultrafiltration is a contemporary water and wastewater filtration tool that has a low pressure-driven membrane, which is tremendously effectual with the supplementary benefit of low energy utilization (Van der Vegt and Iliev 2012). It is a membrane that allows particles smaller than 20 nm to go through it and the aperture sizes vary between 20 nm and 0.1 microns. The function of this membrane system is escalating in the water and wastewater treatment sector and in industrial process severance. A few of the key applications for these membrane systems are in desalination, pretreatment processes, ingestion water treatments, and membrane bioreactors. In the industrialized sector, some definite preferences exist, for instance, as an emphasis on admirable pH and temperature resistance. A stipulation for low foul propensity of filter is also an imperative, even though it is not specifically insisted on in industrial processes. The key applications for these membrane systems are in the victuals and beverage quarter (including a strong stipulation in the dairy industry on behalf of such products), the attention of macromolecules in biotech, the fabrication of ultrapure water for microelectronics, in general industrial wastewater treatment, and oil emulsion waste (Synder Filtration 2015). These membranes are fashioned via assorted suppliers among precise configurations that depend on the contour and material of the membrane. These configurations have a specific use and that is accompanied by advantages and disadvantages. The most crucial influence of the configuration is the mechanical stability on the system and requisite hydrodynamic and fiscal constraint. These membrane module approaches are in capillary or hollow fiber configurations (pipe-shaped membranes), tubular, frame or spiral wound configurations (plate-shaped membranes), and plate. For a spiral wound, towering purity water and capillary configurations would typically be used (Lenntech 2015). The optimization of the system depends mostly on the power consumption, flow velocity, membrane fouling, pressure drop, and module cost (Dhawan 2014). In addition, there are several set ups for the identification of specific membrane configurations. The most frequently used methods incorporate dead end and cross flow filtration setups. The permutation of both dead end and cross surge also represents an achievable type for the filtration process. The forth probable set up is the filtration chamber with suffused membrane filter. This method was initially urbanized for both ultra- and microfiltration through wastewater treatments where the membrane, in

combination with the chamber/reservoir, is fashioned as a membrane bioreactor (MBR). The current most accessible assortment of MBR systems use suffused membranes (Rippenger 2009).

9.8.4 Nanotechnology

Additional staged enhancements are viable in the near future (Tchobanoglous 1981). The notion is humans probed for advancement of the theater membranes through less polluted characteristics, enhanced hydraulic conductivity, and more discriminating denial/transport characteristics. Progress in RO technology includes enhanced membranes with configurations, extra efficient pumping and vigor revival systems, and the progress of process technology, such as membrane distillation (Shannon et al. 2008). Nanofiltration provides a better filtration than ultrafiltration; however, it is as a rule referred to as free reverse osmosis (RO) because of its membrane pore structure. The structure of the membrane is comparatively large when compared to RO membranes, and unlike them, it allows the passage of salts (Rippenger 2009). Nanofiltration membranes have pores with a measurement of around 1–5 nm and the molecular weight cut off for a typical membrane mendacity between 150 and 500 Dalton. Nanofiltration applications are frequently used to tackle organic contaminants and some inorganic salts as they can keep ions and low molecular weight organics. The membranes have more radically advanced water permeability than that of reverse osmosis (RO), which operates at much lower pressures. Owing to its lower energy use and higher flux rates, nanofiltration might replace RO in numerous applications (Shon et al. 2013).

To tackle macrobiotic contaminants in freshwaters, nanofiltration membrane systems are also used for the concentration of dyes, sugars, and other substances. There are a number of developed applications using nanofiltration because it is moderately frequent in the textiles, dairy and food sectors, and in chemical processing; although, the principal applications continue to be in the treatment of wastewaters, fresh processes, and desalination pretreatments (Sutherland 2009). Analogous to ultrafiltration, there are also different shapes of nanofiltration membranes, such as tubular, spiral or flat.

9.8.5 Mechanical Variable Filtration Technology

This technology affirms the treatment used and intended for wastewater handling in which a growing gush of influent is cleaned by a downward gush of sieve media. Throughout the treatment procedure itself, the sieve media is cleaned by the filtered influent; hence, there is no necessity for any bonus sieve media cleaning or fresh water. The automatic variable filtration method consists of double sets of sieve media that can be operated in string or analogous. The two juncture string

configuration is used to turn out incredibly excellent filtrate. This style is ideal for distillation of secondary wastewater for reuse. The automatic variable filtration procedure is operational with actuated valves, sensors, and programmable sense organizers to mechanically change from a serial manner to analogous mode throughout soggy weather circumstances or other preset working situations.

The input benefits of the scheme are:

- Incessantly clean media bed.
- Higher solids capacity.
- Even gush allocation.
- Outlay effectual to inaugurate, low operating and prolongation costs.
- Average reject of 5–15%.
- Easy operation & maintenance.
- Elimination of ancillary equipment.
- Extremely low power consumption.

9.8.6 Reverse Osmosis (RO)

Reverse osmosis is a type of membrane division that uses pressure to compel a solution through a membrane so as to retain the solute and allow the clean solvent to pass to the other side. In general, this membrane deliberately allows water to pass through even as the solutes (for example salt ions) are being separated. It is proficient at sorting out viruses, dissolved solids, bacteria, and other elected dissolved substances and is chiefly used for the desalination of seawater (Bakalar et al. 2009; Frost and Sullivan 2013). The reverse osmosis (RO) membrane is in essence nonporous, and it preferentially passes liquid and retains the majority of the solutes, including ions (Shon et al. 2013). Reverse osmosis and electro dialysis emerged collectively as new technologies in the second half of the twentieth century; they became alternatives to the commonly used techniques of evaporation and distillation. Since then, there have been a number of advancements in most important technologies, including membrane distillation, low temperature distillation, pressure retarded osmosis, graphene membranes, and bio mimetic (International desalination Association 2013).

9.8.7 Microbial Fuel Cells

For microbial stimulate cells, a prospective advanced technology, electrical vigor naturally occurs in the dissipate stream by means of electron transfer to detain the vigor produced by microbes designed for metabolic processes (Kim et al. 2008; Logan et al. 2006). Initially, microbes are matured as a bio film lying on an electrode; the electron contributor is alienated from the electron acceptor by proton barter

membranes, which ascertain an electrical current. Electrical energy is subsequently generated by the corrosion of organic matter. This technology is stable in the stage of improvement and noteworthily advanced in practice. The efficacy and economics are indispensable; it has the potential to create electrical energy directly from organic themes in the waste rivulet.

9.8.8 Innovative Municipal Hygiene Technology

The new municipal hygiene technology intends wastewater treatment by reuse of vigor and mineral deposits with an amalgamation of electroflocculation and anaerobic digestion technology. Electroflocculation treatment is based on severance of the organic contamination from population wastewater through electrocoagulation. The organic slush of the electrocoagulation reactor is made up of sediments in a globular sedimentation store; the slush is subsequently fed to an anaerobic reactor to get renewed biogas, which can be rehabilitated into vigor for captive exploitation. Anaerobic fermentation technology produces optimum biogas owing to two detached processes of hydrolysis, where the long carbon chain complex is wrecked into smaller complexes, for instance, fatty acids and methanogenesis, and the fatty acids get transformed into biogas.

9.9 Innate Treatment Schemes (ITSs)

The foremost basic consideration and depiction of the process of innate treatment schemes (ITSs) is also humanizing and enables us to use the innate process and to develop water excellence (Kadlec and Knight 1996). ITSs use a range of biological, physical, and chemical processes concomitantly to confiscate a wide array of noxious wastes. For instance, this scheme is increasingly being used to detain, maintain, and treat tornado water, thereby converting this “nuisance” attached to a precious source of water. These innate views have the benefit of being capable of eradicating a wide assortment of micro pathogens, constituents, counting nutrients, and noxious wastes. They have long proven to be effectually designed for the treatment of potable water; ITSs are increasingly being used for water retrieval.

9.9.1 Analytical Dissipate

Analytical processes vary in the quantity of dissipate created. The greenest methods produce no dissipate or create merely a diminutive volume of dissipate (Keith et al. 2007). Commonly, the more steps in an analytical scheme, the more reagents consumed, and the higher the volumes of analytical dissipate. Therefore, diminution

in the use of reagents by the techniques discussed above contributes to lessen the manufacture of dissipate. An additional imperative issue is ensuring the appropriate treatments of analytical dissipate. The toxicity of dissipate may be condensed during recycling, degradation, and passivation of dissipate, preferably executed on the line (Garrigues et al. 2010).

9.9.2 Coke Oven (CO) by Product Wastewater Treatment

In India, steel producing plants use this treatment method to convalesce ammonia from coke ovens. Water contamination trouble would subsist if ammonia is not recovered, which is the main contaminate amongst all dissipates from production. In the CO effluent, the majority of the contaminants are liquefied. Additional contaminants are subjected to biological treatment along with residues of phenol and ammonia. The two main processes frequently used for the treatment of coke oven effluents are dribble filter and the activated slush process.

9.9.3 Urine Unraveling Method

Urine is a division of familial wastewater which contains 50% phosphorus and 90% nitrogen. The upgrading of urine unraveling toilets and technology for treating it create compost products that are key for managing nutrients with minimal necessities for exterior assets, for example, additional energy. To produce the identical quantity of fuel based on nitrogen rich fertilizer takes a huge quantity of vigor and nonrenewable resources. Urine unscrambling toilets have already been developed, and advanced research is also going on to further refine and utilize them for wastewater management and creating resources.

9.9.4 Root Zone Treatment

1. Handling of familial wastewater, especially for petite towns, hotels, resorts, rural community, hostels, etc., is effortlessly probable and affordable because it engrosses maintenance cost, low capital, and operation.
2. Root zone treatment canisters also treat eco-friendly built-up effluents, especially effluents from agro based industries, such as those seen at Kids Leather (Tannery effluent), the Chennai CPCB project at Mother Dairy, and the Delhi and Industrial effluent of Proctor and Gamble at Bhopal.
3. Root zone treatment can be applied in Urban Watershed Management by treating the exposed nullah in a decentralized manner and in receipt of the treated dissipates either for dilution purposes or irrigation.

9.9.5 Water Hyacinth Eco-Technology

This technology provides outlaying effectual solutions to dissipate water issues in many precise areas (Trivedy 1998). This is based on waste treatment and was endeavored in Singapore, Malaysia, the US, India, and Japan. India initially designed some for 2–5 years with most studies coming from the United States. Victorious pilot projects are familiar (Mandi 1994; Brix and Schierup 1989). The treatment of wastewater by water hyacinth has been effectively executed by the conurbation of San Diego, USA, to generate an indulgence waste matter quality standard that would be estimated from advanced secondary treatment methods. Current research efforts have exposed that this technology exploits wastewater treatment in universal dispersion. Conventionally, it was used merely for sewage treatment and a few industrial diverse types of dissipate and chemical species are employed for treatment by means of water hyacinth. This technology has shown promise in elimination of venomous organic dissipate, including almost all metals and radioactive dissipate. It has emerged that the plant has a notable capacity to confiscate an exceptionally wide range of substances and a large number of them are yet to be tested.

It is being used in amalgamation with other flora to obtain enhanced recital. Aquatic fish culture is being increasingly used in hyacinth treated water; algal control in water after secondary treatment is furthermore accomplished by water hyacinth. In tremendously underprivileged countries, where water course paucity is acute and hygiene is appallingly low, particularly in rural areas, water hyacinth can be used to make clean water points depleted of waste available. It is also proposed not merely as a water sterilizer but also to generate income for the rustic poor (Trivedy and Thomas 2005).

Biomass operation ought to be a crucial part of the hyacinth based method. It is imperative to recognize economical methods for the discarding and/or exploitation of the large quantity of solids that can be spawned by the water hyacinth treatment process. The microbial environmentalism of hyacinth-based systems, in particular the role of poised and attached escalation, needs to be investigated in detail.

The design parameters developed require validation in miscellaneous situations for diverse kinds of dissipates. Superior effectiveness during microbial growth/higher augmentation of the plant or through additional processes ought to be attained to trim down desired areas. The water hyacinth-based system has shown great promise as a low-cost and efficient water purifier, and its relevance is mounting worldwide.

Initially, it was only used for sewage treatment and now is used in treatment of a broad range of chemical substances. Nowadays, it is a great contributor to the solution of numerous desires akin to raw material for various industries, especially for the rustic poor, milieu protection energy, water furnishing, and fertilizer. The full potential of this plant is yet to be tapped.

9.10 New Technology in Water Handling

According to the most recent third world Academy of Sciences report, of the six billion inhabitants on the globe, in excess of one billion (one in six) do not have access to safe drinking water, and 2.5 billion (more than one in three) do not have access to satisfactory sanitation sources. Today, 31 countries representing 2.8 billion inhabitants, including India, Nigeria, China, Ethiopia, Peru, and Kenya, confront unremitting water problems. Within a generation, the population of the earth will be close to eight billion people, yet the amount of water will be the same. Therefore, we have to discover newer, better ways to treat, recycle, and save the water.

New Approaches

1. Shielding accessible water resources and inventing effectual ways to trim down water utilization for different human uses.
2. New affordable reverse osmosis for desalination.
3. Recycle akin to the gray water that can be used to recharge groundwater to assist in curtailing the salinity levels and to improve the health of swampland.
4. Effective water harvesting.

Method Forward

The new treatment processes for resource revival along with the toting up of metropolitan water and waste management methods will help develop the sustainability of our water resources. The new technologies can significantly lessen water abstraction from our resource constrained world. Retrieving water must be managed suitably to sustain the integrity of the overall treatment system. The vigor utilization in treatment plants also requires active administration to make the complete process efficient and effective. Technologies to meet this challenge before now subsist and work is going on to transform and incorporate them into superior performing, more sustainable systems. The challenges are choosing the appropriate one from the obtainable options and emergent institutional planning for executing them in the most efficient ways.

9.11 Conclusion

Presently, financial crunch in numerous urbanized and developing nations is forcing the execution of low-cost natural and green technological treatment systems for domestic and industrial wastewater solutions. When the technical treatment amenities are installed in many developing countries, the force input is complicated to supply in view of the worldwide energy emergency and its affordability is questionable due to very high outfitting costs. These factors are spurring the employment of environmental engineering ethics for not only misuse solutions but also for conserving biological communities in deprived nations of the globe.

Over the past two decades, ecological regulations have become more stringent, requiring an enhanced quality of manufacturing wastewater effluent. The great number of studies reviewed here is indicative of the extensive and intense investigation that has been done in the field of manufacturing wastewater solutions. These studies cover a broad range of manufacturing pollutants, a broad range of solution technologies, and model solutions with entity substances in genuine effluents containing a combination of diverse importunate substances.

The selection of the most appropriate treatment for industrial wastewater depends primarily on its characteristics and on numerous other parameters, such as ease of use and testing of the technology, pollution control, environmental impact, the overall recital, plant simplicity, experience technologies, and economic parameters, including the capital investment and operational costs. Although a systematic modus operandi exists consisting of model substances prior to stuffing the authentic wastewater, and appraises toxicity and biodegradability throughout and after the degradation process, more pilot-plant scale trials with real industrial wastewater must be executed on a larger scale.

The innovative incorporated technologies entail appraising the absolute wastewater treatment in sequence to be reused in the industry itself. Auspiciously, a lot of technology to meet these demands already exists, and effort is being done to sanitize and incorporate them into the higher theater of further sustainable systems. These are all vicinities in which engineers excel. The companion challenge will be choosing amongst the accessible options and developing institutional planning for putting them into operation in the most effective ways.

This is where we will require aid from other vocations. Permutations and intergradations of a technology were able to treat a broad assortment of high potency and noxious industrials. Such intergradations of treatment technologies can shift the exemplar of wastewater management from treatment and discarding to beneficial consumption and lucrative endeavors.

Acknowledgement The Author Dr.T.Vasantha gratefully acknowledges UGC-PDF, New-Delhi for financial assistance under the scheme Sc/St Post-Doctoral Fellowship for the year 2017-18, No. F./31-1/2017/PDFSS-2017-18-AND-16194.

References

Aithal PS (2015a) Concept of ideal business & its realization using e-business model. Int J Sci Res (IJSR) 4(3):1267–1274. ISSN -2319-7064

Aithal PS (2015b) Mobile business as an optimum model for ideal business. Int J Manag IT Eng (IJMIE) 5(7):146–159. ISSN: 2249-0558, I.F. 5. 299.

Aithal PS (2015c) Concept of ideal banking and realization of it using ubiquitous banking. In: Proceedings of national conference recent trends in management, IT & Social Science, SIMS, Mangalore, 12th, pp 205–213, ISBN: 978-81-929306-7-1

Aithal PS, Aithal S (2015a) Managing anticipated breakthrough technologies of 21st century – a review. Int J Res Dev Technol Manag Sci 21(6):112–133. https://doi.org/10.5281/zenodo.61617

Aithal PS, Aithal S (2015b) An innovative education model to realize ideal education system. Int J Sci Re Manag (IJSRM) 3(3):2464–2469. https://doi.org/10.5281/zenodo.61654
Albadarin AB, Collins MN, Naushad M et al (2017) Activated lignin-chitosan extruded blends for efficient adsorption of methylene blue. Chem Eng J 307:264–272. https://doi.org/10.1016/j.cej.2016.08.089
Anastas PT (2007) Introduction: green chemistry. Chem Rev 107:2167–2168. https://doi.org/10.1021/cr0783784
Anastas PT, Kirchhoff MM (2002) Origins, current status, and future challenges of green chemistry. Acc Chem Res 35(9):686–694. https://doi.org/10.1021/ar010065m
Anastas PT, Warner JC (eds) (1998) Green chemistry: theory and practice. Oxford University Press, Oxford. https://trove.nla.gov.au/version/45703783
Anastas PT, Williamson TC (1996) In green chemistry: designing chemistry for the environment. American Chemical Series Books, Washington, DC
Awual MR, Eldesoky GE, Yaita T et al (2015) Schiff based ligand containing nano-composite adsorbent for optical copper(II) ions removal from aqueous solutions. Chem Eng J 279:639–647. https://doi.org/10.1016/j.cej.2015.05.049
Bakalar T, Bugel M, Gajdosova L (2009) Heavy metal removal using reverse osmosis. Acta Montan Slovaca 14:250–253
Berrone P, Fosfuri A, Gelabert L, Gomez-Mejia LR (2013) Necessity as the mother of 'green' inventions: institutional pressures and environmental innovations. Strateg Manag J 34(8):891–909. https://doi.org/10.1002/smj.2041
Brix H, Schierup H (1989) The use of aquatic macrophytes in water pollution control. Ambio 18 (2):100–107
Cheng TW, Lee ML, Ko MS, Ueng TH, Yang SF (2012) The heavy metal adsorption characteristics on metakaolin-based geopolymer. Appl Clay Sci 56:90–96. https://doi.org/10.1016/j.clay.2011.11.027
Colling AV, Oliveira LB, Reis MM, da Cruz NT, Hunt JD (2016) Brazilian recycling potential: energy consumption and Green House Gases reduction. Renew Sust Energ Rev 59:544–549. https://doi.org/10.1016/j.rser.2015.12.233
Corder GD, Golev A, Giurco D (2015) "Wealth from metal waste": translating global knowledge on industrial ecology to metals recycling in Australia. Miner Eng 76:2–9. https://doi.org/10.1016/j.mineng.2014.11.004
Dangelico RM, Pujari DJ (2010) Mainstreaming green product innovation: why and how companies integrate environmental sustainability. J Bus Ethics 95:471–486. https://doi.org/10.1007/s10551-010-0434-0
Dhawan G (2014) About ultrafiltration. Applied Membranes Inc., Vista
Frost & Sullivan (2013) CEO 360 degree perspective on the global membrane- based water and wastewater treatment, Mountain View
Garrigues S, Armenta S, de la Guardia M (2010) Green strategies for decontamination of analytical wastes. Trends Anal Chem 29:592–601. https://doi.org/10.1016/j.trac.2010.03.009
Guoliang W (2011) A new concept of green education: the cultivation model for successful and practical talents. Int Forum Teach Stud 7(1):45–48
Gutha Y, Munagapati VS, Naushad M, Abburi K (2015) Removal of Ni(II) from aqueous solution by Lycopersicum esculentum (Tomato) leaf powder as a low-cost biosorbent. Desalin Water Treat 54:200–208. https://doi.org/10.1080/19443994.2014.880160
Han W, Liu LC (2009) Discussion on Green Education in Universities. J Daqing Norm Univ 1:39
Hasper M (2009) Green technology in developing countries: creating accessibility through a global exchange forum. Duke Law Technol Rev 7(1):1–14
Hekkert MP, Negro SO (2009) Functions of innovation systems as a framework to understand sustainable technological change: empirical evidence for earlier claims. Technol Forecast Soc Change 76:584–594. https://doi.org/10.1016/j.techfore.2008.04.013
International desalination Association (2013). http://idadesal.org/desalination-101/desalination-overview/

Javadian H, Angaji MT, Naushad M (2014) Synthesis and characterization of polyaniline/γ-alumina nanocomposite: a comparative study for the adsorption of three different anionic dyes. J Ind Eng Chem 20:3890–3900. https://doi.org/10.1016/j.jiec.2013.12.095

Jhansi S, Mishra S (2013) Wastewater treatment and reuse: sustainability options. Consilience J Sustain Dev 10(1):1–15

Kadlec RH, Knight RL (1996) Treatment Wetlands. CRC Lewis Publishers, Boca Raton

Karthikeyan T, Rajgopal S, Miranda LR (2005) Chromium(VI) adsorption from aqueous solution by *Hevea brasiliensis* sawdust activated carbon. J Hazard Mater B 124:192–199. https://doi.org/10.1016/j.jhazmat.2005.05.003

Keith LH, Gron LU, Young JL (2007) Green analytical methodologies. Chem Rev 107:2695–2708. https://doi.org/10.1021/cr068359e

Kim IS, Oh BS, Hyun HW (2008) Moving desalination forward. Proceedings of the Singapore international water week water convention, Singapore, pp 25–26

Lenntech (2015) Tubular-shaped membranes. http://www.lenntech.com/tubularshaped-membranes.html

Logan BE, Hamelers B, Rozendal R, Schroder U, Keller J, Freguia S, Aelterman P, Verstraete W, Rabaey K (2006) Microbial fuel cells: methodology and technology. Environ Sci Technol 40 (17):5181–5192

Luken R, Van Rompaey F (2008) Drivers for any barriers to environmentally sound technology adoption by manufacturing plants in nine developing countries. J Clean Prod 16(1):67–77

Mandi L (1994) Marrakesh wastewater purification experiment using vascular aquatic plants Eichhornia Crassipes and *Lemna Gibba*. Water Sci Technol 29(4):283–287. https://doi.org/10.2166/wst.1994.0210

Marshall FM, Holden J, Ghose C, Chisala B, Kapungwe E, Volk J, Agrawal M, Agrawal R, Sharma RK, Singh RP (2007) Contaminated irrigation water and food safety for the urban and peri-urban poor: appropriate measures for monitoring and control from field research in India and Zambia, Incpetion Report DFID Enkar R8160, SPRU, University of Sussex

Martin-Lara MA, Blazquez G, Trujillo MC, Perez A, Calero M (2014) New treatment of real electroplating wastewater containing heavy metal ions by adsorption onto olive stone. J Clean Prod 81:120–112. https://doi.org/10.1016/j.jclepro.2014.06.036

Massoud MA, Tarhini A, Nasr JA (2009) Decentralized approaches to wastewater treatment and management: applicability in developing countries. J Environ Manag 90(1):652–659. https://doi.org/10.1016/j.jenvman.2008.07.001

MEA (2005) Millennium ecosystem Assessment (MEA), ecosystems and human wellbeing: synthesis. Island Press, Washington, DC

Metcalf and Eddy (1991) Wastewater engineering: treatment, disposal and reuse, 3rd edn, revised by George Tchobanoglous and Franklin L. Burton, McGraw Hill (2018) Inc. International IOP conference series: earth and environmental science. https://doi.org/10.1088/1755-1315/150/1/012013

Nabi SA, Bushra R, Al-Othman ZA, Naushad M (2011) Synthesis, characterization, and analytical applications of a new composite cation exchange material acetonitrile stannic(IV) selenite: adsorption behavior of toxic metal ions in nonionic surfactant medium. Sep Sci Technol 46:847–857. https://doi.org/10.1080/01496395.2010.534759

Narmadha D, Selvam Kavitha VJ (2012) Treatment of domestic waste water using natural flocculants. Int J Life Sci Biotechnol Pharm Res 1(3):2250–3137

Pall Corporation (2015) Fundamentals of water processing. http://www.pall.com/main/water-treatment/fundamentals-of-water-processing8163.page

Parkinson J, Tayler K (2003) Decentralized wastewater management in periurban areas in low-income countries. Environ Urban 15(1):7590. https://doi.org/10.1177/095624780301500119

Paul MR, McKay KJ, Tallon SJ, Catchpole OJ, Mollenhauer T (2012) Wet air oxidation of waste water sludge. A.C.T.: Engineers Australia, Barton, pp 953–960. ISBN 9781922107596

Pawar Avinash Shivajirao (2012) Treatment of distillery wastewater using membrane technologies. Int J Adv Eng Res Stud 1(3):275–283. E-ISSN2249–8974

Pujari D (2009) Eco-innovation and new product development: understanding the influences on market performance. Technovation 26:76–85. https://doi.org/10.1016/j.technovation.2004.07.006

Rippenger S (2009) Anwendungen der Mikro- und Ultrafiltration zur Wasseraufbereitung. F & S Filtrieren und Separieren Nr 5(23):246–252

Schaum C (2016) Abwasserbehandlung der Zukunft: Gesundheits-, Gewässer- und Ressourcenschutz, Habilitation. Schriftenreihe IWAR, 233. Verein zur Förderung des Instituts IWAR der TU Darmstadt e.V., Darmstadt

Schaum C, Cornel P (2016) Abwasserbehandlung der Zukunft: Gesundheits-, Gewässer- und Ressourcenschutz. Österreichische Wasser- und Abfallwirtschaft 68:3–4. https://doi.org/10.1007/s00506-016-0296-5

Sebastian D, Rafael V, Enrique G, Miriam, M (2011) Aerobic membrane bioreactor for wastewater treatment – performance under substrate- limited conditions. https://doi.org/10.5772/17409

Shahat A, Awual MR, Khaleque MA et al (2015) Large-pore diameter nano-adsorbent and its application for rapid lead(II) detection and removal from aqueous media. Chem Eng J 273:286–295. https://doi.org/10.1016/j.cej.2015.03.073

Shannon MA, Bohn PW, Elimelech M, Georgladis JG, Marias BJ, Mayes AM (2008) Science and technology for water purification in the coming decades. Nature 452(20):301–310. https://doi.org/10.1038/nature06599

Sharma G, Naushad M, Pathania D et al (2015) Modification of *Hibiscus cannabinus* fiber by graft copolymerization: application for dye removal. Desalin Water Treat 54:3114–3121. https://doi.org/10.1080/19443994.2014.904822

Shon HK, Phuntsho S, Chaudhary DS, Vignesaran S, Cho J (2013) Nanofiltration for water and wastewater treatment – a mini review. Drink Water Eng Sci 6:47–53. https://doi.org/10.5194/dwes-6-47-2013

Shrivastava P (1995) Environmental technologies and competitive advantage. Strateg Manag J 16:183–200. https://doi.org/10.1002/smj.4250160923

Siddique MNI, Munaim MSA, Zularisam AW (2014) Feasibility analysis of anaerobic co-digestion of activated manure and petrochemical wastewater in Kuantan (Malaysia). J Clean Prod 106:380–388. https://doi.org/10.1016/j.jclepro.2014.08.003

Sires I, Brillas E, Oturan MA, Rodrigo MA, Panizza M (2014) Electrochemical advanced oxidation processes: to- day and tomorrow. A review. Environ Sci Pollut Res Int 21(14):8336–8367. https://doi.org/10.1007/s11356-014-2783-1

Sridhar Acharya P, Aithal PS (2015) Innovations in effective management of energy using green technology. Int J Concep Manag Soc Sci 3(2):18–22. ISSN: 2357 – 2787

Sutherland K (2009) What is nanofiltration. http://www.filtsep.com/view/717/whatis-nanofiltration/

Synder Filtration (2015) Ultrafiltration membranes for research & industry. http://synderfiltration.com/ultrafiltration/membranes/

Tao G, Kekre K, Zhao W, Lee TC, Viswanath B, Seah H (2005) Membrane bioreactors for water reclamation. Water Sci Technol 51(6–7):431–440

Tao GH, Kekre K, Qin JJ, Oo MW, Viswanath B, Seah H (2006) MBR- RO for high-grade water (NEWater) production from domestic used water. Water Pract Technol 1(2):70–77. https://doi.org/10.2166/WPT.2006041

Tchobanoglous G (1981) Wastewater engineering: collection and pumping of wastewater. McGraw-Hill Book Company, New York

Trivedy RK (1998) Advances in wastewater treatment technologies. Vol. 1. Global Science Publications, Aligarh

Trivedy RK, Thomas S (2005) Water hyacinth for pollution control and resource recovery. In: Mathur SM et al (eds) Aquatic weeds, problem, control and management. Himanshu Publications, Udaipur

Turovskiy I (2000) New techniques for wastewater and sludge treatment in Northern Regions

Turovskiy I (2014) New techniques for wastewater and sludge treatment in Northern Regions, Nandeshwar & Satpute. Curr World Environ 9(3): 837–842, 841, December 28, 2000

United Nations Environment Programme (2003) Environmentally sound technologies for sustainable development, revised draft. Division of Technology, Industry and Economics, Osaka

Van der Vegt H, Iliev I (2012) Patent landscape report on membrane filtration and UV water treatment. World Intellectual Property Organization, Geneva

Vijayaraghavan K, Ahmad D, Abdul Aziz ME (2007) Aerobic treatment of palm oil mill effluent. J Environ Manag 82(1):24–31. https://doi.org/10.1016/j.jenvman.2005.11.016

Wang J, Chen C (2009) Biosorbents for heavy metals removal and their future. Biotechnol Adv 27:195–226. https://doi.org/10.1016/j.biotechadv.2008.11.002

Wiesner MR, Hackney J, Sethi S, Jacangelo JG, Laine JM (1994) Cost estimates for membrane filtration and conventional treatment. J Am Water Works Assoc 85(12):33–41

Woisetschlager D, Humpl B, Koncar M, Siebenhofer M (2013) Electrochemical oxidation of wastewater opportunities & drawbacks. Water Sci Technol 68(5):1173–1179. https://doi.org/10.2166/wst.2013.366

Wongburi P, Park JK (2018) Decision making tools for selecting sustainable wastewater treatment technologies in Thailand. IOP Conf Ser Earth Environ Sci 150:012013. https://doi.org/10.1088/1755-1315/150/1/012013

Yu F, Zhang Q, Guo XM (2003a) Wastewater pollution characteristics of Chinese nonferrous metals industry. Nonferrous Met 55:134–139

Yu F, Zhang Q, Guo XM (2003b) Pollution characteristics of main industrial wastewater subsectors in China and control focuses. Environ Prot 21:38–44

Yu F, Zhang Q, Guo XM (2003c) Analysis of wastewater pollution characteristics of mining and mineral processing of China's metal mines. Metal Min 16:40–44

Zhou H, Smith DW (2002) Advanced technologies in water and wastewater treatment. J Environ Eng Sci 1:247–264. https://doi.org/10.1139/S02-020

Chapter 10
Mesoporous Materials for Degradation of Textile Dyes

Diana V. Wellia, Yuly Kusumawati, Lina J. Diguna, Nurul Pratiwi, Reza A. Putri, and Muhamad I. Amal

Contents

Abstract The properties needed for photocatalytic applications, such as large specific surface area, controllable pore size and morphology, and high interparticle connectivity, are among that owed by mesoporous materials. These attributes have been attracted researcher to engineer for further enhancement of the surface and to provide diffusion, charge, or light transfer or reactant access into the cavities. The

D. V. Wellia · N. Pratiwi · R. A. Putri
Chemistry Department, Andalas University, Padang, Indonesia

Y. Kusumawati
Chemistry Department, Sepuluh Nopember Institute of Technology, Surabaya, Indonesia

L. J. Diguna
Department of Renewable Energy Engineering, Prasetiya Mulya University, Tangerang, Indonesia

M. I. Amal (✉)
Research Center Metallurgy and Materials, Indonesian Institute of Sciences, Tangerang Selatan, Indonesia
e-mail: muha137@lipi.go.id

M. Naushad et al. (eds.), *Green Methods for Wastewater Treatment*, Environmental Chemistry for a Sustainable World 35, https://doi.org/10.1007/978-3-030-16427-0_10

synthesis, structural properties, and catalytic performances of mesoporous materials for degradation of textile dyes will be discussed in this chapter. The development of photocatalytic materials, particularly of porous material including metal-incorporated zeolites, metal–organic frameworks, and porous semiconductor photocatalysts, will be described in the beginning of the chapter and followed by the mechanism of the photocatalytic process. Finally, the issue of future challenge will conclude the discussion.

Keywords Mesoporous photocatalyst · Metal oxide · Mesoporous TiO_2 · Mesoporous ZnO · Mesoporous SnO_2 · Supported photocatalyst · Template photocatalyst

10.1 Introduction

Photocatalyst is a material that has a catalytic ability enable after electromagnetic radiation absorption. The range of electromagnetic radiation is commonly in the UV to near-IR range (Shan et al. 2010). It has been widely investigated due to its variety of potential applications for human life, such as degradation of harmful dyes (Mahmoodi et al. 2018; Akpan and Hameed 2009), dye-sensitized solar cells (DSSC) (Chou et al. 2004), and gas sensors (Yamazoe and Miua 1992). To date, many efforts have been made to improve its potential activities such as decreasing the band gap, improving light sensitization, preventing electron–hole recombination, and increasing active surface area by creating porous structure (Yu et al. 2002). The porous structure and size are very important to influence the effectiveness of photocatalytic process (Garforth et al. 1997).

According to IUPAC (International Union of Pure and Applied Chemistry), the materials are classified into three groups based on their pore size: (1) microporous, materials with diameter less than 2 nm; (2) mesoporous, materials with diameter from 2 to 20 nm; and (3) microporous, materials that possess pore size more than 50 nm (Corma 1997). In order to have an efficient photocatalytic process, the most important factors to be considered in engineering materials are pore structure and size. The presence of porous structure in/on the catalyst provides a high surface area for the premier contact of an adsorbate molecule and catalyst. Moreover, it also facilitates the molecule diffusion and charge or light transfer that support the catalytic process (Anpo et al. 1987; Corma 1997). In the case of textile dyes, mesoporous photocatalyst has showed enhancement of the photocatalytic performance (Ali et al. 2012; Chakma and Moholkar 2015; Areerob et al. 2018; Silva et al. 2018).

To date, various methods have been demonstrated to prepare the mesoporous photocatalyst including by using the support material or template agent. In this subchapter, various synthetize techniques to prepare the mesoporous metal oxide photocatalyst are discussed with highlight on the supported photocatalyst and template photocatalyst.

10.2 Mesoporous Metal Oxide Photocatalysts

10.2.1 Mesoporous TiO_2 for Degradation of Textile Dyes

Along with the rapid progress of research in the studies of semiconductor photocatalyst, TiO_2 is widely known as one of the most promising photocatalysts due to its potential properties (Mondal and Sharma 2014; Saravanan et al. 2018) and applications (Xu et al. 2011; Feng et al. 2005; Mishra et al. 2009; Kawahara et al. 2002). The serious problem of environmental wastes could be solved by the understanding of the photocatalytic activity of this material (Dhiman et al. 2017; Chen and Mao 2007). Many reports on the preparation and modification of TiO_2 by creating porous structure have been published recently to enhance the photocatalytic activity of TiO_2. Hossain et al. (2015) reported the fabrication of ordered mesoporous TiO_2 with superior photocatalytic activities. At the same time, Cheng et al. (2015) also introduced the excellent photocatalytic properties of ordered mesoporous TiO_2 by addition of various kinds of metal dopants. Most of all these various preparations, modifications, and characterizations of mesoporous TiO_2 for photocatalysis application have been reviewed by Ismail and Bahnemann (Ismail and Bahnemann 2011). It has also been reported that the presence of porous structure can increase the density of active sites, which lead to the improvement of the intrinsic properties (Li et al. 2013).

Synthesis Method and Reaction

There are various synthesis methods that have been reported on the preparation of mesoporous TiO_2 such as sol–gel, sonochemistry, hydrothermal microwave, and electrodeposition (Bagheri et al. 2015).

Sol–Gel

Sol–gel process consists of two main steps. There are hydrolysis and condensation of precursors. For mesoporous material, the surfactant as a template is dissolved into homogeneous solution of TiO_2 precursor. The slower condensation of the TiO_2 precursor leads to the formation of mesoporous structure, with better accessibility for photocatalysis (Ismail and Bahnemann 2011). The general reaction that involved in the sol–gel process can be schematically represented as follows (Moussaoui et al. 2018):

Hydrolysis

$$M(OEt)_4 + xH_2O \leftrightarrow M(OEt)_{4-x}(OH)_x + xEtOH \tag{10.1}$$

Condensation

$$M(OEt)_4 + xH_2O \leftrightarrow M(OEt)_{4-x}(OH)_x + xEtOH \tag{10.2}$$

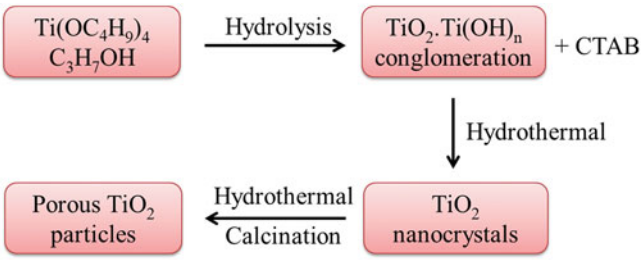

Fig. 10.1 Schematic diagram of preparation of ordered mesoporous TiO_2 via hydrothermal method

Hydrothermal

In the hydrothermal method, the process is normally conducted in pressure vessel steel called autoclaves coated with Teflon liners under controlled temperature and/or pressure with the reaction occurring in aqueous solutions. The temperature can be elevated above the boiling point of water, reaching the saturation vapor pressure (SVP). Both temperature and the amount of solution, especially Ti precursor and the surfactant, determine the generated internal pressure. The example of the mesoporous TiO_2 prepared by using hydrothermal method can be illustrated in Fig. 10.1 (Ismail and Bahnemann 2011).

Microwave Method

Microwave radiation has been applied to prepare various mesoporous TiO_2 nanoparticles in the presence of surfactant. The frequency of microwave heating that is usually used is in between 900 and 2450 MHz. This resulted energy can accelerate the formation of crystalline mesoporous TiO_2 nanopowders with a high surface area and excellent photocatalytic effects for photodegradation of textile dyes (Ismail and Bahnemann 2011).

Sonochemical Method

Ultrasound is a useful method for the synthesis of mesoporous TiO_2 active photocatalyst. This method applies the precursor of TiO_2 under the powerful ultrasound irradiation (20 kHz–10 MHz), without any template. This procedure was claimed to give a good dispersion of the nanoparticles, a marginally large surface area, a good thermal stability, and phase purity (Ismail and Bahnemann 2011).

Experimental Studies of Various Mesoporous TiO_2-based photocatalysys Along with Their Design, with Specific Attention to Various Chemical Reactions Involved

Table 10.1 summarizes the reported experimental studies of various mesoporous TiO_2-based photocatalysts with specific attention to various chemical reactions involved.

Application for Degradation: Mechanism and Some Important Things

Generally, the photocatalysis mechanism can be described by the following equations (Veselý et al. 2005; Wellia 2012):

Table 10.1 Experimental studies of various mesoporous TiO_2-based photocatalysts

Material	Synthesis method/precursor Ti	Template	Doped element (s)/oxide	TiO_2 phase	P_s TiO_2/nm	S_{BET}/$m^2\ g^{-1}$	Vp/$cm^3\ g^{-1}$	Dp/nm	Textile dye (s)/pollutants	Light source(s)	Catalyst loading	Irradiation time/min	% D	References
Mesoporous TiO_2	Sol–gel/titanium (IV) butoxide	$Cati_{14}TAB$		A, B	8.5	437	1.01		Rhodamine B	UV light (366 nm)	200 mg	60	98.58	Moussaoui et al. (2018)
		$C_{16}TAB$											98.72	
		$C_{18}TAB$			9.9	467	0.88						99.95	
		Nonionic: Plantacare UP K55			8.1	508	1.02							
					8.5	400	0.89						98.84	
Mesoporous Cr_2O_3/TiO_2 nanoparticles	Sol–gel/titanium chloride	Octadecylamine	Cr_2O_3	A, R	5–14	166	0.182	4.3	Methylene blue	UV light (254 nm)	0.1 g/100 mL	120	90	Ahmed et al. (2017b)
Mesoporous TiO_2–rGO	Hydrothermal/butyl titanate	Pluronic P123 triblock polymer	Graphene oxide	A					Rhodamine B	Visible light	10 mg	320	81	Zhang et al. (2017)
Mo–N-co-doped mesoporous TiO_2 microspheres	Solvothermal/titanium (IV) isopropoxide		Mo, N	A	10	122.7			Rhodamine B	Visible light	120 mg	240	74	Liu et al. (2017)
Mesoporous TiO_2	Microwave/TTIP			A	2–50	172.3		5	Methylene blue	UV-visible	30 mg	10	99	Alosfur et al. (2018)
													63.4	
Mesoporous TiO_2	Hydrothermal/titanium (IV) oxysulfate (TIOS)	SDS		A	10–20	158	0.53	24.4	Methylene blue	UV-visible	2 mg	60	80	Chowdhury et al. (2016)
													18	

(continued)

Table 10.1 (continued)

Material	Synthesis method/precursor Ti	Template	Doped element (s)/oxide	TiO_2 phase	P_s TiO_2/ nm	S_{BET}/ $m^2\ g^{-1}$	Vp/ $cm^3\ g^{-1}$	Dp/ nm	Textile dye (s)/ pollutants	Light source(s)	Catalyst loading	Irradiation time/min	% D	References
Mesoporous TiO_2	Sol–gel/ solvothermal/ butyl titanate	CTAB	–	A, R	< 50	129.7	0.206	22.6	Methylene blue	UV light	0.1–0.6 g/ L	160	53.4	Xiao et al. (2017)
			Ag			169.3	0.211	18.3					81.7	
			GR			194.5	0.306	15.5					72.5	
			Ag/GR			242.2	0.425	11.1					>98	
Mesoporous Ag/TiO_2	Sol–gel/ TTIP	Chitosan	Ag	A		61.8	0.146	47.45	Methylene blue, indigo carmine	UV light	0.1 g/ 100 mL	120	95	Abdel Messih et al. (2017)

a*A* anatase, *R* rutile, *B* brookite, *rGO* reduced graphene oxide, *CTAB* cetyltrimethylammoniumbromide, *SDS* sodium dodecyl sulfate, *GR* graphene, P_s average particle size, S_{BET} surface area, *Vp* pore volume, *Dp* pore diameter, *% D* % degradation

1. Hydroxyl radical generation

$$TiO_2 \xrightarrow{hv} TiO_2(e^-_{cb}, h^+_{vb}) \rightarrow \text{recombination} \tag{10.3}$$

$$TiO_2(h^+_{vb}) + H_2O_{ads} \rightarrow TiO_2 + HO^\bullet_{ads} + H^+ \tag{10.4}$$

$$TiO_2(h^+_{vb}) + HO^-_{ads} \rightarrow TiO_2 + HO^\bullet_{ads} \tag{10.5}$$

$$TiO_2(e^-_{cb}) + O_{2ads} + H^+ \rightarrow TiO_2 + HO_2^\bullet \rightleftarrows O_2^{\bullet -} + H^+ \tag{10.6}$$

$$TiO_2(e^-_{cb}) + HO_2^\bullet + H^+ \rightarrow TiO_2 + H_2O_2 \tag{10.7}$$

$$TiO_2(e^-_{cb}) + H_2O_2 \rightarrow TiO_2 + HO^\bullet + HO^- \tag{10.8}$$

$$2\,HO_2^\bullet \rightarrow H_2O_2 + O_2 \tag{10.9}$$

$$O_2^{\bullet -} + H_2O_2 \rightarrow HO^\bullet + O_2 + HO^- \tag{10.10}$$

$$H_2O_2 \xrightarrow{hv} 2\,HO^\bullet \tag{10.11}$$

2. Oxidation of electron donor (D, organic molecule) or reduction of electron acceptor (A, metal ion) reaction

$$TiO_2(h^+_{vb}) + D_{ads} \rightarrow TiO_2 + D^+_{ads} \tag{10.12}$$

$$HO^\bullet + D_{ads} \rightarrow D_{oxid} \tag{10.13}$$

$$TiO_2(e^-_{cb}) + A_{ads} \rightarrow TiO_2 + A^-_{ads} \tag{10.14}$$

The photocatalytic activity mainly depends on electron transfer process. There are several factors affecting the efficiency of electron transfer that have been discussed and reported such as the size of photocatalyst, surface composition, and morphology. Creating the porous structure is one of the effective ways to modify the surface morphology that can enhance the photocatalyst performance in degradation process (Mohamed and Bahnemann 2012).

10.2.2 Mesoporous ZnO for Degradation of Textile Dyes

Synthesis Method and Reaction

Nowadays, much attention has been devoted to the preparation of mesoporous photocatalyst to improve its photoactivity and intrinsic structural features. Besides titania, zinc oxide (ZnO) is also one of the promising semiconductor materials for photocatalyst. ZnO has outstanding characteristics such as wide band gap (3.37 eV), nontoxicity, chemical stability, high oxidative capacity, and unique optical and electronic properties (Wang et al. 2014b; Bouzid et al. 2015; Collard et al. 2014).

Researches show that the porosity of ZnO nanostructure has direct effect on its photocatalytic properties as well as the crystallinity and morphology (Reyes et al. 2015). It is possible due to the large surface area, high porosity, and low density of porous structure. In the mesoporous structure, the photocatalyst activity could be enhanced through the channels of semiconductor which act as a light-transfer path for the introduction of incident photons onto the inner surface of the photocatalyst (Ren et al. 2016). Additionally, in degradation process of organic dyes, a mesoporous zinc oxide has adsorption ability because of an increase in the probability of a surface reaction with pollutant molecules (Yin and Liu 2015).

Those exciting mesoporous structures of zinc oxide have been prepared by various techniques such as thermal decomposition (Bijanzad et al. 2015), hydrothermal (Kowsari and Abdpour 2017; Chen et al. 2018), solvothermal (Srinivasan et al. 2015; Wang et al. 2016b), electrospinning (Ren et al. 2016; Ren et al. 2015), and sol–gel process (Abarna et al. 2016). Mostly, the precursors used for synthesizing mesoporous zinc oxide are zinc acetate dihydrate ($Zn(CH_3COO)_2 \cdot 2H_2O$) and zinc(II) hexahydrate ($Zn(NO_3)_2 . 6H_2O$). Some of these methods use template to improve the morphology of zinc oxide, whether natural or synthetic template agent.

In solvothermal method, Srinivasan et al. (2015) synthesized mesoporous zinc oxide using ethylene glycol (EG) and polyethylene glycol (PEG) as solvent and also as structure-directing agent which formed bipyramidal morphology. On the other hand, Wang et al. (2014b) synthesized mesoporous zinc oxide without the addition of template agent and obtained a three-dimensional network of ZnO nanosheet.

Both Kowsari and Abdpour (2017) and Chen et al. (2018) reported hydrothermal method to synthesize mesoporous zinc oxide in the presence of templating agent. FIL (functional ionic liquid) was used as template and formed hexagonal structure (Kowsari and Abdpour 2017). Chen et al. (2018) used amino acid (N-acetyl-D-proline) as template agent and formed multispherical microstructure.

Experimental Studies of Various Materials Along with Their Design, with Specific Attention to Various Chemical Reactions Involved

Experimental studies of various mesoporous ZnO-based photocatalysts are summarized and presented in Table 10.2. Zinc acetate is one of the favorable raw materials to synthesize mesoporous zinc oxide. It easily reacts with ethylene glycol to form 5-membered chelate octahedral complex. Moreover through the thermal process, it grows into one dimension as shown in Fig. 10.2.

The commonly applied structure-directing agents are ethylene glycol (EG) and polyethylene glycols (PEG) with various molecular weights. The synthesis using EG and PEG (200 or 400) leads to the formation of square bipyramidal and spherical morphology, respectively. In the case of PEG-200, the nanocrystalline ZnO spheres displayed radially oriented nanorod features on the surface (Srinivasan et al. 2015).

Application for Degradation: Mechanism and Some Important Things

Due to more surface active sites and the ease of charge carrier transport, mesoporous structures of ZnO have been reported for its excellent photocatalytic activity performance (Wang et al. 2016a). The mechanism involved in the photocatalytic degradation of organic dyes by ZnO can be clearly illustrated below (Tripathy et al. 2016):

Table 10.2 Experimental studies of various mesoporous ZnO-based photocatalysts

Material	Synthesis method/ precursor Ti	Template	Doped element (s)/ oxide	ZnO phase	P_s ZnO/nm	S_{BET}/ $m^2\ g^{-1}$	Vp/ $cm^3\ g^{-1}$	Dp/ nm	Textile dye (s)/pollutants	Light source (s)	Catalyst loading	Irradiation time/min	% D	References
Mesoporous ZnO (nanocrystalline)	Sol–gel	Ethylene glycol Polyethylene glycol		Wurtzite	6–9	77.6	0.33	13.74	Crystal violet	UV light (UV-B and UV-C)	50 mg	165		Srinivasan et al. (2015)
Mesoporous ZnO	Precursor-induced route			Wurtzite	30–50	13.2		11.5	Methyl orange	UV light	10 mg	30	98	Xiao et al. (2015)
Mesoporous microbricks of ZnO	Thermal decomposition			Wurtzite	~30	8.13		22.6	Congo red	Visible light	0.02 g	180	96	Bijanzad et al. (2015)
Mesoporous ZnO	Sol–gel	Bio-template (Jute fiber)		Wurtzite	24–33	20	0.2	19.05	Crystal violet	Visible light	0.1 g	180	80	Abarna et al. (2016)
Mesoporous ZnO	Thermolysis				100	19.82		5.7	Methyl orange Rhodamine B	UV light	18 mg	120	99.7 98.1	Ban et al. (2017)
Mesoporous ZnO	Wet chemical route	Polystyrene			~5	78.3		~26	Rhodamine B	UV light	0.2 g	40	~98%	Tripathy et al. (2016)
Mesoporous ZnO/TiO_2	Hydrothermal		TiO_2	Wurtzite–anatase	10–20	55.98	0.256	2–13	Methyl orange	UV light	20 mg	360	~90	Wang et al. (2014b)

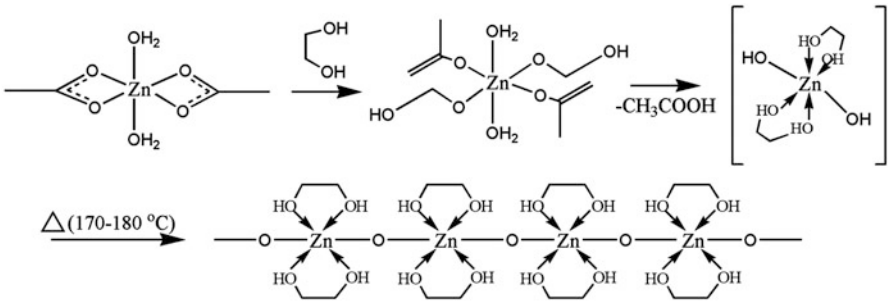

Fig. 10.2 Formation reaction of zinc oxide by solvothermal process

$$\mathrm{ZnO} + h\nu \rightarrow \mathrm{e^-_{CB}} + \mathrm{h^+_{VB}} \tag{10.15}$$

$$\mathrm{e^-_{CB}} + \mathrm{O_2} \rightarrow \mathrm{O_2^{\bullet -}} \tag{10.16}$$

$$\mathrm{H_2O} + \mathrm{O_2^{\bullet -}} \rightarrow \mathrm{HOO^{\bullet}} + \mathrm{OH^-} \tag{10.17}$$

$$2\mathrm{OOH}\grave{O}\ \mathrm{O_2} + \mathrm{H_2O_2} \tag{10.18}$$

$$\mathrm{O_2^{\bullet -}} + \mathrm{dye} \rightarrow \mathrm{dye - OO^{\bullet}} \tag{10.19}$$

$$\mathrm{OOH^{\bullet}} + \mathrm{H_2O} + \mathrm{e^-_{CB}} \rightarrow \mathrm{H_2O_2} + \mathrm{OH^-} \tag{10.20}$$

$$\mathrm{H_2O_2} + \mathrm{e^-_{CB}} \rightarrow \mathrm{OH^{\bullet}} + \mathrm{OH^-} \tag{10.21}$$

$$\mathrm{H_2O_2} + \mathrm{O_2^{\bullet -}} \rightarrow \mathrm{OH^{\bullet}} + \mathrm{OH^-} + \mathrm{O_2} \tag{10.22}$$

$$\mathrm{Dye} + \mathrm{OH^{\bullet}}/\mathrm{O_2^{\bullet -}} + \mathrm{ZnO} \rightarrow \mathrm{Degraded\ dye} \tag{10.23}$$

10.2.3 Mesoporous SnO_2 for Degradation of Textile Dyes

Tin oxide (SnO_2) has been reported as an alternative semiconductor oxides for photodegradation of organic compounds especially for degradation of textile dyes (He and Zhou 2013). However, SnO_2 shows low photocatalytic efficiency because it has wide band gap (~ 3.6 eV) and high recombination rates of photogenerated electron–hole pairs (He and Zhou 2013). This deficiency makes SnO_2 photocatalyst difficult to apply in the environmental application widely and practically (He and Zhou 2013). The fabrication of mesoporous structures of the SnO_2 photocatalyst can be an effective way to overcome the problem (Jing et al. 2014).

Experimental Studies of Various Materials Along with Their Design, with Specific Attention to Various Chemical Reactions Involved

Experimental studies of various mesoporous SnO_2-based photocatalysts are summarized and presented in Table 10.3.

Table 10.3 Experimental studies of various mesoporous SnO_2-based photocatalysts

Material	Synthesis method/ precursor Ti	Template	Doped element (s)/ oxide	SnO_2 phase	P_s SnO_2/ nm	S_{BET}/ $m^2\ g^{-1}$	Vp/ $cm^3\ g^{-1}$	Dp/ nm	Textile dye (s)/ pollutants	Light source (s)	Catalyst loading	Irradiation time/min	% D	Ref.
Mesoporous SnO_2	Electrostatic self-assembly/ tin tetrachloride pentahydrate	$(NH_4)_6Mo_6O_{24}$			5–6	132	0.12	3.5	Methylene orange	UV light	0.05 g	140	60–100	Jing et al. (2014)
Mesoporous SnO_2	Sol–gel/tin tetrachloride pentahydrate	PVP	Ag	R	3.29	37.5	0.088	32.5	Methylene blue	UV light	0.1 g/ 100 mL	120	84	Ahmed et al. (2017a)
									Amaranth				53	
Mesoporous α-Fe_2O_3/SnO_2	Coprecipitation/ butyl titanate		α-Fe_2O_3		6–14	46.6	0.168	9.8	Malachite green	Sunlight	40 mg	240	86	Pradhan et al. (2014)
Mesoporous SnO_2–hexaniobate layered nanocomposite	Sol–gel/tin tetrachloride pentahydrate		Nb_6O_{17}		2.9	140	0.47	2.9	Acid Red G	UV light	0.1 g	90	85	Wang et al. (2010a)

a*R* rutile, P_s average particle size, S_{BET} surface area, *Vp* pore volume, *Dp* pore diameter, % *D* % degradation

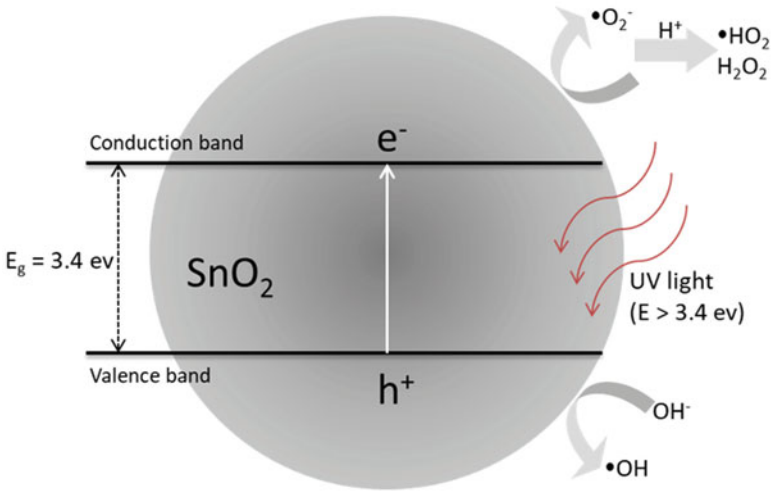

Fig. 10.3 Illustration of photocatalytic mechanism of mesoporous SnO_2

Application for Degradation: Mechanism and Other Important Factors
Generally, photocatalytic mechanism of mesoporous SnO_2 is shown in Fig. 10.3 (Hu et al. 2017), and the relevant reaction equations are detailed as follows (Al-Hamdi et al. 2017):

$$SnO_2 + h\upsilon \rightarrow SnO_2(e^- + h^+) \tag{10.24}$$

$$SnO_2(h^+{}_{VB}) + H_2O_{ads} \rightarrow SnO_2 + HO^\bullet{}_{ads} + H^+ \tag{10.25}$$

$$SnO_2(h^+{}_{vb}) + HO^-{}_{ads} \rightarrow SnO_2 + HO^\cdot{}_{ads} \tag{10.26}$$

$$SnO_2(e^-{}_{cb}) + O_{2ads} \rightarrow SnO_2 + O_2{}^{-\bullet} \tag{10.27}$$

$$O_2{}^{\bullet -} + H^+ \rightarrow HO_2{}^\bullet \tag{10.28}$$

$$O_2{}^{\bullet -} + H_2O \rightarrow HO_2{}^\bullet + OH^- \tag{10.29}$$

$$\text{Dye} + OH^\bullet \text{ or } O_2{}^{\bullet -} \text{or } HO_2{}^\bullet \rightarrow CO_2 + H_2O \tag{10.30}$$

10.3 Supported Mesoporous Photocatalysts

Previous section has discussed about the development of metal oxide materials in the photocatalyst. It has shown that metal oxide semiconductor, especially titanium dioxide, is the most wanted material for this purpose. However, many researchers then revealed that technically it is needed to support the metal oxide with certain material. The purposes of this support are:

1. Increasing the adsorption capability of metal oxide. It is noted that TiO_2 has a poor adsorption capability; such commercial TiO_2 has surface area lower than 50 m^2/g existed as a polar surface (Gu et al. 2010). On the contrary, most of the organic molecule that is wanted to be degraded or converted has a polar structure.
2. Facilitating the removal of catalyst after the treatment process.
3. Preventing the coagulation of metal oxide with certain molecule that causes the UV radiation absorption of the photocatalyst to decrease.

The supporting materials need to meet some requirements in order to enhance the performance of photocatalyst. Based on previous records, the important requirements are mentioned as follows (Shan et al. 2010; Singh et al. 2013; Gu et al. 2010; Srikanth et al. 2017; Li Puma et al. 2008):

1. High surface area to provide as much as possible the adsorption of photocatalyst inside. To meet this requirement, the porous material is preferred. The mesoporous or microporous materials can be considered based on the molecule that is converted or degraded.
2. Good bonding between photocatalyst, either physically or chemically, to provide the stability of supporting photocatalytic. In the case of pollutant degradation, it is desired that the supporting materials also have a good affinity with the pollutant to enhance the removal activity.
3. Transparent to the UV light or other sources of photocatalytic radiation, so they will not interfere the photocatalytic process.
4. Chemically stable. The chemical conversion-supporting material will bring difficulties, for instance, problems of their removal or chance to form coagulated species.
5. Simple regeneration photocatalytic process.

Some materials that meet those criteria have been developed as supporting materials for photocatalytic activity. In this section, three supporting materials that have been used frequently, i.e., silica, zeolite, and carbon, are discussed. The photocatalyst that is frequently combined with these materials is TiO_2.

10.3.1 Silica-Supported Photocatalyst

Silica or silicon dioxide has a chemical formula of SiO_2. The term of silica also revers to $SiO_2.xH_2O$ that include water molecules on the hydrated silica. Silica exists in the crystalline or noncrystalline form. The commonly found natural crystalline silica structure is quartz. Silica is also found in other forms, such as tridymite, cristobalite, stishovite, and coesite. In the room temperature, common stable structure silica is found either as quartz, tridymite, or cristobalite, which all have a tetrahedral coordination. Stishovite and coesite can only be formed in the high pressure and temperature. Stishovite formed at 10 GPa and > 1200 °C, and coesite formed at 2–3 GPa and > 700 °C (Lagaly 1980; Léger et al. 1996; Luo et al. 2007).

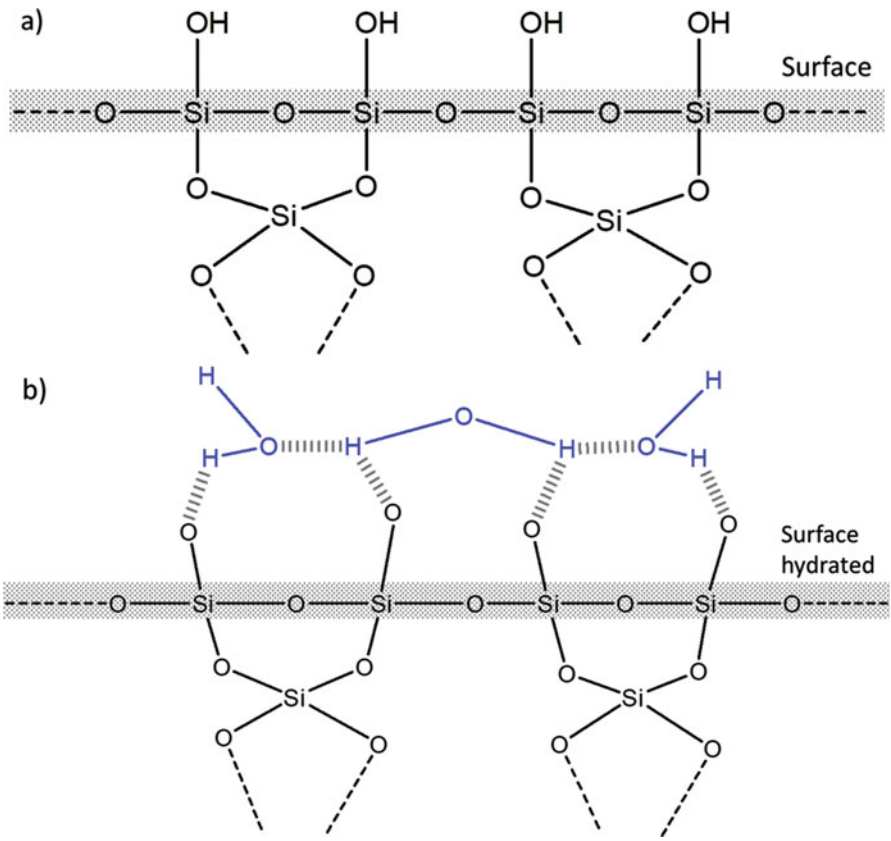

Fig. 10.4 Illustration of surface silica structure with (**a**) hydroxyl group (**b**) siloxane group

The amorphous phase of silica has an irregular structure. The three common forms of amorphous silica are opal, infusorial earth, and diatomaceous earth (Lagaly 1980). Opal is hydrated silica that has structure similar to cristobalite and tridymite (Smith 2013). Infusorial silica is a deposit of silica on the calcareous shell of mollusks, whereas diatomaceous earth is a sedimentary rock formed by accumulation of dead diatom cell walls that contain opal.

The silica surface is composed of hydroxyl group as illustrated in Fig. 10.4. Water heating will remove hydroxyl group from the surface and then will form the siloxane groups. The silica that is composed by siloxane groups is less polar compare to one by hydroxyl groups (Lagaly 1980). These functional groups play role as an active site for adsorption process. Moreover, they have a large surface area, typically about 500–1000 m^2/g (More et al. 2016; Polshettiwar et al. 2010; Brinker et al. 1990). Bearing these properties, silica meets the criteria as support for chemical reaction process, including photocatalytic one.

The application of silica for supporting material in photocatalytic process has been started during the 1960s. Silica-supported TiO_2 photocatalyst is the most

applied material for various photocatalytic processes (Pal et al. 2016; Pang et al. 2015; Kamegawa et al. 2015; Tang et al. 2018). Both types of silica structures, crystalline and amorphous, have been studied for photocatalytic-supporting materials (Jung and Park 1999; Sun et al. 2013b). Other forms of silica such as dispersion form of silica gel (Li et al. 2015a; Liu et al. 2017; Wakimoto et al. 2015) and aerogels (Hu et al. 2016; Lázár et al. 2015; Li et al. 2016; Zu et al. 2015) have also been investigated for its potential in supporting photocatalysis. Recently, mesoporous form of silica has been studied intensively for photocatalyst support, such as SBA-15 (Karimi et al. 2009; Wang et al. 2005), MCM-41 (Das et al. 2010; Dong et al. 2015) or KCC-1 (Polshettiwar et al. 2010). These mesoporous forms are attractive because of the large surface area, arranged pore structure, and tailored pore size (Wang et al. 2014a). They also have interesting textural properties to provide the metal species dispersion (Bacariza et al. 2018).

SBA-15 mesoporous silica is the most common silica form that is used as a support, not only for photocatalyst but for the others. It has a hexagonal array of uniform tubular channel. Its pore diameter ranges from 5 to 30 nm, while the pore thickness ranges from 3 to 6 nm. Both the diameter and the thickness of pores are controllable through their synthesis or preparation, thus making them tunable for various applications (Karimi et al. 2009). TiO_2 is loaded into SBA-15 matrix to enhance the photocatalytic performance of indigo carmine removal. This TiO_2/SBA-15 composite has been developed with high surface area. The TiO_2/SBA-15 surface area reached 674.8 m^2/g, and to extend the UV-Vis absorption range, the TiO_2/SBA15 surface was sensitized by organic molecule, 2,9-dichloroquinacridone. Sol–gel method was applied to prepare this material, with tetraethoxy titanium that was used as a precursor of TiO_2 (Ding et al. 2005; Wang et al. 2005). Sol–gel preparation method is considered as a versatile method with the easiness of controlling the process parameters to obtain the desired properties. Researchers have developed the sol-gel method to load TiO_2 into SBA-15 matrix with titanium isopropoxide as the precursor (Lachheb et al. 2011). The preparation was assisted by sonication technique. As-synthesized composite was applied to degrade methylene blue, and the best photocatalytic activity was observed on the composite with Ti/S ratio about 8 (Lachheb et al. 2011). Acosta-Silva et al. (2011) also studied the sol–gel-prepared TiO_2-SBA-15 to decompose methylene blue. It was observed that the drawbacks of incorporating TiO_2 onto SBA-15 are decreasing the surface area of SBA-15 and hence decreasing the TiO_2 photocatalytic activity. Wei et al. (2018) investigated that the addition of moderate amount of $NiFe_2O_4$ could increase the MB adsorption performance of $NiFe_2O_4$/SBA-15. Moreover, it was also observed that the addition of 20 mg TiO_2 into TiO_2/SBA-15 could enhance the MB photodegradation, with almost 85% of MB degraded after 150 min using TiO_2/SBA-15 whereas only 73% as the result of using sole TiO_2 (Wei et al. 2018). Another study showed that incorporation of titanium into SBA-15 also increased surface area. Das et al. (2010) prepared Ti-SBA15 which has specific surface area 924 $m^2\ g^{-1}$, whereas TiO_2-SBA15 only ranges about 400 $m^2\ g^{-1}$. This value was also higher than SBA-15 surface area which was about 611 $m^2\ g^{-1}$ (Das et al. 2010).

MCM-41 is the other mesoporous silica in addition to SBA-15, which has been manifested as a photocatalyst support. Various metals or metal oxides from Ti, V, Fe, Cu, Nb, Mo, or Zr have been considered to be incorporated into MCM-41 matrix through the hydrothermal method, sol–gel method, impregnation method, or chemical vapor deposition method (Dash et al. 2015). Most of them have been showing a promising photocatalytic activity result to degrade organic pollutant in water (Sharma et al. 2017). Zeolite was commonly used as template matrix for TiO_2. Dong et al. (2015) have prepared TiO_2/MCM-41 through sol–gel method and tested to degrade Acid Red B. The effect of calcination temperature to the photocatalytic performance was primarily studied, and the best photocatalytic activity was observed on the sample which was calcined at 600 °C for 2 h. All of Acid Red with the initial concentration 100 mg/L was successfully degraded after 2 h using 2 .0g/L TiO_2/MCM-41 (Dong et al. 2015). Chen et al. (2016) prepared Ti/MCM-41 photocatalyst to degrade oxytetracycline and found that the removal efficiency was 87% under acidic environmental operation condition (pH = 3).

10.3.2 Zeolite-Supported Photocatalyst

Zeolite is an aluminosilicate porous crystal, commonly found as a mesoporous solid. Ions of Al, Si, and O are the main component which build a tetrahedral structure with oxygen as a connection (Koohsaryan and Anbia 2016; Nada and Larsen 2017; Zhang and Ostraat 2016). Zeolite is considered as a photocatalyst support material due to its unique layered porous structure and abundant availability (Ali et al. 2012). Moreover, they own good ion exchange capability, hydrophilicity, high thermal stability, pollutant adsorption ability, and producibility of a large amount of hydroxyl and peroxide that are beneficial for the photocatalytic process (Kanakaraju et al. 2015; Mahalakshmi et al. 2009; Wang et al. 2011). Natural zeolite is abundantly found in volcanic sedimentary rock (Reháková et al. 2004). Aside from natural zeolite, researchers also attempt to produce synthetic material which has zeolite-like properties. The synthetic zeolite usually possesses three-dimensional networks. The most familiar mesoporous structures are HSM-5, ZSM-5, 13X, 4A, β, HY, Hβ, USY, or Y zeolite (Huang et al. 2008).

The application of zeolite material for enhancing photocatalytic capacity of TiO_2 has showed promising results. Ilinoiu et al. (2013) used natural zeolite to support N-doped TiO_2 processed by microwave-assisted hydrothermal method. The composite showed a photocatalytic activity toward reactive yellow 125 (RY125) dye. It was suggested that the electric field which exists in the zeolite framework provokes the separation between photogenerated electron and holes which is beneficial for photocatalytic process. The optimum photocatalytic process occurred at pH 3. On the contrary, the photocatalytic process became ineffective at the basic condition. Since the attached sulfonate group caused the dyes to have a negative charge at this condition. Meanwhile at the same condition, the photocatalyst also has negative charge. The charge similarity led to a repulsion that decreases the adsorption (Ilinoiu

et al. 2013). The other research applied other form of natural zeolite, mordenite, as supporting material. The TiO_2 loading into mordenite framework enhanced the photodegradation capability of methyl orange. It is worth noting that the optimum photocatalytic activity occurred at acidic condition (pH 4). The reason is at the acidic condition methyl orange exists as ionic quinone form. This ionic form is easier to be adsorbed by zeolite compared to the neutral one (Li et al. 2008). In other research, zeolite made by metakaolin and rice husk was used for supporting material of TiO_2 (Setthaya et al. 2017). Synthetic zeolites were also applied as a support for TiO_2-based photocatalyst to replace natural one, TiO_2/zeolite Y (Mohamed et al. 2005) and multilamellar mesoporous TiO_2/ZSM-5 (Znad et al. 2018), which both showed photocatalytic activity to degrade methyl orange.

10.3.3 Carbon-Supported Photocatalyst

Carbon materials exist in nature as several allotropes including amorphous carbon, graphene, carbon nanotube(s), graphite, fullerene, and diamond. Few of them, such as activated carbon, graphene, and carbon nanotube(s), meet the criteria as a supporting material because they have a large surface area.

Application of activated carbon/nano-ZnO composite as supporting photocatalyst has been studied by Raizada et al. (2014). The activated carbon/nano-ZnO composite was prepared by coprecipitation method with zinc nitrate as a source of ZnO. The prepared composite has shown a higher photocatalytic activity toward malachite green and Congo red compared to ZnO due to increasing adsorption capability (Raizada et al. 2014). The activated carbon in the fiber (activated carbon fiber, ACF) also has been applied as supporting material for photocatalyst. The loading of Fe_2O_3 into ACF with impregnation method has shown the photocatalytic activity to degrade Acid Red B (Lan et al. 2015). Carbon nanosphere also has been applied as supporting material for photocatalyst. Raza et al. (2015) studied that La- and Mo-doped TiO_2 supported on carbon nanosphere have a photocatalytic activity for degrading three kinds of chromophoric dyes, i.e., azo dye represented by Acid Yellow 29, triphenylmethane dye represented by G250, and anthraquinone dye represented by Coomassie Brilliant Blue G250.

The feasibility of graphene as supporting material for photocatalyst was also studied. Pt–TiO_2/graphene photocatalyst prepared through hydrothermal reaction was observed its photocatalytic ability toward acid orange 7 (Hsieh et al. 2015), whereas ZnO nanorod/graphene photocatalyst prepared through a simple one-pot chemical method was observed toward methylene blue and methyl orange (Nipane et al. 2015). The role of graphene is not only to provide a large surface area but also to enhance light harvesting of solar radiation, to inhibit charge recombination, and to provide an electron acceptor site which can induce the peroxide (Nipane et al. 2015). The other examples of photocatalyst supported on graphene material are gold/graphene, Ag_3PO4/graphene, and CdS (Chen et al. 2013; Ye et al. 2012). CdS

also recorded photocatalytic activity for degradation of carbon nanotubes (Ye et al. 2012).

10.4 Templated Mesoporous Photocatalysts

Mesoporous materials with well-controlled morphology have been widely fabricated through sacrificial template-based syntheses (Liu et al. 2013). Basically, the synthesis process includes the growth of desired materials on hard templates such as polymer (Diguna et al. 2006, 2007a, b) and silica (Lee et al. 2003; Taguchi et al. 2003; Smått et al. 2003) or soft templates such as micelles (Kresge et al. 1992; Bradshaw et al. 2014) and bubbles (Peng et al. 2003; Lou et al. 2008). Figure 10.5 shows representative illustration for synthesis of mesoporous materials by using (a) hard template of colloidal crystal and (b) soft template of surfactants. In hard template, rigid materials are typically used and restricted the crystalline growth into the void space, leading to subsequent replication.

The method of template removal depends on the template materials, such as thermal decomposition (calcination) or solvent extraction (dissolution in toluene) for the most commonly used polymer template of polystyrene latex spheres, chemical etching in HF for the silica template, and solvent evaporation for the emulsion template (Wu et al. 2013b). On the other hand, synthesis via soft template does not require prior fabrication steps of templates, and the self-assembly is induced by amphiphilic block copolymers or surfactants. The method associates with the interactions between surfactants and chemical species comprising the mesoporous system. Through these synthesis techniques, the hierarchical structures of macropores with micro-/mesoporous walls can be achieved with a high degree of control over the resulting materials.

Three dimensionally (3D) ordered macroporous structure can be fabricated by using 3D ordered arrays of polymer or silica spheres (colloidal crystals or synthetic opals) as template. After the desired materials are filled in the interstitial volume, the original spheres can be removed, leaving an inverse replica of opal structure, known as an inverse opal or 3D ordered macroporous structure. Inverse opal TiO_2 replicated from polymer template of polystyrene latex spheres has been shown to have higher photocatalytic activity on methylene blue degradation under visible light, particularly for TiO_2 inverse opal reduced by H_2 at 500 °C, compared to the P25 TiO_2 (Xin and Liu 2015). This structure has also been reported to be beneficial for photocatalytic activity in viscous solution, whereas carbon-deposited TiO_2 inverse opal has enhanced visible-light photocatalytic activity on the degradation of methylene blue in viscous polyacrylamide solution (Lee et al. 2013). Moreover, the high photocatalytic performance has been demonstrated by utilizing slow photon effect to enhance the light absorption at the red edge of the photonic band gap, such as in ZnO (Meng et al. 2013; Liu et al. 2014b) and TiO_2 (Wu et al. 2013a) inverse opals in dye molecule degradation of likes rhodamine B (RhB). On the other side, the multiple scattering effect of the macroporous structure has also been reported to facilitate

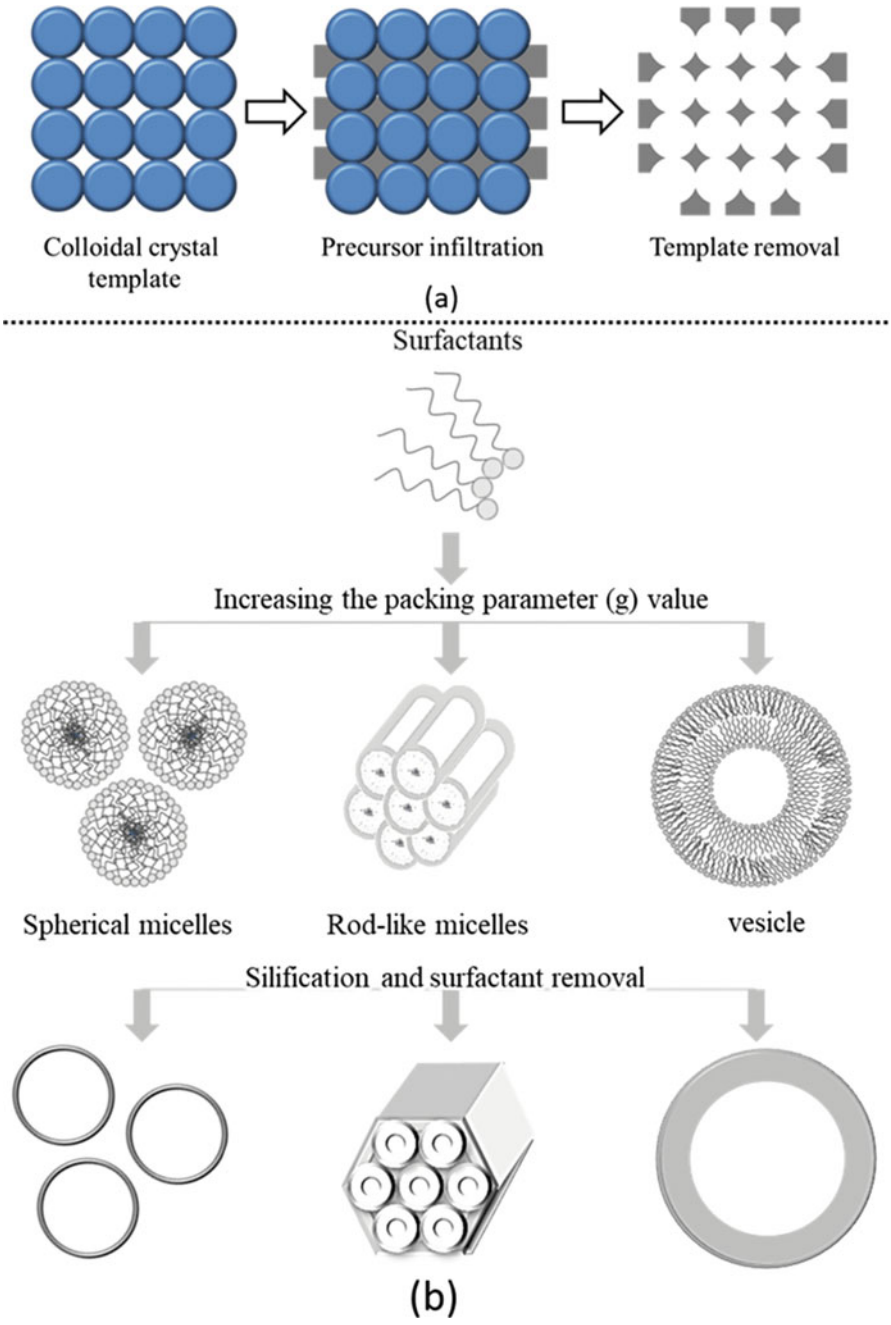

Fig. 10.5 Representative illustrations for synthesis of mesoporous materials based on (**a**) hard-templating and (**b**) soft-templating methods. (**a**) from Yang et al. (2017) and (**b**) from Xia et al. (2016)

visible-light photocatalysis of methylene blue dyes in nonperiodic macroporous N–F-codoped TiO_2 replicated from silica colloidal crystal with mixed sphere sizes (Xu et al. 2010). In case of ternary metal oxides, the photocatalytic activity of Bi_2WO_6 inverse opal on the photodecomposition of methylene blue and salicylic acid under visible-light irradiation has been improved by the factors of 2.2 and 2.4, respectively, in comparison to the Bi_2WO_6 nanofilm prepared with the same method but without the opal template (Zhang et al. 2011). The angle-dependent photodegradation of methylene blue showed the observation of slow photon effect in this Bi_2WO_6 inverse opal. Different mesoporous structures have been further reported by using different template materials such as biosynthesized materials. By using natural rubber latex, mesoporous titania exhibited more significant photodegradation of phenol and rhodamine B compared with Degussa P25 TiO_2 under solar light irradiation (Li et al. 2015b). This higher photocatalytic activity along with the observed red shift of titania absorption edge confirmed that carbon transferred from natural rubber latex has acted as a photosensitizer. Similar effect was also reported for carbon/ZnO nanocomposites prepared using a low-temperature precipitation process and TEMPO (2,2,6,6-tetramethyl-1-piperidinyloxy)-oxidized cellulose as a reactive template, in which it is not only a template but also a carbon provider (Xiao et al. 2018). After calcination, the ZnO structure changed from nanosheets to nanorods with the increase of carbonyl of TEMPO-oxidized cellulose, and the resulted nanocomposites had higher surface area and pore volume and smaller band gap due to more carbon compounded into the ZnO nanocrystals, compared to that prepared without the template. Thus it exhibited a significant photodegradation on methyl orange with 96.11% within 120 min and good reusability.

Various photocatalyst materials have been synthesized using appropriate hard silicate template. The replicated mesoporous $Cd_xZn_{1-x}S$ semiconductors have exhibited excellent photocatalytic performances for the degradation of methylene blue and rhodamine B, whereas the photocatalytic efficiency increased with a decrease in the Cd contents from 1.0 to 0.7 and reduced with the further decrease of Cd composition from 0.7 to 0.0 (Lee et al. 2017). Furthermore, mesoporous $SrTiO_3$ with interconnected pores of ca. 10 nm and surface areas as high as 240 $m^2\ g^{-1}$ has been formed via polycondensation of interpenetrating organic and inorganic polymers, followed by calcination of the organic phase and removal of the silica network via NaOH etching (Kayaalp et al. 2016). The mesoporous $SrTiO_3$ demonstrated the increased photocatalytic degradation of methylene blue up to seven times than for the corresponding nonporous system, as a result of the combined increase of porosity and decrease of crystallite size. For metal-free photocatalysts, mesoporous polymeric graphitic carbon nitride (g-C_3N_4) nanorods have been synthesized via nanocasting approach, i.e., cyanamide condensation within the pores of one-dimensional hexagonal mesostructure of the porous silica nanorods and then followed by the removal of silica by chemical etching (Li et al. 2012). The replicated g-C_3N_4 nanorods demonstrated a high photocatalytic activity for hydrogen generation from water in the presence of triethanolamine as a sacrificial electron donor and Pt nanoparticles as a co-catalyst compared to that obtained with a

conventional g-C_3N_4, and the As-formed H_2 could be further used to reduce 4-nitrophenol to 4-aminophenol. Uniform g-C_3N_4 nanorods have been also proposed for photoenzymatic catalysis in photocatalytic regeneration of NAD+ to NADH, the biological form of hydrogen (Liu et al. 2014a). Moreover, g-C_3N_4 nanospheres, comprised of interconnected 2D nanosheets, were also prepared by employing high area silica nanospheres as sacrificial templates (Zhang et al. 2014). This nanospherical g-C_3N_4 structure with sharp edges drastically improved H_2 evolution with an apparent quantum yield of 9.6% at 420 nm with 3 wt% Pt, favoring both charge separation and mass transport in photocatalysis. Instead of high surface area, the enhanced photocatalytic activity of mesoporous silica-templated g-C_3N_4 has been reported due to the presence of more delocalized electrons and the increased photogenerated electron–hole pair separation lifetimes (Li et al. 2015a, b, c).

Another synthesis strategy of mesoporous materials is via soft-templating method, which relies on the ability of structure-directing agents such as nonionic surfactants, amphiphilic block copolymers, and some ionic surfactants to readily self-assemble via non-covalent interactions such as hydrogen bonds or electrostatic bonds into ordered mesoscale arrays. Templating involves co-assembly of structure-directing agents and appropriate precursor molecules of desired photocatalyst materials. Subsequent cross-linking of the precursors at the interface causes phase separation to occur, which effectively forms a continuous ordered replica of the organic mesoscale template. The posttreatment is conducted to remove the structure-directing agent from the photocatalyst materials. With such complex physicochemical phenomena, formation of reliable self-assembly template structures; susceptibility of solution pH and ionic constituents; stability of micelle structure against the growth direction of desired materials, morphologically even crystal–crystal phase transition during thermal treatment; and complete removal of template by posttreatment are very critical and challenging problems in this method (Gu and Schüth 2014). Different hierarchical ZnO mesoporous structures have been formed from variation in molecular geometry, hydrophobic/hydrophilic properties of amino acid-based surfactants used, and different solvents to change packing parameters and micellization behaviors of surfactants (Kim et al. 2012). Metal oxide compounds of Fe_2O_3–Ga_2O_3 nanostructures have been successfully synthesized using glycoluril template, and it showed Fe_2O_3 content-dependent photocatalytic degradation of azo dye (Bagheri and Mahjoub 2016). Under UV light, 3% content of Fe_2O_3 had the highest dye removal efficiency of 99.8% after 15 min irradiation in comparison with reference P25 showing 54% removal after 120 min irradiation. Synthesis of mesoporous g-C_3N_4 has been conducted through self-polymerization of dicyandiamide by using various soft templates, such as nonionic surfactants, amphiphilic block copolymers, and some ionic surfactants (Wang et al. 2010b). The resulting g-C_3N_4 possessed high surface area particularly when Pluronic P123 amphiphilic block copolymer is used as structure-directing agent. However, the inefficient process of removing the template residue during the synthesis led to side reactions, resulting in high carbon content in the carbon nitride samples due to the strong hydrogen bonds between PEO blocks in Pluronic P123 and dicyandiamide. By using the same Pluronic P123 as soft template, mesoporous

g-C_3N_4 was then synthesized from melamine precursors regarding its less reactivity than dicyandiamide (Yan 2012). The prepared g-C_3N_4 showed not only high surface area but also redshifts its absorbance edge up to 800 nm and shows photocatalytic activity even when the irradiation light k is more than 700 nm. Mesoporous carbon nitrides with high surface area, high porosity, and low C/N ratio were further synthesized using water as the solvent, taking advantage of both supramolecular assembly of melamine cyanurate hydrogen-bonded complex through hydrogen bonding and different structure-directing agents of nonionic surfactants including Pluronic P123 (Peer et al. 2017). The synthesized high surface area carbon nitrides showed the improved light absorption and enhanced photocatalytic activity in a rhodamine B dye degradation reaction under visible-light irradiation compared to bulk melamine-derived carbon nitride. Unique yolk–shell nanostructured photocatalyst consisting of TiO_2 nanoparticles core and porous silica shell with controllable pore size was fabricated through a facile single-step dual-templating approach utilizing oil-in-water microemulsions and amphiphilic protein molecules (Fujiwara et al. 2017). The addition of optimum amount of protein as a sacrificial template improved photocatalytic activity of yolk–shell structured photocatalyst on the degradation of 2-propanol owing to the extended porosity of the silica shell.

Bubble template approach has been proposed for synthesis of mesoporous photocatalysts due to the unnecessary posttreatments of removing chemical species derived from soft template agents. Through acidic hydrothermal condition, hierarchical hollow spheres of rutile-phase TiO_2 have been fabricated using potassium titanium oxalate as the precursor and O_2 bubbles as soft template originated from H_2O_2 decomposition (Li et al. 2006). Under UV irradiation, hollow TiO_2 spheres showed faster degradation of rhodamine B compared to the rutile-phase TiO_2 nanorods. Bismuth vanadate ($BiVO_4$) hollow spheres were synthesized by using urea as surfactant as well as provider of NH_3 bubble template (Sun et al. 2013a). The synthesized samples showed efficient photocatalytic activity on degradation of rhodamine B and 2-propanol with high stability and durability after several cycling runs of degradation. Hollow spheres of $Sn_2Nb_2O_7$ have been successfully formed using soft template of CO_2 and NH_3 bubbles generated in situ from the decomposition of urea as soft templates under hydrothermal routes (Zhou et al. 2013). The As-obtained hollow spheres have a large specific surface area of 58.3 $m^2\ g^{-1}$ and show improved photocatalytic H_2 production in lactic acid aqueous solutions, about four times higher than that of the bulk, under visible-light irradiation. Nih-CdTe quantum dot (QD) hollow nanospheres were synthesized from CdTe QDs as the building blocks, nickel salts (Ni^{2+}), and ascorbic acid (H_2A). The visible light worked as a catalyst to generate in situ H_2 gas bubbles which acted as templates, thus leading to the formation of hollow structure (Li et al. 2014). The average diameter and shell thickness of the obtained hollow nanospheres ranged from 10–20 nm and 3–6 nm, respectively. The nanospheres exhibited excellent

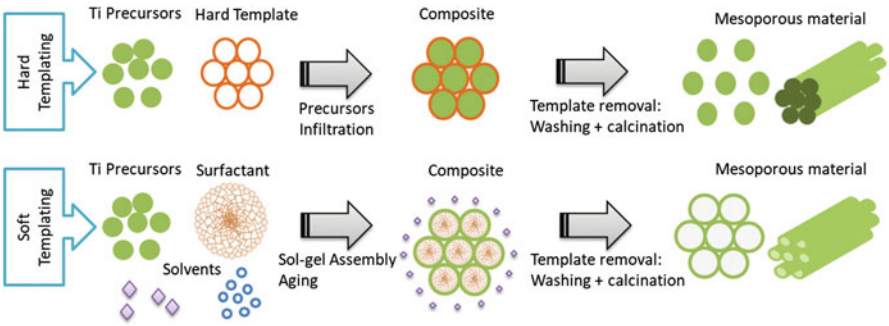

Fig. 10.6 The simplified scheme of template-assisted for the preparation of ordered mesoporous TiO_2 (Bonelli et al. 2017)

photocatalytic activity and stability for H_2 generation with a rate constant of 21 μmol h^{-1} mg^{-1}. Here, the QDs serve as antenna chromophores to harvest light, and Ni^{2+}-centered complexes formed in situ with dangling bonds (Te^{2-}) on the surface of the QDs serve as reaction centers to capture the photoexcited electrons of the QDs for H_2 generation. Porous polymeric g-C_3N_4 synthesized by using sulfur–bubble template showed high-efficient visible-light performance for H_2 evolution of 50.1 μmol h^{-1} relatively to pure g-C_3N_4 of 8.4 μmol h^{-1} (He et al. 2015). The sulfur-mediated g-C_3N_4 also showed 92% degradation of RhB after 50 min under visible-light irradiation, while the pure g-C_3N_4 degraded 48% at the same conditions.

Other interesting mesoporous structures with the unique surface characteristics and the relevant photocatalytic properties can be further explored to take the advantages of template-based routes. Although many significant improvements have been achieved in the template-mesoporous photocatalyst, further efforts are required to solve some issues, such as small-scale, low-yield production of mesoporous materials, the unclear interaction mechanisms between building components, and the low solar light utilization. In the future, the green, cost-effective, and industry-scale synthesis of mesoporous photocatalysts would be highly desirable.

Especially for porous material, like mesoporous TiO_2, it could be synthesized with or without using organic surfactant templates (Ismail and Bahnemann 2011). Generally, there are two main arrays used to construct ordered mesoporous TiO_2, i.e., by using soft-templating methods and by using hard-templating methods as illustrated in Fig. 10.6 (Li et al. 2014). However, template-free methods can also produce mesoporous TiO_2 with disordered mesostructures, which derived from the irregular packing of building blocks (Li et al. 2014). The development of mesoporous TiO_2 in order to increase the photocatalytic properties has also been done by adding single or multi-dopants (i.e., transition metal, noble metal, or nonmetal) (Wei et al. 2018). Various synthesis route, surfactant types, and techniques (i.e., dopant types) which have been applied in the modification of mesoporous TiO_2 are illustrated in Fig. 10.6.

10.5 Challenges for Catalysis

In photocatalytic application, pursuing the strategy to achieve efficient photogenerated charge separation and transport in nanoscale semiconductor particles is the most critical challenge faced over the decades. In fact, several approaches have been conducted to improve the interfacial charge transfer efficiency such as doping with metal or nonmetal impurities, surface modification, and coupling with other semiconductors having narrow band gap. Innovative strategy needs to be formulated in order to boost efficiency. Factors affecting the electron transfer ability have to be clearly understood, and the mechanism through which these factors influence the activity should be obviously verified. Correlation of the interfacial transfer of electrons and the kinetics of charge recombination with the photocatalytic activities is the key challenge that still exists and needs to be examined in semiconductor-based photocatalysis. This correlation provides the fundamentals behind the photocatalysis and subsequently the real industrial application of photocatalytic reactions as well as the photocatalytic system design. Therefore, some insights and directions that should be thoroughly addressed are as follows (Mohamed and Bahnemann 2012):

1. More detailed knowledge on the kinetics and mechanisms of electron transfer is required under different parameters such as crystal size, crystalline structure, surface area, and morphology.
2. Investigation of electron transfer characteristics on well-defined semiconductor single crystals is conducted, and then the information obtained is correlated with those in polycrystalline nanoparticles.
3. The experimental observations and the corresponding theoretical model of interfacial electron transfer kinetics need to be correlated in the photocatalytic system.
4. Temperature effects on the kinetics of electron transfer still need to be evaluated in details for several photocatalytic systems.

Various kinetic and mechanistic studies on photoinduced electron transfer have been widely carried out for the thermodynamically favorable reactions such as the photocatalytic reduction of organic halides and metal ions. However, the kinetic and mechanistic details of the energetically unfavorable reactions are still lacking such as those for H_2O or CO_2 photocatalytic reduction.

10.6 Challenges with Past Developments and Direction for Further Research of Photocatalyst

In photocatalytic application, the small number of studies conducted on ordered mesoporous titania is likely related to the difficulties faced in designing it as a material with the ordered porous structure. Ever since the synthesis of mesoporous TiO_2 in 1995 (Antonelli and Ying 1995), many efforts have been made to control the

crystallization and to increase its crystallinity while maintaining its mesoscale order (Ismail and Bahnemann 2011). In case of the traditional mesoporous ZnO materials, the relatively low photocatalytic activity and efficiency are due to the low inherent porosity and instability (Wang et al. 2016b). Therefore, a simple and economical approach is necessary to easily synthesize 1D mesoporous ZnO materials having desired high porosity and satisfactory pore sizes (Wang et al. 2016b). In comparison to the common synthesis method used for ZnO nanostructures, the precursor route is green, low-cost, and facile synthesis with good reproducibility. Hence, this method is a promising candidate for the practical application of ZnO as a photocatalyst (Xiao et al. 2015). Various ZnO morphologies can be fabricated through solution-based chemical processing depending on the used solvents, surfactants as structure-directing agents, synthesis conditions, the precursors, etc. (Srinivasan et al. 2015). Despite great progress made in the field of ZnO synthesis, control over shape, morphology, and structure, there still remains a remarkable challenge (Collard et al. 2014).

The future direction of development should be made in the understanding of the process and improvement of the degradation efficiency for a number of different compounds. Even though many progresses have been made, some challenges from the past development still need attention. One of those is the role of defects in the photocatalytic processes, while the losses of recombination have been detrimental for photocatalytic efficiency, yet defects could also improve the separation of electron hole and could also act as photocatalyst active surface centers. Another interesting challenge is how to enhance the photocatalytic activity under solar and/or visible irradiation particularly. Although this study has been developed through various approaches such as doping, lattice defects, and others, detailed explanations and further work are still needed. Furthermore, the separation system and the toxicity of photocatalyst have been receiving less attention. Due to these challenges, observation of the unpredictable effects of photocatalyst materials in the environment is fully needed (Djurisic et al. 2014).

References

Abarna B, Preethi T, Karunanithi A, Rajarajeswari GR (2016) Influence of jute template on the surface, optical and photocatalytic properties of sol-gel derived mesoporous zinc oxide. Mater Sci Semicond Process 56:243–250. https://doi.org/10.1016/j.mssp.2016.09.004

Abdel Messih MF, Ahmed MA, Soltan A, Anis SS (2017) Facile approach for homogeneous dispersion of metallic silver nanoparticles on the surface of mesoporous titania for photocatalytic degradation of methylene blue and indigo carmine dyes. J Photochem Photobiol A 335:40–51. https://doi.org/10.1016/j.jphotochem.2016.11.001

Acosta-Silva YJ, Nava R, Hernández-Morales V, Macías-Sánchez SA, Gómez-Herrera ML, Pawelec B (2011) Methylene blue photodegradation over titania-decorated SBA-15. Appl Catal B 110:108–117. https://doi.org/10.1016/j.apcatb.2011.08.032

Ahmed MA, Abdel Messih MF, El-Sherbeny EF, El-Hafez SF, Khalifa AMM (2017a) Synthesis of metallic silver nanoparticles decorated mesoporous SnO2 for removal of methylene blue dye by

coupling adsorption and photocatalytic processes. J Photochem Photobiol A 346:77–88. https://doi.org/10.1016/j.jphotochem.2017.05.048

Ahmed MA, Abou-Gamra ZM, Salem AM (2017b) Photocatalytic degradation of methylene blue dye over novel spherical mesoporous Cr2O3/TiO2 nanoparticles prepared by sol-gel using octadecylamine template. J Environ Chem Eng 5(5):4251–4261. https://doi.org/10.1016/j.jece.2017.08.014

Akpan UG, Hameed BH (2009) Parameters affecting the photocatalytic degradation of dyes using TiO2-based photocatalysts: a review. J Hazard Mater 170(2):520–529. https://doi.org/10.1016/j.jhazmat.2009.05.039

Al-Hamdi AM, Rinner U, Sillanpää M (2017) Tin dioxide as a photocatalyst for water treatment: a review. Process Saf Environ Prot 107:190–205. https://doi.org/10.1016/j.psep.2017.01.022

Ali I, Asim M, Khan TA (2012) Low cost adsorbents for the removal of organic pollutants from wastewater. J Environ Manag 113:170–183. https://doi.org/10.1016/j.jenvman.2012.08.028

Alosfur FKM, Ridha NJ, Jumali MHH, Radiman S (2018) One-step formation of TiO2 hollow spheres via a facile microwave-assisted process for photocatalytic activity. Nanotechnology 29 (14):145707. https://doi.org/10.1088/1361-6528/aaabee

Anpo M, Shima T, Kodama S, Kubokawa Y (1987) Photocatalytic hydrogenation of propyne with water on small-particle titania: size quantization effects and reaction intermediates. J Phys Chem 91(16):4305–4310. https://doi.org/10.1021/j100300a021

Antonelli DM, Ying JY (1995) Synthesis of hexagonally packed Mesoporous TiO2 by a modified sol–gel method. Angew Chem Int Ed 34(18):2014–2017. https://doi.org/10.1002/anie.199520141

Areerob Y, Cho JY, Jang WK, Oh WC (2018) Enhanced sonocatalytic degradation of organic dyes from aqueous solutions by novel synthesis of mesoporous Fe3O4-graphene/ZnO@SiO2 nanocomposites. Ultrason Sonochem 41:267–278. https://doi.org/10.1016/j.ultsonch.2017.09.034

Bacariza MC, Graça I, Bebiano SS, Lopes JM, Henriques C (2018) Micro- and mesoporous supports for CO2 methanation catalysts: a comparison between SBA-15, MCM-41 and USY zeolite. Chem Eng Sci 175:72–83. https://doi.org/10.1016/j.ces.2017.09.027

Bagheri M, Mahjoub AR (2016) Template assisted fast photocatalytic degradation of azo dye using ferric oxide–gallia nanostructures. RSC Adv 6(90):87555–87563. https://doi.org/10.1039/C6RA16317C

Bagheri S, Mohd Hir ZA, Yousefi AT, Abdul Hamid SB (2015) Progress on mesoporous titanium dioxide: synthesis, modification and applications. Microporous Mesoporous Mater 218:206–222. https://doi.org/10.1016/j.micromeso.2015.05.028

Ban J, Xu G, Zhang L, Lin H, Sun Z, Lv Y, Jia Z (2017) Mesoporous ZnO microcube derived from a metal-organic framework as photocatalyst for the degradation of organic dyes. J Solid State Chem 256:151–157. https://doi.org/10.1016/j.jssc.2017.09.002

Bijanzad K, Tadjarodi A, Akhavan O (2015) Photocatalytic activity of mesoporous microbricks of ZnO nanoparticles prepared by the thermal decomposition of bis(2-aminonicotinato) zinc (II). Chin J Catal 36(5):742–749. https://doi.org/10.1016/S1872-2067(14)60305-3

Bonelli B, Esposito S, Freyria FS (2017) Mesoporous Titania: synthesis, properties and comparison with non-porous Titania. In: Janus M (ed) Titanium dioxide. Intechopen, London, pp 119–141. https://doi.org/10.5772/intechopen.68884

Bouzid H, Faisal M, Harraz FA, Al-Sayari SA, Ismail AA (2015) Synthesis of mesoporous ag/ZnO nanocrystals with enhanced photocatalytic activity. Catal Today 252:20–26. https://doi.org/10.1016/j.cattod.2014.10.011

Bradshaw D, El-Hankari S, Lupica-Spagnolo L (2014) Supramolecular templating of hierarchically porous metal-organic frameworks. Chem Soc Rev 43(16):5431–5443. https://doi.org/10.1039/C4CS00127C

Brinker CJ, Brow RK, Tallant DR, Kirkpatrick RJ (1990) Surface structure and chemistry of high surface area silica gels. J Non-Cryst Solids 120(1):26–33. https://doi.org/10.1016/0022-3093(90)90187-Q

Chakma S, Moholkar V (2015) Sonochemical synthesis of mesoporous ZrFe2O5 and its application for degradation of recalcitrant pollutants. RSC Adv 5(66):53529–53542. https://doi.org/10.1039/C5RA06148B

Chen X, Mao SS (2007) Titanium dioxide nanomaterials: synthesis, properties, modifications, and applications. Chem Rev 107(7):2891–2959. https://doi.org/10.1021/cr0500535

Chen G, Sun M, Wei Q, Zhang Y, Zhu B, Du B (2013) Ag3PO4/graphene-oxide composite with remarkably enhanced visible-light-driven photocatalytic activity toward dyes in water. J Hazard Mater 244–245:86–93. https://doi.org/10.1016/j.jhazmat.2012.11.032

Chen H, Peng YP, Chen KF, Lai CH, Lin YC (2016) Rapid synthesis of Ti-MCM-41 by microwave-assisted hydrothermal method towards photocatalytic degradation of oxytetracycline. J Environ Sci 44:76–87. https://doi.org/10.1016/j.jes.2015.08.027

Chen X, Zhang H, Zhang D, Miao Y, Li G (2018) Controllable synthesis of mesoporous multi-shelled ZnO microspheres as efficient photocatalysts for NO oxidation. Appl Surf Sci 435:468–475. https://doi.org/10.1016/j.apsusc.2017.11.045

Cheng G, Xu F, Stadler FJ, Chen R (2015) A facile and general synthesis strategy to doped TiO2 nanoaggregates with a mesoporous structure and comparable property. RSC Adv 5 (79):64293–64298. https://doi.org/10.1039/C5RA11099H

Chou TP, Fryxell GE, Li XS, Cao G (2004) Development of titania nanostructures for the exploration of electron transport in dye-sensitized solar cells. Proc SPIE Nanophotonic Mater 5510. https://doi.org/10.1117/12.563083

Chowdhury IH, Ghosh S, Naskar MK (2016) Aqueous-based synthesis of mesoporous TiO2 and ag–TiO2 nanopowders for efficient photodegradation of methylene blue. Ceram Int 42(2, Part A):2488–2496. https://doi.org/10.1016/j.ceramint.2015.10.049

Collard X, El-Hajj M, Su BL, Aprile C (2014) Synthesis of novel mesoporous ZnO/SiO2 composites for the photodegradation of organic dyes. Microporous Mesoporous Mater 184:90–96. https://doi.org/10.1016/j.micromeso.2013.09.040

Corma A (1997) From microporous to mesoporous molecular sieve materials and their use in catalysis. Chem Rev 97(6):2373–2420. https://doi.org/10.1021/cr960406n

Das SK, Bhunia MK, Bhaumik A (2010) Highly ordered Ti-SBA-15: efficient H2 adsorbent and photocatalyst for eco-toxic dye degradation. J Solid State Chem 183(6):1326–1333. https://doi.org/10.1016/j.jssc.2010.04.015

Dash SK, Parida K, Rath D (2015) Synthesis of a mesoporous silica. In: Alio M (ed) A comprehensive guide to Mesoporous silica, 1st edn. Nova Publication, New York, pp 43–67

Dhiman P, Naushad M, Batoo KM et al (2017) Nano FexZn1−xO as a tuneable and efficient photocatalyst for solar powered degradation of bisphenol a from aqueous environment. J Clean Prod 165:1542–1556. https://doi.org/10.1016/j.jclepro.2017.07.245

Diguna LJ, Murakami M, Sato A, Kumagai Y, Ishihara T, Kobayashi N, Shen Q, Toyoda T (2006) Photoacoustic and Photoelectrochemical characterization of inverse opal TiO2 sensitized with CdSe quantum dots. Jpn J Appl Phys 45(6S):5563–5568. https://doi.org/10.1143/JJAP.45.5563

Diguna LJ, Shen Q, Kobayashi J, Toyoda T (2007a) High efficiency of CdSe quantum-dot-sensitized TiO2 inverse opal solar cells. Appl Phys Lett 91(2):023116. https://doi.org/10.1063/1.2757130

Diguna LJ, Shen Q, Sato A, Katayama K, Sawada T, Toyoda T (2007b) Optical absorption and ultrafast carrier dynamics characterization of CdSe quantum dots deposited on different morphologies of nanostructured TiO2 films. Mater Sci Eng C 27(5):1514–1520. https://doi.org/10.1016/j.msec.2006.06.036

Ding H, Sun H, Shan Y (2005) Preparation and characterization of mesoporous SBA-15 supported dye-sensitized TiO2 photocatalyst. J Photochem Photobiol A 169(1):101–107. https://doi.org/10.1016/j.jphotochem.2004.04.015

Djurisic AB, Leung YH, Ng AMC (2014) Strategies for improving the efficiency of semiconductor metal oxide photocatalysis. Mater Horiz 1(4):400–410. https://doi.org/10.1039/C4MH00031E

Dong Y, Fei X, Zhang H, Yu L (2015) Effects of calcination process on photocatalytic activity of TiO2/MCM-41 Photocatalyst. J Adv Oxid Technol 18:322–330. https://doi.org/10.1515/jaots-2015-0219

Feng X, Zhai J, Jiang L (2005) The fabrication and switchable Superhydrophobicity of TiO2 Nanorod films. Angew Chem Int Ed 44(32):5115–5118. https://doi.org/10.1002/anie.200501337

Fujiwara K, Kuwahara Y, Sumida Y, Yamashita H (2017) Controlling photocatalytic activity and size selectivity of TiO2 encapsulated in hollow silica spheres by tuning silica shell structures using sacrificial biomolecules. Langmuir 33(25):6314–6321. https://doi.org/10.1021/acs.langmuir.7b01528

Garforth A, Fiddy S, Lin YH, Ghanbari-Siakhali A, Sharratt PN, Dwyer J (1997) Catalytic degradation of high density polyethylene: an evaluation of mesoporous and microporous catalysts using thermal analysis. Thermochim Acta 294(1):65–69. https://doi.org/10.1016/S0040-6031(96)03145-0

Gu D, Schüth F (2014) Synthesis of non-siliceous mesoporous oxides. Chem Soc Rev 43(1):313–344. https://doi.org/10.1039/C3CS60155B

Gu L, Chen Z, Sun C, Wei B, Yu X (2010) Photocatalytic degradation of 2, 4-dichlorophenol using granular activated carbon supported TiO2. Desalination 263(1):107–112. https://doi.org/10.1016/j.desal.2010.06.045

He Z, Zhou J (2013) Synthesis, characterization, and activity of tin oxide nanoparticles: influence of solvothermal time on photocatalytic degradation of Rhodamine B. MRC 02(03):13–18. https://doi.org/10.4236/mrc.2013.23A003

He F, Chen G, Yu Y, Zhou Y, Zheng Y, Hao S (2015) The sulfur-bubble template-mediated synthesis of uniform porous g-C3N4 with superior photocatalytic performance. Chem Commun 51(2):425–427. https://doi.org/10.1039/C4CC07106A

Hossain MK, Akhtar US, Koirala AR, Hwang IC, Yoon KB (2015) Steam-assisted synthesis of uniformly mesoporous anatase and its remarkably superior photocatalytic activities. Catal Today 243:228–234. https://doi.org/10.1016/j.cattod.2014.07.045

Hsieh SH, Chen WJ, Wu CT (2015) Pt-TiO2/graphene photocatalysts for degradation of AO7 dye under visible light. Appl Surf Sci 340:9–17. https://doi.org/10.1016/j.apsusc.2015.02.184

Hu E, Wu X, Shang S, Tao XM, Jiang SX, Gan L (2016) Catalytic ozonation of simulated textile dyeing wastewater using mesoporous carbon aerogel supported copper oxide catalyst. J Clean Prod 112:4710–4718. https://doi.org/10.1016/j.jclepro.2015.06.127

Hu W, Yuan X, Liu X, Guan Y, Wu X (2017) Hierarchical SnO2 nanostructures as high efficient photocatalysts for the degradation of organic dyes. J Solgel Sci Technol 84(2):316–322. https://doi.org/10.1007/s10971-017-4511-z

Huang M, Xu C, Wu Z, Huang Y, Lin J, Wu J (2008) Photocatalytic discolorization of methyl orange solution by Pt modified TiO2 loaded on natural zeolite. Dyes Pigments 77(2):327–334. https://doi.org/10.1016/j.dyepig.2007.01.026

Ilinoiu EC, Pode R, Manea F et al (2013) Photocatalytic activity of a nitrogen-doped TiO2 modified zeolite in the degradation of reactive yellow 125 azo dye. J Taiwan Inst Chem Eng 44(2):270–278. https://doi.org/10.1016/j.jtice.2012.09.006

Ismail AA, Bahnemann DW (2011) Mesoporous titania photocatalysts: preparation, characterization and reaction mechanisms. J Mater Chem 21(32):11686–11707. https://doi.org/10.1039/C1JM10407A

Jing Y, Yan W, Xiaowen X (2014) Preparation of Mesoporous SnO2 by electrostatic self-assembly. J Chem 2014:713573. https://doi.org/10.1155/2014/713573

Jung KY, Park SB (1999) Anatase-phase titania: preparation by embedding silica and photocatalytic activity for the decomposition of trichloroethylene. J Photochem Photobiol A 127(1):117–122. https://doi.org/10.1016/S1010-6030(99)00132-X

Kamegawa T, Ishiguro Y, Seto H, Yamashita H (2015) Enhanced photocatalytic properties of TiO2-loaded porous silica with hierarchical macroporous and mesoporous architectures in water purification. J Mater Chem A 3(5):2323–2330. https://doi.org/10.1039/C4TA06020B

Kanakaraju D, Kockler J, Motti CA, Glass BD, Oelgemöller M (2015) Titanium dioxide/zeolite integrated photocatalytic adsorbents for the degradation of amoxicillin. Appl Catal B 166–167:45–55. https://doi.org/10.1016/j.apcatb.2014.11.001

Karimi Z, Mahjoub AR, Aghdam FD (2009) SBA immobilized phosphomolybdic acid: efficient hybrid mesostructured heterogeneous catalysts. Inorg Chim Acta 362(10):3725–3730. https://doi.org/10.1016/j.ica.2009.04.029

Kawahara T, Konishi Y, Tada H, Tohge N, Nishii J, Ito S (2002) A patterned TiO2 (anatase)/TiO2 (rutile) bilayer-type photocatalyst: effect of the anatase/rutile junction on the photocatalytic activity. Angew Chem Int Ed 41(15):2811–2813. https://doi.org/10.1002/1521-3757(20020802)114:15<2935::AID-ANGE2935>3.0.CO;2-6

Kayaalp BE, Lee JY, Kornowski A, Gross S, D'Arienzo M, Mascotto S (2016) Cooperative assembly synthesis of mesoporous SrTiO3 with enhanced photocatalytic properties. RSC Adv 6(93):90401–90409. https://doi.org/10.1039/C6RA13800D

Kim SH, Olson TY, Satcher JH Jr, Han TYJ (2012) Hierarchical ZnO structures templated with amino acid based surfactants. Microporous Mesoporous Mater 151:64–69. https://doi.org/10.1016/j.micromeso.2011.11.015

Koohsaryan E, Anbia M (2016) Nanosized and hierarchical zeolites: a short review. Chin J Catal 37(4):447–467. https://doi.org/10.1016/S1872-2067(15)61038-5

Kowsari E, Abdpour S (2017) In-situ functionalization of mesoporous hexagonal ZnO synthesized in task specific ionic liquid as a photocatalyst for elimination of SO2, NOx, and CO. J Solid State Chem 256:141–150. https://doi.org/10.1016/j.jssc.2017.08.038

Kresge CT, Leonowicz ME, Roth WJ, Vartuli JC, Beck JS (1992) Ordered mesoporous molecular sieves synthesized by a liquid-crystal template mechanism. Nature 359:710–712. https://doi.org/10.1038/359710a0

Lachheb H, Ahmed O, Houas A, Nogier JP (2011) Photocatalytic activity of TiO2–SBA-15 under UV and visible light. J Photochem Photobiol A 226(1):1–8. https://doi.org/10.1016/j.jphotochem.2011.09.017

Lagaly G (1980) K. K. Unger: porous silica — its properties and use as support in column liquid chromatography. Elsevier scientific publishing co., Amsterdam, Oxford, New York 1979. 226 Seiten, Preis: $ 46.25. Ber Bunsenges Phys Chem 84(1):111–111. https://doi.org/10.1002/bbpc.19800840140

Lan H, Wang A, Liu R, Liu H, Qu J (2015) Heterogeneous photo-Fenton degradation of acid red B over Fe2O3 supported on activated carbon fiber. J Hazard Mater 285:167–172. https://doi.org/10.1016/j.jhazmat.2014.10.057

Lázár I, Kalmár J, Peter A, Szilágyi A, Győri E, Ditrói T, Fábián I (2015) Photocatalytic performance of highly amorphous titania–silica aerogels with mesopores: the adverse effect of the in situ adsorption of some organic substrates during photodegradation. Appl Surf Sci 356:521–531. https://doi.org/10.1016/j.apsusc.2015.08.113

Lee J, Kim J, Hyeon T (2003) A facile synthesis of bimodal mesoporous silica and its replication for bimodal mesoporous carbon. Chem Commun 10:1138–1139. https://doi.org/10.1039/B301535A

Lee S, Lee Y, Kim DH, Moon JH (2013) Carbon-deposited TiO2 3D inverse opal photocatalysts: visible-light photocatalytic activity and enhanced activity in a viscous solution. Appl Mater Interfaces 5(23):12526–12532. https://doi.org/10.1021/am403820e

Lee YY, Moon JH, Choi YS, Park GO, Jin M, Li D, Lee JY, Son SU, Kim JM (2017) Visible-light driven photocatalytic degradation of organic dyes over ordered mesoporous CdxZn1-xS materials. J Phys Chem C 121(9):5137–5144. https://doi.org/10.1021/acs.jpcc.7b00038

Léger JM, Haines J, Schmidt M, Petitet JP, Pereira A, da Jornada JAH (1996) Discovery of hardest known oxide. Nature 383:401. https://doi.org/10.1038/383401a0

Li Puma G, Bono A, Krishnaiah D, Collin JG (2008) Preparation of titanium dioxide photocatalyst loaded onto activated carbon support using chemical vapor deposition: a review paper. J Hazard Mater 157(2):209–219. https://doi.org/10.1016/j.jhazmat.2008.01.040

Li X, Xiong Y, Li Z, Xie Y (2006) Large-scale fabrication of TiO2 hierarchical hollow spheres. Inorg Chem 45(9):3493–3495. https://doi.org/10.1021/ic0602502

Li F, Sun S, Jiang Y, Xia M, Sun M, Xue B (2008) Photodegradation of an azo dye using immobilized nanoparticles of TiO2 supported by natural porous mineral. J Hazard Mater 152 (3):1037–1044. https://doi.org/10.1016/j.jhazmat.2007.07.114

Li XH, Wang X, Antonietti M (2012) Mesoporous g-C3N4 nanorods as multifunctional supports of ultrafine metal nanoparticles: hydrogen generation from water and reduction of nitrophenol with tandem catalysis in one step. Chem Sci 3(6):2170–2174. https://doi.org/10.1039/C2SC20289A

Li W, Wu Z, Wang J, Elzatahry AA, Zhao D (2013) A perspective on mesoporous TiO2 materials. Chem Mater 26(1):287–298. https://doi.org/10.1021/cm4014859

Li ZJ, Fan XB, Li XB, Li JX, Ye C, Wang JJ, Yu S, Li CB, Gao YJ, Meng QY, Tung CH, Wu LZ (2014) Visible light catalysis-assisted assembly of Nih-QD hollow nanospheres in situ via hydrogen bubbles. J Am Chem Soc 136(23):8261–8268. https://doi.org/10.1021/ja5047236

Li D, Zhu Q, Han C, Yang Y, Jiang W, Zhang Z (2015a) Photocatalytic degradation of recalcitrant organic pollutants in water using a novel cylindrical multi-column photoreactor packed with TiO2-coated silica gel beads. J Hazard Mater 285:398–408. https://doi.org/10.1016/j.jhazmat.2014.12.024

Li J, Chen Y, Wang Y, Yan Z, Duan D, Wang J (2015b) Synthesis and photocatalysis of mesoporous titania templated by natural rubber latex. RSC Adv 5(28):21480–21486. https://doi.org/10.1039/C4RA15566A

Li X, Masters AF, Maschmeyer T (2015c) Photocatalytic hydrogen evolution from silica-templated polymeric graphitic carbon nitride—is the surface area important? ChemCatChem 7 (1):121–126. https://doi.org/10.1002/cctc.201402567

Li ZD, Wang HL, Wei XN, Liu XY, Yang YF, Jiang WF (2016) Preparation and photocatalytic performance of magnetic Fe3O4@TiO2 core–shell microspheres supported by silica aerogels from industrial fly ash. J Alloys Compd 659:240–247. https://doi.org/10.1016/j.jallcom.2015.10.297

Liu Y, Goebl J, Yin Y (2013) Templated synthesis of nanostructured materials. Chem Soc Rev 42 (7):2610–2653. https://doi.org/10.1039/C2CS35369E

Liu J, Huang J, Zhou H, Antonietti M (2014a) Uniform graphitic carbon nitride nanorod for efficient photocatalytic hydrogen evolution and sustained photoenzymatic catalysis. ACS Appl Mater Interfaces 6(11):8434–8440. https://doi.org/10.1021/am501319v

Liu J, Jin J, Li Y, Huang HW, Wang C, Wu M, Chen LH, Su BL (2014b) Tracing the slow photon effect in a ZnO inverse opal film for photocatalytic activity enhancement. J Mater Chem A 2 (14):5051–5059. https://doi.org/10.1039/C3TA15044E

Liu H, Gong H, Zou M, Jiang H, Abolaji RS, Tareen AK, Yang M (2017) Mo-N-co-doped mesoporous TiO2 microspheres with enhanced visible light photocatalytic activity. Mater Res Bull 96:10–17. https://doi.org/10.1016/j.materresbull.2016.12.041

Lou XW, Archer LA, Yang Z (2008) Hollow micro−−/nanostructures: synthesis and applications. Adv Mater 20(21):3987–4019. https://doi.org/10.1002/adma.200800854

Luo SN, Swadener JG, Ma C, Tschauner O (2007) Examining crystallographic orientation dependence of hardness of silica stishovite. Phys B Condens Matter 399(2):138–142. https://doi.org/10.1016/j.physb.2007.06.011

Mahalakshmi M, Vishnu Priya S, Arabindoo B, Palanichamy M, Murugesan V (2009) Photocatalytic degradation of aqueous propoxur solution using TiO2 and Hβ zeolite-supported TiO2. J Hazard Mater 161(1):336–343. https://doi.org/10.1016/j.jhazmat.2008.03.098

Mahmoodi NM, Abdia J, Oveisia M, Asli MA, Vossoughi M (2018) Metal-organic framework (MIL-100 (Fe)): synthesis, detailed photocatalytic dye degradation ability in colored textile wastewater and recycling. Mater Res Bull 100:357–366. https://doi.org/10.1016/j.materresbull.2017.12.033

Meng S, Li D, Wang P, Zheng X, Wang J, Chen J, Fang J, Fu X (2013) Probing photonic effect on photocatalytic degradation of dyes based on 3D inverse opal ZnO photonic crystal. RSC Adv 3 (38):17021–17028. https://doi.org/10.1039/C3RA42618A

Mishra A, Fischer MK, Bäuerle P (2009) Metal-free organic dyes for dye-sensitized solar cells: from structure: property relationships to design rules. Angew Chem Int Ed 48(14):2474–2499. https://doi.org/10.1002/anie.200804709

Mohamed HH, Bahnemann DW (2012) The role of electron transfer in photocatalysis: fact and fictions. Appl Catal B Environ 128:91–104. https://doi.org/10.1016/j.apcatb.2012.05.045

Mohamed RM, Ismail AA, Othman I, Ibrahim IA (2005) Preparation of TiO2-ZSM-5 zeolite for photodegradation of EDTA. J Mol Catal A Chem 238(1):151–157. https://doi.org/10.1016/j.molcata.2005.05.023

Mondal K, Sharma IA (2014) Photocatalytic oxidation of pollutant dyes in wastewater by TiO2 and ZnO nano-materials–a mini-review. In: Misra A, Bellare JB (eds) Nanoscience & technology for mankind. The National Academy of Sciences India, New Delhi, pp 36–72

More PM, Umbarkar SB, Dongare MK (2016) Template-free sol–gel synthesis of high surface area mesoporous silica based catalysts for esterification of di-carboxylic acids. C R Chim 19 (10):1247–1253. https://doi.org/10.1016/j.crci.2016.02.001

Moussaoui Y, Kachbouri S, Elaloui E (2018) The effect of surfactant chain length and type on the photocatalytic activity of mesoporous TiO2 nanoparticles obtained via modified sol-gel process. Iran J Chem Chem Eng, avalaible online at http://www.ijcce.ac.ir/article_29528_0.html. Accessed Aug 2018 In press)

Nada MH, Larsen SC (2017) Insight into seed-assisted template free synthesis of ZSM-5 zeolites. Microporous Mesoporous Mater 239:444–452. https://doi.org/10.1016/j.micromeso.2016.10.040

Nipane SV, Korake PV, Gokavi GS (2015) Graphene-zinc oxide nanorod nanocomposite as photocatalyst for enhanced degradation of dyes under UV light irradiation. Ceram Int 41 (3 Part B):4549–4557. https://doi.org/10.1016/j.ceramint.2014.11.151

Pal A, Jana TK, Chatterjee K (2016) Silica supported TiO2 nanostructures for highly efficient photocatalytic application under visible light irradiation. Mater Res Bull 76:353–357. https://doi.org/10.1016/j.materresbull.2015.12.040

Pang D, Qiu L, Zhu R, Ouyang F (2015) Silica supported SO42-/TiO2 for photocatalytic decomposition of acrylonitrile under simulant solar light irradiation. Chem Eng J 270:590–596. https://doi.org/10.1016/j.cej.2015.02.055

Peer M, Luardi M, Jensen KF (2017) A facile soft-templated synthesis of high surface area and highly porous carbon nitrides. Chem Mater 29(4):1496–1506. https://doi.org/10.1021/acs.chemmater.6b03570

Peng Q, Dong Y, Li Y (2003) ZnSe semiconductor hollow microspheres. Angew Chem Int Ed 42 (26):3027–3030. https://doi.org/10.1002/anie.200250695

Polshettiwar V, Cha D, Zhang X, Basset JM (2010) High-surface-area silica Nanospheres (KCC-1) with a fibrous morphology. Angew Chem Int Ed 49(50):9652–9656. https://doi.org/10.1002/anie.201003451

Pradhan GK, Reddy KH, Parida KM (2014) Facile fabrication of mesoporous α-Fe2O3/SnO2 nanoheterostructure for photocatalytic degradation of malachite green. Catal Today 224:171–179. https://doi.org/10.1016/j.cattod.2013.10.038

Raizada P, Singh P, Kumar A, Sharma G, Pare B, Jonnalagadda SB, Thakur P (2014) Solar photocatalytic activity of nano-ZnO supported on activated carbon or brick grain particles: role of adsorption in dye degradation. Appl Catal A Gen 486:159–169. https://doi.org/10.1016/j.apcata.2014.08.043

Raza W, Haque MM, Muneer M, Fleisch M, Hakki A, Bahnemann D (2015) Photocatalytic degradation of different chromophoric dyes in aqueous phase using La and Mo doped TiO2 hybrid carbon spheres. J Alloys Compd 632:837–844. https://doi.org/10.1016/j.jallcom.2015.01.222

Reháková M, Čuvanová S, Dzivák M, Rimár J, Gaval'ová Z (2004) Agricultural and agrochemical uses of natural zeolite of the clinoptilolite type. Curr Opin Solid State Mater Sci 8(6):397–404. https://doi.org/10.1016/j.cossms.2005.04.004

Ren X, Ying P, Yang Z, Shang M, Hou H, Gao F (2015) Foaming-assisted electrospinning of large-pore mesoporous ZnO nanofibers with tailored structures and enhanced photocatalytic activity. RSC Adv 5(21):16361–16367. https://doi.org/10.1039/C4RA15421E

Ren X, Hou H, Liu Z, Gao F, Zeng J, Wang L, Li W, Ying P, Yang W, Wu T (2016) Shape-enhanced photocatalytic activities of thoroughly mesoporous zno nanofibers. Small 12 (29):4007–4017. https://doi.org/10.1002/smll.201600991

Reyes MK, Dashdorj U, Amarjargal A, Park CH, Kim CS (2015) Simple and rapid synthesis of mesoporous nanosheet-based ZnO hierarchical structure loaded with metal nanoparticles. Ceram Int 41(2, Part A):2022–2027. https://doi.org/10.1016/j.ceramint.2014.09.126

Saravanan R, Manoj D, Qin J, Naushad M, Gracia F, Lee AF, Khan MM, Gracia-Pinilla MA (2018) Mechanothermal synthesis of ag/TiO2 for photocatalytic methyl orange degradation and hydrogen production. Process Saf Environ Prot 120:339–347. https://doi.org/10.1016/j.psep.2018.09.015

Setthaya N, Chindaprasirt P, Yin S, Pimraksa K (2017) TiO2-zeolite photocatalysts made of metakaolin and rice husk ash for removal of methylene blue dye. Powder Technol 313:417–426. https://doi.org/10.1016/j.powtec.2017.01.014

Shan AY, Ghazi TIM, Rashid SA (2010) Immobilisation of titanium dioxide onto supporting materials in heterogeneous photocatalysis: a review. Appl Catal A Gen 389(1):1–8. https://doi.org/10.1016/j.apcata.2010.08.053

Sharma G, Bhogal S, Naushad M et al (2017) Microwave assisted fabrication of La/cu/Zr/carbon dots trimetallic nanocomposites with their adsorptional vs photocatalytic efficiency for remediation of persistent organic pollutants. J Photochem Photobiol A Chem 347:235–243. https://doi.org/10.1016/j.jphotochem.2017.07.001

Silva TL, Cazetta AL, Souza PSC, Zhang T, Asefa T, Almeida VC (2018) Mesoporous activated carbon fibers synthesized from denim fabric waste: efficient adsorbents for removal of textile dye from aqueous solutions. J Clean Prod 171:482–490. https://doi.org/10.1016/j.jclepro.2017.10.034

Singh S, Mahalingam H, Singh PK (2013) Polymer-supported titanium dioxide photocatalysts for environmental remediation: a review. Appl Catal A Gen 462–463:178–195. https://doi.org/10.1016/j.apcata.2013.04.039

Smått JH, Schunk S, Lindén M (2003) Versatile double-templating synthesis route to silica monoliths exhibiting a multimodal hierarchical porosity. Chem Mater 15(12):2354–2361. https://doi.org/10.1021/cm0213422

Smith DK (2013) Opal, cristobalite, and tridymite: noncrystallinity versus crystallinity, nomenclature of the silica minerals and bibliography. Powder Diffract 13(1):2–19. https://doi.org/10.1017/S0885715600009696

Srikanth B, Goutham R, Narayan RB, Ramprasath A, Gopinath KP, Sankaranarayanan AR (2017) Recent advancements in supporting materials for immobilised photocatalytic applications in waste water treatment. J Environ Manag 200:60–78. https://doi.org/10.1016/j.jenvman.2017.05.063

Srinivasan P, Subramanian B, Djaoued Y, Robichaud J, Sharma T, Bruning R (2015) Facile synthesis of mesoporous nanocrystalline ZnO bipyramids and spheres: characterization, and photocatalytic activity. Mater Chem Phys 155:162–170. https://doi.org/10.1016/j.matchemphys.2015.02.018

Sun J, Chen G, Wu J, Dong H, Xiong G (2013a) Bismuth vanadate hollow spheres: bubble template synthesis and enhanced photocatalytic properties for photodegradation. Appl Catal B 132–133:304–314. https://doi.org/10.1016/j.apcatb.2012.12.002

Sun Z, Bai C, Zheng S, Yang X, Frost RL (2013b) A comparative study of different porous amorphous silica minerals supported TiO2 catalysts. Appl Catal A Gen 458:103–110. https://doi.org/10.1016/j.apcata.2013.03.035

Taguchi A, Smått JH, Lindén M (2003) Carbon monoliths possessing a hierarchical, fully interconnected porosity. Adv Mater 15(14):1209–1211. https://doi.org/10.1002/adma.200304848

Tang X, Feng Q, Liu K, Luo X, Huang J, Li Z (2018) A simple and innovative route to remarkably enhance the photocatalytic performance of TiO2: using micro-meso porous silica nanofibers as carrier to support highly-dispersed TiO2 nanoparticles. Microporous Mesoporous Mater 258:251–261. https://doi.org/10.1016/j.micromeso.2017.09.024

Tripathy N, Ahmad R, Kuk H, Hahn Y-B, Khang G (2016) Mesoporous ZnO nanoclusters as an ultra-active photocatalyst. Ceram Int 42(8):9519–9526. https://doi.org/10.1016/j.ceramint.2016.03.030

Veselý M, Zita J, Veselá M, Chovancová J, Chomoucká J, Možíšká P (2005) 6. Physical & applied chemistry 6.1. lectures. Chem List 99:s49–s652

Wakimoto R, Kitamura T, Ito F, Usami H, Moriwaki H (2015) Decomposition of methyl orange using C60 fullerene adsorbed on silica gel as a photocatalyst via visible-light induced electron transfer. Appl Catal B Environ 166–167:544–550. https://doi.org/10.1016/j.apcatb.2014.12.010

Wang L, Kong A, Chen B, Ding H, Shan Y, He M (2005) Direct synthesis, characterization of cu-SBA-15 and its high catalytic activity in hydroxylation of phenol by H2O2. J Mol Catal A Chem 230(1):143–150. https://doi.org/10.1016/j.molcata.2004.12.027

Wang QQ, Lin BZ, Xu BH, Li XL, Chen ZJ, Pian XT (2010a) Preparation and photocatalytic properties of mesoporous SnO2–hexaniobate layered nanocomposite. Microporous Mesoporous Mater 130(1):344–351. https://doi.org/10.1016/j.micromeso.2009.11.033

Wang Y, Wang X, Antonietti M, Zhang Y (2010b) Facile one-pot synthesis of nanoporous carbon nitride solids by using soft templates. ChemSusChem 3(4):435–439. https://doi.org/10.1002/cssc.200900284

Wang C, Shi H, Li Y (2011) Synthesis and characteristics of natural zeolite supported Fe3+-TiO2 photocatalysts. Appl Surf Sci 257(15):6873–6877. https://doi.org/10.1016/j.apsusc.2011.03.021

Wang B, Zhang L, Li B, Li Y, Shi Y, Shi T (2014a) Synthesis, characterization, and oxygen sensing properties of functionalized mesoporous silica SBA-15 and MCM-41 with a Pt(II)–porphyrin complex. Sensors Actuators B Chem 190:93–100. https://doi.org/10.1016/j.snb.2013.08.036

Wang Y, Zhu S, Chen X, Tang Y, Jiang Y, Peng Z, Wang H (2014b) One-step template-free fabrication of mesoporous ZnO/TiO2 hollow microspheres with enhanced photocatalytic activity. Appl Surf Sci 307:263–271. https://doi.org/10.1016/j.apsusc.2014.04.023

Wang J, Li X, Xia Y, Komarneni S, Chen H, Xu J, Xiang L, Xie D (2016a) Hierarchical ZnO nanosheet-nanorod architectures for fabrication of poly(3-hexylthiophene)/ZnO hybrid NO2 sensor. ACS Appl Mater Interfaces 8(13):8600–8607. https://doi.org/10.1021/acsami.5b12553

Wang X, Huang L, Zhao Y, Zhang Y, Zhou G (2016b) Synthesis of mesoporous ZnO nanosheets via facile solvothermal method as the anode materials for lithium-ion batteries. Nanoscale Res Lett 11(1):37–37. https://doi.org/10.1186/s11671-016-1244-9

Wei JQ, Chen XJ, Wang PF, Han YB, Xu JC, Hong B, Wang XQ (2018) High surface area TiO2/SBA-15 nanocomposites: synthesis, microstructure and adsorption-enhanced photocatalysis. Chem Phys 510:47–53. https://doi.org/10.1016/j.chemphys.2018.05.012

Wellia DW (2012) Green preparation of visible light active titanium dioxide films, thesis

Wu M, Liu J, Jin J, Wang C, Huang S, Deng Z, Li Y, Su BL (2013a) Probing significant light absorption enhancement of titania inverse opal films for highly exalted photocatalytic degradation of dye pollutants. Appl Catal B Environ 150–151:411–420. https://doi.org/10.1016/j.apcatb.2013.12.037

Wu SH, Mou CY, Lin HP (2013b) Synthesis of mesoporous silica nanoparticles. Chem Soc Rev 42(9):3862–3875. https://doi.org/10.1039/C3CS35405A

Xia Y, Wang J, Chen R, Zhou D, Xiang L (2016) A review on the fabrication of hierarchical ZnO nanostructures for photocatalysis application. Crystals 6(11):148. https://doi.org/10.3390/cryst6110148

Xiao S, Li H, Liu L, Lian J (2015) Glucose-assisted generation of assembled mesoporous ZnO sheets with highly efficient photocatalytic performance. Mater Sci Semicond Process 39:680–685. https://doi.org/10.1016/j.mssp.2015.05.051

Xiao L, Youji L, Feitai C, Peng X, Ming L (2017) Facile synthesis of mesoporous titanium dioxide doped by ag-coated graphene with enhanced visible-light photocatalytic performance for methylene blue degradation. RSC Adv 7(41):25314–25324. https://doi.org/10.1039/C7RA02198D

Xiao H, Zhang W, Wei Y, Chen L (2018) Carbon/ZnO nanorods composites template by TEMPO-oxidized cellulose and photocatalytic activity for dye degradation. Cellulose 25(3):1809–1819. https://doi.org/10.1007/s10570-018-1651-4

Xin L, Liu X (2015) Black TiO2 inverse opals for visible-light photocatalysis. RSC Adv 5(88):71547–71550. https://doi.org/10.1039/C5RA10280D

Xu J, Yang B, Wu M, Fu Z, Lv Y, Zhao Y (2010) Novel N-F-codoped TiO2 inverse opal with a hierarchical meso−−/macroporous structure: synthesis, characterization, and photocatalysis. J Phys Chem C 114(36):15251–15259. https://doi.org/10.1021/jp101168y

Xu QC, Wellia DV, Yan S, Liao DW, Lim TM, Tan TTY (2011) Enhanced photocatalytic activity of C–N-codoped TiO2 films prepared via an organic-free approach. J Hazard Mater 188 (1):172–180. https://doi.org/10.1016/j.jhazmat.2011.01.088

Yamazoe N, Miua N (1992) Some basic aspects of semiconductor gas sensors. In: Yamauchi S (ed) Chemical sensor technology. Elsevier, Amsterdam, pp 19–42. https://doi.org/10.1016/C2009-0-13117-3

Yan H (2012) Soft-templating synthesis of mesoporous graphitic carbon nitride with enhanced photocatalytic H2 evolution under visible light. Chem Commun 48(28):3430–3432. https://doi.org/10.1039/C2CC00001F

Yang XY, Chen LH, Li Y, Rooke JC, Sanchez C, Su BL (2017) Hierarchically porous materials: synthesis strategies and structure design. Chem Soc Rev 46(2):481–558. https://doi.org/10.1039/C6CS00829A

Ye A, Fan W, Zhang Q, Deng W, Wang Y (2012) CdS–graphene and CdS–CNT nanocomposites as visible-light photocatalysts for hydrogen evolution and organic dye degradation. Catal Sci Technol 2(5):969–978. https://doi.org/10.1039/C2CY20027A

Yin M, Liu S (2015) Controlled ZnO hierarchical structure for improved gas sensing performance. Sensors Actuators B Chem 209:343–351. https://doi.org/10.1016/j.snb.2014.11.129

Yu J, Yu JC, Hoa W, Jiang Z (2002) Effects of calcination temperature on the photocatalytic activity and photo-induced super-hydrophilicity of mesoporous TiO2 thin films. New J Chem 26 (5):607–613. https://doi.org/10.1039/b200964a

Zhang K, Ostraat ML (2016) Innovations in hierarchical zeolite synthesis. Catal Today 264:3–15. https://doi.org/10.1016/j.cattod.2015.08.012

Zhang L, Baumanis C, Robben L, Kandiel T, Bahnemann D (2011) Bi2WO6 inverse opals: facile fabrication and efficient visible-light-driven photocatalytic and photoelectrochemical water-splitting activity. Small 7(19):2714–2720. https://doi.org/10.1002/smll.201101152

Zhang J, Zhang M, Yang C, Wang X (2014) Nanospherical carbon nitride frameworks with sharp edges accelerating charge collection and separation at a soft photocatalytic interface. Adv Mater 26(24):4121–4126. https://doi.org/10.1002/adma.201400573

Zhang JJ, Liu X, Ye T, Zheng GP, Zheng XC, Liu P, Guan XX (2017) Novel assembly of homogeneous reduced graphene oxide-doped mesoporous TiO2 hybrids for elimination of Rhodamine-B dye under visible light irradiation. J Alloys Compd 698:819–827. https://doi.org/10.1016/j.jallcom.2016.12.279

Zhou C, Zhao Y, Bian T, Shang L, Yu H, Wu LZ, Tung CH, Zhang T (2013) Bubble template synthesis of Sn2Nb2O7 hollow spheres for enhanced visible-light-driven photocatalytic hydrogen production. Chem Commun 49(84):9872–9874. https://doi.org/10.1039/C3CC45683H

Znad H, Khalid A, Hena S, Auwal MR (2018) Synthesis a novel multilamellar mesoporous TiO2/ZSM-5 for photo-catalytic degradation of methyl orange dye in aqueous media. J Environ Chem Eng 6(1):218–227. https://doi.org/10.1016/j.jece.2017.11.077

Zu G, Shen J, Wang W, Zou L, Lian Y, Zhang Z (2015) Silica–titania composite aerogel photocatalysts by chemical liquid deposition of titania onto nanoporous silica scaffolds. ACS Appl Mater Interfaces 7(9):5400–5409. https://doi.org/10.1021/am5089132

Index

M. Naushad et al. (eds.), *Green Methods for Wastewater Treatment*, Environmental Chemistry for a Sustainable World 35, https://doi.org/10.1007/978-3-030-16427-0